Loughborough University

The Development of Rubber-Thermoplastic Blends from Ground Tyre Rubber and Waste Polypropylene

by

Shantha M. Egodage

Supervisor – Mr. J. F. Harper

August, 2009

Abstract

The aim of this thesis was to develop and process viable rubber-thermoplastics blends from ground tyre rubber (GTR) and waste polypropylene (WPP). The use of WPP with waste rubber in blends is novel, although limited studies have been carried out on virgin polypropylene (PP)-waste rubber blends. The Delink pretreatment for the GTR is also a novel technique used for property enhancement. To achieve the aim, a number of GTR/WPP blends were prepared, in different blend compositions (from 0 to 100 wt% of each polymer), at different processing parameters, and with two compatibilizing systems. One system called dimaleimide contained N-N' meta-phenylene dimaleimide (HVA-2) as the compatibilizer and either di(tert-butylperoxyisopropyl) benzene (DTBPIB) or 2-2'-dithiobenzothiazole (MBTS) as an activator. The other system contained phenolic resin compatibilizer (SP 1045H resin) and stannous chloride ($SnCl_2$) activator in two forms; anhydrous and dihydrated. The compatibilizer level varied from 0 to 5 pphp, while the activator level varied from 0 to 1 pphp. In a separate investigation, the GTR was pre-treated with Delink up to 9 phr, and GTR treated with the resultant optimum Delink level of 3 phr (DGTR) was blended with WPP to prepare DGTR/WPP blends. All these blends were processed using a Haake Rheocord PolyLab System. The processing characteristics and the mechanical properties of these blends were investigated. The effects were explained by dynamic mechanical properties, melting and crystallization behaviour, sol/gel characteristics and by blend morphology.

Morphological observations of the blends showed a two phase systems, in which GTR was dispersed as domains in the continuous WPP matrix at low GTR contents. At 70 wt% GTR, the GTR dispersed phase changed to a continuous phase. The degree of crystallinity in the WPP remained unchanged up to 60 wt% GTR, but thereafter increased slightly. The processing characteristics and the mechanical properties of the GTR/WPP simple blends were found to be varied with its composition, which directly influenced the phase morphology and the degree of crystallinity. The melt flow index, hardness, tensile strength, secant modulus at 2% strain, and tear resistance decreased with GTR content, while the melt viscosity, the elongation at break and the impact failure energy increased. The blend containing 50 wt% of each polymer produced the best balance of properties.

The effect of processing parameters on the tensile properties is small. A processing temperature of 180 ^{0}C, processing speed of 90 rpm, and processing time of 5 minutes, when processed under a single step adding procedure produced best properties.

The melt viscosity, tensile strength and elongation at break for the 50/50 blends containing HVA-2 showed an increase with HVA-2 level, while the impact energy showed an optimum at a 3 pphp level. The addition of DTBPIB, increased melt viscosity further, and produced a stable phase morphology with the formation of interfacial crosslinks which led to a remarkable improvement in mechanical properties. The optimum DTBPIB level was 0.6 pphp. The addition of MBTS produced a slight increase in tensile properties and a decrease in impact properties. The melt viscosity, tensile strength and elongation at break for the 50/50 blends containing SP resin increased with SP resin level, however, impact properties remained unchanged. The addition of the $SnCl_2$ in any form slightly increased elongation at break but not tensile strength. The blends prepared by adding GTR to the resin modified WPP produced better properties, with a maximum at 4 pphp of SP resin at 0.8 pphp of $SnCl_2$. Thermal properties, swelling behaviour and gel/sol from the boiled xylene extractions for the blends containing compatibilizing systems were correlated with the impact and tensile properties. The remarkable property enhancement in dimaleimide compatibilized blends clearly proved that dimaleimide system was more effective than the resin compatibilizing system as a compatibilizer for GTR/WPP blends. The DGTR/WPP simple blends showed slight improvements in properties compared to the GTR/WPP simple blends at every GTR content. The DGTR/WPP blends produced greater enhancements in properties with the dimaleimide compatibilizing system. No such improvement was noticed with the resin compatibilizing system. The DGTR/WPP (70/30) blend containing the dimaleimide system produced the best property enhancement. The increases in tensile strength, elongation at break, secant modulus and impact failure energy of this blend, over the GTR/WPP (70/30) simple blend were 250%, 420%, 52% and 295%, respectively. All possible chemical reactions for each reactive blend were proposed.

The aim was to develop viable GTR/WPP blends. The enhanced properties of both GTR/WPP and DGTR/WPP blends proved that the viable blends could be produced from the GTR and the WPP, especially with the dimaleimide compatibilizing system.

Acknowledgements

I am very grateful to my principal supervisor, Mr. John. F. Harper of the Materials Department, Loughborough University, UK, for his guidance, patience, time, encouragement and commitment throughout the PhD study program. I am also grateful to my additional supervisor Dr. Shantha Walpalage of the Chemical and Process Engineering Department (DCPE), University of Moratuwa, Sri Lanka for his guidance and encouragement given to me during my stay in Sri Lanka. A special mention of my Research Director, Prof. Marianne Gilbert, for her great cooperation and valuable technical advices.

I wish to express my gratitude to the Head of the Department and all my Colleagues in the Academic staff of DCPE, University of Moratuwa, Sri Lanka for nominating me for a postgraduate degree program. I appreciate the valuable support extended to me in numerous ways by the Officials of Local Secretariat Office – IRQUE Project, University of Moratuwa, Sri Lanka. The World Bank helped me to drive this project by granting all the financial assistance required. The Loughborough University also helped me by providing the cost of my maintenance during my stay in UK.

My special thanks are also due to the Academic and Technical Staff in the Materials Department of Loughborough University, who have helped and supported me in many ways: Dr. Jane Clarke, Dr. Ali Ansarifar, Dr. David Ross, Andy Woolley, Ray Owens, Andrew Lau, John Bates, Frank Page, Trevor Atkinson, June Lennie, and Sue Zhou.

Finally, my gratitude must go to my husband Bandula Egodage, daughter Nipuni Egodage and my parents Mr. & Mrs. Thejasiri Maduwage for their understanding and their whole-hearted support for the completion of this project. To them I dedicate this thesis.

Shantha M. Egodage
August, 2009

Table of Contents

Table of Figures

Table of Tables

Nomenclature

$(\Delta H_f)_c$ - Enthalpy of fusion of pure crystalline polypropylene

ρ - Density

γ - Interfacial tension coefficient

χ_{12} - Thermodynamic interaction parameter/Flory interaction parameter

ΔH_c - Heat of crystallization

ΔH_f - Heat of fusion

v_i - Molar volume of polymer i (=1 or 2)

δ_i - Solubility parameter of polymer i (=1 or 2).

ϕ_i - Volume fraction of polymer i (=1 or 2)

Δl - Interphase thickness

v_s - Volume of the segment taken/volume of repeating unit of polymer chain

ATR - Attenuated total reflection

b - Lattice parameter

B - Interaction energy density

BR - Butadiene rubber

CBS - N-cyclohexyl-2-benzothiozole sulphenamide

C-S - Carbon-sulfur bonds

D - Cooling rate

D_F - Displacement at failure (impact) force

DGTR - Delink treated ground tyre rubber, at 3 phr of Delink

dH_c/dT - Heat flow at temperature T_c

D_M - Displacement at peak (impact) force

DMTA - Dynamic mechanical thermal analysis

DPC - Dicumyl peroxide

DSC - Differential scanning calorimetry

DTBPIB - Di(tert-butylperoxyisopropyl)benzene

DTGA - Differential thermogravimetric analysis

ENR - Epoxidised natural rubber

EOC - Ethylene-octyl copolymer

EPDM - Ethylene propylene diene monomer

F_F - Failure (impact) force

F_M - Peak force

FTIR - Fourier transform infrared spectroscopy

GTR - Ground tyre rubber

HBTP - Hexamethylene N, N' bis(tert-butyl peroxy) carbamate

HDPE - High density polyethylene

H_p - Peak height of the exotherm

HPHTS - High-pressure high-temperature sintering

HVA-2 - N, N'-metaphenylene dimaleimide

k - Boltzmann constant

$KMnO_4$ - Potassium permanganate

LCA - Life cycle assessment

LCST - Lower critical solution temperature

LLDPE - Linear low density polyethylene

LNR - Liquid natural rubber

M - Torque

m - Weight of the material processed

MA - Maleic anhydride

m_{av} - Average mass

MBT - 2-mercaptobenzothiozole

MBTS - 2-2'-dithiobenzothiazole

MFI - Melt flow index

MMA - Methyl methacrylate

m_{nom} - Nominal load

n - Rotor speed

NBR - Nitrile rubber

N_i - Number of moles of polymer i (=1 or 2)

NIR - Near infrared spectroscopy

NMR - Nuclear magnetic resonance

PE - Polyethylene

PET - Polyethylene terephthalate

phr - Parts by weight per hundred parts by weight of rubber

PMMA - Polymethyl methacrylate

PP - Polypropylene

pphp - Parts by weight per hundred parts by weight of the WPP and GTR combined

PS - Polystyrene

PVC - Polyvinyl chloride

R - Universal gas constant

r_i - Number of segments of polymer i (=1 or 2)

RTR - Reclaimed–tyre rubber

SEM - Scanning electron microscopy

S_i - Slope of the high temperature side of the thermogram

SP 1045 - alkyl phenol (para, t-octyl phenol) formaldehyde resin

S-S - Sulfur-sulfur bonds

T - Temperature

$t_1(=0)$ - Initial time

$t_{1/2}$ - Half-time of crystallization

$t_2(=t_{ss})$ - Time at the end of processing (= time to reach steady state)

T_∞ - End crystallization temperature

T_c - Crystallization temperature

t_c - Crystallization time

T_{co} - Onset crystallization temperature

T_g - Glass transition temperature

TGA - Thermogravimetric analysis

T_{ge} - End of the glass transition

T_{go} - Extrapolated onset glass transition

t_i - Cut off time interval

T_m - Melting temperature

t_{max} - Time taken to reach torque maximum

T_{max} - Maximum torque from the moving average trend line

T_{min} - Torque at 8 minutes

TMTD - Tetramethylthiuram disulfide

T_p - Peak crystallization temperature

T_{ss} - Steady state torque

t_{ss} - Time taken to reach steady state

UCST - Upper critical solution temperature

UGTR - Ultrasonically treated GTR

UV - Ultraviolet

V - Volume

W - Specific Energy

W - Specific energy

W_1 - Weight of the specimen

W_2 - Swollen weight of the specimen

W_3 - Final dry weight of the specimen

w_{De} - Delink added to the GTR

W_F - Failure (impact) energy

W_{GTR} - Weight fraction of ground tyre rubber present in the blend

W_M - Energy to peak force or fracture initiation energy

W_P - Fracture propagation energy

WPE - Waste polyethylene

WPP - Waste polypropylene

WTD - Waste tyre dust

W_{WPP} - Weight fraction of waste polypropylene present in the blend

XIF - Xylene insoluble fraction

XIF_B - Xylene-insoluble fraction of the blend

XIF_{GTR} - Xylene-insoluble fraction of the ground tyre rubber

XIF_{WPP} - Xylene-insoluble fraction of the waste polypropylene

X_f - Relative crystallinity

ZDMC - Dimethyldithiocarbomate

ZnO - Zinc oxide

ΔG_{mix} - Gibbs free energy

ΔH_{mix} - Enthalpy of mixing

ΔS_{mix} - Entropy of mixing

ΔT - Supper cooling temperature

ΔW - Half width of the crystallization exotherm

psw - per sample weight

prsw - per GTR weight in the sample

Chapter 1
Introduction

1.1 Polymer Waste Recycling

Over the last two decades of the twentieth century, the general public has become increasingly aware that the energy and raw material resources of the earth are not inexhaustible and also that pollution of the environment for the present and future generations cannot be allowed to continue. This increasing awareness has provided a powerful driving force for the development of strategies for the reuse of especially non-degradable waste materials or their destruction in a safer manner. Polymer waste is a major fraction of the solid wastes collected in the whole world [1-4]. These wastes include post production, post industrial and post consumer polymeric materials mainly from the automotive industry and packaging industry. This waste consists of rubber waste, thermoplastic waste and thermoset composite waste, of which rubber waste and the commodity thermoplastic waste are relatively greater [5].

Polymer waste can either be disposed of in a safe manner [6-10] or recycled and reused [2, 11-42]. Alternatively, these wastes could be utilized to recover energy [6, 10, 43-46] or to recover fuels and other valuable chemicals [46-63], which are feedstock for other industries. Life cycle assessment (LCA) methodology has illustrated that recycling is more advantageous when compared to disposal of polymer wastes [64-70].

The polymer waste can be processed alone [71, 72], or can be processed with other polymer chemicals [71, 73-76]. This waste also can be added to its parent polymer at limited levels [2, 77-80], or can be incorporated into non-polymeric materials [7-9, 63, 81-86]. However, the major potential is to incorporate this polymer waste into polymeric materials. Waste rubber can be incorporated into other virgin rubbers [85-92], or waste plastics can be incorporated into other virgin thermoplastics [14, 93, 94] to produce polymer blends. Alternatively, waste rubbers and waste thermoplastics can be mixed together to produce rubber-thermoplastic blends from polymer wastes [95, 96].

1.2 Ground Tyre Rubber (GTR) and Waste Polypropylene (WPP) Blends

Rubber-thermoplastic blends are a popular form of new thermoplastic engineering material having a better balance of properties than is obtainable with a single polymer [97]. The main reason for blending is economy. In addition, rubber-thermoplastic blends are prepared to produce useful materials with a wide range of applications, to improve the polymer processability, and to meet the market forces of recycling [98-102].

Rubber thermoplastic blends made from virgin polymers have been studied by several researchers [100, 103-110]. The incorporation of rubber into the thermoplastics improved the impact strength and ductility of the resulting blend [89, 111]. However, the additions of rubber also resulted in a significant deterioration in mechanical properties such as tensile strength, modulus, tear strength, hardness, etc., [100, 111-113].

Rubber thermoplastic blends using waste rubber and virgin commodity thermoplastics, such as polyethylene (PE), [101, 113-115] or polypropylene (PP), [102, 111, 112, 114, 116, 117] have also been studied. These also showed improved impact strength, with decreased tensile strength, modulus and hardness. However, limited studies have been undertaken into waste rubber/waste thermoplastic blends.

Tyre rubber, polyethylene (PE) and polypropylene (PP) are the major components in any polymer waste collection. Tyre rubber contains both natural rubber and styrene butadiene rubber as major components, and other rubbers such as butadiene rubbers and butyl rubbers as minor components [118]. In addition the tyre rubber will also contain 20-40 wt% carbon black and 10-15 wt% low molecular weight additives [118, 119]. Waste polypropylene (WPP) is valued in rubber-thermoplastic blends more than polyethylene. Compared to PE, PP has a higher rigidity and hardness, and excellent electrical and chemical resistance at higher temperatures [120]. Further, PP is used indoors and outdoors and also in engineering applications.

The mechanical properties of any type of rubber thermoplastic blend mainly depend on the properties of the rubber and thermoplastic phases and their composition

[9, 99-101, 110, 113, 121-123]. Rubber rich blends produce a soft thermoplastic elastomer while plastic rich blends produce a rubber toughened thermoplastic [99, 102, 111]. Further, blend properties depend on melt viscosity of the matrix phase [9, 111], processing conditions [100, 111, 122, 124-127] and moulding techniques [9, 122, 128]. In the case of blends with waste rubbers, the shape of the particle surface [89, 102, 114, 129-131] and the size of the particle [2, 102, 112, 114, 116] have also been shown to have a significant effect on blend properties. However, the property improvement with smaller particles is not justifiable due to additional cost associated with the size reduction.

The major challenge to blending of rubber and thermoplastics is the incompatibility between the two phases, and is enhanced when both polymers are wastes. Common thermoplastics are semi crystalline while waste rubber is amorphous thermoset. Because of this incompatibility, simple blending will not ensure a blend with desirable properties [89, 111, 127, 132]. Hence, selection of a proper compatibilization technique, and thereby a compatibilizing system is highly important.

1.3 Compatibilizing Systems

Compatibilization is the process of improving homogeneity and stability of a blend of immiscible polymers. Compatibility of a blend can be improved by adding a substance called compatibilizer, which has an ability either to crosslink both phases or to improve surface adhesion between them, or by stabilizing morphology during processing. The compatibilizing techniques that are practiced in the polymer industry are categorized as chemical techniques such as the addition of a block or a graft copolymer, dynamic vulcanization or polymer pretreatment [133], and physical techniques such as gamma, ultraviolet, ultrasonic and microwave techniques [95, 134-139]. Physical techniques, compared to chemical techniques are not effective in improving properties of rubber-thermoplastic blends. Further, physical techniques need relatively higher energies, although they are environmentally safe.

The addition of a suitable block or graft copolymer has been used for blends made from commodity thermoplastics and the main rubbers in the GTR namely natural rubber (NR) and styrene butadiene rubber (SBR) [100, 140-143]. Dynamic vulcanization is the

commonest reactive compatibilizing technique used in rubber-thermoplastic blends [124]. Common vulcanizing systems used in rubber processing, have been used to vulcanize the rubber phase in the rubber-thermoplastic blends made from PP and NR or SBR or GTR. These systems included sulfur and sulfur-donor systems [100, 127, 144, 145], organic peroxides [100, 146, 147], maleimides [105, 145, 148-151] and phenolic resins [100, 152-154]. Of the above vulcanizing systems, sulfur [121, 155] and peroxide systems [102, 111, 155-158] have been incorporated into the blends made from PP and waste rubbers. Limited studies have been reported on phenolic resins [111] or on maleimides [159] with blends made from PP and waste rubbers, and especially not for blends made from WPP and GTR.

The maleimides with an activator, such as the peroxides and sulfur accelerators of the thiazole type, have proved an efficient vulcanizing system especially in blends made from virgin NR and PP [145, 150], and ethylene propylene diene monomer (EPDM) and PP [160-162]. The penolic resins in the presence of an activator, like a halogen donor or a metal compound, also behaved as an efficient compatibilizer for blends made from virgin NR and PP [154], EPDM and PP [163-165], and nitrile rubber (NBR) and PP [104, 106, 166, 167]. The above studies reveal the suitability of using maleimides and the phenolic resins in crosslinking diene rubbers in the rubber-thermoplastic blends.

Surface modifications of rubber waste have been used to improve its compatibility with thermoplastics in rubber-thermoplastic blends. This has been done both chemically [102, 113, 156, 168] and physically [119, 131]. In addition, a blend's compatibility could be improved by converting rubber waste to its initial un-vulcanized state, prior to its melt mixing with the thermoplastic. Delink-R, a mix of common industrial rubber chemicals, was successful in this conversion [38, 42, 169, 170]. Therefore, Delink treated rubber was incorporated into virgin rubber compounds to minimize the product cost with balanced properties [38, 171]. However, its incorporation to thermoplastics to produce rubber-thermoplastic blends, and especially to produce GTR/WPP blends, is not yet reported. The rubber chemicals present in the GTR treated with this novel compatibilizing system might develop new crosslinks within the unsaturated rubbers in the GTR phase, and between phases, during melt mixing with the WPP and hence would improve overall blend properties.

1.4 Aim and Objectives of the Project

Polymer blending permits the combination of the attractive features of several materials into one, to improve the deficient characteristics of a particular polymer, and to reduce the price of the end product. Reuse of this waste solves the waste disposal problem that the polymer industry currently faces and will overcome a major environment problem.

The scope of the present study is to develop useful materials from polymer waste for various commercial applications. The market for rubber-thermoplastic blends has grown dramatically because of the ability to recycle, and to process them in conventional thermoplastic machinery. The aim of the project is to develop and process viable rubber-thermoplastic blends from ground tyre rubber (GTR) and waste polypropylene (WPP), as they are the major components in any polymer waste collection.

The objectives of the project are

- To investigate the suitability of the GTR and the WPP in producing rubber-thermoplastic blends
- To develop simple rubber-thermoplastic blends from the GTR and the WPP, to investigate the effect of blend composition and processing parameters on mechanical properties, and thereby to identify the optimum blend composition and process conditions
- To examine the mechanical property enhancement in the GTR/WPP reactive blends made with dimaleimide and phenolic resin compatibilizing systems, and to identify optimum compatibilizer composition in each system
- To identify the Delink treatment conditions and the optimum Delink level, and finally to develop the simple blends and the reactive blends from the Delink treated ground tyre rubber (DGTR) and the WPP
- To propose the most appropriate reaction mechanism for each reactive blend
- By studying the chemical and physical characteristics of the blends to explain the observed mechanical property trends
- To identify the 'best' methods and formulations for the production of viable GTR/WPP blends

Chapter 1
Introduction

1.1 Polymer Waste Recycling

Over the last two decades of the twentieth century, the general public has become increasingly aware that the energy and raw material resources of the earth are not inexhaustible and also that pollution of the environment for the present and future generations cannot be allowed to continue. This increasing awareness has provided a powerful driving force for the development of strategies for the reuse of especially non-degradable waste materials or their destruction in a safer manner. Polymer waste is a major fraction of the solid wastes collected in the whole world [1-4]. These wastes include post production, post industrial and post consumer polymeric materials mainly from the automotive industry and packaging industry. This waste consists of rubber waste, thermoplastic waste and thermoset composite waste, of which rubber waste and the commodity thermoplastic waste are relatively greater [5].

Polymer waste can either be disposed of in a safe manner [6-10] or recycled and reused [2, 11-42]. Alternatively, these wastes could be utilized to recover energy [6, 10, 43-46] or to recover fuels and other valuable chemicals [46-63], which are feedstock for other industries. Life cycle assessment (LCA) methodology has illustrated that recycling is more advantageous when compared to disposal of polymer wastes [64-70].

The polymer waste can be processed alone [71, 72], or can be processed with other polymer chemicals [71, 73-76]. This waste also can be added to its parent polymer at limited levels [2, 77-80], or can be incorporated into non-polymeric materials [7-9, 63, 81-86]. However, the major potential is to incorporate this polymer waste into polymeric materials. Waste rubber can be incorporated into other virgin rubbers [85-92], or waste plastics can be incorporated into other virgin thermoplastics [14, 93, 94] to produce polymer blends. Alternatively, waste rubbers and waste thermoplastics can be mixed together to produce rubber-thermoplastic blends from polymer wastes [95, 96].

1.2 Ground Tyre Rubber (GTR) and Waste Polypropylene (WPP) Blends

Rubber-thermoplastic blends are a popular form of new thermoplastic engineering material having a better balance of properties than is obtainable with a single polymer [97]. The main reason for blending is economy. In addition, rubber-thermoplastic blends are prepared to produce useful materials with a wide range of applications, to improve the polymer processability, and to meet the market forces of recycling [98-102].

Rubber thermoplastic blends made from virgin polymers have been studied by several researchers [100, 103-110]. The incorporation of rubber into the thermoplastics improved the impact strength and ductility of the resulting blend [89, 111]. However, the additions of rubber also resulted in a significant deterioration in mechanical properties such as tensile strength, modulus, tear strength, hardness, etc., [100, 111-113].

Rubber thermoplastic blends using waste rubber and virgin commodity thermoplastics, such as polyethylene (PE), [101, 113-115] or polypropylene (PP), [102, 111, 112, 114, 116, 117] have also been studied. These also showed improved impact strength, with decreased tensile strength, modulus and hardness. However, limited studies have been undertaken into waste rubber/waste thermoplastic blends.

Tyre rubber, polyethylene (PE) and polypropylene (PP) are the major components in any polymer waste collection. Tyre rubber contains both natural rubber and styrene butadiene rubber as major components, and other rubbers such as butadiene rubbers and butyl rubbers as minor components [118]. In addition the tyre rubber will also contain 20-40 wt% carbon black and 10-15 wt% low molecular weight additives [118, 119]. Waste polypropylene (WPP) is valued in rubber-thermoplastic blends more than polyethylene. Compared to PE, PP has a higher rigidity and hardness, and excellent electrical and chemical resistance at higher temperatures [120]. Further, PP is used indoors and outdoors and also in engineering applications.

The mechanical properties of any type of rubber thermoplastic blend mainly depend on the properties of the rubber and thermoplastic phases and their composition

[9, 99-101, 110, 113, 121-123]. Rubber rich blends produce a soft thermoplastic elastomer while plastic rich blends produce a rubber toughened thermoplastic [99, 102, 111]. Further, blend properties depend on melt viscosity of the matrix phase [9, 111], processing conditions [100, 111, 122, 124-127] and moulding techniques [9, 122, 128]. In the case of blends with waste rubbers, the shape of the particle surface [89, 102, 114, 129-131] and the size of the particle [2, 102, 112, 114, 116] have also been shown to have a significant effect on blend properties. However, the property improvement with smaller particles is not justifiable due to additional cost associated with the size reduction.

The major challenge to blending of rubber and thermoplastics is the incompatibility between the two phases, and is enhanced when both polymers are wastes. Common thermoplastics are semi crystalline while waste rubber is amorphous thermoset. Because of this incompatibility, simple blending will not ensure a blend with desirable properties [89, 111, 127, 132]. Hence, selection of a proper compatibilization technique, and thereby a compatibilizing system is highly important.

1.3 Compatibilizing Systems

Compatibilization is the process of improving homogeneity and stability of a blend of immiscible polymers. Compatibility of a blend can be improved by adding a substance called compatibilizer, which has an ability either to crosslink both phases or to improve surface adhesion between them, or by stabilizing morphology during processing. The compatibilizing techniques that are practiced in the polymer industry are categorized as chemical techniques such as the addition of a block or a graft copolymer, dynamic vulcanization or polymer pretreatment [133], and physical techniques such as gamma, ultraviolet, ultrasonic and microwave techniques [95, 134-139]. Physical techniques, compared to chemical techniques are not effective in improving properties of rubber-thermoplastic blends. Further, physical techniques need relatively higher energies, although they are environmentally safe.

The addition of a suitable block or graft copolymer has been used for blends made from commodity thermoplastics and the main rubbers in the GTR namely natural rubber (NR) and styrene butadiene rubber (SBR) [100, 140-143]. Dynamic vulcanization is the

commonest reactive compatibilizing technique used in rubber-thermoplastic blends [124]. Common vulcanizing systems used in rubber processing, have been used to vulcanize the rubber phase in the rubber-thermoplastic blends made from PP and NR or SBR or GTR. These systems included sulfur and sulfur-donor systems [100, 127, 144, 145], organic peroxides [100, 146, 147], maleimides [105, 145, 148-151] and phenolic resins [100, 152-154]. Of the above vulcanizing systems, sulfur [121, 155] and peroxide systems [102, 111, 155-158] have been incorporated into the blends made from PP and waste rubbers. Limited studies have been reported on phenolic resins [111] or on maleimides [159] with blends made from PP and waste rubbers, and especially not for blends made from WPP and GTR.

The maleimides with an activator, such as the peroxides and sulfur accelerators of the thiazole type, have proved an efficient vulcanizing system especially in blends made from virgin NR and PP [145, 150], and ethylene propylene diene monomer (EPDM) and PP [160-162]. The penolic resins in the presence of an activator, like a halogen donor or a metal compound, also behaved as an efficient compatibilizer for blends made from virgin NR and PP [154], EPDM and PP [163-165], and nitrile rubber (NBR) and PP [104, 106, 166, 167]. The above studies reveal the suitability of using maleimides and the phenolic resins in crosslinking diene rubbers in the rubber-thermoplastic blends.

Surface modifications of rubber waste have been used to improve its compatibility with thermoplastics in rubber-thermoplastic blends. This has been done both chemically [102, 113, 156, 168] and physically [119, 131]. In addition, a blend's compatibility could be improved by converting rubber waste to its initial un-vulcanized state, prior to its melt mixing with the thermoplastic. Delink-R, a mix of common industrial rubber chemicals, was successful in this conversion [38, 42, 169, 170]. Therefore, Delink treated rubber was incorporated into virgin rubber compounds to minimize the product cost with balanced properties [38, 171]. However, its incorporation to thermoplastics to produce rubber-thermoplastic blends, and especially to produce GTR/WPP blends, is not yet reported. The rubber chemicals present in the GTR treated with this novel compatibilizing system might develop new crosslinks within the unsaturated rubbers in the GTR phase, and between phases, during melt mixing with the WPP and hence would improve overall blend properties.

1.4 Aim and Objectives of the Project

Polymer blending permits the combination of the attractive features of several materials into one, to improve the deficient characteristics of a particular polymer, and to reduce the price of the end product. Reuse of this waste solves the waste disposal problem that the polymer industry currently faces and will overcome a major environment problem.

The scope of the present study is to develop useful materials from polymer waste for various commercial applications. The market for rubber-thermoplastic blends has grown dramatically because of the ability to recycle, and to process them in conventional thermoplastic machinery. The aim of the project is to develop and process viable rubber-thermoplastic blends from ground tyre rubber (GTR) and waste polypropylene (WPP), as they are the major components in any polymer waste collection.

The objectives of the project are

- To investigate the suitability of the GTR and the WPP in producing rubber-thermoplastic blends
- To develop simple rubber-thermoplastic blends from the GTR and the WPP, to investigate the effect of blend composition and processing parameters on mechanical properties, and thereby to identify the optimum blend composition and process conditions
- To examine the mechanical property enhancement in the GTR/WPP reactive blends made with dimaleimide and phenolic resin compatibilizing systems, and to identify optimum compatibilizer composition in each system
- To identify the Delink treatment conditions and the optimum Delink level, and finally to develop the simple blends and the reactive blends from the Delink treated ground tyre rubber (DGTR) and the WPP
- To propose the most appropriate reaction mechanism for each reactive blend
- By studying the chemical and physical characteristics of the blends to explain the observed mechanical property trends
- To identify the 'best' methods and formulations for the production of viable GTR/WPP blends

Chapter 2

Literature Review

Rubber is not regarded as an environmentally friendly material. Once rubber is vulcanized for commercial applications it behaves as a thermoset which consists of a three dimensional network between rubber molecules. It is difficult to breakdown the strong chemical network. Similarly, thermoplastics are also not regarded as environmentally friendly materials as they are not biodegradable. With specific advantages over traditional materials such as wood, metal, glass, paper and fabrics, their usage has increased. However, the usage of thermoset was limited. For an example, the usage of thermoplastics in Western Europe in 2002 was 85% of all polymers, while that of thermosets was only 15 % [5]. Polymer waste collection also increases accordingly. As the volume of rubber waste and commodity thermoplastic waste are greater than thermoset composite waste, this present work is focused on these two materials.

2.1 Polymer Waste Disposal

Polymer waste, both rubber waste and plastic waste, can be disposed in a safer manner either by using in certain physical applications or by incineration to recover fuel value. Therefore polymer waste disposal can be reviewed under two general categories namely, physical methods and applications, and incineration.

2.1.1 Rubber Waste Disposal

The main source of rubber waste is scrap tyres. Other sources are worn-out footwear, belting, hose, sponge, foam and mechanical rubber goods. This waste may be unvulcanized or vulcanized and also may contain nylon and rayon. Rubber waste disposal has been a burden tqo the industry ever since the use of tyres became a significant fraction of waste rubber piles.

2.1.1.1 Physical Methods and Applications

The uses of rubber waste, which utilize the excellent energy absorbing properties of vulcanized rubber and its resistance to environmental degradation, are classified as physical applications. Whole scrap tyres have been used in artificial fish reefs, in highway abutment crash barriers, in erosion control measures, in splitter industries and for trivial uses such as bumpers, children's swings and flower planters, etc. [6]. Ground rubber waste can be used as an absorbent in the cleaning up of crude oil spills [7] or it can be used alone or mixed with soil as a lightweight backfill [8] or as landfill drainage layer [9].

2.1.1.2 Incineration

Rubber waste has been used as a fuel supplement in power plants, cement kilns and industrial boilers, etc. There are possibilities for disposing of large amounts of rubber waste in municipal incineration (steam generation) systems [6]. It has been reported that rubber waste has more energy value per pound than coal and hence the utilization of rubber waste as a fuel appears to be a good answer for the rubber waste disposal problem. However, the incineration of scrap and waste rubber, which are rich in hydrocarbons, is not the most desirable approach in the long-run particularly when the total natural resource situation is considered. The incineration of rubbers for energy may lead to air pollution [10]. Used or waste rubber is better returned to the production cycle as a useful material such as reclaim, reinforcing carbon black or other carbon compound.

2.1.2 Plastic Waste Disposal

Plastic waste can be a single thermoplastic or a mixture of commodity thermoplastics such as polyethylene (PE), polypropylene (PP), polystyrene (PS), polyethylene terephthalate (PET), polyvinyl chloride (PVC), polymethyl methacrylate (PMMA) and nylon. Sources of plastic waste include containers used for beverages, household containers, packaging films, housings of electrical and electronic appliances, grocery and garbage bags, cables, sheets, battery containers, car bumpers, pipes and accessories,

window frames, carpet fiber, etc. Plastic waste, which is generally none bio- and photo-degradable, has become a major social and environmental problem throughout the world.

2.1.2.1 Physical Methods and Applications

In most countries, plastic waste is managed by dumping on land surfaces, at sea or in wetlands or by burial in excavated pits or by engineering sanitary landfills [10]. However, due to environmental law restrictions, leachate hazards, a reduction in available landfill capacity, disruption of aesthetic values, and the rising costs and generation of explosive greenhouse gases such as methane, disposing of this waste in landfill has become undesirable [10, 43, 45].

2.1.2.2 Incineration

Plastic waste has a high content of hydrocarbons and thereby has a good calorific value and hence can be utilized as an energy source. Recovering energy from plastic waste is not an economical method when compared to conventional power plants due to the initial investment in construction, operating costs and maintenance costs [10, 44]. The incineration of plastic waste can also meet with strong social opposition as it releases carbon dioxide, light hydrocarbons, carbon monoxide, nitrogen oxides, sulfur oxides and dioxins into the environment [43, 46]. However, methane emission from incineration is very low and is only one third that from land filling [10]. The gases emitted from land filling can be collected and used in small scale energy recovery units. The costs of waste disposal by land filling and by incineration are increasing in response to public fears of the hazards involved. Hence, the recycling of plastic waste has been suggested.

2.2 Polymer Waste Recycling

Recycling or utilizing scrap/waste polymer as a raw material, rather than using it in physical applications or as a fuel, has been increasingly important over the last three decades due to the shortage of virgin raw materials. This is importance because of the

increased levels of pollutants in the environment caused by growing stockpiles of polymer waste. Hence, companies, research centers, trade associations, government agencies and private recycling firms in countries where rubber and plastics are consumed on a large scale have expanded their efforts in finding viable polymer recycling methods. Polymer waste recycling can be reviewed under three categories, namely feedstock recycling, rubber recycling and plastic recycling.

2.2.1 Feedstock Recycling

Feedstock recycling, which is also known as chemical recycling or tertiary recycling, is the technique used to convert waste polymer into its original monomer/s, other polymeric components or valuable chemicals. These products could be considered as useful feedstock for downstream industrial processes or as transportation fuels.

2.2.1.1 Feedstock Recycling of Rubber Waste

Rubber waste can be converted into valuable materials by several methods. The commonly practiced method is destructive distillation or pyrolysis. A study on different pyrolyzing processes of scrap tyres has been reported [63], one approach was the direct carbonization at 2000^{0}C for the manufacture of carbon black and another approach was to pyrolyze scrap tyres at a temperature between 500 ^{0}C and 900 ^{0}C for the manufacture of liquid oil as the main product and gas and solid char as by-products. The pyrolytic oil produced can be utilized as a source of chemicals or tackifying resins [63] and as a substitute for diesel fuel [62]. The pyrolytic char could be used in water and gas purification or could be ground to a low-quality carbon black [60]. The char and the oil could also be used as a fuel in existing furnaces [59]. When sulfur was separated, the recovered materials such as rubber, carbon black, and oil extender can be used for many applications in the manufacturing sector [58].

In addition, another approach involving the biodegradation of rubbers has been reported, in which rubber was fermented [43]. However, it was concluded that the toxic substances

usually present in vulcanized rubber kill the microorganisms which had already grown and retarded the process of biodegradation.

2.2.1.2 Feedstock Recycling of Plastic Waste

Feedstock recycling of plastic waste includes depolymerization, partial oxidation and cracking approaches. Condensation polymers such as polyamides and polyesters can be depolymerized via reversible synthesis reactions into diacids and diols or diamines [46]. In contrast to condensation polymers, addition polymers, such as those used in the production of polyolefins are difficult to depolymerize into their original monomers [58]. However, PMMA was thermally depolymerized to methyl mecthacrylate (MMA), at a yield of 98% [57]. Partial oxidation of plastic waste using oxygen or steam generated a mixture of hydrocarbons and synthesis gases like carbon dioxide (CO_2) and hydrogen (H_2) [46].

Cracking processes at elevated temperatures and pressures breakdown long polymer chains into useful low molecular weight compounds. Commodity thermoplastics were thermally degraded and hydrogenated [56], and/or catalytically degraded [54, 55] to liquid fuels such as gasoline and diesel fuel. In addition, these plastics were thermally and catalytically cracked to a variety of hydrocarbon products typically between C-1 and C-15 and then to carbon and hydrogen [49-53, 61]. The carbon could be utilized as carbon black and activated carbon while hydrogen could be used as a clean fuel and a raw chemical material.

Without processing alone, the addition of plastic waste to coal in the coke manufacturing process was reported [47]. In this process, coal and added plastics were carbonated and converted into coke, tar, oil, and coke oven gas in a coke oven chamber.

These studies suggested that the yield and the composition and hence physiochemical properties of the obtained fuels and hydrocarbon products were depended on the type of polymer and catalysts used, and also on the type of reactors and the processing conditions. The results confirmed the viability of the cracking method as a commercial recycling process in producing fuel components. However, all these cracking processes

require significant operating temperatures and are strongly endothermic leading to large adiabatic temperature falls across reactors. Further, the constructions of such reactors as well as the catalysts that use then are fairly expensive. These deficiencies could be overcome by improving the economics of the process itself by using exhausted zero cost catalysts, which will also help feedstock recycling [48].

Use of the above processes to recover activated carbon, carbon black and fuel oil would be economical and it may become a necessity, if a shortage of carbon black feed stock occurred. A recycling process by which polymer waste can be economically converted into a basic raw material in large volume is important to solve the waste disposal problem.

2.2.2 Rubber Recycling

Used or waste rubber products can be reused after repairing such as in the tyre re-treading industry. Otherwise, they can be recycled and reused in the polymer industry itself. Hence, rubber recycling can be referred to as reuse of rubber waste by depolymerization or devulcanization after removing steel and fiber, which are already incorporated in the waste material. There are three main rubber recycling methods namely, chemical methods, mechanical methods and electromagnetic wave methods.

2.2.2.1 Chemical Methods

Recycling by chemical methods like reclaiming, catalyzing and grafting, etc produces rubber, which is capable of being processed, compounded and revulcanized [172]. "Reclaiming" is the process that applies heat and chemical agents to ground vulcanized waste rubber [32]. By-products of petroleum refining such as dipentene, naphtha, unsaturated resin oils, and various other chemicals like alkylated phenol sulfides, aliphatic and aromatic mercaptans, alkyl and aryl amines have been used as effective reclaiming agents [172]. In order to simplify the reclaiming technology, systems were introduced to soften vulcanized rubber by chemical reactions with phenylhydrazine-ferrous chloride catalyst in the presence of atmospheric oxygen [35] and in the absence of

oxygen [33]. The major benefit of using reclaimed rubber is the relatively low cost compared to virgin rubber. In addition, this rubber has advantages on processing. The problems associated with flow, knit, nerve, die-swell and bloom are lessen [34]. However, these rubbers showed poor mechanical properties such as green strength, toughness and tensile strength, when compared to virgin rubber [33, 34, 37]. With the advent of radial tyres requiring high green strength for processing, the usage of reclaim rubber in tyres further declined. These results propose that the reclaiming processes cause extensive mechanical and chemical main chain scissions to give highly branched chain segments, which differ greatly from new rubber. Hence, the usage of reclaim rubber is limited to applications which need low product performance.

In order to improve the properties of reclaim rubber, a phase transfer catalyst namely quaternary ammonium chloride catalyst, was used. It was successful in cleaving polysulfide crosslinks without breaking off the main chain [22]. Alternatively, certain chemical probes like thiol-amine reagent, lithium aluminium hydride, triphenylphosphene, dithiothreitol phenyl lithium and methyl iodide, devulcanize the rubber by breaking the sulfur crosslinks without disturbing the main chain [21]. Delink-R, which consists of rubber curatives, accelerators and activators, has also been used to break the sulfur crosslinks present in the ground rubber waste. These broken crosslinks were re-linked upon moulding at high temperatures [38, 42]. A rubber accelerator called tetra methyl thiuram disulfide (TMTD) alone has also been successfully used as a reclaiming agent [39].

An investigation was reported which involved modifying rubber granules by grafting with ethyl acrylate onto ground-polybutadiene-vulcanizate waste rubber using a redox method, and also via gamma rays [20], and by matathesis of acrylic diene [19]. Devulcanization also could be achieved by dissolving small pieces of vulcanized rubber in o-dichlorobenzene. Most, or all, of the poly-, di- and monosulfidic crosslinks originally present were cleaved without excessive degradation [29]. Hence this process could be used in converting waste/used rubber into a usable material.

In addition, a biotechnological possibility of selective breaking of S-S and S-C bonds has been reported [18]. It was shown that microorganisms, both bacteria and archaea, mainly sulfur oxidizing species, were able to break bonds selectively. As rubber formed by this

microbial desulfurization technique has more flexible rubber chains on its surface, it could be used to produce rubber which could facilitate binding upon vulcanization.

2.2.2.2 Mechanical Methods

Mechanical methods of rubber recycling include grinding of rubber waste by different techniques, namely, ambient grinding, cryogenic grinding and wet/solution grinding [2, 30]. In addition, rubber can be recycled by shear extrusion pulverization and ambient air milling techniques [2]. Grinding produces irregular shaped particles with many small hair-like appendages that attach to other appendages on other particles, or attach to the virgin rubber matrix, producing an intimately bonded mixture [2, 31]. The particle size of ground rubber varies from 10 to 200 mesh depending upon the grinding technique used. Further details of particle characteristics of ground rubber are given in Section 2.6.2.4 and Section 2.8.2.

The chemical and mechanical methods discussed above result in inferior properties and contamination with rubber waste, and also hazardous waste release to the environment. They also do not convert rubber waste to a usable material efficiently, effectively and environmentally friendly. Hence electromagnetic wave technologies, namely microwave and ultrasonic, were considered for the reprocessing of rubber waste.

2.2.2.3 Electromagnetic Wave Methods

Applying a controlled dose of microwave energy at a specified frequency could devulcanize the vulcanized rubber [24, 29]. Materials that have been processed by this technique include ethylene propylene diene monomer (EPDM) hose end trim, butyl bladders and a tyre tread material. These rubbers contained either polar groups or polar components. Although the rubber waste could be devulcanized, without depolymerization, the microwave technique is a batch process and is rather expensive compared to the rubber recycling methods discussed earlier.

The application of ultrasonic waves to the process of devulcanization is an attractive field of study. The continuous rubber devulcanization process was performed in a coaxial extruder, in which an ultrasonic unit was fitted at the die end [27, 28]. In these studies, the ultrasonic frequency of the transducer was maintained at a constant value of 20 MHz. The ultrasonic treatment for styrene butadiene rubber (SBR) resulted in a considerable degree of main chain scission and modification, in addition to a significant break down of sulfidic crosslinks [26]. However, the selective cleavage of inter-chain silicone-carbon bonds without breaking main chain silicone-oxygen bonds in silicone rubber was achieved [25]. It has been reported that a controlled devulcanization of sulfur vulcanized natural rubber could be achieved by varying both the ultrasonic frequency of the transducer and the amplitude of the vibrating element [23]. These results suggest that ultrasonic technology could be used to convert rubber waste to a usable material without re-compounding.

2.2.3 Plastic Recycling

In a similar way to the rubber waste products repair, plastics waste products also could be reused after surface refurbishing. This could be done either by polishing to remove small surface irregularities, or by the application of a coating. However, even though the surface properties were improved by this method, environmental stress cracking and crazing resulted due to the reaction of the plastics with some solvents used in polishing or in coating [10].

2.2.3.1 Steps in the Plastic Recycling Process

The major steps involved in plastic recycling are sorting of waste materials, comminution, decontamination and reprocessing to form recycled component [10]. Identification and sorting of plastic waste is very important as most of the recycling processes prohibit certain types of plastics [10]. In the early days of recycling, plastic waste was sorted out manually by visual inspection, according to the Society of Plastics Industry (SPI) code [17], and by simple tests based on some characteristics of plastics such as density, solubility and heating behaviors, like flammability, odor of vapor fumes, softening or

melting temperatures [10]. Due to the decreasing cost effectiveness and the reduced efficiency of these techniques, they have been superseded by a number of new techniques based on density differences and electrostatic separation [17]. Electronic device with near infrared (NIR) spectroscopy, too, were utilized for online identification of plastics in recycling streams [15].

After preliminary sorting, comminution is carried out with granulators and grinders in order to convert sorted plastics into a form which is more convenient for downstream possessing operations. This can be carried out at room temperature or at lower temperatures with carbon dioxide and liquid nitrogen as refrigerants [16]. Cryogenic impact milling could be used to produce fine powder from flakes of mixed plastic waste [14].

These plastic crumbs are separated at the secondary stage with developed techniques and then depending on the application, they are granulated or pulverized into powder. Tribo-electrostatic separation has been used in order to remove PVC crumbs from mixed plastic waste, which consisted of PE, PP, PS, PVC and PET [12, 13]. This technique was also used to separate PET crumbs from a mixed plastic waste [11]. In addition, density difference separation techniques, which include the float-sink method, centrifugal method and froth flotation, can also be used for sorting purposes [17, 40, 41]. However, separation of PVC from PET using this technique was difficult as the densities of the two materials are very close to each other [10].

Plastic wastes have in their composition additives, other polymers, monomers and so on. These additional materials cause changes in processing characteristics and in properties, as well as forming and/or emitting harmful substances [17]. Hence, they are subjected to a filtration process in the molten state before they undergo final processing into the recycled component. These materials as well as the level of polymer degradation can be identified by IR spectroscopy, thermal analysis and thermo-chemical analysis [10]. Also, near infrared (NIR) spectroscopy combined with neural network analysis has proven to be useful in predicting plasticizer content in PVC [173].

2.2.3.2 Biodegradable Plastics

As an environment friendly option for plastic waste recycling, biodegradable plastics have been produced. Biodegradable materials from plastic wastes were prepared by incorporating biodegradable natural materials such as starch, wood, vegetable matrices, and agro materials as well as lignocellulostic fillers like saw dust, straw and coir [174, 175]. Both fresh and waste biopolymers were added in these studies.

2.3 Life Cycle Assessment Methodology

Life cycle assessment (LCA) methodology is the best environmental management tool that can be used to compare the alternative eco-performances of different recycling and disposing systems [70]. A LCA study of tyres was performed in comparing conventional combustion and supplement fuel in cement kiln [69]. Better results were shown with fuel substitution in cement kilns. In the same study, reuse as filling material based on cryogenic grinding and mechanical grinding processes was analyzed. This study showed a worse result for the grinding processes in terms of environment impact with respect to other alternatives. This was due to their high energy consumption. In another LCA study of shredder residue management, a comparison of land filling, supplemental fuel in cement kilns and fuel oil recovery was carried out [68]. The materials contained in shredder residue were rubber, plastics, glass, and fibers. It was concluded that material and energy recovery alternatives to land filling are beneficial because of conservation of non-renewable resources and reduction of waste disposal. In a separate study assessing profitability of car and truck tyre re-treading, LCA recommended re-treading as the most sustainable recovery alternative compared to other tyre recycling processes [67]. These LCA studies revealed that rubber recycling is advantageous compared to deposal, mainly in land filling.

In a study on LCA with waste plastics, the phases of collection, compaction, sorting, reprocessing and refuse disposal were individually analyzed and quantified in terms of energy and material compositions as well as environmental emissions [70]. The results in terms of the energy saving in the production of recycled plastics compared to that of virgin polyolefin were remarkable. However, in another study, some inefficiency of

recycling, mainly the energy consumption in collection, transportation of low density plastic materials, and water consumption in plastic recycling were detected [45]. In a separate study, LCA of mechanical and feedstock recycling options for the management of plastic packaging wastes was analyzed and compared with conventional options like incineration and land filling [66]. The results of this study confirmed that the recycling scenarios were always preferable to those of non-recycling. Based on a survey of the plastic recycling industry in the USA, the validity of plastic recycling was reconfirmed and suggestions to implement policies that could promote the recycling of plastics were made [65]. Evaluation of issues in production, recycling and international trade of plastics via an optimal life cycle model, formulated by the Chinese plastic sector also showed that plastic waste recycling was economically and environmentally advantageous [64].

2.4 Polymer Waste – Processing and Applications

2.4.1 Ground/Milled Rubber Waste

Ground rubber waste can be processed alone under high temperature and high pressure conditions, or it can be incorporated into its parent polymer. Alternatively, ground rubber waste can be incorporated into other rubbers and thermoplastics. It also can be incorporated into non-polymeric material for specific applications.

2.4.1.1 Processing Alone

High–pressure high-temperature sintering (HPHTS) technology was utilized to produce a solid mass from 100% vulcanized rubber powder. However, only 30-40% of the original mechanical properties were retained with the sintered rubber [71]. Utilization of ground rubber waste as a mat for railway track applications was reported. It was shown that the dynamic stiffness steadily increased with increasing frequency, and it shifted to higher absolute values with increasing static pre-loads [72]. These results suggest that the usage of ground rubber waste alone is not successful for most applications.

2.4.1.2 Processing with Polymer Chemicals

As an improvement over the earlier processes, a method was proposed in which the ground rubber waste was revulcanized, with vulcanizing ingredients, under normal conditions of time, temperature and pressure without adding parent virgin rubber [75]. It was found that the ground rubber could be converted to a plastic or elastomeric material according to the percentage of the vulcanizing ingredients added. A large range of cheap and high quality materials were processed and used as low-transmitting vibration blocks for industrial machines or as resilient coverings absorbing noises in houses [74]. In a separate study a vulcanized rubber powder produced by HPHTS technique, with additives of maleic acid, maleic anhydride, phthalimide and some organic acids, showed enhanced properties compared to the same material processed without such additives [71].

Ground rubber can also be used to prepare water dispersible amphiphilic particulate phase semi-interpenetrating polymer networks [74]. In this study, a mixture of toluene, acrylic acid monomer and azobisisobutyronitrile was used to prepare swollen rubber particles before subjecting them to suspension polymerization. It was recommended that the water dispersible recycled rubber composite particles prepared in this way were suitable for a variety of aqueous applications such as additives in waterborne emulsions and vehicles for wastewater treatment.

2.4.1.3 Blending with Rubbers

Ground rubber waste is incorporated into its parent rubber in order to reduce the cost of the raw material. Ground rubber is widely used in tyre applications including treads, carcasses, inner-liners, sub-treads and bead components and also in mechanical goods, footwear, solid tyres, mats and retreads, normally at levels of 5 to 20 phr [2].

The effect of using ground rubber waste in the parent compound was evaluated by considering tensile properties and making comparison with kaolin clay. A significant drop in tensile properties was reported even when adding low levels of ambient ground rubber scrap and also with fine rubber powders, produced with second stage grinding [79]. However, the addition of cryogenically ground rubber waste into parent compounds at up

to 40 phr resulted in little or no change in hardness, tear strength and compression set, but, the tensile properties were found constant only up to 10 phr addition [80].

An alternative method was reported in which the vulcanized rubber waste was initially milled without grinding and then mixed with sulfur [78]. However, a higher fraction of milled rubber increased the stiffness and caused brittle fracture. These observations suggest that either ground or milled rubber waste could only be used for applications with low product performance.

Ultrasonic technology has also been used to disperse ground rubber waste crumbs in parent rubber compounds [77]. In this study, ground rubber waste was used as a filler in window seal formulations. It was shown that a fine dispersion could be prepared by this technology and hence the properties of the compound improved. The deterioration in some mechanical properties on incorporation of up to 200 phr was marginal compared to the results reported for rubber ground by other methods.

Ground rubber waste could be blended with other rubbers to enhance their properties for specific applications. A study on incorporating 10 phr-devulcanized rubber into new tyre tread compound reported excellent mechanical properties [92]. The devulcanized rubber used in this study was prepared from tyre rubber waste by a continuous devulcanization process carried out in an extruder under high shearing forces. Actual road tests showed that tread wear behavior with the new compound was almost equal to that for the standard type compound.

Work on incorporating ground natural rubber prophylactic waste into EPDM has been reported [91]. In this study, processing characteristics showed that the curing properties such as optimum cure time, scorch time and induction time decreased with increase in ground rubber loading. Increased tensile strength with up to 30 phr of ground rubber addition and maximum elongation at break, at 20 phr, were reported. Similar trends in properties were observed with rubber powder in natural rubber blends [87]. The powder used in this study was a fine convoluted rubber powder obtained from the sanding process when polishing rubber balls. The effects of GTR on cure characteristics, tensile properties and swelling behavior of natural rubber compounds were reported [123]. Cure characteristics for this study were in agreement with previous studies. Further, the

increased ground rubber loading produced better resistance to swelling and reduced elongation at break. However, tensile strength and modulus values exhibited slight increases up to 10 phr loading. In a separate study, dynamic mechanical properties and swelling behavior of natural rubber and reclaim rubber blends were examined [90]. Fracture morphology of rubber compounds containing ground rubber showed that the deterioration of mechanical properties with increased ground rubber loading was due to poor adhesion between the two phases caused by de-wetting of rubber particles followed by void formation [88]. Results of the above studies suggest that the ground rubber waste could be utilized to prepare blends with different rubbers. Further, the ground rubber loading could be varied to produce the properties required for specific applications.

The ground rubber waste can be used for synthetic turf in playgrounds, factory floors and park path, and for mats, floor tiles, under cushion, etc. when applied with a binder such as polyurethane or latex [63, 85, 86].

In Addition, ground rubber waste could be added to common thermoplastics such as PE, PP, PS, polyester resins and epoxy resins, and to other polymeric materials without causing processing difficulties [112, 131, 176]. Technical developments, characteristics and evaluation of rubber-thermoplastic blends will be discussed in detail in Section 2.6.

2.4.1.4 Incorporation into Non-Polymeric Materials

Ground rubber waste can also be utilized in reinforced bituminous binders in all weather-wearing courses in flexible roads [7, 81], substrates for sound attenuation and roof coatings [8] and rubberized concrete component [82-84].

2.4.2 Ground Plastic Waste

As an option to plastic waste recycling, recycled or regenerated plastics can be utilized alone to create products or can be blended with other thermoplastics and rubbers. These can also be incorporated into non-polymeric materials.

2.4.2.1 Processing Alone

The use of 100% mechanical ground post-consumer plastic waste into high quality products has been reported [76]. Results of this work suggested that the properties of blow moulded bottles prepared with 100% post-consumer HDPE exceeded the material specifications for virgin plastic designs. It was further observed that the samples made from 100% PP from shredder residue displayed sufficient material strength for future reprocessing. However, properties in post-consumer recycled HDPE deteriorated due to rapid thermo-oxidative degradation occurring at reprocessing [73].

2.4.2.2 Blending with Thermoplastics

Preparation of blends or composites with plastic wastes has been practiced. This is generally done in order to enhance the properties of a single plastic material which exhibits average mechanical properties. Due to poor interfacial strength between two phases, a blend made from PP and LDPE showed inferior mechanical properties [94]. This study further showed improved properties of the blend in the presence of a third material; namely a compatibilizing agent. The compatibilizers used in this work included EPDM, ethylene propylene rubber (EPR) and polyethylene graft polymer. In the same way, certain fillers, coupling agents and property enhancers could also be added [10]. Alternatively, a composite material could be developed by cryogenic milling but without compatibilizers [93]. Composite material produced from mixed post consumer plastics, which consists of dissimilar generic polymers, exhibited interesting mechanical properties. Despite porosity in the milled plastics, an alloy between immiscible plastics could be prepared [14]. These studies indicate the suitability of using plastic waste in the manufacture of commercial plastic products.

2.4.2.3 Incorporation into Non-Polymeric Materials

Plastic waste can also be incorporated to make an asphalt concrete mixture called, plastiphalt [139].

Results of these studies confirmed the significance of the incorporation of plastic wastes in other plastic materials. In addition to the above applications, as a solution for plastic waste recycling, plastic waste could be utilized to generate new materials either with fresh rubber or with secondary waste rubber.

2.5 Mixing and Polymer Blends

2.5.1 Thermodynamics of Mixing

Polymer processing proceeds as a rule at elevated temperatures, where mixed components are viscous liquids. Their mixing should be considered as the mixing of two liquids and the relationships developed for polymer mixtures [177, 178] could be applied for polymer blends when they are melt mixed. According to the general principles of thermodynamics, the formation of a thermodynamically stable system is accompanied by a decrease in Gibbs free energy, ΔG_{mix}:

$$\Delta G_{mix} = \Delta H_{mix} - T\,\Delta S_{mix} \qquad \text{Equation 2.1}$$

where, ΔH_{mix} and ΔS_{mix} are enthalpy of mixing and entropy of mixing, respectively. T is the absolute temperature. The necessary condition for the system stability is that $\Delta G_{mix} < 0$, which is fulfilled if $\Delta H_{mix} < 0$ and $T\Delta S_{mix} > 0$, or $\Delta H_{mix} > 0$ but $|T\Delta S_{mix}| > |\Delta H_{mix}|$ [179].

For a binary system, the Flory-Huggins-Staverman equation for the Gibbs free energy of mixing per unit volume can be expressed in the following form [179].

$$\frac{\Delta G_{mix}}{V} = \frac{RT}{v_s}\left[\frac{\varphi_1}{r_1}\ln\varphi_1 + \frac{\varphi_2}{r_2}\ln\varphi_2 + \chi_{12}\varphi_1\varphi_2\right] \qquad \text{Equation 2.2}$$

where, V is the total volume, v_s is the volume of the segment taken which is equal to the volume of the repeating unit of the polymer chain (the same for both polymers), r_i is the number of segments of polymer i (=1 or 2), which is proportional to the degree of polymerization, $r_i=v_i/v_s$ (v_i is the molar volume of polymer i), ϕ_i is the volume fraction of polymer i, R is the universal gas constant, and χ_{12} is the thermodynamic interaction parameter, which is also called the 'Flory interaction parameter'.

The first two terms on the right hand side of the Equation 2.2 represent the combinatorial entropy of mixing, and the last term comes from the interaction enthalpy, which is originally assigned to enthalpy of mixing. This equation has been quite successful in describing many of qualitative features of polymer blend thermodynamics [180].

The entropy of mixing can be written as [177, 178]

$$\Delta S_{mix} = -R(N_1 \ln\varphi_1 + N_2 \ln\varphi_2) \qquad \text{Equation 2.3}$$

where, N_i is the number of moles of polymer i (=1 or 2). The entropy of mixing depends on the number of molecules present and hence is a function of the molecular weight. This entropy of mixing is decreasing towards zero, as the degrees of polymerization of the components approach the values typically found in commercially important polymers [180, 181]. This low entropy is a direct result of the high configurational entropy that is characteristic of polymer chains [180].

The enthalpy of mixing, ΔH_{mix}, on the other hand, primarily depends on the energy change associated with the changes in nearest neighbour contacts and is much less dependent on the molecular weight [181]. Since the entropy of mixing of high molecular weight polymers is quite small, the blend stability usually occurs when the enthalpy of mixing is negative, for that the mixing has to be exothermic. This would require unlike polymer molecules to be associated with one another more strongly than like polymer molecules [179]. This is related to the specific interactions between unlike polymers (Section 2.5.4).

The enthalpy of mixing in non-polar systems can be written as [178],

$$\Delta H_{mix} = V(\delta_1 - \delta_2)^2 \phi_1 \phi_2 \qquad \text{Equation 2.4}$$

where, V is the total volume of the mixture and δ_i is the solubility parameter of polymer i (=1 or 2). This enthalpy of mixing is positive, and for most of the polymer pairs, it is larger than the entropy of mixing. As a result, polymer blends are rarely thermodynamically stable. However, where the solubility parameters of the two polymers are very close to each other, the enthalpy of mixing approaches zero and a negative ΔG_{mix} results.

The binary system is at a critical point when [179],

$$\frac{\partial^2 \Delta G_{mix}}{\partial \varphi_1^2} = \frac{\partial^3 \Delta G_{mix}}{\partial \varphi_1^3} = 0 \qquad \text{Equation 2.5}$$

Critical values of composition and interaction parameters can be expressed as,

$$(\varphi_1)_{crit} = \frac{1}{1 + \left(\frac{r_2}{r_1}\right)^{1/2}} \qquad \text{Equation 2.6}$$

$$(\chi_{12})_{crit} = \frac{1}{2}\left(\frac{1}{r_1^{1/2}} + \frac{1}{r_2^{1/2}}\right)^2 \qquad \text{Equation 2.7}$$

For a symmetrical blend (equal degrees of polymerization for both polymers), the critical value of the interaction parameter is given by $(\chi_{12})_{crit} = 2/r$. If $\chi_{12} < (\chi_{12})_{crit}$, the blend is always miscible and if $\chi_{12} > (\chi_{12})_{crit}$, the blend may phase separated into two coexisting phases.

2.5.2 Types of Polymer Blends

Miscibility is a function of the microstructure of the polymers, (eg., molecular weight, tacticity, presence of comonomer, etc.) and thermodynamic variables such as temperature,

pressure and blend composition [180]. A completely miscible polymer blend will result, if the following two conditions are met [182, 183].

Condition-1, $\Delta G_{mix} < 0$ and

Condition-2, $\left(\frac{\partial^2 \Delta G_{mix}}{\partial \phi_2^2}\right)_{T,P} > 0$

The Gibbs free energy (ΔG_{mix}) in a binary system can behave in three different ways, as shown in Figure 2.1 [182]. Curve-A does not satisfy even a single condition and hence represents an immiscible system. Curve-B satisfies both conditions for all compositions and represents a completely miscible system. Curve-C satisfies condition-1 for all compositions, but does not satisfy condition-2 in the middle composition region, where the mixture phase separates. Hence, curve-C represents a partially miscible system. Accordingly, polymer blends can be classified as completely miscible blends, partially miscible blends and as immiscible blends. Partially miscible blends are often called compatible blends and 100% compatible blends are thus miscible blends [180].

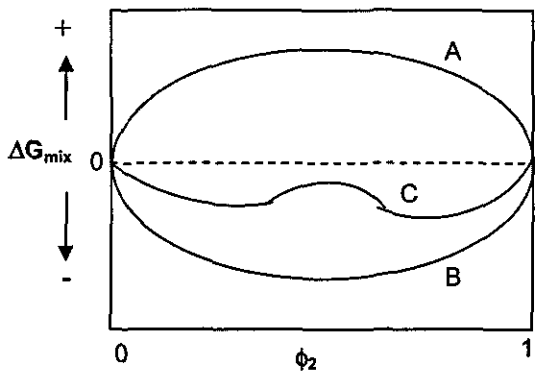

Figure 2.1 Free energy of mixing for binary mixtures; A- immiscible, B- completely miscible, C – partially miscible [182]

2.5.3 Polymer Blend Phase Diagrams

The phase behaviour of a binary system is described by a temperature-composition (T-ϕ) diagram, at ambient pressure [183]. In fact, every blend will be miscible under some

conditions of temperature and composition [180]. Of the five types of phase behaviours (Figure 2.1), hourglass (a) is commonly found in high molecular weight polymer blends, this represents an immiscible blend. The lower critical solution temperature (LCST) phase behaviour (c) is also found in high molecular weight polymer blends, but upper critical solution temperature (UCST)/LCST phase behaviour (d) has rarely been reported. The other phase behaviours are found for small molecules, and for low molecular weight polymer blends. However, different phase behaviours occur for different polymer pairs [179, 180].

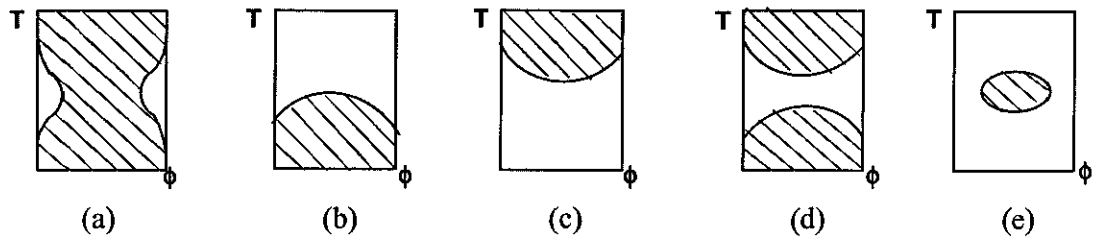

Figure 2.2 Polymer blend phase diagram types (shaded area represents immiscible region); (a) hourglass (b) UCST (c) LCST (d) UCST/LCST (e) loop [180]

2.6.4 Phase Separation and De-mixing

Phase separation of an immiscible polymer blend is relatively slow compared to mixtures of small molecules. This is due to the high viscosity and the slow diffusion (10^{-10} cm^2/sec or less) of long molecules, which are associated with high molecular weight and high levels of molecular entanglements. As a result, the phase separation in an immiscible polymer blend does not reach macroscopic size, but is found on the micron scale [180].

The phase diagram indicates regions of thermodynamic stability, metastability and instability (Figure 2.3). The nature of phase separation depends on where in the phase diagram it takes place. Near to the phase boundary, in the metastable region, phase separation takes place due to a 'nucleation and growth' mechanism. This separation only proceeds by overcoming the activation energy of nucleation. Once the nucleus is formed, it grows by a diffusion of macromolecules towards the nucleus. The macromolecules diffuse from a region of relatively high concentration to the vicinity of the growing nucleus, which is a region of relatively low concentration. This mechanism produces

spheres, with sharp boundaries, of the second phase within a matrix of the first phase. These spheres grow by increasing their diameter with time, whilst their composition remains constant. Further from the phase boundary, in the unstable region, phase separation takes place by a 'spinodal decomposition' mechanism. In this region, there is no barrier to phase separation and it occurs by a continuous and spontaneous process. Spinodal decomposition tends to produce interconnected cylinders of the second phase within a matrix of the first phase. Unlike nucleation and growth, the composition and size increase with time in this mechanism. Spinodal decomposition produces fine phases with blurred interphases until the later stage of decomposition [184].

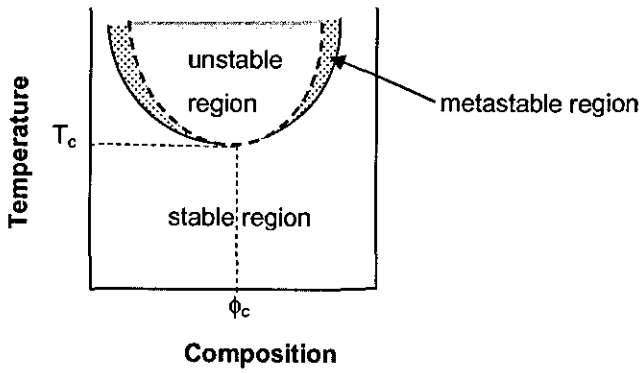

Figure 2.3 LCST phase diagram [183]

Two polymeric melts, will in general, have different free volumes, which relates to their thermal expansion coefficients (Table A.1 in Appendix A.1). This is associated with differences in chain architecture and chain flexibility. Even though this difference is small for most of the polymer pairs, there will be a net volume contraction upon mixing. Such contraction leads to an additional negative contribution to ΔH_{mix} (favourable for mixing) and an additional positive contribution to $-T\Delta S_{mix}$ (unfavourable for mixing). This additional contribution becomes more unfavourable with increasing temperature and leads to LCST demixing. The compressibility (change of volume with pressure) increases with increase in temperature and result in phase separation at higher temperatures.

LCST phase separation can be caused by specific interactions as well. In polymer blends, where specific interactions play a role, LCST demixing is dominated by such interactions rather than compressibility effects, as the difference in thermal expansivity between polymers is relatively small [183]. Unlike the compressibility effect, specific interactions

can cause interaction parameters to become negative (Section 2.5.4). In contrast to dispersive interactions, where heat is consumed upon mixing, specific interactions give rise to heat release upon mixing, and hence give a negative contribution to ΔH_{mix}. Further, these interactions are entropically unfavourable because the degrees of freedom are 'frozen in' in one specific interaction channel. This leads to an additional entropy loss term in the free energy of mixing, which is positive. This unfavourable entropy loss becomes more important with increasing temperature and leads to LCST demixing.

2.5.4 Flory Interaction Parameter and Interphase

In immiscible polymer blends, the phases are not separated by a plane, but separate by a region of inter-diffusion of the two types of polymers [108]. This region is called an interphase, a third phase in the immiscible polymer blend. This interphase has its own properties.

According to the Helfand-Tagami lattice theory, the interphase thickness, Δl, can be expressed as [180, 182, 185]:

$$\Delta l = 2b/(6\chi_{12})^{1/2} \qquad \text{Equation 2.8}$$

where, b is the lattice parameter (assumed the same for both components). Equation 2.8 shows that the interphase thickness is dependent on the thermodynamic interaction of the two components and their molecular weights. Further, this equation shows that the interphase thickness increases with a decrease in the value of χ_{12}.

The Flory interaction parameters, χ_{12}, is related to the interaction energy density, B, that has units in Pa, according to the following equation [180, 182].

$$B = \chi_{12} R T / v \qquad \text{Equation 2.9}$$

where, v is an arbitrary reference volume (also defined as $\sqrt{v_1 v_2}$)

This interaction energy density can be estimated from the solubility parameters of the components in the blend using the following equation [180].

$$B = (\delta_1 - \delta_2)^2 \qquad \text{Equation 2.10}$$

By combining the Equations 2.9 and 2.10, the Flory interaction parameter can be related to the solubility parameters of the two polymer components, as follows [178, 182].

$$(\delta_1 - \delta_2)^2 = \chi_{12}\, R\, T / v \qquad \text{Equation 2.11}$$

Equation 2.11 shows that polymer blends with components having similar or closer solubility parameters increase in blend miscibility and consequently a thicker interphase is obtained.

According to the Helfand-Tagami lattice theory, the interfacial tension coefficient, γ, can be expressed as [180, 182, 185]:

$$\gamma = (\chi_{12}/6)^{1/2} b\, \rho\, k\, T \qquad \text{Equation 2.12}$$

where, k is the Boltzmann constant and ρ is the bulk density (same for both components). This equation implies that the interfacial tension coefficient decreases with a decrease in the value of χ_{12}. This results in an improved adhesion between the phases.

The above relationships explain that the blend structure is mainly depended on the interaction energy density and on the Flory interaction parameter. Figure 2.4 summarises the role of interaction energy density on interphase thickness, adhesion, interfacial tension and hence on particle size of the dispersed phase.

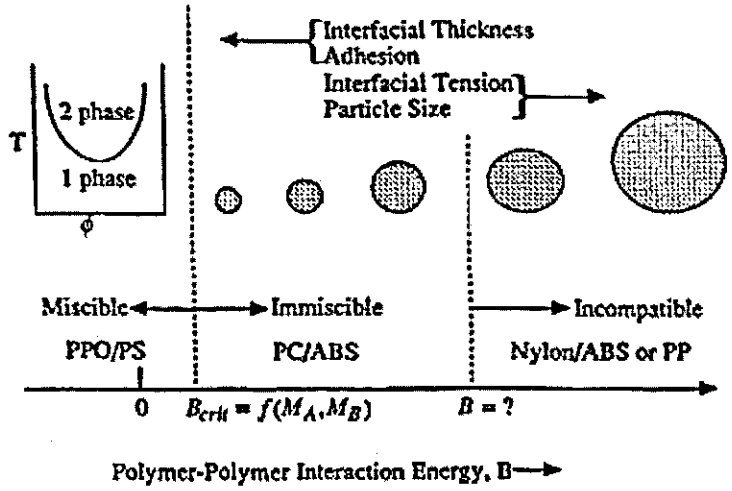

Figure 2.4 Role of polymer-polymer interaction energy on blend structure [184]

2.6 Rubber-thermoplastic Blends

The review of this subject is based on blends produced with common polymers used in the industry. The majority of thermoplastics considered are polypropylene (PP) and polyethylene (PE) and the rubbers are natural rubber (NR), styrene butadiene rubber (SBR) and ethylene propylene diene monomer (EPDM).

2.6.1 Commercial Considerations

Rubber-thermoplastic blends are a type of polymer blend. They have a better balance of properties than obtainable with a single polymer. Hence, blending of rubber and thermoplastics is an appealing alternative for existing applications. The resulting blend material has a hard block/soft block arrangement (Figure 2.5) in which the soft blocks provide the elasticity and softness, while the hard blocks give structure and allow the bulk material to melt and deform as the temperature and pressure increased [97]. This new material can be processed and reprocessed with low cost machinery in the same manner as other thermoplastics [102], and also the scrap produced during processing can be recycled [101]. In addition, processing of these materials does not require factory compounding or vulcanization processes [100] and hence they have faster production

cycles compared to cured thermoset rubber [99]. Rubbers in the blend absorb some amount of heat and allow the thermoplastic fraction to cool faster than pure thermoplastics [98]. These facts contribute to a reduced processing cost compared to pure thermoplastics and thermoset rubbers. In addition, these blends have increased design freedom [99].

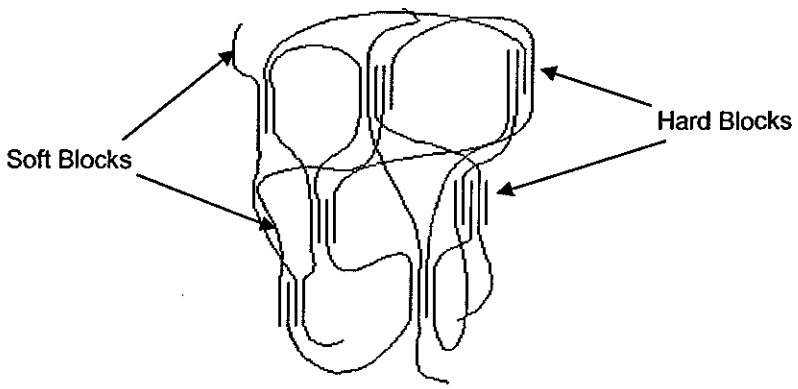

Figure 2.5 Soft block/hard block arrangement in a block copolymer [124]

An option to both rubber and plastic waste recycling is that either waste rubber, or waste plastic, could be incorporated into virgin thermoplastics or virgin rubbers respectively. Alternatively a waste rubber (ground to crumb or powder) and a waste thermoplastic could be utilized to prepare a blend [95, 96].

2.6.2 Factors Affecting Blend Properties

Blend properties mainly depend upon the type of rubber and thermoplastics used to prepare blends, the blend composition, and the adhesion between the two materials [101, 106]. Further, the adhesion between the two materials depends on the shape and size of the dispersed phase formed during the melt mixing process, and thereby on the melt viscosity of the matrix phase and processing conditions. In the case of waste rubbers, the size and shape of the particle surface vary with the grinding technique used [186]. In addition, blend properties will vary with the moulding techniques that are used to make test specimens.

2.6.2.1 Type of Polymer

(a) *Type of Rubber*

The quality of a blend is generally evaluated by its physical and mechanical properties. A study evaluating the effect of type of rubber on blend properties has been reported [102]. In this study, an initial comparison was carried out with EPDM/PP and SBR/PP blends. The rubbers and thermoplastics used in this initial study were virgin materials. The EPDM/PP blend showed higher ultimate tensile strength, and ultimate elongation. Similarly, EPDM/LDPE blends showed better tensile properties compared to NR/LDPE blends, with the poorest properties from SBR/LDPE blends [121] . The better properties with EPDM were attributed to the similarities in the EPDM and PP or LDPE structures compared to NR and SBR with PP or LDPE structures. In agreement, was a study on the replacement of EPDM by NR or epoxidized natural rubber (ENR) in EPDM/PP blends which showed reduction in tensile properties [110]. However, blends with NR compared to ENR, showed difficulty in processing but better tensile properties. The lower performance of ENR compared to NR, should be expected because of the introduction a polar substance to a non-polar system.

Blends of waste-EPDM/PP blends compared to waste-SBR/PP exhibited similar or poorer properties [102]. Respective blends with virgin rubbers showed better tensile properties with EPDM. This difference in results suggests that rubber type is not so important when waste rubbers are used. The rubber waste may behave as a filler in the blend.

(b) *Virgin Rubber versus Waste Rubber*

Waste-NR/PP blends when compared to NR/PP blends prepared with the same rubber content showed slightly higher tensile strength and Young's modulus but with lower elongation at break [89]. Waste-NR with both LDPE and LLDPE compared to those blends with virgin-NR also showed similar variation in tensile properties [101]. These observations suggest that the weaker molecular entanglements in the rubber chain in virgin rubbers producing inferior mechanical properties. Further, the presence of carbon black filled crosslinked rubber particles and other curatives in the waste rubber allowed

the rubber particles to reach higher stresses and provided mechanical strength to the particles. At the same time these ingredients limited the flow and mobility of the particles reducing the elongation capabilities. However, viscosity increases with the addition of carbon black filled waste-EPDM to PP were as not as pronounced as expected [111]. It was concluded that the waste rubber did not behave as a rigid solid filler, but that it had a deformable nature. This filler behavior was confirmed by the observations of increased surface roughness of extrudates at high shear rates for waste-NR/linear low density polyethylene (LLDPE) and waste–NR/LDPE blends, compared to blends with virgin rubber respectively [101].

(c) *Type of Thermoplastic*

The effect of the type of virgin thermoplastic in waste rubber blends was studied by comparing a waste-EPDM/Ethylene-octyl copolymer (EOC) blend and a waste-EPDM/PP blend [102]. The waste-EPDM/EOC blend showed better tensile properties. The results of another study also showed better tensile properties with waste-NR-SBR/EOC blends, compared to waste-NR-SBR/PP blends [111]. These results reveal that the properties of a blend with waste rubbers depend on the characteristics of the thermoplastics used. The differences in properties with different thermoplastics may be due to structure differences and similarities and the polarity of the polymers.

These results agreed with similar studies which used virgin rubbers. In a study comparing NR/copolymer-PP blend and NR/homopolymer-PP blend, greater ductility, and impact strength at low temperatures were shown with the NR/copolymer-PP blends [100]. In a separate study, NR/LLDPE blends exhibited higher viscosities, compared to NR/LDPE blends [101]. Further, the optical photographs obtained in this study illustrated higher surface irregularities with LLDPE/NR blends. These variations in properties were stated to be due to the differences in crystallinity of the thermoplastics used.

2.6.2.2 Blend Composition

It has been shown that rubber rich blends produce a soft thermoplastic elastomer while plastic rich blends produce a rubber toughened thermoplastic [102]. When the rubber

content falls below 65%, the blend acquires properties closer to the thermoplastic than the rubber [99, 111]. The role of rubber in a rubber modified thermoplastics is to improve the impact strength and ductility, as in toughened thermoplastics such as PS and PP [89, 111, 127]. Generally, additions of rubber to a thermoplastic matrix result in a significant deterioration of mechanical properties [113]. In confirming this, the tensile strength, secant modulus and the hardness of rubber-thermoplastic blends were reported to decrease with an increase in rubber content [102, 111, 187]. The stiffness also decreased with increase in rubber content [100].

Waste rubber showed the same trend in results as virgin rubbers [102, 111]. The mechanical properties deteriorated with increase in waste rubber content. In a separate study, an increase in ground tyre rubber (GTR) content, in GTR/LDPE blends, produced an increased viscosity and modulus, slightly increased tensile stress and drastically reduced elongation at break [100]. Further, in contrast to the general belief, an increase in GTR content in GTR/LLDPE blends resulted in a reduced impact strength [113, 122].

2.6.2.3 Melt Viscosity of Matrix Phase

Some characteristic properties of thermoplastics also influence the quality of the blend. In a study blending EPDM with PP having different melt flow index (MFI) values, a higher ultimate elongation was recorded with the PP having the lower MFI [102]. Similar trends were observed with SBR/PP blends. In addition, blends of PP with waste-EPDM, waste-SBR and waste-NR-SBR also displayed the same trend in results [111]. In these studies, the consistency index in the power law equation, which varies with the resistance to flow, showed an increase in value with decrease of MFI. These results suggest that higher molecular weight thermoplastics, which are associated with both lower MFI and crystallinity, improve the compatibility with amorphous rubber material.

2.6.2.4 Size and Shape of Waste Rubber Particle

Particle size of the ground rubber has also been shown to have a significant effect on blend properties [102, 114]. Higher tensile properties were exhibited with a decreased

particles size of GTR in GTR/LLDPE blends [113]. Further, blends of PP with waste-EPDM and waste-SBR showed an increase in ultimate elongation and tensile strength with a decrease in particle size of rubbers used [102]. Similarly, blends of PP with waste-SBR-NR [112] and with waste tyre dust (WTD) [116] exhibited improved mechanical properties with reduced rubber particle size These results suggest that the higher contact surface area associated with smaller sized dispersed rubber particles could improve adhesion between the two phases effectively leading to a high quality blend. In general, due to thermo-mechanical stresses applied on grinding, crosslinked rubber creates active sites on its particle surfaces. Further, smaller particles result in a more homogeneous distribution of the dispersed phase and hence better properties in the physical blend. However, the improvement with smaller particles in the dispersed phase is marginal and is not justifiable due to the additional cost associated with size reduction [114].

In addition, it has been reported that the particle shape of the waste rubber affects blend properties. For the same rubber particle size, ambient ground rubber based GTR/PP and GTR/LLDPE blends, compared to cryogenically ground rubber based blends, showed better processability, toughness [131] and mechanical properties [130]. GTR/PP and GTR/LDPE blends made with wet milling and roller ground rubber compared to cryogenically GTR, showed lower elongation values. However, no significant variation of ultimate strength was noticed.

Cryogenically ground rubber showed a smoothed flat fracture surface while wet milling ambient ground rubber and roller ground rubber showed multi-lobed morphology and hairy snow like surfaces respectively [89, 102, 114, 129]. The polymer chains present in the blend can penetrate into the cavities on ambient ground rubber particle surfaces, providing in a physical binding between polymer and rubber particles [114]. On the other hand, the smoothed surface particles diminish interactions with the matrix phase. It was explained at the microscopic level that flat smoothed surfaces had less surface area for the same particle size than multi-lobed and hairy snow like surfaces [102]. Hence, this increased surface area and mechanical interlocking obtained with wet milling and roller grinding gave better adhesion between the rubber and thermoplastic phases. In addition, the higher degree of surface oxidation contained in the ambient ground rubber particles may provide better adhesion to the polymers present in the blend [2].

Literature further revealed that an optimum particle size for the rubbery phase in rubber toughened thermoplastics should be somewhere in the range of a micrometer [113]. The toughening effect varies with the nature of the thermoplastic matrix used. As an example, in the case of psuedoplastic polymers, the optimum rubber particle size was found to be about 0.1-0.5 μm. GTR particles, even when ground to the smallest size possible by any technique, are an order of magnitude larger than this optimum size. This confirms the behavior of GTR as a filler when incorporated into a thermoplastic matrix.

2.6.2.5 Processing Conditions

In addition to the material factors, processing conditions could also affect the properties of the blend. Blends could be prepared by melt mixing techniques or solution casting techniques [127]. Because of the mechanical and thermal degradation which take place in melt mixing, melt mixed blends, compared to solution casted blends, showed inferior properties. Melt mixing avoids problems of contamination, solvent and water removal etc [124]. However, the properties of the solution casted blends varied with the solvent used, depending upon the extent of interaction between the blend components and casting solvent. Generally, melt mixed blends are prepared by high shear intense high energy processes either in a twin screw extruder or in an internal mixer. The quality of a blend was reported to depend on the type of equipment used [127]. Higher elongations resulted from blends processed by two-step or batch mixing with an internal mixer, compared to continuous mixing with a co-rotating extruder. However, no tensile strength variations were noticed. Image analysis of blends prepared with two step batch mixing showed even dispersion of waste-NR-SBR in a PP matrix. Further, when the average residence time was maintained constant, all blends processed both with an internal mixer and screw extruder, showed similar properties [111]. Theoretically, the quality of a blend will vary with the extent of thermo-mechanical stresses built up by the action of rotating elements in the specific equipment during processing. However, the above results suggest that processing conditions also have a greater influence on the quality of a blend.

Processing parameters such as temperature, mixing procedure, mixing speed/residence time, influence the homogeneity of the blend and hence its properties [122]. The homogeneity of the blend is improved when the viscosities of the two components are

comparable [100]. In order to produce the maximum mixing effect, both components should be in the semisolid state. In general, the temperature at which the blending takes place is to be slightly greater than the melting point of the thermoplastic used, which is always greater than the softening points of common elastomers [100]. Further, blends of NR/LLDPE processed at temperatures lower than their melting temperatures exhibited poor properties. However, enhanced properties of blends of EPDM, SBR and NR/SBR with PP were obtained with elevated mixing temperatures [111]. Additionally, GTR/waste-PE blends showed better tensile properties at a temperature of 160 ^{0}C compared to those at a temperature of 300^{0}C [122]. Deterioration of tensile properties at higher temperatures was also shown with NR/PE blends [120]. These observations suggest a severe destruction of the three-dimensional network of the crosslinked rubber, as well as waste-PE, at very high temperatures. This tendency was enhanced with the oxygen atmosphere [100, 125]. The extent of oxidative degradation depends on the nature of the rubber [100]. Further, too high temperature could provoke the carbonization of rubber with a filler-like effect reducing tensile properties [122]. In addition, the lower viscosity of thermoplastics at higher temperatures may result in a less effective mixing producing agglomeration of the components. However, surface irregularities of the extrudates could be reduced when processing at higher temperatures [126]. These results suggest that the best properties of a blend can only be obtained when processing at an optimum temperature.

A study based on GTR/waste-PE showed that higher levels of depolymerization occurred at increased mixing speeds [102]. Hence, blends prepared at higher mixing rates showed inferior properties. Further, due to the ageing and mechanical degradation of the rubber phases in the blend, at longer blending times, tensile strain showed decreased values. However, it was concluded that the processing speed, blending time and temperature had negligible effects on the change in tensile properties in EPDM/PP blends [102]. Further, the mixing procedure did not produce a significant variation in the ultimate strength of the blends. Another study based on NR/LLDPE [100] illustrated that the level of mixing increased directly with the mixing speed before the optimum rate was reached, providing better properties. Further, it was suggested that the optimum mixing speed was dependent on the processing temperature. These observations demonstrate the importance of optimizing process conditions when preparing a rubber-thermoplastic blend.

2.6.2.6 Moulding Techniques

In addition to the processing conditions, the type of moulding technique used to make test specimens, affects the properties of the blends. Specimens made by injection moulding, compared to compression moulding showed better mechanical properties [122]. This suggests that the higher mixing level, and hence enhanced mechanical properties, were obtained with the high packing pressures associated with the injection moulding techniques. Further, due to the air entrapment at interfaces, blends made with waste rubber having larger particles were unable to be moulded using compression moulding [122]. However, the crosslinked-rubber/PP blends prepared in a reciprocating screw injection moulding machine under high shear moulding, and in a ram injection moulding machine under low shear moulding, did not show significant difference in tensile properties [128].

The results discussed above reveal that, in addition to the composition of the blend, the compatibility between the two phases is the main factor influencing the quality of a blend. Further, they reveal that compatibility, and thereby mechanical properties, could be improved if the phases had similar structures, a low level of crystallinity in the thermoplastics, decreased particle size of the dispersed rubber phase, two-step batch mixing, and with optimum process conditions. MFI was reported as the key factor in enhancing the mechanical properties of the blend as opposed to particle size and blending time [102]. However, the selection of both materials to be blended, and the processing conditions, varied with the required properties of a blend for a specific application.

2.6.3 Applications of Rubber-Thermoplastics Blends

As these blends have characteristics of both rubber and thermoplastic, they have been utilized for a variety of engineering applications, mainly in the automobile industry, for recreation surfacing and flooring products [102, 133]. It was reported that 94% of car bumpers manufactured by the Fiat Company were made from rubber–thermoplastic blends [188]. Auto fascias, and trim and injection moulded auto exterior and interior parts, also were manufactured with blend materials [124]. Alternatively, they were used to produce shoe soles, scrubbing brushes, table cloths and elastic films [97].

Similarly, blends of polymer wastes could be utilized for different applications mainly due to their improved impact strength, increased flexibility and good skid resistance [98]. Blends from ultra-fine car tyre rubber and waste-PP have been commercially used to produce roof slates [130]. In addition, ground rubber powder/thermoplastic blend has been used for shoe soles, mats, sheets and containers [2]. Waste-rubber/waste-PP and waste-rubber/waste-HDPE has been used to produce moulded articles for low strength applications like waste paper baskets and food trays [98]. These blend materials were used for the production of fender liners, splash guards, recreational products, sport surfaces, speed humps, road emergency sign supports and motorway sound barriers [102, 175]. They could also be used in the synthetic lumber industry [98]. A thick sheet, which could be welded on site to form an irrigation ditch profile, was manufactured from tyre rubber crumbs and waste-PE [188].

2.7 Polymer Blend Compatibility

Polymer blending is an effective way of achieving a desirable combination of properties that are often absent in single component polymers. This two- or multi- phase polymer system can either be a copolymer or a mechanical blend. In general, a miscible polymer blend, a copolymer or properly mixed homogeneous mechanical blend, should have one phase and exhibiting a single peak in a tan δ curve produced during dynamic mechanical analysis [100]. This peak should correspond to the glass transition temperature, T_g, of the blend and it should be between the glass transition temperatures of the polymers used. Heterogeneous, immiscible blends are phase separated, exhibiting the glass transition temperatures of the individual polymers (Figure 2.6). If there is partial miscibility the glass transition temperatures will move close together compared with the individual polymers [180, 181].

It has been reported that both waste-SBR/PP and waste-EPDM/PP blends exhibited two peaks at the two different temperatures associated with the T_g of the rubber and thermoplastic respectively [100, 111]. Further, peak heights varied with blend composition. These observations indicate either immiscibility or incompatibility of the two phases in the blend. Hence, homogeneity and thereby the quality of a blend could be improved with the development of compatibility between two dissimilar phases.

The degree of compatibility of a blend can be estimated by observation of the morphology. In miscible blends, due to specific interactions, homogeneity is observed at least at the nano-meter scale, if not at the molecular level. In partially miscible blends, part of one component is dissolved in the other and the blend exhibits fine phase morphology. Immiscible blends have coarse morphology, and poor adhesion between phases. Most polymer blends are immiscible [189].

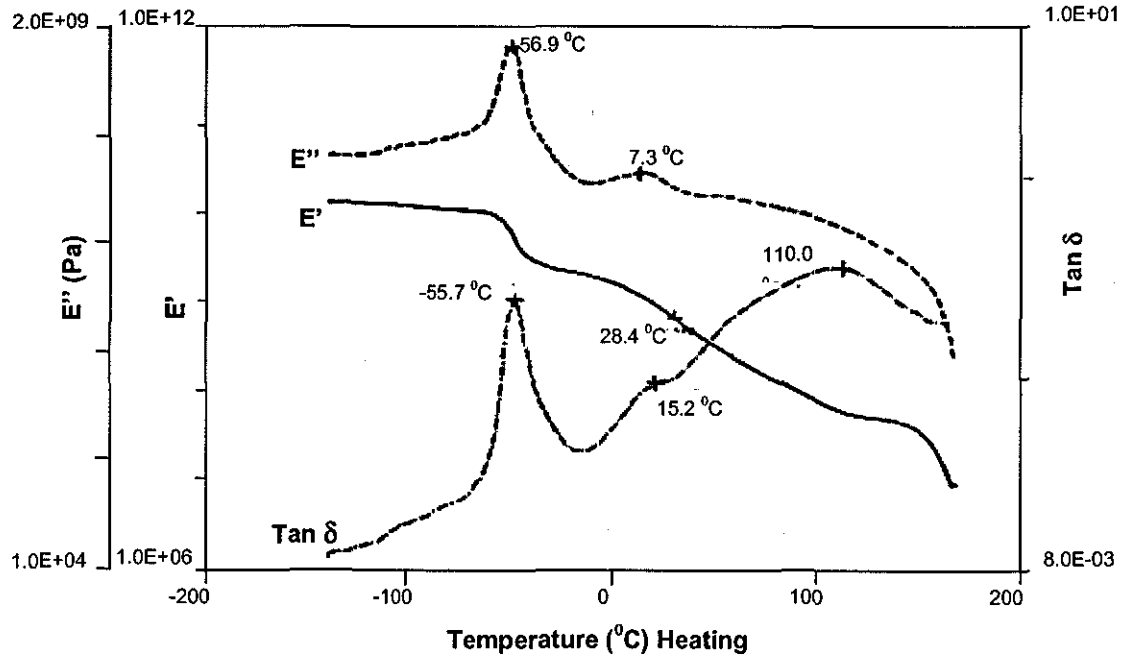

Figure 2.6 Typical dynamic mechanical analysis curves for NR/PP blend showing immiscible behaviour [100]

2.7.1 The Role of Compatibilizers

The miscibility of a blend will occur or will improve, if ΔH_{mix} is negative and hence if the value of χ_{12} is negative (Section 2.5). A negative value of χ_{12} will result due to the presence of strong attractive interactions between the components. These attractions, which are often called specific interactions, are not present in either component by itself but appear when both are present. In addition, a negative value of χ_{12} will result if one or both components are statistical copolymers, in which the sequential distribution of the

monomeric units obeys known statistical laws like Bernouliaan and Markovian statistics. Thus the miscibility of immiscible blends or partially miscible blends could be improved by introducing specific interactions externally via compatibilizers [181].

The interaction between the phases occurs across the interphase (Figure 2.7) and hence the driving force for phase separation is located at the interphase. The size of the phase domains produced during mixing is controlled partly by interfacial tension, as is the adhesion between phases. The mechanical behaviour of the blend will depend on the nature of the interphase and its ability to transmit stresses from one phase to the other [180, 181].

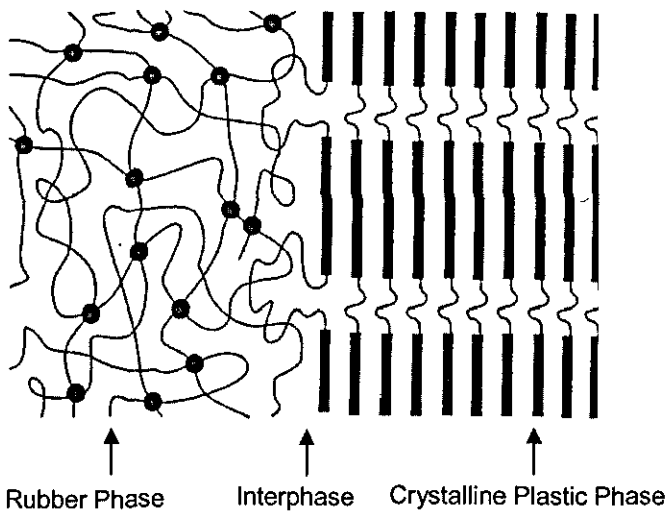

Figure 2.7 Formation of an interphase between rubber and plastic phases [124]

Polymeric additives are generally used as compatibilizers to modify the interphase [180]. The function of a compatibilizer is analogous to that of a surfactant stabilizing a water/oil emulsion [185]. When a compatibilizer is added, it migrates to the interphase and reduces the interfacial coefficient and the size of the phase domains (a finer dispersion of the minor component). The smaller domain size leads to a higher surface area and hence the percentage of interphase increases [190]. Similarly, the interphase thickness increases. This thicker interphase reduces the entropy of mixing, and lowers the enthalpy of mixing, and thereby provides a negative free energy of mixing leading to an improved stability of the polymer blend.

When the two polymers are blended on the industrial scale, high shear intensive mixing will take place. In this process, initially melting of the polymer pellets takes place. Secondly, mixing and phase separation occurs during shearing and extension of the polymers, so that coalescence of the particles is likely to happen. This introduces another possible mechanism for the activity of compatibilizers in reducing domain sizes. This is associated with steric stabilization to prevent or slow down the coalescence of dispersed particles [181]. The size of particles during shear is determined by the balance of two forces. The first comes from the repulsive interaction between the two components, which is represented by the interfacial tension which tends to make the particles grow bigger. The second force is shearing itself. This stretches each particle into a string, which then breaks up into a series of spherical particles, which are smaller than the original one. The efficiency of the shear to accomplish such breakup of the particles depends on the force transmitted from the matrix to the dispersed phase. This is a function of the viscosities of both phases and on the viscosity ratio. In addition the elastic forces tend to stabilize particles with a somewhat larger size [181, 191].

As a summary, the objectives of the compatibilization process are to reduce interfacial tension facilitating dispersion, and thereby to stabilize morphology against the high stress and strain of processing, and to enhance adhesion between the phases in the solid state thus improving the properties of the polymer blend [181]. Therefore, the role of compatibilizers can be shown schematically in Figure 2.8. This figure also shows the factors that affect properties of a blend with no compatibilizers. As discussed earlier (Section 2.6.2), the end properties will vary with the properties of the individual polymers and with the blend phase morphology, which will further vary with the interfacial tension in melt resulted through compatibility between polymers. The blend morphology will also vary with the processing conditions and with the relative melt rheology.

With a low degree of compatibility, insufficient mechanical properties will result. Compatibility between phases in a blend could be improved by chemical and/or physical treatments.

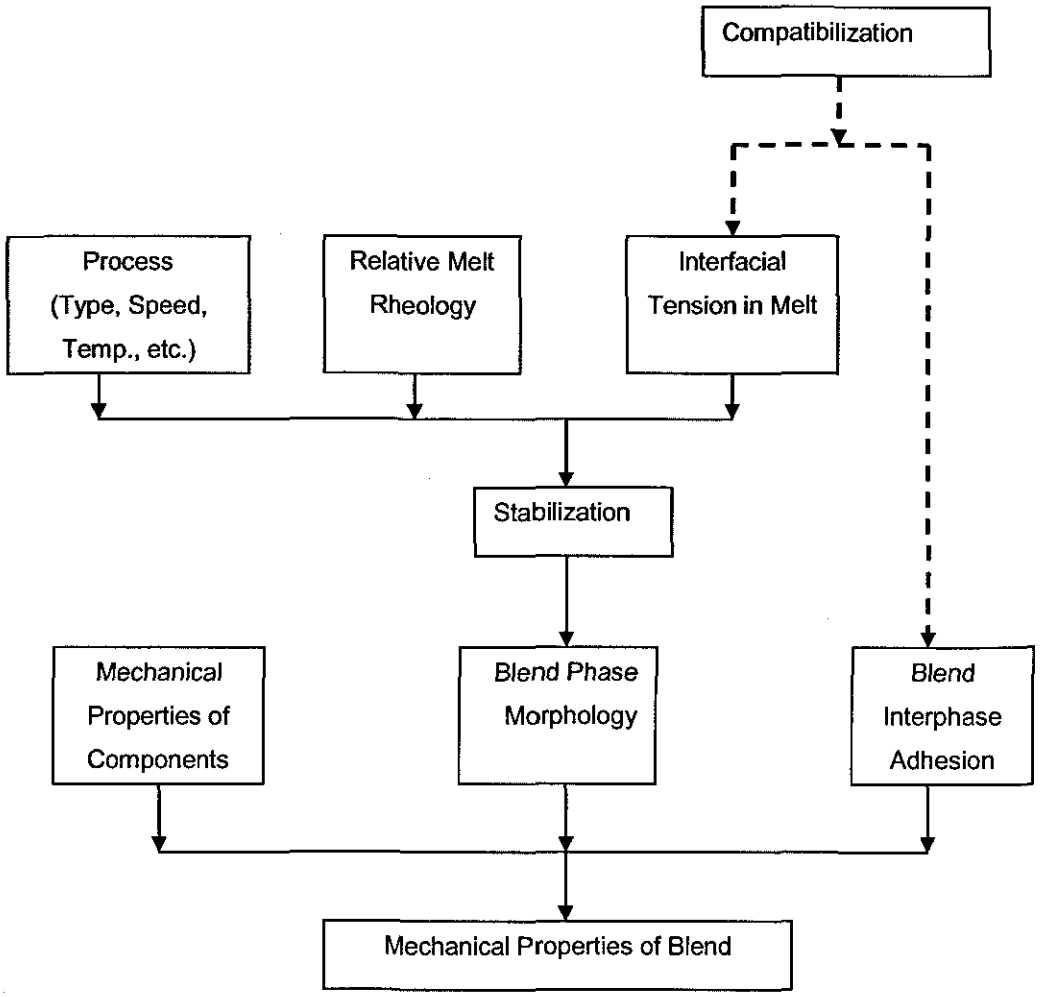

Figure 2.8 The role of compatibilizers (marked in dotted lines) [180]

2.7.2 Chemical Compatibilizing Techniques

Chemical compatibilizing techniques can be classified as non-reactive compatibilizing, and reactive compatibilizing techniques [133]. Non-reactive compatibilizing includes addition of a block or graft copolymer, which is miscible with each homopolymer in the blend. The copolymer creates an interphase between two phases (Figure 2.9) [145].

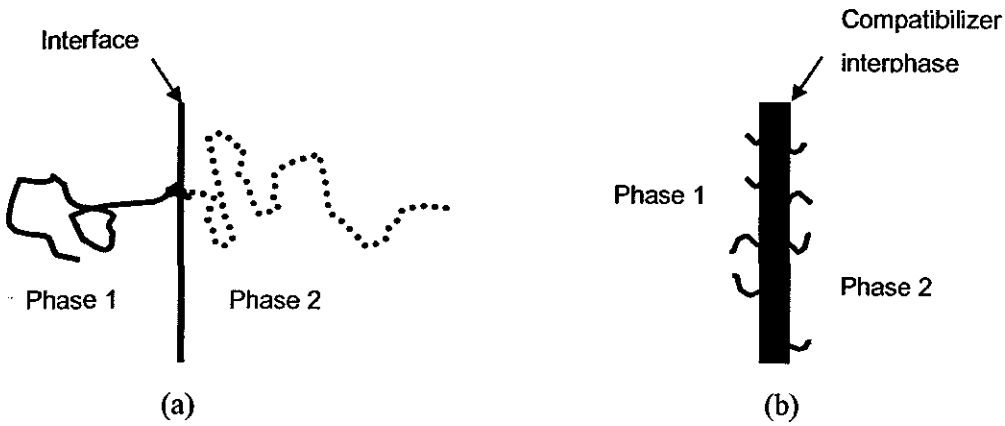

Figure 2.9 Function of a compatibilizing block copolymer (a) Interface of the polymer blend and (b) Creation of thick interphase [145]

Dynamic vulcanization is the commonest reactive compatibilizing technique used to improve the properties of rubber-thermoplastic blends. Depending on the amount of compatibilizer, crosslinking within the dispersed phase or graftlinking/grafting between the phases will occur (Figure 2.10) [192]. Grafting improves the compatibility of the blend. Materials with ionic groups can also be added to improve the compatibility of blends [193]. They are effectively crosslinked through the association of ionic groups forming clusters. However, polar plasticizers have to be incorporated into ion containing polymer blends in order to reduce the melt viscosity resulting from strong ionic associations, and to improve processability. Alternatively, two component compatibilizing systems can be incorporated into blends to improve adhesions between two polymers respectively. In the case of blends with waste rubber, one component is used to improve the surface characteristics of the rubber phase and the other is for the thermoplastic phase. Applicability of these compatibilizing techniques varies with the nature of the polymers present in the blend. The dynamic vulcanization and surface treatment techniques have been commonly practiced with waste polymers.

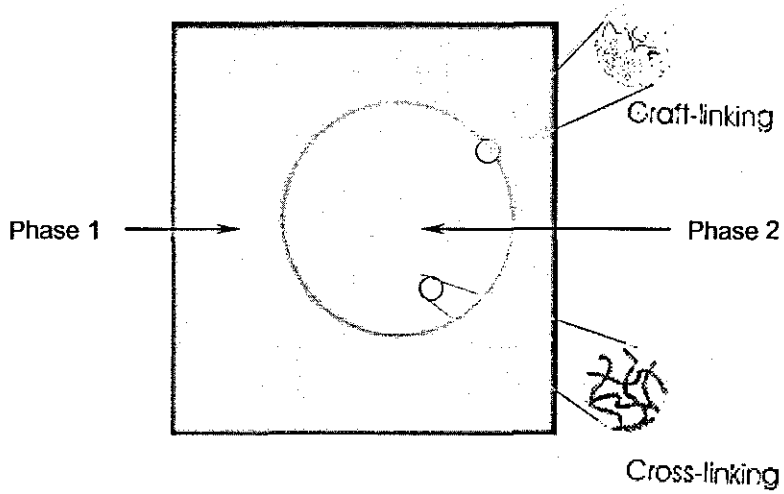

Figure 2.10 Formation of crosslinks and graft-links [192]

2.7.2.1 Non-reactive Compatibilization

(a) NR/PP Blends

The addition of liquid natural rubber (LNR) into NR/PP blends produced an increase in torque during processing and better tensile properties [100]. This torque increment with LNR suggested a partial crosslinking between phases and a compatibilizing role for LNR in NR/PP blends. Incorporation of EPDM and chlorinated polyethylene (CPE) into NR/PP improved the tensile properties of the blend [100, 141].

(b) NR/PE Blends

LNR in NR/HDPE blends also had a prominent role in the curing, but only with low concentrations [100]. Higher concentrations of LNR (greater than 27%) produced plasticizing effects thus decreasing mechanical properties. Further, the compatibilization capability of LNR was confirmed with a single peak in dynamic mechanical analysis. In addition, LNR improved the compatibility of NR/LDPE blends and NR/LLDPE blends [100].

The addition of a di-block copolymer called poly(hydrogenated butadiene-b-isoprene), into NR/LLDPE produced improved mechanical properties and morphological characteristics [143]. In addition, the incorporation of EPDM, chlorinated polyethylene and chlorosulphonated polyethylene into NR/HDPE blends also produced improved mechanical properties, while the most significant effect was noticed with EPDM [142]. Further, scanning electron micrographs showed more uniform and finely dispersed phases with all these third components. These observations confirm the improved interactions between homopolymers in the presence of a compatibilizer with a suitable similar structure.

(c) Waste-rubber/PP Blends

Incorporation of several compatibilizers, including styrene-butadiene-styrene, styrene-ethylene-butylene-styrene (SEBS), maleic anhydride-grafted styrene-ethylene-butylene-styrene (SEBS-g-MA), maleic anhydride-grafted polypropylene, into scrap rubber dust/PP blends were reported [140]. These blends exhibited increase in impact strength and elongation at break. But due to decrease in matrix strength with the addition of compatibilizers, tensile strength and modulus were slightly decreased. In a separate study [117], bitumen-treated-rubber-waste/PP blends also exhibited greater elongations with SEBS and SEBS-g-MA.

2.7.2.2 Dynamic Vulcanization

Dynamic vulcanization is the process of vulcanizing rubber during its intimate melt mixing with a non-vulcanizing thermoplastic polymer. The resultant material is called a thermoplastic vulcanizate [124].

Dynamic vulcanization can be carried out for all compositions of the rubber-thermoplastic blends [100]. Rubber rich blends exhibit phase inversion during dynamic vulcanization [127, 164]. However, when dynamic vulcanization was carried out on thermoplastic rich blends, where rubber was already in the dispersed phase, no phase inversion was reported. Micrographs of the dynamically vulcanized EPDM/PP showed EPDM as a dispersed phase in a PP matrix while uncured blends showed two continuous

phases for EPDM and PP respectively [164, 194]. Dynamic mechanical studies showed two separate transitions, both in cured and uncured systems, corresponding to the two phases [109]. The separate transitions explained that the miscibility of the two polymers could not be brought about with dynamic vulcanization.

Even though the miscibility of the two phases could not be improved, dynamic vulcanization improved blend properties. During dynamic vulcanization, crosslinked rubber particles were formed and hence more torque was exerted and more effective mixing resulted [195]. Higher mixing levels produced blends with fine dispersed phases, which led to enhanced properties [125]. Compared to uncured blends, thermoplastic vulcanizate showed improved elasticity, reduced compression set, improved ultimate mechanical properties, long term resistance to elevated temperatures, greater resistance to attack by chemicals and fluids, improved ozone resistance, improved fatigue resistance, greater melt strength and more reliable thermoplastic fabricability [97, 107, 124, 132]. However, due to increased level of the curing system, thermoplastic vulcanizates showed flow irregularities [127].

Dynamic vulcanization techniques were also practiced with waste rubbers. In general, waste rubber contains carbon black filled vulcanized rubber particles. The surfaces of these particles have active sites formed during the grinding processes. Literature reveals that 90% of the double bonds are available even after the rubber is vulcanized [111]. Hence, the presence of these double bonds in the waste rubber provides opportunities for grafting and crosslinking reactions which improve the compatibility with the thermoplastic phase [102].

Dynamic vulcanization can be carried out with a suitable vulcanizing system in specific rubber-thermoplastic blends. Common vulcanizing systems used in the industry are discussed below.

(a) *Vulcanizing with Sulfur and Sulfur Donor Systems*

Sulfur is the most effective vulcanizing agent used in rubber processing. A conventional sulfur vulcanizing system, as well as an efficient sulfur vulcanizing system, was used in making NR/PP blends [100, 127, 144, 145]. Mechanical properties, such as ultimate

tensile strength, elongation at break and tear strength continuously improved in proportion to the amount of vulcanizing system. Impact energy also improved and failure occurred in a ductile manner produced using the blends with sulfur systems. Blends without these systems showed a brittle fracture. The blends were prepared in these studies at various blend ratios, from 30 wt% to 70 wt% of each material. In addition, sulfur donor systems, such as tetramethylthiuram disulfide (TMTD) with N-cyclohexyl-2-benzothiozole sulphenamide (CBS), zinc oxide and stearic acid also showed enhanced physical properties [100, 145].

The sulfur vulcanizing systems were also used in ground tyre rubber (GTR)/PP blends and reclaimed-tyre rubber (RTR)/PP blends [155]. It was reported that the blends with RTR showed better impact properties compared to the blends with GTR, having rubber content up to 40 wt%. The blends with thermo-mechanically decomposed GTR and LDPE also showed improved tensile and impact properties compared with GTR/LDPE blends [121]. However, surface blooming and odor resulting from residual chemicals in the blends were reported in all blends vulcanized with sulfur systems. In addition, hindrance of the activity of ultraviolet stabilizers, used in NR/PP blend, was reported with the sulfur-donor systems [100].

(b) *Vulcanizing with Peroxides*

Dicumyl peroxide (DPC) has been utilized to produce dynamically vulcanized blends including NR/PP, GTR/PP, NR/LLDPE, and NR/LDPE [100, 146, 155-158]. These blends showed improved tensile and impact properties with the DCP level (up to 7 pphp). The addition of coagents or modifiers, such as maleimide, maleic anhydride (MA), acrylic acid, and acrylamide with DCP, to blends further improved their mechanical properties [113, 157, 196]. The activity of such coagents or modifiers was reported as an enhancement of the grafting reaction, thereby improving the adhesion between the two phases. In a separate study, an addition of DCP to GTR/EPDM/acrylated-PP (30/30/40) showed enhanced mechanical properties, with an optimum level of DCP at 1 phr [158] .

The use of different organic peroxides, including DCP and di(tert-butylperoxyisopropyl)benzene (DTBPIB), for NR/PP (60/40) blends has been

reported [146]. All blends showed an increase in tensile strength and elongation at break and decrease in compression set with the peroxide level up to 7 pphp.

In addition, a mixed system of sulfur and DCP has also been reported [127, 155]. Comparisons of sulfur, DCP, and mixed systems, showed that DCP greatly reduced the particle size in the dispersed phase. The largest particles occurred with sulfur vulcanizing systems. The mixed systems showed intermediate particles. Hexamethylene N, N' bis(tert-butyl peroxy) carbamate (HBTP) was also used in preparing NR/PP blends [195]. The results of swelling index tests showed that crosslinking increased with HBTP loadings up to 3%. Similar with sulfur and DCP, the mechanical properties also exhibited a continuous increase with HBTP loading. However, the degree of crosslinking acquired by HBTP was lower than that of the blend dynamically vulcanized by a system containing tetramethyl thiurum disulfide (TMTD) and 2-mercaptobenzothiozole (MBT) with zinc oxide and stearic acid [195].

The use of peroxide leads to undesirable side reactions, because of the free radicals that are generated. In the case of blends with PE, the peroxide radicals lead to crosslinking of the PE, yielding to very viscous blends that are difficult to process [157]. In the case of PP, the peroxide free radicals abstract the hydrogen from PP, generating a more stable tertiary free radical, which undergoes chain scission [192]. Therefore the NR/PP blends dynamically vulcanized by peroxide showed better processing characteristics compared to those vulcanized by sulfur [147]. Sulfur proved more beneficial as a vulcanizing agent in GTR/LDPE blends compared to DCP vulcanizing agent [121].

(c) *Vulcanizing with Maleimides*

Dimaleimides were also used in dynamic vulcanization. Several types of maleimides, including N, N'-metaphenylenedimaleimide (HVA-2), were used for EPDM/PP blends, which showed some compatibility between the two polymers [162]. The maleimide added systems illustrated stable blend morphology with a smaller dispersed phase and better interfacial adhesion, and hence exhibited better tensile properties with shear yielding in the PP matrix. HVA-2 with dihydroquonoline activators have also been used with EPDM/PP blends, having 5 to 30 wt% EPDM [161, 197]. These systems accelerated the crosslinking reaction in the EPDM, without any degradation. Further, the blends prepared

with these systems showed increased interfacial adhesions, and hence improved impact energies both at room temperature and at temperatures below 0 ^{0}C [197].

The incorporation of HVA-2 to NR/PP (85/15) blends showed improved impact strength at low temperature, flexural modulus, yield stress and tensile strength [151]. The level of HVA-2 added in that study was only up to 1 pphp. In a separate study, NR/PP (20/80) blends exhibited enhanced tensile strength and Izod impact strength, with HVA-2 and Epolene [149]. The addition of wax further improved the adhesion of the two phases, as they behaved as coupling agents. Five levels, up to 3 pphp of HVA-2, were used in the study and the optimum level was reported as 0.2 pphp.

HVA-2 with activators such as organic peroxides and 2-2'-dithiobenzothiazole (MBTS) produced enhanced mechanical properties in dynamically vulcanized NR containing blends [145, 198]. NR/PP blends containing 50-60 wt% NR showed increases in tensile strength and elongation at break with increase in HVA-2 content [145]. In this study 7.5 phr of HVA-2 with 1.5 phr MBTS was used, and produced very high gel contents, indicating a fully cured NR phase. In addition, increases in tensile strength and tear strength were reported with an increase in HVA-2 level in NR/PP (80/20) blends [145]. HVA-2 used in this study was limited to 1.5 pphp. In a separate study, the effect of HVA-2 with DCP in waste tyre dust/PP has been investigated [159]. The blends with the compatibilizing system showed noticeable enhancement in overall proprieties with improvements in swelling resistance to toluene and oil and thermal stability

HVA-2 has also been incorporated into ternary EPDM/NR/PP blends, at levels of 3 parts per 100 parts of NR [105]. These blends contained 50 wt% of PP, and the EPDM to NR ratio was varied. All these blends exhibited increases in melt viscosity, tensile strength and modulus compared to the blends without HVA-2, but with decreased elongation at break. This decrease in elongation is due to the restriction of molecular mobility and deformability of the matrix. Further, the blends with HVA-2 showed better heat resistance and greater crystallinity of the blends. These results show that HVA-2 can be used as a curing agent for blends containing NR and PP.

(d) *Vulcanizing with Phenolic Resins*

Phenolic resins have also been used in the dynamic vulcanization of rubber-thermoplastic blends prepared with PP and diene rubbers. Alkyl-phenol-formaldehyde resin, which is commercially known as SP-1045, was used with zinc oxide activator for NR/PP blends [100]. The levels of SP resin and zinc oxide used for this study were 15 phr and 5 phr respectively. These blends showed relatively improved mechanical properties compared to a blend prepared without any compatibilizing system. The SP 1045 resin with some other phenolic resins called CRJ-352 and SP 1056 were added to both NR/PP and SBR/PP blends having different blend compositions [153]. In that study, up to 7.5 phr resins were added with zinc oxide up to 2.5 phr. The blends prepared with those resins and zinc oxide showed relatively higher mechanical properties.

Stannous chloride, in levels up to 6 pphp, also has been used to activate phenolic resins in the preparation of NR/PP blends [152]. It was reported that the blends with phenolic resin activated by zinc oxide produced better mechanical properties compared to those activated by stannous chloride. However, it is difficult to compare the blend properties directly as the levels of zinc oxide (2 pphp) and stannous chloride (1 pphp) added were different. A mix of zinc oxide and stannous chloride has also been used as an activator in EPDM/PP blends which were vulcanized by phenolic resin [163].

An incorporation of modified PP to EPDM/PP blends has been reported [165]. The PP modification in that study was with 4 parts of phenolic resins and 0.8 parts of stannous chloride. The blends with modified PP showed relatively higher elongations at break but with slightly lower tensile strengths. In another study [199], NR/HDPE blends with modified HDPE showed enhanced tensile strengths and elongations at break compared to blends with unmodified HDPE and NR. The reason given for that enhancement was the formation of a better interphase, which improved adhesion between phases. The active sites in the phenolic resin would react with unsaturation in the HDPE molecules, which were formed during termination reactions of the polymerization process.

Dynamic vulcanization of waste-SBR/PP blends with SP 1045 phenolic resin and stannous chloride also showed a similar trend in results [111]. Further, blends without dynamic vulcanization at high rubber contents did not even show rubber-like properties.

At low rubber contents, dynamic vulcanization produced high tensile strengths and elongations at break. However, dynamic vulcanization of NR-SBR commingled waste tire rubber and PP, with phenol resin system, did not produce any significant enhancement in mechanical properties [111].

The EPDM/PP blends dynamically vulcanized by phenolic resin showed improvements in compression set, oil resistance and processing characteristics compared to blends vulcanized by sulfur and peroxide vulcanizing systems [164]. That was due to an in-situ formation of a graft copolymer between EPDM and PP in the presence of phenolic resins. In agreement to that result, NR/PP blends dynamically vulcanized by phenolic resin and zinc oxide also showed better tensile properties and ageing and ozone resistance compared to those vulcanized by peroxide, and sulfur and peroxide mixed cured systems [152]. These results showed the importance of using phenolic resin in dynamic vulcanization for blends of PP and diene rubbers.

In another study, blends of epoxidised natural rubber (ENR) and phenolic resin modified PP were prepared with peroxide, sulfur and mixed system as the vulcanizing agents [154]. In that study, blends dynamically vulcanized by sulfur showed higher elongations while blends vulcanized by phenolic resin showed higher tensile strength. Hence, the mixed system showed better overall properties. Similarly, the blends of NR and phenolic resin modified HDPE showed best overall properties with mixed cure system [199].

Dynamically vulcanized blends, as discussed above, showed superior mechanical properties. However, with the addition of larger quantities of vulcanizing agents, processing difficulties were reported in most of these studies. These results suggest that an optimum concentration of the vulcanizing agent in the blend is required to obtain superior physical properties without the surface irregularities that are associated with the excessive crosslink formation. Further, the overall improvement in properties of dynamically vulcanized blends confirms that dynamic vulcanization can be employed as a means of technological compatibilization of all rubber-thermoplastic blends. However, rubber-thermoplastic vulcanizates are more expensive to make than those with simple rubber-thermoplastic blends because the reaction requires time to change the phase from a continuous elastomer phase to a continuous plastic phase [97, 164].

2.7.2.3 Pretreatment of Ground Tyre Rubber

Surface modifications of ground rubber have been widely used to enhance compatibility with a polymer matrix. A study was reported on coating GTR with methyl isobutyl ketone solutions containing different quantities of DCP (up to 0.4 wt%) and triallyl cyanurate (up to 1.0 wt%) at room temperature, before melt mixing with LLDPE to prepare GTR/LLDPE blends [113]. The blends containing coated GTR, compared to the blend containing uncoated GTR, showed improved impact energies. The waste rubber powder was also treated with solutions containing different compositions of allylamine and benzoyl peroxide prior to blending with PP and maleated-PP [156]. The levels of allylamine and peroxide were up to 1.5 wt% each. It was noted that the blends with treated rubber powder showed enhanced tensile and elongation at break compared to un-treated blends at different compositions. But elongation at break decreased with peroxide level, leaving tensile strength unchanged. Both tensile strength and elongation at break decreased with allylamine level. FTIR spectra of the above blends showed grafting of allylamine in the rubber powder to maleated-PP.

In another study [102], waste-EPDM and waste-SBR were treated with potassium permanganate ($KMnO_4$) solution, in order to modify their surfaces with hydroxyl groups, prior to blending with maleated-PP and with regular-PP. However, the effect of maleated-PP compared to regular-PP in the blend properties was not evaluated. GTR was also reported as being treated with $KMnO_4$ prior to blending with recycled-LDPE and recycled-HDPE [95]. The $KMnO_4$ treated blends exhibited better compatibilization with higher tensile properties, compared to blends with un-treated rubbers.

In addition to surface modification, the GTR was modified with chemical systems to improve compatibility with the thermoplastic phase in the blends. The GTR was thermally treated with functional monomers of acrylic acid, methacrylic acid, 2-hydroethyl methacrylate, acrylamide and 1-allyl-2-thiourea. This treatment was carried out in an internal mixer at 140 ^{0}C. The treated GTR was melt mixed with LLDPE in the presence of a matrix phased compatibilizer of ethylene-co-glycidyl methacrylate. These blends exhibited significant increases in impact energy compared to GTR/LLDPE blends [113].

The GTR was also treated with vulcanizing systems prior to melt mixing with a thermoplastic. The GTR was thermally treated at 160 ^{0}C with MA and DCP and then added to EPDM/acrylated-HDPE blends [168]. It was reported that blends containing the treated-GTR, where 50 wt% of the rubber phase was replaced by the treated-GTR, showed greater physical properties than blends with untreated-GTR. In another study [200], waste tyre dust (WTD) was treated with 4 wt% and 2 wt% of natural rubber latex and sulfur respectively, prior to blending with PP. The treated-WTD showed improved tensile properties, swelling resistance and morphology, but did not show any change in the degradation processes analyzed by thermogravimetry.

In another experiment, GTR also thermomechanically decomposed in both presence and absence of paraffinic oil prior to blending with LDPE [121]. The percentages of acetone extracted from the blend with decomposed-GTR were higher than that with GTR. Further, the GTR decomposed with paraffin oil was less extractable compared to the decomposed blend without oil. This may be due to the imposition of high mechanical shearing forces on the GTR during processing without oil. The blends with decomposed GTR also exhibited enhanced mechanical properties after heat ageing.

The above performances suggest that the adhesion between phases could be improved by modification of GTR in GTR/thermoplastic blends, thereby improving the blend morphology and the mechanical properties. However, as this is a two step reaction process, the total time consumed to prepare the blends is considerable. Also this treatment needs special sophisticated machinery.

The above results suggest that the homogeneity and compatibility of a blend can be improved by having proper dispersion, by crosslinking particles in both dispersed and matrix phases, or by improving surface adhesion between dissimilar phases. It was reported that no significant difference in ultimate strength was noticed with the type of reactive compatibilizing technique [102]. Compared to non-reactive compatibilization, reactive compatibilization produces thicker interphases (Table 2.1). However, all techniques showed better properties compared to simple rubber-thermoplastic blends.

Table 2.1 Interphase thickness of polymer blends [185]

Type of Blend	Thickness (nm)
Immiscible	2
Block copolymer	4-6
Polymer/copolymer	30
Reactive compatibilization	30-60

2.7.3 Physical Compatibilizing Techniques

Compatibility of the blends could be improved by means of physical techniques, in addition to chemical compatibilization techniques. High energy treatments including corona discharge [119], plasma and electron beam radiation [131] have been used to modify rubber particle surfaces. Ground rubber modified by these treatments had an increased concentration of oxygen containing functional groups on the surface which led to better adhesion of waste rubber powder to the thermoplastic matrix. In addition, electromagnetic wave techniques could be used to modify the surfaces of rubber particles and to vulcanize the rubber phase in rubber-thermoplastic blends.

2.7.3.1 The Gamma Radiation Technique

Work based on gamma radiation vulcanizing of the rubber phase in EPDM/medium density polyethylene blends was reported [134]. In this study, extension after yielding showed enhancement with an increase in irradiation dose. In addition, the gamma radiation was utilized to oxidize the GTR surface prior to blending with HDPE and maleated-PE [95]. It was reported that the oxidation was not effective enough to improve the mechanical properties of the blends.

2.7.3.2 The Ultraviolet Radiation Technique

Ultraviolet (UV) energy has also been applied to modify the surface properties with monomers and photosensitizers. The utilization of UV radiation for surface modification of GTR in GTR/PP and GTR/maleic anhydride grafted PP blends has been reported [138]. Allylamine and benzophenone was used as the monomer and the sensitizer respectively. The results of this study revealed that the mechanical properties of GTR/PP blends significantly improved upon loading with the UV-modified GTR, due to increased chemical interaction between the allylamine of the GTR and the PP matrix. However, UV monomer grafting is not suitable for large-scale processes.

2.7.3.3 The Ultrasonic Wave Technique

It has been proven that ultrasonic technology can be used to devulcanize rubber waste, which can then be reprocessed and revulcanized to create other rubber products with sufficient mechanical properties (Section 2.2.2.3). This implies that active sites on the rubber particles can be formed by ultrasonic treatment which could improve surface adhesion between the two phases. Ultrasonically treated NR/PP blends, compared to untreated blends showed greater improvement in tensile properties and in toughness [135]. Further, the micrographs of the treated blends showed relatively smaller rubber particles as the dispersed phase. The ultrasonically treated GTR (UGTR) in UGTR/HDPE blends also exhibited enhanced tensile and impact properties compared to GTR/HDPE blends [137]. The blends treated ultrasonically after preparing the GTR/HDPE in an internal mixer, showed further enhancement in properties. The property enhancement was much greater with the addition of a vulcanizing agent during ultrasonic treatment. This property enhancement is due to the formation of interfacial bridge compounds within the blend during the ultrasonic treatment. Alternatively, it could be due to the improved homogeneity with fine dispersions formed during ultrasonic treatment [108]. By confirming these factors, another work [136] reported on in-situ copolymer formation at the interfaces during ultrasonic treatment. This was shown as a result of the decreased amount of extractable components in the blend and through the improved mechanical properties. These results propose that the compatibilization of immiscible polymers can be obtained by ultrasonic treatment. Further, this technology with varied supply energy

densities may be beneficial in forming blends with different crosslinking levels, leading to specific properties.

2.7.3.4 The microwave Technique

Microwave technology has been practiced for heating [201], polymerizing [202], crosslinking [203, 204] and depolymerization [33], of certain polymeric materials in both the rubber and plastics industry. This technique has also been used in processing of some polymer composites [205, 206]. Polar polymers or polymers with polar additives can process using this technique since field polarizations, including electronic polarization, atomic polarization, dipole steering polarization and interfacial polarization, take place in such polymers under the action of microwave [202]. No literature was found concerning the preparation of rubber-thermoplastic blends with either microwave technique.

2.8 Polymers used in the Present Study – Ground Tyre Rubber (GTR) and Waste Polypropylene (WPP)

2.8.1 Selection of Polymers

The aim of this project was to prepare and evaluate rubber-thermoplastic blends from polymer waste. Of the waste materials collected in the whole world, polymer waste, especially waste tyre rubber and commodity thermoplastics, make a major contribution. Polyethylene (PE) is the most widely used thermoplastic, polyvinyl chloride (PVC) is second and polypropylene (PP) is third. However, recycling of PVC is difficult with the emissions of harmful acidic substances during thermal treatment. Common thermoplastic processing equipment cannot be used to process PVC [120]. Hence, converting waste materials such as waste tyre rubber, waste polypropylene (WPP) and waste polyethylene to usable resultant materials is of great importance.

Rubber waste in powder form, including ground tyre rubber (GTR), has been incorporated into virgin commodity thermoplastics, such as PE [95, 100-102, 114, 118,

119, 121, 122, 131, 137] and PP [89, 102, 111-113, 116, 128, 136, 138, 140, 146, 156, 158, 200, 207], to produce rubber toughened thermoplastics. PP and PE in many ways have similar characteristics. The significant differences are: PP is less dense, has a higher rigidity and hardness, and has a higher softening temperature meeting dimensional stability at higher temperatures requirements [120, 208]. Further, PP offers excellent electrical and chemical resistance at higher temperatures [17, 133]. Because of these inherent properties, PP can be used in both indoor and outdoor applications and also in engineering applications. However, PP is notch-brittle, particularly at low temperatures and under impact loading [209]. None-the-less, the use of WPP compared to WPE in rubber-thermoplastic blends is valued.

Even though, the blends from waste tyre rubber and WPP have been used commercially for treating sport surfaces [133] and in roof slate production [130] and for the production of low performance applications like waste paper baskets and food trays [98], a detailed study on such blends has not been reported, especially with compatibilization. However, scientific studies [102, 95] have reported on blends of waste tyre rubber with WPE.

2.8.2 Ground Tyre Rubber

Tyre rubber is classified under different names such as cuts, shreds, granules, powder etc., according to sizes (Table 2.2). Tyre rubber is vulcanized and has a three dimensional chemical network which combines individual rubber chains. This chemical network will be broken during recycling processes, including grinding, via a free radical mechanism [210]. Chain scission and/or crosslink scission can take place, and hence a chemical structure with broken crosslinks and chains results (Figure 2.11). The random crosslink scission, together with random chain scission, results in the formation of soluble branched rubber chains and fragments of the gel structure [210]. The presence of carbon black, which is chemically or physically anchored to the rubber chains, complicates the chemical structure and it can be pictured schematically as in Figure 2.12.

Table 2.2 Different forms of tyre waste [2]

Tyre-derived Fraction	Approximate Size Ranges
Cuts	12 - 3 mm of the whole tyre
Shreds	300 - 50 mm
Tyre Chips(with inherent wire)	50 – 10 mm
Tyre Chips(95% wire free)	50 – 10 mm
Tyre Granules	10 -1 mm
Typical Crumb Rubber (CRM) Coarse	2000 – 420 μm (10 – 40 US Mesh)
Typical Crumb Rubber (CRM) Fine	420 – 180 μm (40 – 80 Mesh)
CRM Powder	180 – 75 μm (80 – 200 Mesh)
Super Fine CRM	< 75 μm (200 Mesh)

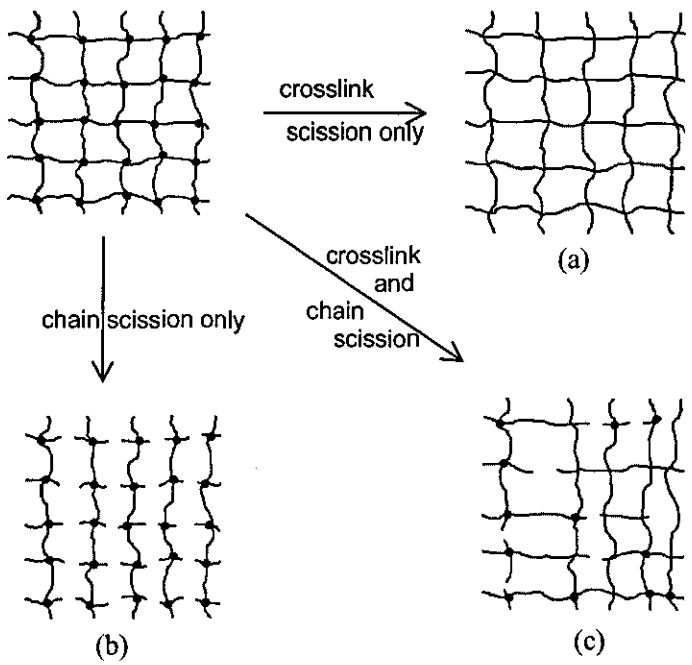

Figure 2.11 Schematic representation of the physical effects which can be expected during the recycling processes (a) Scission of all crosslinks (b) Scission of rubber chains at points between crosslinks (c) Scission of some crosslinks and chains between crosslinks [210]

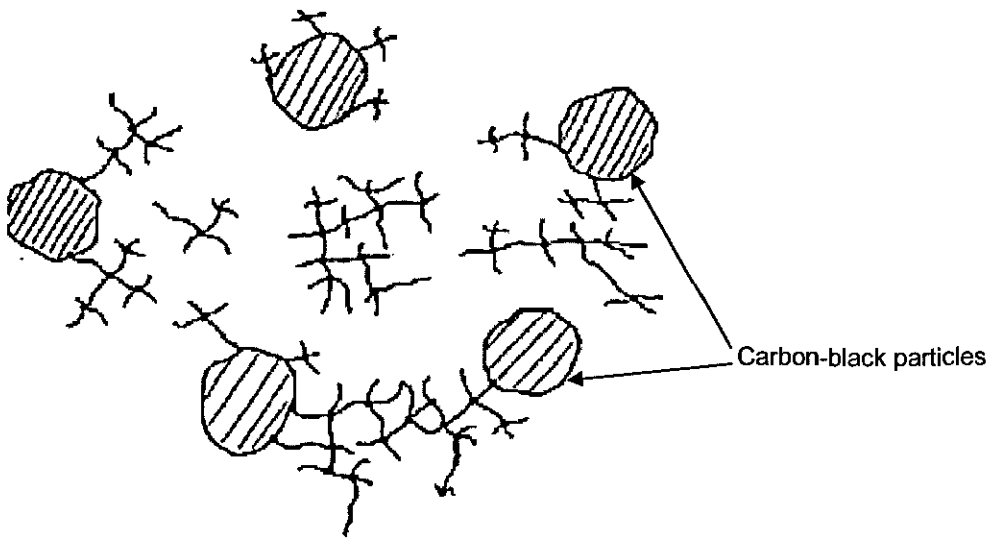

Figure 2.12 Schematic diagram of carbon black and crosslinks in GTR structure [210]

GTR, even though it is vulcanized, contains 90% of the double bonds found in un-vulcanized rubber [102, 112]. The presence of these double bonds in the GTR provides opportunities for grafting and/or crosslinking reactions which improve its compatibility with the thermoplastic phase [102]. The surfaces of the GTR particles have active sites formed during the grinding processes [102, 112]. The presence of these active sites will further improve the compatibility.

Ground tyre rubbers show different surface characteristics corresponding to the grinding techniques. In general, compared to cryogenic grinding, ambient grinding gives rougher particles with higher surface area [131]. Further, ambient ground rubber, compared to cryogenically ground rubber shows a narrow particle size distribution, but, the average particle size is large (Figure 2.12). The separation of reinforcing materials, such as fibre and metal, from rubber is more effective with cryogenic grinding. The ambient ground rubber contains 0.5% fibre and 0.1% steel while the contamination level of cryogenically ground rubber is below the detection limit [2]. The effect of particle size and shape of GTR on properties of GTR/ thermoplastic blends is discussed in Section 2.6.2.4.

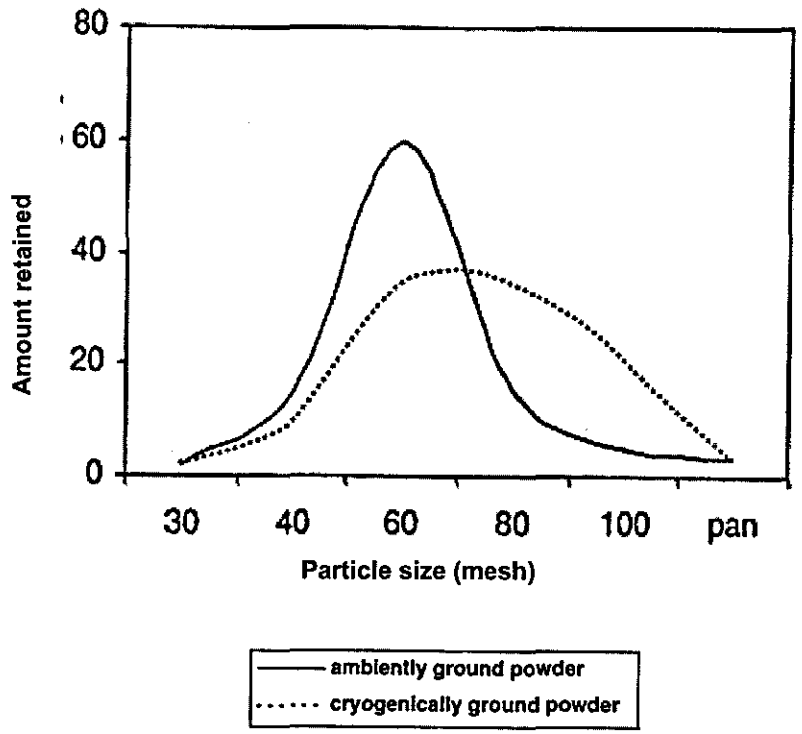

Figure 2.13 Particle size distribution obtained from sieve analysis for ambiently and cryogenically ground rubber [2]

GTR contains both natural rubber (NR) and synthetic rubbers. The synthetic rubbers contain styrene butadiene rubber (SBR) as a major component, and other rubbers such as butadiene rubbers and butyl rubbers as minor components. The non-rubber compounds in GTR consist of fillers like carbon black and silica along with zinc oxide (ZnO), traces of metal and acetone extractable volatiles [158]. The components of the GTR vary with the type of tyre, and further with the part of tyre. Unlike passenger car tyres, truck tyres contain a higher percentage of NR (up to 66%) compared to synthetic rubbers [211, 212]. The composition of ground tyre rubbers varies in the range 40-55 wt% rubber, 20-40 wt% carbon black and 10-15 wt% low molecular weight additives [118, 119].

2.8.3 Waste Polypropylene (WPP)

Structurally polypropylene is a vinyl polymer, similar to polyethylene, but with a methyl group attached to alternative carbon atoms in the backbone [213]. The chemical structure of PP is given as:

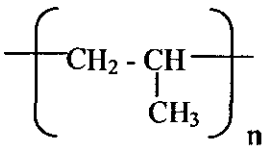

PP can be found in three forms; isotactic, syndiotactic and atactic. The crystalline properties of the linear isotactic form make it the most commercially attractive with a melting point of around 166 ^{0}C [107]. This form of PP has all methyl groups arranged on the same side of the chain, which is shown as:

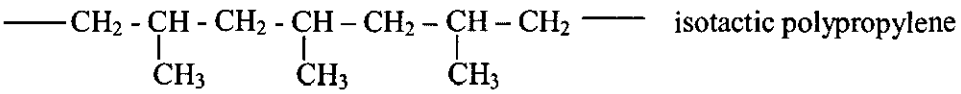

Usually isotactic PP includes at least 95% isotactic configuration, and the other 5% correspond to all other configurations [213]. Commercially available isotactic PP may contain lower percentages of the isotactic configuration, and is a semi crystalline polymer. The glass transition temperature of isotactic PP is in a temperature range -10 ^{0}C to 5 ^{0}C [107].

WPP suffers chemical and physical changes during processing and service life, but the main properties of virgin PP remain unchanged or insignificantly varied [214]. Generally, single cycle recycling of PP does not cause significant changes in average molecular weight, polymer chain structure and morphology. On the other hand, if PP is repeatedly recycled, the molecular weight could be affected as a consequence of the weakness of the tertiary carbon in the PP chain and its oxidation [214]. With the formation of pro-oxidative moieties, a substantial portion of the stabilizers are consumed, with the consequent decrease of long-term stability and mechanical properties [215]. However, it

has been reported that the degradation of waste PP begins at a lower temperature than in the case of virgin PP, but the difference is not high enough to commend the thermal stability of waste PP over virgin PP [214]. Furthermore during their application and recovery, waste polymers come in contact with non-polymeric impurities and other polymers, which contaminate and affect the performance of the waste polymers [215].

2.8.4 Compatibility of WPP with GTR

GTR contains mainly natural rubber (NR) and styrene butadiene rubber (SBR) and hence these two rubbers have only been considered when evaluating compatibility with PP. Compatibility of NR and SBR with PP can be considered using the microstructures of the individual polymers, i.e.

NR:

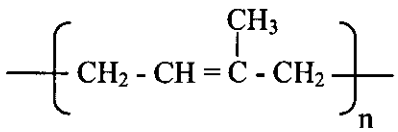

SBR:

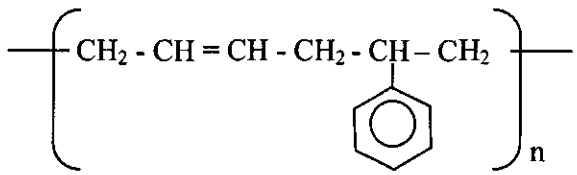

PP:

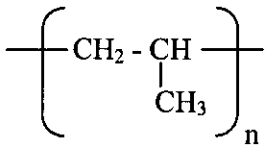

At the molecular level, both NR and PP, and SBR and PP are incompatible which will give rise to a two phase blend [105]. Further, NR and SBR are amorphous rubbers, while PP is a semi crystalline thermoplastic material. However, NR is strain induced crystallisable [216].

Solubility parameters of NR, SBR and PP are 16.2, 17.6 and 18.8 $(J/cm^3)^{1/2}$ respectively [217]. Thus the difference in solubility parameters between NR and PP is 2.6 $(J/cm^3)^{1/2}$ and, between SBR and PP is 1.2 $(J/cm^3)^{1/2}$. Both the major rubbers in GTR, as well as PP,

are non-polar. As ΔH_{mix} is always positive for non-polar systems (see Equation 2.4), the difference in solubility parameters of the polymers in the blend needs to be very small to obtain a negative value for ΔG_{mix}. However, since the difference in solubility parameters of GTR and PP are not so small, ΔG_{mix} will not be negative. This results in an incompatible blend. However, these solubility parameters are fairly close to each other and thus a stable dispersion of GTR particles in the PP matrix is possible [100]. Also mixing involves melting of PP, thus increasing ΔH_{mix}.

Commercial grade PP, which is normally used in industries, is made of not only $-CH_3$ groups, as branches on the polymer backbone, but also groups such as propane and butane, etc. These side chains and branches are likely to cause an increase in the level of incompatibility with the GTR in the blend [100, 105]. Further, other rubbers, crosslinks, carbon black and other compounding ingredients in the GTR may slightly affect the level of incompatibility of the polymers in the blend.

The Flory interaction parameter, χ_{12}, can be approximately calculated according to Equation 2.11 (see Appendix A.3). These calculated values of χ_{12}, for NR-PP systems and SBR-PP systems (based on their repeating units), at 180 ^{0}C, are 0.09 and 0.03 respectively. Two polymers in a blend will be miscible when the value of χ_{12} is less than the critical value, $(\chi_{12})_{crit}$. The critical value calculated for the GTR and PP blend having equal weights of each polymer is 0.001(see Appendix A.3). The χ_{12} values obtained thus also clearly show that the two major rubbers present in GTR, and PP at the melt mixing temperature of 180 ^{0}C are incompatible.

2.8.5 Toughening and Fracture Mechanisms

2.8.5.1 Fracture in PP

The fracture of semicrystalline polymers can occur by ductile tearing like rubbers, or by a crazing mechanism principle [192, 218]. Crazing is a dilatational process that yields the formation and extension of cavities in the polymer ahead of any inhomogeniety. These cavities called crazes are essentially cracks, but bridged by fibrils of oriented polymeric

materials [219]. The crazes grow normal to in the direction of the applied stress, as shown in Figure 2.14.

The initiation and propagation of crazes in semicrystalline polymers depend on the structural arrangement, such as inter-lamellar slip and separation, defolding of lamellae, etc. For a specimen with a crack, the structural transformations (stress and strain induced molecular motions associated with rotation and slip of lamellae, transformation of lamellae to fibrils, etc.) at the crack tip increase specific energy, which is needed to cause crack propagation. This process is called crack tip blunting [192, 220].

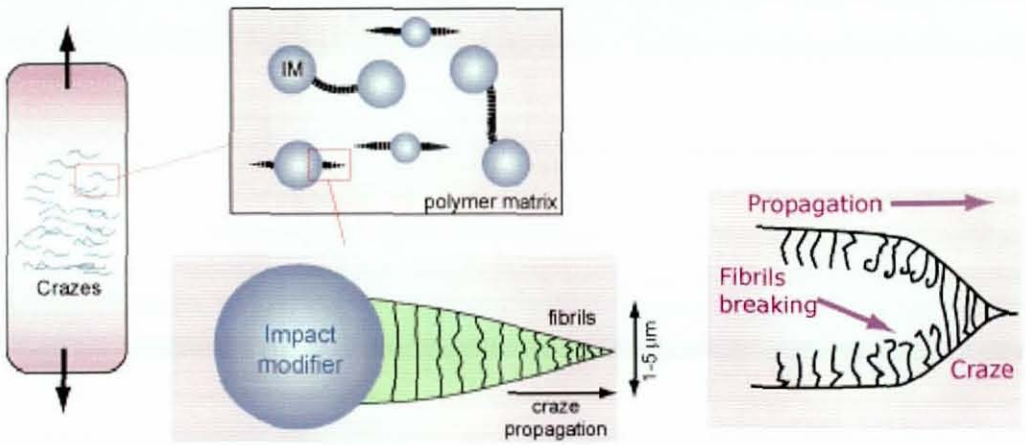

Figure 2.14 Crazing Mechanism [219]

Shear yielding is an efficient impact energy absorbing mechanism due to the irreversible nature of plastic deformation [221]. Shear bands are developed at an angle 45^0 to the main direction of stress, where the shear stress is maximized (Figure 2.15) [220]. These bands do not involve changes in the volume of the polymer (dilatation) seen in crazing [218]. Further, shear banding involves localized orientation of the polymer, and hence it is highly temperature and strain rate dependent.

Crazing and shear yielding are in general assumed to be independent processes, and the failure mechanism that requires the lowest stress is dominant [192, 218, 222]. When craze stress is less than the yield stress, a brittle fracture occurs, and when yield stress is less than the craze stress, a ductile fracture occurs. The evaluation of the fracture mechanism is rather complex, and is strongly depended on the characteristics of the polymer, the type

of test, and processing and testing conditions [192, 218, 223-225]. The type of tests used for fracture analysis includes the tensile test, dynamic mechanical test, and impact test. Common impact tests include un-instrumented Charpy and Izod tests, and the instrumented falling dart test. For example, the notched and the un-notched specimens used for Charpy impact tests behave very differently.

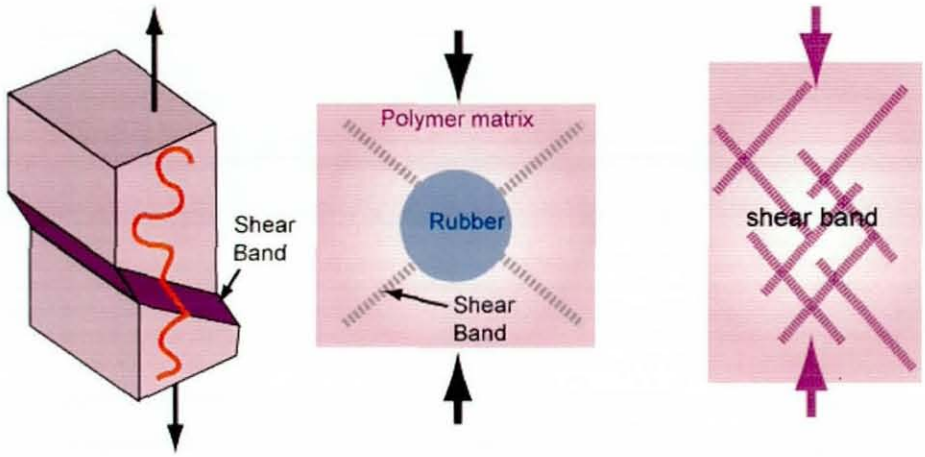

Figure 2.15 Shear Yielding Mechanism [221]

The yield stress is more sensitive to process parameters than craze stress. The yield stress increases with strain rate and with decreasing temperature [192, 207, 225]. The yield stress of a semicrystalline polymer also increases with increase in crystallinity and lamellae thickness [192, 220, 226]. The craze stress increases with increasing entanglement density and molecular weight of the polymer [192, 225].

PP, at low temperatures and under impact loading, shows predominantly notch-brittle failure. Crazing has been recognized as the main fracture mechanism in virgin PP [227-229]. But, PP is a ductile polymer at room temperature being above its T_g, and shear yielding is the primary fracture mechanism [162, 225, 230]. Shear yielding has been studied in PP mostly under compression [220]. It was reported that the structure of the shear bands alters with the testing temperature in a coarse spherulitic PP. The discrete shear bands became diffuse with increasing temperature, especially near to the T_g.

2.8.5.2 Toughening of PP

Toughness is defined as the ability to resist fracture by absorbing energy. The toughness of PP at low temperature can be increased if crazing can be suppressed. An efficient way to toughen PP is to incorporate a dispersed rubbery phase, which has excellent elasticity and toughness [192, 218, 220, 231, 232]. Alternatively, the toughness of PP can be improved by incorporating rigid organic and inorganic fillers [228, 233-235]. The objective of the present study is to prepare rubber-thermoplastics blends, and hence this review is focused only on toughening PP with a rubber phase.

The primary function of a rubber phase is to relieve the triaxial stress state in front of a crack tip or an inhomegeniety by internal cavitation [103, 192]. Cavitation is a dilatational process and is very effective in changing the stress state [220]. The ease of cavitation of the rubber in a particular stress state depends on the local rubber concentration, particle size, particle dispersion and morphology of the particles [103, 192, 236]. It also depends on the thermal stresses in the blend [192, 218]. Cavitation is usually divided into two kinds of behaviours, namely internal or particle cavitation, and interfacial debonding [192].

The particle cavitation involves the formation of a hole/void within the core of the dispersed rubber phase. In creating space for the growing void, the surrounding rubber is stretched biaxially and therefore subjected to substantial hoop stresses, especially in the region close to the cavity. These stresses are released when the crack cleaves through the particle, so that the stretched rubber shell retracts leaving a craterlike depression in the fracture surface (Figure 2.16). The presence of biaxial tensile stresses in the cavitated rubber provides a degree of strain hardening to the system [192].

Interfacial debonding (Figure 2.17) occurs when the interfacial tension between the rubber and the PP matrix is high. Debonding is especially important in PP composites because of its low polarity and consequently low surface energy [220].

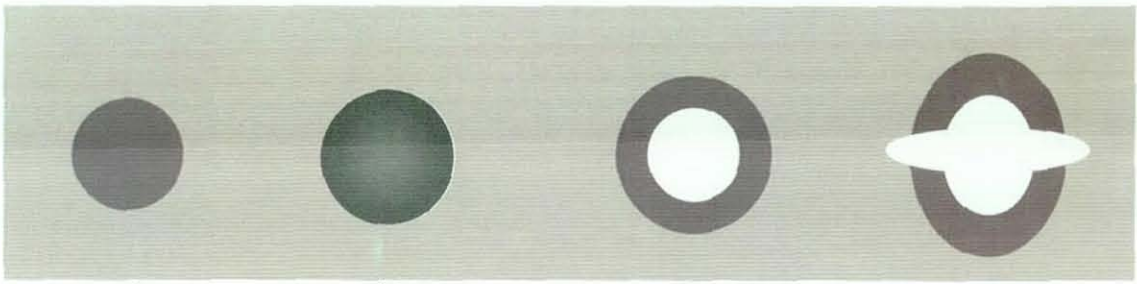

Figure 2.16 Cavitation in a rubber particle (a) initial state (b) volume change due to tension (c) void appearing releasing stress (d) creation of a craterlike depression [192]

The secondary function of the rubber phase is to act as a stress concentrator to promote multiple crazing and/or shear yielding and to suppress brittle fracture as a result [162, 192, 218]. Crazes are generated near the equator of a rubber particle and propagate normal to the applied tensile stress and terminate when a neighboring rubber particle is encountered (Figure 2.14). The resulting multiple crazes can absorb more impact energy. Contrary to crazing, shear yielding does not induce any significant material volume variation [221]. In the presence of rubber particles, more diffuse regions of plastic deformation may also appear in addition or substitution to shear bands. Shear yielding is also an efficient barrier to the propagation of crazes and cracks, delaying material failure (Figure 2.15).

The cavitation generated by the rubber phase also absorbs energy, but relatively low amounts compared to shear yielding and crazing. However, it can efficiently concentrate stress due to its much lower stiffness than the matrix polymer [192, 218]. Good interfacial adhesion between the matrix and rubber is also necessary to provide stress transfer and effective crack tip blunting [192, 218].

The toughened PP often deforms in a ductile manner even at low temperatures and under impact loading with greater impact energies, but strongly depends on the characteristics of the two phases [151], the compatibility between the phases [103, 192, 207, 236, 237], and on the processing and test conditions [237, 238]. The influences of the above factors on blend properties are discussed in detail in Section 2.6.2.

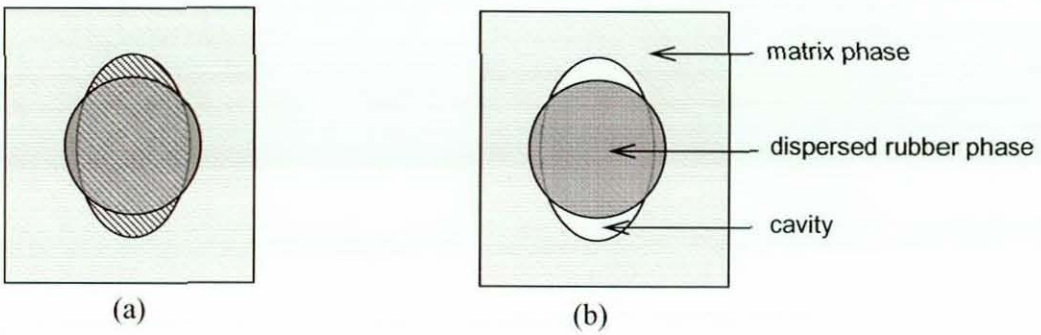

Figure 2.17 Interfacial debonding (a) before (b) after [220]

2.8.5.3 Fracture in Rubber-toughened PP

The non-elastic deformation mechanisms in rubber-toughened PP have been identified as shear yielding, multiple crazing and cavitation [207, 227, 236-240]. Fracture surfaces of the ethylene propylene rubber (EPR)/PP blends showed cavitation with highly stretched and elongated cavities, matrix-rubber debonding, and shear banding along the draw direction [239]. Fracture surfaces of styrene butadiene styrene rubber (SBS)/PP blends showed particle cavitation along with matrix-rubber debonding [229]. The crosslinked rubber/PP blends [207] and EPDM/PP blends [237] demonstrated shear yielding as the preferred fracture mechanism. These studies did not show crazing on the fracture surfaces suggesting that the craze stress of PP in those blends is higher than the yield stress. It also suggests that the craze stress of PP is higher than the stresses for rubber cavitation and interfacial debonding at the processing conditions studied.

A study on styrene-ethylene-propylene rubber (SEP) toughened polypropylene demonstrated shear yielding around SEP particles smaller than 0.3 μm, and crazing and cavitation around larger particles (>0.3 μm) [227]. Fracture surfaces of the SBR/PP and EPDM/PP blends illustrated shear yielding as the dominant fracture mechanism for those with particles smaller than 0.5 μm, and crazing around larger particles [236]. These studies discovered that the fracture mechanisms of rubber toughened PP are strongly dependent on the particle size of the dispersed phase and the smaller rubber particles were not capable of initiating crazes in PP matrix.

2.9 Compatibilizing Techniques Selected for the Present Study

The results discussed in the Section 2.6.2 and Section 2.7.2 explained that blends can be tailored for specific applications by proper selection of the type and the composition of polymers, and a suitable compatibilization technique. These results also showed that enhanced blend properties could be obtained, with the blends having smaller dispersed rubber particles, better particle distribution, good cohesive strength in the rubber phase, and better interfacial adhesion. Further, it has been shown that greater ability of rubber phase to promote cavitation and to act as a stress concentrator and easy to develop stress concentration zones in the matrix, all result in a better compatible rubber-thermoplastic blend.

However, it is practically difficult for the melt mixing process to produce a PP/rubber blend in which all of the above conditions are realized. In the case of PP/NR and PP/SBR blends, the ability to promote cavitation and to act as a stress concentrator, and dispersion of the rubber particles in the matrix are favourable, when the molecular weight of the NR/SBR is low. However, to develop stress concentration zones in PP, and to dissipate energy through cohesive fracture between particles, the molecular weight needs to be high. Similarly, development of a stress concentration zone is favourable when the PP content is lower, but energy dissipation by cohesive fracture is favourable when it is higher. Hence, in order to optimize the above conditions, an attractive technique, which could generate stable blend morphology and could also improve interfacial adhesion, is required. Selection of suitable compatibilizing systems for the GTR/WPP blend, and details of the selected systems are discussed in this section.

2.9.1 Selection of Compatibilizing Techniques

Among the chemical compatibilizing systems, non-reactive systems cannot be used for GTR/WPP blends, due to the noticeably poor compatibility between the two polymers (Section 2.8.4). Dynamic vulcanization has been proven as a promising compatibilizing technique to provide some of the conditions discussed above (Section 2.7.2.2). Pretreatment of waste rubber also showed enhanced blend properties due to improved adhesions to the thermoplastic phase and to improved cohesive strength with the rubber

phase (Section 2.7.2.3). However, all these chemical compatibilizing systems release hazardous chemicals or fumes to the surrounding environment. Physical compatibilizing techniques, including gamma, ultraviolet, microwave and ultrasonic technique, do not release any hazardous materials to the environment. However, all these physical compatibilizing systems are not effective in improving the properties of rubber-thermoplastic blends and/or are not suitable for large scales processes (Section 2.7.3). Therefore dynamic vulcanization and GTR pretreatment were selected as possible compatibilizing techniques in the present study.

2.9.2 Selection of Compatibilizing Systems for Dynamic Vulcanization

GTR/WPP blends are melt mixed at temperatures higher than the melting point of PP, 166 ^{0}C. Hence, the crosslinks formed by the vulcanizing system during dynamic vulcanization are to be thermally stable at higher temperatures. Of the vulcanizing systems used in dynamic vulcanization, peroxide, maleimide and resin vulcanizing systems produced thermal and oxygen resistant C-C crosslinks. Sulfur crosslinks, S-S and S-C, are not sufficiently thermally stable, and hence sulfur vulcanizing systems are not commercially used in dynamic vulcanization. Further, sulfur vulcanizing systems generate unpleasant odors during both production and processing. Although the peroxide vulcanizing system generates thermally stable rubber network, it has only a limited temperature range of processing and there is a risk of uncontrolled degradation of the PP during dynamic vulcanization. Because of these reasons, maleimide and resin vulcanizing systems were selected. These systems are effective in crosslinking the rubber phases in rubber-thermoplastic blends, and are also effective in improving compatibility between the two polymers. Hence these systems were chosen and are hereafter referred to as the compatibilizing systems.

2.9.2.1 Dimaleimide Compatibilizing System

Maleimide vulcanizing is commonly used with unsaturated rubbers, such as NR, SBR and butadiene rubber (BR), in order to produce vulcanized rubber with good ageing characteristics [160, 241]. One of the attractive features of a maleimide vulcanizing

system is that the physical properties of the vulcanized rubber are independent of the vulcanizing temperature and it does not markedly affect the ability of rubbers to crystallize when stretched [160]. Maleimides, containing an appropriate second functional group can be used as a self-accelerating vulcanizing agent. It has been shown that dimaleimides are more effective than mono-maleimides as vulcanizing agents [160, 241]. Further, the vulcanizing activity of the dimaleimides is dependent on the structure, and the characteristics of the bridging group which joins the maleimide rings. The maleimides showed efficient vulcanizing with an initiator such as peroxides and sulfur accelerators of the thiazole type. Because of these reasons, a dimaleimide was selected to use as a compatibilizing agent in the present study.

N-N'metaphenylene dimaleimide, which is commercially called HVA-2, has been used to crosslink the rubber phase in NR/PP [105, 149, 151, 198] and in SBR/PP [198]. HVA-2 was found to be an effective vulcanizing agent in the presence of an organic peroxide or MBTS [145, 159, 160, 198, 241]. Also in the absence of initiators, HVA-2 was able to cure NR and SBR, but the degree of crosslinking was relatively low [160, 241]. Further, HVA-2 is capable of reacting with polymer radicals formed by chain scission during blending [145, 151].

Tyre rubber contains both natural rubber and synthetic rubbers like SBR and BR. Since HVA-2 was successful as a compatibilizing agent for dynamic vulcanization of NR/PP and SBR/PP blends, it was expected that HVA-2 could enhance compatibility in the GTR/WPP blends.

2.9.2.2 Addition of Organic Peroxides to Dimaleimide System

Organic peroxides are often used for controlled degradation of PP in extrusion processes [103]. The degradation of PP occurs through a sequence of radical reactions; peroxide decomposition to free radicals (Section 6.1.1), hydrogen-abstraction, chain scission and termination [124]. The peroxide radicals preferentially abstract the tertiary hydrogen atoms of the PP main chain [103].

Organic peroxides are also used to crosslink rubbers that contain no sites for attack by other type of vulcanizing agents [212]. The peroxide radical abstracts a hydrogen atom from the rubber chain and form a C-C crosslink, which is heat stable [242]. The efficiency of crosslinking depends on the peroxide concentration, and the degree of chain scission at the process temperature [103, 124].

These peroxides were used as a vulcanizing agent for the rubber phase in rubber-thermoplastic blends (Section 2.7.2.2). The main factors that influence the properties of the NR/PP blend were identified as typical crosslinking temperature, the crosslink efficiency and relative amounts of decomposition products, and the degree of PP degradation [146]. In practice, sulfur or coagents such as dimaleimides and triallyl cyanurate are used to suppress chain scission at high temperatures [212]. The coagent increases the crosslink density in the rubber phase of the rubber-thermoplastic blends and improves the grafting between PP and rubber [198]. Of the peroxides used for NR/PP blends, dicumyl peroxide (DCP) and di(tert-butylperoxy isopyopyl) benzene (DTBPIB) exhibited better properties, DTBPIB is the best [146]. The crosslinking temperatures of DCP and DTBPIB are 160 ^{0}C and 170 ^{0}C respectively [198]. As these temperatures are closer to the melt mixing temperatures of GTR/WPP blends, 180 ^{0}C, high crosslinking efficiency would be expected.

Because of all the above reasons, HVA-2 was selected to use as the compatibilizing agent. DTBPIB and MBTS were selected as the activators for the maleimide compatibilizing system.

2.9.2.3 Resin Compatibilizing System

Phenolic resins are the condensation products of phenols and aldehydes [243]. They are generally classified into two main classes; resoles and novolak. Resoles have reactive methylol groups, whereas novolaks do not have any reactive functionality. Further, resoles have two structures between aromatic rings, dibenzyl ether and/or methylene links. The two groups are formed under different conditions; however, both structures are typically formed in resole resin synthesis [163, 244]. Due to the presence of reactive groups, the resole resins are used for vulcanizing of rubbers. The resole resins with a

higher number of ether bridges were shown as more effective in vulcanizing unsaturated rubbers [163]. However, they were not used in traditional rubber vulcanizates since the volatiles released from their breakdown generated voids in the vulcanizates.

Resin vulcanizing has been used with rubbers like NR, SBR, butadiene rubber (BR), nitrile rubber (NBR) and EPDM [163, 212]. The vulcanizates produced are thermally stable and exhibit low compression set and good dynamic properties [245]. Cure rate and the crosslink density can be improved when a suitable activator, such as a halogen donor and a metal compound is used. The metal compounds, that are commonly used include iron oxide, titanium oxide, magnesium silicate, silicon dioxide and preferably ZnO [163, 243, 246]. The common halogen donors used are of metal halides of Lewis acids such as stannous chloride, ferric chloride, zinc chloride and aluminum chloride.

Phenolic resin has also been used to vulcanize the rubber phase in blends made with diene rubbers and thermoplastics [163]. Phenolic resin activated by zinc oxide has been successfully used for NR/PP and SBR/PP blends [153, 154]. Not much work was reported on the use of stannous chloride activated phenolic resin for PP blends with NR and SBR. However, this resin system has been used for recycled-SBR/PP blend, and showed improved blend properties [111]. In this work, the effect of several other activators such as aluminum chloride, tin chloride and iron chloride were studied. Stannous chloride produced the blends with best properties.

The stannous chloride activated phenolic resin was successful as a compatibilizer for NBR/PP [104, 106, 166, 167] and EPDM/PP blends [164, 243]. PP modification with stannous chloride activated phenolic resin prior to melt mixing with rubbers showed enhancement in blend properties, compared to direct incorporation of the resin system in the blends. Those blends showed reduced domain size for the dispersed rubber phase and improved interfacial adhesion, and hence resulted in improved mechanical properties. Further, the micrographs of those blends explained the formation of a graft copolymer between the two phases.

The GTR in this study is a mix of diene rubbers like NR, SBR and BR. WPP has a similar structure to virgin PP. Therefore an improvement in blend properties would be expected, if the GTR/WPP blends were dynamically vulcanized with the stannous chloride

activated phenolic resin. Of the resins used in previous studies (Section 2.7.2.2d), SP 1045 resin was selected to use in the present study, as it is a balance of both dibenzyl ether and methylene bridges. Further, this resin has been used in the preparation of EPDM/PP and NBR/PP blends.

2.9.3 Selection of GTR Pretreatment Technique

The results reported in Section 2.7.2.3 showed that the compatibility of waste tyre rubber(WTR)/thermoplastic blends could be improved when the WTR is pretreated. This pretreatment can either be a surface modification or a vulcanizing process of the tyre rubber particles, or a breakdown of the tyre rubber to a rubber having similar characteristics to its virgin rubber/s.

Surface modification of the tyre rubber could be achieved using, both, chemical (Section 2.7.2.3) and physical (Section 2.7.3) techniques. The surface modified rubber particles provide better interfacial adhesion with the thermoplastic phase in the rubber-thermoplastic blends. However, these treatments need special sophisticated equipments. Vulcanizing and also breaking of the tyre rubber could be carried out using common rubber machinery available in any rubber industry, like in an internal mixer or an open mill. The pre-cured rubber particles improve the cohesive strength of the rubber phase itself. They also provide a dispersed phase with smaller particles. However, these particles do not provide any additional interfacial adhesion in order to show greater enhancement in blend properties.

Normally, blends prepared with virgin rubbers show improved properties compared to blends prepared with waste rubbers. Hence, breakdown of tyre rubber to a rubber similar to its virgin rubber would be the best option to improve the properties of the GTR/WPP blends. This section discusses the selection of a suitable pretreatment technique to breakdown the GTR.

2.9.3.1 Selection of Delink Process for GTR Pretreatment

Tyre rubber consists of a chemically crosslinked network structure and hence it is difficult to break using only mechanical means. This crosslinked structure could be broken down using selected chemical techniques (Section 2.2.2.1) and electromagnetic wave techniques (Section 2.2.2.3). The electromagnetic wave techniques need special machinery. Some are batch processes and are rather expensive compared to the mechanical and chemical recycling techniques.

Several chemical agents have been used to treat the tyre rubber (Section 2.2.2.1), but most of them produced a depolymerised rubber rather than a devulcanized rubber. The chemical agents that promote devulcanization are expensive and cannot be used on an industrial scale. However, a chemical system called Delink, which consists of common industrial rubber chemicals, has been reported to effectively convert tyre crumbs, made with 100% natural rubber, into rubber having comparable properties to virgin rubber [42, 169, 170]. The Delink treated rubber has been used to replace up to 50 wt % virgin rubber in making rubber products [38, 171]. However, its incorporation into thermoplastics to produce rubber-thermoplastic blends has not been reported. Hence, the Delink system was chosen to treat the GTR prior to melt-mixing with the WPP.

2.9.3.2 Delink Process

This novel technology [42], which was invented by Kormer and Sekhar, is based on chemical devulcanization and is used to recycle sulfur and/or metal oxide vulcanized rubbers. This process involves an addition of the Delink, to crumb rubber at temperatures below 70 ^{0}C, in a two roll mill and/or in an internal mixer. The devulcanized product, called De-Vulc, is ready for moulding and vulcanization. This delink process is elegant, simple and is neither energy nor labour intensive. The reaction scheme of devulcanization and re-vulcanization is given in Figure 2.18.

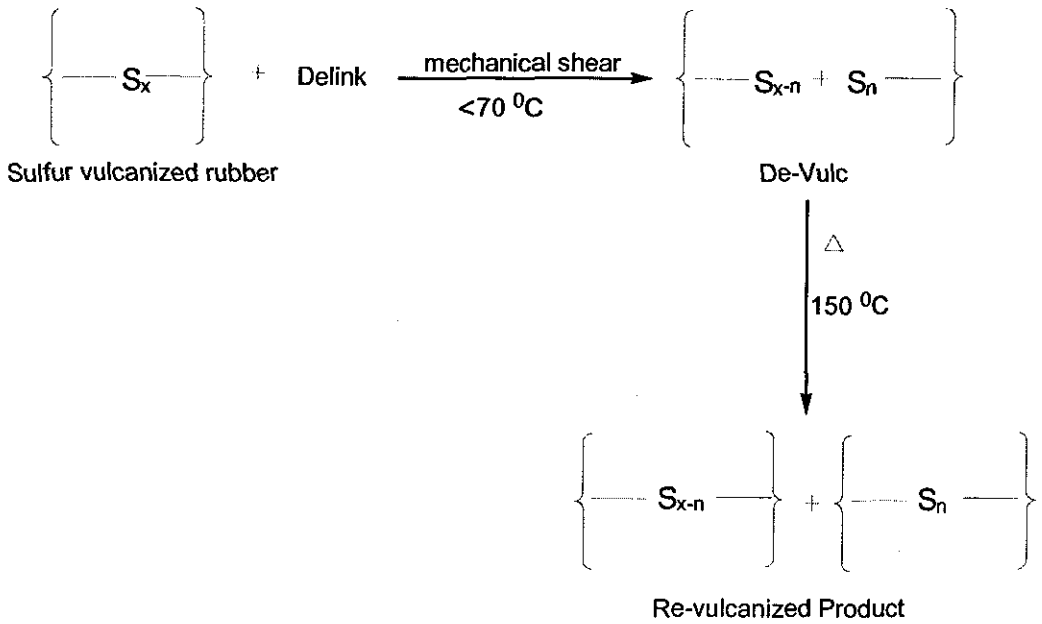

Figure 2.18 Delink Process and Sekhar-Kormer-Stonikova Reaction [247]

2.9.3.3 Delink Composition

The Delink mixture comprises one or more rubber accelerator and one or more rubber activator, and is capable of initiating proton exchange in a controlled manner at temperatures below 70 ^{0}C, by opening up or delinking the sulfur vulcanized network of rubber.

The ultra fast and/or fast accelerators, preferably zinc salt of thiocarbamates such as zinc dimethyldithiocarbomate (ZDMC) and 2-mercaptobenzothiazole (MBT) or their derivatives, in a molar ratio in the range of 1:1 to 1:12, are commonly used [42]. Hence, the Delink composition may comprise of ingredient such as ZDMC in the range 4.8 to 7.2 pphp (by weight) and MBT in the range of 16 to 24 pphp. These accelerators are activated by the activators, preferably ZnO and stearic acid. Each activator may be in the range 1.6 to 2.4 pphp. The presence of a small amount of sulfur aids ultimate vulcanization but is not essential. Similarly, the presence of diol may help in the dispersion of the powders and perhaps activates the mixture, but this is not essential. Sulfur may be present in the range 1.2 to 1.8 pphp and a diol such as diethylene glycol may be present in the range 9.6 to 14.4 parts by weight.

As discussed above, maleimide and resin compatibilizing systems were selected to investigate their effect on GTR/WPP blend properties. In addition, the influence of GTR pretreatment with Delink on blend properties was studied. Preparation of the GTR/WPP blends at varied compositions and at different processing conditions, addition of maleimide and resin compatibilizing systems to the GTR/WPP blends, pretreatment of the GTR with Delink system, and the preparation of blends with the Delink-treated GTR are discussed in the next Chapter.

Chapter 3

Experimental

Waste polypropylene (WPP) and ground tyre rubber (GTR) were selected as the base materials for this study (Section 2.8.1). These two materials were characterized by Fourier transform infrared spectroscopy (FTIR), melt flow analysis, differential scanning calorimetry (DSC), dynamic mechanical analysis (DMA) and by thermogravimetric analysis (TGA). Blends from GTR and WPP were prepared in an internal mixer under specific process conditions.

The literature review revealed (Sections 2.6.2 and 2.7) that the properties of rubber-thermoplastic blends mainly depend on the properties of the rubber and thermoplastic phases, blend composition, processing conditions and compatibility between the polymers. In the case of blends with waste rubbers, in addition to the above factors, the size and shape of the rubber particles have been shown to influence blend properties (Section 2.6.2.4). Smaller particles and particles having highly convoluted surfaces showed improved properties. However, the improvement associated with smaller particles is only marginal and is not justifiable due to the additional cost associated with the size reduction. Further, it has been shown that an optimum particle size for the rubbery phase in a rubber toughened thermoplastics should be somewhere in the range of a micrometer. Waste rubber particles, even when ground to the smallest size possible by any technique, are an order of magnitude larger than this optimum size. Hence, the effect of particle size and shape were not studied in the present work.

The first part of the project investigated the effect of blend composition, and the process parameters, on blend properties. The blend composition varied from 0 wt% to 100 wt% of each material. Processing characteristics and mechanical properties of the blends were measured to identify the optimum blend composition to use in the latter part of this study. The mechanical properties measured included non destructive property like hardness, and destructive properties like tensile strength, tear resistance, and impact properties. Trends in the properties obtained were related to blend structure. The Blend structure was

examined by swelling characteristics, thermal analysis, optical microscopy and scanning electron microscopy. Processing parameters were optimized using the tensile properties of blends having a composition of 50 wt% of each. Processing parameters considered in this study were processing temperature, rotor speed, and processing time.

The second part of the project was to study the use of compatibilizing systems for GTR/WPP blends having a composition of 50 wt% each. Two compatibilizing systems, namely dimaleimide system and resin system were chosen (Section 2.9.2). For the dimaleimide compatibilizing system, N-N'metaphenylene dimaliemide (HVA-2) was selected to use as the compatibilizing agent, and di(tert-butylperoxyisopropyl) benzene (DTBPIB) and 2-2'-dithiobenzothiazole (MBTS) were used as the activators (Section 2.9.2.1 and Section 2.9.2.2). For the resin compatibilizing system, alkyl phenol (para, t-octyl phenol) formaldehyde resin (SP 1045H), called hereafter as SP resin, was selected to use as the compatibilizing agent and stannous chloride in both anhydrous and dihydrate forms were used as activators (Section 2.9.2.3). Two different mixing schedules were used. In the first mixing schedule (schedule-a), both GTR and WPP were added together at the commencement of the mixing. In the second schedule (schedule-b), the WPP was first modified and then the GTR was added to the modified WPP. Processing characteristics and the mechanical properties mentioned earlier were measured to evaluate the blends. Trends in the properties obtained were explained by swelling characteristics, thermal analysis, sol and gel from boiled xylene extracts, and scanning electron microscopy (SEM).

The ability of WPP modification using the resin system was evaluated compared to modification of PP. This evaluation was based on tensile properties of the modified WPP or PP and %solvent extraction residues from acetone extractions. The extents of modifications were further studied by FTIR spectra taken after acetone and p-xylene extractions. Similarly, the modification of the GTR with the resin system was studied.

The third part of the project aimed to investigate property enhancement with the pre-treated GTR. The Delink system was selected to pre-treat the GTR (Section 2.9.3.1). The Delink components and their mixes were characterized by DSC. The processing temperature of the Delink process was first estimated using DSC thermograms obtained

under isothermal conditions at different temperatures, and then practically determined while mixing in the internal mixer. The optimum Delink level was determined by first evaluating the tensile properties of the Delink treated GTR. The GTR treated with the optimum Delink level (DGTR) was then added to the WPP to prepare the blends at different compositions. The influence of GTR pretreatement on the blend properties (tensile and impact properties) was studied. Finally, DGTR/WPP blends were prepared with the dimaleimide compatibilizing system. Blends at three different compositions were prepared (30, 50 and 70 wt% of DGTR) in this part of the project to compare the resultant tensile and impact properties. These properties were then related to the morphology and fracture behaviour of the blends. The raw materials used and the methodologies practiced in the present study, are discussed in this chapter.

3.1 Materials

3.1.1 Base Polymers

The waste polypropylene (WPP) used in this study was a mix of used injection moulded products, and was supplied by Plastic Reclamation Limited, UK.

Ground tyre rubber (GTR) having the code 1249/Y-1151/F36 was supplied by the Alruba Rubber Company, UK. The GTR consisted of equal quantities of tread components from car and truck tyres. Car tyre treads contain lower rubber content (40-45%) with higher carbon black content (35-40%), while the truck tyre treads contain higher rubber content (approx. 60%) with lower carbon black content (approx. 30%) [248]. The rubber in car tyre treads was essentially a mix of synthetic rubbers; styrene butadiene rubber (SBR) and butadiene rubber (BR). Truck tyre treads contain up to 65% of natural rubber (NR); the rest being synthetic rubbers. NR in the GTR will account for 30-35 wt% of the rubber. Particle size reduction was achieved by ambient grinding. The average particle size given by the supplier was 40-mesh, which is equivalent to 420 microns [249].

3.1.2 Components of the Compatibilizing Systems

N-N'metaphenylene dimaleimide (HVA-2) and alkyl phenol (para, t-octyl phenol) formaldehyde (SP 1045H) were the two compatibilizing agents selected for the present study (Section 2.9.2). HVA-2 (Figure 3.1) is known as a primary vulcanizing agent and as a secondary accelerator for NR and SBR [105, 161]. It also acts a vulcanize promoter in sulfur and sulfur donor systems, and a coagent in peroxide vulcanizing systems [212]. It can be viewed as a multifunctional radical acceptor which promotes the combination of dissimilar polymer radicals to give a copolymer by reducing the interfacial tension.

SP 1045H (Figure 3.2) is the same as SP 1045, which is manufactured by the Schenectady International Incorporation, USA [244, 250]. This resin has an amorphous structure with various chain lengths and has multiple reactive sites like methylol groups and hydroxyl groups. It contains both methylene and ether bridged monomeric units formed during resin synthesis. It is also highly aliphatic due to its long alkyl chain.

Di(tert-butylperoxyisopropyl) benzene (DTBPIB) and 2-2'-dithiobenzothiazole (MBTS) were the activators used for the dimaleimide system. Stannous chloride anhydrous ($SnCl_2$) and stannous chloride dihydrate ($SnCl_2.2H_2O$) were used as activators for the resin compatibilizing system. The chemical structures of DTBPIB and MBTS are given in Figure 3.3 and Figure 3.4, respectively. Virgin PP was used to compare with WPP, after their modifications with SP resin activated by stannous chloride.

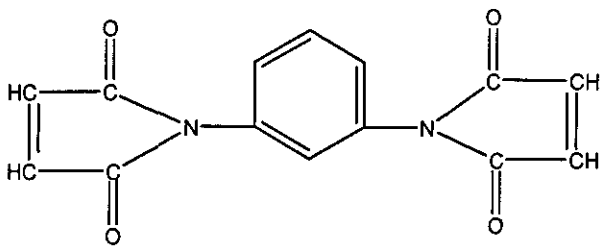

Figure 3.1 Chemical structure of HVA-2

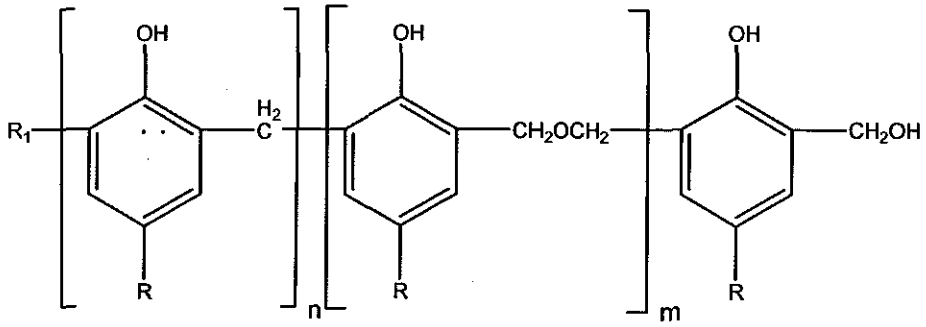

n, m = 0-15

R1= -H or -CH_2OH

R= -$C(CH_3)_2$-CH_2-$C(CH_3)_3$

Figure 3.2 Chemical structure of SP 1045H [250]

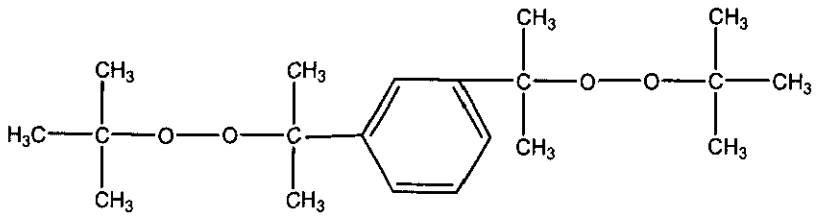

Figure 3.3 Chemical structure of DTBPIB

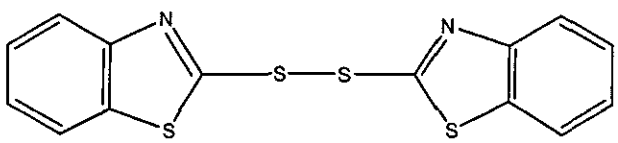

Figure 3.4 Chemical structure of MBTS

Delink was selected to pre-treat the GTR (Section 2.9.3.1). The Delink used for the present study consisted of zinc dimethyldithiocarbomate (ZDMC), 2-mercaptobenzothiazole (MBT), sulfur, zinc oxide (ZnO), stearic acid and diethylene glycol. The following formulation, which was given by the inventors in their study [42], was used in the present study.

MBT	20 parts
ZDMC	6
ZnO	2
Stearic acid	2
Sulfur	1.5
Diethethlene glycol	12

MBT (Figure 3.5) is a semi-ultra accelerator, while ZDMC (Figure 3.6) is an ultra-accelerator. Both accelerators are used for the vulcanization of rubbers such as NR, SBR, EPDM, butyl rubber (IIR), isoprene rubber (IR) and nitrile rubber (NBR). MBT is not fully effective in vulcanization unless activated by zinc oxide [251]. Stearic acid will activate the accelerator still further. ZDMC also activates with ZnO and stearic acid. MBT gives the compound considerably higher processing safety than ultra-accelerators. MBT has a very broad plateau and can therefore be vulcanized at higher temperatures during a short time. Further, MBT has a slight depolymerizing action on rubber, which favorably influences the processability of the compound. In general ZDMC gives a fast cure, high modulus and short scorch times. It is not conducive to pre-vulcanizing at room temperature but has a strong accelerating effect at temperatures above 100 °C.

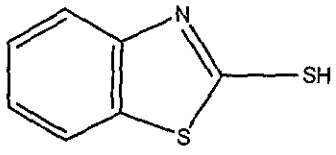

Figure 3.5 Chemical structure of MBT

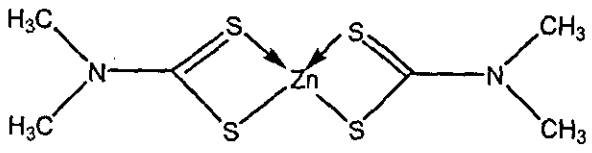

Figure 3.6 Chemical structure of ZDMC

A combination of ZDMC and MBT produces a synergistic accelerator complex, as shown in Figure 3.7. When MBT is used with ZDMC, the rate of vulcanization increases gradually [251]. Hence, a small amount of ZDMC is good to activate the MBT accelerator.

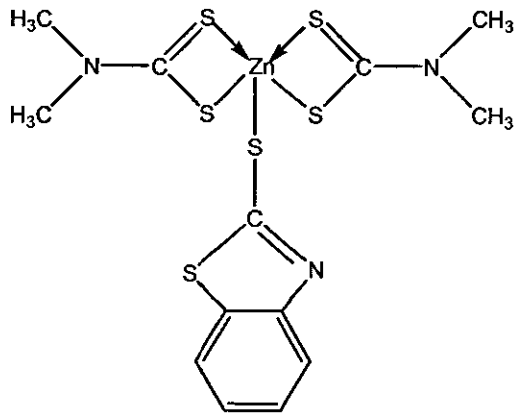

Figure 3.7 Synergistic accelerator complex from MBT and ZDMC [252]

3.1.3 Other Chemicals

The antioxidant called Ralox-46 was incorporated into all blends to prevent degradation of the GTR during processing at high temperatures. Toluene was used as the solvent for swelling experiments, and the extractions were carried out with acetone and with boiled p-xylene. The antioxidant-2246 was used for the boiled xylene extraction. All rubber chemicals used in the experiments were of industrial grade, and the solvents were of general purpose or laboratory grade.

The product name, chemical name, molecular formula, and the supplier for each chemical, are listed in Table 3.1.

Table 3.1 Details of chemicals used

Product Name	Chemical Name	Molecular Formula/Structure	Abbreviation	Supplier
Vulcafac 13PDM Powder	N-N'metaphenylene dimaleimide	$C_{14}H_8O_4N_2$	HVA-2	Safic-Alcan UK Limited
SP 1045H	Alkyl phenol formaldehyde resin	Polymer	SP resin	Schenectady Europe SAS, France
Perkadox 14-40B-PD	Di-(tert-butylperoxyisopropyl) benzene, 40% on whiting and silica carrier	$C_{20}H_{34}O_4$	DTBPIB	Akzo Nobel Polymer Chemicals, Netherlands
Perkacit MBTS	2-2'--dithiobenzothiazole	$C_{14}H_8N_2S_4$	MBTS	Flexsys Antwerp, Belgium
Tin(II) Chloride anhydrous	Stannous Chloride	$SnCl_2$	$SnCl_2$	Fisher Scientific, UK
Tin(II) Chloride dihydrate	Stannous Chloride, dihydrate	$SnCl_2.2H_2O$	$SnCl_2.2H_2O$	Fisher Scientific, UK
Perkacit ZDMC	Zinc dimethyldithiocarbomate	$C_6H_{12}N_2S_4Zn$	ZDMC	Flexsys Antwerp, Belgium

Perkacit MBT	2-mercaptobenzothiazole	$C_7 H_5 N S_2$	MBT	Flexsys Antwerp, Belgium
Powder sulfur	Sulfur	S_8	S	Safic-Alcan UK Limited
Zinc oxide powder	Zinc Oxide	ZnO	ZnO	Safic-Alcan UK Limited
Stearic Acid	Octadecanoic acid	$CH_3(CH_2)_{16}COOH$		Fisher Scientific, UK
Diethylene Glycol, 99%	Bis(2-hydroxyethyl) ether	$[HO(CH_2)_2]_2 O$	DEG	Fisher Scientific, UK
Ralox 46	2,2'-Methylene-bis-(6-tert.-butyl-4-methylphenol)	$[C_6H_2 [C(CH_3)_3] (CH_3) OH]_2 CH_2$		Safic-Alcan UK Limited
p–Xylene, 99%	1, 4-Dimethylbenzene	$C_6H_5 (CH_3)_2$	Xylene	Fisher Scientific, UK
p–Xylene, laboratory grade	1, 4-Dimethylbenzene	$C_6H_5 (CH_3)_2$	Xylene	SK Laboratory Chemicals, Sri Lanka
Antioxidant 2246	2,2'-Methylene-bis-(6-tert.-butyl-4-methylphenol)	$[C_6H_2 [C(CH_3)_3] (CH_3) OH]_2 CH_2$		SK Laboratory Chemicals, Sri Lanka
Acetone, 99+%	2-Propanone	$CH_3 C O CH_3$	Acetone	Fisher Scientific, UK
Toluene, 99+%	Methybenzene	$C_6H_5 CH_3$	Toluene	Fisher Scientific, UK
Toluene, general purpose	Methybenzene	$C_6H_5 CH_3$	Toluene	SK Laboratory Chemicals, Sri Lanka

3.2 Compound Formulation

3.2.1 Specimen Code for First Part of Project

The code used to identify the blends (eg.50:50/180/90/8P) was as follows: the first set of numbers details the GTR to WPP weight ratio. The second number after the first slash represents the processing temperature. The third number after the second slash details the rotor speed and the last number after the third slash represents the processing time. The last letter associated with the last number in the specimen code indicates the type of first material added to the mixer, P is for waste polypropylene and R is for ground tyre rubber. No letter was given for the case when both materials were added together

3.2.2 Evaluation of Blend Composition

In order to evaluate the influence of blend composition on properties, a variety of blends were prepared by varying the GTR level from 0 wt% to 100 wt % in 10 wt% intervals. In this study, the rotor speed was set at 30 rpm and the temperature at 180 ^{0}C. The processing time was set at 8 minutes. Each blend was prepared twice to ensure reproducibility.

3.2.3 Evaluation of Process Parameters

A furher set of blends was prepared to evaluate the influence of process conditions on the resultant blend properties. Process conditions considered in this study were melt-mixing temperature, speed of processing and time of processing. The effect of processing schedule was also studied.

3.2.3.1 Selection of Blend Composition

A study of the results for various blend compositions (Section 5.1) revealed that the 50:50 blend had reasonable set of mechanical properties. Further, it exhibited the lowest specific energy requirement. As the main objective of this project was to develop a blend with waste polymerss; waste tyre rubber and waste plastic, energy costs are important. Therefore by considering these factors, the 50:50 blend was selected as the control blend.

3.2.3.2 Selection of Process Conditions

(a) *Processing Temperature*

Blending via melt mixing of two polymers will not occur until the melting points of these two materials are reached [195]. DSC thermograms (Section 4.1.4.1) showed that the equilibrium melting point of the WPP was around 166 ^{0}C. Hence, the processing temperature was varied from 170 ^{0}C to 210 ^{0}C at 10 ^{0}C intervals. Additionally, in order to study the mixing behaviour of blends below the melting point of the WPP, one blend was prepared at 160 ^{0}C. In these experiments the rotor speed was set at 30 rpm. The processing characteristics monitored in the previous part of the study showed that the torque always stabilized within 5 minutes. Hence, the processing time for this part of the study was kept at 5 minutes.

(b) *Processing Speed*

The processing speed was varied from 15 rpm to 120 rpm, initially at intervals of 15 rpm and then at 5 rpm intervals between the selected rotor speed range. The best properties of the blends studied in the previous part of this study were obtained at 180 ^{0}C. Hence, the processing temperature of this study was set at 180 ^{0}C. The processing time was kept constant at 5 minutes as in the previous section.

(c) *Processing Time*

Previous parts of this study showed that the optimum temperature and rotor speed were 180 ^{0}C and 90 rpm respectively. Hence, these parameters were selected for this part of the study. A melt temperature versus time curve for these particular process conditions showed that the melting temperature of waste polypropylene was reached within 2 minutes. Hence, mixing times of 2, 5, 8, 12 and 16 minutes were used. Table 3.2 lists all the blends produced in order to optimize the processing parameters.

Table 3.2 Blends prepared to assist in the optimisation of processing parameters

Specimen Code	Composition (GTR:WPP)	Processing Temperature, ^{0}C	Rotor speed, rpm	Processing time, min
50:50/160/30/5	50:50	160	30	5
50:50/170/30/5	50:50	170	30	5
50:50/180/30/5	50:50	180	30	5
50:50/190/30/5	50:50	190	30	5
50:50/200/30/5	50:50	200	30	5
50:50/210/30/5	50:50	210	30	5
50:50/180/15/5	50:50	180	15	5
50:50/180/45/5	50:50	180	45	5
50:50/180/60/5	50:50	180	60	5
50:50/180/75/5	50:50	180	75	5
50:50/180/90/5	50:50	180	90	5
50:50/180/105/5	50:50	180	105	5
50:50/180/120/5	50:50	180	120	5
50:50/180/90/2	50:50	180	90	2
50:50/180/90/8	50:50	180	90	8
50:50/180/90/12	50:50	180	90	12
50:50/180/90/16	50:50	180	90	16

(d) *Mixing Procedure Analysis*

In order to study the effect of mixing procedure on the blend properties, WPP and GTR were added separately. The second material was added 3 minutes after the addition of the first material. The order of addition of material was changed for each experiment. The resultant blend was always taken out of the mixer after processing for a further 5 minutes.

Table 3.3 lists the four blends prepared to evaluate the effect of processing schedule on the blend properties.

Table 3.3 Blends prepared to evaluate mixing procedure

Specimen Code	Description of the schedule
50:50/180/90/8P	WPP was added first and after 3 minutes, GTR was added
50:50/180/90/8R	GTR was added first and after 3 minutes WPP was added
50:50/180/90/5	Both WPP and GTR were added at the same time and processed for 5 minutes
50:50/180/90/8	Both WPP and GTR were added at the same time and processed for 8 minutes

3.2.4 Specimen Code for Second Part of Project

The code used for the identification of the blends used in the second part of the project (eg. 50:50/1H/0.2D-a) was as follows: the first set of numbers details the GTR to WPP weight ratio, which is always 50:50 for this part of study. The second number after the first slash represents the amount of compatibilizing agent used, which is given in parts by weight per hundred parts by weight of the WPP and GTR combined, pphp. The letter associated with the second number is for the compatibilizing agent, H is for HVA-2 and S is for SP 1045H resin. The third number after the second slash represents the amount of activator given in pphp. The letter associated with the third number in the specimen code indicates the type of activator; D is for DTBPIB, M is for MBTS and TA is for $SnCl_2$ and

TD is for $SnCl_2.2H_2O$. The letter at the end of the code represents the mixing schedule used in preparation of the blend.

3.2.5 Compositions Used for the Study of Compatibilizing Systems

The dynamically vulcanized rubber-thermoplastic blends have shown significant enhancement in overall properties (Section 2.7.2.2). However, with the addition of higher levels of vulcanizing agents, processing difficulties resulted. Further the results showed inferior properties with highly crosslinked rubber particles if no interfacial crosslinks were formed. Therefore, the determination of an optimum level of each component in the compatibilizing systems was of value.

3.2.5.1 Dimaleimide Compatibilizing System

The addition of HVA-2 to NR/PP blends having different compositions were studied previously [145, 149, 151] and were reported in Section 2.7.2.2c. Different HVA-2 levels were considered for those studies. The maximum HVA-2 level for NR/PP having 50 to 60 wt% of NR was reported as 7.5 phr. MBTS and DCP were also used as activators in some of the studies. The addition of MBTS was limited to 1.5 phr and DCP was to 1 phr. However, the maximum peroxide level used to vulcanize NR/PP blends with peroxide as the vulcanizing agent, were reported as 7 pphp (Section 2.7.2.2b). In order to compare the results of the present study with those of previous studies, a range dimaleimide levels was chosen with the maximum level of each component in the system selected to exceed the range of maximum levels used in the previous studies.

With the intension of optimizing the composition of the dimaleimide compatibilizing system in the present study, HVA-2 was first added to the GTR/WPP blends without any activators. For this study, the HVA-2 level was varied from 0 to 8 pphp in 1 pphp intervals. Secondly, the two activators, DTBPIB and MBTS, were also added to the blends with the HVA-2. Results obtained in this part of the study (Section 6.1) explained that the blend properties deteriorated with the addition of HVA-2 beyond 5 pphp. Hence, for the study of preparation of blends with activators, the HVA-2 level was varied from

0 to 5 pphp in 1 pphp intervals, while levels of the two activators were varied from 0 to 1 pphp in 0.2 pphp intervals.

3.2.5.2 Resin Compatibilizing System

Similar to the blends prepared with the dimaleimide compatibilizing system, blends with the resin compatibilizing system were prepared in which SP resin was first added to the GTR/WPP blends at levels varied from 0 to 8 pphp in 1 pphp intervals. The activator, $SnCl_2$ was added at levels varied from 0 to 1 pphp in 0.2 pphp intervals.

Literature revealed that PP modification with the resin system prior to melt mixing with rubbers favourably influenced the blend properties (Section 2.7.2.2d and Section 2.9.2.3). Therefore the effect of WPP modification on GTR/WPP blends was investigated. WPP modification was carried out at different levels of the resins system, but the SP resin to $SnCl_2$ weight ratio was maintained at 5:1. This ratio was selected based on the results of the first part of this study, in which the blends were prepared according to the mixing schedule-a (Section 6.2), and also on the previous studies reported in the literature [104, 165-167]. Both anhydrous and dihydrate forms of stannous chloride were used as activators in those previous studies. The water content in the dihydrate form should have evaporated during melt mixing and hence should have given the same effect as an activator. However, the effect of the two forms was also investigated in the present study.

3.2.6 Processing Conditions Used for Study of Compatibilizing Systems

From the effect of processing parameters on blend properties study (Section 5.2) it was determined that the best tensile properties were exhibited at a processing temperature of 180 ^{0}C, rotor speed of 90 rpm and for a processing time of 5 minutes. Further, better properties were produced when both materials were added together. These optimized processing parameters were for the 50:50 blend, which was selected as the control blend for this study. The compatibilizers were added to the melt-mix, 2 minutes from the start of mixing, when the WPP and GTR was melt-mixed. This stage was identified by the stabilization of torque (Section 5.2). The mixing schedule in which both materials were

added together at the start of the mixing was called 'schedule-a'. This 'schedule-a' was used for blends with the dimaleimide compatibilizing system and for some blends with the resin compatibilizing system. For the other blends, the WPP was first modified with resin system and then the GTR was added. This procedure was practiced in a previous study for the preparation of NBR/PP blends [106]. The second mixing schedule was called 'schedule -b'.

Table 3.4 and Table 3.5 list the blends prepared for compatibilization with the dimaleimide system, without, and with activators, respectively. Table 3.6 and Table 3.7 list the blends prepared for compatibilization with the resin system, without, and with activators, respectively.

Table 3.4 Blends prepared using the dimaleimide compatibilizing system without activators

Specimen Code	Blend Composition (GTR:WPP)	HVA-2, pphp	Mixing Schedule
Control Blend	50:50	0	a
50:50/1H-a	50:50	1	a
50:50/2H-a	50:50	2	a
50:50/3H-a	50:50	3	a
50:50/4H-a	50:50	4	a
50:50/5H-a	50:50	5	a
50:50/6H-a	50:50	6	a
50:50/7H-a	50:50	7	a
50:50/8H-a	50:50	8	a

Mixing schedule-a

0 min	add WPP and GTR
2 min	add compatibilizing agent/system and antioxidant*
5 min	dump

(* for the control blend, antioxidant was added at the start of mixing at 0 minute)

Mixing schedule-b

0 min	add WPP
1.5 min	add SP 1045H resin and/or activator ($SnCl_2$ or $SnCl_2.2H_2O$)
2.5 min	add GTR and antioxidant
5 min	dump

Table 3.5 Blends prepared using the dimaleimide compatibilizing system with activators

Specimen Code	Blend Composition (GTR:WPP)	HVA-2, pphp	DTBPIB, pphp	MBTS, pphp	Mixing Schedule
50:50/0H/0.2D-a	50:50	0	0.2	-	a
50:50/1H/0.2D-a	50:50	1	0.2	-	a
50:50/2H/0.2D-a	50:50	2	0.2	-	a
50:50/3H/0.2D-a	50:50	3	0.2	-	a
50:50/4H/0.2D-a	50:50	4	0.2	-	a
50:50/5H/0.2D-a	50:50	5	0.2	-	a
50:50/3H/0.4D-a	50:50	3	0.4	-	a
50:50/3H/0.6D-a	50:50	3	0.6	-	a
50:50/3H/0.8D-a	50:50	3	0.8	-	a
50:50/3H/1.0D-a	50:50	3	1.0	-	a
50:50/0H/0.2M-a	50:50	0	-	0.2	a
50:50/1H/0.2M-a	50:50	1	-	0.2	a
50:50/2H/0.2M-a	50:50	2	-	0.2	a
50:50/3H/0.2M-a	50:50	3	-	0.2	a
50:50/4H/0.2M-a	50:50	4	-	0.2	a
50:50/5H/0.2M-a	50:50	5	-	0.2	a
50:50/3H/0.4M-a	50:50	3	-	0.4	a
50:50/3H/0.6M-a	50:50	3	-	0.6	a
50:50/3H/0.8M-a	50:50	3	-	0.8	a
50:50/3H/1.0M-a	50:50	3	-	1.0	a

3.2.7 Modification of WPP with Resin Compatibilizing System

In order to investigate WPP modification with a resin system, blends with two different compositions of the resin system were prepared. They were 4 pphp (parts by weight of a compatibilizing component per hundred parts of WPP by weight) of SP resin with 0.8 pphp of activator, and 8 pphp of SP resin with 1.6 pphp of activator. Both $SnCl_2$ anhydrous and dihydrate were used for modification. These modified WPP were compared with modified PP at the respective compositions. The extent of modification was investigated using FTIR spectra of gels obtained by acetone and xylene extractions.

A separate sample identification code was used for this part of the study (eg. 4S/0.8TA/WPP). It was as follows: the first number represents the amount of compatibilizing agent added in pphp. The letter associated with the first number identified the compatibilizing agent, eg. S for the SP 1045H resin. The second number after the first slash represents the amount of activator added in pphp, and the set of two letters associated with the number is for the type of activator; TA for the $SnCl_2$ and TD for the $SnCl_2.2H_2O$. The third set of letters in the identification code is for the polymer that was modified; WPP for waste polypropylene and PP for virgin polypropylene.

Table 3.6 Blends prepared using the resin compatibilizing system without activators

Specimen Code	Blend Composition (GTR:WPP)	SP resin, pphp	Mixing Schedule
Control Blend-a	50:50	0	a
50:50/1S-a	50:50	1	a
50:50/2S-a	50:50	2	a
50:50/3S-a	50:50	3	a
50:50/4S-a	50:50	4	a
50:50/5S-a	50:50	5	a
50:50/6S-a	50:50	6	a
50:50/7S-a	50:50	7	a
50:50/8S-a	50:50	8	a

Table 3.7 Blends prepared using the resin compatibilizing system with activators

Specimen Code	Blend Composition (GTR:WPP)	SP resin pphp	$SnCl_2$ pphp	$SnCl_2.2H_2O$ pphp	Mixing Schedule
50:50/0S/0.2TA-a	50:50	0	0.2	-	a
50:50/1S/0.2TA-a	50:50	1	0.2	-	a
50:50/2S/0.2TA-a	50:50	2	0.2	-	a
50:50/3S/0.2TA-a	50:50	3	0.2	-	a
50:50/4S/0.2TA-a	50:50	4	0.2	-	a
50:50/5S/0.2TA-a	50:50	5	0.2	-	a
50:50/3S/0.4TA-a	50:50	3	0.4	-	a
50:50/3S/0.6TA-a	50:50	3	0.6	-	a
50:50/3S/0.8TA-a	50:50	3	0.8	-	a
50:50/3S/1.0TA-a	50:50	3	1.0	-	a
Control Blend-b	50:50	0	-	-	b
50:50/2S-b	50:50	2	-	-	b
50:50/3S-b	50:50	3	-	-	b
50:50/4S-b	50:50	4	-	-	b
50:50/5S-b	50:50	5	-	-	b
50:50/2S/0.4TA-b	50:50	2	0.4	-	b
50:50/3S/0.6TA-b	50:50	3	0.6	-	b
50:50/4S/0.8TA-b	50:50	4	0.8	-	b
50:50/5S/1.0TA-b	50:50	5	1.0	-	b
50:50/4S/0.8TD-b	50:50	4	-	0.8	b

WPP/PP modification was carried out in the internal mixer under the processing conditioned mentioned in Section 3.2.6. However, mixing was performed with a new mixing schedule called 'schedule-c'. This mixing procedure has been used previously [166]. The WPP/PP samples prepared for this part of the study are given in Table 3.8.

Mixing schedule-c

0 min	add WPP or PP
2 min	add SP 1045H resin
4 min	add activator ($SnCl_2$ or $SnCl_2.2H_2O$)
6 min	dump

Table 3.8 Samples prepared for WPP/PP modification

Specimen Code	SP resin, pphp	$SnCl_2$, pphp	$SnCl_22H_2O$, pphp	Mixing Schedule
4S/0.8TA/WPP	4	8	-	c
8S/1.6TA/WPP	8	1.6	-	c
8S/1.6TD/WPP	8	-	1.6	c
4S/0.8TA/PP	4	8	-	c
8S/1.6TA/PP	8	1.6	-	c
8S/1.6TD/PP	8	-	1.6	c

3.2.8 Crosslinking Capability of GTR with Resin Compatibilizing System

The ability of the GRT to crosslink using the resin system was studied. This ability was investigated for both activators using processing characteristics, moulding capability and by gel content after acetone extraction. In this part of the study, 8 pphp (parts of a compatibilizing agent by weight per hundred parts of GTR by weight) of SP resin with 1.6 pphp of activator was mixed to the GTR, in the internal mixer under the processing conditioned given in Section 3.2.6. Mixing was carried out according to the mixing schedule-c, with replacement of WPP/PP by GTR.

Table 3.9 Samples prepared for GTR crosslinking

Specimen Code	SP resin, pphp	$SnCl_2$, pphp	$SnCl_2 2H_2O$, pphp	Mixing Schedule
GTR	-	-	-	c
8S/1.6TA/GTR	8	1.6	-	c
8S/1.6TD/GTR	8	-	1.6	c

3.2.9 Specimen Code for Third Part of Project

The code used (eg. 50:50-DGTR/3H/0.6D-f) for the identification of the blends used in the third part of the project was similar to that (eg. 50:50 /3H/0.6D-a) used in the second part of the study (Section 3.2.4). The additional four letters in the code separated by a dash from the first set of numbers, which details the GTR to WPP weight ratio, represents the type of GTR used; DGTR if for GTR treated with 3 phr of Delink and PGTR is for processed GTR without Delink (Section 3.2.11).

3.2.10 Evaluation of Delink Level

3.2.10.1 Selection of Delink level

The inventors of the Delink system [42] suggested adding 6 parts of Delink to 100 parts (pphp) of tyre crumbs made with 100% natural rubber, as this Delink treated rubber showed comparable properties to virgin rubbers. The Delink level required depends on the type of rubber being devulcanized and the final form of the devulcanized product desired, and hence the inventors in a separate study [169] suggested adding 2-6 pphp of Delink. It has been shown that the optimum Delink level was 6 pphp, when 30 wt% Delink treated rubber was blended with virgin natural rubber [38]. Further, 6 pphp of Delink was used in treating buffing dust in order to incorporate it into virgin natural rubber at 0 to 50 wt% levels [171]. Hence, the effect of Delink treatment on the tensile

properties of the GTR was investigated by varying the Delink level from 3 to 9 phr at 3 phr intervals.

3.2.10.2 Selection of Treatment Conditions

It has been reported that devulcanization using Delink occurred in 7 to 10 minutes when processed in a two-roll mill [42]. The devulcanization was also completed in 5-6 minutes when processed in an internal mixer [169]. Alternatively, devulcanization can be achieved by processing first in an internal mixer and subsequently milled in an open mill. Irrespective of the equipment used, it was recommended to process for less than 10 minutes at a temperature below 70 ^{0}C [42].

Torque versus time curve for the GTR when processed at 40 ^{0}C and at 90 rpm showed that the maximum temperature of the melt was always below 70 ^{0}C. Processing at a temperature greater than 40 ^{0}C showed an increase in melt temperature above 70 ^{0}C. Hence 40 ^{0}C and at 90 rpm processing conditions were selected for the Delink process. The time of processing was taken as 7 and 10 minutes. The mixing schedule used for the Delink process, called 'schedule –d' was as follows:

Mixing schedule-d

0 min	add GTR
2 min	add Delink
7/10 min	dump

Moulding of the processed GTR mixes was carried out at two different temperatures; at 150 ^{0}C, the normal rubber vulcanizing temperature and at 200 ^{0}C, the temperature at which the blends were moulded.

A separate code of identification of the Delink treated GTR was applied (eg. 3De/7/150). The first number in the code represents the level of Delink added, and the two letters 'De' which follow is for the Delink. The second number after the first slash represents the processing time and the third number after the second slash represents the moulding

temperature. The Delink treated GTR samples prepared for this part of study are given in Table 3.10.

Table 3.10 Delink treated GTR prepared for the evaluation of Delink level

Specimen Code	Delink, phr	Processing time, min	Moulding temperature, ^{0}C	Mixing Schedule
0De/7/150	0	7	150	d
3De/7/150	3	7	150	d
6De/7/150	6	7	150	d
9De/7/150	9	7	150	d
0De/7/200	0	7	200	d
3De/7/200	3	7	200	d
6De/7/200	6	7	200	d
9De/7/200	9	7	200	d
0De/10/150	0	10	150	d
3De/10/150	3	10	150	d
6De/10/150	6	10	150	d
9De/10/150	9	10	150	d
0De/10/200	0	10	200	d
3De/10/200	3	10	200	d
6De/10/200	6	10	200	d
9De/10/200	9	10	200	d

3.2.11 Preparation of DGTR/WPP Blends

The results of the study of Delink level (Section 7.1) showed that the best tensile properties were obtained at 3 phr of Delink when processed at 40 ^{0}C and at 90 rpm for 10 minutes, and therefore these conditions were selected for the rest of the project. The GTR processed with 3 phr of Delink was then labelled Delink treated ground tyre rubber

(DGTR). The GTR processed under the same conditions, but without the Delink, was labelled processed ground tyre rubber (PGTR).

DGTR/WPP blends at different compositions were prepared to investigate the effect of blend composition. The levels used for this study varied from 10 to 90 wt% in 20 wt% intervals of each material. Properties of these blends were compared with PGTR/WPP blends at the same compositions. For the blends with DGTR, it was not advisable to add both materials together at the commencement of mixing as in mixing schedule-a (Section 3.2.6). Re-linking of the Delink treated GTR can occur at the start of mixing within the GTR phase itself, without promoting interfacial linkages with the molten WPP. Because of this, the DGTR was added to the mixer when the WPP was melted after 2 minutes from the start of mixing. The mixing time for the DGTR, or the PGTR, was kept at 5 minutes. The mixing schedule used for this study 'schedule-e' is given below. The blends prepared for this part of study are given in Table 3.11.

Mixing schedule- e

0 min	add WPP
2 min	add PGTR or DGTR with antioxidants*
7 min	dump

(* for the DGTR/WPP with compatibilizing systems, the systems were also added at this stage of mixing)

In addition, the pure PGTR and the pure DGTR were reprocessed at 180 ^{0}C and 90 rpm for 5 minutes. These reprocessed polymers were called as RPGTR and RDGTR.

Table 3.11 DGTR/WPP and PGTR/WPP blends prepared for evaluation of blend composition

Specimen Code	WPP, wt%	PGTR, wt%	DGTR, wt%	Mixing Schedule
10:90-PGTR-e	90	10	-	e
30:70-PGTR-e	70	30	-	e
50:50-PGTR-e	50	50	-	e
70:30-PGTR-e	30	70	-	e
90:10-PGTR-e	10	90	-	e
10:90-DGTR-e	90	-	10	e
30:70-DGTR-e	70	-	30	e
50:50-DGTR-e	50	-	50	e
70:30-DGTR-e	30	-	70	e
90:10-DGTR-e	10	-	90	e

3.2.12 Preparation of DGTR/WPP Blends with Compatibilizing Systems

DGTR/WPP blends were prepared with both compatibilizing systems used in the previous parts of the present study. The optimum level of each compatibilizing system was used in preparation of DGTR/WPP blends. Properties of these blends were compared with the PGTR/WPP prepared under the same processing conditions. The levels of the compatibilizing systems used and the processing conditions are discussed below.

3.2.12.1 DGTR/WPP Blends with Dimaleimide Compatibilizing System

The optimum level of the dimaleimide vulcanizing system was obtained as 3 pphp of HVA-2 and 0.6 pphp of DTBPIB (Section 6.1). Hence, this optimum level was used in preparation of DGTR/WPP blends with the dimaleimide compatibilizing system. The mixing 'schedule-e' (Section 3.2.11) was followed to prepare most of the blends. A new mixing schedule called 'schedule-f' was also followed to prepare blends, in order to

investigate the sequence of incorporating the dimaleimide system to the DGTR/WPP blends. In this 'schedule-f', HVA-2 and/or DTBPIB were added after 4 minutes from the start of mixing. The mixing 'schedule-f' is given as below. The full set of blends prepared for this study is given in Table 3.12.

Mixing schedule- f

0 min	add WPP
2 min	add PGTR or DGTR with antioxidants
4 min	add HVA-2 and/or DTBPIB
7 min	dump

Table 3.12 DGTR/WPP and PGTR/WPP blends prepared with the dimaleimide compatibilizing system

Specimen Code	WPP wt%	PGTR wt%	DGTR wt%	HVA-2 pphp	DTBPIB pphp	Mixing Schedule
50:50-DGTR/3H-e	50	-	50	3	-	e
50:50-DGTR/3H/0.6D-f	50	-	50	3	0.6	f
50:50-DGTR/3H/0.6D-e	50	-	50	3	0.6	e
30:70-DGTR/3H/0.6D-e	70	-	30	3	0.6	e
70:30-DGTR/3H/0.6D-e	30	-	70	3	0.6	e
50:50-PGTR/3H/0.6D-f	50	50	-	3	0.6	f
50:50-PGTR/3H/0.6D-e	50	50	-	3	0.6	e
30:70-PGTR/3H/0.6D-e	70	30	-	3	0.6	e
70:30-PGTR/3H/0.6D-e	30	70	-	3	0.6	e

3.2.12.2 DGTR/WPP Blends with Resin Compatibilizing System

The optimum level of the resin vulcanizing system was obtained as 4 pphp of SP resin and 0.8 pphp of $SnCl_2$ (Section 6.2). This optimum level was used in preparation of

DGTR/WPP blends with the resin compatibilizing system. For this part of the study, mixing 'schedule-e' and another mixing schedule called 'schedule-g' were followed. In the mixing 'schedule-g', the WPP was first modified with SP resin system and then the PGTR or DGTR was added. Schedule-g is given as follows:

Mixing schedule- g

0 min	add WPP
2 min	add SP system
4 min	add PGTR or DGTR with antioxidants
7 min	dump

Table 3.13 DGTR/WPP and PGTR/WPP blends prepared with the resin compatibilizing system

Specimen Code	WPP wt%	PGTR wt%	DGTR wt%	SP Resin pphp	$SnCl_2$ pphp	Mixing Schedule
50:50-DGTR/4S-g	50	-	50	4	-	g
50:50-DGTR/4S/0.8TA-g	50	-	50	4	0.8	g
50:50-DGTR/4S/0.8TD-g	50	-	50	4	0.8	g
50:50-DGTR/4S/0.8TA-e	50	-	50	4	0.8	e
50:50-DGTR/4S/0.8TD-e	50	-	50	4	0.8	e
50:50-PGTR/4S-g	50	50	-	4	-	g
50:50-PGTR/4S/0.8TA-g	50	50	-	4	0.8	g
50:50-PGTR/4S/0.8TD-g	50	50	-	4	0.8	g

3.3 Preparation of Delink

Components of the Delink were weighed individually, according to the formulation given in Section 3.1.2. Delink was prepared in 50 g. batches each time. Components in powder or pellet form, like ZDMC, MBT, ZnO and stearic acid, were first mixed using mortar

and pestle, until the mix became a fine powder. Finally diethylene glycol was added to the mix to make a smooth paste.

3.4 Compound Processing and Characterization

The blends of GTR and WPP were prepared by melt mixing in a Haake Rheocord Polylab system manufactured by the Thermo Haake Company, UK. This is a computer controlled torque rheometer, which can also be used as a mini batch mixer. This mixer controls the temperature and rotor speed and measures torque, melt temperature and melt pressure against time. The mixing chamber of the mixer is made up of three plates, two removable plates and a non-removable plate. Roller rotors (Figure 3.8), which were used for melt mixing, were fixed to the mixer through the non-removable plate as shown in Figure 3.9(a). The non-removable plate and one removable plate were rectangular in shape, and were served as covering plates. The other removable plate, which contained a cavity to the shape of the mixing chamber, was assembled in the middle. This plate had a thermocouple at the centre opposite to the opening to the feed hopper, and was used to monitor the chamber temperature or the melt temperature.

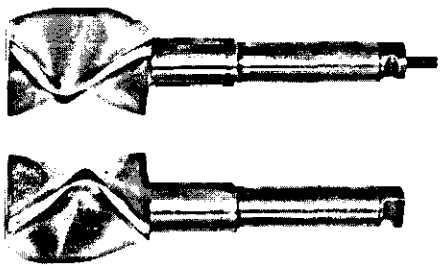

Figure 3.8 Roller rotors used in the Haake mixer

The processing conditions, which were specified under the different compound formulations, were set prior to the addition of the polymer/s. The mixer was preheated for 30 minutes until the chamber temperature stabilized. A batch weight of 50 g was maintained for all blends processed. The WPP, the GTR and specified chemicals were added to the mixer, through the feeding hopper (Figure 3.9 (b)), according to the specified mixing schedule. For the blends prepared with compatibilizing systems, the GTR and the

chemicals were added to the mixer at different time intervals, according to the specified schedule, by lifting up the ram. The ram was closed directly after the addition. The resultant blend came out from the mixer as a single mass and it was cut into small pieces while still hot. The mixer was cleaned and purged between each blend. In the case of the Delink process, the resultant Delink treated GTR came out from the mixer in powder form, and was stored in the same form.

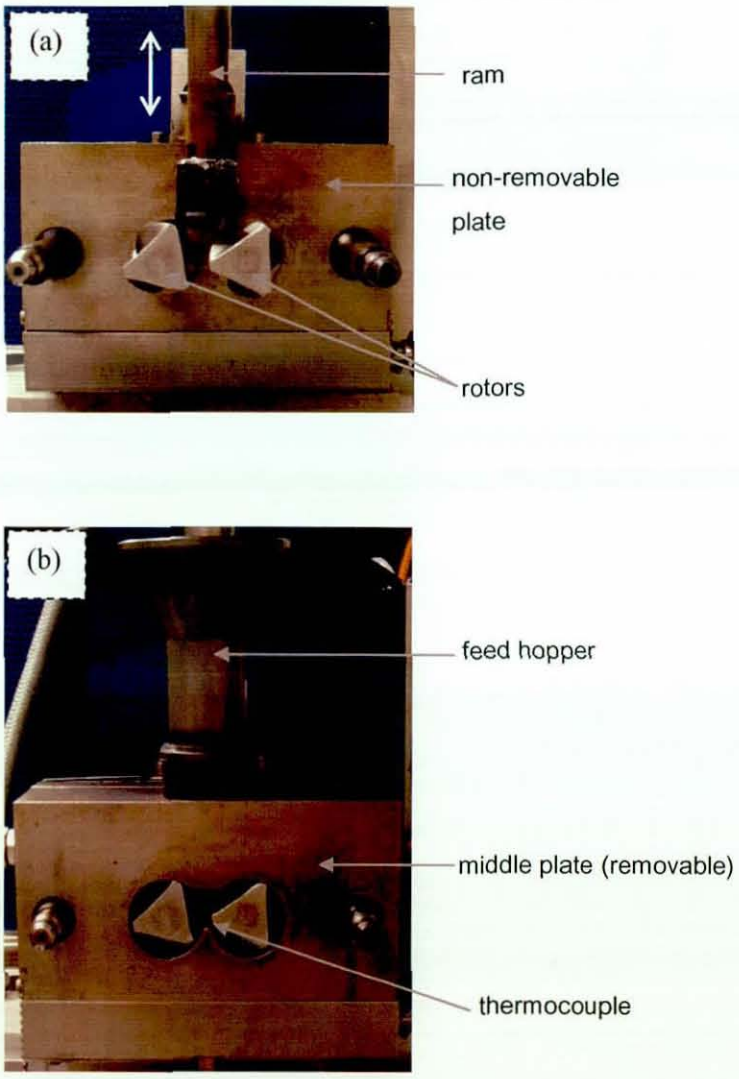

Figure 3.9 Assembly of the Haake mixer (a) positioning of rotors and ram during mixing (ram movement shown by the white arrow) (b) assembly of hopper and the middle removable plate

For the blends prepared in the first part of the project, processing characteristics were studied in detail. The recorded torque versus time data produced a graph with a very scattered nature. For analysis, a smoothed curve was plotted with a trend line. A moving average with a period of 10 was selected to plot the trend line. Maximum torque, torque at steady state and time taken to reach steady state were calculated from the plotted smoothed curve (Figure 3.10). Blends containing 70 wt% of GTR, and above showed two maxima. As the other blends only had one maximum torque, only the initial maximum torque was considered for comparison and analysis of results.

Steady state was defined as the state when the torque was at 110% of the value recorded after 8 minutes.

The torque reduction rate was defined as follows:

$$\text{Torque Reduction Rate} = \frac{(T_{max} - T_{ss})}{(t_{ss} - t_{max})} \qquad \text{Equation 3.1}$$

Where, T_{max} is the maximum torque from the moving average trend line, in Nm

t_{max} is the time taken to reach torque maximum, in minutes

T_{ss} is the steady state torque, where, $T_{ss} = 1.1*T_{min}$

T_{min} is the torque at 8 minutes, in Nm

t_{ss} is the time taken to reach steady state, in minutes

When processing conditions were considered the steady state process time was considered as the time for complete melt mixing, and was set at 5 minutes. This time was also used in the second part of the project. For the third part of the project, the mixing time was varied. Torque at completion of the mixing process was therefore considered as the steady state torque.

The energies necessary to process the blends, until they reached steady state conditions were calculated from the retrieved torque-time data. The specific energy required to process the blends at a given temperature and shear rate were obtained by multiplying the integral of the area beneath the torque development curve, by the rotor speed, per gram of processed material, as described in Equation 3.2 [253]. The integral of the area beneath the curve was calculated using an approximation method, using a trapezoidal algorithm.

$$\text{Specific Energy, } W = \frac{2\pi n \int_{t_1}^{t_2} M\, dt}{m} \qquad \text{Equation 3.2}$$

Where, n is the rotor speed, in rpm

M is the torque, in Nm

$t_1 (= 0)$ is the initial time minutes

$t_2 (= t_{ss})$ is the time at the end of processing (= time to reach steady state), in minutes

m is the weight of the material processed, in grams

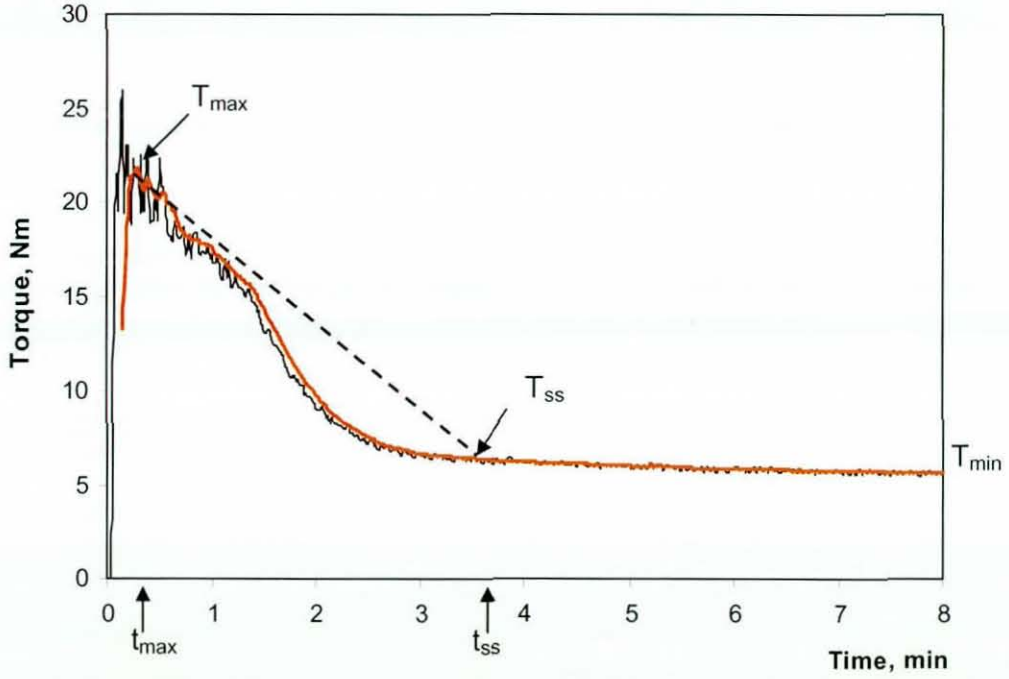

Figure 3.10 Typical torque-time curve obtained from the mixer

3.5 Melt Flow Analysis

Melt flow index (MFI), which is also known as melt mass flow rate (MFR), reflects the ease of flow of a molten polymer at specific process conditions [133]. Melt flow tests were performed using an Extrusion Plastomerer, Model MP600, manufactured by Tinius Oslen, USA, according to BS EN ISO 1133, Procedure A:2005.

5 g of material was charged to the barrel of the melt indexer. During charging, material was compressed with the packing rod using hand pressure. The charged material was preheated to 230 ^{0}C for 5 minutes. A weighted piston with a nominal load of 2.16 kg was then immediately placed in the charged cylinder. The material was allowed to extrude for a preset period of time and the extrudate was cut off using a cutting tool. The melt flow index, expressed in grams per 10 minutes, is given by the following equation [254].

$$MFI(T, m_{nom}) = \frac{600 m_{av}}{t_i} \qquad \text{Equation 3.3}$$

Where, T is the test temperature, in^{0}C

m_{nom} is the nominal load, in kilogram

m_{av} is the average mass, in gram

t_i is the cut off time interval, in seconds

600 is the factor used to convert grams per second into grams per 10 minutes (600s)

3.6 Moulding of Test Specimens

The small pieces of the blend from the Haake mixer were allowed to cool to room temperature. Test specimens were prepared from these pieces by compression moulding in an electrically heated hydraulic press. The press was preheated to equilibrium at 200 ^{0}C. The specified weight (10 - 35 g.) of the blended material was placed into a suitable mould and this was placed into the hydraulic press. Initially it was compressed under 500 kN/m^2 pressure for 4 minutes, and then the pressure was slowly increased to 1000 kN/m^2 for another 4 minutes. Finally it was cooled for 2 minutes under 1000 kN/m^2 pressure in a cooling press. The moulded material was then removed from the mould. The specific type and size of mould used, and post moulding preparations used are given in the following sections.

Unlike the blends, the PGTR and the Delink treated GTR taken from the Haake mixer were in powder form. These powders were compressed using the hydraulic press to make moulded sheets. A specified weight of 25 g. was placed in a square shaped mould having

90 mm each side and compressed under 1000 kN/m^2 pressure for 10 minutes at the specified temperature. The moulded sheets were then removed from the mould and cooled in air.

3.6.1 Hardness Test Specimens

A 10 mm thick disc shaped frame mould was placed between two steel plates to form the mould. The diameter of the disc was 25 mm. A constant weight of material of 10 g. was placed into the mould.

3.6.2 Tensile Test Specimens

A square shaped aluminium frame was sandwiched in between two steel plates to form the mould. The frame was 80 mm square by 1.5 mm thick. A constant weight of material of 13 g. was compressed to form the sheet. For the second and third parts of the project, a 90 mm square frame was used. The thickness of the frame was 2 mm, and a constant weight of material of 19 g. was compressed.

The moulded sheet was cut into strips, 12mm wide, using an electrically operated band saw. These strips were shaped into dumbbells using a template. A high speed router machine with a tungsten carbide blade was used to shape the dumbbells. The dimensions of the test specimen made are given in Figure 3.11.

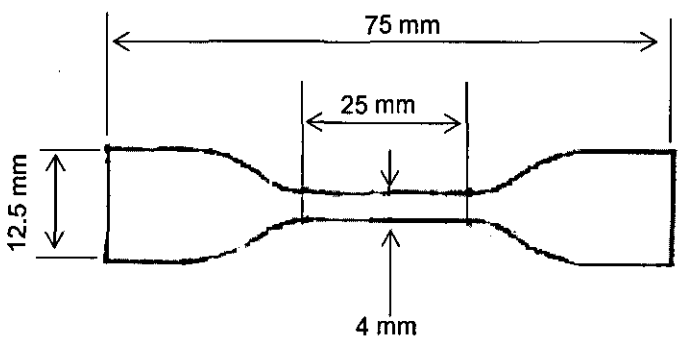

Figure 3.11 Dimensions of the dumbbell test specimen

3.6.3 Tear Test Specimens

A 1 mm thick square shaped frame was placed between two steel plates to form the mould. The sides of the frame were 150 mm long. A constant weight of material of 25 g. was placed inside the frame. Trouser test pieces were prepared from the moulded sheet according to the specimen dimensions given in Figure 3.12. A 75 mm longitudinal cut was made at the centre of the test specimen. The cut was made using a knife with a scalpel blade.

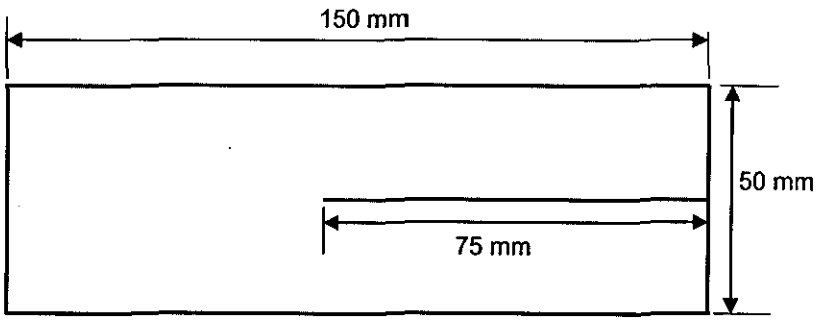

Figure 3.12 Dimensions of the tear test specimen

3.6.4 Impact Test Specimens

A 2 mm thick square shaped frame was placed between two steel plates to form the mould. The sides of the frame were 120 mm long. A constant weight of material of 33 g. was placed inside the frame. Impact test specimens, 60 mm square, were cut from the moulded sheet, according to BS EN ISO 6603-1:2000.

3.7 Mechanical Properties

The blends prepared according to the formulations and processing conditions given in the previous sections were evaluated in terms of mechanical behaviour such as hardness, tensile properties, impact properties and tear resistance. The testing procedures and conditions used for the blend evaluations are given in detail in this section.

3.7.1 Hardness

The hardness test is a non destructive test and a simple way to measure the modulus of a rubber material [255]. Hardness tests were performed using a Dead Load Hardness Tester, manufactured by H. W. Wallace & Co. Ltd., U.K, according to BS EN ISO 868:2003. The hardness values were determined after penetration of the indenter for 30 seconds into the specimen. This test was performed at a room temperature of 21±1 ^{0}C. Test results were recorded using the International Rubber Hardness Degree (IRHD) scale.

3.7.2 Tensile Properties

Tensile testing for the first part of the project was performed according to BS EN ISO 527:1996 [256] using a Lloyd Tensometer L10000. This tensometer utilized a 500N load cell and was operated by a computer controlled system. A Lloyd instrument data analysing software package was used to determine the tensile properties. A crosshead speed of 50 mm/min was set. Elongation was determined using the crosshead displacement and the gauge section as the original length. Tensile testing for the second and third parts of the project was performed using a Hounsfield Tensile Testing machine with a 1000N load cell. The crosshead speed was set at 50 mm/min. Qmat software was used to determine the properties, and elongation was determined using a laser extensometer. As the dimensions of specimens slightly varied, all specimens were measured before testing. The thickness and the width of the test specimens were measured in several places using a bench type thickness gauge and a vernier calliper respectively. The average values of the measurements were used for calculations.

Load against extension data was recorded until the specimen fractured. Maximum load, extension at maximum load, load at break, and extension at break were also determined by the software. Tensile strength, elongation at break, secant modulus at 2% strain and Young's modulus were calculated using the following equations [256]. A typical stress-strain curve is given in Figure 3.13.

$$\text{Tensile Strength (MPa)} = \frac{\text{Maximum Load (N)}}{\text{Original Cross Sectional Area (mm}^2\text{)}} \qquad \text{Equation 3.4}$$

$$\%\ \text{Elongationat Break} = \frac{\text{Extension at Break (mm)}}{\text{Guage Length (mm)}} \times 100 \qquad \text{Equation 3.5}$$

$$\text{Secant Modulus (MPa)} = \frac{\text{Load at 2\% Strain} \times 100\ \text{(N)}}{2 \times \text{Original Cross Sectional Area (mm}^2\text{)}} \qquad \text{Equation 3.6}$$

$$\text{Young's Modulus (MPa)} = \frac{(\text{Load at 0.25\% Strain - Load at 0.05\% Strain}) \times 100\ \text{(N)}}{(0.25 - 0.05) \times \text{Original Cross Sectional Area (mm}^2\text{)}} \qquad \text{Equation 3.7}$$

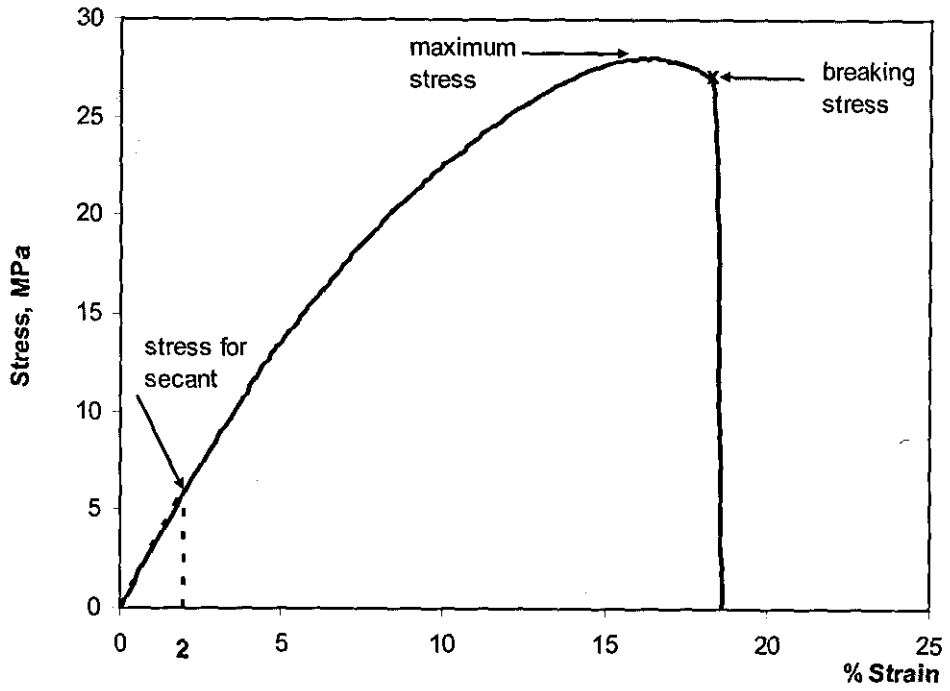

Figure 3.13 Typical stress - strain curve from tensile test

3.7.3 Tear Resistance

Tear resistance tests were performed according to BS EN ISO 6383-1:2004 [257] using a Lloyd Tensometer L10000. A 500 N-load cell was attached to the tensometer and tests were performed at a crosshead speed of 100 mm/min. Thicknesses at three different

equidistant points between the tip of the slit and the opposite end of each specimen were measured using a bench type thickness gauge before testing. The average values of the measurements were used for calculations. The initial grip separation was set at 75 mm. The test specimens were clamped to the grips with its major axis coincident with an imaginary line joining the centre of the grips.

Load against extension data was recorded until the specimen was split. A typical curve is given in Figure 3.14. Disregarding the loads recorded in tearing the first 20 mm and the last 5 mm of the un-slit length, the mean value of the tearing load over the remaining 50 mm of the un-slit length was obtained. The tear resistance of the specimen was calculated according to the following equation [257].

$$\text{Tear Resistance (N/mm)} = \frac{\text{Tearing Force (N)}}{\text{Thickness (mm)}} \qquad \text{Equation 3.8}$$

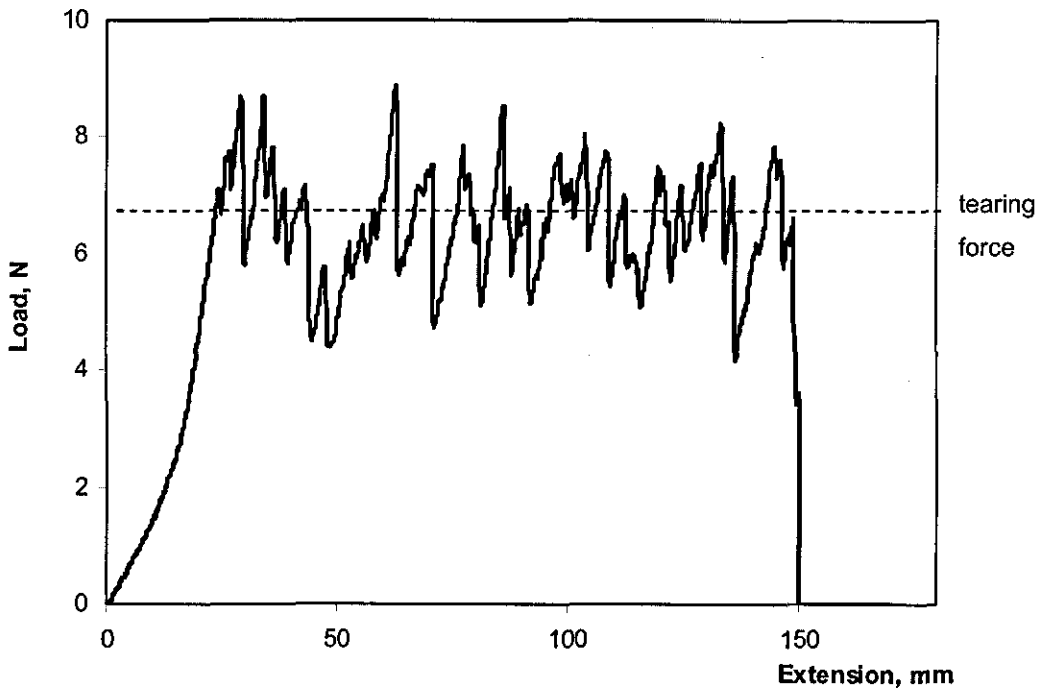

Figure 3.14 Typical load vs. extension curve from tear test

3.7.4 Impact Properties

Impact tests were performed, according to BS EN ISO 6603-2:2002, using a Rosand Falling Dart Impact tester. The test specimens were placed on the specimen supporting ring and then clamped. The impact test was conducted at a velocity of 3 m/s and at a corresponding height of 0.46 m. The applied impact load was 4 kg. Tests were conducted at a room temperature of 20±2 ^{0}C. Impact falling weight analysis software was used to determine the properties. Peak force, F_M, energy to peak force or fracture initiation energy, W_M, displacement at peak force, D_M, failure force, F_F, failure (impact) energy, W_F, and displacement at failure force, D_F, were recorded. All these properties were normalized by dividing by the thickness of each specimen. In addition to these properties, fracture propagation energy, W_P, stiffness, and ductility index were considered for comparison of results. Fracture propagation energy is the impact energy absorbed after the maximum force until failure. Stiffness is the initial slope of the impact curve [133]. Ductility index is the ratio of the fracture propagation energy to the total energy absorbed during an impact event [124]. A typical force vs. displacement curve is given in Figure 3.15. Fracture propagation energy, stiffness and ductility index were calculated according to the following equations.

$$\text{Fracture Propagation Energy} = \text{Failure Energy} - \text{Fracture Initiation Energy (J)} \qquad \text{Equation 3.9}$$

$$\text{Stiffness (N/m)} = \frac{\text{Peak Force(N)}}{\text{Deformation at Peak Force(m)}} \qquad \text{Equation 3.10}$$

$$\text{Ductility Index} = \frac{\text{Fracture Propagation Energyy}}{\text{Failure Energy}} \qquad \text{Equation 3.11}$$

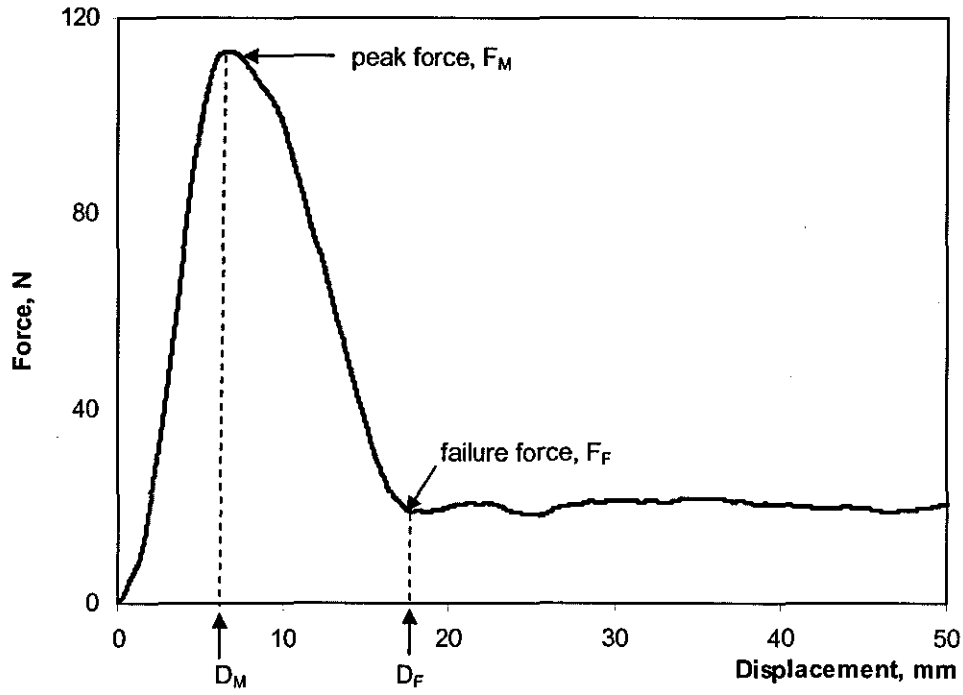

Figure 3.15 Typical force vs. displacement curve from falling dart impact test

3.8 Thermal Analysis

3.8.1 Thermogravimetric Analysis (TGA)

Polymers are thermally stable until the decomposition process starts. Two main types of decomposition processes, chain depolymerization and random decomposition, may occur separately or in combination. Both processes cause sample mass losses which can be measured by TGA [258].

Thermogravimetric analysis was carried out using a Hi-Res Modulated TGA 2950 instrument manufactured by TA instruments. Degradation behaviours of WPP and GTR were studied. 15 to 25 mg of the polymer was placed in the aluminium pan and heated at a rate of 10 ^{0}C/min from room temperature to 700 ^{0}C. The test was carried out under normal atmosphere. A typical TGA thermogram is given in Figure 3.16. This thermogram gives both % weight remaining in the pan and the differential of the weight against

temperature, dw/dT. The composition of the GTR was determined using these two curves; TGA curves and differential thermogravimetric analysis (DTGA) curve. Both starting and completion degradation temperatures for each component was identified by the turning points of the DTGA curve. The corresponding weights were obtained by the TGA curve. The weight of each component was calculated by the weight difference obtained, as an examples, a, b, c, d and e as marked in Figure 3.16.

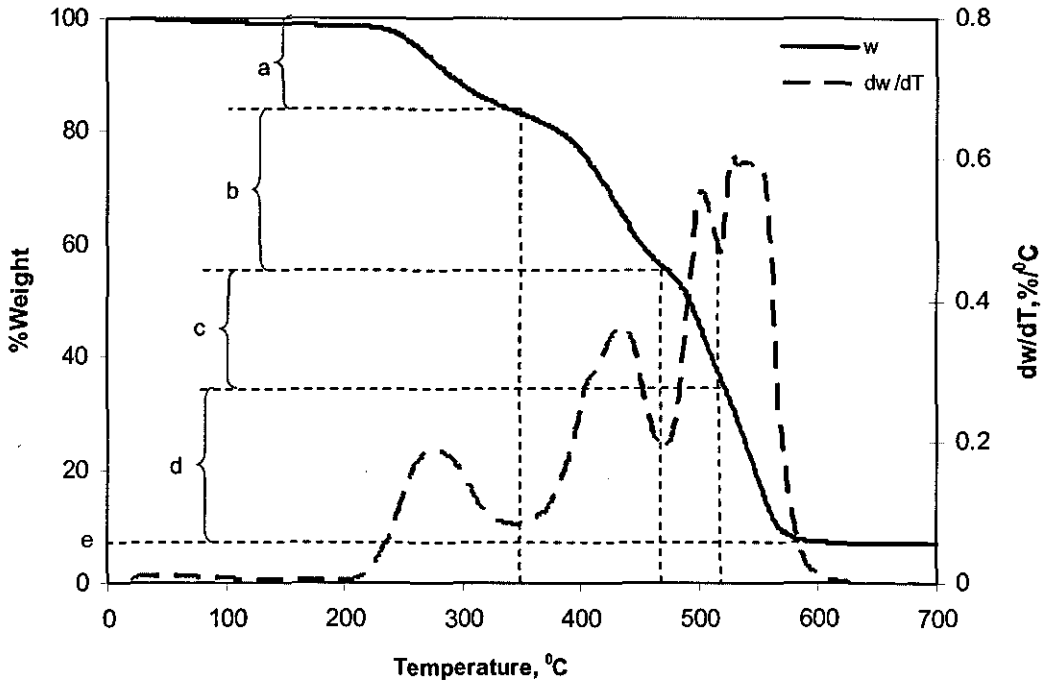

Figure 3.16 Typical thermogram from thermogravimetric analysis

3.8.2 Differential Scanning Calorimetry (DSC)

Thermal properties (Section 3.8.2.2) of WPP, blends, rubber chemicals, and gels from solvent extractions were determined using a DSC 2010 Thermal Analyser manufactured by TA instruments, USA. This thermal analyzer possessed a computer controlled system and the operating parameters were programmed with a "Thermal Solutions" software package. A weight of 10.0 to 15.0 mg was placed on an aluminium pan and then placed in the specimen cell. The test was performed with nitrogen purge gas at a flow rate of 35 ml/min. Testing conditions were varied according to the thermal property to be

determined and with the material tested. Specific testing conditions used for different materials are given in the following section.

3.8.2.1 Testing Conditions

Thermal properties and degrees of crystallinity of the WPP and the blends prepared were determined. Accordingly, specimens were heated at a rate of 10 ^{0}C/min from 20 ^{0}C to 200 ^{0}C followed by isothermal heating for 3 minutes at 200 ^{0}C. This isothermal heating was performed to ensure a complete melting of crystals. The specimens were then cooled to 20 ^{0}C, at a rate of 10 ^{0}C/min. Isothermal cooling was carried out for 3 minute at 20 ^{0}C. In order to eliminate the thermal history, the cycle was repeated under the same conditions.

For the determination of glass transition temperature of the WPP, the specimen was heated from -40 ^{0}C to 25 ^{0}C at a heating rate of 5 ^{0}C/min.

In order to investigate the presence of WPP and other added chemicals in the gel and sol of boiled xylene extracts, the specimens were heated from 30 ^{0}C to 250 ^{0}C at a heating rate of 10 ^{0}C/min. The same testing conditions were maintained when characterizing the Delink components and their mixes using melting endotherms. Components of the two compatibilizing systems were also characterized at the same processing conditions.

The safe processing conditions for the Delink process were investigated using DSC thermograms taken under isothermal conditions. Isothermal temperatures were varied from 40 ^{0}C to 80 ^{0}C in 10 ^{0}C intervals, and heating continued up to 20 minutes. The DGTR used for the test was prepared manually using a mortar and pestle. Mixing was carried out until the mix became uniformly dispersed.

3.8.2.2 Determination of Thermal Properties

Heat flow versus temperature and time data was recorded on a thermogram (Figure 3.17 and Figure 3.18). The thermal properties such as melting temperature (T_m), peak

crystallization temperature (T_p), onset crystallization temperature (T_{co}), heat of fusion (ΔH_f) and heat of crystallization (ΔH_c) were determined with universal analysis software. T_{co} is the temperature where the thermogram initially departs from the baseline on the high temperature side of the thermogram. ΔH_f and ΔH_c are the areas enclosed by the base line and the endotherm and exotherm peaks. The readings of T_p and ΔH_c were taken during the first thermal cycle and those of T_m and ΔH_f were taken during the second heating cycle. Supper cooling (ΔT), the peak height (H_p), the width of half-height of the crystallization exotherm (ΔW) and the slope of the high temperature side of the thermogram (S_i) for each blend were calculated. ΔT is the temperature difference between the melting temperature (T_m) and the T_{co}. ΔW, after normalization of the peak to constant mass of WPP component in the blend, characterizes the size distribution of the crystal present in the blend. S_i is a measure of rate of nucleation. Relative crystallinity, X_t, against crystallization time, t_c, curves for the WPP was plotted. Half-time of crystallization, $t_{1/2}$, was calculated using this curve (Figure 3.19).

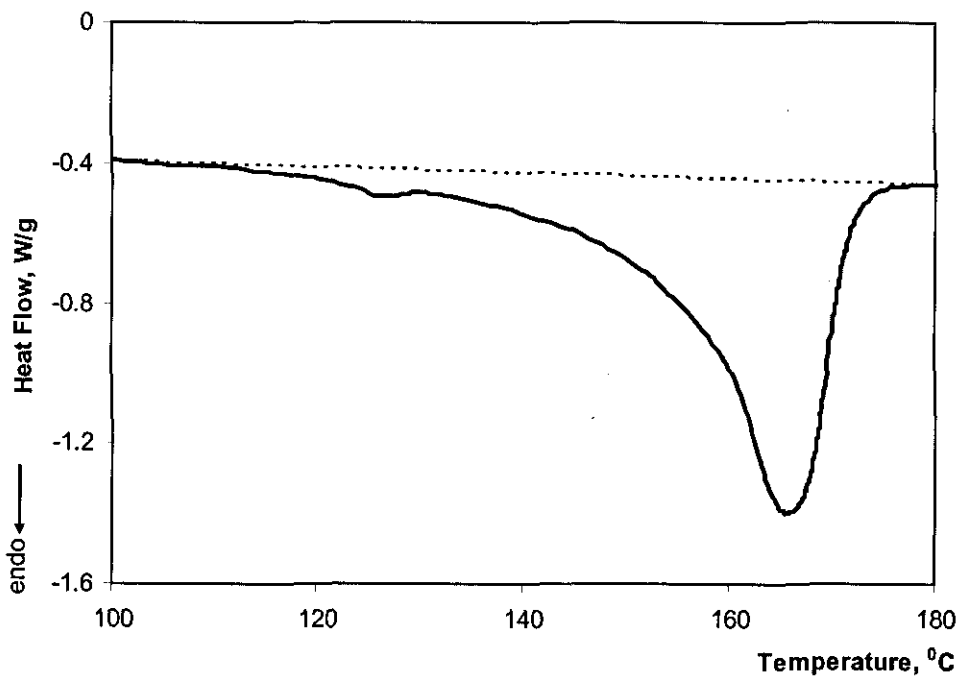

Figure 3.17 Section of typical heating curve from DSC thermogram

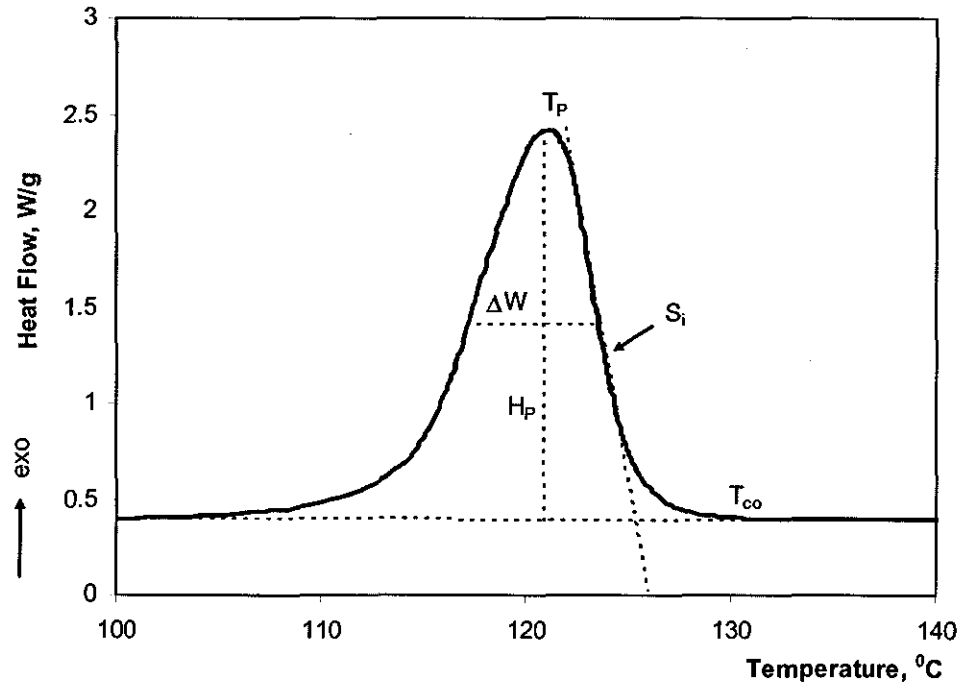

Figure 3.18 Section of typical cooling curve from DSC thermogram

The relative crystallinity as a function of temperature is defined as follows [259],

$$\text{Relative Crystallinity at time t}, X_t = \frac{\int_{T_0}^{T_{co}} (dH_c/dT_c)dT_c}{\int_{T_0}^{T_\infty} (dH_c/dT_c)dT_c} \qquad \text{Equation 3.12}$$

Where, T_∞ is the end crystallization temperature

T_c is the crystallization temperature

dH_c/dT is the heat flow at temperature T_c

Crystallization time is given by the following equation [259].

$$\text{Crystallization time}, t_c = \frac{T_{co} - T_c}{D} \qquad \text{Equation 3.13}$$

Where, D is the cooling rate

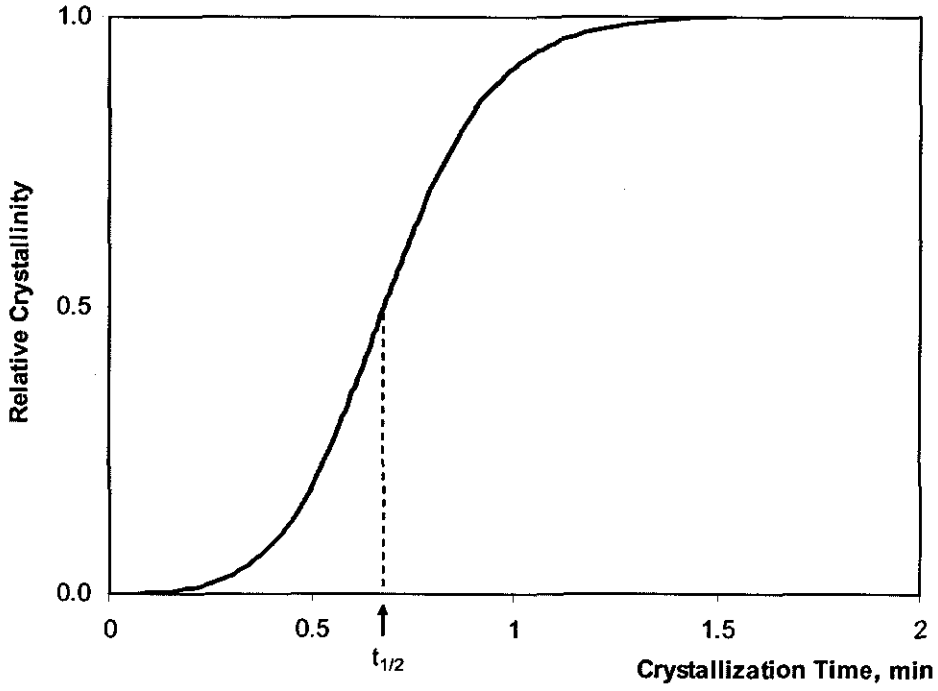

Figure 3.19 Relative crystallinity vs. Crystallization time curve

The degree of crystallinity of a blend was calculated using the following equation [260].

$$\% \text{ Crystallinity of the blend} = \frac{\Delta H_f}{(\Delta H_f)_c} \times 100 \qquad \text{Equation 3.14}$$

Where, ΔH_f is the enthalpy of fusion of the blend

$(\Delta H_f)_c$ is the enthalpy of fusion of pure crystalline polypropylene and is taken from literature [213] as 209 J/g.

The percentage degree of crystallinity of WPP in the blend was calculated using the following equation.

$$\% \text{ Crystanllinity of WPP in the blend} = \frac{\% \text{ Crystallinity of the blend}}{\text{Weight fraction of WPP in the blend}}$$

Equation 3.15

The glass transition temperature (T_g) of the WPP was determined from the DSC. The specimen was heated at a heating rate of 3 ^{0}C/min, from -10 ^{0}C to 15 ^{0}C. This test was

also carried out under a nitrogen atmosphere. The transition observed under the DSC thermogram (Figure 3.20) is small and overlapped with the transition due to moisture present in the specimen. The glass transition region was defined by the difference of onset and end glass transition temperatures (T_{ge}-T_{go}). The mid temperature of the transition region was considered as the T_g of the WPP [261]. T_{go}, the extrapolated onset glass transition was located as the point where the tangent to the transition intersects the slope at the lower temperature side. T_{ge}, the end of the glass transition, was located as the point where the extended slope at the higher temperature side intersects the obtained DSC curve.

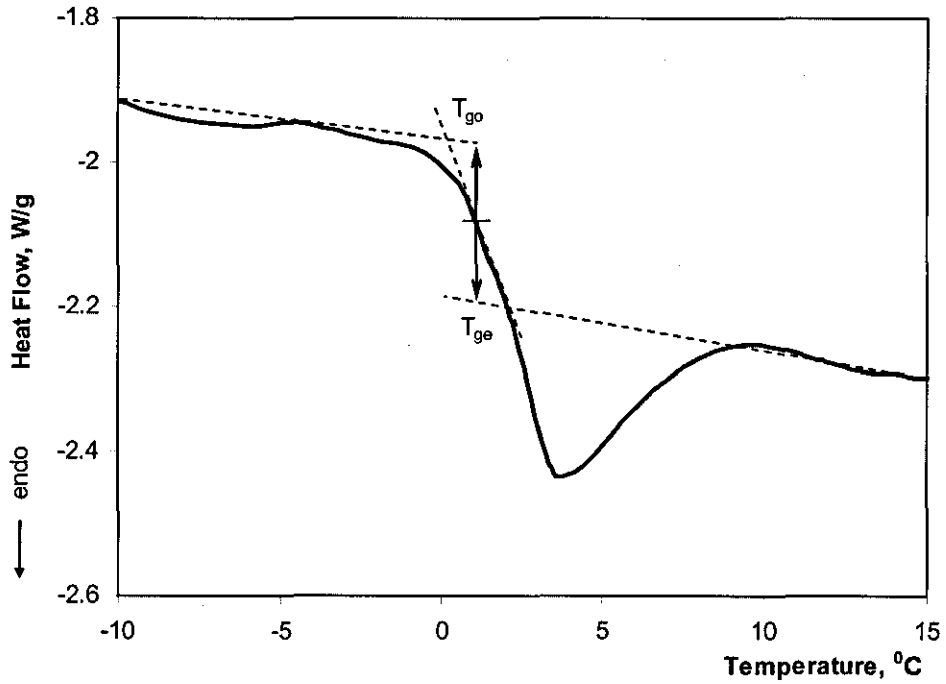

Figure 3.20 Glass transition region of a heating curve of a DSC thermogram

3.8.3 Dynamic Mechanical Analysis (DMA)

The dynamic mechanical properties of WPP and selected blends were investigated by subjecting specimens to forced dynamic bending using a DMA device manufactured by TA Instruments, UK. Rectangular specimens, with dimensions, 13mm×60mm×2mm were cut from compression moulded sheets. The width and thickness of the specimens were varied slightly in all specimens. The specimens were clamped using a dual cantilever

system and were bent at a constant frequency of 10 Hz and strain amplitude of 64 microns. The testing temperature ranged from -100 ^{0}C to 100 ^{0}C with a selected heating rate of 3 ^{0}C/min. A typical DMA trace is given in Figure 3.21. The temperatures corresponding to the peaks in the bending tan delta versus temperature plot were taken as the glass transition temperatures (T_g) of the two phases.

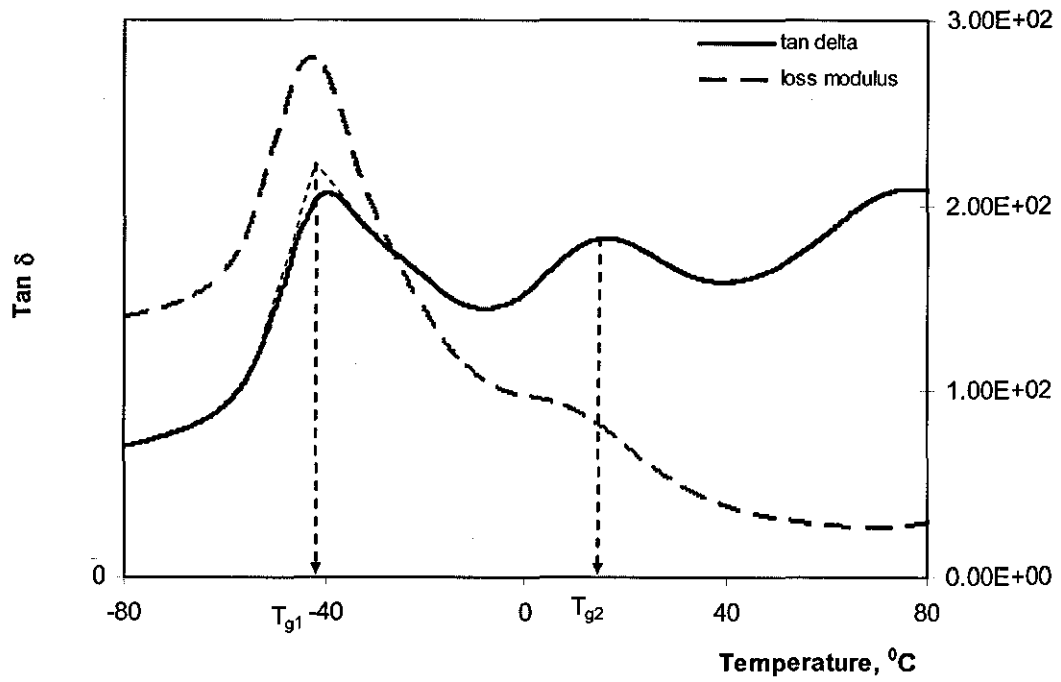

Figure 3.21 Typical DMA trace, showing two glass transitions for two phases

3.9 Sol/Gel Analysis

3.9.1 Swelling Characteristics

Swelling indices of the WPP, GTR vulcanizates, and vulcanizates of Delink treated GTR, and vulcanizates of different blends were obtained using an equilibrium swelling method. Toluene was used as the solvent. Specimens, with dimensions, 15mm×15mm×2 mm were cut from compression moulded sheets and weighed to determine their initial weights in a range from 0.6 to 0.7 g. The specimens were immersed in the solvent at an ambient temperature of 25 ^{0}C for 72 hours. For the vulcanizates of the Delink treated rubber, the

specimens were immersed at 40 ^{0}C for 7days. A constant volume of 100 ml of the solvent was used. After removal from the solvent, the specimens were wiped with tissue to remove any excess solvent from the surface. The specimens were then re-weighed to determine their swollen weight. The swollen specimens were dried at 70 ^{0}C for 2 hours using a vacuum oven and weighed again to obtain the final dry weight. Swelling indices were calculated according to the Equation 3.16.

$$\text{Swelling Index} = \frac{W_2 - W_3}{W_3} \qquad \text{Equation 3.16}$$

Where W_2 is the swollen weight of the specimen

W_3 is the final dry weight of the specimen

3.9.2 Solvent Extraction

Solvent extractions of the WPP, the GTR and their vulcanizates and also the vulcanizates of the blends were determined by using toluene, acetone and xylene as solvents. Solvent extraction residues of the above vulcanizates were determined by toluene extraction according to Equation 3.17.

$$\%\text{Solvent Extraction Residue} = \frac{W_3}{W_1} \times 100 \qquad \text{Equation 3.17}$$

Where W_1 is the initial weight of the specimen

W_3 is the final dry weight of the specimen

The %residue of the GTR and Delink treated GTR, which were available in powder form, was also determined using toluene as the solvent, but the specimens were first placed in a special specimen holder prior to immersion in the solvent. The specimen holder was 40mm×40mm in size and made from 100 micron wire mesh. Sample weight and the testing conditions were maintained as mentioned above. The residues from the specimens were kept in the holders, dried and were weighed. The resultant residue contained only

crosslinked rubber and hence %solvent extraction residue in this case was labeled as %gel content.

%Gel content per weight of GTR in the Delink treated GTR was determined according to Equation 3.18.

$$\%\text{Gel Content in the rubber} = \frac{W_3}{W_1} \times (100 + w_{De}) \qquad \text{Equation 3.18}$$

Where w_{De} is the Delink added to the GTR (3, 6 and 9 phr)

It was found that the SP resin completely dissolved in acetone at 30 ^{0}C. The uncombined SP resin present in the modified WPP or in the modified PP will be extracted to the sol phase. Hence, to determine the degree of WPP or PP modification with the resin compatibilizing system, modified WPP or modified PP specimens were immersed in acetone for 7 days at 30 ^{0}C. For this extraction, small pieces, approximately 5mm×5mm, were used. These pieces were cut from the 2mm thick moulded sheets. A sample weight of 0.3 to 0.4 g. was maintained. A constant volume of 100 ml acetone was used, and was replaced by fresh toluene after 3 days. The specimens immersed in toluene were kept inside an oven at 30 ^{0}C. The resultant WPP or PP mass was dried at 70 ^{0}C for 2 hours in a vacuum oven. This extraction test was repeated using xylene as the solvent. In this case, drying was carried out at 100 ^{0}C for 2 hours. The dried pieces were stored for FTIR studies

In order to investigate the crosslinking capability of GTR by the resin compatibilizing system, vulcanizates of the resin modified GTR was immersed in acetone while keeping it in a specimen holder. A sample weight in the range 0.6 to 0.7 g. was used. The same extraction and drying conditions, which were used for acetone extraction for modified WPP, were maintaind. The %gel content was calculated according to Equation 3.17.

3.9.3 Boiled Xylene Extraction

Xylene insoluble fraction and degree of crosslinking of WPP, GTR and selected blends were determined by boiled xylene extraction according to BS ISO 10147:2004.

A specimen having a weight of 0.6 to 0.7 g. was placed inside a specimen holder, which was used for solvent extraction of rubber powders. This specimen was 15mm x10mm in size and was cut from a 2 mm thick vulcanized sheet. Antioxidant 2246 at a concentration of 1% was added to xylene. The specimen with the holder was immersed in 150 ml of boiled xylene and was extracted for 8 hrs inside a fume hood. The extracted specimen was dried in an oven at 150 ^{0}C for 3 hours. The xylene insoluble fraction and the degree of crosslinking are defined by Equation 3.19 and Equation 3.20, respectively. These two parameters are used to describe the character of the crosslinking reaction [161, 162].

$$\text{Xylene Insoluble Fraction, XIF}\,(\%) = \frac{\text{Residual Weight of Specimen after Extraction}}{\text{Original Weight of Specimen}} \times 100$$

Equation 3.19

$$\text{Degree of Crosslinking}\,(\%) = \frac{\text{Xylene Insoluble Fraction of the Blend}}{\text{Weight of the Elastomer in the Blend}} \times 100$$

Equation 3.20

The WPP and the GTR also created residual masses during boiled xylene extraction (Section 6.1.12). Hence the degree of crosslinking was corrected for the pure rubber and polypropylene present in the blend and the degree of crosslinking of the blend was calculated according to Equation 3.21.

$$\text{Degree of Crosslinking of the Blend}\,(\%) = \frac{XIF_B - (XIF_{GTR} \times W_{GTR} + XIF_{WPP} \times W_{WPP})}{\left(1 - \frac{XIF_{GTR}}{100}\right) \times W_{GTR}}$$

Equation 3.21

Where, XIF_B - Xylene-insoluble fraction of the blend, %

XIF_{GTR}- Xylene-insoluble fraction of the ground tyre rubber, %

XIF_{WPP}- Xylene-insoluble fraction of the waste polypropylene, %

W_{GTR} - Weight fraction of ground tyre rubber present in the blend

W_{WPP} - Weight fraction of waste polypropylene present in the blend

The xylene used for this part of the study was of industrial grade and hence it was purified before performing extractions. The xylene was double distilled using a steam distillation apparatus and the distillate, in the boiling range 138 to 145 ^{0}C, was collected and used for the experiments. The boiling points of the three isomers of xylene; para-, meta- and ortho- xylene are 138, 139 and 144 ^{0}C respectively [262].

3.10 Fourier Transformation Infrared Spectroscopy (FTIR)

FTIR spectra of WPP, GTR and selected blends were recorded in the range 4000-500 cm^{-1}, using a Mattson 3000 FTIR spectrophotometer. The spectra were obtained in the transmission mode, at a resolution of 4 cm^{-1}. The peaks obtained on the recorded spectra were determined using Winfirst software.

Thin films of WPP, the selected blends, the residues from acetone and xylene extractions of modified WPP and PP were prepared using an electrically heated hydraulic press. A small piece of material was pressed between two plates at 200 ^{0}C temperature. It was difficult to control the thickness by this method, but it is rapid and adequate for qualitative analysis. A 1cm^2 piece from the thinnest part of the film was cut and was placed inside the spectrophotometer.

The FTIR spectra of GTR, HVA-2, SP1045H resin, MBTS, DTBPIB and some gels from xylene extracts, which were in powder form, were obtained using a potassium bromide (KBr) pellet. About 0.01 g of powdery material was mixed with 1 g of finely ground KBr. This powder was placed in a special die and was pressed at 100 MPa. This thin pellet was removed from the die and attached, using a special frame, inside the spectrophotometer.

Some gels of xylene extracts were not in the powder form and were obtained as single masses. The thin films made out of these gels showed tiny cracks all over the specimen and hence it was not possible to obtain clear spectrum. The spectra of such gels were obtained using the pyrolysis technique. In order to compare the results, gels of selected xylene extracts and GTR were also obtained using this technique. The liquid/gel obtained

by pyrolysis was pressed between two glass plates and was placed inside the spectrophotometer.

The bottom layers of the sols of the boiled xylene extracts were first separated using a separation funnel and then were subjected to centrifuging for further separation. The centrifuging was carried out for 5 minutes at 10000 rpm speed. The spectra of sols of selected xylene extracts were also obtained by pressing liquids/gels between the same plates used in the pyrolysis technique.

Moulded sheets prepared from Delink treated GTR, especially at 200 ^{0}C, showed surface blooming. The bloomed components were analysed using attenuated total reflection (ATR) technique.

3.11 Morphology

3.11.1 Optical Microscopy

The morphology of films of selected blends was studied using a Reichert MEF-3 microscope, equipped with a Kohler illumination system. This microscope is for reflected light work and is of the inverted type. The films were microtome using glass knives by holding the blend samples on the microtome stage using ice. The microtome films were mounted in the usual way, between slide and cover slip, with silicone oil used as a liquid to hold the sections flat. The thickness of the microtome films was 10 μm. These films were observed under bright field illumination and the micrographs were obtained using ×5 and ×10 objective lens magnifications. The images were captured use of a digital camera.

3.11.2 Scanning Electron Microscopy (SEM)

Studies of the morphology of the tensile fracture surfaces of WPP and selected blends were carried out using two scanning electron microscopes. Images at lower

magnifications (×15 and above) were recorded using a Leo Cambridge S 360 scanning electron microscope. Images with higher magnifications (×150 and above) were recorded using a Leo 1530VP field emission gun scanning electron microscope (FEGSEM). The fractured ends of the specimens were cut and mounted on aluminium stubs using silver in methyl isobutyl ketone. These specimens were sputter coated with a thin layer of gold to avoid electrostatic charging during examination.

3.12 Statistical Analysis

All the above tests were repeated to ensure repeatability and reproducibility. The WPP, GTR, the blends, Delink GTR, modified WPP, and modified PP were processed at least two times to determine flow curves and processing characteristics. A minimum of two sheets were moulded and three to four specimens were tested from each moulded sheet, thus a minimum of six specimens were used in determining all four mechanical properties. DSC thermograms were obtained with three specimens, while FTIR spectra were obtained with two specimens, and TGA and DMA thermograms were obtained with a single specimen. A minimum of three specimens were used in swelling experiments, solvent extractions and in boiled xylene extraction.

Arithmetic mean values were reported as the average values for the properties measured and/or calculated. Standard deviations were calculated and used to draw error bars in all graphs, or to give values in all tables, in parenthesis.

The properties measured only twice are presented in duplicate in graphs, or in tables in parenthesis. When the duplicate results are given in parenthesis in tables, it is deliberately stated as an end note at the bottom of the table.

Chapter 4 Results and Discussion - Part I

Raw Material Characterization

The main raw materials used in the present study were of waste polypropylene (WPP) and of ground tyre rubber (GTR). Physical appearance, chemical composition and thermal properties of the two materials were investigated by optical microscopy, Fourier transformation infrared spectroscopy (FTIR), differential scanning calorimetry (DSC), dynamic mechanical analysis (DMA) and by thermogravimetric analysis (TGA).

4.1 Waste Polypropylene (WPP)

4.1.1 Physical Appearance

Waste polypropylene is a mix of several products of black and white in colour. It is available as granules of different sizes, as shown in Figure 4.1.

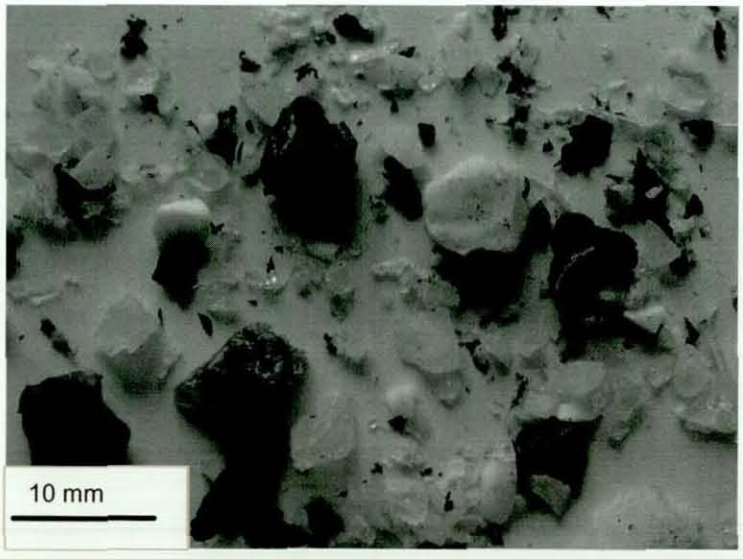

Figure 4.1 Waste polypropylene granules

The optical micrograph of a film of WPP (Figure 4.2) showed tiny black spots, which are additives like carbon black and pigments or impurities present in the WPP. These additives or impurities may affect the performance of the WPP.

Figure 4.2 Optical micrograph of WPP film (×10)

4.1.2 Melt Flow Analysis

The melt flow index of the WPP was obtained as 12.5 g/10 min at 230 ^{0}C at 2.16 kg load. The melt viscosity was obtained as 1720 Pa/sec, and the melt density was 0.7763 g/cm^{3}. The MFI of polypropylene (PP) lies in the range 0.5 to 136 g/10 min [208]. The injection moulded grade of commercial PP has a MFI in a range of 6 to 55 g/10 min, while blow moulded and extruded grades have 1.8 to 12, and 1.8 to 3 g/10 min, respectively [263]. The results obtained confirmed that the WPP used in this study is an injection moulded grade. The MFI of PP can linearly increase with the number of reprocessing cycles due to chain scission [215] or initially remain constant during the initial reprocessing cycles, and thereafter increase considerably [264]. Thus the variations in MFI will finally depend on the reprocessing conditions. MFI will decrease with chain branching and crosslinking, and this is common with polyethylene (PE) [73, 133]. However, these two reactions will not take place with PP and hence no reduction of MFI for WPP was reported for these two reasons.

4.1.3 Chemical Composition

4.1.3.1 Fourier Transformation Infrared Spectroscopy (FTIR)

Figure 4.3 displays the FTIR spectrum of the WPP film and the peak assignments are given in Table 4.1. In this spectrum, hydrocarbon compounds are represented by a strong band of multiple peaks near 2951 cm^{-1} and at 1458 cm^{-1}. Such bands correspond to different vibrational modes of the methylene and methyl groups. The characteristic band corresponding to the vibrational movement of C–H from the methyl group, which appears at 1375 cm^{-1}, can also be seen. Additionally, the spectrum display many sharp peaks of medium intensity in the region between 1200 and 800 cm^{-1}. They are assigned to C-C stretching vibrations. These peaks are the major characteristic peaks of a PP spectrum [265].

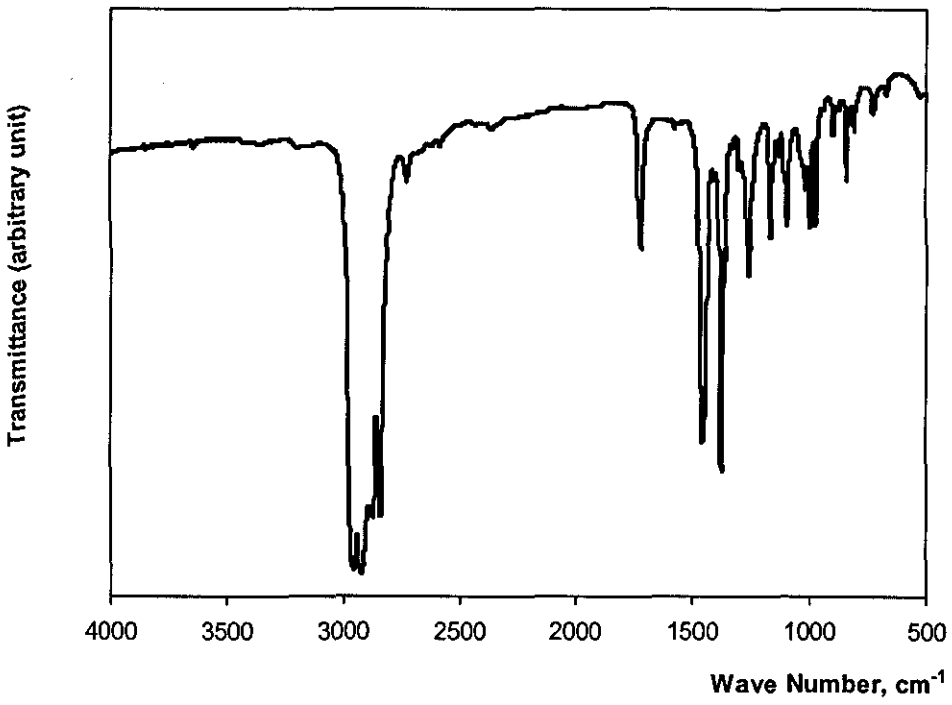

Figure 4.3 FTIR Spectrum of WPP

Table 4.1 Peak assignments in FTIR spectrum of WPP [266]

IR band , cm^{-1}	Assignment
Multiple peaks between 2980-2850	C-H asymmetric stretching of methyl group
	C-H asymmetric stretching of methylene group
	C-H symmetric stretching of methyl group
	C-H symmetric stretching of methylene group
1723	C=O stretching vibrations of carbonyl group
1458	C-H bending (out-of-phase) of methyl group
	C-H scissoring of methylene group
1375	C-H bending (in-phase) of methyl group
1263	C-H twisting vibration of methylene group
1167	C-H wagging vibration of methylene group
Multiple peaks between 1200 -800	C-C stretching vibration
972	=C-H out-of-plane-bending vibration
840	$=CH_2$ wagging vibration
728	C-H rocking vibration of methylene group

In addition, a medium intensity peak near 1723 cm^{-1} is noticeable. This peak is attributed to the C=O stretching in the carbonyl group, which is generally not present in a virgin PP spectrum [265]. However, it is noticeable with commercial PP [267] and may be due to the presence of some additives, like nucleating agents or antioxidants. This peak is also reported as present in the FTIR spectrum of degraded PP [267, 268], as carbonyl groups are formed during the oxidative degradation process. With the formation of carbonyl groups, a certain level of unsaturation is also formed during the oxidative degradation process and hence another prominent peak is shown in the spectrum in conjunction with the C=O stretching peak [267]. The latter peak is apparent in the range 1680-1640 cm^{-1} and is attributed to the C=C stretching in the alkenes. However, the latter peak does not appear in the WPP spectrum (Figure 4.3). The latter peak is also reported as not present in degraded PP when exposed to gamma radiation [265]. Although this prominent peak does not appear in the WPP spectrum, two weak peaks are present at 840 and 972 cm^{-1}, which

correspond to the C-H wagging and bending vibrations of C-H in the alkenes. This suggests the presence of some unsaturation in the WPP.

Moreover, a weak peak at 728 cm^{-1} is observable. This peak corresponds to CH_2 rocking deformation and it is commonly observed with PE and not with PP [213, 269]. There appears to be a certain level of PE present in the WPP. The presence of PE in the WPP was confirmed by the DSC thermogram obtained (Section 4.1.4.1).

4.1.3.2 Nuclear Magnetic Resonance Spectroscopy (NMR)

In the NMR method, the configuration of each segment of the polymer chain can be identified. Hence the method can be used to distinguish even similar polymers. All types of PP, isotactic, syndiotactic, atactic and stereo block PP, show three main chemical shifts from 1-2-dicholobenzene-d_4, in the range δ = 49.3 to 23.2 ppm in the ^{13}C NMR spectra. These chemical shifts will vary with the type PP, but will lie within that specified range. Isotactic-PP and syndiotactic-PP can be distinguished [213]. PE, either linear, branched, low density or high density, shows more than three chemical shifts from 1-2-dicholobenzene-d_4, and they are in the range δ = 36 to 10.9 ppm [270]. Hence, the ^{13}C NMR method can be used to detect PE present in PP. The chemical shifts appearing in the ^{1}H NMR spectra of PE and PP are overlapping, and hence the ^{1}H NMR method cannot be used to distinguish PE from PP.

Isotactic PP cannot be dissolved in any deuterated solvents at room temperature, whereas atactic PP solutions are easily formed with various solvents. As a consequence, dissolutions are usually conducted at high temperatures (130 ^{0}C to 170 ^{0}C) with halogenated aromatic compounds (mono-, di- or trichlorobenzene) or decaline. As PP can easily undergo thermo-oxidative degradation at high temperatures, the dissolution temperature is limited to between 140 ^{0}C and 145 ^{0}C, and the solvent must contain antioxidants. Further, at least 30 hours are necessary to obtain a stable, aggregate-free solution, at 145 ^{0}C [213]. In the mean time, the spectrum has to be recorded at a high temperature to ensure high resolution. Because of these reasons, liquid state it was not

possible to carry out a ^{13}C NMR test with the WPP. The solid state NMR test also failed due to difficulty in producing WPP in power form.

4.1.4 Thermal Properties

4.1.4.1 Melting and Re-crystallization Temperatures

DSC thermograms of the WPP obtained at first and second heating cycles and cooling cycle are shown in Figure 4.4 and Figure 4.5 respectively. These thermograms show the thermal behaviour of the WPP in a temperature range 80 ^{0}C to 180 ^{0}C. Figure 4.4 exhibits a broad melting endotherm, a common characteristic for thermoplastics [271]. The melting point of semi-crystalline plastic is strongly affected by distributions in morphology, its impurity concentration and distribution, its processing history, as well as the residual strain and orientation. Further, this figure exhibits a major endothermic peak around 166 ^{0}C and a second small endothermic peak around 126 ^{0}C. This feature was observed during both first and second heating cycles. The first major peak is associated with the melting of WPP. The melting point of isotactic-PP is reported as 166 ^{0}C [107]. The temperature at which the second minor peak occurs is similar to the melting point of PE [120, 272]. The FTIR spectrum of WPP indicated the presence of PE (Figure 4.3). Hence this DSC thermogram confirms the presence of PE in the WPP. Further, the amount of PE present appears to be very little and may be presence as an impurity.

Figure 4.5 shows a sharp exothermic peak around 120 ^{0}C. This is associated with the re-crystallization of WPP. The onset crystallization temperature is shown as 130 ^{0}C and the end crystallization temperature is shown as 105 ^{0}C. PE crystallizes in the temperature range 115 ^{0}C – 120 ^{0}C [272]. The re-crystallization peak of PE overlaps that of WPP. Hence, this figure does not show a separate exothermic peak for re-crystallization of PE.

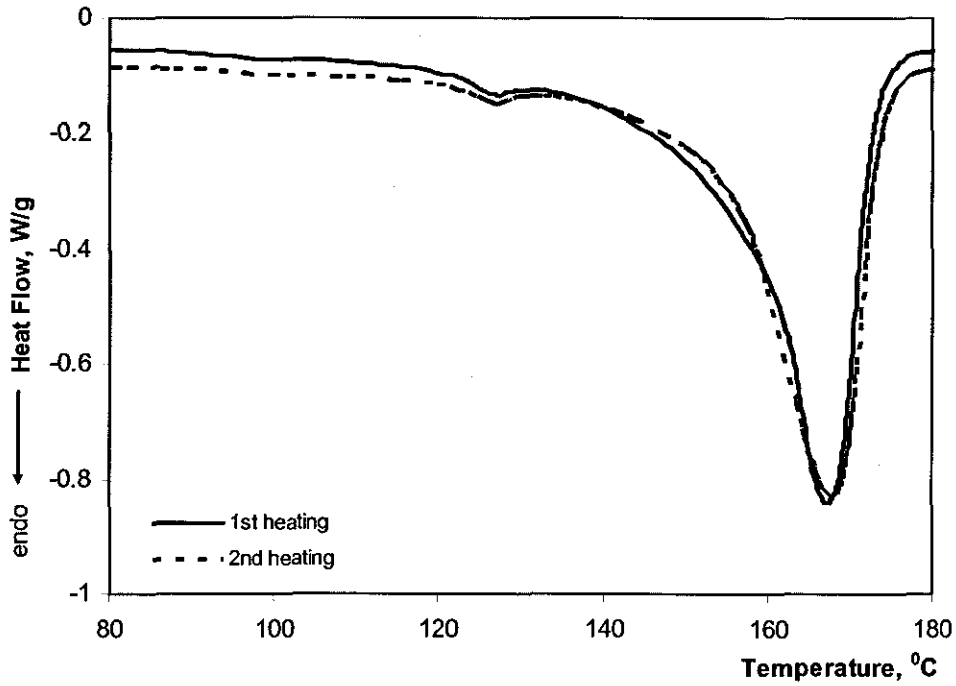

Figure 4.4 Section of the first and second heating cycles of WPP

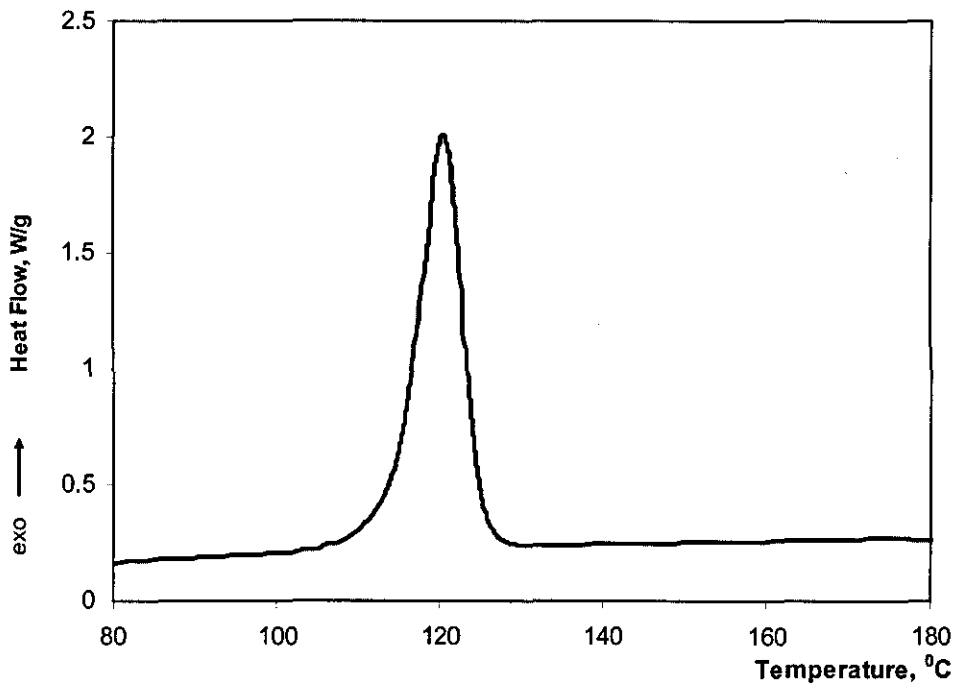

Figure 4.5 Cooling cycle of WPP

4.1.4.2 Glass Transition Temperature (T_g)

The glass transition temperature of isotactic-PP is difficult to detect by DSC as the concentration of amorphous PP is small [273]. The atactic-PP exhibits its T_g around –20 ^{0}C in DSC thermograms. However, the DSC thermogram for the WPP (Figure 4.6) shows a glass transition in a temperature range 0 ^{0}C to 4 ^{0}C and hence the T_g of the WPP was determined (Section 3.8.2.2) as 1 ^{0}C. It has been reported [107] that the T_g of virgin PP recorded in DSC thermograms is around -10 to 5 ^{0}C. The T_g of virgin PP will vary with the fraction of the isotactic-PP present. The T_g of commercially available PP and also WPP could be further varied with the influence of additives, such as stabilizers, carbon black and other pigments and processing aids, etc.

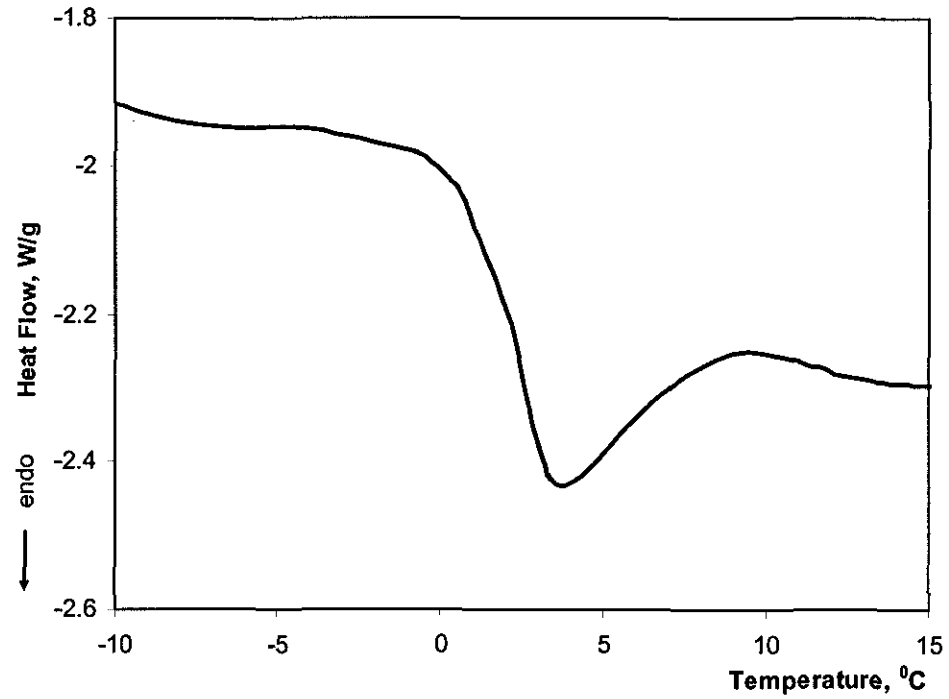

Figure 4.6 Section of the first heating cycle of WPP

Figure 4.7 shows a typical tan δ curve obtained from the DMA for the WPP. The T_g determined by the DMA (Section 3.8.3) was 15 ^{0}C, and was different to that determined by the DSC. This T_g difference for the same WPP explains that its dependence on the measuring technique.

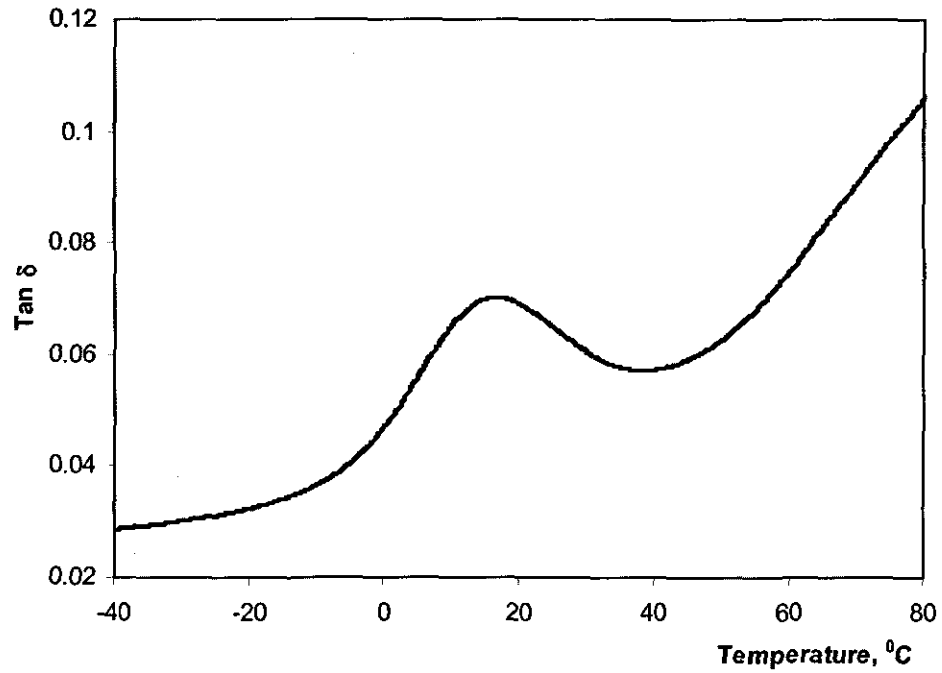

Figure 4.7 Tan δ curve for WPP, showing its glass transition

4.1.4.3 Degradation Temperature

Figure 4.8 shows the thermogravimetric analysis and differential thermogravimetric analysis (DTGA) thermograms for the WPP. Degradation of the WPP in air starts at 230 ^{0}C and completes at 445 ^{0}C having a residue of 3 wt%. The degradation of virgin PP is reported as occurring around 210 ^{0}C in air and around 300 ^{0}C in nitrogen [258]. In a separate study [214], it was shown that the degradation of recycled PP in nitrogen began at a lower temperature (300 ^{0}C) than virgin PP (305 ^{0}C). However, no conclusions were drawn on the thermal stability of the recycled PP compared to virgin PP as the temperature difference was not high enough.

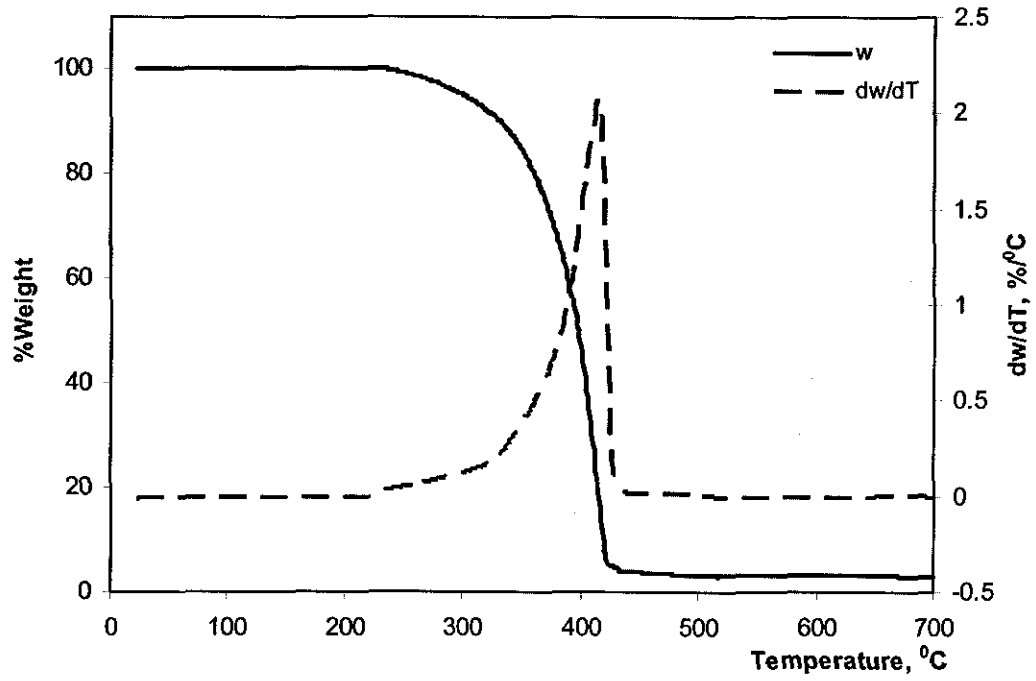

Figure 4.8 TGA thermogram and DTGA curve for WPP

4.2 Ground Tyre Rubber (GTR)

4.2.1 Physical Appearance

The GTR particles were spongy and free flowing. Those particles observed under the optical microscope exhibited highly convoluted surfaces (Figure 4.9) and hence it is confirmed that the GTR used in this study was ambient ground. Cryogenically ground particles are smooth and angular [88, 129].

The SEM image of a GTR particle obtained at a higher magnification (Figure 4.10) clearly exhibited fine particles dispersed in the GTR. These particles can be mainly carbon black filler, and other additives, present in the GTR. Presence of these particles on SEM images will facilitate to identify the GTR phase separated from the WPP and hence to understand the morphology of a GTR/WPP blend.

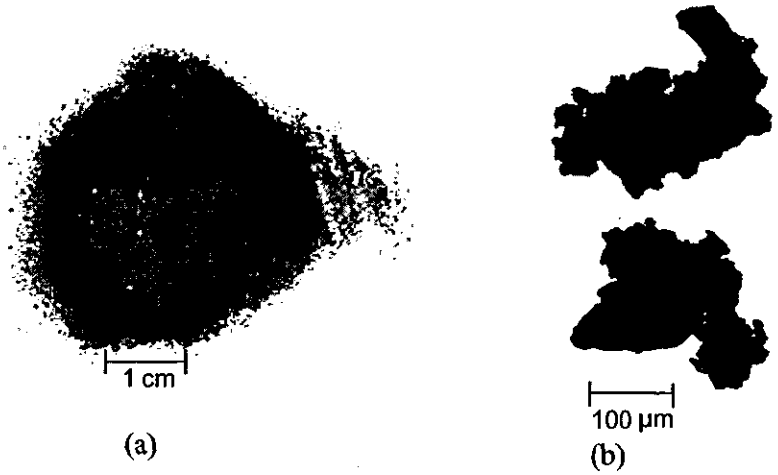

Figure 4.9 (a) GTR (b) GTR particles under optical microscope (×10)

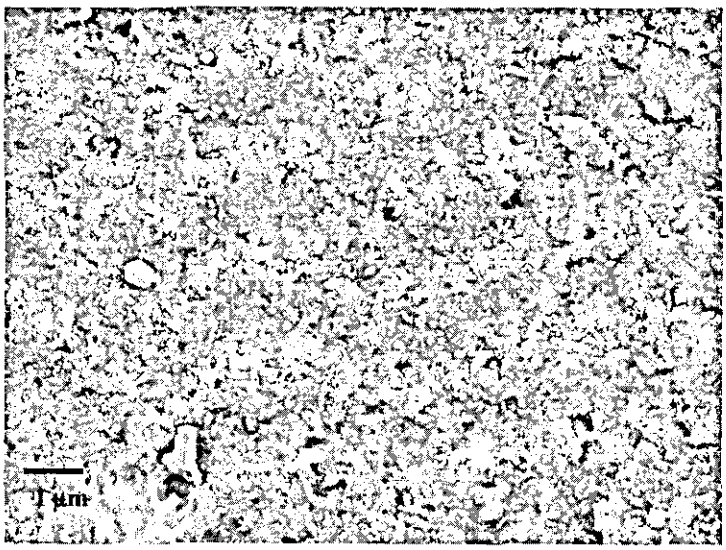

Figure 4.10 Scanning electron micrograph of a GTR particle at a higher magnification

4.2.2 Chemical Composition

4.2.2.1 Fourier Transformation Infrared Spectroscopy (FTIR)

Figure 4.11 illustrates the FTIR spectrum acquired with GTR using two methods, namely KBr pellet and pyrolysis. The FTIR spectra acquired using KBr pellet did not show a proper base line due to the large GTR particles used and hence due to poor dispersivity in

KBr. The spectra acquired using both methods showed similar major peaks assignments, which are given in Table 4.2.

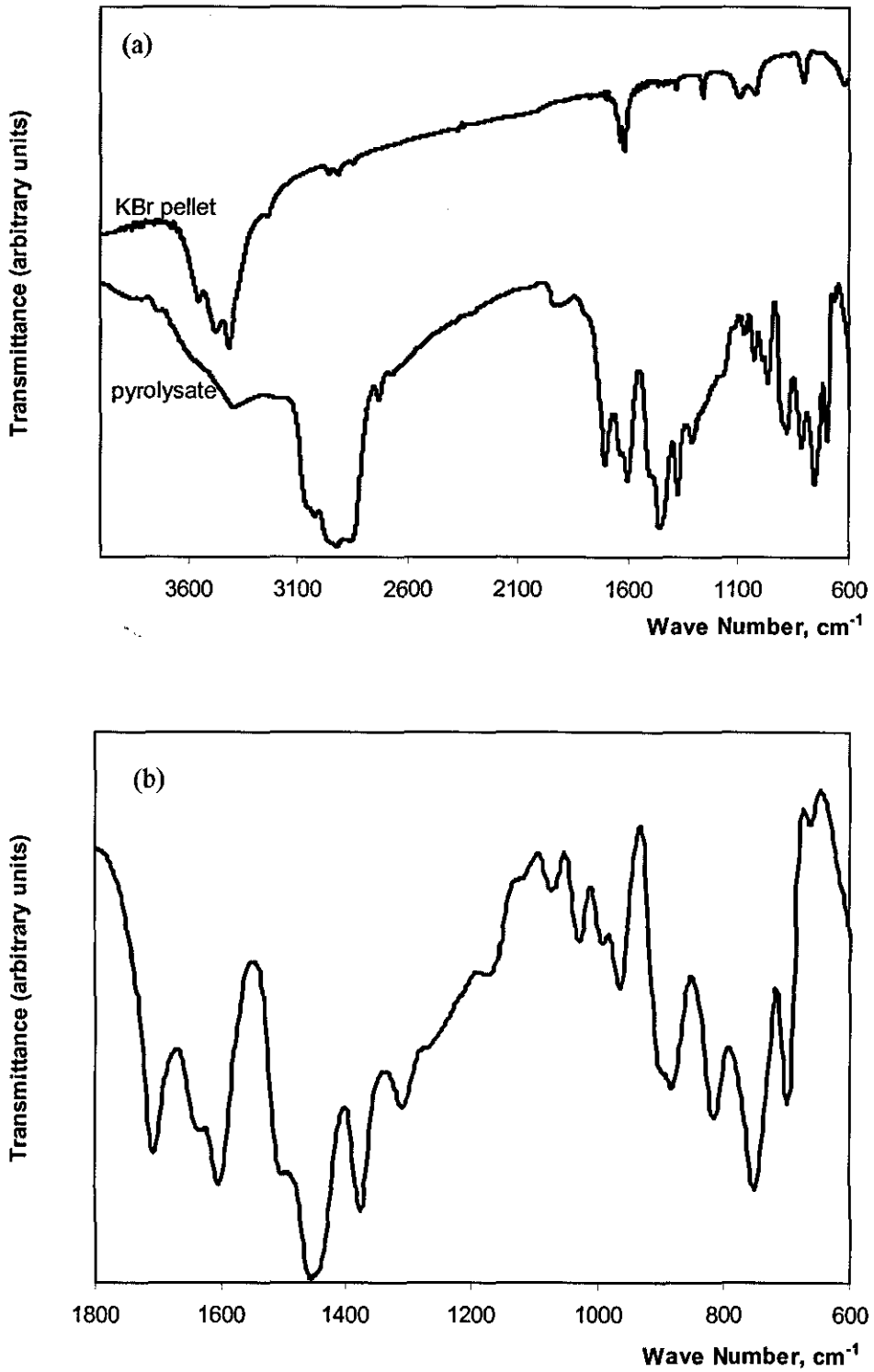

Figure 4.11 FTIR spectrum of GTR (a) full spectrum (b) spectral region of pyrolysate

Table 4.2 Peak assignments in FTIR spectrum of GTR [266, 274]

IR band , cm^{-1}	Assignment
3450	O-H stretching in phenolic groups
2930	C-H asymmetric stretching of methylene group
2870	C-H symmetric stretching of methylene group
1640	C=C symmetric stretching vibration
1500 and 1600	C=C stretching vibration of aromatic ring in styrene
1460	C-H scissoring of methylene group
1380	C-C stretching vibration of $C-CH_3$ group
990, 970, 890	C-H bending vibrations in alkenes, (of groups
and 815	$-CH=CH-$, $-CH=CH_2$, $>C=CH_2$, $-CH=C<$)
700 and 760	=C-H and C=C bending vibrations of aromatic groups in styrene

The peak around 3450 cm^{-1} corresponds to the O-H stretching in the phenolic hydroxyl and carboxylic groups present on the surface of carbon black. The peaks at 2950 cm^{-1} and 2870 cm^{-1} represent C-H asymmetric and symmetric stretching of methylene groups respectively. The peak at 1640 cm^{-1}, which is due to C=C in the alkenes, confirms the presence of unsaturation sites of alkene units. These units can be isoprene units and/or butadiene units. The peak 1460 cm^{-1} represents C-H scissoring of methylene group. The peaks 970-800 cm^{-1} represents C-H bending vibrations of $CH=CH-$, $-CH=CH_2$, $>C=CH_2$, $-CH=C<$ groups in alkenes. These peak assignments suggested that the GTR consists of unsaturated rubbers and carbon black.

In the case of heavily filled rubbers like GTR, it is necessary to characterize the blends from the spectra obtained from pyrolysate and not from the rubbers themselves [275]. Hence the selected spectral region, obtained using pyrolysate, can be used to identify the rubbers present in the GTR (Figure 4.11 (b)). The peak at 1380 cm^{-1} represents C-C stretching of the $C-CH_3$ group in natural rubber, while the peaks 815, 890 and 970 cm^{-1} represent C-H bending vibrations of $-CH=C<$, $>C=CH_2$ and $CH_2=CH-$ respectively. The peaks at 990 and 970cm^{-1} represent out of plane bending vibrations $CH_2=CH-$ and trans $-CH=CH-$ of butadiene. The peaks at 1600 and 1500 cm^{-1} represent C=C stretching

vibrations of aromatic ring, while 700 and 760 cm^{-1} represent =C-H and C=C out of plane bending vibrations of aromatic ring in polystyrene.

These peak assignments represent most of the prominent peaks which appear in NR, SBR and BR spectra [274], and hence confirmed their presence in the GTR. These assignments further indicated the presence of some unsaturation in rubbers in the GTR. FTIR spectra with similar prominent peak assignments were reported for waste tyre rubber in previous studies [138, 156, 275].

4.2.2.2 Thermogravimetric Analysis

Figure 4.12 shows TGA and DTGA thermograms for the GTR in air. These thermograms exhibit four steps in weight loss with corresponding maximum peaks, which are associated with four different components present. The first weight loss associated with the peak at 280 ^{0}C is attributed to the volatilization of processing oil or any other low boiling point components. The next weight loss associate with two peaks is due to degradation of hydrocarbon components present in the GTR, while the third weight loss is due degradation of carbon black when reacting with oxygen present in atmospheric air. The non-volatile residue corresponds mainly to inorganic fillers.

NR largely decomposes at lower temperatures compared to SBR [275, 276]. BR also decomposes at higher temperatures like SBR. Further, at a 20 ^{0}C/min heating rate, degradation of pure NR has been reported to start at 330 ^{0}C and completes at 495 ^{0}C, while degradation of SBR and BR starts at 370 ^{0}C and completes at 515 ^{0}C [276]. In the present study, the degradation of the first hydrocarbon component occurs in the 350 to 474 ^{0}C temperature range, and that of the second hydrocarbon component in the 474 to 518 ^{0}C range. This observation confirms the presence of NR and SBR and/or BR in the GTR.

The quantitative analysis of rubbers in the GTR can be determined (Section 3.8.1) through the correlation of peak heights in the DTGA thermogram to the content of each component [275]. However, this determination works well only when the DTGA

thermograms of each rubber are separated, which is necessary to prevent any overlapping of different peaks. With the experimental conditions maintained in the present study, it was difficult to identify separate peaks for each rubber and hence, the composition of the GTR was estimated with the degradation transitions observed. The rubber hydrocarbons may undergo oxidation during heating in air atmosphere, exhibiting a lower value compared to the actual content present in the GTR. The GTR contains 17 wt% low molecular boiling point components, 49 wt% rubber hydrocarbons (28% NR and 21 wt% synthetic rubbers), 27 wt% carbon black and 7 wt% ash or residue. This composition is within the composition range given in literature (Section 582.8.2).

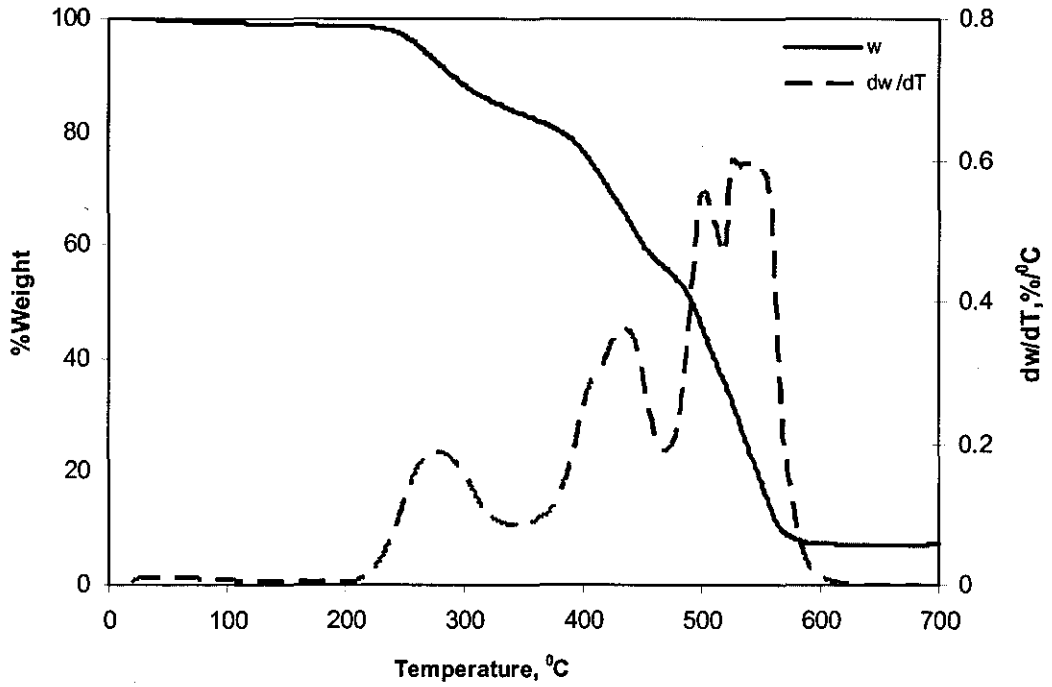

Figure 4.12 TGA thermogram and DTGA curve for GTR

4.2.3 Glass Transition Temperature

Tan δ curve for the GTR, obtained from the DMA test, showed a broad peak in a temperature range -70 to 10 ^{0}C (Figure 4.13). This peak was for the glass transition of the rubbers in the GTR, and hence T_g of the GTR was determined (Section 3.8.3) as -30 ^{0}C. The glass transitions of diene rubbers, including NR and SBR, also fall within this

temperature range [216, 217]. This observation is also supported to the presence of NR and SBR in the GTR.

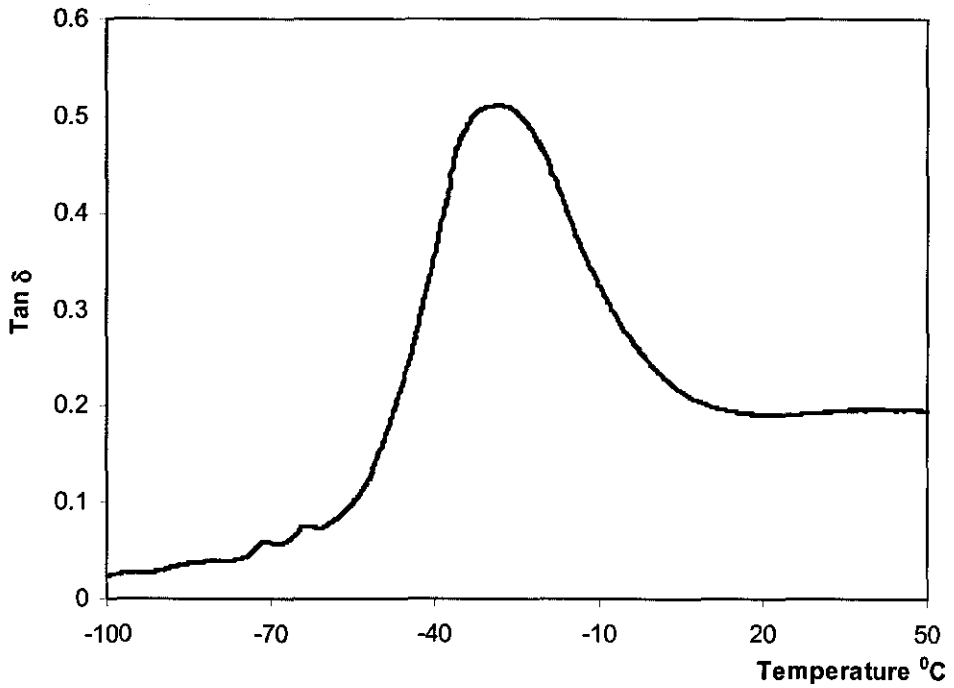

Figure 4.13 Tan δ curve for GTR, illustrating its glass transition

4.2.4 Degradation Temperature

Figure 4.12 shows that the degradation of the GTR in air starts at 200 ^{0}C. However, the degradation of the guayule rubber is reported as occurring at 230 ^{0}C in air and at 330 ^{0}C in nitrogen [277]. The lower onset degradation recorded for the GTR is due to presence of larger amounts of low molecular weight components in the GTR. The high molecular weight components in the waste rubber will degrade during previous processes and will produce low molecular weight components in the GTR. Alternatively, the low onset degradation of the GTR could be due to variations in heating rates used in the two studies [276] and/or due to presence of acids in the rubbers [277]. However, the low onset degradation suggested the necessity of an addition of a suitable antioxidant to the GTR to prevent further degradation.

4.3 Summary

The WPP used in the present study has a melt flow index of 12.5 g/10 min at 230 ^{0}C at 2.16 kg load, and hence it was identified as a mix of injection moulded products. The optical image for the WPP exhibited tiny black spots indicating its contamination. The FTIR spectrum and the DSC thermogram for the WPP revealed that the presence of PE as a contaminant. Further, the TGA thermogram revealed that the solid residue in the WPP as 3 wt%. The melting temperature, the re-crystallization temperature and the glass transition temperature in the DSC thermogram for the WPP were determined as 166 ^{0}C, 120 ^{0}C and 1 ^{0}C, respectively. The degradation temperature for the WPP in air was recorded as 230 ^{0}C. These thermal characteristics suggested the suitability of processing of the WPP at 180 ^{0}C in similar to virgin PP.

The microscopic images for the GTR identified it as ambient ground. The FTIR spectra and the tan δ curve for the GTR used in the present study revealed that it was a mix of NR, SBR and/or BR. The TGA and DTGA thermogram further revealed that the GTR contained 17 wt% low molecular boiling point components, 28 wt% NR, 21 wt% SBR and /or BR, 27 wt% carbon black, and 7 wt% residue. The glass transition temperature and the onset degradation temperature for the GTR were determined as -30 ^{0}C and 200 ^{0}C, respectively. The low onset degradation of the GTR suggested of using a suitable antioxidant to prevent degradation during melt mixing carried out at 180 ^{0}C under high shear forces.

Chapter 5 Results and Discussion - Part II Simple Blends

5.1 Effect of Blend Composition

Blends with different compositions (Table 3.3) were prepared as described in Section 3.2.2. These blends were analyzed initially by processing characteristics (Section 3.4) and mechanical properties (Section 3.7). The results obtained in this initial analysis were further investigated by thermal analysis (Section 3.8), sol/gel analysis (Section 3.9) and morphology (Section 3.11).

5.1.1 Processing Characteristics

5.1.1.1 Torque and Blend Temperature Developments

The melt mixing behaviours of waste polypropylene (WPP), ground tyre rubber (GTR), and the blends of these two polymers, were studied. Torque developments during melt mixing for WPP, GTR, a blend containing equal amounts of the two materials (50:50/180/30/8) and a blend containing 80 wt% GTR (80:20/180/30/8) are shown in Figure 5.1. The curve for the 50:50/180/30/8 blend in Figure 5.1 is typical of the torque development curves produced for the majority of the blends. However, the blends containing 70 wt%, 80 wt% and 90 wt% of GTR were significantly different at the early stages of mixing. The blend temperature development curves for WPP, GTR and the above two blends are given in Figure 5.2. These figures represent a single set of experimental data.

The melt mixing behaviors of the pure materials and the blends are different to each other. The melt mixing behaviours of different blends are discussed separately.

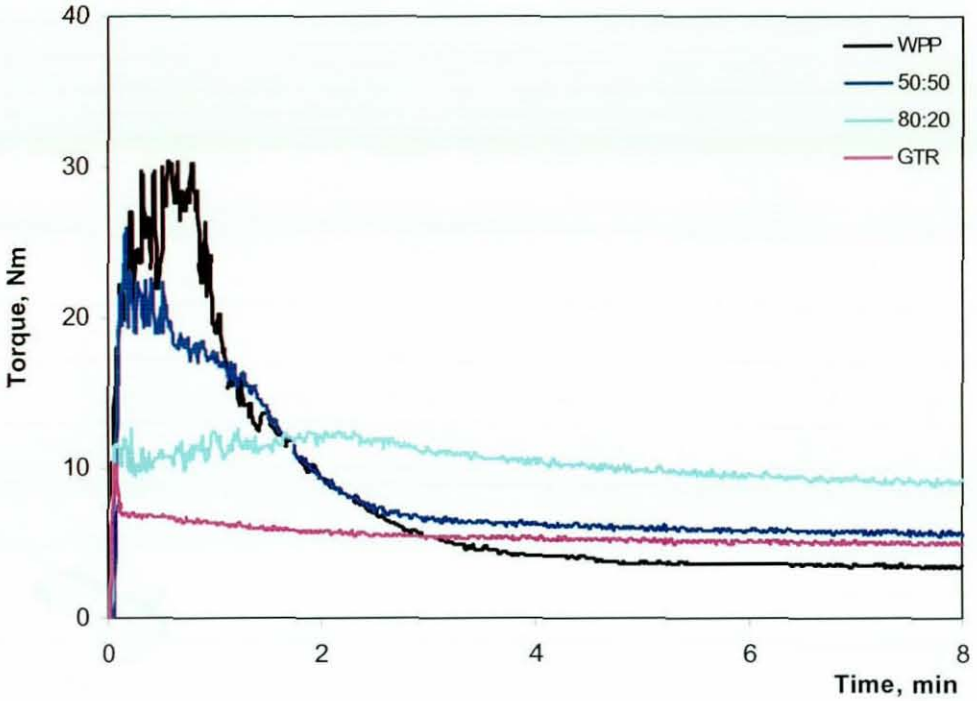

Figure 5.1 Torque developments for WPP, GTR and selected (GTR:WPP/180/30/8) blends

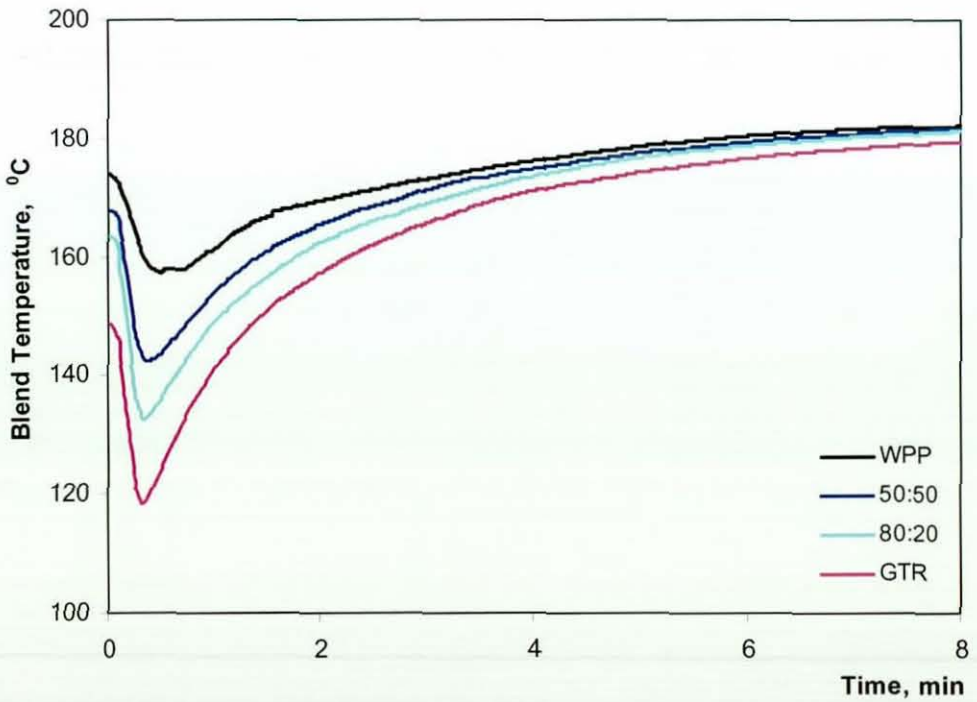

Figure 5.2 Temperature developments for WPP, GTR and selected (GTR:WPP/180/30/8) blends

(a) Waste Polypropylene

The torque development curve for the pure WPP exhibits a sharp peak initially (Figure 5.1). The increase in torque associated with the initial peak is due to the resistance exerted on the rotors by loading with un-molten WPP. When the WPP is subjected to mechanical and thermal shearing stresses, it first softens and then melts. As a result, the torque decreases and stabilizes upon the completion of the melt mixing process. The blend temperature development curve shows a decrease in temperature at loading of cold waste polypropylene (Figure 5.2). The blend temperature increases thereafter and stabilizes at the completion of the mixing, around the processing temperature of 180 ^{0}C.

(b) Ground Tyre Rubber

GTR can be considered as a particulate solid. When particulate solids are subjected to thermal stresses, they form agglomerants of primary particles held together by van der Waals or dipole-dipole forces [191]. In agreement with this, agglomerants of primary GTR particles were observed on completion of the pure GTR mixing process. Most of the agglomerants observed were very small and behaved as free particles. The other agglomerants were large and lumpy. Both the small and large agglomerants were soft.

The blend temperature for pure GTR decreases initially and then increases towards a stabilized temperature at the completion of the mixing process (Figure 5.2). Compared to WPP, GTR absorbs large amount of heat energy at the initial stage of the mixing process and hence exhibits a greater decrease in blend temperature. Although the blend temperature development of the two pure materials is the same, the torque development nature is different. The GTR shows an initial increase in torque at loading (Figure 5.1) which falls and stabilizes suddenly, without exhibiting a gradual decrease. This indicates that the GTR does not melt nor softens during the mixing process.

(c) 50:50/180/30/8 Blend

The torque development and the nature of the blend temperature development of the 50:50/180/30/8 blend are very similar to those of pure WPP. When the WPP and GTR are loaded the torque development curve exhibits an initial increase (Figure 5.1) while the

blend temperature development curve (Figure 5.2) exhibits a decrease. The mix homogenizes as the WPP is subjected to mechanical and thermal shearing stresses and softens. As a result, the torque decreases and stabilizes upon the completion of the melt mixing process. However, the initial drop in blend temperature is high for the 50:50/180/30/8 blend compared to WPP. This is due to the presence of a higher GTR content, which absorbs more energy than WPP. Similar torque development and blend temperature development curves were observed with all blends containing less than 70 wt% GTR. However, the torque range and the blend temperature range varied with the blend composition. These ranges lie in between those of pure WPP and pure GTR, according to their composition.

The resultant blends observed at the completion of mixing took the form of a large single mass. None of the GTR agglomerants, which were uncombined in the single mass, were observed.

(d) 80:20/180/30/8 Blend

The 80:20/180/30/8 blend also showed similar torque and blend temperature developments when the polymer was loaded, but changed thereafter (Figure 5.1 and Figure 5.2). Even though the blend temperature increased after the initial drop, the initially increased torque neither does decreased suddenly as shown with pure GTR, nor gradually as shown with WPP and the 50:50/180/30/8 blend. The torque actually increased, but slightly at the early stage of mixing. With an increase in temperature beyond its melting point of 166 ^{0}C, WPP melts, and as a result, the torque decreases with time towards a final plateau region. The slight torque increase at the early stage of mixing may be due to coalescence of GTR particles to form large GTR agglomerants, which create greater torques.

At the completion of the mixing process, tiny GTR agglomerants, which were not combined in the single mass of the resultant blend, were observed. These agglomerants behaved as free particles. This indicates that the amounts of WPP in these blends are insufficient to entrap the GTR agglomerants and to combine them in a single mass consisting of a formation of a GTR continuous phase.

5.1.1.2 Torque Properties

The information retrieved from torque development curves has regularly been used to analyze processing characteristics of melt-mixed compounds [89, 110]. The following processing characteristics were determined from the torque development curves: maximum torque (T_{max}), time taken to reach maximum torque (t_{max}), steady state torque (T_{ss}), time taken to reach steady state (t_{ss}), torque reduction rate (T_{max}-T_{ss}/t_{ss}-t_{max}) and the specific energy requirement to reach steady state (W). These melt mixing properties, for all blends, are shown in Table 5.1. The variations of these properties with GTR content are shown in Figure 5.3 (maximum torque and steady state torque), and Figure 5.4 (specific energy requirement).

(a) Waste Polypropylene and Ground Tyre Rubber

The un-molten WPP is hard, but GTR is soft and in particulate form. Hence, pure WPP exhibits a greater maximum torque than pure GTR (Figure 5.3). Due to the high torque at the early stage of mixing, pure WPP compared to pure GTR exhibits a greater specific energy requirement (Figure 5.4).

The steady state torque is an indicator of the viscosity of the melt mix and hence it is used to assess its processability [110]. WPP melts with an increase in temperature which thereby increases its molecular flexibility and mobility. Due to this high molecular mobility, viscosity decreases. As a result, pure WPP exhibits a low steady state torque (and a fast torque reduction rate (Table 5.1). Further, it reaches its steady state within 5 minutes (Table 5.1).

GTR contains chemically crosslinked rubber molecules formed during previous vulcanization processes. Due to the non-melting behavior of GTR, which is associated with its crosslinked structure, it does not decrease its viscosity with increase in temperature. Hence, compared to pure WPP, pure GTR exhibits a higher steady state torque. However, due to the particulate nature of pure GTR, this value is not high. The pure GTR reaches its steady state within 2.5 minutes (Table 5.1). Even though it reaches

its steady state quickly, due to its low maximum torque and high steady state toque, pure GTR shows a slow torque reduction rate (Table 5.1).

Table 5.1 Some processing characteristics of the blends

GTR:WPP	t_{max}, min	t_{ss}, min	T_{max}-T_{ss}/t_{ss}-t_{max}, Nm/min
0:100	0.8(0.0)	4.5(0.0)	6.5(0.3)
10:90	0.7(0.0)	4.1(0.1)	8.7(0.7)
20:80	0.4(0.1)	4.2(0.1)	7.3(0.6)
30:70	0.5(0.0)	4.1(0.0)	6.9(0.0)
40:60	0.3(0.0)	4.6(0.4)	5.3(0.3)
50:50	0.3(0.0)	4.5(0.3)	4.1(0.3)
60:40	0.3(0.0)	4.6(0.5)	2.9(0.1)
70:30	0.3(0.0)	4.8(0.1)	1.4(0.1)
80:20	0.2(0.0)	4.8(0.1)	1.1(0.2)
90:10	0.2(0.0)	5.1(0.2)	0.1(0.0)
100:0	0.2(0.0)	2.5(0.0)	0.8(0.1)

(b) Blends

The maximum torque decreases with increase of GTR content in the blend (Figure 5.1). This variation is expected as pure WPP exhibited a higher maximum torque than pure GTR, at their non-melting stage.

The GTR in the blends, which was already crosslinked during previous processes, limits the mobility of the WPP at higher temperatures and hence the steady state torque increases with GTR content. However, this increase is not linear, which is generally expected with the incorporation of fillers into thermoplastics [87]. The viscosity increase is possibly due to agglomeration of the GTR particles and the formation of new crosslinks at higher temperatures. As this combined effect increases with higher GTR contents, a relatively higher increase in steady state torque is exhibited. On the other hand, at low GTR contents, tiny GTR particles may homogeneously disperse in the blends and have no

significant effect on viscosity. These results indicate a decrease in processability with increase in GTR content. An increase in steady state torque with increase in rubber content in virgin rubber-thermoplastics blends has also been reported previously [106]. Also an increase in steady state torque with increase in recycled rubber content in virgin polypropylene-recycled rubber blends has been reported [89]. However, the increase exhibited was linear. WPP, when compared to virgin PP, has a higher tendency to undergo degradation during high temperature mixing [215]. This is because during long term exposure to sunlight, humidity, air and other environmental conditions, the saturated polymer chains have already undergone chain scission to a certain extent. Further, the WPP contains some chemical additives and contaminants (Figure 4.2), which influence the mixing torque. Hence, the differences noticed in the two studies are attributed to the difference in types of polypropylenes used.

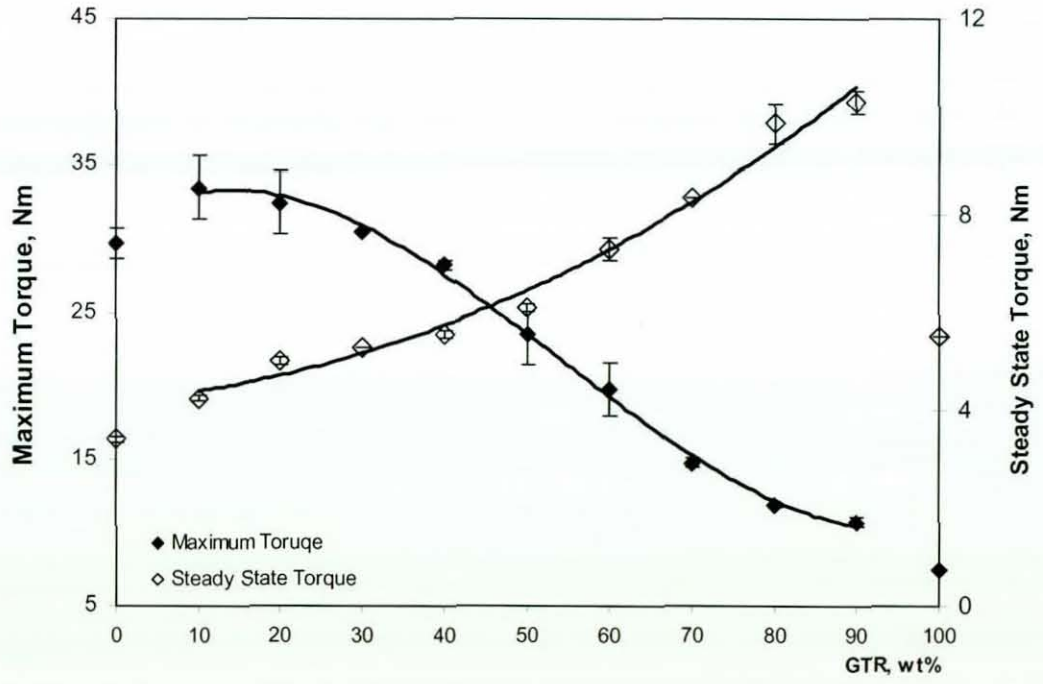

Figure 5.3 Maximum and steady state torques vs. Ground tyre rubber content

The difference between maximum torque and steady state toque, generated during the melt mixing process, decreases with increase in GTR content. Further, the time taken to reach maximum torque, t_{max}, slightly decreases with increase in GTR content (Table 5.1). The greatest difference in t_{max} values can be seen between the two 'pure' polymers. But, it

is only 0.6 minutes. However, the time taken to reach steady state, t_{ss}, does not show such a gradual decline. All the blends took around 4-5 minutes to reach their steady states. Because of these factors, torque reduction rate decreases with increase in GTR content (Table 5.1).

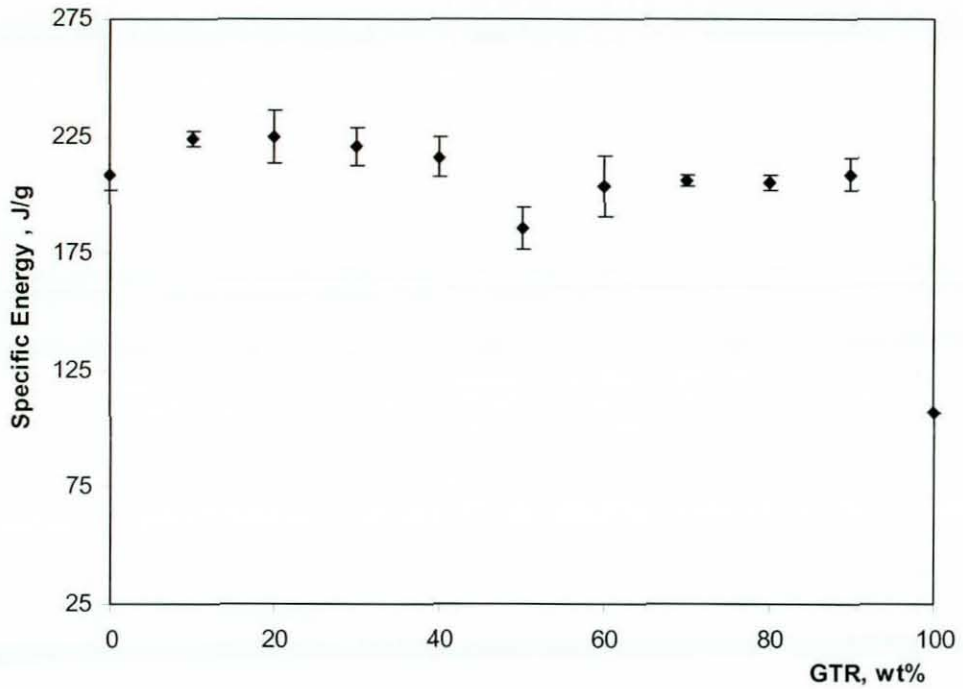

Figure 5.4 Specific energy requirement vs. Ground tyre rubber content

Figure 5.4 shows the specific energy requirement to reach steady state against GTR content. The WPP shows a low specific energy requirement compared to WPP rich blends, and this can be attributed to the additional energy associated with the mixing of two materials. WPP rich blends exhibit higher energies compared to GTR rich blends. WPP rich blends show greater maximum torques at the initial stage of mixing (Figure 5.3), rapid torque reduction rates (Table 5.1) and lower steady state torques at the final stage of mixing (Figure 5.3), and hence, the energy requirement at the early stage is greater but at the later stage is lower. In contrast, GTR rich blends exhibit lower initial torques, slow torque reduction rates and slightly higher final steady state torques and hence, these blends consume lower energy at the early stage but higher energy at the later stage. Hence, the resultant specific energy requirement is more or less similar. However, with an average energy consumption at both stages, the 50/50/180/30/8 blend shows the minimum specific energy requirement.

5.1.2 Melt Flow Index (MFI)

The melt flow indices of blends containing up to 60 wt% GTR are given in Figure 5.5. It was not possible to obtain melt flow index (MFI) for blends containing higher GTR contents as the flow properties of these blends were too low and erratic for measurement using the standard low shear conditions normally employed for thermoplastics. The MFI decreases with increase in GTR content due to replacement of WPP, which has low melt-viscosity, by non-flowing GTR. However, this decrease is not linear, and a rapid decline occurs above 30 wt% GTR. This is in agreement with the steady state torque variation measured under high shear conditions and at relatively lower temperature conditions.

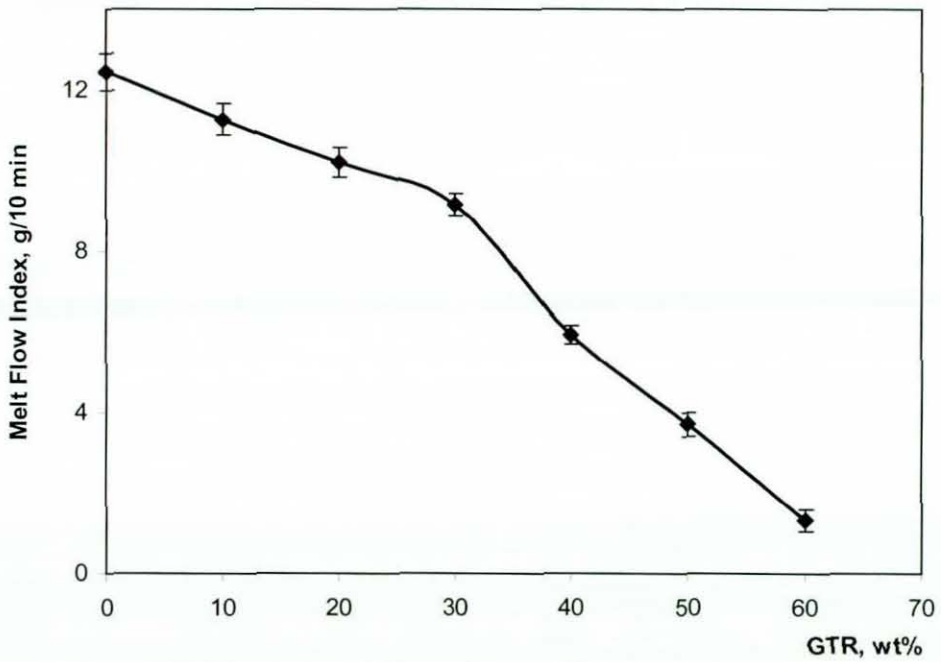

Figure 5.5 Melt flow index vs. Ground tyre rubber content

5.1.3 Mechanical Properties

The mechanical properties that were used to assess the effect of blend composition included hardness, tensile properties, tear resistance and impact properties. The property variation against GTR content is discussed in this section. Although the pure WPP was considered for the evaluation, the pure GTR were not considered. Difficulty was found in producing smooth compression moulded sheets from the pure GTR in a similar way to

WPP and all the blends. As the moulded sheets were of loosely bonded GTR particles, the specimens cut from the sheets were easily damaged.

5.1.3.1 Hardness

The hardness of the WPP, and the blends, are given in Table 5.2. This table shows that hardness decreases with an increase in GTR content. Further, this decrease accelerates with GTR content.

Table 5.2 Hardness of waste polypropylene and blends

GTR:WPP	Hardness, IRHD
0:100	86 (1)
10:90	85 (1)
20:80	84(1)
30:70	82(1)
40:60	82(1)
50:50	76(1)
60:40	76(1)
70:30	70(1)
80:20	61(1)
90:10	56(1)

WPP is rigid and has a higher hardness than all the blends. The replacement of hard WPP by soft GTR decreases the hardness of the blend. At low GTR contents, the tiny agglomerants are dispersed homogeneously in the hard WPP matrix (Figure 5.22a) and hence the resulting blend does not show a large drop in hardness. At high GTR contents, GTR agglomerants remain close to each other and hence hardness falls to a greater extent. This decrease is enhanced with the conversion of the GTR dispersed phase to a continuous phase at 70 wt% GTR (Figure 5.22d). The secant modulus also shows the same trend in variation (Section 5.1.3.2).

5.1.3.2 Tensile Properties

Stress-strain curves for the blends were plotted using the recorded load against extension data. Typical stress-strain curves for pure WPP, and selected blends, are illustrated in Figure 5.6. The variations of tensile strength and % elongation at break with GTR content are shown in Figure 5.7 while the variation of secant modulus at 2% strain is shown in Figure 5.8. Table 5.3 gives the tensile properties of the blends as a percentage of the tensile properties of pure WPP.

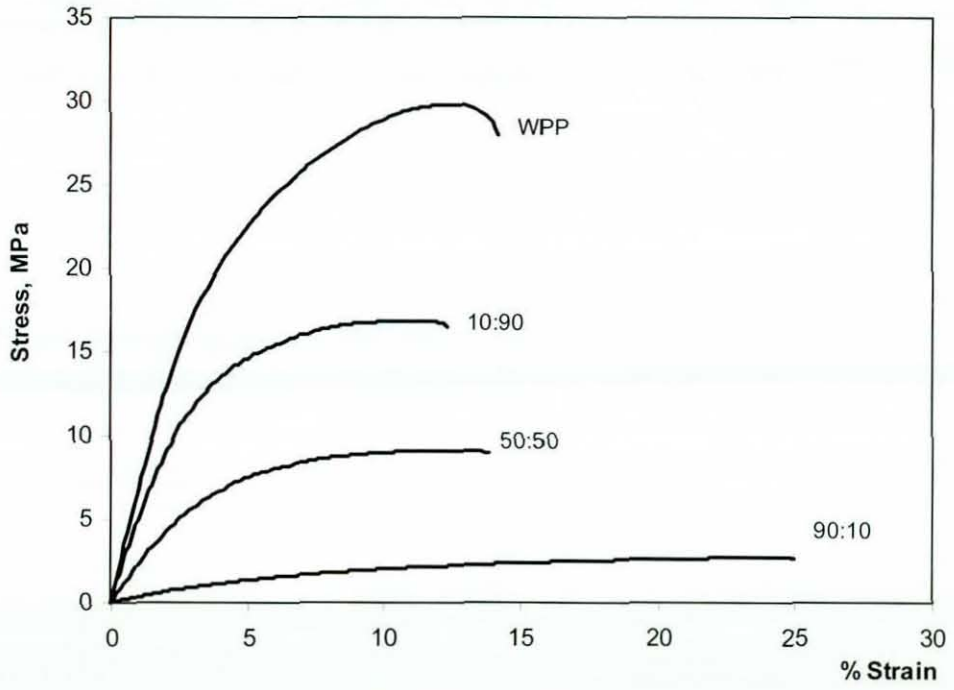

Figure 5.6 Stress vs. Strain for WPP and selected (GTR:WPP/180/30/8) blends

The Stress-strain curve for WPP exhibits a plastic response (Figure 5.7), which is a common characteristic feature for semi crystalline polymers [107, 111, 120]. It shows an increase in stress against strain followed by a slight decrease before failure. This suggests that the failure in WPP occurred by sliding of crystalline regions may be due to interference of impurities in WPP [218]. The addition of GTR changes the nature of the stress-strain curves considerably. The blends containing low GTR contents show a plastic response, an increase in stress against strain, but do not show a decrease in stress before failure. This indicates that failure in such blends occurred by the alignment of crystalline

regions at the onset of necking, which was interrupted by the GTR dispersed phase. The blends containing high GTR contents showed a high-extension rubbery response, indicating a transition of the GTR phase to a continuous phase. An indication of this phase change was given by the torque development curves obtained at high GTR contents. Further, the phase change was clearly observed with the optical micrographs (Figure 5.22). Similar stress-strain variations were reported for blends of waste-ethylene propylene diene monomer and polypropylene [111].

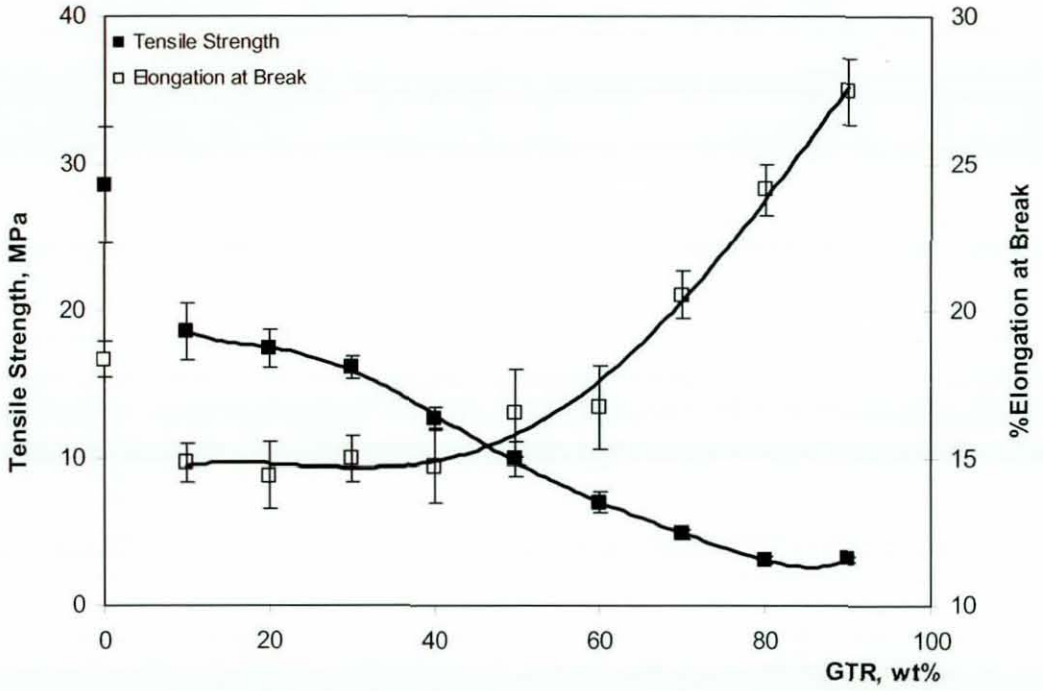

Figure 5.7 Tensile strength and elongation at break vs. Ground tyre rubber content

WPP is a semi crystalline polymer and has a high degree of physical entanglements associated with the crystalline regions [111, 120]. Hence, WPP has a high tensile strength (Figure 5.7) and modulus (Figure 5.8). Further, these physical entanglements stretch during straining and the result is a somewhat higher elongation at break (Figure 5.7).

GTR is an amorphous thermoset containing some chemical crosslinks which has low tensile strength and modulus, and high elongation at break. With the incorporation of the soft GTR phase into WPP tensile strength and secant modulus (at 2% strain) significantly fall: the addition of 10 wt% GTR lowers tensile strength by 35% and secant modulus by 29% (Table 5.3). This significant drop in tensile properties is due to a disruption of the

stretching process of the WPP by the GTR phase and also poor interfacial adhesion between these two phases (Section 5.1.3.3). A similar drop can be seen when solid fillers are incorporated in thermoplastics [278].

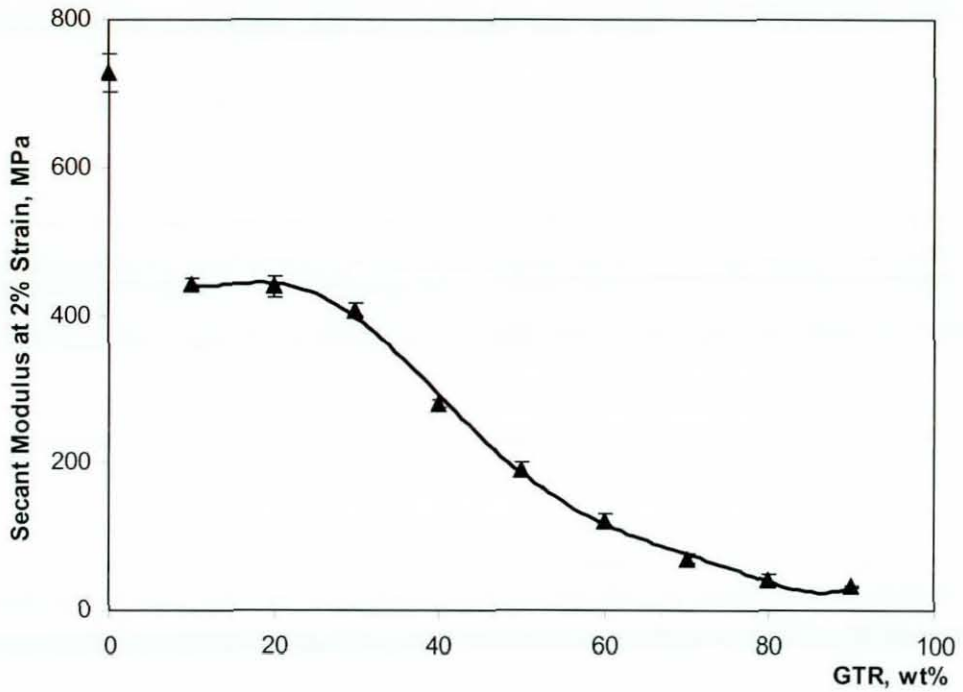

Figure 5.8 Secant modulus vs. Ground tyre rubber content

The strength of the GTR/WPP blend depends in part on the strength of the WPP which in turns depends on the degree of crystallinity and on its continuity. It has been observed that the crystallinity of the blend decreased with the increase in GTR content (Table 5.7). A greater amount of tiny GTR agglomerants, which were physically anchored to the WPP matrix, were observed in the blends with low GTR contents (Figure 5.22). With further increase in GTR content, the amount and the size of the dispersed GTR phase increased, and hence the GTR phase exerted its rubbery behavior. Hence, the tensile strength and modulus show a gradual slow decrease up to 30 wt% GTR and a rapid decline thereafter up to 60 wt% GTR. This decrease is enhanced by a distinct phase separation due to the poor interfacial adhesions between phases (Figure 5.12), which restricts the load transfer between phases during straining. With the formation of a continuous GTR phase at 70 wt% GTR (Figure 5.22(d)), the drop in tensile strength and modulus slows, deviating from the rapid decrease observed up to that point. This may also be attributed to the

increase in strain induced crystallization caused by the natural rubber components present in the continuous GTR phase. The faster crystallization rate noticed at high GTR content (Figure 5.20 and Table 5.9) may also result in this property enhancement. The crystallites formed at lower crystallization temperatures under faster crystallization are expected to be small, less perfect and connected by larger concentration of tie molecules [222]. The decrease in tensile strength and modulus with increase in waste rubber content is a common observation in many studies [89, 102, 116, 128, 200].

Table 5.3 Tensile properties of blends as percentages of WPP

GTR, wt%	% Tensile Strength	% Secant Modulus	% Elongation at Break
10	65	71	77
20	61	70	75
30	56	60	78
40	44	46	77
50	39	31	86
60	24	22	87
70	17	12	107
80	10	8	126
90	11	7	143

The percentage elongation at break (Figure 5.7) drops 30 %with the addition of 10% GTR and then remains unchanged up to 40 wt% GTR. The percentages obtained are fairly low. This is again due to the poor adhesion between phases. With a further increase in GTR content, elongation at break increases gradually due to increased stretching of the GTR agglomerants in the continuous phase [116]. The GTR agglomerants contain of long flexible crosslinks and low levels of crosslinks, which promote stretching during straining [212].

5.1.3.3 Tensile Fracture

The fracture behaviour of the WPP and the blends was studied by observing the surfaces of the tensile fractured specimens using optical microscopy and the tensile fracture surfaces using scanning electron microscopy (SEM).

Figure 5.9 illustrates three microscopic images of the surface of a tensile fractured specimen of WPP observed at different distances from the fractured end. Stress whitening was observed at the fractured end and the crazes were visible under optical microscopy on the stress whitening region (Figure 5.9c). These crazes ran normal to the tensile direction indicated by the arrow [219, 279]. The dark spots in the micrographs are either voids [240] or particulate ingredients and contaminants present in the WPP (Section 4.1.1). There are some scratches also apparent on the surface, which were formed when the sheet was moulded. Generally, crazes are initially formed on the surface and grow inward [230]. A stable crack nucleates and propagates through the array of closely spaced crazes resulting in tearing along the array of crazes. Figure 5.1b and Figure 5.9c show clearly the craze growth along the length of the tensile specimen during straining. Crazing has already been recognized as a fracture mechanism for virgin PP (Section 2.8.5.1) at room temperature.

Figure 5.10, is a SEM image of a WPP tensile fracture surface, it shows a rough brittle fracture surface. This fractograph exhibits tiny voids, which are more likely to be associated with an unidentified nucleating agent or a pigment or a contaminant present in the WPP. During continued deformation, voids are formed because of the debonding of the one or more of the above mentioned particles from the high crystallinity WPP matrix. The high stress concentration at the particles facilitates their separation [230]. These voids act as points of nucleating for the crazes which then lead to brittle fracture.

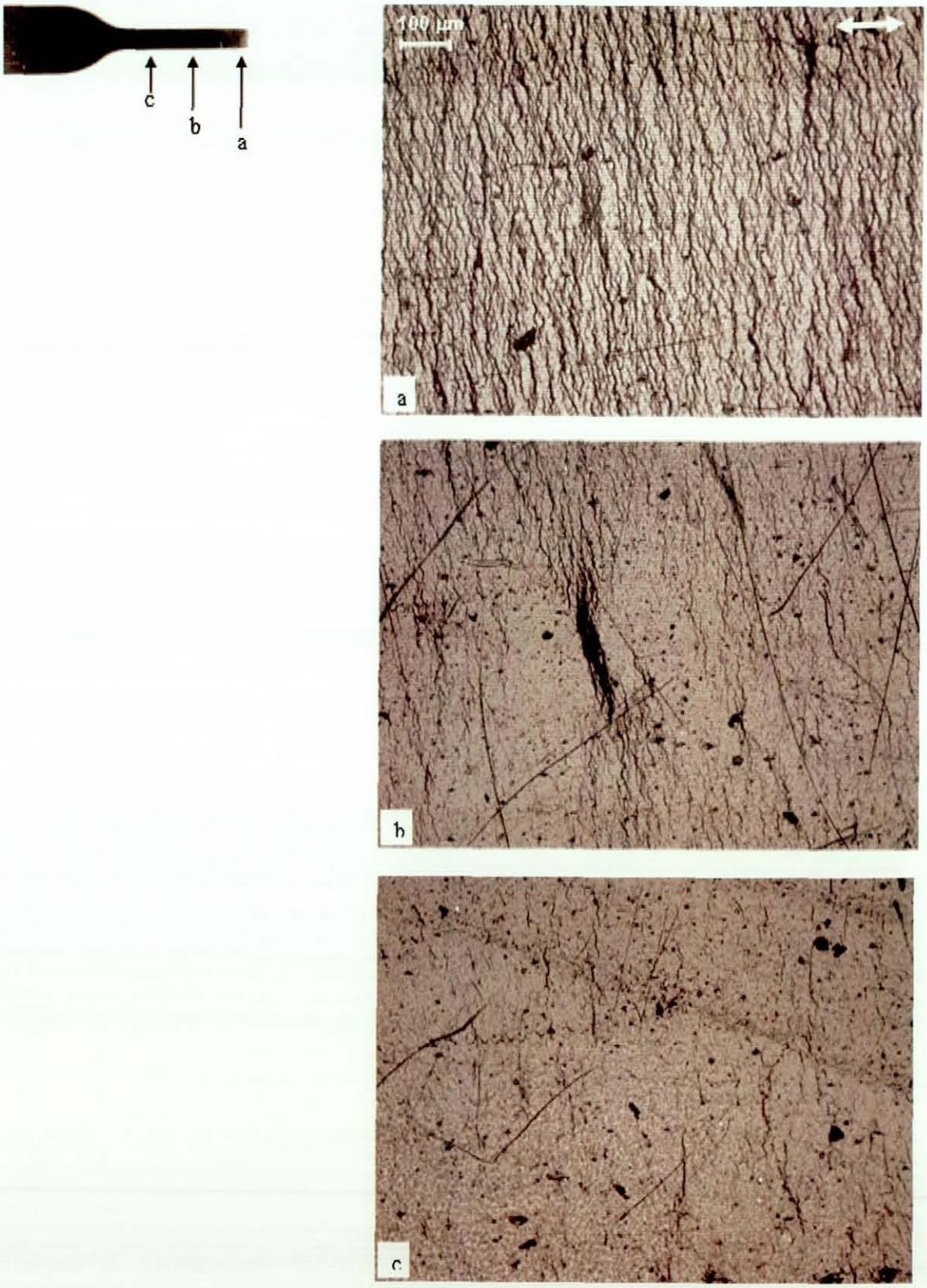

Figure 5.9 Stress cracks observed on the surface of a WPP tensile fractured specimen

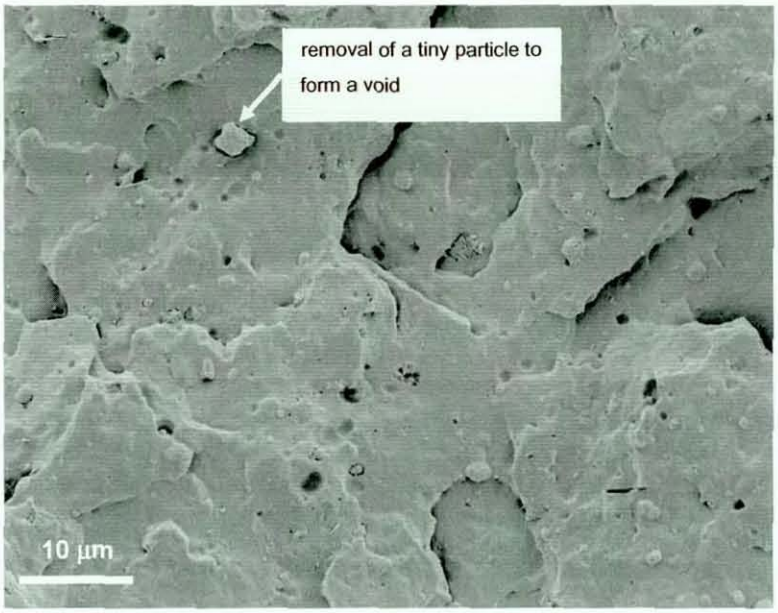

Figure 5.10 Tensile fractograph of waste polypropylene

Incorporation of GTR into WPP changes its fracture behaviour. Figure 5.11, illustrates the microscopic images of stress cracks formed on the surface of the tensile fractured specimen of a 50:50 blend. These images do not show of craze across the width of the test specimen, and also no stress whitening on the fractured end. This implies that failure of the blend did not occur due to crazing. This is in agreement with the stress-strain curves obtained for blends (Figure 5.6). However, a certain number of tiny crazes were noticed along the surface closer to the large voids. It seems that the crazes were formed in the WPP phase and were localized at the interface between two phases.

In general, rubber in PP has two functions: it has to relieve the volume strain by cavitation and it acts as a stress concentrator to promote multiple crazing and/or shear yielding (Section 2.8.5.2). Both these functions are directly related to the concentration and particles size and distribution of the rubber phase. It has been reported [236] that rubber particles less than 5 µm in size initiate shear yielding whereas those larger than 5 µm initiate crazing. The GTR particles used in the present study are of 420 µm in size and hence it is hard to expect the formation of particles smaller than 5 µm in the dispersed phase during melt mixing. However, if the GTR particles are cavitated, then the volume

strain is lowered and shear yielding can be expected. Simultaneously, multiple crazes will develop in WPP regions around the cavitated GTR particles.

The fracture behaviour of the blends can be clearly understood from the SEM images of the fractured surfaces, which are shown in Figure 5.12. All these fractographs show similar facture behaviour. On the fractured surfaces many GTR particles are present; some of them are encapsulated by the WPP. The others are nearly clean suggesting that during fracture propagation, the fracture front preferentially passed around the interface rather than going through the particles. In agreement, with this suggestion are big holes which were created due to removal of the GTR particles at the fracture. This is an indication that the debonding stress is smaller than the cleavage stress of the GTR particles, in other words a rather poor adhesion between phases [200, 223]. When the adhesion between phases is relatively poor, interfacial debonding may occur and avoid internal cavitation. This debonding occurs due to different levels of shrinkage between two polymers during cooling, if there are no proper adhesion between the polymers. Blends with incompatible polymers show this nature of fracture [89]. At the molecular level, NR, SBR and /or BR in the GTR and PP are incompatible (Section 2.8.4) and high interfacial tension leads to poor interfacial adhesion. Alternatively, when the cohesive strength within the GTR phase is poor, due to a high GTR content present in the blend, debonding occurs between GTR particles with the resultant formation of a small cavity (Figure 5.12(c)). Because of this voiding at the interface, GTR/WPP blends do not show improved tensile properties.

In addition to voiding at the interface, fibrillation can be seen in the WPP regions on the tensile fracture surfaces of the blends (Figure 5.12). This is not seen on the fracture surface of the WPP (Figure 5.10). The appearance of fibrillation indicates that a certain level of shear yielding in the WPP occurred during straining, and is responsible for the relatively enhanced ductility of the blends [230, 239]. It has been reported [231] that multiple crazing is favoured for blends with strong interfacial adhesion whereas shear yielding occurs in blends with poor interfacial adhesion.

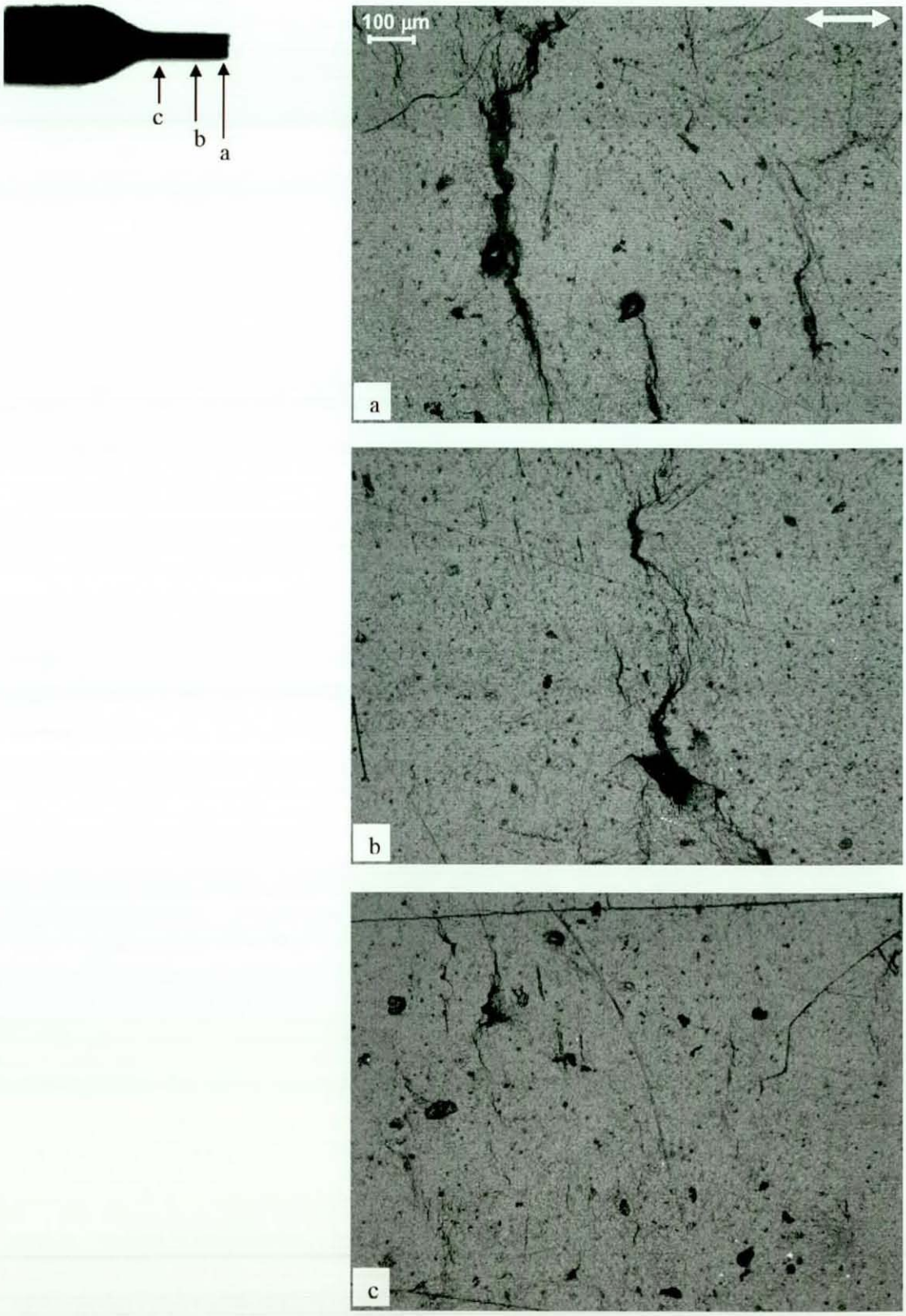

Figure 5.11 Stress cracks observed on the surface of a 50:50 blend tensile fractured specimen

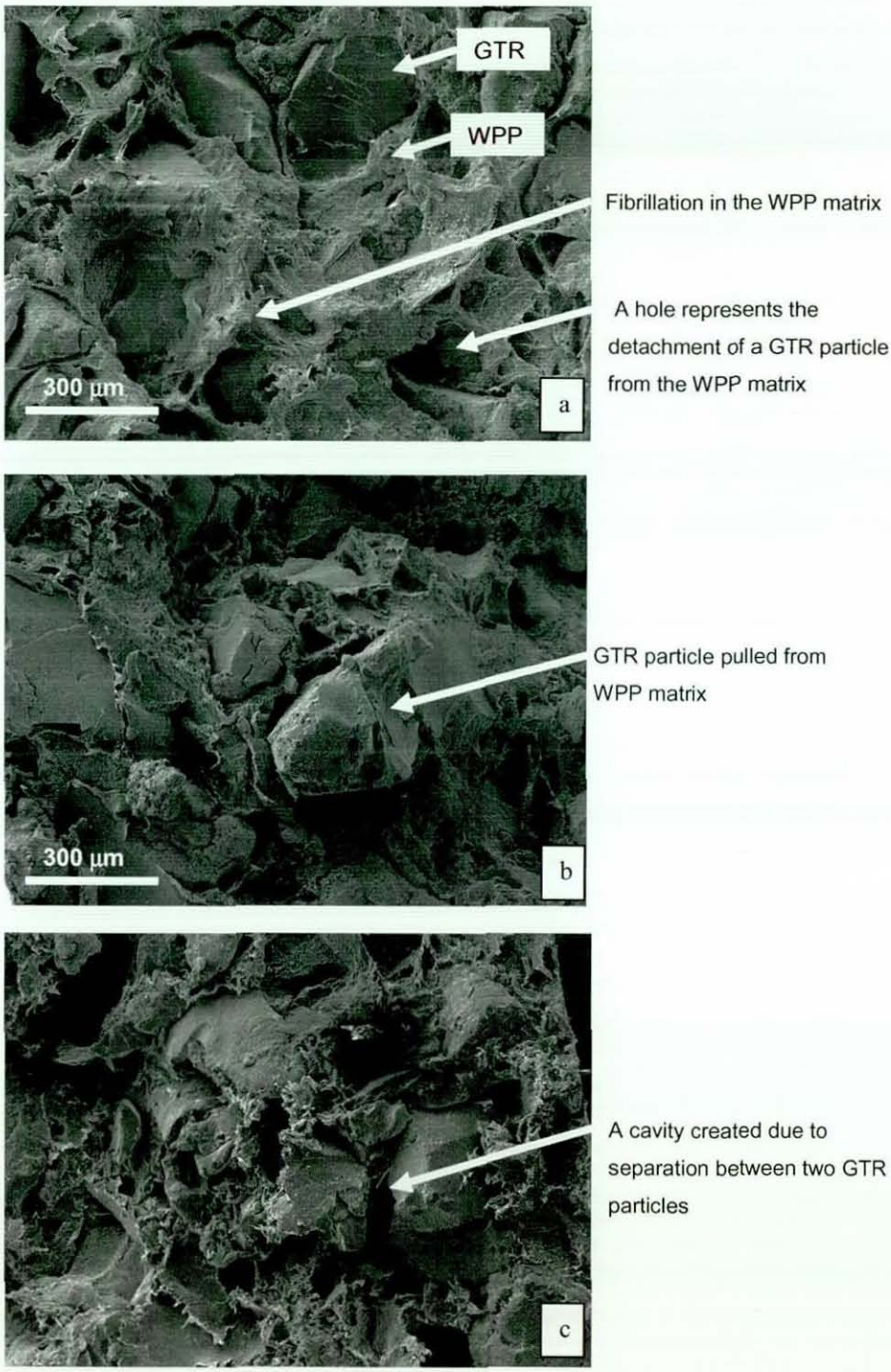

Figure 5.12 Tensile fractographs of (GTR:WPP/180/30/8) blends
(a) 20:80 (b) 50:50 (c) 80:20

5.1.3.4 Tear Resistance

Stick and slip or knotty tearing behavior was observed when tear testing the blends. This behavior is generally shown by filled polymer systems [109, 280]. It was not possible to record the tear resistances for the blends containing 30 wt% GTR or below because the specimens cracked close to the tip of the slit without tearing through the rest of the specimen. The tear resistance of blends containing 30 wt% of GTR, or more, are given in Table 5.4.

Table 5.4 Tear resistance of blends

GTR:WPP	Tear Resistance, N/mm
30:70	9.4(0.4)
40:60	8.0(0.4)
50:50	6.2(0.4)
60:40	4.3(0.3)
70:30	2.9(0.2)
80:20	1.9(0.1)
90:10	1.4(0.1)

During tearing, GTR particles are subjected to large tensile strains which result in extensive craze formation. In the GTR/WPP blend, a void form at the interface due to poor interfacial adhesions (Section 5.1.3.3) and a crack is initiated in response to an applied stress. Once a crack is formed it runs from one GTR particle to another with little hindrance. The bigger agglomerants of the GTR dispersed phase were unable to bridge the growing crack during tearing and the fracture path proceeds uninterrupted. Thus the tear resistance decreased with increase in dispersed phase size, which increased with GTR content (Figure 5.22). The slow incremental decrease in tear resistance after 70 wt% GTR was again due to the phase inversion of GTR from dispersed to continuous. A similar decrease of tear resistance with increase of rubber content in NBR/PP blends has been reported [106]. In this study, tear strengths were reported against blend compositions varying from 0% to 100% NBR. A negative deviation from the additive line after 30 wt%

rubber was reported. It was concluded that this negative deviation was due to the poor interfacial adhesion between two phases.

5.1.3.5 Impact Properties

The force-displacement curves produced during impact testing of the WPP and selected blends are given in Figure 5.13. The curves represent the impact force experienced at the tip of the falling dart plotted against displacement through the specimen, when the impact test was performed at 20±2 ^{0}C. In this test, the energy involved in the impact is consumed by both the fracture process and the specimen as vibrational energy within the sample [192]. Hence, the blends with different compositions exhibit different failure modes. The variation of failure mode with GTR content is illustrated in Figure 5.14.

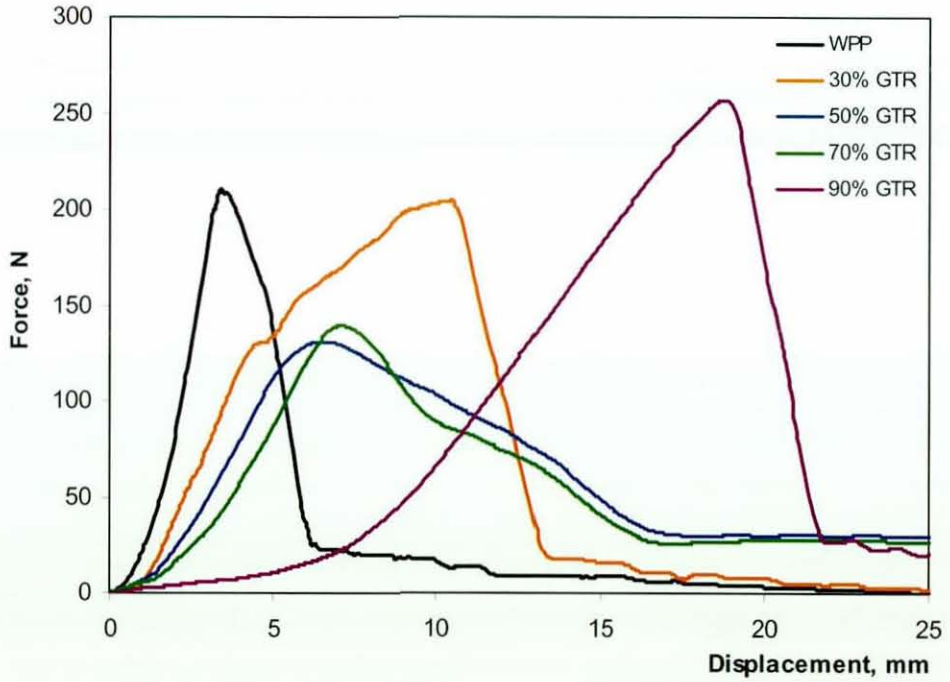

Figure 5.13 Force vs. Displacement (impact loading) for WPP and selected blends

The force-displacement curves in Figure 5.13 show two different types of fracture behaviors. Generally, the fracture process under impact load can be divided into an initiation stage and a fracture propagation stage. During the initiation stage, deformation

takes place until a fracture is initiated. Fracture propagation starts after the fracture has been initiated. In the force-displacement curve, fracture initiation is considered as occur near the force maximum. The WPP and the blends containing GTR up to 40 wt% show a sharp drop in force after a fracture has been initiated. This implies that the additional energy needed for fracture propagation is very low. This type of fracture is referred to as brittle fracture, and is represented by a large hole in the specimen, which was created when the dart passed through the specimen (Figure 5.14). Brittle fracture for the WPP is expected as the testing temperature is below its brittle to ductile transition temperature range (Section 4.1.4.2). For the blends containing more than 40 wt% of GTR, additional energy is needed for fracture propagation, and this fracture is ductile. In this fracture, the dart drew the material out as it passed through the specimen, exhibiting only a crack (Figure 5.14). However, in the case of highly ductile fracture, no clear transition was observed and determination of the beginning of fracture propagation was somewhat arbitrary [192, 237].

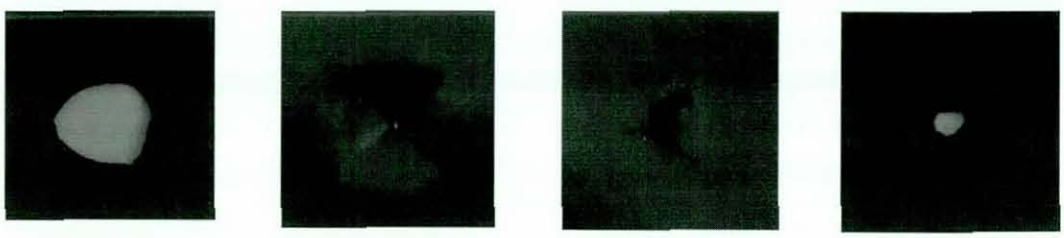

Figure 5.14 Macroscopic images of specimens after impact test for blends having different GTR contents

The impact properties of the WPP and the blends determined from these curves are given in Table 5.5, while the fracture initiation, propagation and failure energies as a function of GTR content are given in Figure 5.15. The impact properties tabled include force needed to initiate a fracture called peak force (F_M), fracture initiation displacement (D_M), fracture propagation displacement (D_P), ductility index, and stiffness. The ductility index is the ratio of fracture propagation energy to failure energy. The stiffness of the blend is given by the initial slope of the force-displacement curve.

The WPP, a semi crystalline polymer, exhibits the high peak force associated with high yield stress, low displacement both at peak force and at failure, and hence high stiffness. Further, it shows higher fracture initiation energy compared to propagation energy, which is associated with the brittle fracture, and thereby provides a low ductility index. A similar brittle fracture due to crazing occur with PP when it subjected to impact loads at room temperature [224, 281].

The addition of GTR into WPP reduces the peak force, but increases the fracture initiation displacement (Table 5.5) resulting in enhanced fracture initiation energy (Figure 5.15). The stiffness as well as the ductility index drop. These variations are ascribed to the presence of relatively soft and flexible GTR particles in the WPP matrix, which lead to absorption of more energy during fracture. Also this probably reflects the longer path of the propagating fracture around the rubber particles [226]. With increase in GTR content up to 40 wt%, (as with the increase of amount and size of GTR agglomerants (Figure 5.22)), the peak force further decreases and the initiation displacement increases, reducing the stiffness of the blends. The impact failure energy gradually increases as a result of increase in initiation energy. The lower propagation energy and hence low ductility correspond to the brittle fracture exhibited by these blends.

With a further increase in GTR content, the larger GTR agglomerants present in the blends absorbed more energy and also blocked fracture propagation, resulting a greater fracture propagation displacement and greater fracture propagation energy compared to initiation energy. As a result, the failure mode changes from brittle to ductile, which is associated with shear yielding (Figure 5.1). The ductility index increases and the stiffness of the blend decreases with the GTR content. However, in this work the resultant failure energy was lower than expected, which is mainly attributed to the poor interfacial adhesions, observed under scanning electron microscopy (Figure 5.12). The poor interfacial adhesion causes premature failure, and the energy dissipated by cavitation is relatively low compared to that dissipated by multiple crazing or shear yielding (Section 2.8.5.2). With the GTR phase inversion from dispersed to continuous, plastic deformation before fracture initiation becomes larger, fracture initiation energy increases rapidly and hence impact failure energy increases rapidly. But, due to the poor cohesion within the GTR phase (Figure 5.22d), the blends with 70 and 80 wt% GTR show a ductile

fracture with a small punch indentation in the specimen. The blend with 90 wt% GTR shows a complete small punch hole.

These results indicate that a certain level of GTR is required to change the fracture from brittle to ductile, thereby improving ductility of the GTR/WPP blend. Otherwise, the WPP predominates and exhibits properties similar to thermoplastics. However, all the blends show higher impact failure energies than WPP. One main reason for the incorporation of rubber into thermoplastics like PP is to improve impact strength and the literature reveals an increase with an increase in rubber content [113, 151, 226, 237]. However, the variation of impact properties against rubber content is not linear, and was specific to each study. Those differences may be due to differences in types of rubbers and testing conditions used. The observed changes in crystallization and melting behaviour of WPP in GTR blends in the present study (Section 5.1.5), although not dramatic, can result in improved impact properties of the WPP phase as compared to pure WPP. The GTR agglomerants can improve the fracture resistance of WPP by varying its crystalline structure (eg. providing spherulite in smaller size due to faster crystallization observed at high GTR contents).

Table 5.5 Impact properties of blends

GTR:WPP	F_M*, N/mm	D_M, mm	D_P, mm	Ductility Index	Stiffness, N/m
WPP	111(7)	4.1(0.2)	2.7(0.2)	0.43(0.03)	47(2)
10:90	106(6)	5.6(0.2)	4.0(0.3)	0.37(0.01)	25(2)
20:80	100(6)	7.0(0.5)	4.4(0.4)	0.35(0.00)	25(2)
30:70	82(3)	7.5(0.6)	5.1(0.4)	0.34(0.03)	23(2)
40:60	70(4)	7.7(0.5)	5.4(0.3)	0.37(0.02)	22(2)
50:50	68(4)	7.0(0.6)	8.9(0.3)	0.55(0.00)	21(2)
60:40	68(5)	6.7(0.5)	10.4(0.7)	0.64(0.01)	21(2)
70:30	79(6)	7.4(0.5)	9.3(0.4)	0.64(0.03)	21(1)
80:20	105(4)	11.1(0.5)	4.4(0.4)	0.41(0.03)	19(1)
90:10	129(5)	18.7(0.5)	3.0(0.5)	0.23(0.00)	14(1)

* *normalized by dividing by the thickness of each specimen*

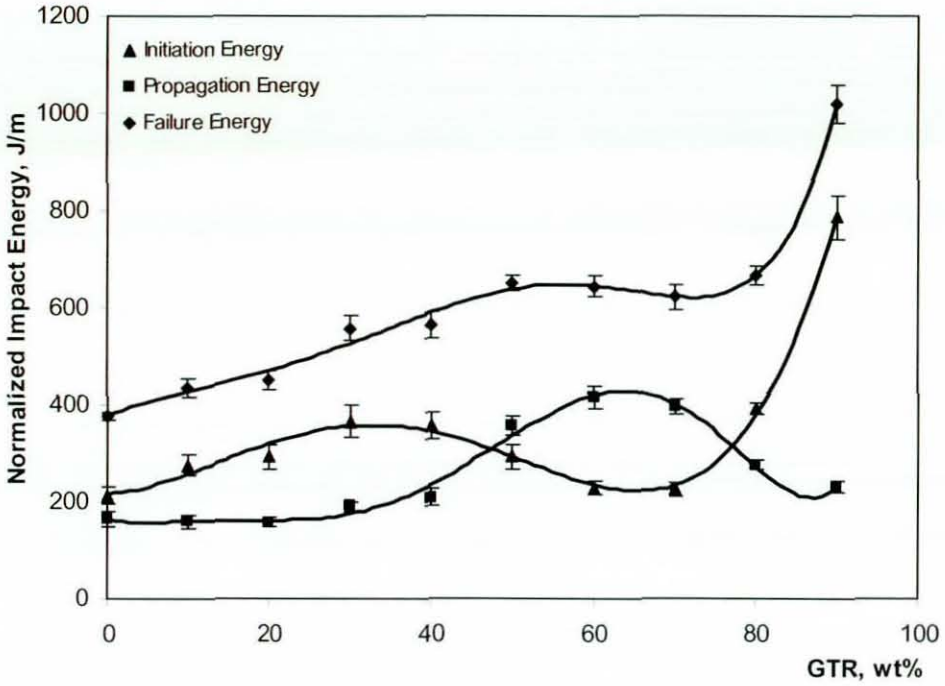

Figure 5.15 Impact energy (normalized by dividing by the thickness of each specimen) vs. Ground tyre rubber content

The mechanical properties discussed above explained that their variation with the blend composition. The hardness, tensile strength, secant modulus and tear resistance decreased with the GTR content while %elongation at break, and impact failure energy increased. These property variations can be related to the variations in dynamical mechanical properties, melting and crystallization behavior, blend morphology and sol/gel characteristics, which are discussed in Section 5.1.4, Section 5.1.5, Section 5.1.6, and Section 5.1.7, respectively.

5.1.4 Dynamic Mechanical Properties

Dynamic mechanical properties of polymers and polymer blends are highly dependent on the material structure [109, 195, 282]. Thus the molecular level changes that occur in a polymer under the application of a sinusoidal stress are reflected in dynamic mechanical measurements. Hence, these properties can be correlated to the variation of the mechanical properties determined.

The variation of the elastic or storage modulus (E′), the loss modulus (E″) and the dissipation or loss factor (tan δ) with temperature for the WPP and a few selected blends are presented in Figure 5.16, Figure 5.17 and Figure 5.18 respectively. Three distinct regions of mechanical behaviour can be observed for WPP: a glassy region, a glass to rubber transition region and a rubbery region. For the blends, the glass to rubber transition region is not separated since the transition regions of the two polymers are overlapping. In the glassy region, at low temperatures the molecular chains are frozen into a rigid network yielding high storage modulus and low loss. In the transition region, as temperature is increased long range motion of chain segments starts to occur leading to a remarkable drop in storage modulus, with a pronounced loss factor peak. This transition represents the α-transition of the polymer. Secondary transitions like β and γ transitions of low magnitudes can also be observed, and are due to some limited micro-Brownian movement either within the main chain or the side groups attached to the chain. The last region is the flow region, where the amorphous chains completely flow and a terminal fall off in modulus is accompanied by a continuous increase in loss factor. Figure 5.16 shows a reduction in modulus with the GTR content over the temperature range studied. This is associated with the presence of more soft GTR regions in the blends and is in agreement with the results of secant modulus (Section 5.1.3.2) and hardness (Section 5.1.3.1) obtained.

Figure 5.17 and Figure 5.18 exhibit two distinct peaks for every blend, indicating immiscibility between the two phases in the blend (Section 2.7). This is in agreement with the microscopic studies (Section 5.1.6), and also a common observation for the blends with recycled-rubber and polypropylene [102, 111]. The peak at lower temperature (around -40 ^{0}C) is associated with the T_g of the GTR phase whereas the peak at higher temperature (around 15 ^{0}C) is that for the WPP. The WPP shows a remarkable peak for its α-transition in the loss modulus curve (Figure 5.17). It also shows a peak with low magnitude at -40 ^{0}C. This small peak having lower activation energy is associated with the secondary β-transition of the WPP. This peak is not observed in other blends as it overlaps with the α-transition peak of the GTR. The glass transition temperature (T_g), which is associated with the α-transition, was taken as the peak in the tan δ curve (Figure 5.18). If it is taken as the peak in the loss modulus curve (Figure 5.17), the T_g of the WPP phase would be about 5 ^{0}C lower. In general, E″ goes through a peak at a slightly lower

temperature than does the tan δ [282]. The obtained T_g values for both phases are given in Table 5.6.

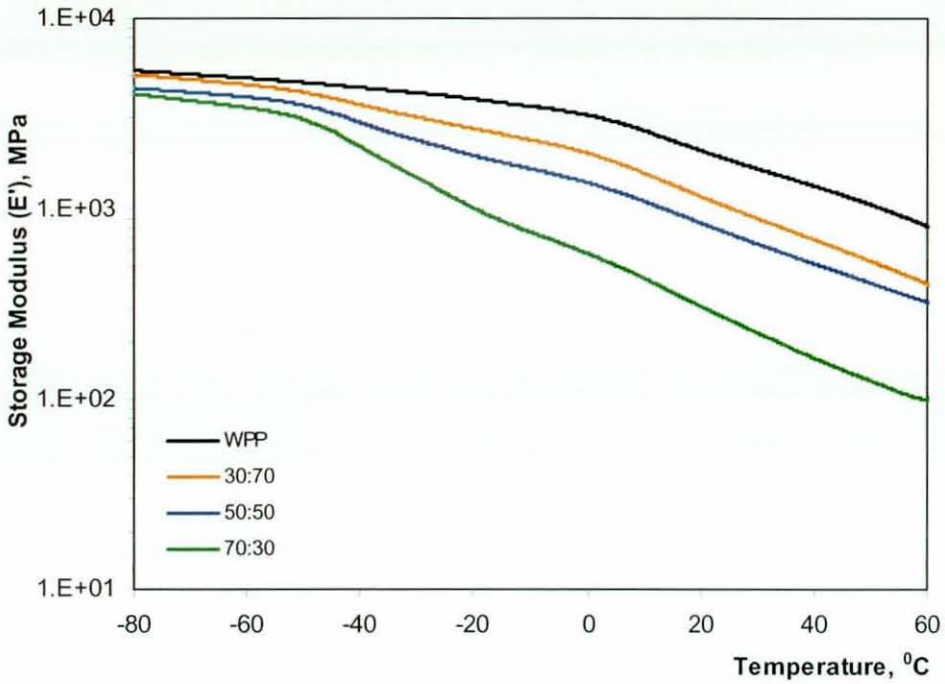

Figure 5.16 Storage modulus vs. temperature for WPP and (GTR:WPP) selected blends

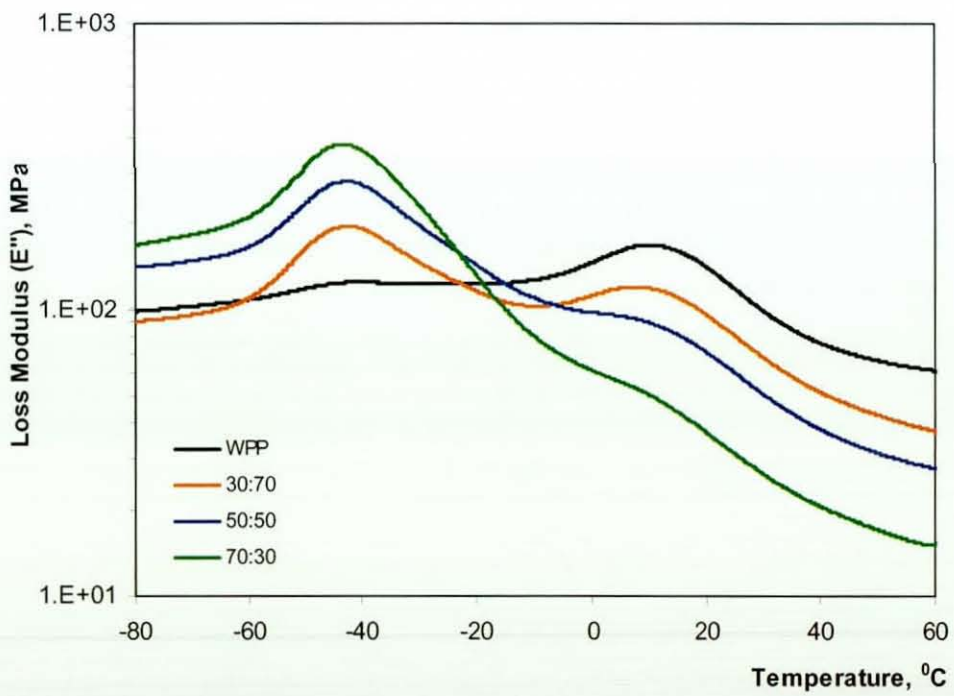

Figure 5.17 Loss modulus vs. temperature for WPP and (GTR:WPP) selected blends

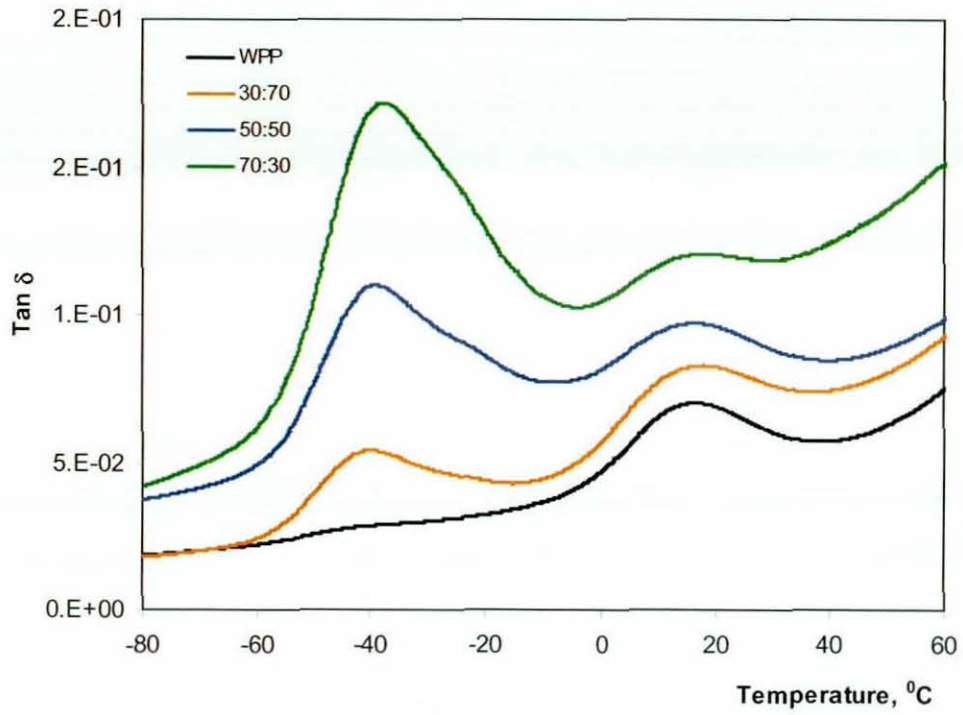

Figure 5.18 Tan δ vs. temperature for WPP and (GTR:WPP) selected blends

The magnitude of the transition peak for the amorphous GTR is much higher than that for the semi crystalline WPP (Figure 5.17 and Figure 5.18), because the chain segments of the amorphous polymer are free from the resistant imposed by the crystalline polymers in the glass transition region [282]. In addition, the magnitude of the transition peak for the specific polymer varies with the content of that polymer present in the blend. Similar observations have been reported previously with waste-rubber/PP blends [102, 112]. With the increase of the specific polymer in the blend, the corresponding glass transition starts at a lower temperature and ends at a higher temperature, broadening that transition (Table 5.6), resulting the T_g of the GTR phase shifts to a slightly lower temperature. However, the T_g of the WPP does not show any variation with the GTR content, indicating no plasticizing effect caused by the GTR on the WPP phase. A decrease in the T_g of PP with rubber content in EPDM/PP blends due to a plasticizing effect has been reported [237]. In those blends, the T_g of EPDM did not change with the rubber content. This may be due to the formation of a copolymer and relatively enhanced compatibility between the two polymers. However, in another study [158], no T_g variation of the HDPE phase with GTR content was shown.

Table 5.6 Glass transition temperatures of each polymer

GTR, wt%	T_g of GTR, ^{0}C	Width of GTR transition, ^{0}C	T_g of WPP, ^{0}C	Width of WPP transition, ^{0}C
0	-	-	15	60
30	-41	52	15	58
50	-40	58	15	50
70	-38	66	15	38
100	-30*	94*	-	-

* see Section 4.2.3

5.1.5 Melting and Crystallization Behaviour

The non-isothermal crystallization conditions approach more closely the industrial conditions of polymer processing, so that the study of crystallization under non-isothermal conditions is of great importance [283]. Therefore the non-isothermal crystallization behaviour of WPP in GTR/WPP blends was investigated by differential scanning calorimetry (DSC) to detect changes in melting and the degree of crystallization. DSC thermograms of the second heating cycle and the first cooling cycle obtained for WPP, and selected blends, are shown in Figure 5.19 and Figure 5.20 respectively. Figure 5.19 displays a major melting endotherm for the WPP phase around 165 ^{0}C, and a second minor endotherm around 125 ^{0}C, which is similar to the melting point PE (Section 4.1.4.1). Characteristic thermal properties of the blends determined from the major melting endotherms are given in Table 5.7. This table also includes some properties extracted from the melting endotherm of the first heating cycle. Whereas the properties determined from the second minor endotherms are given in Table 5.8. Table 5.9 summarises the properties determined from the crystallization exotherms (Figure 5.20). Thermal properties measured during the second heating cycle are a function of the material characteristics and thermal history during the first cooling cycle [260]. Hence, enthalpy of fusion (ΔH_f) and enthalpy of crystallization (ΔH_c) of individual rubber-thermoplastic blends show similar values.

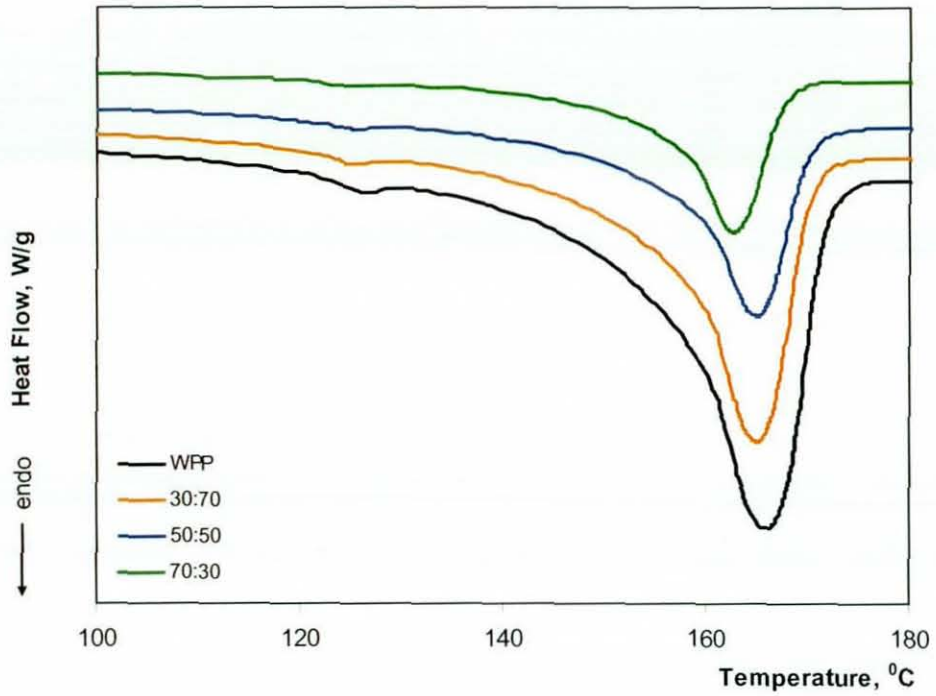

Figure 5.19 Second heating cycle of WPP and selected (GTR:WPP) blends

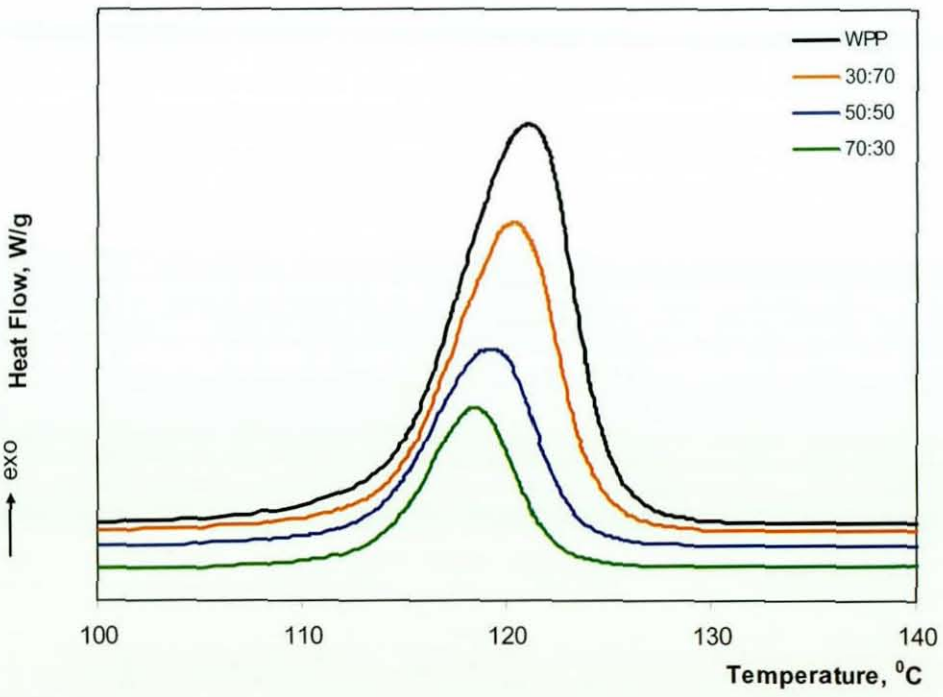

Figure 5.20 First cooling cycle of WPP and selected (GTR:WPP) blends

Table 5.7 Characteristic properties obtained from major melting endotherms

GTR:WPP	$T_{m,}$ ^0C	ΔH_{f1}, J/g	ΔH_f, J/g	%Crystallinity*	
				Blend	WPP phase
WPP	165.8(0.3)	88(2)	93(2)	44(1)	44(1)
10:90	165.5(0.5)	80(3)	86(1)	41(0)	45(0)
20:80	165.0(0.8)	70(3)	77(0)	37(0)	46(1)
30:70	164.9(0.5)	60(1)	65(1)	31(0)	45(0)
40:60	164.5(0.6)	47(3)	56(2)	27(1)	45(1)
50:50	164.2(0.2)	38(3)	46(4)	22(2)	44(4)
60:40	163.4(0.5)	32(2)	38(2)	18(1)	45(2)
70:30	162.7(0.2)	26(1)	30(1)	14(1)	48(2)
80:20	162.0(0.1)	18(1)	20(0)	10(0)	48(0)
90:10	161.8(0.1)	9(1)	11(1)	5(1)	50(3)

**Calculated according to Equations 3.14 and 3.15*

Table 5.8 Characteristics properties obtained from second minor endotherms

GTR:WPP	T_{m2}, ^0C	ΔH_{f2}, J/g
0:100	126.0(0.1)	0.8(0.0)
10:90	125.1(0.0)	0.7(0.1)
20:80	125.9(0.6)	0.7(0.0)
30:70	125.1(0.1)	0.6(0.0)
40:60	125.7(0.1)	0.4(0.0)
50:50	125.0(0.0)	0.4(0.0)
60:40	124.8(0.1)	0.3(0.1)
70:30	124.3(0.0)	0.3(0.0)
80:20	124.3(0.0)	0.2(0.0)
90:10	124.3(0.0)	0.1(0.0)

Table 5.9 Characteristic properties determined from crystallization exotherms

GTR:WPP	T_p, ^0C	T_{co}, ^0C	ΔT, ^0C	ΔH_p , J/g	ΔW, ^0C	ΔH_c, J/g
WPP	121.1(0.2)	130.7(0.4)	35	2.0(0.1)	6.4(0.1)	92(1)
10:90	121.0(0.5)	130.5(0.2)	35	1.9(0.0)	6.3(0.1)	85(3)
20:80	120.8(0.4)	130.5(0.4)	35	1.8(0.1)	5.9(0.3)	74(4)
30:70	120.2(0.3)	129.7(0.2)	35	1.6(0.1)	6.1(0.1)	66(1)
40:60	119.5(0.6)	128.8(0.2)	35	1.2(0.1)	6.0(0.1)	58(3)
50:50	119.5(0.3)	128.8(0.3)	35	1.0(0.0)	5.9(0.2)	46(2)
60:40	118.8(0.5)	127.7(0.1)	35	1.0(0.0)	5.4(0.1)	36(3)
70:30	118.5(0.2)	127.2(0.6)	35	0.8(0.0)	5.0(0.1)	29(2)
80:20	118.1(0.6)	126.6(0.2)	35	0.6(0.1)	4.6(0.1)	19(1)
90:10	118.0(0.5)	126.3(0.2)	35	0.5(0.1)	4.2(0.1)	9 (1)

Figure 5.19 shows that the size of the major transition varies with the content of the WPP in the blend, and that of the minor transition varies accordingly with the content of the PE in the blend. Hence this observation reconfirms the presence of PE in WPP. This figure further shows that the melting temperature for the WPP in the blends (T_m) and the melting temperature at the second endotherm (T_{m2}) decrease slightly, and the transitions narrow, with an increase of GTR content. These shifts in temperature are significant, but are small, and lie within a 4 ^0C temperature range for the major endotherm (Table 5.7) and within a 2 ^0C temperature range for the minor endotherm (Table 5.8). These temperature shifts may be due to the decrease of crystalline content in the blends, which result in a faster melting process. A similar variation was reported for GTR/HDPE blends [158].

Generally, the presence of a rubber can affect the crystallization behaviour, which can be characterized by determining the peak crystallization temperature (T_p), the onset crystallization temperature (T_{co}), the width of half-height of the exotherm (ΔW), the peak height of the exotherm (H_p), and the enthalpy of crystallization. With increase in GTR content, the onset crystallization temperature and the peak crystallization temperature show significant shifts to lower temperatures. The super cooling temperature (ΔT)

remains unchanged (Table 5.9). The super cooling temperature is simply the difference between the melting and the onset crystallization temperatures, and it depends on nucleation and the rate of crystallization [284]. The same super cooling temperature at all GTR contents implies that the induction time for crystallization is not varied with the GTR content in the blend, and demonstrates that neither the rubbers incorporated into WPP nor their additives (carbon black, processing agents, stabilizers, etc) had any significant influence on nucleation of crystallites in WPP.

Similar to the melting transition, the crystallization transition also narrows with an increase in GTR content, but the sharpness of the exotherm decreases (Figure 5.20). The peak height of the exotherm, the width of half-height of the exotherm and the enthalpy of crystallization decrease with increase in GTR content (Table 5.9). The decrease in ΔW indicates a faster crystallization while the decrease in peak height of the exotherm and the enthalpy of crystallization indicate a lower degree of crystallinity with an increase in GTR content. The fall in the above temperatures and also the faster crystallization with increase in GTR content may be due to the low levels of crystalline regions present in the blends. Further, the faster crystallization can be due to stretching of WPP chains which were the result of processing due to the shear action of large rubber particles in the blends at high GTR contents (Figure 5.22). On the other hand the inclusion of a more flexible GTR phase could disturb the packing of the WPP chains [155]. It also has been shown in literature [140] that the addition of the scrap rubber dust result in a less regular spherulite texture with sharp spherulite boundaries in the PP matrix, which is associated with homogeneous nucleation. The nucleation effect of the rubber phase and thereby a further reduction of the spherulite size of the PP matrix phase has also been observed in EPDM/PP blends [237].

The GTR consists of several low molecular weight ingredients (Section 4.2.2.2). These ingredients may migrate to crystalline regions in the WPP during processing. These migrants, as well as defects and voids formed in the crystalline regions during processing, may affect overall crystallization rate, either by decreasing or increasing primary nucleation and/or secondary nucleation. It has been reported [285] that any carbon black present in PP composites promotes heterogeneous nucleation. A nucleation activity could vary with temperature. As a temperature-changing process, the non-isothermal

crystallization is complicated and needs further studies to comment on the variations in crystallization rate.

In general crystallization rate variation can be clearly observed by the relative crystallinity against crystallization time plots (Figure 5.21). The time taken to complete 50% of crystallization, which is also called the half-time of crystallization ($t_{1/2}$), gives a quantitative comparison. The WPP gives a half-time of crystallization as 1 minute. However, it was difficult to compare these rates for the blends prepared in the present study due to variations in both crystalline content and onset crystallization temperature. This plot was used in evaluating the effect of blend composition under isothermal crystallization [259] and in evaluating the effect of cooling rate under non-isothermal crystallization [272, 283, 285]. Curve in this figure exhibit a sigmoid shape indicating a primary crystallization or nucleation during the early stages and a secondary crystallization during the later stages.

The enthalpy of fusion developed in the first heating cycle was varied in the second heating cycle owing to the melting of imperfections or rearrangement of molecules [284]. However, the enthalpy of fusion in both cycles, and hence the degree of crystallinity of the blends shows a decrease with increase in GTR content (Table 5.7), suggesting that the mechanical properties of the blends are governed by the WPP phase. The enthalpy of fusion associated with the second endotherm (ΔH_{f2}) also shows a small decrease with increase in GTR content (Table 5.8). The degree of crystallinity of the WPP phase in the blends remains unchanged up to 60 wt% GTR, but it increases slightly (by approximately 3%) with further increases in GTR content. This is attributed to the change in blend morphology at 70 wt% GTR (Figure 5.22). The change of dispersed GTR phase to continuous phase causes shear induced crystallization, which result in a higher degree of crystallinity in the WPP phase. The decrease in degree of crystallinity of blends with increase in rubber content is a common observation in rubber-thermoplastics blends, whether the rubbers used were virgin or waste [105, 131, 237]. It was reported that the crystallinity of the PP matrix was not at all or slightly affected by the dispersed rubber phase, within the rubber content studied up to 50 wt% [237, 279].

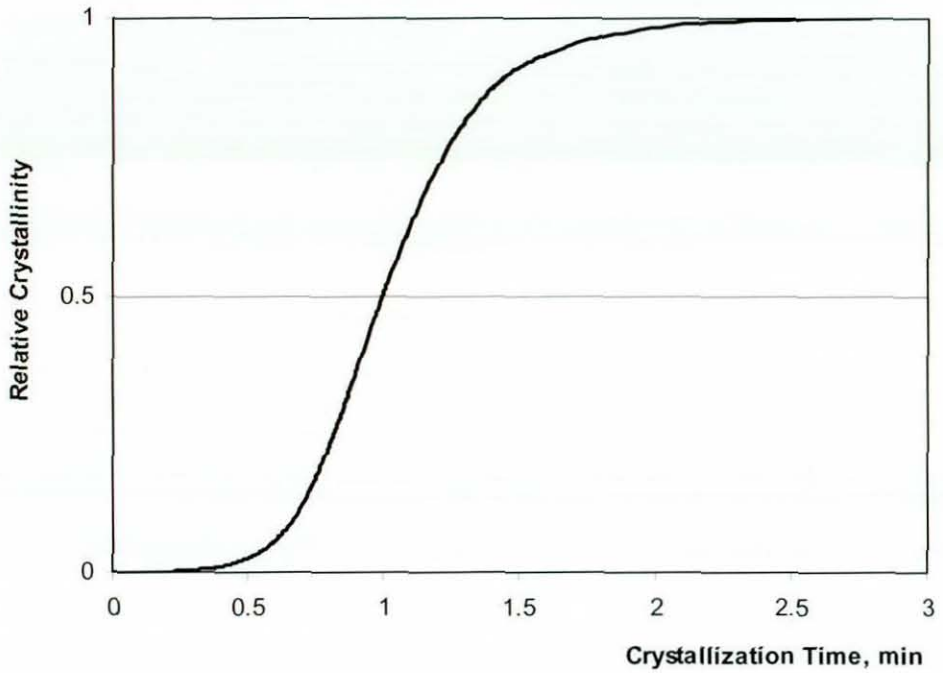

Figure 5.21 Relative crystallinity vs. Crystallization time for WPP

5.1.6 Blends Morphology

Figure 5.22 shows optical micrographs of microtome films of selected blends. These blends show a two phase system as expected. This is due to the incompatibility of the GTR and WPP at the molecular level (Section 2.8.4). The GTR appears black in the micrographs and is easily distinguishable. The blends containing 10 - 50 wt% GTR show GTR as dispersed domains in the continuous WPP matrix phase (Figure 5.22(a)-(c)). This is associated with the relatively higher viscosity of GTR at the processing condition (Figure 5.23and Figure 5.5). If the viscosities were similar, the high volume fraction component will be the continuous phase and the low volume fraction would be the dispersed phase [145]. These micrographs also show GTR particles of different sizes, with the appearance of larger particles increasing with GTR content. This proves that GTR particle agglomeration or coalescence takes place during processing, and that greater agglomeration occurs at higher GTR contents. The micrograph at 70 wt% GTR shows a separation of the WPP from the GTR phase, and a change in GTR phase morphology from dispersed to continuous (Figure 5.22(d)). It was not possible to prepare microtome films from the blends containing 80 - 100 wt% GTR due to the removal of

tiny particles, during sectioning. The occurrence of coalescence and the formation of co-continuous phase morphology at higher rubber concentrations have been previously reported for virgin rubber-thermoplastic blends [104, 106].

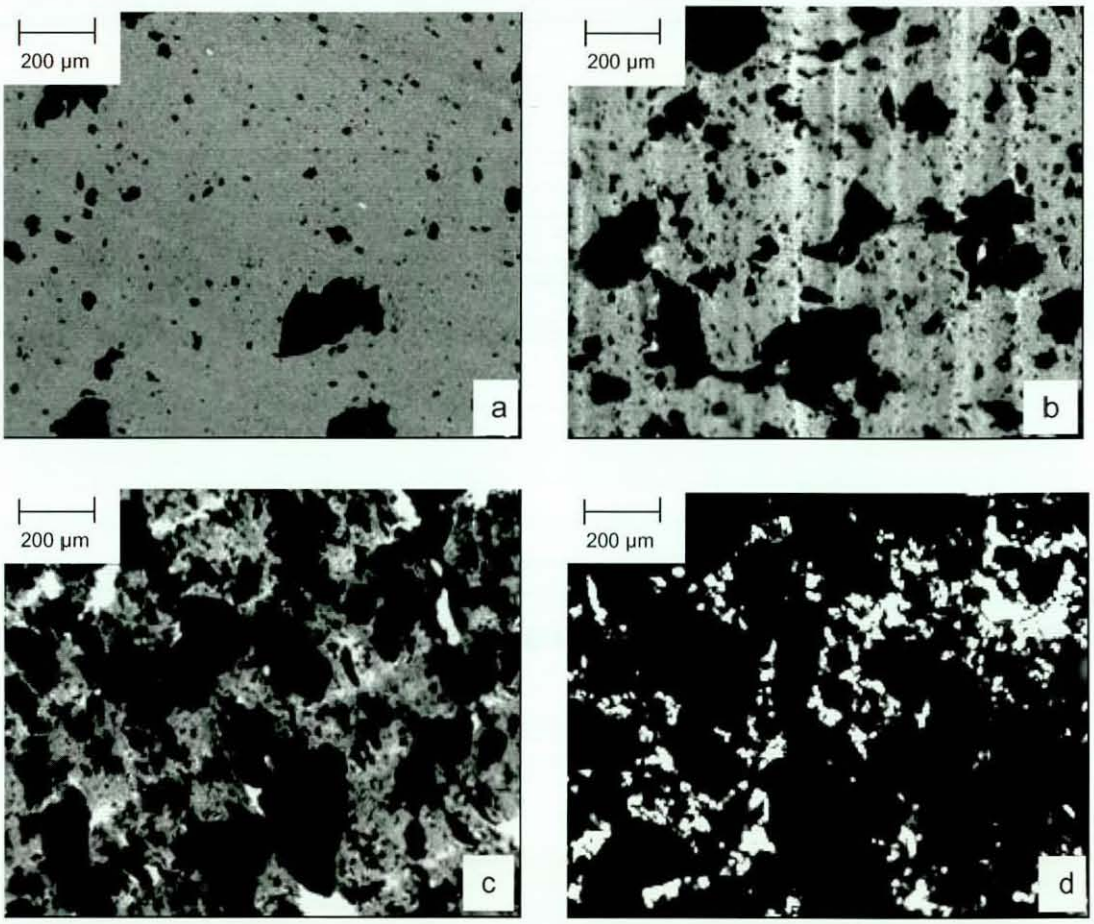

Figure 5.22 Optical micrographs of WPP and GTR:WPP/180/3/8 Blends

(a) 10:90 (b) 30:70 (c) 50:50 (d) 70:30

5.1.7 Sol/gel Characteristics

The swelling index (Equation 3.16) and the %solvent extraction residue (Equation 3.17) depend on the blend structure. The WPP neither dissolved nor was swollen in toluene and hence the swelling index and the %solvent extraction residue remain unchanged for the blends with low GTR contents (Figure 5.23). With an increase in GTR agglomerates with

increase in GTR content (Figure 5.22), the swelling index increased and the soluble components in the GTR migrated to the toluene thus decreasing the %residue. With the GTR phase inversion at 70 wt% GTR, the swelling index increased rapidly. Variations of these two properties are in agreement with the variations in mechanical properties observed. An increase in swelling index with waste tyre dust (WTD) content, up to 60 wt% , in WTD/PP blends has also been reported previously [116, 200].

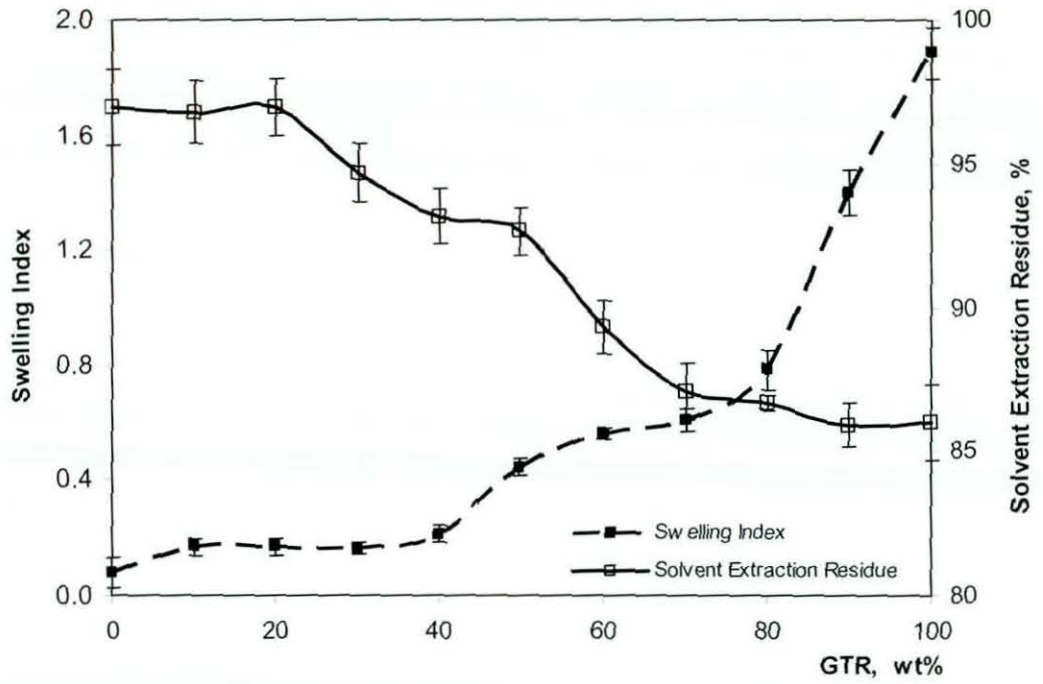

Figure 5.23 Swelling index and solvent extraction residue vs. Ground tyre rubber content

5.1.8 Infrared Spectroscopy

Figure 5.24 shows the FTIR spectrum acquired for the 50:50/180/30 blend, with the spectra for GTR and WPP. The spectrum of the blend shows a combination of peak assignments acquired from the individual spectra of the GTR and the WPP. It has been shown that IR spectrum of multiphase systems are a summing of the spectra of individual constituents [269]. Hence, this observation confirms that the blend prepared for this study is a two phase system.

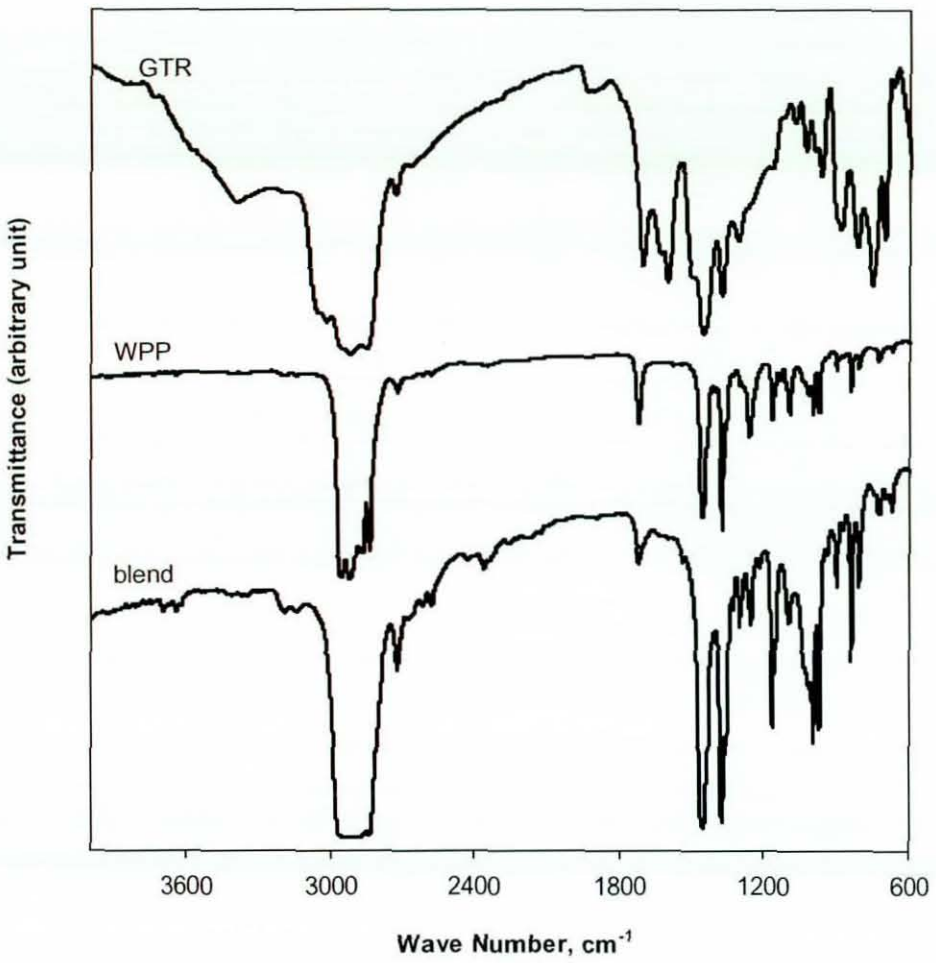

Figure 5.24 FTIR spectra of GTR, WPP and 50:50/180/30 blend

5.2 Effect of Process Parameters

The results of the blend composition study showed that the GTR/WPP blend was a two phase system and indicated the immiscibility between the two polymers. Further, the non-melting behaviour of GTR during processing has been shown. The GTR behaved like a filler. Therefore, improvements in the miscibility of polymers in the GTR/WPP blend cannot be expected by optimizing the processing parameters, although the miscibility is a function of thermodynamic variables (Section 2.5.2).

The quality of a blend depends on the mixing efficiency [122]. Distributive mixing provides homogeneity of the blend while dispersive mixing improves the interactions of

the two phases due to a reduction in dispersed phase size [191]. Not only that, shear induced phase adhesion is also expected by varying the thermo-mechanical stresses acting on the polymers in the blend. Stronger interfacial adhesions in an immiscible blend improve blend compatibility (Section 2.5.4).

The effect of the blend composition study, however, showed that the specific process conditions used were insufficient to promote shear induced phase adhesion. Shear stresses applied to the melt can vary with processing temperature and rotor speed variations. Time of mixing may also influence the level of applied thermal heating and mechanical shear stresses in the melt.

The process conditions considered for this study were therefore processing temperature, processing speed, processing time and mixing schedule. Blends were prepared at different process conditions (Table 3.2 and Table 3.3), according to the method described in Section 3.2.3.2. Process conditions were optimized by analyzing the torque during mixing and the tensile properties of the resultant blends for the specimens prepared as described in Section 3.6.2.

5.2.1 Processing Temperature

5.2.1.1 Processing Characteristics

The melt mixing behavior of 50:50 blends processed at different temperatures were investigated. Rotor speed and processing time were kept constant as 30 rpm and 5 minutes, respectively. Figure 5.25 and Figure 5.26 illustrate the torque development curves and temperature development curves for selected blends, respectively. Three curves for the blends processed at 170 ^{0}C, 180 ^{0}C and 210 ^{0}C show a sudden increase followed by a gradual reduction in torque (Figure 5.25). With further increase in time, a steady state torque was noticed. However, the blend processed at 160 ^{0}C did not show a sudden reduction in torque within the time period but a lower steady state torque with temperature increase. Variations in processing characteristics with temperature for all blends are given in

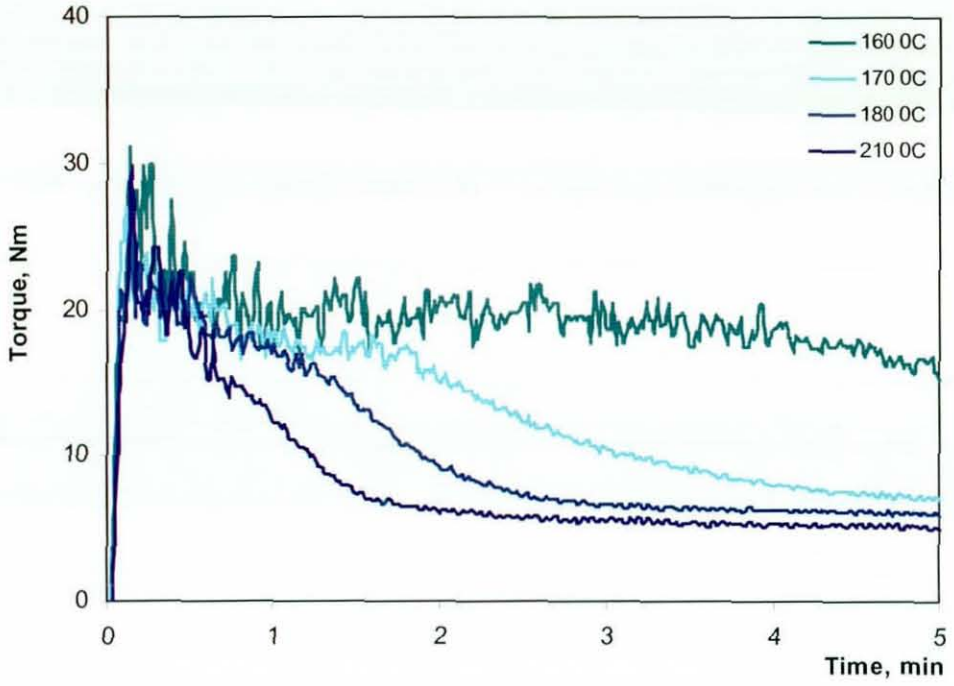

Figure 5.25 Torque-time curves for 50:50 blends processed at different temperatures

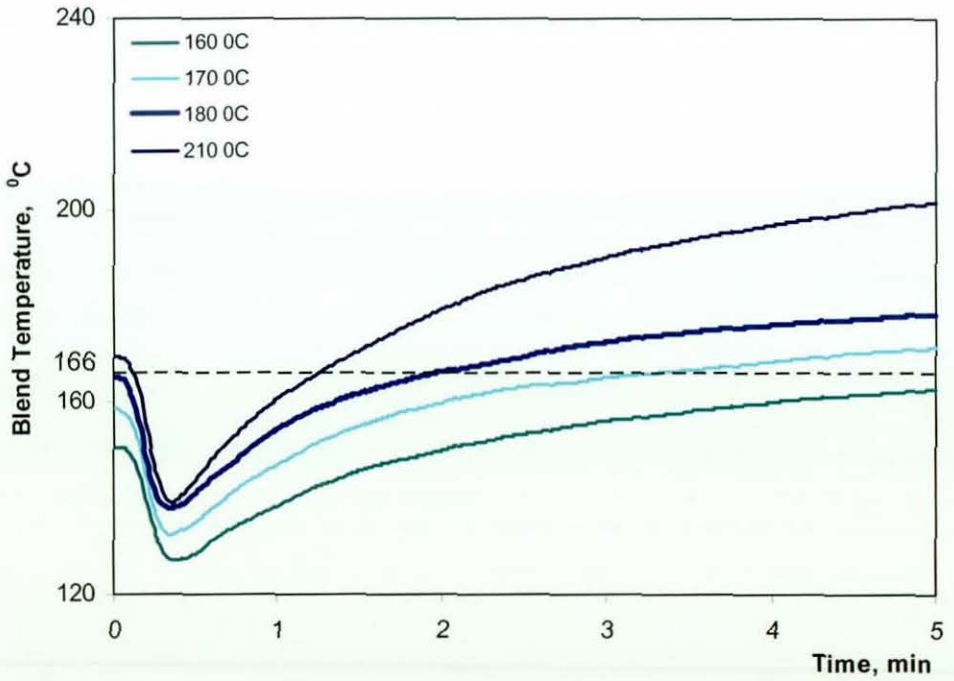

Figure 5.26 Temperature-time curves for 50:50 bends processed at different temperatures

Table 5.10 Processing characteristics of 50:50 blends processed at different temperatures

Sample Code	T_{max}, Nm	T_{ss}, Nm	Time to reach T_m of WPP, min	Specific Energy, J/g
50:50/160/30/5	26.8(0.5)	14.5(1.2)	>5(0.1)	351(17)
50:50/170/30/5	24.8(0.4)	7.7(0.6)	3.3(0.1)	252(5)
50:50/180/30/5	23.5(0.7)	6.0(0.2)	1.8(0.1)	202(4)
50:50/190/30/5	22.5(0.4)	5.8(0.0)	1.4(0.1)	182(9)
50:50/200/30/5	22.8(0.5)	5.2(0.1)	1.4(0.0)	148(10)
50:50/210/30/5	22.5(0.7)	4.8(0.3)	1.3(0.0)	154(4)

The maximum torque decreases with increase in temperature up to 180 ^{0}C. Thereafter no significant variation of this torque is noticed. The greater maximum torques at lower temperatures are due to the higher viscosities of the blends at those temperatures. This observation is supported by the blend temperature development curves obtained during processing (Figure 5.26). These curves show a decrease in blend temperature at the beginning, followed by a gradual increase towards a plateau. The temperature drop is similar for all blends, but at lower processing temperatures the value reached is lower, viscosity higher and torque therefore higher. Further, the maximum torque and the minimum blend temperature exhibit a linear relationship (Figure 5.27).

Steady state torque relates to the viscosity of the resultant blend and hence it can be used to explain the processability of the blend [110]. The blend temperature of the blend processed at 160 ^{0}C does not exceed the melting temperature of the WPP (166 ^{0}C) (Figure 5.26). Hence, due to the very high viscosity of the WPP phase, a greater increase in steady state torque is observed at 160 ^{0}C processing temperature. The other blends exceed the melting temperature of the WPP during processing. The viscosity of the WPP phase decreases with an increase in blend temperature and hence the viscosity of the resultant blend decreases accordingly. This results in a lower steady state torque at higher processing temperature. As expected, an intense reduction in viscosity at higher temperatures was not observed. The WPP cannot be degraded when using the processing

conditions used in the present study as the degradation of WPP starts at 230 ^{0}C under normal atmosphere (Section 4.1.4.3). These results suggest that fast processability can be obtained at higher processing temperatures.

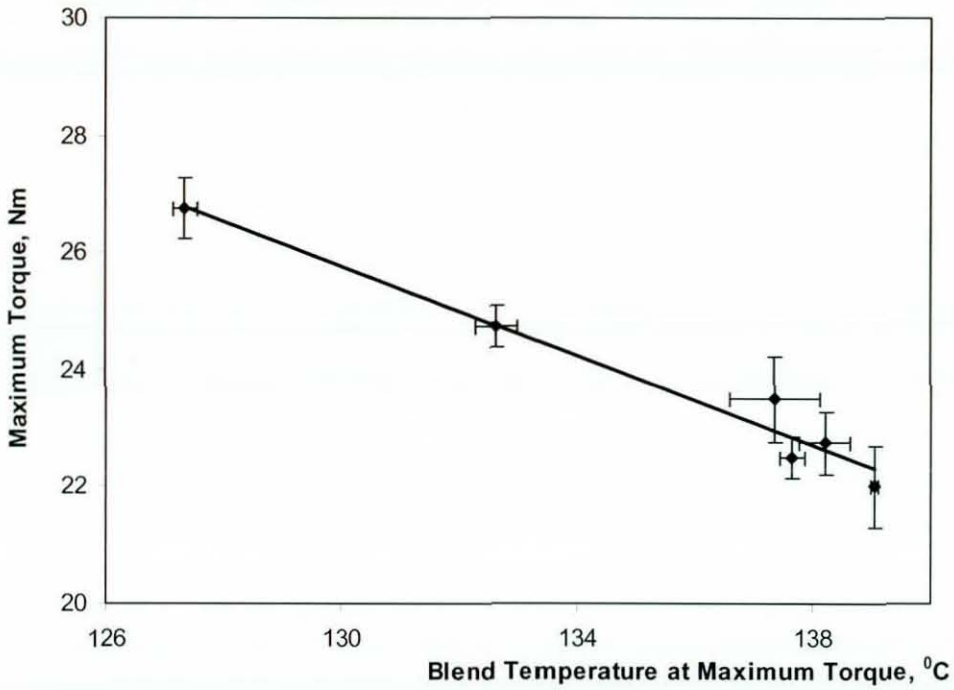

Figure 5.27 Maximum torque vs. blend temperature for 50:50 blends processed at different temperatures

As expected, the specific energy requirement decreases with the increase in processing temperature. This is associated with the greater reduction in torque during the early stage of mixing and the lower steady state torque at higher processing temperatures (Table 5.10).

5.2.1.2 Tensile Properties

The tensile properties obtained with a 50:50 blend processed at different temperatures are given in Figure 5.28. Although the tensile strength variation is small, the highest tensile strength was obtained for the blend processed at 180 ^{0}C. The highest elongation at break was also obtained at 180 ^{0}C and 190 ^{0}C. These tensile property variations can be explained by reference to the blend temperature development curves (Figure 5.26).

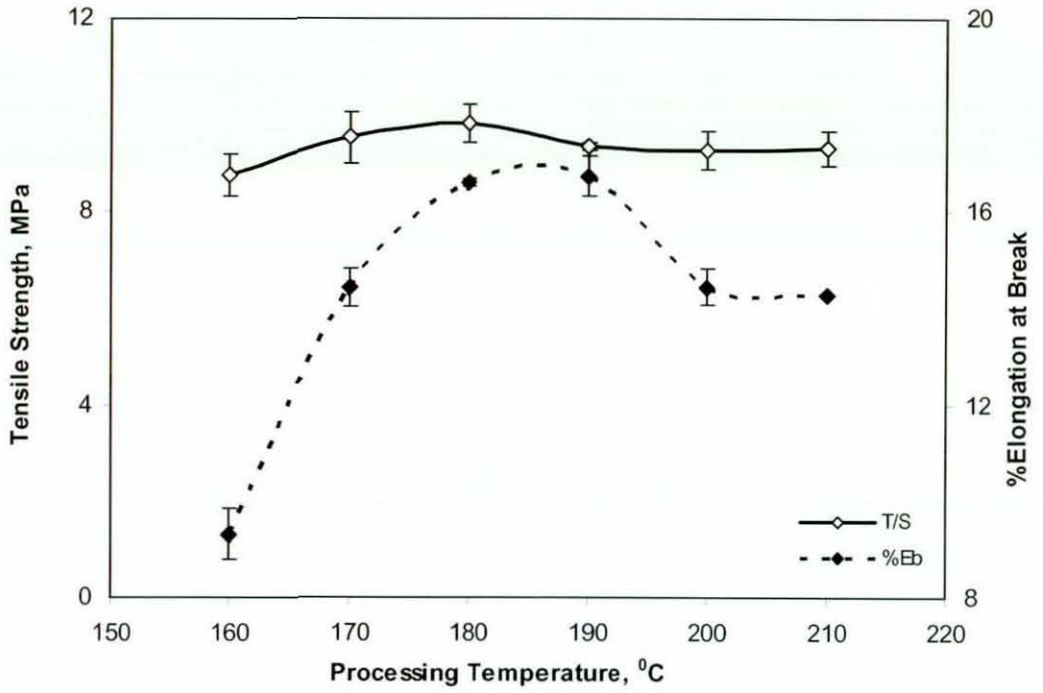

Figure 5.28 Tensile properties vs. processing temperature

In general, during melt mixing, materials commence mixing with each other when they reach their melting temperatures [191]. As the GTR does not melt at the processing temperatures, and is a particulate solid, mixing commences when the melting temperature of the WPP is reached. Table 5.10 shows that the time taken to reach the melting temperature of WPP decreases with an increase in processing temperature. Hence, the effective mixing time will increase with an increase in processing temperature, resulting in a higher degree of distributive mixing [191]. The low viscosity associated with a fast reduction in torque produces a high melt viscosity ratio at the early stage of mixing and hence dispersive mixing will not occur at higher processing temperatures. Further, at higher temperatures, the molten WPP may promote GTR particle agglomeration in a similar way to particulate filler agglomeration in thermoplastics [122, 126, 184]. In addition, GTR will degrade at higher processing temperatures [122, 286], since its degradation starts at 200 ^{0}C under normal atmosphere (Section 4.2.4). Because of the above reasons, the blends processed at higher temperatures show poor tensile properties. Due to insufficient effective mixing time, the blends processed at lower temperatures also show poor tensile properties. This is clearly shown in Figure 5.29, which shows the variation of tensile properties with an effective mixing time. The optimum tensile

properties were observed at an effective mixing time of 3.2 minutes, which corresponded to 180 ^{0}C. A similar trend in variation of tensile properties was reported in a study blending LLDPE and NR [100]. The optimum process temperature in that study was reported as 135 ^{0}C, which is little above the melting point of LLDPE.

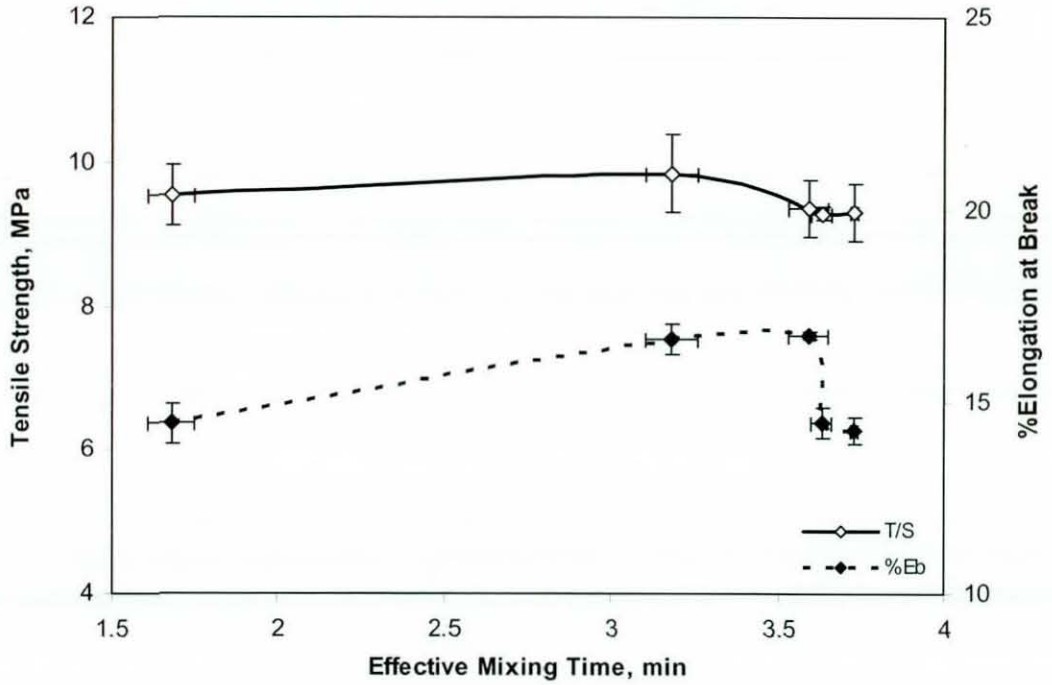

Figure 5.29 Tensile properties vs. effective mixing time

5.2.2 Processing Speed

5.2.2.1 Processing Characteristics

Torque development curves for 50:50 blends processed at a constant temperature of 180 ^{0}C and at selected rotor speeds are given in Figure 5.30. Processing time was kept constant at 5 minutes. These curves show similar trends to previous studies, but the torque at the initial stage of mixing reduces rapidly with increase of rotor speed. The blend temperature developments for selected blends are shown in Figure 5.31. This figure shows that the blend temperature at a specific time increases with increase of rotor speed. Table 5.11 summarizes the processing characteristics of the blends obtained at different

rotor speeds. Figure 5.32 shows the variation of steady state torque, and final blend temperature, with rotor speed.

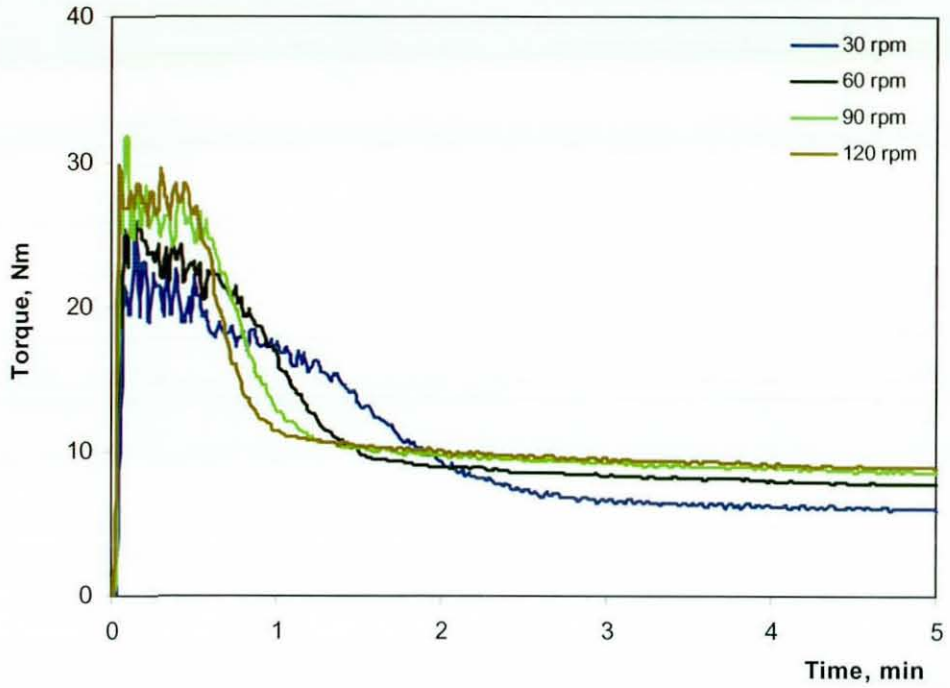

Figure 5.30 Torque-time curves for 50:50 blends processed at different rotor speeds

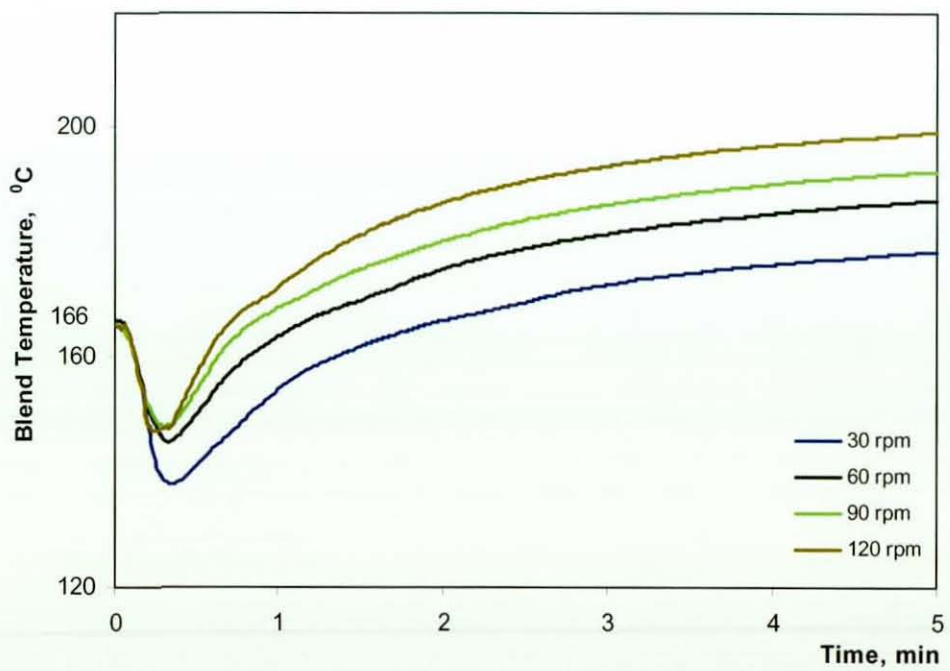

Figure 5.31 Temperature-time curves for 50:50 blends processed at different rotor speeds

Table 5.11 Processing characteristics of 50:50 blends processed at different rotor speeds

Rotor Speed, rpm	T_{max}, Nm	Specific Energy, J/g
15	23.7(1.2)	118(11)
30	23.9(1.2)	202(14)
45	24.3(0.1)	366(13)
60	25.5(0.6)	426(18)
75	25.5(0.4)	544(12)
90	26.5(1.4)	608(16)
105	26.5(0.4)	771(10)
120	27.5(0.5)	922(15)

Generally, the surface velocity of the rotors and hence the shear rate generated increases with increase of rotor speed [278]. Therefore, due to increase of both shear rate and blend temperature, blends processed at high rotor speeds showed faster reductions in torque during the initial stage of mixing. Due to the higher shear stresses generated at higher rotor speeds during the loading of polymers, maximum torque slightly increases with increase of rotor speed (Table 5.11). As expected, the specific energy requirement increases with rotor speed, as given in Equation 3.2. This implies that processing at a lower rotor speed is more economical and energy saving.

According to the Power Law for both Newtonian and non-Newtonian fluids, shear stress increases with shear rate [287, 288]. This relationship is linear for Newtonian fluidsThe apparent viscosity is given by the gradient of the shear stress versus shear rate curve. Figure 5.32 also shows an increase in steady state torque with an increase in rotor speed. Further, a negative deviation from linearity is shown at higher rotor speeds. Torque, and rotor speed, is directly proportional to the shear stress, and the shear rate, respectively. This implies that the 50:50 blend shows a characteristic non-Newtonian psuedoplastic behavior, and hence indicates the processability of blends as thermoplastics [125]. The viscosity reduction is also indicated by the increase in steady state blend temperature with rotor speed.

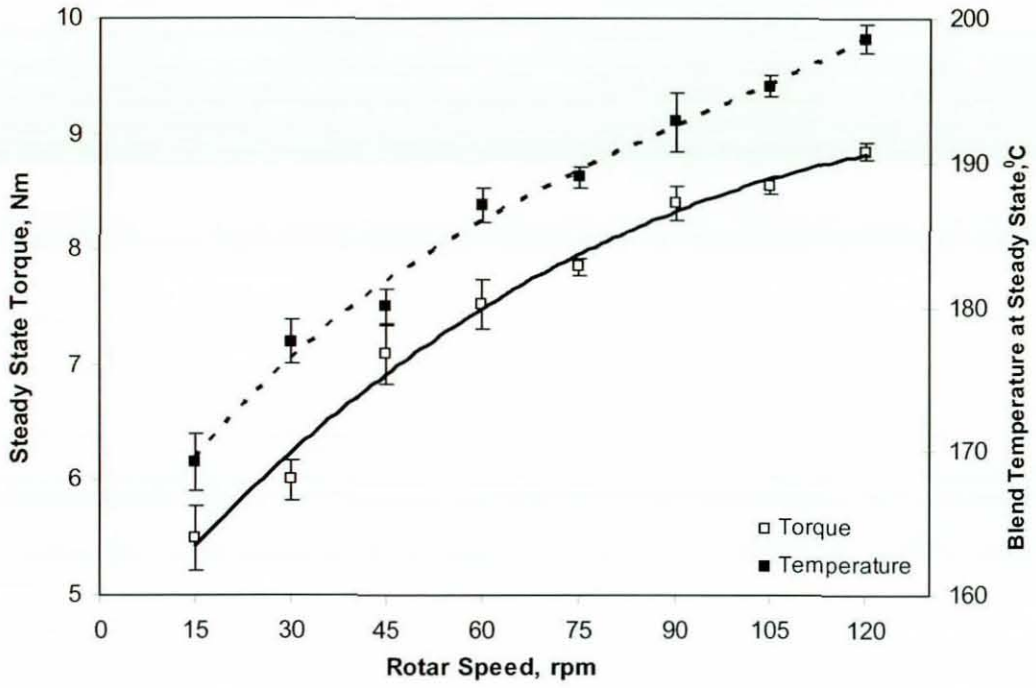

Figure 5.32 Torque and blend temperature at steady state vs. rotor speed

5.2.2.2 Tensile Properties

Figure 5.33 shows the variation of tensile strength, and % elongation at break, with rotor speed. Although the properties do not significantly vary, both show a small increase followed by a decrease with increase in rotor speed, passing through an optimum point at 90 rpm.

The effective mixing time increases with increase in rotor speed (Figure 5.31), in a similar way to the increase with processing temperature (Section 5.2.1.1). This shows that a higher degree of distributive mixing is achieved at higher rotor speeds. The GTR agglomerants will break up at the early stage of mixing under intense stress fields during flow [191, 278]. Hence, the degree of dispersive mixing at the early stage of mixing is greater at higher rotor speeds. This increased degree of dispersive mixing can be lowered with the agglomeration of like particles which occurs at higher mixing speeds for excessive time [289]. This influence is also associated with a decrease in WPP viscosity

with rotor speed (Section 5.2.2.1). These factors suggest that the mixing efficiency will be at an optimum at a certain mixing rate [100].

The GTR particles contain reactive sites on their surface, which were formed during the grinding processes [111, 113]. These active sites may react with free radicals formed in WPP during high shear mixing. Further, the curatives present in the GTR, which were not reacted in the previous vulcanization processes, may also come to the surfaces of the GTR particles during high shear mixing [133]. These ingredients aid bonding with WPP, improving the adhesive strength of the blend. Alternatively, they may form crosslinks within the GTR phase, improving the cohesive strength of the blend. As a result, the tensile properties of the blend may be increased. This degree of phase adhesion and cohesion depends on the amount of new active sites formed and finally on the degree of dispersive mixing. This explanation would be consistent with the gradual increase in steady state torque with increase in rotor speed.

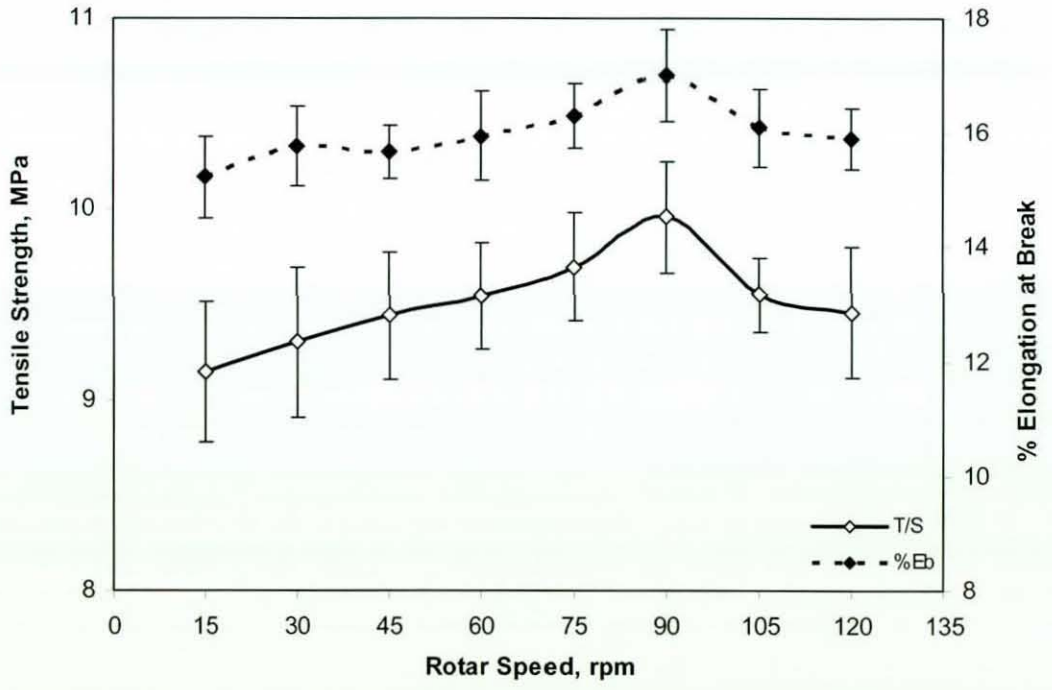

Figure 5.33 Tensile strength and elongation at break vs. rotor speed

5.2.3 Processing Time

5.2.3.1 Processing Characteristics

Figure 5.34 shows typical curves of torque and blend temperature developments for the 50:50/180/90/16 blend. This figure shows a gradual but slight decrease in torque with time, indicating a degradation of either the GTR phase or WPP phase or both. The blend temperature does not show a decrease with extended time of processing and it reaches a plateau. Degradation of rubbers and PP at higher processing times has been reported [100, 122], when they were processed at a higher temperature under a higher mixing speed. The degradation behaviour of the 50:50 blends is clearly exhibited in Figure 5.35. The linear decrease of torque against blend temperature, changes to a rapid decrease after 190 ^{0}C. A similar, but relatively small, decrease was noticed at higher processing temperatures, when mixing at a lower speed for a shorter processing time.

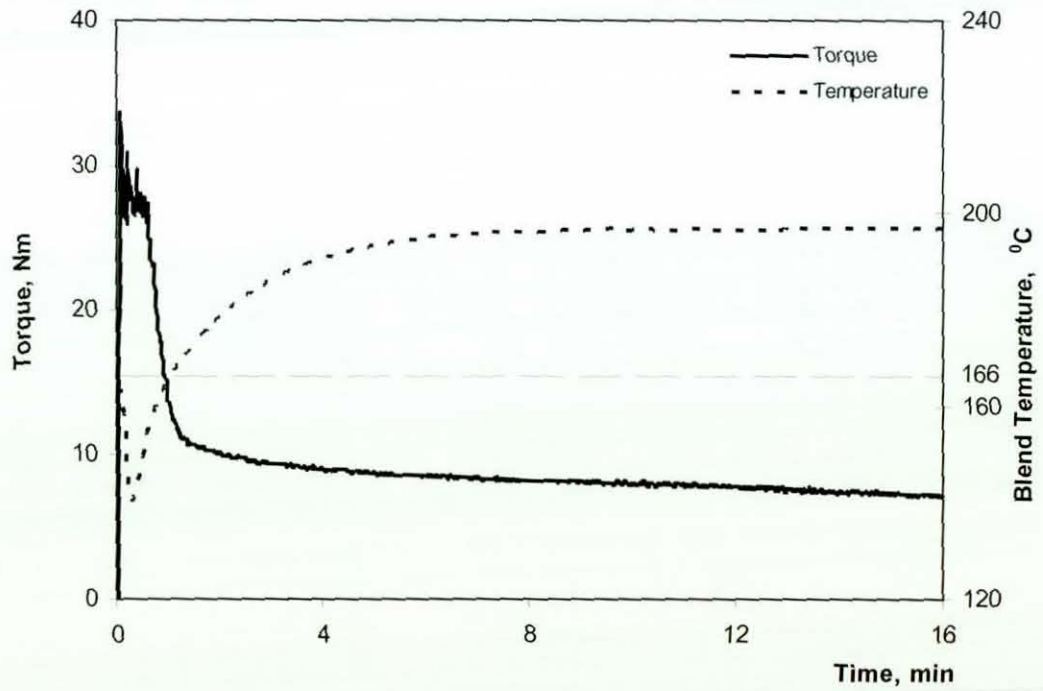

Figure 5.34 Torque and temperature vs. time for a 50:50/180/90/16 blend

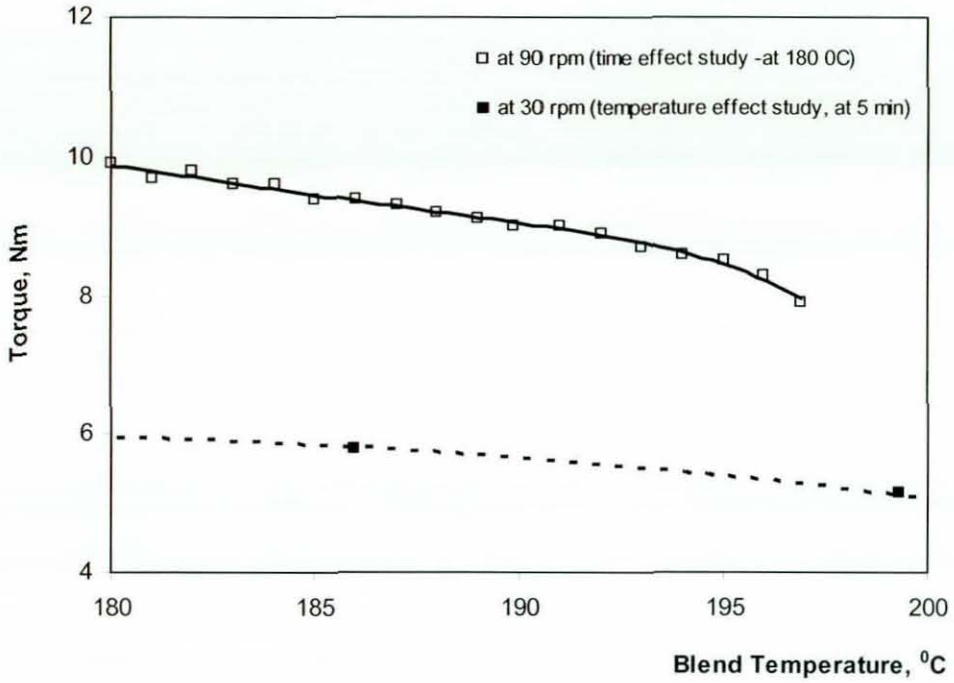

Figure 5.35 Torque vs. Blend temperature

5.2.3.2 Tensile Properties

Figure 5.36 shows the variation of tensile strength and elongation at break with processing time. The degree of distributive mixing increases with increase in processing time, improving the homogeneity of the blend. But the degree of dispersive mixing will decrease due to GTR agglomeration which occurs at increased processing times, even at low processing temperatures. The coalescence of like particles during mixing for longer times is a common observation for polymer blends [184, 191]. Mixing efficiency is a compromise between distributive mixing and dispersive mixing, when related to the processing time, and hence, the best tensile properties were observed at 5 minutes processing time. The blends processed for 2 minutes show poor properties due to improper mixing. The blend temperature at 2 minutes was only 176 ^{0}C, which is only 10 ^{0}C greater than the melting temperature of the WPP. These results clearly show that, optimum blend properties can be obtained at a certain processing time, processing temperature and a processing speed. However, processing at a higher temperature and at

lower rotor speed for shorter time is more economical when consideration is given the specific energy required when processing 50:50 blends.

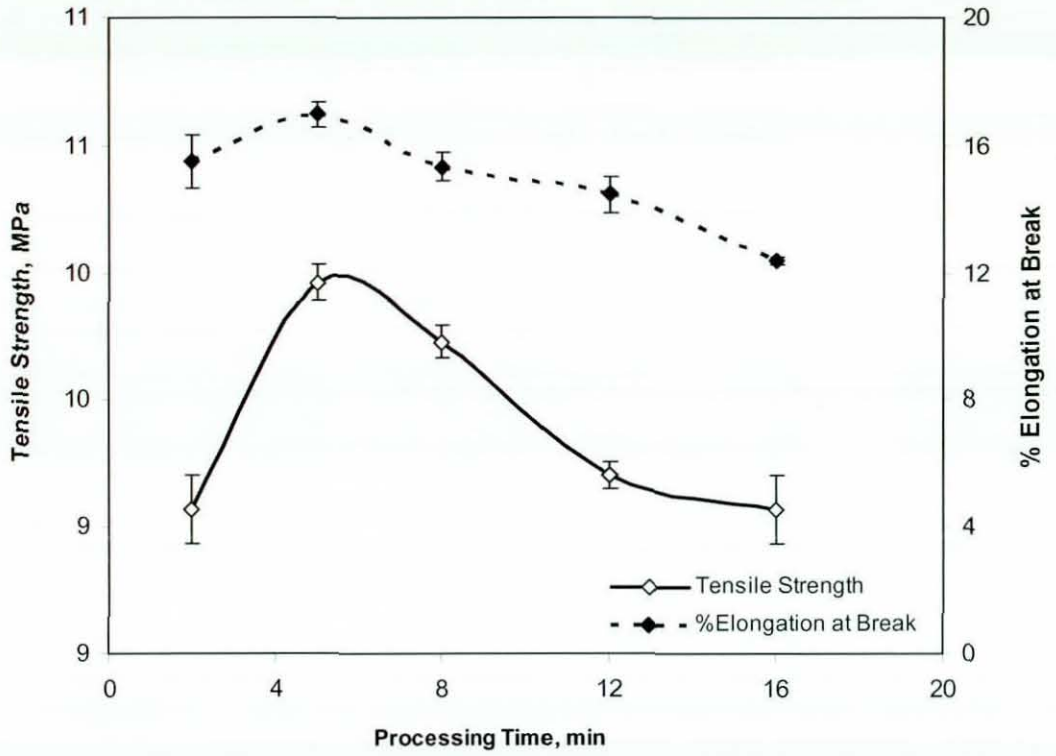

Figure 5.36 Tensile strength and elongation at break vs. processing time

5.2.4 Mixing Procedure

5.2.4.1 Processing Characteristics

The mixing procedure was evaluated using three 50:50blends. In one blend (50:50/90/180/8P), WPP was added first while in the second blend (50:50/90/180/8R), GTR was added first. The third blend was prepared by feeding both polymers together (50:50/90/180/8). Figure 5.37 and Figure 5.38 exhibit the torque developments and blend temperature developments for the blends processed with the different mixing procedures. Torque development for the 50:50/90/180/8 blend was described in Section 5.1.1.1. In contrast to that torque development, Figure 5.37 exhibits two maxima in torque for the 50:50/90/180/8P blend. Only a single maximum torque is exhibited for the

50:50/90/180/8R blend. However, all three blends show the same level of torque after processing for 8 minutes.

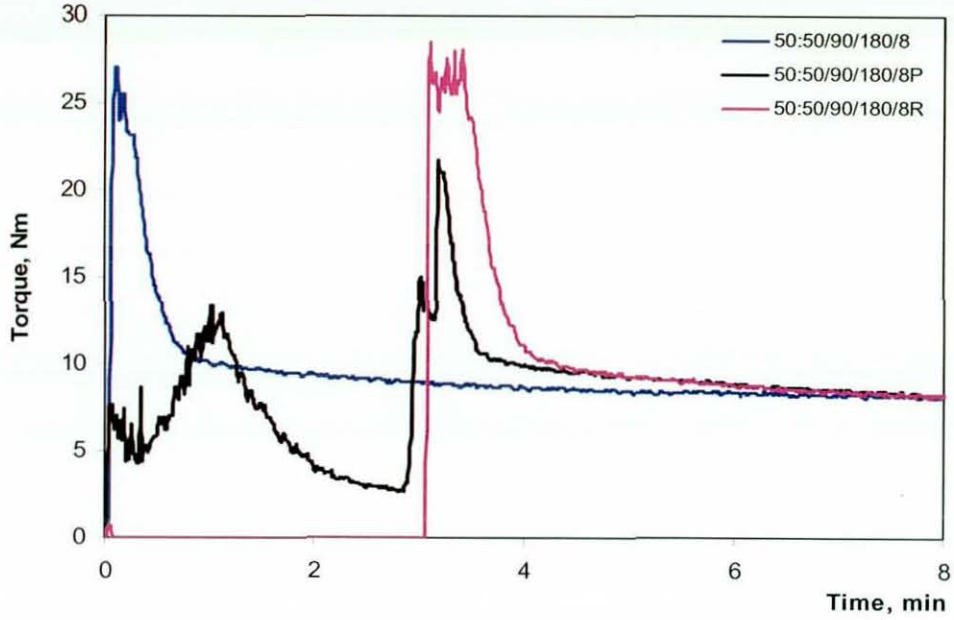

Figure 5.37 Torque-time curves for 50:50 blends processed with different mixing procedures

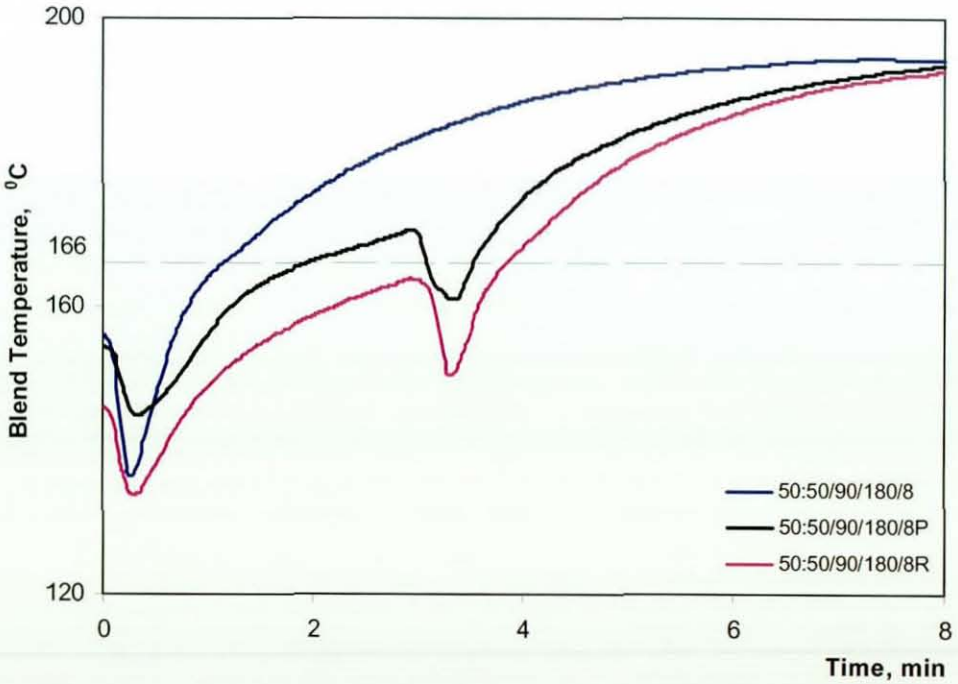

Figure 5.38 Temperature-time curves for 50:50 blends processed with different mixing procedures

The torque development of the 50:50/90/180/8P blend can be explained as follows. The first peak relates to the loading with WPP, while the second peak relates to that of GTR loading. The first peak appeared after a relatively long time compared to the peak for the 50:50/90/180/8 blend. This is because the WPP, which is in pellet form, will first roll over the rotors generating lower torques until it softens [290]. The first peak, compared to the second, shows a lower torque. The low value of the first peak is due to the low resistance exerted on the rotors due to the chamber being partially filled. When the GTR portion is added, the chamber volume is filled and hence the resistance exerted on the rotors by the polymer inside the chamber is high. As a result, the torque is high which corresponds to the second peak being higher. Similar torque developments were reported when blending rubber and thermoplastics in an internal mixer [89, 110].

The torque development for the 50:50/90/180/8R blend shows only one peak. This peak relates to the loading of the WPP. There is no torque exhibited when loading GTR which may be due to both the low volume of GTR in the chamber and its particulate nature.

5.2.4.2 Tensile Properties

Figure 5.39 gives the tensile properties of the blends processed using different mixing procedures. It also includes the tensile properties of the 50:50/180/90/5 blend, for comparison. The blends in which the polymers were added in two steps showed similar effective mixing times (Figure 5.39), and hence showed similar properties. The effective mixing time of the 50:50/180/90/5 blend was similar to the two step blends, and hence all three blends show similar elongations at break. The blends in which both polymers were added together showed slightly greater tensile strengths. But the elongation at break of the 50:50/180/90/8 blend falls due to degradation. These results suggest that the single step adding procedure is more effective. They also suggest that the processing sequence has no effect on tensile properties.

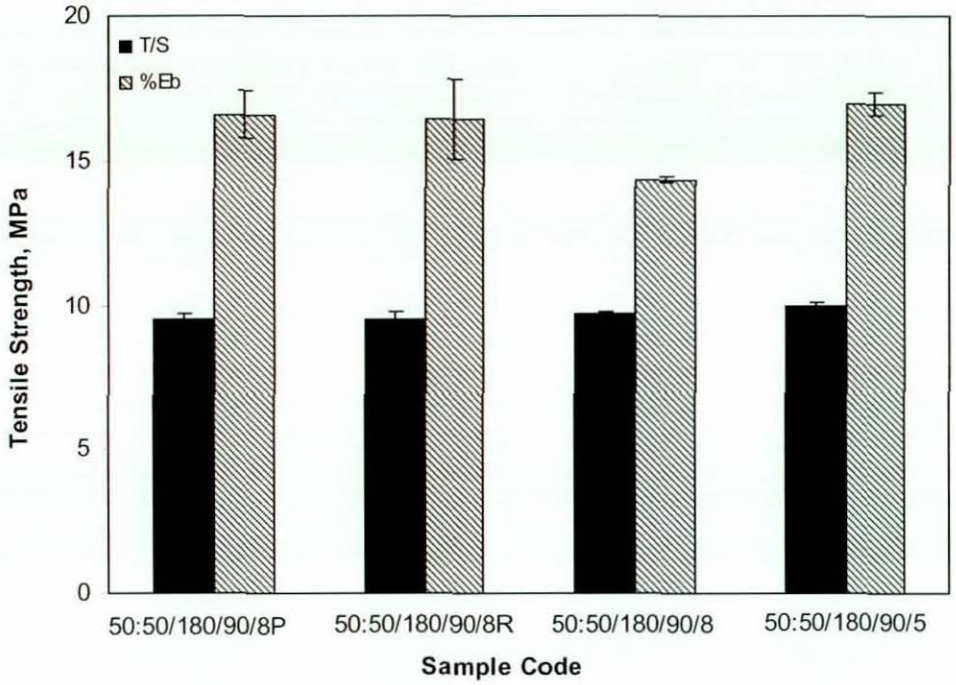

Figure 5.39 Tensile properties of 50:50 blends with different mixing procedures

5.3 Summary

The processing characteristics analyzed from the torque development curves show that the steady state torque of the GTR/WPP blends increases with increase in GTR content, indicating an increase in blend viscosity with GTR content. Melt flow index also decreases with GTR content. Most of the blends showed similar specific energy requirements. However, the 50:50/180/30/8 blend exhibited the minimum.

The optical micrographs for the GTR/WPP simple blends exhibited two-phase morphology, indicating incompatibility between GTR and WPP. At low GTR contents, the GTR was dispersed as domains in the continuous WPP matrix. The size of the domains increased with increase in GTR content. At 70 wt% of the GTR, the GTR dispersed phase changed to a continuous phase, resulting in co-continuous phase morphology. Confirming this two-phase morphology, two distinct peaks, for two glass transitions, were recorded on the tan δ curves in the dynamic mechanical analysis. The

magnitude of the transition peak for the specific polymer varied with its content in the blend.

The mechanical properties were also found to vary with the blend composition, due to the replacement of strong semi crystalline WPP by the soft amorphous GTR. The response to tensile loading ranged from a plastic response with WPP rich blends to a high extension–rubbery response with GTR rich blends. Fracture in the WPP due to tensile straining was identified as crazing, while that for all blends was identified mainly as interfacial debonding with some shear yielding. Under impact loads brittle fracture occurred in blends containing up to 40 wt% GTR and ductile fracture thereafter. The hardness, tensile strength, secant modulus, and tear resistance of the blends decreased with GTR content while % elongation at break and impact failure energy increased. In support, the swelling index increased with the GTR content while the solvent extraction residue decreased. The best balanced properties were obtained at 50 wt% of each polymer.

The property variation was small up to 30 wt% of the GTR, but increased thereafter up to 60 wt% of the GTR. This variation was changed again from 70 wt% of the GTR. The different variations at different composition ranges were related to the degree of crystallinity of the blend, and the phase morphology of the blend. The degree of crystallinity of the WPP remained unchanged up to 60 wt%, but increased slightly thereafter with the phase change. The slow variations in properties at low GTR contents suggest that a certain level of GTR is required to give rubbery properties to a GTR/WPP simple blend. However, none of the properties obtained for the blends were as high as expected. These inadequate properties are associated mainly with interfacial debonding and with the poor cohesive strength of the GTR phase.

Tensile properties slightly improved with an increase in the degree of both dispersive and distributive mixing associated with an increase in processing temperature, processing speed and processing time. But, the properties deteriorated with excessive mixing at higher processing parameters. This implies that the blend properties will be optimum at a certain mixing rate and processing temperature, for a particular mixing time. The best properties for the 50:50 blend were obtained at a processing temperature of 180 ^{0}C, a processing speed of 90 rpm, and processing time of 5 minutes, with a single step adding

procedure. However, the property enhancement obtained at optimum process conditions is lower than expected, and is mainly due to the poor interfacial adhesions between the two polymers. Thus the shear induced phase adhesion cannot be sufficiently developed in the GTR/WPP blends by varying the melt mixing processing conditions. This section of the present study shows the necessity of a suitable compatibilizer to improve phase adhesion and thereby improve the properties of the blends, significantly.

Chapter 6 Results and Discussion-Part III Reactive Blends

Reactive blends were prepared using a GTR/WPP simple blend having equal amounts of each polymer. The 50:50 simple blend was considered as the control blend. With the intention of generating both interfacial crosslinks and crosslinks within the GTR phase, thereby enhancing mechanical properties of the control blend, two compatibilizing systems were used. They were a dimaleimide system and a resin system. The suitability of such systems on property enhancement was investigated and is discussed in this chapter. The possible reactions that could occur during the melt mixing process are also discussed.

6.1 Dimaleimide Compatibilizing System

The dimaleimide compatibilizing system used in the present study consists of two components; a compatibilizing agent called N, N'-metaphenylenedimaleimide (HVA-2), and activators called 2-2'-dithiobenzothiazole (MBTS) and di-(tert-butyl peroxy-isopropyl) benzene (DTBPIB). The HVA-2 level was varied up to 8 pphp, and the activators up to 1 pphp (Section 3.2.5). The reactive blends with the dimaleimide compatibilizing system were prepared according to 'schedule-a' and under the processing conditions specified in Section 3.2.6. The processing characteristics, swelling behaviours, sol/gel analysis after solvent extraction, thermal properties, mechanical properties such as hardness, tensile and impact properties, and morphology of the blends were studied. The results obtained with and without the two activators are discussed in this section.

6.1.1 Possible Chemical Reactions during Melt Mixing

The GTR and WPP will generate free radicals during melt mixing when subjected to high shearing forces. These radicals will then recombine to form new crosslinks in the GTR phase and between phases. An addition of a chemical compatibilizing system will

enhance these reactions. Possible chemical reactions that could occur during melt mixing are discussed in this section.

6.1.1.1 Radical Formation in the GTR Phase

GTR contains NR, SBR and/or BR (Section 4.2). It has a complex chemical network structure due to vulcanization in previous processes. The GTR will generate free radicals during melt mixing which is carried out under intensive mechanical shearing forces, similar to the rubber mastication process [212]. Compared to C-C bond, S-S or C-S bond has lower dissociation energy, and hence S-S crosslinks may undergo breakage first to form radical ends with S atoms (Scheme 6.1). In addition, the unsaturated rubbers contained in the GTR may also form highly reactive radicals by H-abstraction from the α-methylene C-atom in the rubber main chain, when they were subjected to intensive mechanical shearing forces (Scheme 6.2).

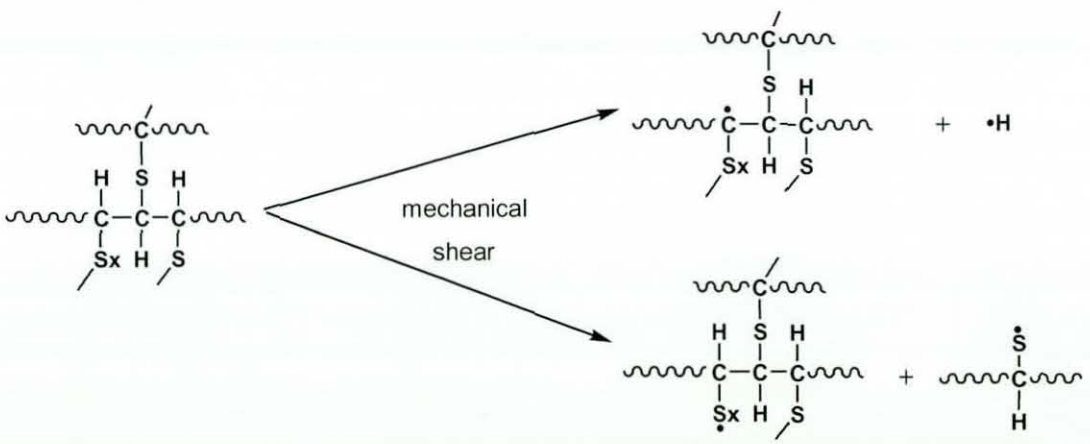

Scheme 6.1 Radical formation in the GTR during melt mixing [159]

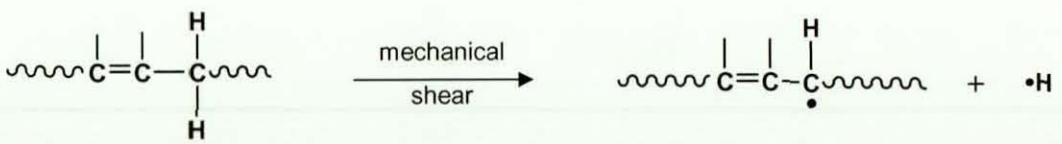

Scheme 6.2 Radical formation in the unsaturated rubbers in the GTR during melt mixing [212]

6.1.1.2 Formation of Crosslinks in the GTR Phase by Dimaleimide System

Dimaleimides, including HVA-2, are used to crosslink unsaturated rubbers like NR and SBR [160, 212, 241]. The reaction of crosslinking unsaturated rubbers by HVA-2 are given in Scheme 6.3. It has been reported [241] that dimaleimides alone crosslink NR at higher temperatures, but only to a relatively slight extent. A catalytic free radical source, such as organic peroxide or sulfur accelerators of a thizole type like MBTS, is usually incorporated to increase the degree of crosslinking [160, 212, 241].

HVA-2 shows a sharp melting endotherm on a DSC thermogram with an equilibrium melting temperature of 204 ^{0}C (Figure 6.1). MBTS also exhibits a sharp melting endotherm with an equilibrium melting temperature of 180 ^{0}C. A mixture of HVA-2 and MBTS, at a ratio of 5:1 by weight, shows broad melting endotherms with lowered melting temperatures for both the MBTS (174 ^{0}C) and HVA-2 (194 ^{0}C). This DSC thermogram suggests the occurrence of a chemical reaction between two chemicals, even at static conditions, but at higher temperatures. The lowering of the melting temperatures is in agreement with the behaviour of MBTS as a crosslinking promoter for HVA-2. MBTS will generate free radicals under high shearing forces at high temperatures, as shown in Scheme 6.4. These radicals influence radical formation in rubber chains which will then unite to form crosslinks within the GTR phase in the presence of HVA-2.

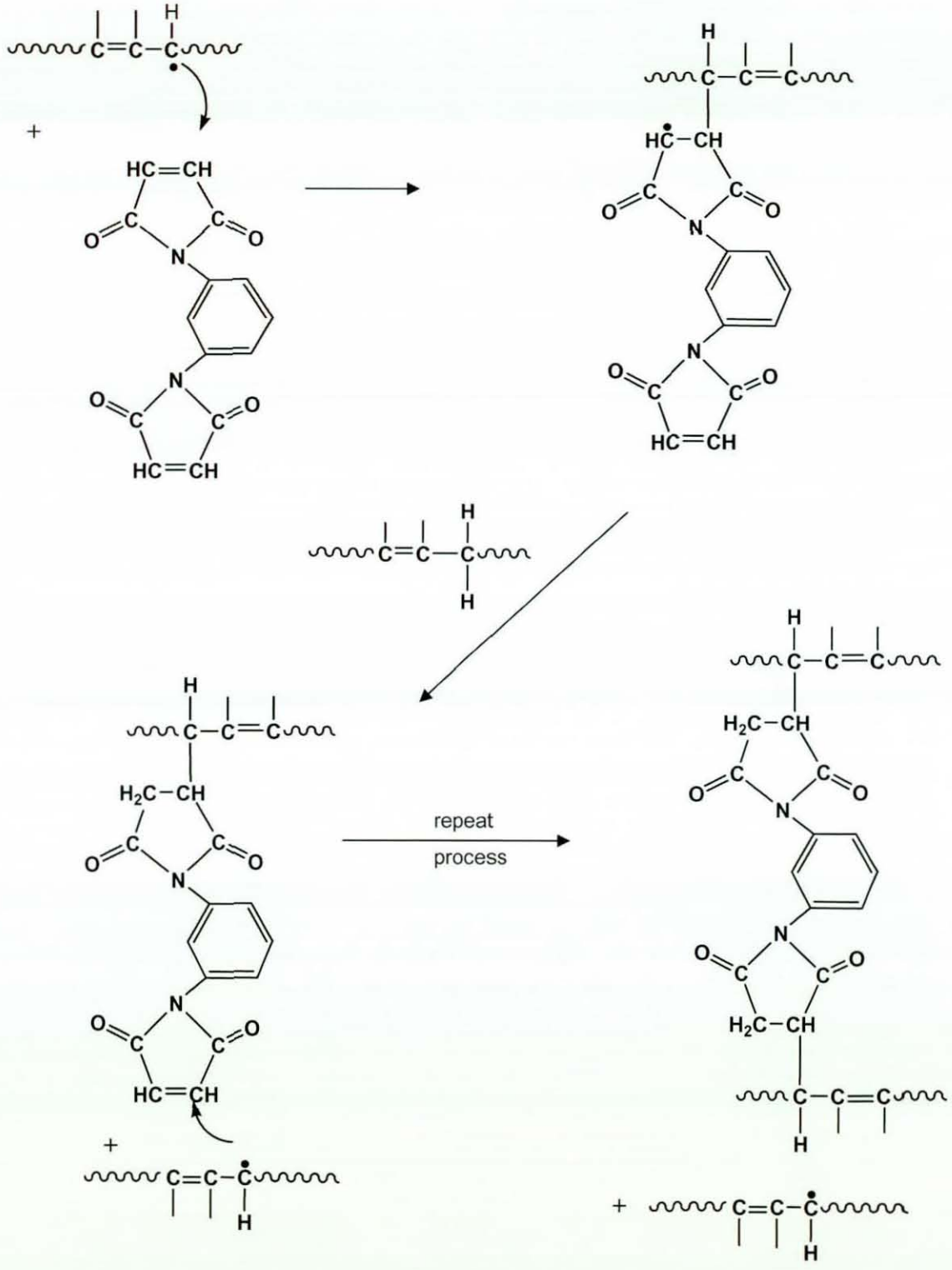

Scheme 6.3 The reaction scheme for the formation of crosslinks in the GTR phase by HVA-2 [212]

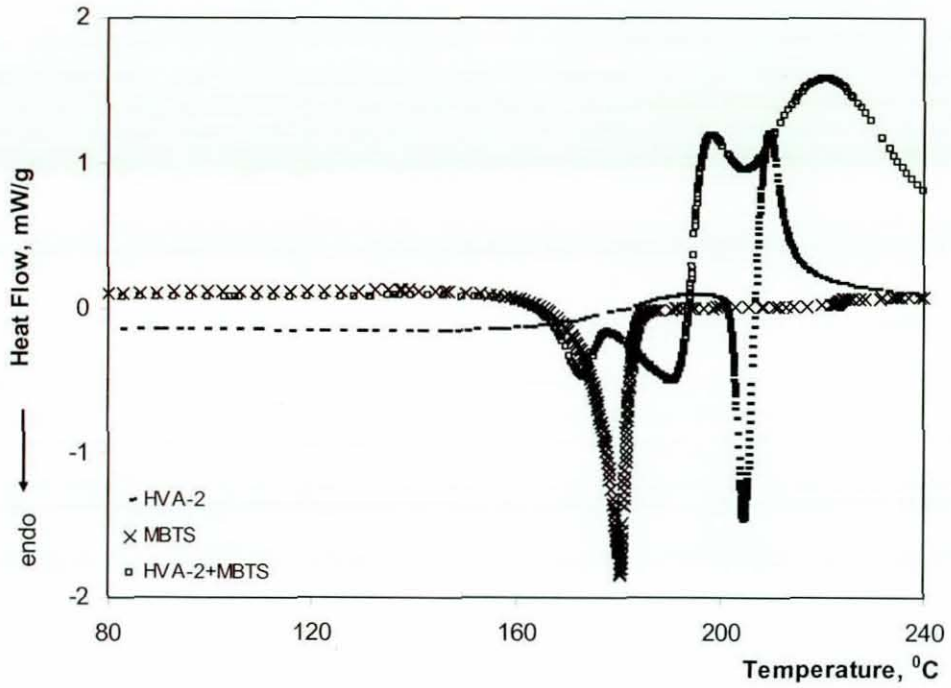

Figure 6.1 DSC thermograms of HVA-2, MBTS and their mixture

Scheme 6.4 Free radical formation in MBTS [212]

6.1.1.3 Formation of Crosslinks in the GTR Phase by Organic Peroxides

Organic peroxides are also used to crosslink rubbers derived from isoprene and butadiene [212, 242]. The first step in this peroxide crosslinking is the homolytic cleavage of the peroxide molecule to form two peroxy radicals (Scheme 6.5). Accordingly, DTBPIB will decompose at high temperatures under high shear stresses, as shown in Scheme 6.6. A DSC thermogram (Figure 6.2) showed that the commencement of DTBPIB decomposition occurred at 130 ^{0}C with a peak decomposition temperature at 180 ^{0}C. This observation confirms the occurrence of DTBPIB decomposition during melt mixing in the present study. The decomposition products of DTBPIB, which can abstract

hydrogen atoms from the unsaturated rubbers, are tert-butaloxy-, methyl- and di-(hydroxyl-i-propyl) benzene radicals [146]. The H-abstraction capacity depends mainly on the nature of the primary radicals and the dissociation energy of the covalent bond, and then on the steric hindrance, polarity and electron resonance. Both methyl and peroxy radicals are good in H-abstraction [124].

Scheme 6.5 Homolytic dissociation of organic peroxide [212]

The next step in the peroxide crosslinking is either H-abstraction from an allylic position on the rubber molecule or the addition of the peroxide-derived radical to a double bond of the rubber molecule [212]. For isoprene rubber, the abstraction route predominates over the radical addition. The rubber radicals then unite to give a C-C crosslink (Scheme 6.7). The peroxide is not part of the crosslink and does not affect the stability of the rubber by introducing a foreign structure [242]. However, in the presence of oxygen, the radical on the rubber chain couples with an oxygen molecule to form a hydroperoxyl radical [242]. This leads to rubber degradation.

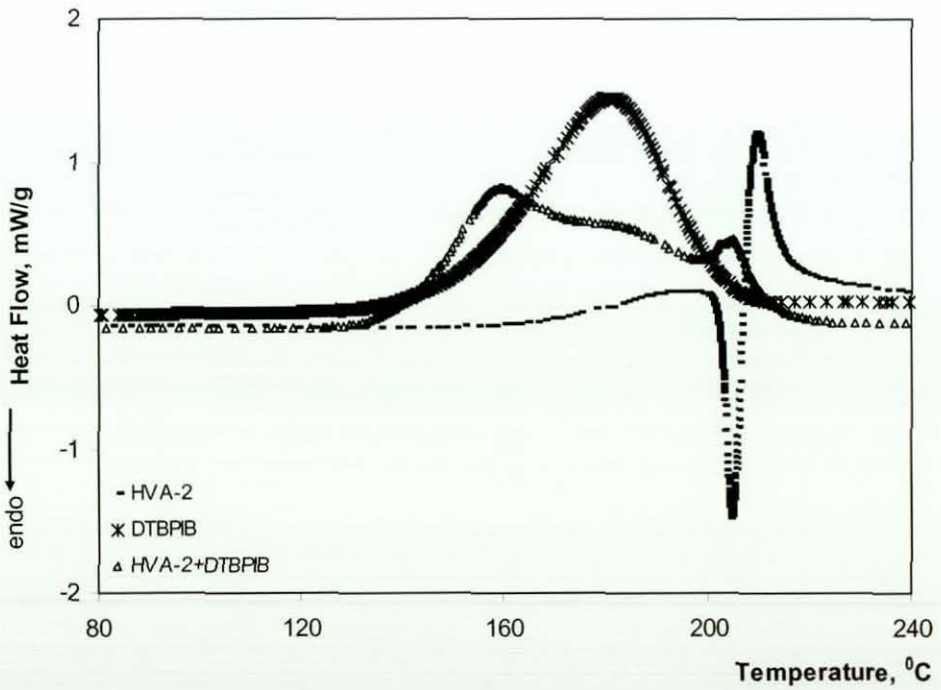

Figure 6.2 DSC thermograms of HVA-2, DTBPIB and their mixture

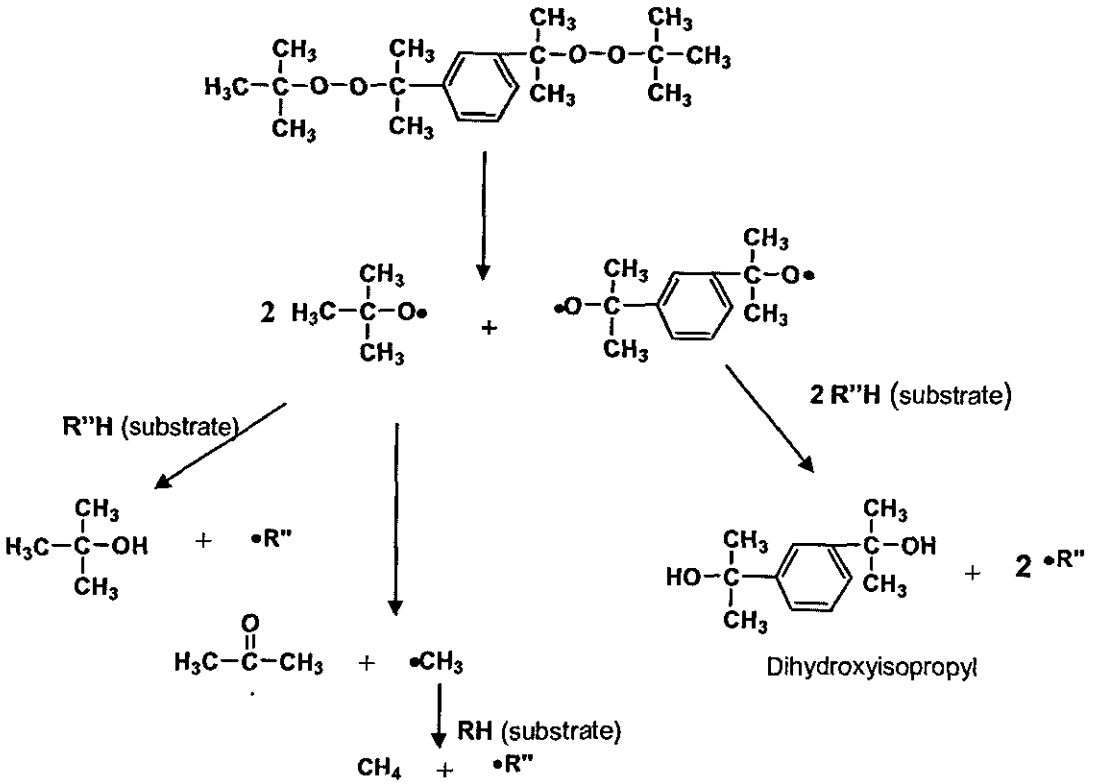

Scheme 6.6 Decomposition mechanism of DTBPIB and hydrogen abstraction reactions from a substrate [124, 146]

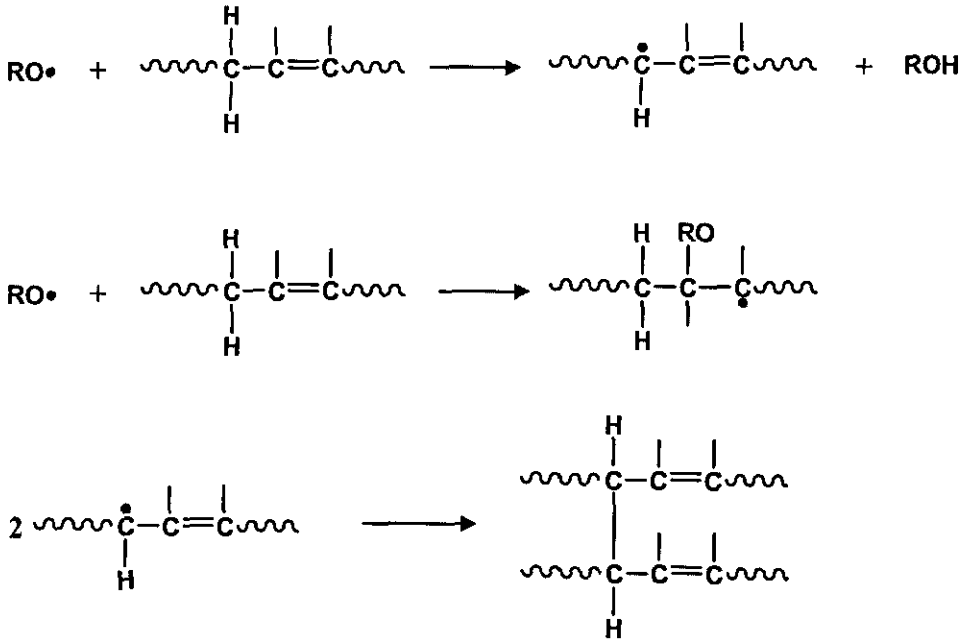

Scheme 6.7 The reaction scheme for the crosslinking of unsaturated rubbers in the GTR phase by organic peroxide [212]

The peroxy radical can abstract H atoms from any available source in the composition, not only from the rubbers. If hydrogen is transferred from a non-polymeric ingredient, the vulcanizing efficiency of the peroxide is usually reduced [242]. The non-polymeric radical that is formed will couple, graft or decompose without yielding a crosslink.

6.1.1.4 Degradation of WPP by Organic Peroxides

The highly reactive radicals generated from the DTBPIB not only give a high degree of crosslinking in the GTR phase, but also lead to some degradation of the WPP phase (Scheme 6.8). The degradation of WPP by organic peroxides occurs through a sequence of radical reactions; peroxide decomposition, H-abstraction, β-scission and termination. As the overall degradation rate is controlled by the peroxide decomposition rate [156], processing time should be equivalent to 6-7 half-lives of the peroxide to ensure practically complete decomposition. It has been reported that the half-life of DTBPIB is only 6.5 seconds at 200 ^{0}C [146]. These peroxides complete decomposition in less than 1 min at 200 ^{0}C. The secondary decomposition reaction of the tert-butaloxy radical to acetone and a methyl radical (Scheme 6.6), has no effect on the degradation of WPP, as the methyl radical is equally reactive in H-abstraction from WPP [212].

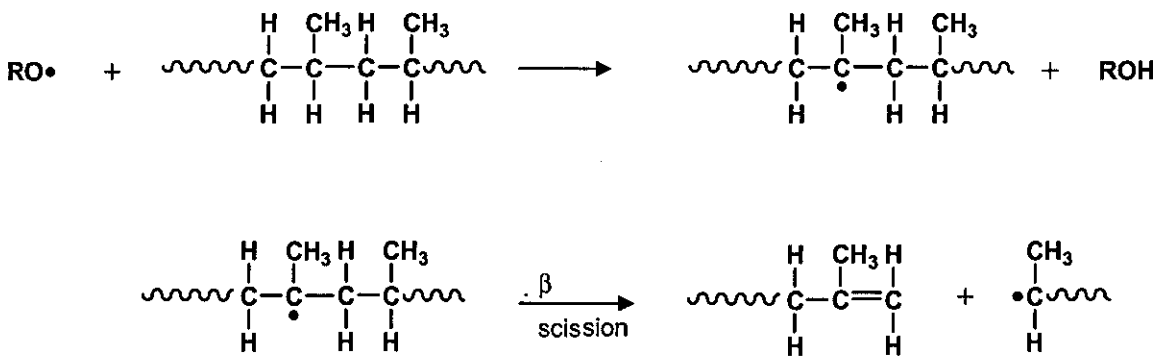

Scheme 6.8 Simplified reaction scheme for peroxide degradation of WPP by β-scission [212]

6.1.1.5 Formation of Interfacial Crosslinks

An addition of a coagent, like sulfur, m-phenylenebismaleimide, triallyl cyanurate, etc., into organic peroxide suppresses the chain scission of PP [212]. The PP radical generated due to H-abstraction by the peroxy radical will then react with the coagent to form a crosslink between the two phases. This reaction is similar to the grafting of functional monomers onto PP [124]. This is in support of this is the occurrence of a chemical reaction between HVA-2 and DTBPIB as shown by the DSC thermogram for a mixture at 5:1 weight ratio (Figure 6.2). The exothermic peak associated with peroxide decomposition was shifted to the lower temperature side, while the melting endotherm assigned to HVA-2 partially disappeared. The disappearance of the peak assigned to HVA-2 suggests that an interaction between HVA-2 and DTBPIB even under the static conditions. By considering this chemical reaction occurred between HVA-2 and DTBPIB, a chemical reaction for the formation of interfacial crosslinks between the two polymers in the GTR/WPP blends can be proposed, as given in Scheme 6.9.

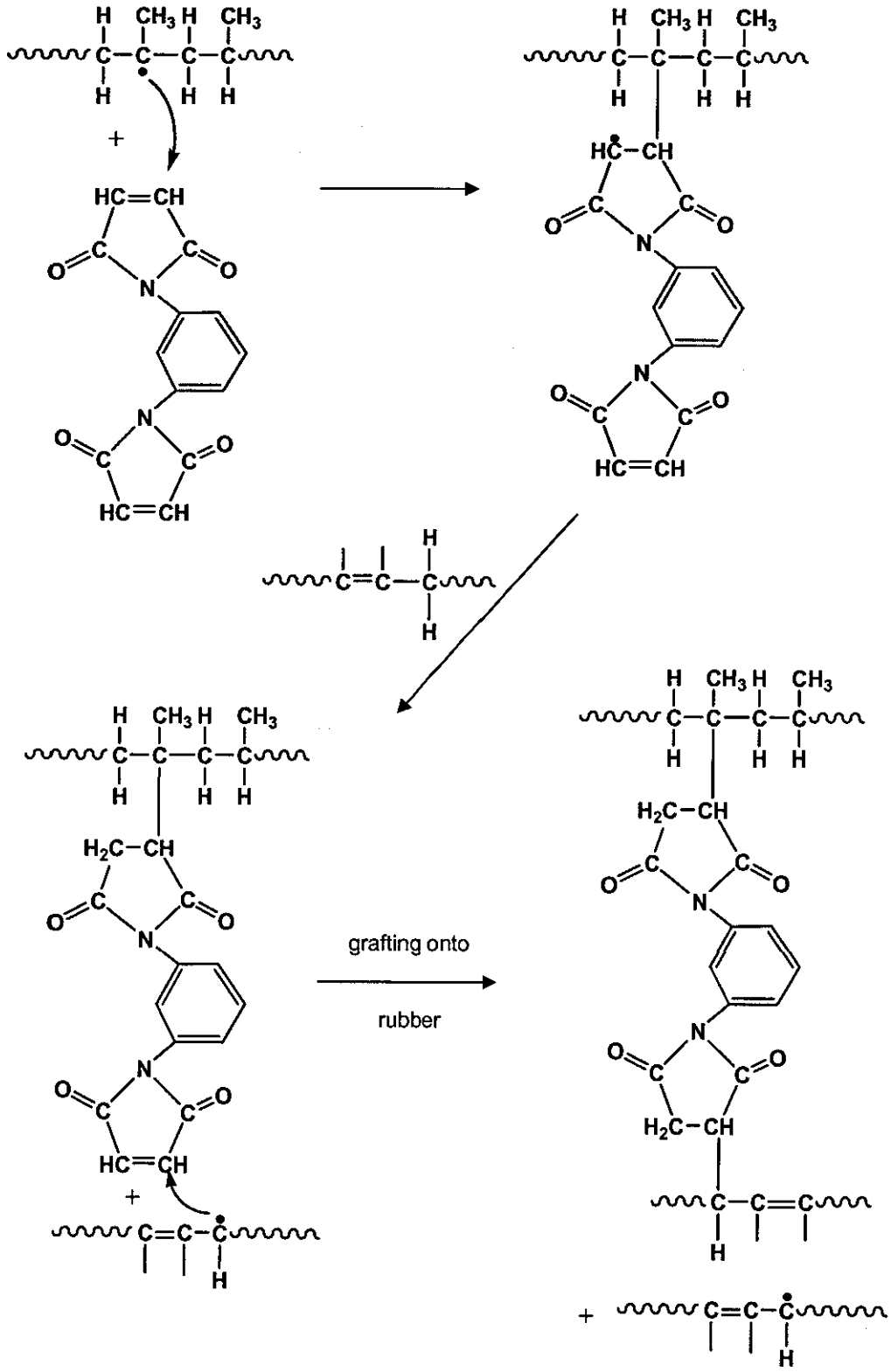

Scheme 6.9 Proposed reaction scheme for the formation of interfacial crosslinks in the presence of HVA-2 and DTBPIB

6.1.2 Processing Characteristics

Torque-time curves for the control blend and a few selected blends are given in Figure 6.3. All blends exhibited the same trend in torque development during the first stage of mixing. The break in the curves at 2 minutes is due to the ram being raised in order to add the compatibilizing system and/or anti-oxidants during mixing of GTR and molten WPP A slight, but gradual, decrease in torque thereafter is observed with the control blend, which is attributed to a decrease in viscosity with increase in blend temperature. In contrast, the blends containing HVA-2 alone exhibit a slight increase in torque towards stabilization. The torque increase with HVA-2 is indicative of an increase in the viscosity of the blend and hence a slight reduction in processability. The torque at completion of the melt mixing, for blends with HVA-2, is given as the steady state torque, in Table 6.2. This table shows an increase in steady state torque with increase in HVA-2 level up to 5 pphp, then a leveling off, followed by a slight decrease thereafter. The formation of a graft copolymer during the mixing of two polymers is known to cause a substantial increase in the viscosity of the blend [151]. Crosslinking in the GTR phase could also be expected to result in an increase in the viscosity. The possible mechanism for crosslink formation within the GTR phase is shown in Scheme 6.3. An increase in steady state torque with the addition of 1 pphp of HVA-2 into EPDM/PP (15/85) blends has been previously reported [151]. An increase in 40% in steady state torque with the addition 3 pphr of HVA-2 to EPDM/NR/PP ternary blends has also been reported [105]. However, the maximum increase in torque in the present study was only 21%, and this is attributed to the lack of unsaturated rubbers in the GTR phase.

The blends containing both HVA-2 and MBTS show similar variation in torque against time. Further, these blends show higher steady state toques compared to blends containing HVA-2 alone. This increase in torque with the addition of MBTS indicates that it is acting as a crosslinking promoter within the GTR phase (Section 6.1.1.2) [212, 241].

The blends containing both HVA-2 and DTBPIB show a sudden torque increase when the compatibilizing system is added, and a decrease thereafter towards stabilization. The height of this second peak, which is related to the amount of crosslinks formed in the GTR phase [146] and between the phases, increases with HVA-2 level. The second peak

does not appear in the blends without DTBPIB. The decrease in toque after the second peak could be associated with degradation of WPP and/or with a size reduction of the GTR phase [147].

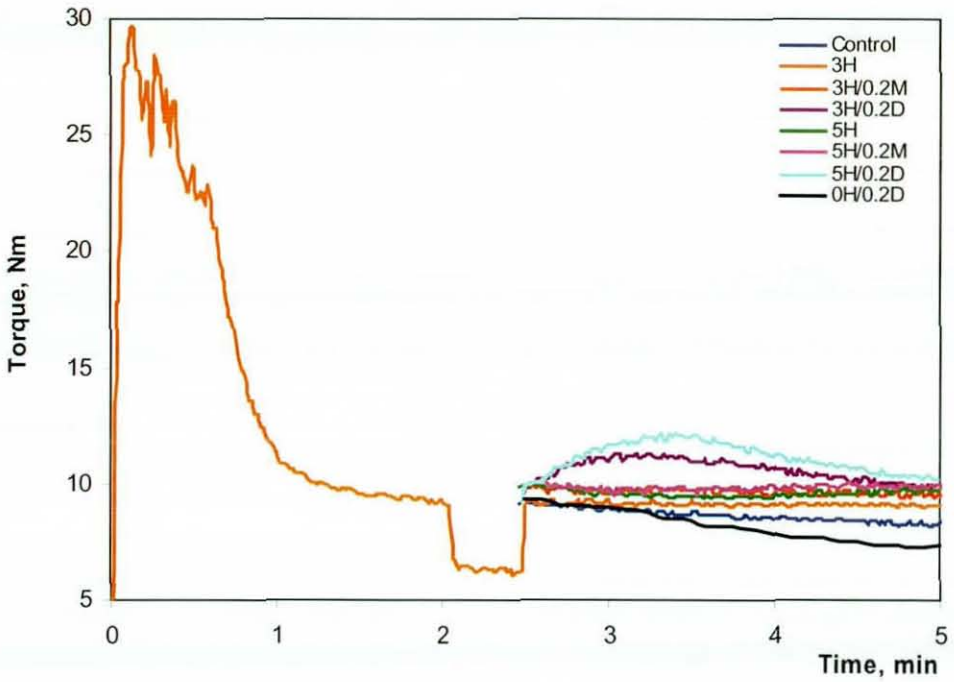

Figure 6.3 Torque vs. time curves for blends containing HVA-2 with and without 0.2 pphp of activators

In general, peroxides generate free radicals at higher temperatures which lead to undesirable side reactions when polyolefin is present in the blend as the plastic phase. In the case of blends prepared with unsaturated rubbers and PP, the peroxy radicals abstract H-atoms not only from allylic carbons of rubber (Scheme 6.7), but also from the tertiary carbons of PP (Scheme 6.8) [162]. The more stable tertiary free radical generated undergoes β–chain scission; which results in some degradation of the PP (Scheme 6.8) [291]. Similarly, the DTBPIB in the GTR/WPP blends generates highly active radicals (Scheme 6.6), and produces a high degree of crosslinking in the presence of HVA-2 (Scheme 6.3 and Scheme 6. 9), but with some degradation of the WPP phase. However, the blend containing DTBPIB alone does not show any increase in torque at the latter stage of mixing and drastically decreases with time. The viscosity decrease of the WPP due to chain scission (Scheme 6.8) overrules the viscosity increase due to crosslinking by

DTBPIB in the GTR phase (Scheme 6.7), resulting in an overall decreased torque at the final stage of the mixing. This confirms the degradation of the WPP phase and suggests the necessity of HVA-2 for crosslink formation in the GTR/WPP blends. The formation of crosslinks within the rubber phase by dicumyl peroxide (DCP) and DTBPIB was reported for NR/PP blends [146]. However, this study also reported some degradation of the PP phase.

Table 6.1 Steady sate torques for blends containing HVA-2 with and without 0.2 pphp of activators

HVA-2, pphp	Steady State Torque, Nm		
	without activators	with 0.2 pphp of MBTS	with 0.2 pphp of DTBPIB
0	8.4(8.3)	-	-
1	8.7(8.9)	9.2(9.1)	8.9(8.7)
2	9.0(9.2)	9.4(9.4)	9.3(9.5)
3	9.2(9.3)	9.4(9.5)	9.5(9.8)
4	9.6(9.5)	9.7(9.6)	10.0(9.9)
5	9.6(9.7)	9.8(9.9)	10.4(10.2)
6	9.7(9.6)	-	-
7	9.7(9.5)	-	-
8	9.6(9.5)	-	-

duplicate results are given in parenthesis

It is clear from Table 6.1 that the steady state torque increase is considerably higher for blends with HVA-2 and DTBIPB, compared to those for blends with HVA-2 and MBTS, for a specific HVA-2 level. This greater increase in torque for blends with HVA-2 and DTBPIB could be due to an involvement of the WPP phase in the crosslinking process. This suggests an interfacial crosslink formation between the phases (Scheme 6.9).

The blend temperature–time curves for the control blend and the blends with HVA-2 alone and with both activators are given in Figure 6.4. The blend temperature increases with the addition of HVA-2 and further with the activators. The highest temperature

increase is for the blend containing HVA-2 and DTBPIB. This is due to the heat evolved by the exothermic reaction, which occurs due to the decomposition of DTBPIB at 180 ^{0}C. The decomposition of DTBPIB and the exothermic reaction with HVA-2 is clearly shown on the DSC thermogram (Figure 6.2). This exothermic reaction, which provides a negative enthalpy of mixing, is an indication of an improved stability of the blend (Section 2.5.1).

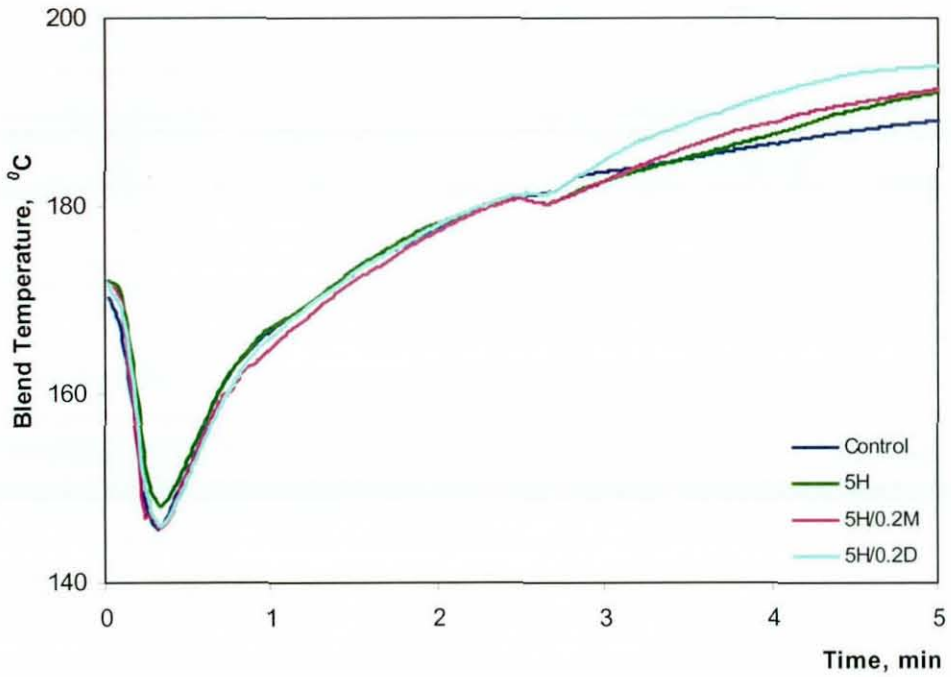

Figure 6.4 Blend temperature vs. time curves for blends containing HVA-2 with and without 0.2 pphp of activators

Figure 6.5 displays the torque-time curves for blends containing different DTBPIB levels. An increase in both steady state torque and torque at the second peak with the DTBPIB level is clearly shown. Table 6.2, which tabulates torques for all DTBPIB levels, shows a 50% increase in steady state torque with the addition of 1 pphp of DTBPIB to 3 pphp of HVA-2 over that of the control blend. This greater increase in torque with DTBPIB level is due to increased levels of crosslink formation in the GTR phase and between the phases. However, no increase in steady state torque is noticed with MBTS level. Further, no sudden increase in torque with the addition of the HVA-2 and MBTS compatibilizing system to the GTR/WPP blends is noticed, even at higher MBTS levels. This suggests

that there is no interfacial crosslink formation by the HVA-2 and MBTS compatibilizing system within the levels used in the present study.

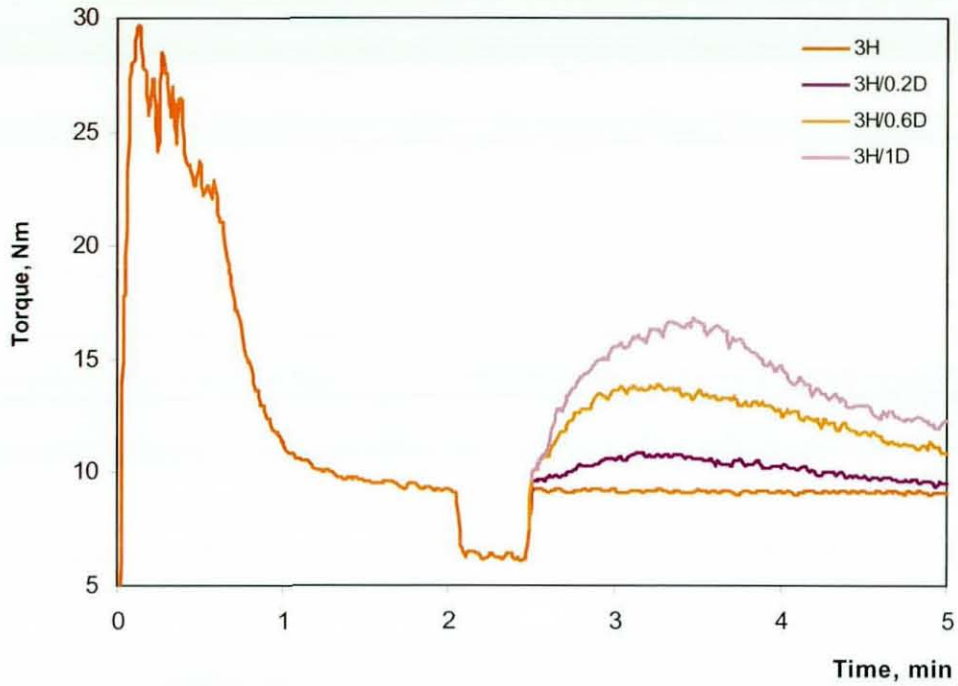

Figure 6.5 Torque vs. time curves for blends containing different levels of DTBPIB with 3 pphp of HVA-2

Table 6.2 Toques at steady state and at second peak for blends containing different levels of DTBPIB with 3 pphp of HVA-2

Activator, pphp	Steady State Torque, Nm		Second Peak in Torque with
	MBTS	DTBPIB	DTBPIB, Nm
0	8.7(9.0)		
0.2	9.5(9.6)	9.5(9.8)	11.3(10.9)
0.4	9.5(9.6)	9.9(10.1)	12.6(12.9)
0.6	9.7(9.6)	10.9(10.7)	13.8(14.3)
0.8	9.6(9.5)	11.4(11.3)	15.2(14.8)
1.0	9.5(9.6)	12.3(12.1)	16.6(16.3)

duplicate results are given in parenthesis

6.1.3 Melt Flow Analysis

Table 6.3 gives the melt flow indices for the control blend and a few selected blends. It shows a significant increase in viscosity with the addition of 1 pphp HVA-2 in the GTR/WPP blends, as measured by the melt flow index (MFI). This increase in viscosity is remarkably high with the addition of 3pphp of HVA-2. It was not possible to measure the MFI of the blends containing more than 3 pphp HVA-2 due to their very high viscosity. The higher viscosity of blends containing HVA-2 and DTBPIB or MBTS is due to the presence of crosslinks within the GTR phase or interfacial interactions within the phases. A significant increase in viscosity with the addition of 1 phr of HVA-2 into NR/PP (15/85) blends has also been previously reported [151].

Table 6.3 Melt Flow indices of selected blends with and without activators

Blend	MFI, g/10 min
Control	3.7(0.3)
1H	2.5(0.1)
3H	0.8(0.1)
3H/0.2M	0.5(0.1)
3H/0.2D	0.3(0.0)

6.1.4 Swelling Behaviour

Crosslinked rubber, in general, is insoluble in toluene, but is highly swollen by the solvent [292]. The swelling index of the GTR (Equation 3.16) was measured as 1.9 (Section 5.1.7). While the %solvent extraction residue of the GTR (Equation 3.17), was obtained as 86%. This indicates that the GTR contained some soluble rubber, and a considerable residue which of course contained the carbon black, the majority of which was bound chemically or physically to the rubber. As expected, the WPP exhibited 100% residue with negligible swelling.

Table 6.4 shows the swelling indices and the %solvent extraction residues of the control blend, and blends containing HVA-2 with and without MBTS and DTBPIB activators. The control blend recorded a very low swelling index with a relatively high solvent extraction residue. The WPP phase may restrict diffusion of toluene to the inside of the specimen. This may also be due to formation of physical crosslinks at the GTR phase or between the phases during the high shear melt mixing process. During melt mixing, PP chains were adsorbed onto the active sites of the GTR surface.

Table 6.4 Swelling characteristics of blends containing different levels of HVA-2, with (0.2 pphp) and without activators

HVA-2, pphp	Swelling Index			%Solvent Extraction Residue		
	without activators	with MBTS	with DTBPIB	without activators	with MBTS	with DTBPIB
0	0.50(0.01)			92(0)		
1	0.41(0.01)	0.39(0.02)	0.37(0.02)	95(0)	94(0)	94(1)
2	0.38(0.01)	0.34(0.03)	0.38(0.03)	95(0)	95(0)	94(0)
3	0.33(0.01)	0.34(0.02)	0.34(0.02)	95(0)	95(1)	94(0)
4	0.33(0.01)	0.29(0.00)	0.31(0.03)	96(0)	95(0)	95(1)
5	0.33(0.01)	0.27(0.01)	0.28(0.02)	95(0)	95(0)	95(0)
6	0.32(0.01)			96(0)		
7	0.32(0.01)			95(0)		
8	0.36(0.01)			95(0)		

The addition of HVA-2 decreases the swelling index, which further decreases in the presence of MBTS and of DTBPIB. The addition of HVA-2 alone increases the solvent extraction residue, but no significant change was observed with HVA-2 level. The swelling of a crosslinked elastomer is dependent upon the average length of the polymer chains between crosslinks [162, 292]. The HVA-2 vulcanizing system produces C-C crosslinks, which are shorter and stronger than the polysulfidic crosslinks available in the GTR. Hence, the decrease in swelling index and the increase in residue suggest the formation of additional crosslinks in the GTR phase. A further decrease in swelling index

with HVA-2 level in the presence of MBTS and DTBPIB, suggests the formation of increased levels of new crosslinks within the GTR phase. This also suggests the formation of interfacial crosslinks and scission of polymer chains in the blend. Further increases in the activator level results in a slight decrease in swelling index and an increase in solvent extraction residue (Table 6.5), and suggests the formation of more crosslinks with the chain ends generated by chain scission. However, swelling alone cannot be used to characterize the degree of crosslinking or degree of chain scission since it is theoretically possible to cut crosslinks and polymer chains without the formation of a soluble material. This also reflects the constant value of solvent extraction residue obtained for all reactive blends.

Table 6.5 Swelling characteristics of blends containing different levels of HVA-2, with (0.2 pphp) and without activators

Activator,	Swelling Index		%Solvent Extraction Residue	
pphp	with MBTS	with DTBPIB	with MBTS	with DTBPIB
0.2	0.34(0.02)	0.34(0.02)	95(1)	94(0)
0.4	0.33(0.01)	0.31(0.02)	95(0)	94(0)
0.6	0.33(0.02)	0.31(0.02)	96(1)	95(1)
0.8	0.34(0.03)	0.31(0.01)	95(0)	95(1)
1.0	0.31(0.01)	0.31(0.02)	95(0)	95(0)

6.1.5 Hardness

The variation of hardness of blends containing HVA-2 with and without activators is given in Table 6.6. The hardness gradually increased with increase in HVA-2 level, up to 4 pphp, and then reached a plateau. This increase in hardness is attributed to the formation of new crosslinks within the GTR phase. Once the crosslink formation within the GTR phase reaches saturation, the hardness remains unchanged. The excess HVA-2 content may be entrapped in the blend as filler. Comparatively higher hardness values shown with MBTS for the blends with lower HVA-2 levels explain the activity of MBTS as a promoter or accelerator for effective crosslink formation within the GTR phase.

Further increase in hardness with the DTBPIB is due to the involvement of the WPP phase in the crosslinking process.

Table 6.6 Hardness of blends containing different levels of HVA-2, with and without 0.2 pphp of activators

HVA-2, pphp	Hardness, IRHD		
	without Activators	with MBTS	with DTBPIB
0	80(1)	-	-
1	82(1)	89(1)	88(2)
2	83(1)	89(1)	91(2)
3	84(2)	89(1)	92(3)
4	89(2)	89(1)	92(2)
5	89(1)	89(1)	93(2)
6	90(1)	-	-
7	88(1)	-	-
8	88(1)	-	-

6.1.6 Tensile Properties

Typical stress-strain curves for the control blend and a few selected blends are illustrated in Figure 6.6. All these blends show a plastic response and do not show any yielding before failure. However, the stress and strain capabilities varied between each blend. Interfacial adhesions formed during melt mixing in the blend containing HVA-2 and DTBPIB (see Figure 6.15) allows specimens to undergo greater deformation before failure. Figure 6.7 shows the variation of tensile strength with HVA-2 level for the blends with (0.2 pphp) and without MBTS and DTBPIB activators. The variations of elongation at break and secant modulus at 2% strain are shown in Figure 6.8 and Figure 6.9, respectively. Table 6.7 gives the tensile properties for the blends containing 3 pphp of HVA-2 with activators at different levels.

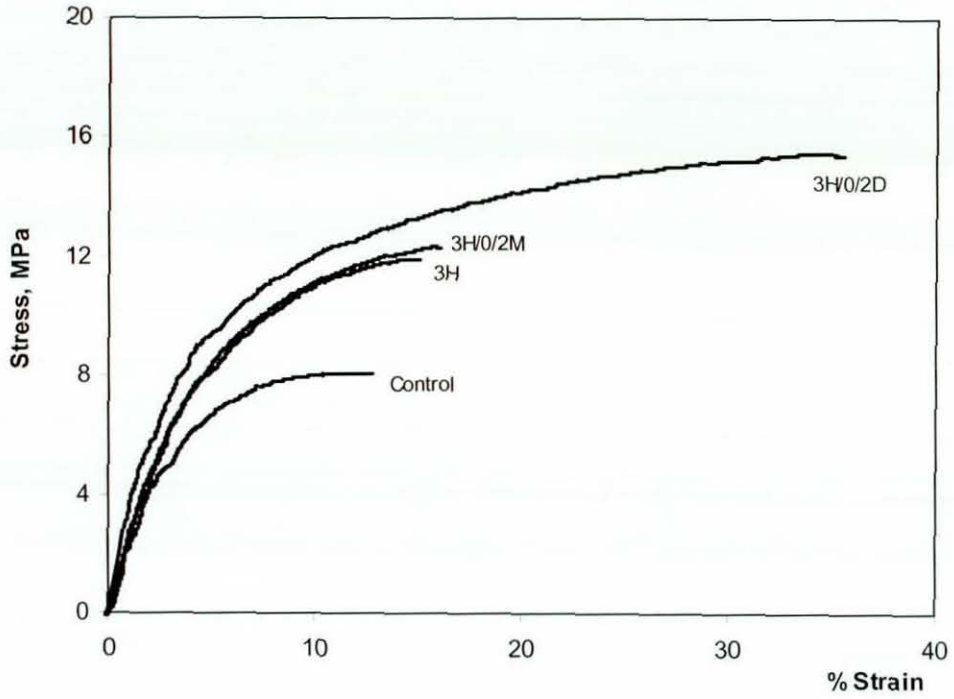

Figure 6.6 Typical stress-strain curves of the control blend and few selected blends

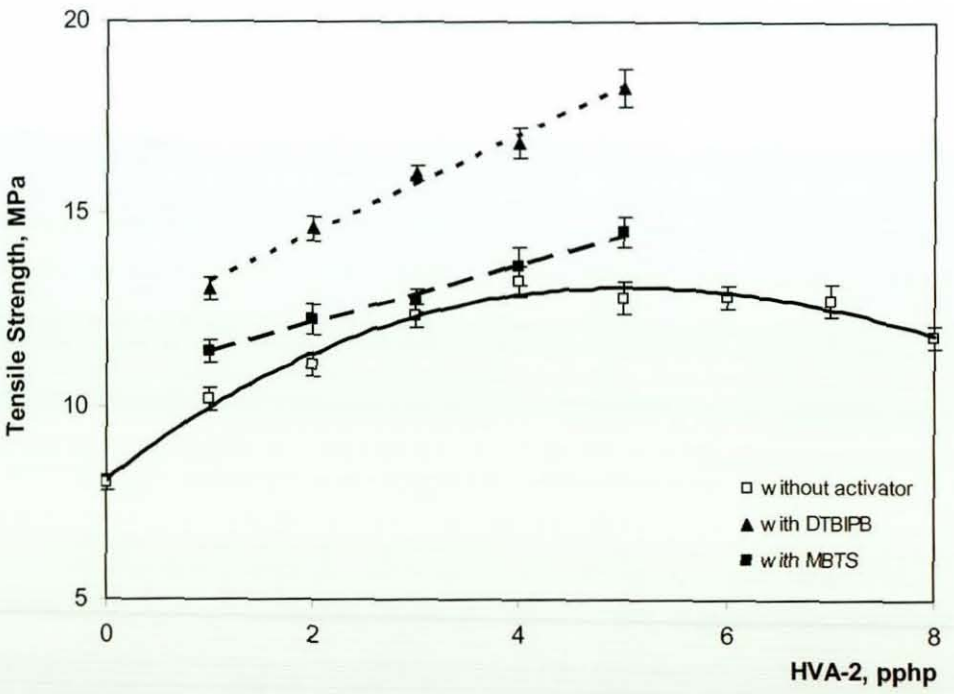

Figure 6.7 Tensile strength vs. HVA-2 level with (0.2 pphp) and without activators

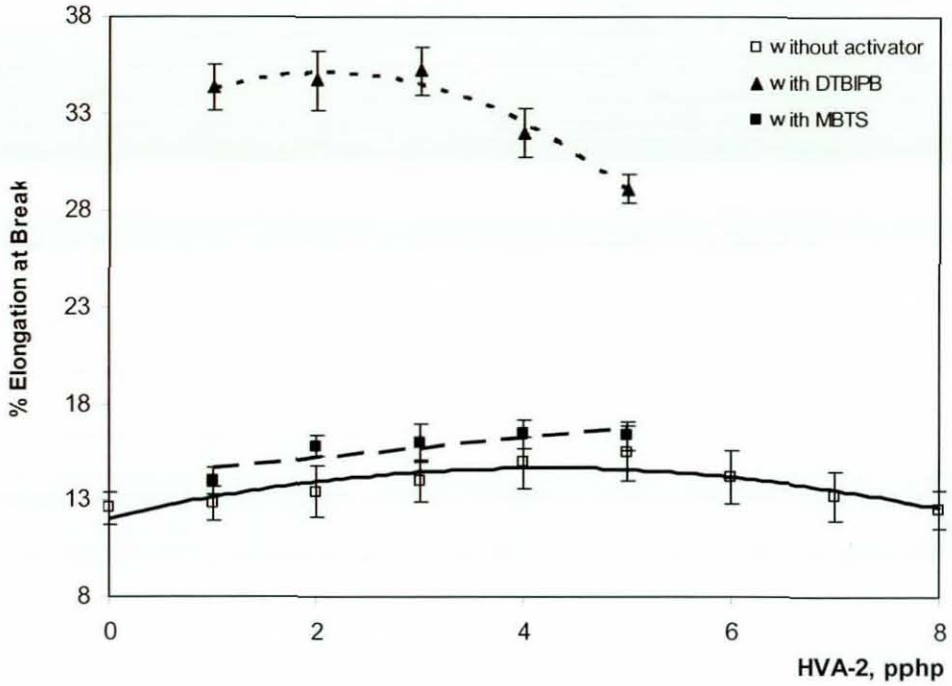

Figure 6.8 % Elongation at break vs. HVA-2 level with (0.2 pphp) and *without* activators

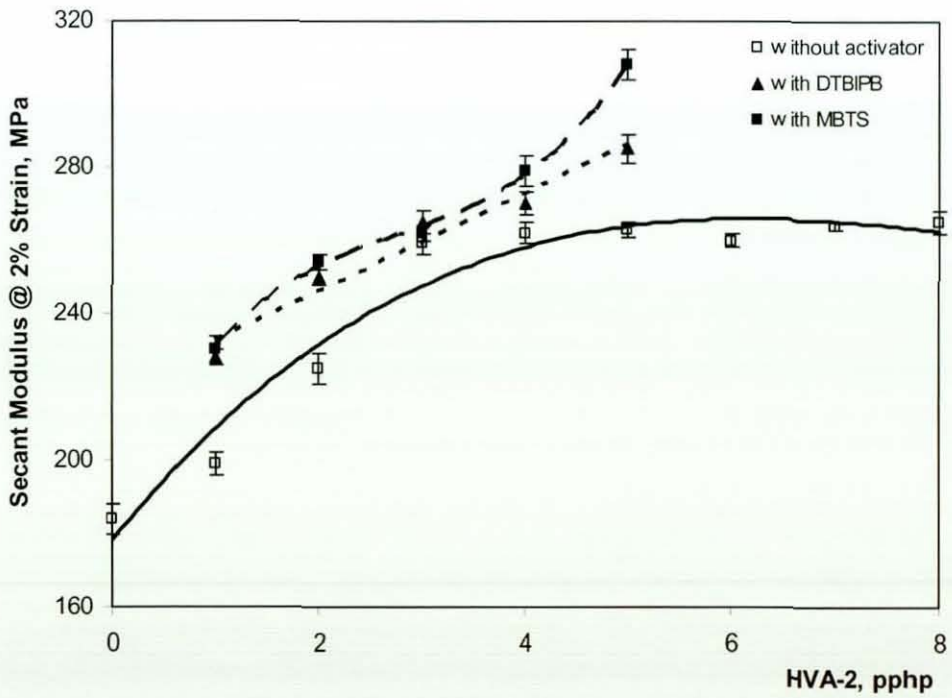

Figure 6.9 Secant modulus vs. HVA-2 level with (0.2 pphp) and without activators

Table 6.7 Tensile properties of blends, containing 3 pphp of HVA-2, with activator levels

Activator, pphp	MBTS			DTBPIB		
	Tensile Strength, MPa	% Elongation at Break	Secant Modulus, MPa	Tensile Strength, MPa	% Elongation at Break	Secant Modulus, MPa
0.2	12.7(0.6)	16.0(1.0)	259(4)	16.1(0.4)	35.2(1.2)	265(6)
0.4	13.4(0.6)	16.6(1.5)	273(4)	18.3(0.6)	36.6(1.7)	269(7)
0.6	14.6(0.5)	17.2(1.6)	281(7)	19.3(0.8)	39.2(1.0)	274(8)
0.8	13.7(0.4)	15.2(1.2)	283(3)	19.6(0.4)	37.7(1.6)	265(7)
1.0	12.5(0.5)	13.9(1.3)	289(4)	18.5(0.5)	35.1(1.7)	263(4)

(a) *Influence of HVA-2 Addition*

Tensile strength increases initially with HVA-2 level and then reaches a plateau, appearing to reach an optimum level at 4 pphp. A 63% increase in tensile strength for the 50:50/4H blend over that of the control blend was observed. The crosslinking of the GTR phase increased the cohesive strength of the blend allowing it to undergo greater deformation before failure (Figure 6.6). In a separate study an approximate 75% increase in tensile strength, over the control blend, was reported with the addition of 0.2 wt% of HVA-2 in a NR/PP (20/80) blend [149]. Another study showed only a 20% increase with 0.2 phr of HVA-2 for NR/PP (15/85) blends [151]. Also no further increase in strength with HVA-2 content was recorded in either study.

Elongation at break increases gradually with HVA-2 level up to a 5 pphp level and decreases thereafter (Figure 6.8). This variation is small, and the highest increase is only 20%. A drop in the elongation at break at high HVA-2 level is due to formation of more crosslinks (Scheme 6.3), which restrict the slip of the GTR chains past each other. As expected, secant modulus at 2% strain increase with HVA-2 level reaching a plateau at high levels.

(b) *Influence of MBTS Addition*

The tensile strength continuously, but slightly, increases with HVA-2 level when a constant level (0.2 pphp) of MBTS was added to the blend (Figure 6.7). This is due to the increase in crosslink formation in the GTR phase by the MBTS. The MBTS free radicals generated under high shearing forces at high temperatures (Scheme 6.4) influenced the formation of radicals in the GTR phase (Scheme 6.1) and then united to form additional crosslinks in the GTR phase (Scheme 6.3). Further increases in the MBTS, increase the tensile strength considerably, up to a maximum at 0.6 pphp for 3 pphp of HVA-2 (Table 6.7). Tensile strength thereafter decreases with an increase in degree of crosslinking, which increases with the activator level (see Table 6.15). The maximum increase over the control blend for the blend with MBTS was 25%. A 200% increase in tensile strength was reported when using 4.5 phr of HVA-2 with 0.9 pphp of MBTS for NR/PP (60/40) blend [150]. However, the results obtained in the present study cannot be compared accurately with the results of the previous study due to differences found in processing conditions and in moulding techniques used to make test specimens.

The elongation at break, and the secant modulus, also continuously but slightly increases with HVA-2 level when a constant level (0.2 pphp) of MBTS was added. This is associated with relatively increased degree of crosslinking within the GTR phase. However, the increase in degree of crosslinking is limited for such blends (see Table 6.14) and is not as high as expected. Further increase in MBTS level for the blends containing 3 pphp of HVA-2, did not produce a considerable increase in the degree of crosslinking (see Table 6.15), and therefore, no significant improvement in elongation at break is observed. This implies a poor utilization of the MBTS in effective crosslink formation. The non-reacted MBTS may remain in the blend as a filler. However, maximum elongation at break is shown at 0.6 pphp of MBTS for blends containing 3 pphp of HVA-2. A decrease of properties thereafter is associated with phase separation. The highly crosslinked rubber phase may separate from the matrix phase due to the high viscosity ratio during melt mixing. The tensile properties of the blends at this composition are comparable with the blend containing 5 pphp of HVA-2 and 0.2 pphp of MBTS.

(c) *Influence of DTBPIB Addition*

With addition of a constant level (0.2 pphp) of DTBPIB to the blends containing HVA-2, the tensile strength and the secant modulus continuously increase with HVA-2 level (Figure 6.7 and Figure 6.9). These increases were relatively large compared to the increases produced with the addition of the MBTS at the same level. Further increases in the DTBPIB, increase the tensile strength significantly, up to a maximum at 0.6 pphp for 3 pphp of HVA-2 and thereafter decreases (Table 6.7). The maximum increase over the control blend for the blend with DTBPIB was 140%. The secant modulus continuously increases with the DTBPIB level. The relatively improved tensile strength and the secant modulus for the blends with HVA-2 and DTBPIB, compared to those with HVA-2 and MBTS, is mainly associated with the increase in both interfacial crosslink formation (Scheme 6.9) and crosslink formation within the GTR phase by the DTBPIB (Scheme 6.7) and the HVA-2 (Scheme 6.3). In all cases, the morphology is stabilized by a reduced coalescence rate of GTR particles during the melt mixing process [140]. This improves the compatibility of the blends (see Section 6.1.10) and hence results in stabilized phase morphology (see Figure 6.14). A 100% increase in tensile strength over the control blend was reported for virgin NR/PP (80/20) blend [148]. That increase was at 1.5 pphp of HVA-2 and it was initiated with a low concentration of peroxide.

As expected, the addition of DTBPIB to blends containing HVA-2 increases elongation at break drastically for all of the HVA-2 levels studied. Unlike the gradual increase in tensile strength with HVA-2 content, an optimum elongation at break, at 3 pphp of HVA-2, is observed (Figure 6.8). This is due to the additional crosslinks formed within the GTR phase, which restrict the stretching of the GTR molecules. However, due to the formation of additional interfacial crosslinks with DTBPIB, the elongation at break further increased with DTBPIB content up to a maximum of 0.6 pphp (Table 6.7). However, any further increase in both types of crosslinks resulted in a decrease in the elongation at break. The maximum increase in elongation at break over the control blend, 210%, was observed at 0.6 pphp DTBPIB with 3 pphp HVA-2. This suggests the necessity for an optimum level of both HVA-2 and DTBPIB to achieve best properties.

6.1.7 Tensile Fracture

The fracture behaviour of the compatibilized blends was studied by observing the surface of the tensile fractured specimens. Unlike the surfaces of tensile fractured specimens of the WPP and the simple blends (see Figure 5.9 and Figure 5.11), reactive blends with both HVA-2 and DTBPIB exhibited a similar fracture appearance throughout the length of the fractured specimen. During tensile testing, greater elongation of the specimen occurred before failure providing sufficient time for crack development throughout the linear portion. However, the images of reactive blends with HVA-2 alone, and with HVA-2 and MBTS, were very similar to those for simple blends, and can also be represented by the Figure 5.11 in Section 5.1.3.3. The surfaces of these blends showed large voids localized at the interface between two phases towards the fractured end of the specimen. Tiny crazes formed in the WPP phase were apparent on the surface at the other end. This is consistent with their respective stress-strain curves (Figure 6.6).

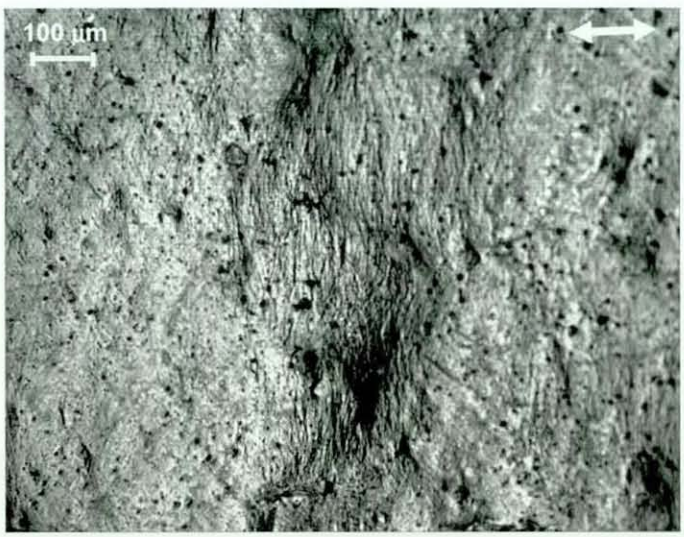

Figure 6.10 Optical microscopic image of stress cracks on the surface of a 50:50/3H/0.6D blend tensile fractured specimen

Figure 6.10 illustrates an optical microscopic image of the surface of a tensile fractured specimen of a blend containing HVA-2 and DTBPIB. The white arrow gives the direction of tensile forces applied. This figure shows tiny multiple cracks developed throughout the specimen. There are no large void assisted cracks on the surface indicating no separation

between phases at fracture. The tiny dark spots in the micrographs are either voids [240] or particulate ingredients and contaminants present in the blends. Since more particulate ingredients were present in this blend, the spots in this image are greater in quantity than that for the control blend (Figure 5.12). These multiple tiny stress cracks are clearly visible when observed under scanning electron microscope at a higher magnification (Figure 6.11).

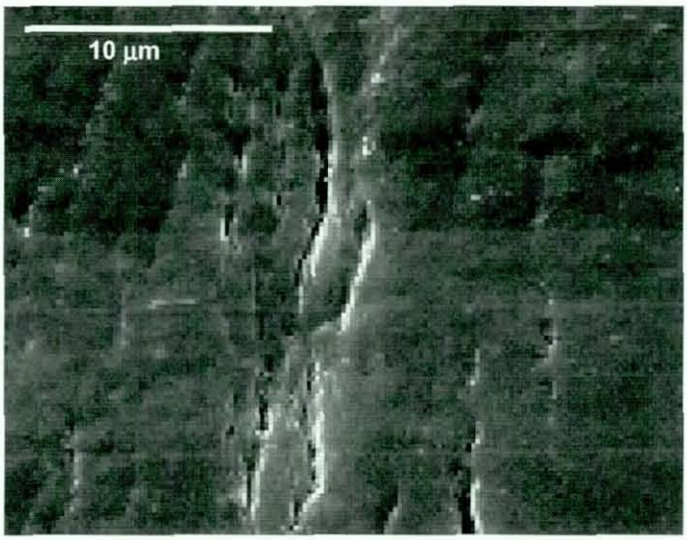

Figure 6.11 SEM image of stress cracks on the surface of a 50:50/3H/0.6D blend tensile fractured specimen

Figure 6.12 shows scanning electron microscopic images of tensile fracture surfaces of the control blend and the blends with HVA-2 alone, at room temperature. All these fractographs exhibit non-homogeneous fracture surfaces overall, with voids created due to the removal of GTR particles from the WPP phase, indicating poor interfacial adhesions. Further, the GTR particles can be clearly identified separating from the WPP phase. Some fibrillation is seen around loosely bound GTR particles (Figure 6.13a) which suggest that a certain level of shear yielding occurred around such GTR particles. Limited regions show a rough surface (Figure 6.13b), suggesting brittle failure of the WPP phase. However, interfacial debonding is the predominant failure mechanism in these blends, and it occurred even at low loads and resultant low tensile properties (Figure 6.7, Figure 6.8 and Figure 6.9). Interfacial debonding or cavitation at the interface was the

preferred failure mechanism for the un-compatibilized blends in the two phase systems (Section 2.8.5.3).

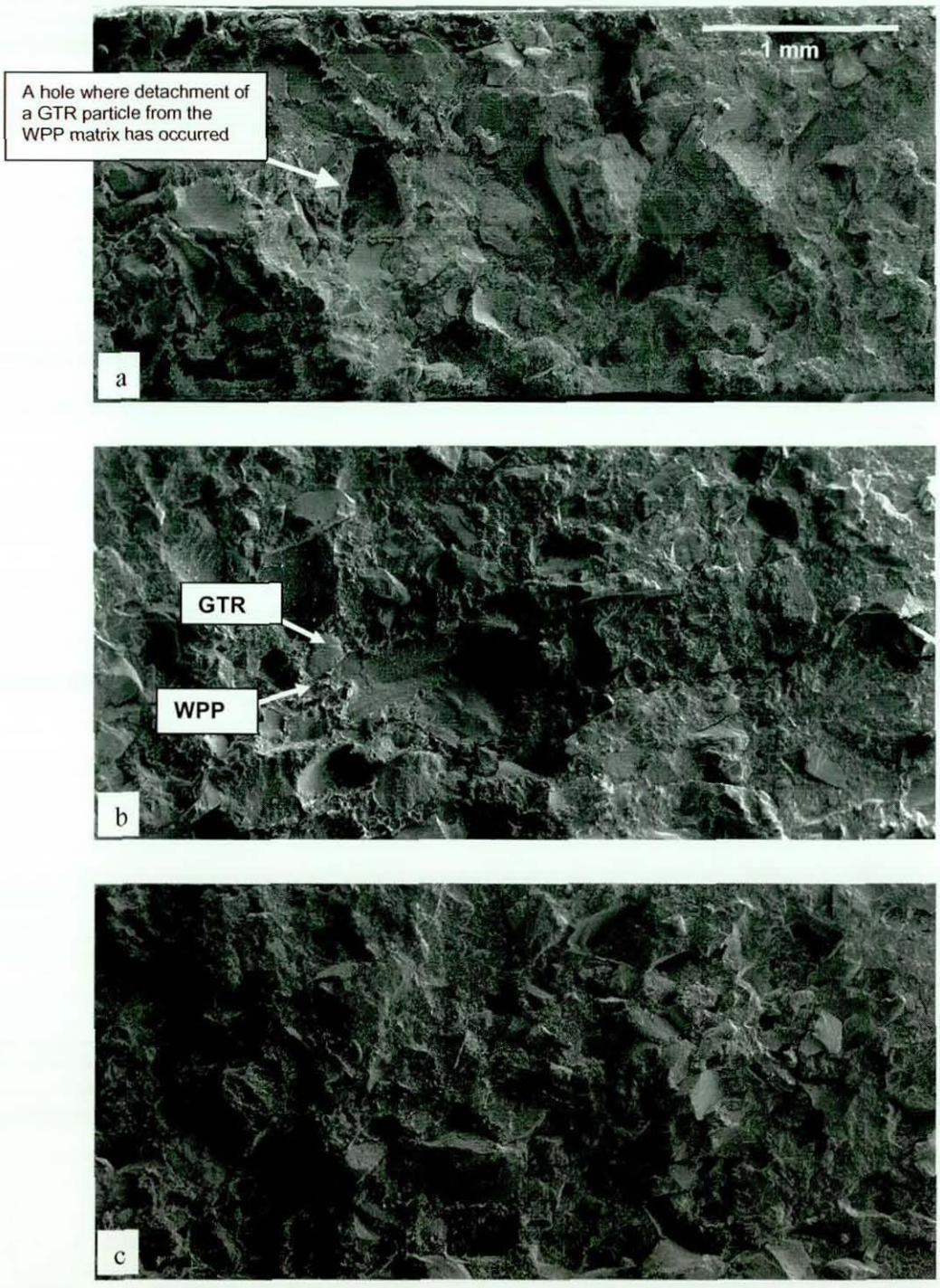

Figure 6.12 Tensile fractographs of 50:50 blends

(a) Control (b) 3H (c) 8H

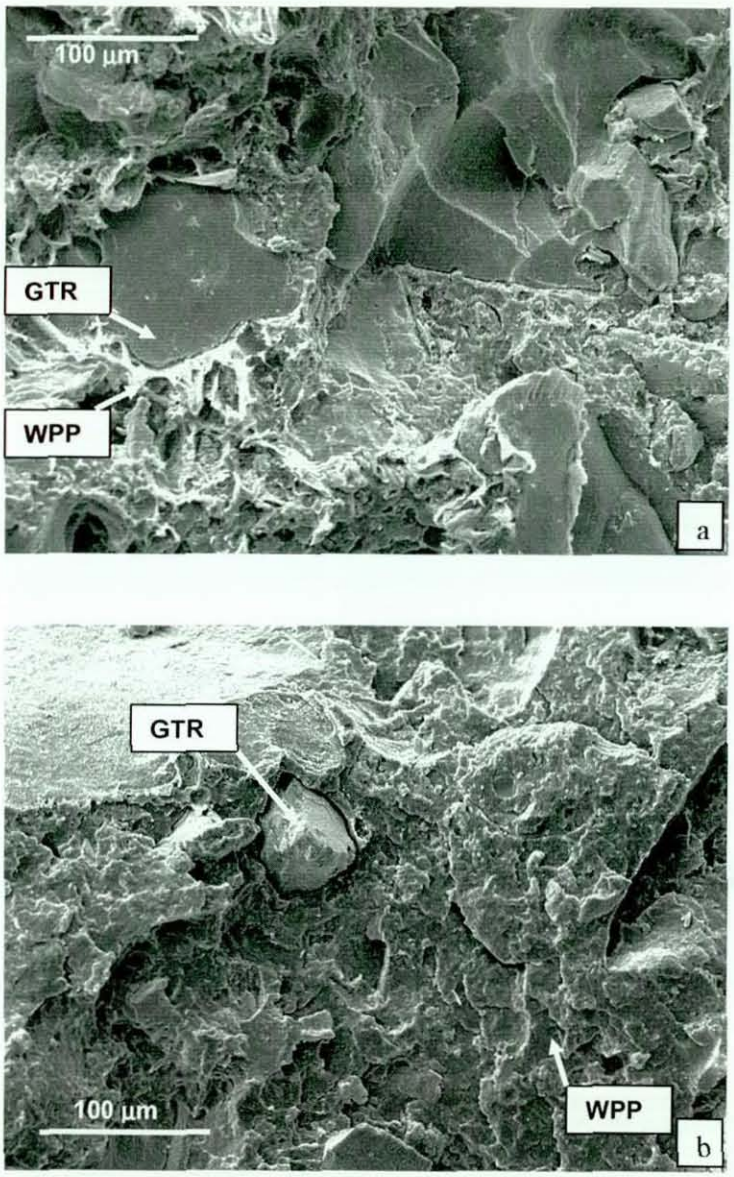

Figure 6.13 Different regions of a tensile fracture surface showing:

(a) shear yielding around loosely bound GTR particle (b) brittle failure

Figure 6.14 shows tensile fractographs for blends containing HVA-2 with activators. The fractograph for the blend containing HVA-2 with MBTS shows a non-homogeneous fracture surface, which is similar to that for the blends with HVA-2 alone (Figure 6.14a). These observations reveal that the crosslinking within the GTR phase does not affect the blend morphology.

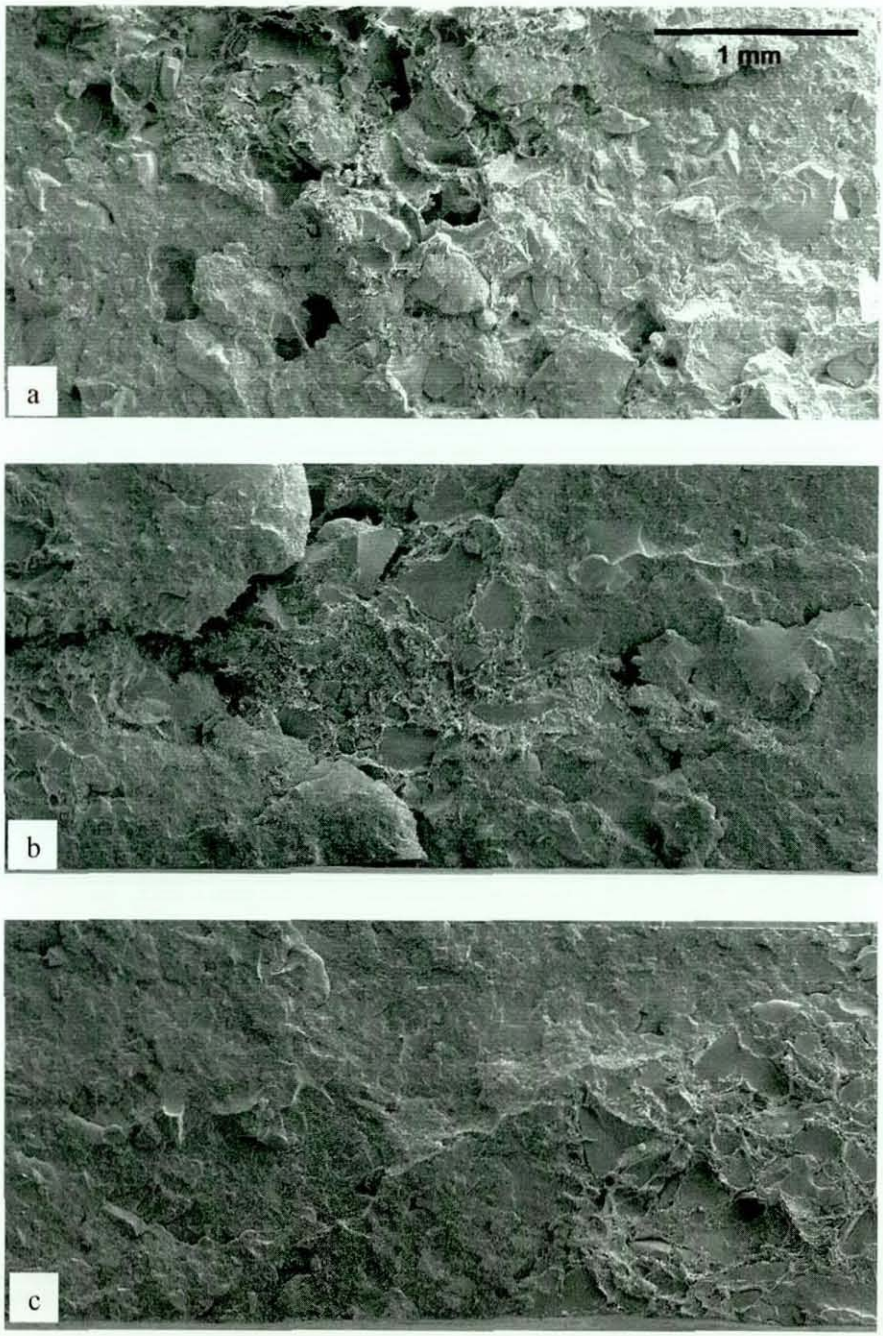

Figure 6.14 Tensile fractographs of 50:50 blends

(a) 3H/0.2M (b) 3H/0.2D (c) 3H/0.6D

In contrast, Figure 6.14b shows more regular shapes and a homogeneous blend. The removal of GTR particles is greatly reduced, and almost no voids due to GTR removal are noticeable in such blends. Further, this blend shows a rough fracture surface, which indicates better tensile properties (Figure 6.7, Figure 6.8 and Figure 6.9). The features of

homogeneity and roughness increase for the blend with higher DTBPIB levels (Figure 6.14c). A similar morphology is observed with cryogenically fractured surfaces (see Figure 6.24). In these fracture surfaces, the GTR particles appear to be entrapped in the WPP phase or covered with the WPP. These covered particles suggest that the blend containing HVA-2 and DTBPIB produce interfacial crosslinks and/or graft copolymers at the interface during melt mixing (Scheme 6.9) which strengthens interfacial adhesion (Figure 6.15). As discussed before, the 3H/0.6D blend exhibits a relatively higher tensile strength.

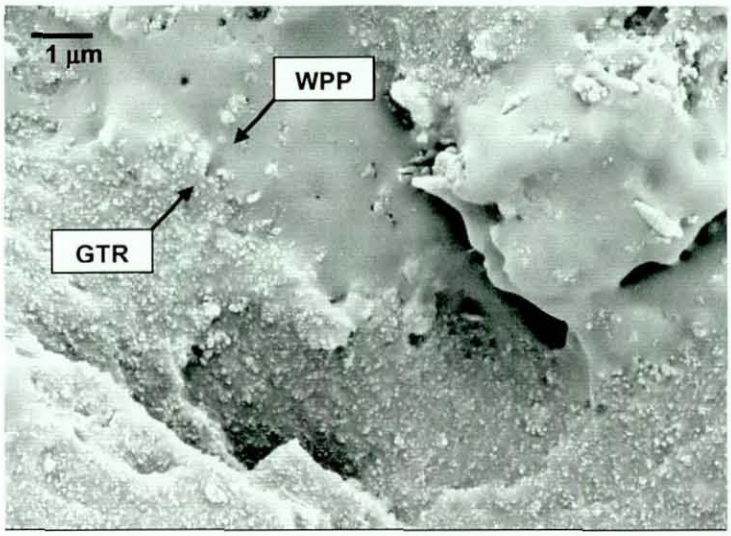

Figure 6.15 A strong interface between polymers in the 3H/0.6D blend

The improved interfacial adhesions (Figure 6.15) improve the compatibility between phases and increase the stress at failure. Further, these adhesions suppress the production of voids, which might grow into cracks. Also the interactions between the stress concentration zones promotes shear yielding [162]. Therefore, the failure can be occurred either due to shear yielding, multiple crazing, internal cavitation or a combined effect of all mechanisms. A fractograph (Figure 6.16) reveals that internal cavitation of the GTR phase also proceeded during tensile straining. Shear yielding, internal cavitation and multiple crazing were identified previously as failure mechanisms for the compatibilized rubber-thermoplastic blends (Section 2.8.5.3).

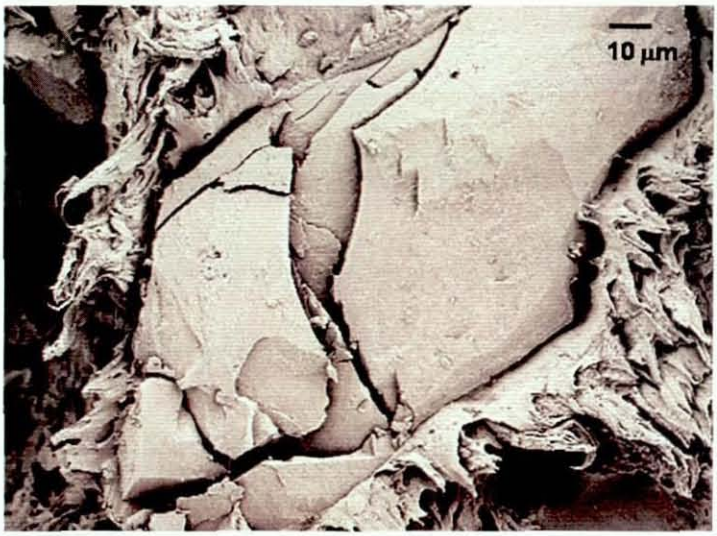

Figure 6.16 Cleavage of a GTR particle in the 3H/0.6D blend during tensile straining

6.1.8 Impact properties

Table 6.8 and Figure 6.17 show the impact properties obtained from the falling dart impact tests performed at 20 ± 1^{0}C. Peak force, which has been shown to correspond to the yield point in the failure process, and stiffness are given in Table 6.8, while the fracture initiation, propagation and failure energies as a function of HVA-2 level are shown in Figure 6.17. The stiffness of the blend is given by the initial slope of the force-displacement curve. The failure mode for each blend is given in Table 6.8 and the image that represents the mode is given in Figure 6.18.

The impact failure of the control blend is a ductile failure process in which the dart drew the material out as it passed through the specimen (Figure 6.18). With the addition of just 1 pphp of HVA-2 to the control blend, the peak force increases, while the stiffness decreases (Table 6.8), suggesting greater deformation before fracture initiation. The fracture initiation energy increases and the propagation energy decreases, resulting in overall higher impact failure energy (Figure 6.17), but with a semi brittle fracture of the specimen (Figure 6.18). As noticed with the torque-time curves (Figure 6.3), this variation is attributed to the formation of more crosslinks in the GTR phase by the HVA-2 (Scheme 6.3). The free radicals formed in the GTR during high shear melt mixing (Scheme 6.1 and Scheme 6.2) will facilitate the formation of crosslinks. A relatively high

degree of crosslinking will provide additional strength to the GTR phase, which will allow GTR molecules to stretch to a greater extent before the failure started. This crosslink formation increases with increase in HVA-2 level up to a maximum level. Once the free radicals formed during mixing are completely utilized, HVA-2 added to the blend may remain un-reacted and behave like a filler. This variation in the degree of crosslinking with the addition of HVA-2 can be verified by the results obtained in the swelling experiments (Section 6.1.4) and boiled xylene extraction experiments (Section 6.1.12). The peak force and hence the stiffness slightly decrease at high HVA-2 levels (Table 6.8) due to lowering the force associated with enhanced phase separation. The highly crosslinked GTR phase will separate from the WPP phase under the application of lesser impact loads due to the greater viscosity difference of the two phases at the processing conditions. Similarly, the impact failure energy passes through a maximum at 3 pphp of HVA-2 suggesting this as the optimum level for the GTR/WPP (50/50) blend.

Table 6.8 Failure mode and peak force of blends having different HVA-2 levels

HVA-2, pphp	Failure Mode	Peak Force*N/mm	Stiffness*. N/mm^2
0	Ductile	67(2)	10(1)
1	Ductile	71(3)	8(1)
2	Ductile	73(4)	8(1)
3	Ductile	73(4)	10(2)
4	Ductile	72(5)	9(0)
5	Semi brittle	71(3)	8(1)
6	Semi brittle	68(4)	8(1)
7	Semi brittle	68(4)	6(1)
8	Semi brittle	65(4)	7(1)

**normalized by dividing by the thickness of each specimen*

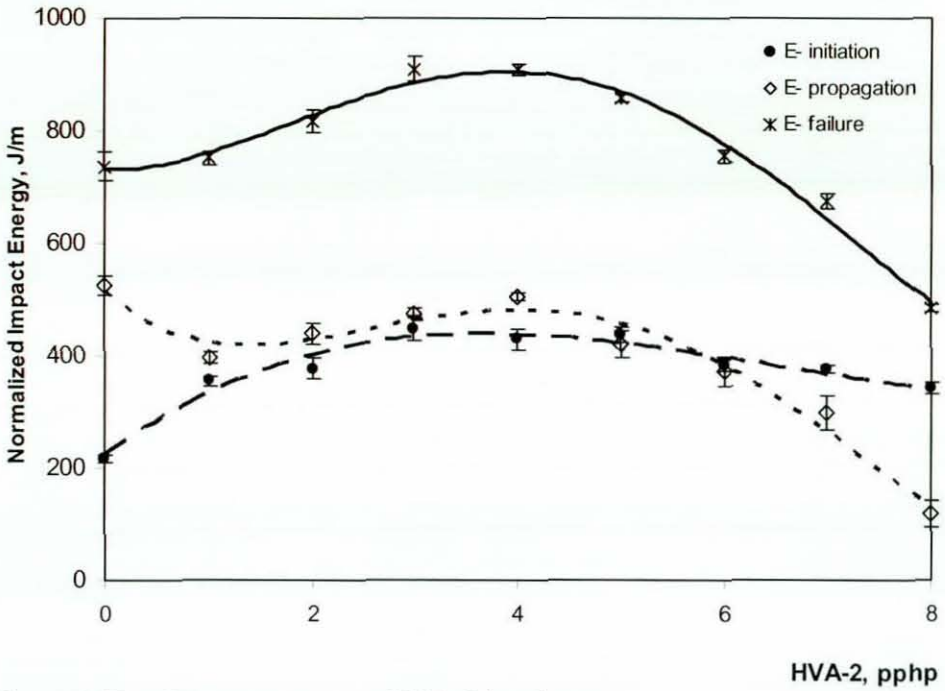

Figure 6.17 Impact energy vs. HVA-2 level

Brittle Semi brittle Ductile

Figure 6.18 Impact failure modes under impact loading

The effect of the addition of an activator on the impact properties of the blends containing different HVA-2 levels is shown in Table 6.9, while the effect of the activators on impact properties are given in Table 6.10. The peak force and the stiffness decrease with the HVA-2 level in the presence of a constant level (0.2 pphp) of MBTS. Therefore, the fracture initiation energy decreases, and the fracture propagation energy remains unchanged, resulting in a further decrease in overall impact failure energy. These variations are attributed to the increased level of phase separation caused by the increased degree of crosslinking in the GTR phase. A further increase in MBTS level, greater than 0.2 pphp, decreases the impact failure energy and results in brittle failure. However, the peak force increases with this increase in MBTS level. These results corresponds with the

results for tensile properties (Section 6.1.6), and confirm behaviour of MBTS as a filler at higher levels.

Table 6.9 Impact properties of blends containing different levels of HVA-2 with 0.2 pphp of activator

HVA-2, pphp	Failure Mode	Peak Force*, N/mm	Initiation Energy*, J/m	Propagation Energy*, J/m	Failure Energy*, J/m	Stiffness*, N/mm^2
			MBTS			
1	Semi Brittle	75(3)	469(28)	415(27)	886(60)	8(1)
2	Semi Brittle	75(4)	468(29)	417(30)	889(31)	8(1)
3	Ductile	69(6)	433(33)	432(40)	872(20)	8(1)
4	Ductile	68(6)	420(41)	412(35)	859(44)	7(1)
5	Ductile	65(5)	381(35)	431(30)	812(54)	7(0)
			DTBPIB			
1	Ductile	101(10)	390(26)	734(22)	1124(95)	15(1)
2	Ductile	108(7)	426(27)	720(41)	1146(92)	14(1)
3	Ductile	124(12)	456(43)	724(68)	1180(73)	18(1)
4	Ductile	149(12)	458(26)	750(38)	1208(68)	20(2)
5	Ductile	192(16)	460(32)	771(64)	1231(98)	26(2)

**normalized by dividing by the thickness of each specimen*

With the addition of DTBPIB to the blends containing HVA-2, a significant increase in the peak force and in the stiffness of the blends resulted. The propagation energy drastically increased providing more ductility to the blend. This effect was greatest at the higher HVA-2 levels. The impact failure energy also increased accordingly. The failure energy further increased with the increase in DTBPIB level (Table 6.10). These improved impact properties are due to better adhesion caused by the formation of interfacial crosslinks [162, 291]. A stronger interface (Figure 6.15) will prevent interfacial debonding under impact loads, will dissipate more energy, and will transfer load effectively from the WPP phase to the GTR phase. In a previous study [197], it was reported that the interfacial adhesion was one of the most important factors affecting the impact of multilayer polymer blends.

Table 6.10 Impact properties of blends containing 3 pphp of HVA-2 with different activator levels

Activator, pphp	Failure Mode	Peak Force*, N/mm	Initiation Energy*, J/m	Propagation Energy*, J/m	Failure Energy*, J/m	Stiffness*, N/mm^2
			MBTS			
0.2	Ductile	69(6)	468(29)	417(30)	872(20)	8(1)
0.4	Semi Brittle	69(2)	460(24)	343(15)	798(60)	8(1)
0.6	Semi Brittle	71(1)	382(21)	302(20)	684(21)	8(1)
0.8	Semi Brittle	74(6)	368(19)	221(16)	597(12)	8(1)
1.0	Semi Brittle	73(2)	287(14)	270(17)	577(11)	8(1)
			DTBPIB			
0.2	Ductile	124(12)	456(43)	724(68)	1180(73)	18(1)
0.4	Ductile	146(8)	422(33)	731(20)	1153(93)	18(1)
0.6	Ductile	165(11)	422(40)	785(60)	1207(42)	26(2)
0.8	Ductile	130(9)	428(42)	785(75)	1213(30)	24(2)
1.0	Ductile	139(13)	493(44)	780(21)	1273(47)	23(2)

**normalized by dividing by the thickness of each specimen*

6.1.9 Melting and Crystallization Behaviour

Structural changes in the WPP phase of the blends with the addition of HVA-2 with and without activators can be evaluated using melting and crystallization properties obtained by differential scanning calorimetry (DSC). The DSC thermograms, both melting endotherms and crystallization exotherm, for the control and the blends with (0.2 pphp) and without MBTS, were very similar, and did not vary significantly with the HVA-2 level. However, some considerable deviations in the DSC thermograms were observed for the blends containing HVA-2 and DTBPIB (Figure 6.19 and Figure 6.20). Thermal properties obtained from the DSC thermograms (Section 3.8.2.2) of blends containing different levels of HVA-2 with (0.2pphp) and without MBTS and DTBPIB are given in Table 6.11.

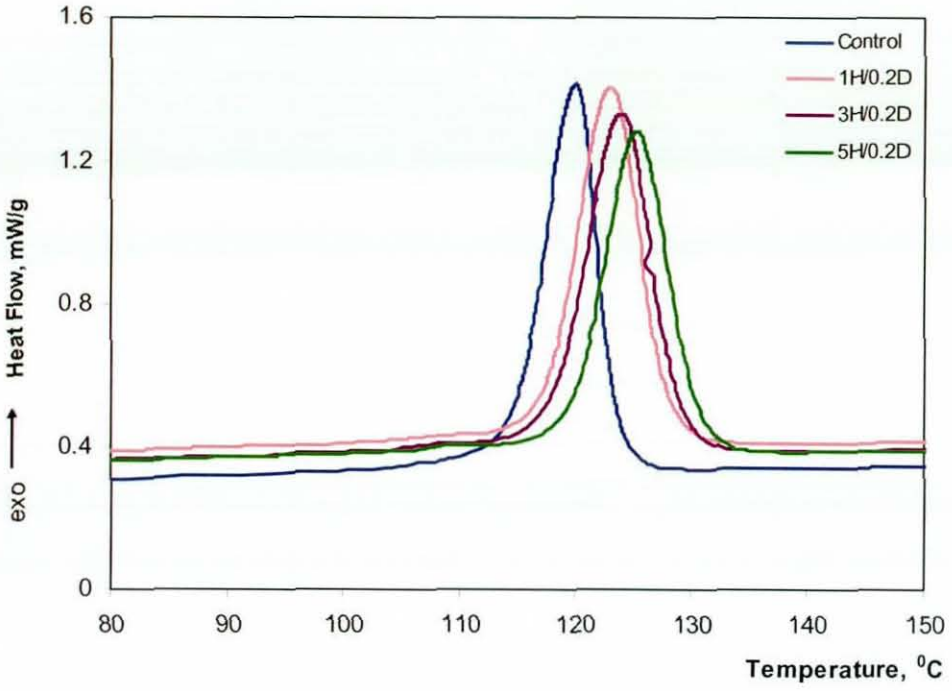

Figure 6.19 Second heating cycle of the control blend and selected blends containing HVA-2 and DTBPIB

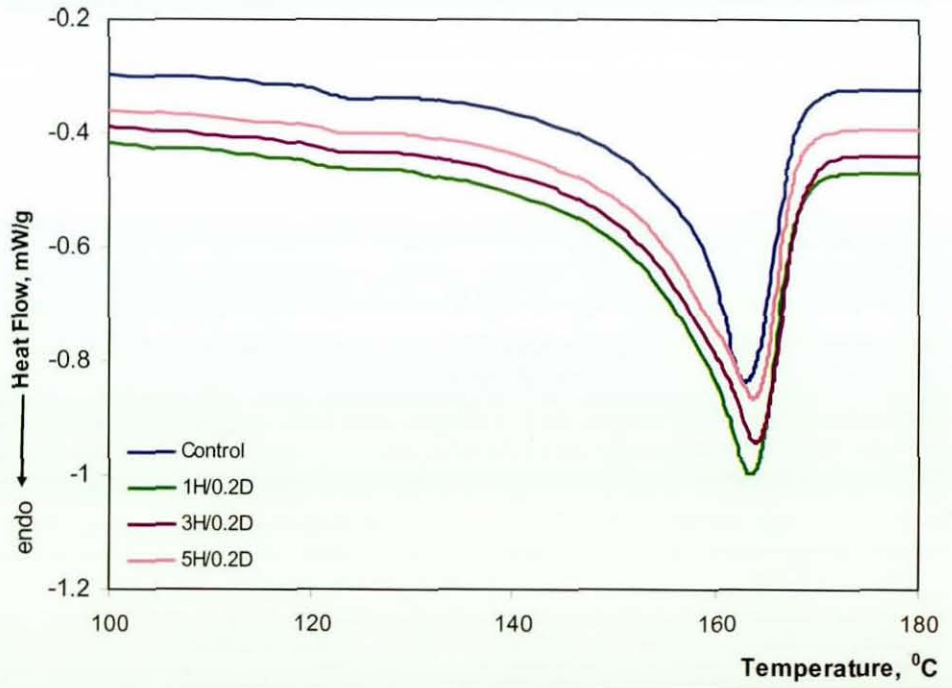

Figure 6.20 Cooling cycle of the control blend and selected blends containing HVA-2 and DTBPIB

Table 6.11 Thermal properties obtained from DSC thermograms of blends containing HVA-2 with (0.2 pphp) and without activators

HVA-2, pphp	T_{co}, ^{0}C	T_p, ^{0}C	H_c, J/g	T_m, ^{0}C	H_f, J/g	ΔT, ^{0}C	ΔW, ^{0}C	S_i, mW/g^{0}C	$\%X_c$ (Blend)	$\%X_c$ (WPP)
Control	128.8(0.6)	120.2(0.3)	45(1)	163.5(0.5)	44(1)	35	5.2(0.1)	0.3(0.0)	21(1)	43(1)
HVA-2 without Activators										
2	129.7(0.7)	199.9(0.4)	46(1)	163.9(0.7)	46(2)	34	5.0(0.2)	0.4(0.1)	22(1)	45(2)
4	130.1(0.6)	120.2(0.3)	41(1)	164.4(0.4)	41(1)	34	5.3(0.3)	0.3(0.1)	20(2)	43(1)
6	129.4(0.2)	120.7(0.5)	42(1)	163.3(0.6)	42(1)	34	5.3(0.3)	0.3(0.0)	20(1)	43(1)
8	128.8(1.0)	120.0(0.5)	44(0)	162.8(0.9)	45(2)	34	4.7(0.3)	0.4(0.0)	22(2)	45(2)
HVA-2 with 0.2 pphp of MBTS										
1	128.9(0.8)	119.5(0.5)	38(1)	164.2(1.2)	39(1)	35	5.3(0.2)	0.3(0.1)	19(1)	38(1)
2	128.7(0.5)	120.2(0.2)	39(0)	163.3(0.6)	39(1)	35	5.1(0.1)	0.4(0.0)	19(1)	39(1)
3	129.4(0.2)	120.4(0.3)	39(1)	164.0(0.9)	39(1)	35	5.2(0.1)	0.4(0.0)	19(1)	40(1)
4	128.4(0.8)	120.9(0.6)	41(0)	163.1(0.4)	43(1)	35	5.2(0.1)	0.4(0.1)	20(1)	40(1)
5	129.4(0.4)	120.7(0.6)	39(1)	163.0(0.4)	40(1)	34	5.0(0.1)	0.4(0.0)	19(1)	40(0)
HVA-2 with 0.2 pphp of DTBPIB										
1	133.3(0.5)	122.9(0.2)	43(1)	163.5(0.4)	44(1)	30	6.4(0.1)	0.3(0.0)	21(1)	42(1)
2	134.5(0.6)	123.3(0.3)	43(1)	163.4(0.4)	43(1)	29	6.4(0.1)	0.3(0.1)	21(1)	43(1)
3	134.9(0.4)	123.8(0.4)	43(6)	163.5(0.8)	43(1)	29	6.4(0.1)	0.2(0.0)	21(1)	43(1)
4	135.4(0.3)	124.5(0.2)	43(1)	163.7(0.5)	43(1)	28	6.4(0.1)	0.2(0.0)	20(0)	43(1)
5	136.5(0.2)	125.2(0.3)	41(1)	163.9(0.8)	40(1)	27	6.3(0.1)	0.2(0.0)	19(1)	40(1)

Table 6.11 shows that the melting temperatures of all blends are in a range 163.5 ± 1^{0}C. This suggests that the chemical reactions due to the presence of HVA-2 either with MBTS or DTBPIB in the blends did not disturb the integrity of the WPP matrix structure. Although degradation of the WPP occurred at high temperature and shearing during the melt mixing process, the identical melting temperature (T_m) suggests the presence of HAV-2, either with MBTS or DTBPIB, significantly limited the crosslinking reactions of the WPP phase, and instead promoted the formation of crosslinking in the GTR phase or at the interface. If the presence of HVA-2 and MBTS or DTBPIB in the blends promoted crosslinking in the WPP phase, the T_m should be greatly affected as branches introduce the defects into the crystals, thus reduces the T_m [159]. This observation also infers that the presence of any activator did not restrict the rearrangement of the WPP molecules during melting and kept chain scission at a minimum. Chain scission increases the melt entropy of polymers and lowers the T_m. However, in a previous study [105], a slight increase in T_m for dynamically vulcanized EDPM/NR/PP blends with HVA-2 was exhibited, compared to the blends without it. It was reported that this slight increment may be due to the restriction in the mobility of the PP phase caused by the crosslinking of the rubber phase. Although such an increase is not noticed in the present study, a drop in the degree of crystallinity, by 2-6%, is noticed for the blends with MBTS activator (Table 6.11). Enhanced crosslinking in the GTR phase and at the interface may cause restrictions in crystal formation [197] in the WPP phase.

The properties obtained from the crystallization exotherms, including peak crystallization temperature (T_p), onset crystallization temperature (T_{co}), heat of crystallization (ΔH_c), half width of the crystallization exotherm (ΔW) and slope of the high temperature side of the thermogram (S_i), do not significantly vary with the HVA-2 level, even in the presence of 0.2 pphp of MBTS (Table 6.11). The super cooling (ΔT) is therefore the same for these blends. These results suggest that the HVA-2 had no influence on the WPP phase [162], and reconfirm the crosslink formation in the GTR phase. However, T_p and T_{co} for the blends containing HVA-2 and 0.2 pphp of DTBPIB differ from the above blends by 2-5 ^{0}C and 3-7 ^{0}C, respectively (Figure 6.15). Also these temperatures increase with increase in HVA-2 level indicating an acceleration of the crystallization process in the WPP due to the interfacial crosslinks formed. However, it has been reported [105] that the addition of HVA-2 alone into EPDM/NR/PP blends can influence the crystallization

process by improving the packing of the polymer chains into a crystalline structure at high temperature, thus restricting the unfolding of the polymer chains.

The blends containing HVA-2 and 0.2 pphp of DTBPIB further exhibit lower super cooling (Table 6.11), indicating a rapid rate of nucleation. Due to this rapid rate of nucleation, small crystals will form, however, due to a slow rate of crystallization, which is indicated by S_i, some crystals will grow to the optimum size. Thus, the crystallite size distribution will be broader, and this is clearly shown by a relatively large ΔW. This confirms that the presence of both HVA-2 and DTBPIB affected the crystalline structure of the WPP phase resulting in the coexistence of different crystalline structures. The crystallization exotherms of these blends further show a second minor peak, which cannot be seen in the exotherm for the control blend (Figure 6.20). This may be associated with the formation of different crystalline structures. Alternatively this could be associated with crystallization of the PE in the WPP. The crystallization exotherms of PP and PE are not overlapped in these blends, as the crystallization occurred at relatively higher temperatures (Table 6.11).

The variation of thermal properties with the activator level is given in Table 6.12. These properties for the blends containing 3 pphp of HVA-2 with MBTS are identical and do not vary with MBTS level. However, an increase in T_p and T_{co}, and rate of nucleation, with increase in DTBPIB level, is noticed for the blends containing 3 pphp of HVA-2 with DTBPIB. The small crystals formed due to rapid nucleation at high DTBPIB provide enhanced tensile properties. These results are in agreement with the torque-time curves (Figure 6.5), the xylene insoluble fraction (Figure 6.26) and the DSC thermograms of gels from boiled xylene extractions obtained (Figure 6.28), and reconfirm the formation of more interfacial crosslinks in these blends. However, the rate of crystallization, the crystal size distribution and the degree of crystallinity do not vary with the DTBPIB level.

Table 6.12 Thermal properties obtained from DSC thermograms of blends containing 3 pphp of HVA-2 with different levels of activators

Activator, pphp	T_{co}, ^0C	T_p, ^0C	H_c, J/g	T_m, ^0C	ΔH_f, J/g	ΔT ^0C	ΔW, ^0C	Si, mW/g^0C	$\%X_c$ (Blend)	$\%X_c$ (WPP)
HVA-2 only	128.2(0.1)	120.8(0.3)	42.8(0.3)	164.1(0.5)	43(1)	35	5.2(0.1)	0.3(0.0)	21(0)	43(0)
With MBTS										
0.2	129.4(0.2)	120.4(0.3)	39(1)	164.0(0.9)	39(1)	35	5.2(0.1)	0.4(0.0)	19(1)	40(1)
0.4	128.9(0.1)	120.5(0.1)	42(1)	163.8(0.3)	41(0)	35	5.1(0.1)	0.4(0.0)	20(1)	41(1)
0.6	128.5(0.5)	120.6(0.1)	40(0)	163.8(0.2)	41(1)	35	5.1(0.1)	0.4(0.0)	20(0)	41(1)
0.8	128.5(0.6)	120.3(0.2)	41(1)	163.6(0.4)	41(0)	35	5.4(0.1)	0.4(0.0)	20(0)	41(1)
1.0	129.2(0.1)	120.3(0.2)	41(1)	163.6(0.2)	42(1)	34	5.6(0.1)	0.3(0.0)	20(1)	41(1)
With DTBPIB										
0.2	134.9(0.4)	123.8(0.4)	43(1)	163.5(0.8)	43(1)	29	6.4(0.0)	0.2(0.0)	20.6(0.5)	43(1)
0.4	136.3(0.5)	126.5(0.6)	43(0)	163.2(0.5)	44(1)	27	6.4(0.1)	0.2(0.0)	20.8(0.2)	43(0)
0.6	137.9(0.3)	127.2(0.5)	41(0)	162.9(0.6)	43(1)	25	6.0(0.3)	0.2(0.0)	20.7(0.5)	43(1)
0.8	139.3(0.3)	127.1(0.6)	45(1)	162.9(0.4)	44(1)	24	6.2(0.4)	0.2(0.0)	21.2(0.9)	44(1)
1.0	135.5(0.7)	125.2(0.8)	43(1)	163.7(0.7)	42(0)	24	6.1(0.2)	0.2(0.0)	20.2(0.4)	42(1)

6.1.10 Dynamic Mechanical Properties

Structural changes in both phases of the blends with the addition of HVA-2, with and without activators can be evaluated using properties obtained by dynamic mechanical analysis (DMA). Variations of storage modulus, loss modulus and of tan δ with temperature for blends containing HVA-2 alone are given in Figure 6.21, Figure 6.22 and Figure 6.23, respectively. Glass transition temperatures determined from tan δ curves and storage modulus for selected blends containing HVA-2 with and without activators are given in Table 6.13.

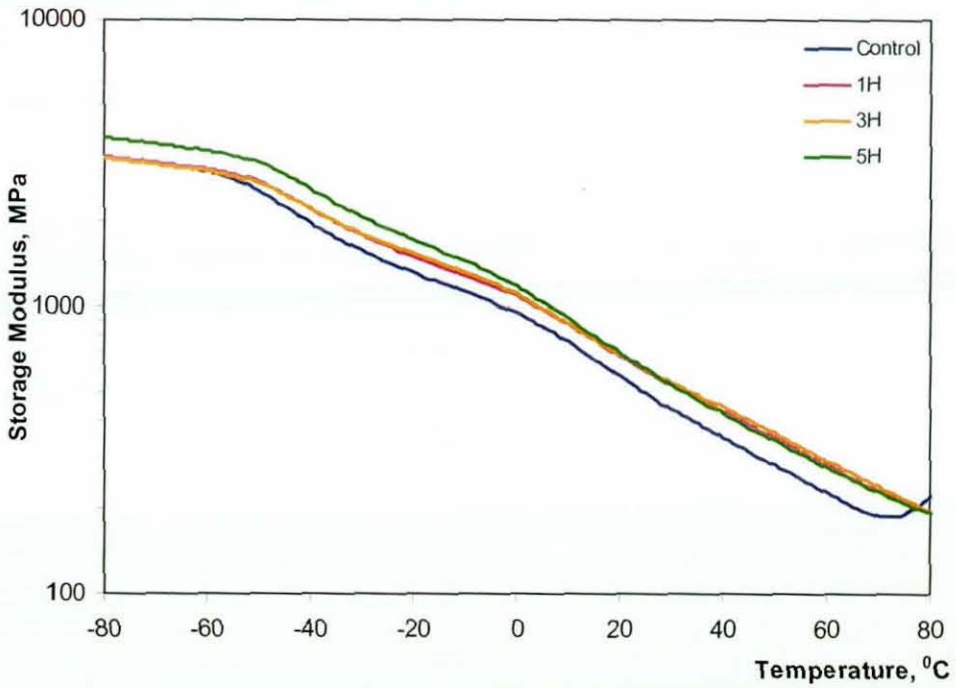

Figure 6.21 Storage modulus vs. temperature for blends with HVA-2 alone

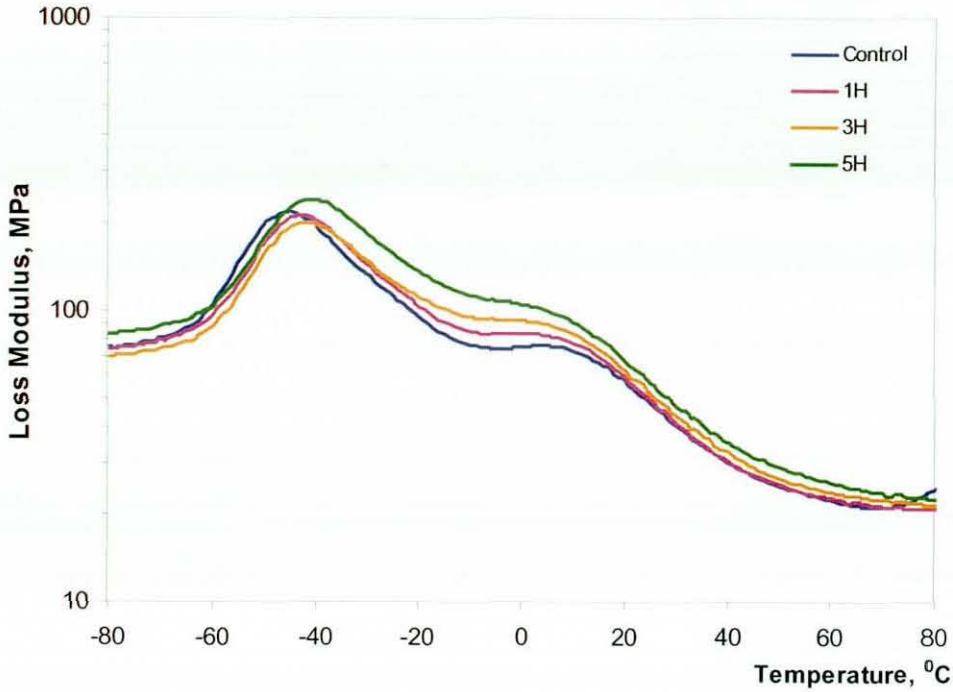

Figure 6.22 Loss modulus vs. temperature for blends containing HVA-2 alone

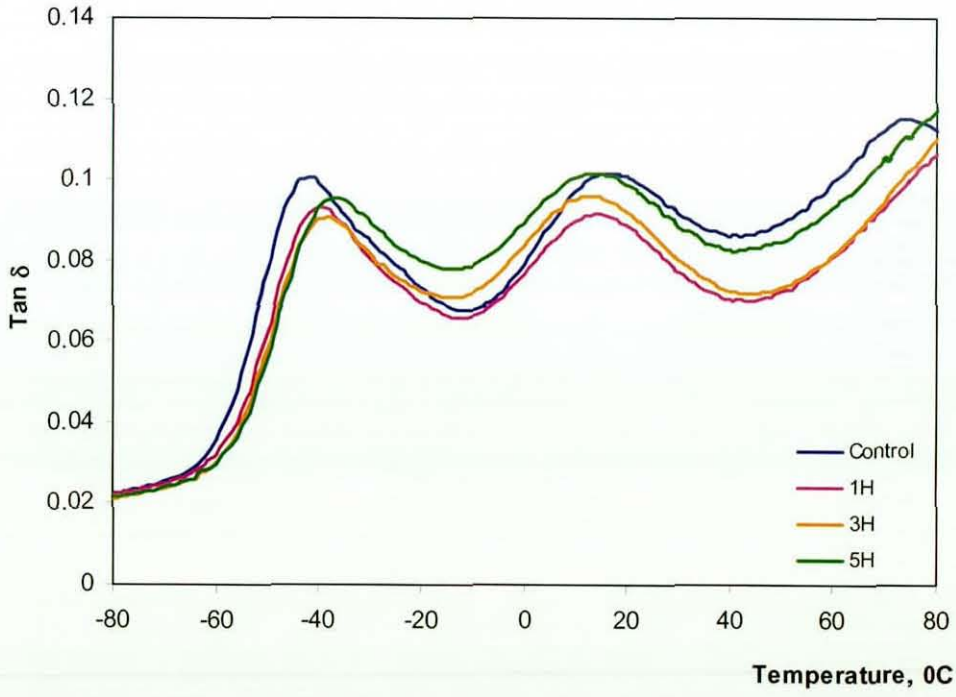

Figure 6.23 Tan δ vs. temperature for blends containing HVA-2 alone

Table 6.13 Dynamic mechanical properties of selected blends containing HVA-2 with and without activators

Sample Code	T_g of GTR, ^0C	T_g of WPP, ^0C	Temperature Difference, ^0C	Storage Modulus @ 20 ^0C
Control	-42	15	57	574
1H	-39	15	54	665
3H	-38	14	52	682
5H	-37	14	51	689
1H/0.2M	-39	14	54	675
3H/0.2M	-37	14	51	687
5H/0.2M	-37	14	50	715
3H/0.6M	-37	14	51	731
1H/0.2D	-38	16	54	663
3H/0.2D	-37	15	52	625
5H/0.2D	-36	15	51	723
3H/0.6D	-36	16	52	660

Both the storage modulus and loss modulus show higher values for the blends containing HVA-2, over the temperature range recorded. Further, the glass transition temperature (T_g) of the GTR shifts to a higher temperature with the addition of HVA-2 thus decreasing the difference in T_g of the phases (Table 6.13). The shift in T_g of the GTR is high at high HVA-2 levels. These results confirm the formation of additional crosslinks in the GTR phase by the HVA-2, as proposed in Scheme 6.3. It was reported in a previous study [105] that an increase in T_g of the rubber phase occurred after dynamic vulcanization with HVA-2. This was for EPDM/PP blends. The shift in T_g of the WPP to a lower temperature is limited only to 1 ^0C. This result confirms that the crosslinking reaction in the GTR proceeded selectively.

With the addition of activators into the blends containing HVA-2, the storage modulus at 20 ^0C increases continuously with the HVA-2 level and further with the activator level (Table 6.13). Similar trends are noted for the secant modulus at 2% strain, obtained under

tensile straining (Figure 6.9).The blends show greater shifts in the T_g of the GTR to a high temperature, confirming an increased degree of crosslinking in the GTR phase. This shift is relatively high for blends containing HVA-2 with DTBPIB, and is due to the formation of interfacial crosslinks (Scheme 6.9). Participation of the WPP in the crosslinking process increases the T_g of the WPP, slightly. As expected, no large increase in the T_g of the WPP was observed, thus confirming the limited selectivity for crosslinking within the WPP phase. Closeness of the T_g values for the reactive blends compared to that for the control blend explained enhanced compatibility of the reactive blends.

6.1.11 Blend Morphology

Blend morphology was studied using SEM images of the surfaces fractured in liquid nitrogen. The cryo-fractographs, which are illustrated in Figure 6.24, show regular shapes and brittle fracture. However, Figure 6.24b exhibits a more brittle surface with many tear lines. The roughness of the fractured surface increases with the addition of the compatibilizing system (Figure 6.24b). The nature of this figure provides further evidence for effective crosslinking in both phases, thus explaining the significant improvement in mechanical properties. This kind of observation has been reported [105] for EPDM/NR/PP blends when dynamically vulcanized with HVA-2.

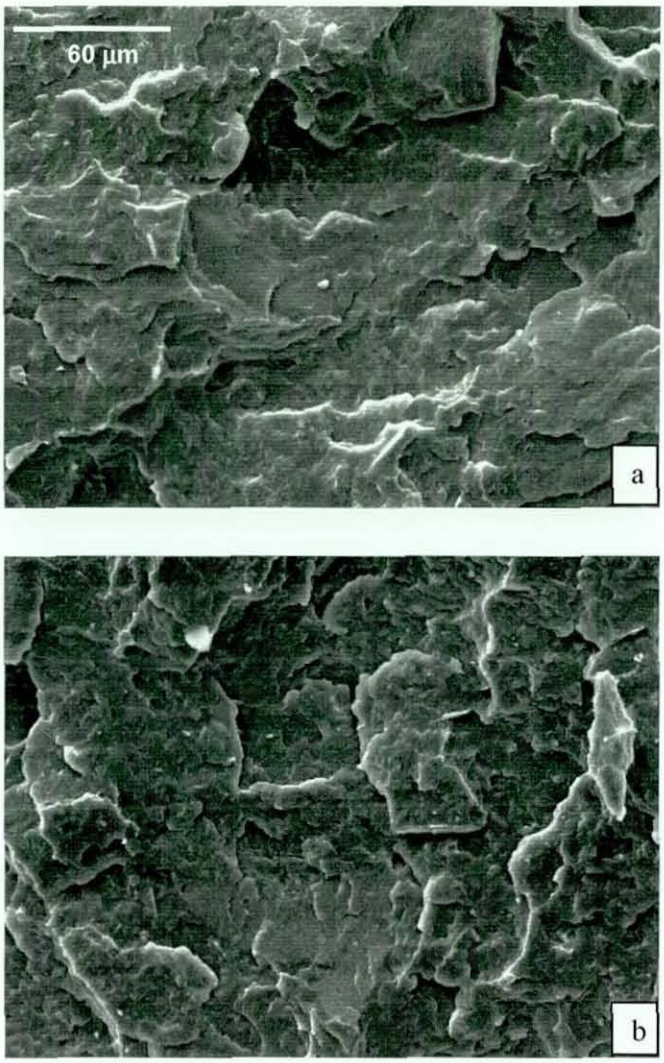

Figure 6.24 SEM images of cryo-fractured surfaces of
(a) Control blend (b) 3H/0.6D blend

6.1.12 Boiled Xylene Extraction

Un-crosslinked PP and un-crosslinked rubbers, in general, completely dissolve in boiled xylene. However, both WPP and GTR show residues due to the presence of particulate additives and impurities of particle sizes greater than 100 µm, and the xylene insoluble fractions were measured as 15 % and 12% respectively.

The xylene insoluble fractions of the control blend and the blends containing HVA-2 with and without MBTS and DTBPIB activators are shown in Figure 6.25. The degree of crosslinking calculated according to Equation 3.21 in Section 3.9.3 for the above blends are given in Table 6.14. The xylene insoluble fraction of the control blend showed a much higher value, 38%, compared to the insoluble fractions of the individual polymers, confirming the formation of crosslinks during melt mixing.

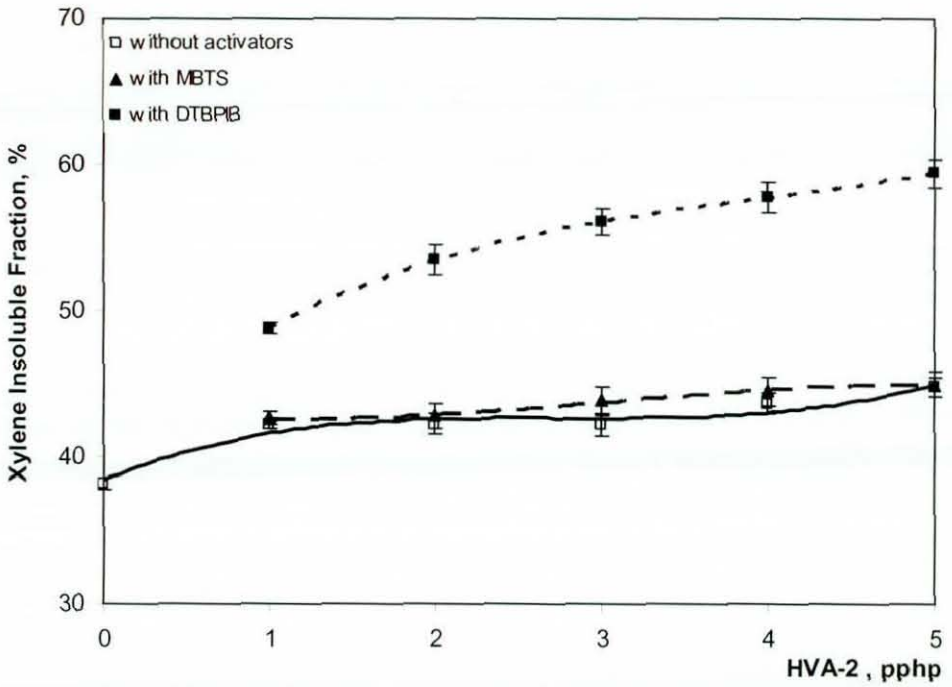

Figure 6.25 The xylene insoluble fraction for blends containing HVA-2 with (0.2 pphp) and without activators

The xylene insoluble fraction increases with the addition of HVA-2 to the control blend (Figure 6.25 and Table 6.14). This increase remains unchanged up to 3 pphp of HVA-2. Further, the xylene insoluble fraction increases continuously but slightly with HVA-2 level in the presence of MBTS, and remarkably in the presence of DTBPIB. This xylene insoluble fraction does not show a significant increase with MBTS level, but increases drastically with the DTBPIB level up to 0.6 pphp (Figure 6.26 and Table 6.15). These observations are in agreement with the swelling characteristics (Section 6.1.4), and with the mechanical properties (Section 6.1.6 and Section 6.1.8).

Table 6.14 Degree of crosslinking of blends containing HVA-2 with (0.2 pphp) and without activators

HVA-2, pphp	Degree of Crosslinking, %			Degree of crosslinking of the blend compared to the control blend, %		
	without activators	with MBTS	with DTBPIB	without activators	with MBTS	with DTBPIB
0	56(1)					
1	66(0)	68(1)	85(2)	18	21	52
2	67(1)	69(1)	95(2)	20	23	70
3	68(1)	72(2)	101(2)	21	29	80
4	71(2)	76(2)	107(2)	27	36	91
5	75(1)	78(2)	112(2)	34	39	100

The degree of crosslinking was high at higher HVA-2 contents, but was always less than 100%, even with MBTS. However, the degrees of crosslinking in the blends at high HVA-2 contents, in the presence of DTBPIB, were greater than 100%, thus confirming the adhesion of the WPP phase to the GTR phase hence also confirming that the WPP was also involved in the crosslinking process. This adhesion can be due to the formation of interfacial crosslinks and/or the formation of graft copolymers (Figure 6.15). This effect is similar for an increase in DTBPIB content, but is significant at higher contents. The proposed chemical reaction for the formation of interfacial crosslinks in the presence of DTBPIB and HVA-2 is given by Scheme 6.9 in Section 6.1.1.5.

The blend with DTBPIB alone produced in the lowest xylene insoluble fraction at 38% and the degree of crosslinking at 55 %, which is caused by degradation of the WPP (Scheme 6.7). This is in agreement with the processing characteristics obtained (Figure 6.3). These results are further confirmed by the appearance of the gel and sol obtained, and with the DSC thermograms of the gels.

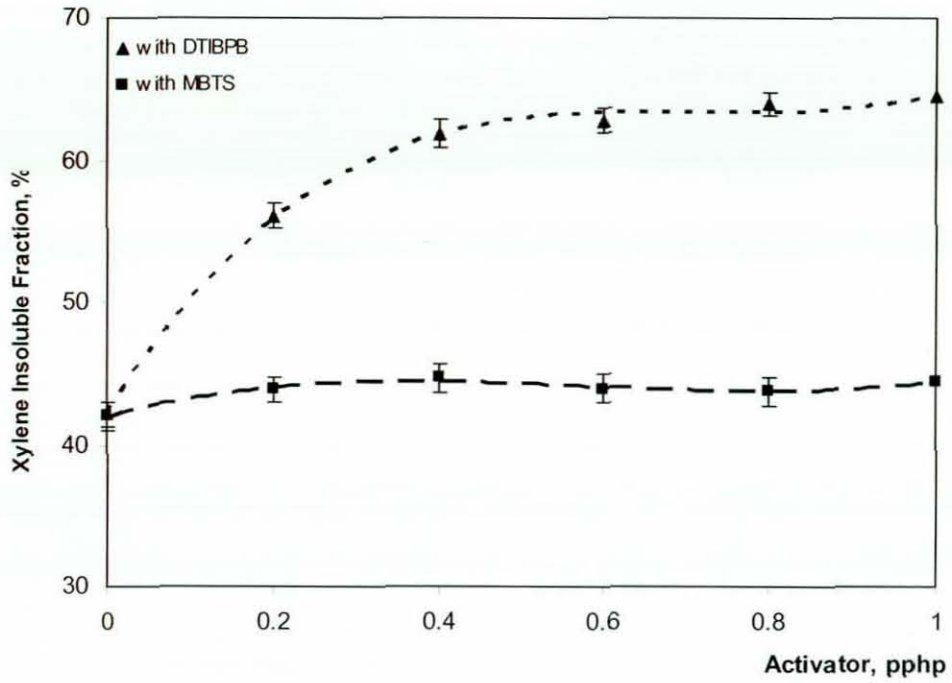

Figure 6.26 Xylene insoluble fraction of blends containing 3 pphp of HVA-2 with different activator levels

Table 6.15 Degree of crosslinking of blends containing 3 pphp of HVA-2 with different activator levels

Activator, pphp	Degree of Crosslinking, %	
	with MBTS	with DTBPIB
0	68(2)	-
0.2	72(1)	101(2)
0.4	72(1)	115(2)
0.6	72(1)	118(2)
0.8	76(1)	121(2)
1.0	78(1)	123(1)

Figure 6.27 shows the appearances of gel fractions and sol fractions obtained during boiled xylene extraction while Figure 6.28 illustrates the DSC thermograms of the gel

fractions. The gel from the control blend was a free flowing fine powder (Figure 6.27) which did not exhibit any peak assignment for the melting point of PP at 166 ^{0}C (Figure 6.28). The gel from the 3H blend was a coarse powder which could be crushed under finger pressure. The DSC thermogram for the 3H blend also did not exhibit a peak for PP, but the 5H blend exhibited a small peak assigned to PP which revealed that a limited crosslinking reaction occurred in the GTR/WPP blends, at the interface.

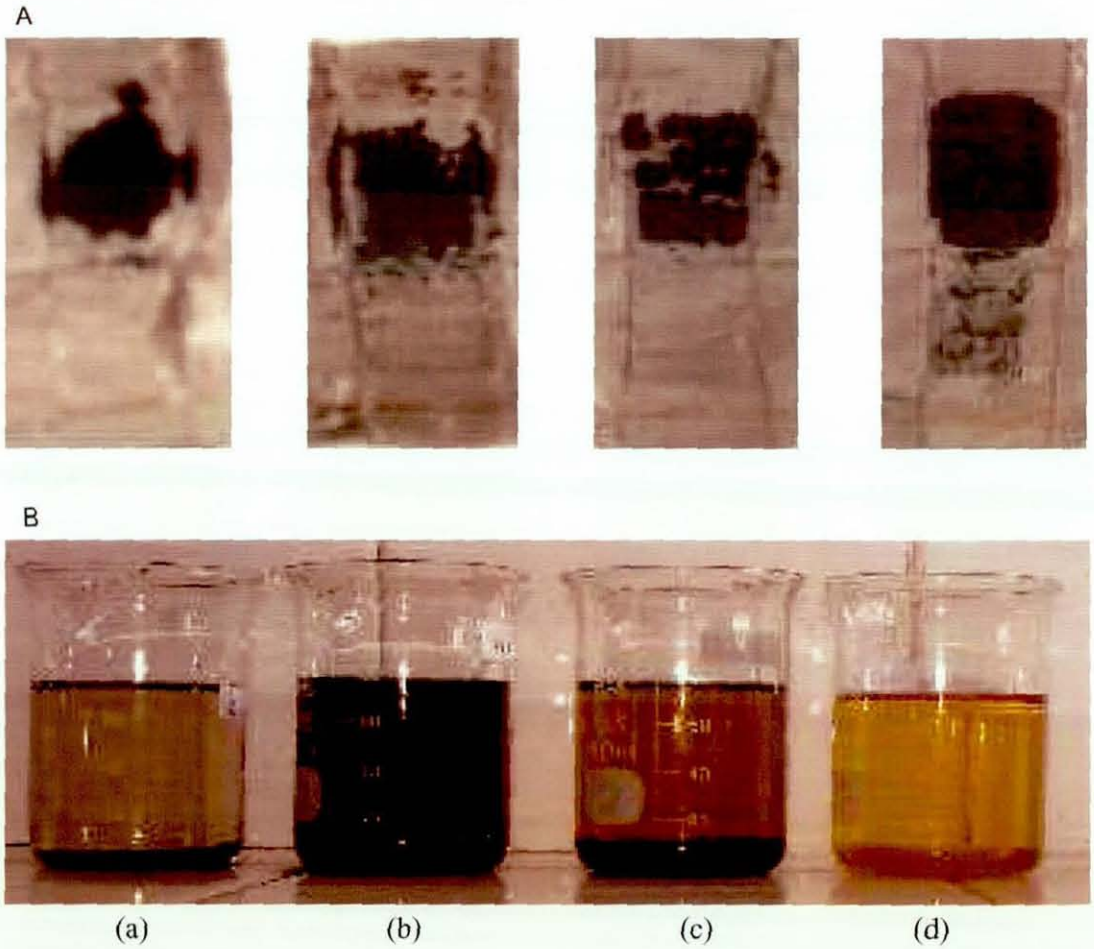

Figure 6.27 Gels and sols from the blends after boiled xylene extraction; A- gel, B-sol

(a) Control (b) 3H (c) 3H/0.6M (d) 3H/0.6D

The gels from the blends containing HVA-2 with MBTS were also free flowing coarse powders. The gel from the 3H/0.2M blend did not show any peak assignment for the PP. However, that from the 5H/0.2M blend exhibited a small peak, similar to the gel from the 5H blend. These results suggest that a certain level of HVA-2 is required before crosslinking between the phases in the GTR/WPP blend commenced, either with or

without MBTS. Alternatively crosslinking reactions proceeded at the GTR phase selectively (Scheme 6.3).

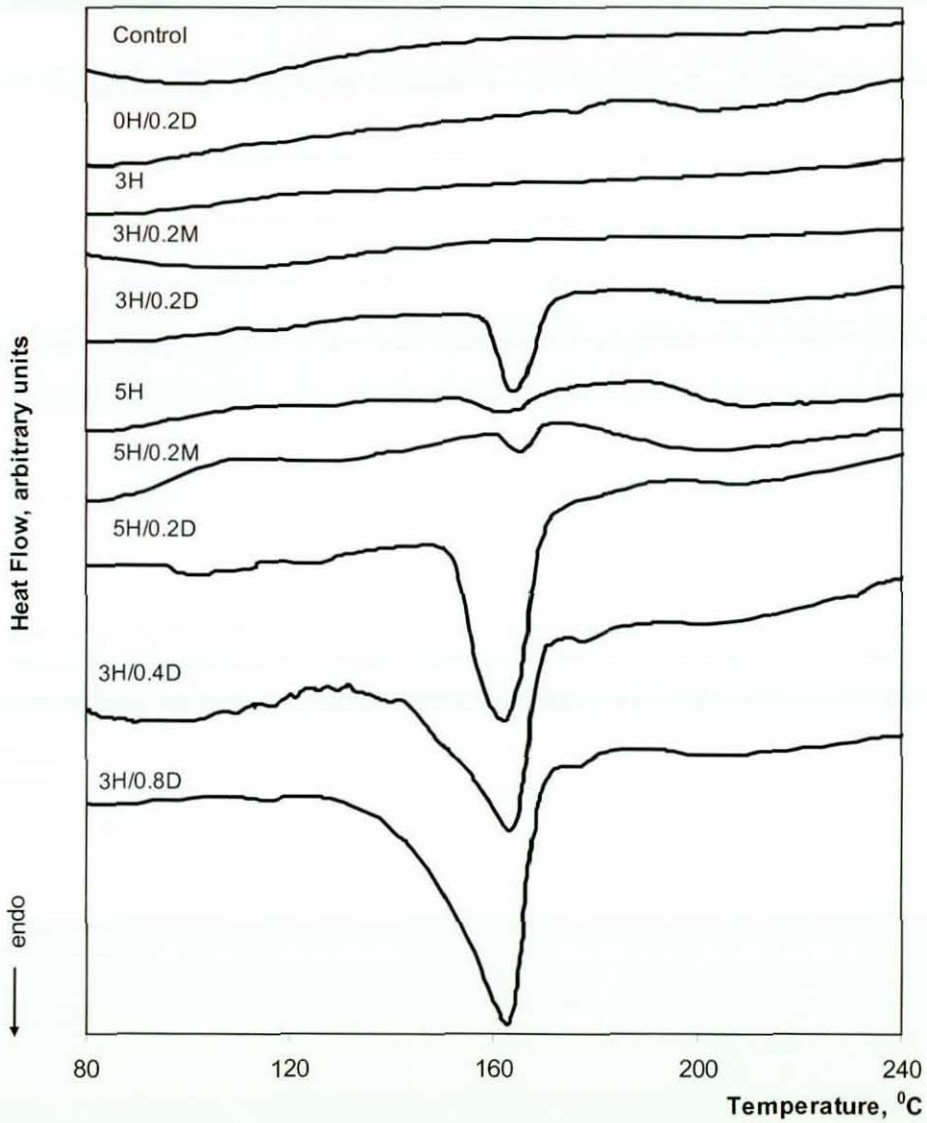

Figure 6.28 DSC thermograms of gel of blends after boiled xylene extraction

The gels from the blends containing HVA-2 and DTBPIB were combined into single masses and show significant peaks assigned to WPP, indicating that the selectivity is retained in the WPP phase. These peaks become larger and also broader with an increase in the HVA-2 level and further in the DTBPIB level, and confirm the formation of increased levels of interfacial crosslinking. However, the appearance of the gel from the blend with DTBPIB alone was very similar to that of the control blend. It did not show

the peak assigned to WPP, and hence confirms the failure in formation of interfacial crosslinks with DTBPIB alone for the WPP/GTR blends, although these have been reported with virgin NR/PP blends [146].

Figure 6.29 shows the FTIR spectra of the gel fractions obtained during xylene extraction. The spectrum for the gel from the control blend exhibits peaks between 2960 cm^{-1} and 2850 cm^{-1} and at 1460 cm^{-1} which represent hydrocarbon compounds. They also exhibit a dominant peak at 1680 cm^{-1} which indicates a greater content of carbon black present in the gel. The presence of more hydrocarbons in the gels, especially alkanes, from the blends containing 3 pphp of HVA-2, with and without MBTS is supported by the increased intensity of the above peaks. Additionally, both spectra show significant multiple peak assignments between 1200 cm^{-1} and 800 cm^{-1}, which are associated with C-C stretching vibrations, and confirm the presence of more alkanes. This observation indicates the presence of the GTR phase (see FTIR spectrum for the GTR given in Figure 4.11 in Section 4.2.2.1) in such gels.

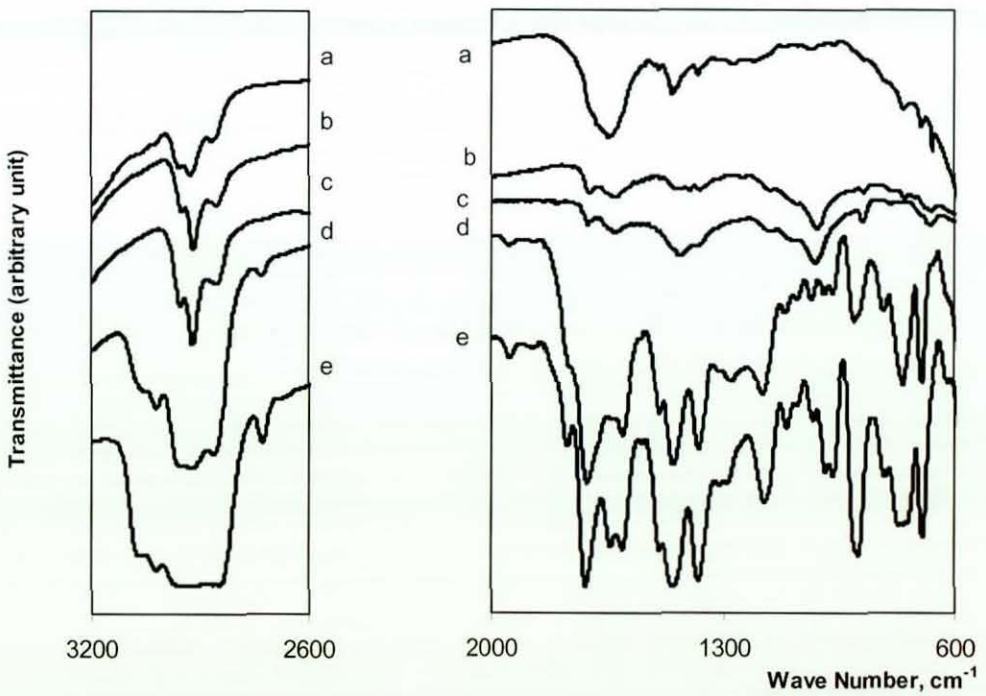

Figure 6.29 FTIR spectra of gels from blends after boiled xylene extraction:
(a) Control (b) 3H (c) 3H/0.6M (d) 5H/0.2M (e) 5H/0.2D

The spectrum for the gel from the 5H/0.2M blend exhibits some additional peaks. These peaks between 3080 cm^{-1} and 3020 cm^{-1}, which correspond to C-H stretching vibrations in alkenes, represent the presence of more GTR in the gel compared to that in the gel from the control blend. Further, the appearance of significant peak assigned to WPP at 1380 cm^{-1} (see FTIR spectrum of the WPP given in Figure 4.3 in Section 4.1.3.1) in this spectrum confirms the presence of WPP in the gel from the 5H/0.2M blend. In addition, a prominent peak at 1720 cm^{-1}, which corresponds to C=O stretching vibrations, indicates the presence of HVA-2 in the gel. The presence of HVA-2 in the gel is confirmed with the appearance of a peak at 1182 cm^{-1}, which corresponds to C-N stretching vibrations. The peak at 1380 cm^{-1} also represents C-H stretching vibrations of the aromatic rings presence in the HVA-2. The appearance, with greater intensities, of the peaks at 1182 cm^{-1}, 1380 cm^{-1} and 1720 cm^{-1} in the spectrum for the gel from the 5H/0.2D blend suggests the presence of HVA-2 in greater content. These spectrum further shows higher intensities for the prominent peaks, assigned to both the GTR and the WPP, and hence confirm their presence in greater quantities. These observations are in agreement with the degree of crosslinking resulted (Table 6.14 and Table 6.15), and the intensity of endothermic peaks recorded on DSC thermograms (Figure 6.28).

The sol component of the control blend was partly clear but showed a black precipitate at the bottom of the flask (Figure 6.27). This black precipitate indicates dissolution of carbon black and some other particulate additives in the xylene. The sol from the blend containing HVA-2 alone was a turbid solution with fine black dispersed particles, but with a considerable black precipitate. The sols from the blends containing HVA-2 and MBTS were a clear light brown solution with black precipitates. The quantity of precipitates obtained from the blends containing HVA-2 with and without MBTS were the same. These observations imply that increased level of fine particles are entrapped in the gel in the presence of HVA-2 with MBTS. This is in agreement with the slightly increased xylene insoluble fraction for such blends (Figure 6.25). The light brown colour of the sol was due to the combined effect of the dissolution of the HVA-2 and less black pigments in the xylene.

The sol from the blend containing DTBPIB was a clear yellow coloured solution, with a thick white gel at the bottom. The yellow colour was due to the dissolution of the HVA-2 in the xylene and the white gel may be un-crosslinked WPP. The absence of black

precipitates in this blend suggests the entrapment of carbon black and other particulate additives in the network that was formed during blending, which result in a further enhancement of the mechanical properties.

FTIR spectra for the sols of the blends are given in Figure 6.30. Although the sols were centrifuged to separate from xylene, a considerable quantity of xylene was present as an impurity. Therefore all of these spectra were identical and were similar to the xylene spectrum.

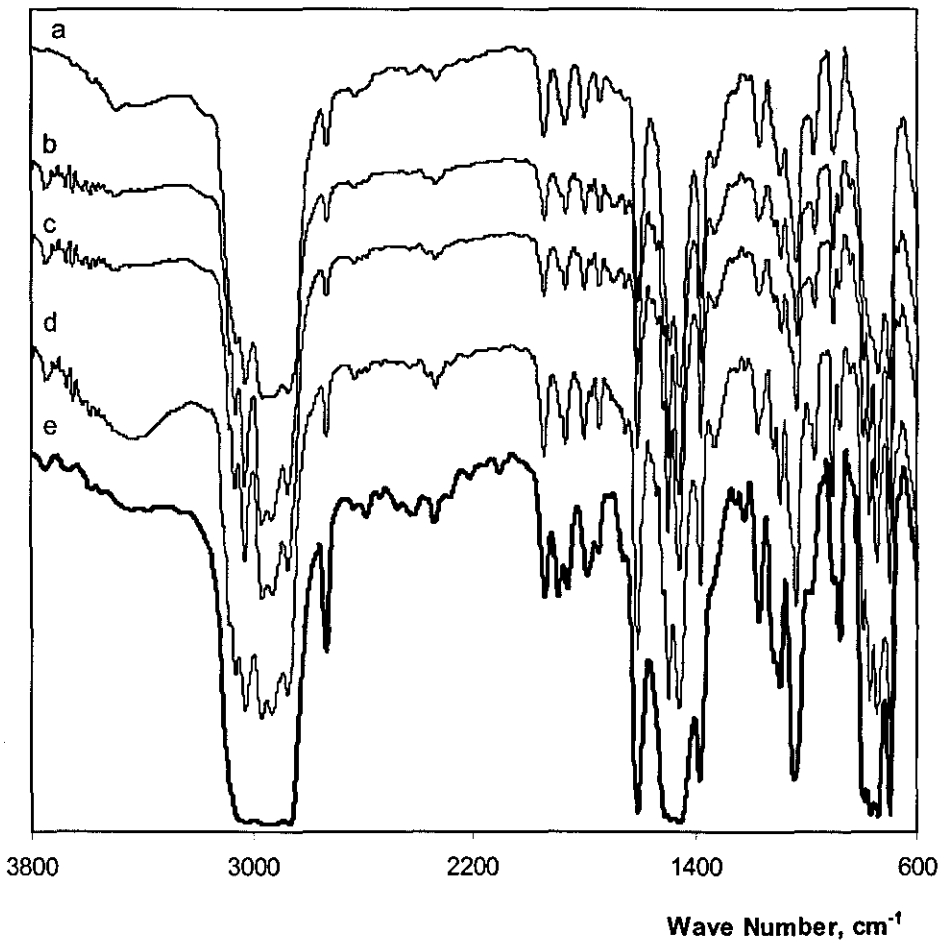

Figure 6.30 FTIR spectra of sol from blends after boiled xylene extraction:
(a) 5H/0.2D (b) 5H/0.2M (c) 5H (d) Control (e) Xylene

6.2 Resin Compatibilizing System

The resin compatibilizing system used in the present study consisted of two components; a crosslinking agent called SP 1045H resin (SP resin), and an activator called stannous chloride ($SnCl_2$). The stannous chloride was used in both anhydrous and dihydrate forms. The SP resin level was varied up to 8 pphp level, and the activator up to 1 pphp level (Section 3.2.5.2). The reactive blends with the resin compatibilizing system were prepared according to the 'schedule-a', in which the both polymers were added together at the commencement of mixing, under the processing conditions specified in Section 3.2.6. The reactive blends the resin compatibilizing system were also prepared according the 'schedule-b', in which the GTR was added to the SP resin modified-WPP. The processing characteristics, swelling behaviours, sol/gel analysis after solvent extraction, thermal properties, mechanical properties such as tensile and impact properties of the blends were studied. The results obtained for the blends containing SP resin with and without $SnCl_2$ are discussed in this section. Further, the possibility of WPP modification, and GTR crosslinking, by the resin compatibilizing system were investigated in order to understand and to explain the above property trends. For the study of this section, mixing 'schedule–c' was followed (Section 3.2.7).

6.2.1 Possible Chemical Reactions during Melt Mixing

The SP resin contains dimethylene ether bridges and methylol end groups (Figure 3.2), which could undergo dehydration to react with diene rubbers. Simplified structures for the SP resin (Structure-I and Structure-V) have been chosen to explain the possible reaction schemes. Structure-I has a monophenol linkage while Structure-V has a bisphenol.

The SP resin, during melt mixing with GTR/WPP blends, will undergo two main reactions; self-condensation or hardening of the resin, and the formation of crosslinks with diene rubbers in the GTR [293]. The possible self-condensation reaction is given in Scheme 6.10.

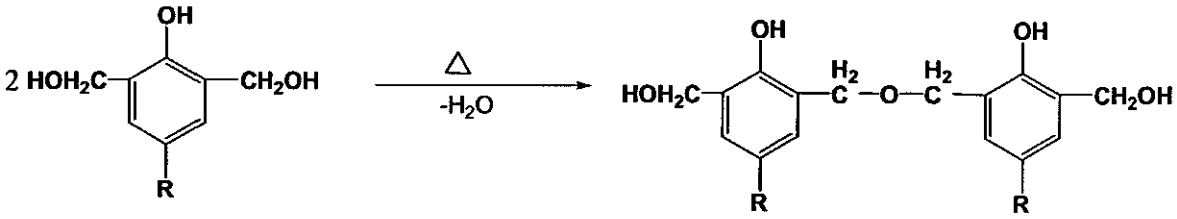

SP resin (Structure-I) Self-condensed product (Structure-II)

Scheme 6.10 Self condensation of SP resin [293]

The presence of a conjugated diene and an olefin is required for the crosslinking reaction [246]. Although the diene rubbers in the GTR, such as NR, SBR and/or BR, were crosslinked, they still contain double bonds, which could participate in a crosslinking reaction (Section 4.2.2.1). In general, the phenolic resins are not in a suitable form to participate in this reaction, and hence will undergo an elimination reaction to provide conjugated diene structures. Therefore, the first step in crosslinking is dehydration of the SP resin to give intermediates or reactive species, as shown in Scheme 6.11.

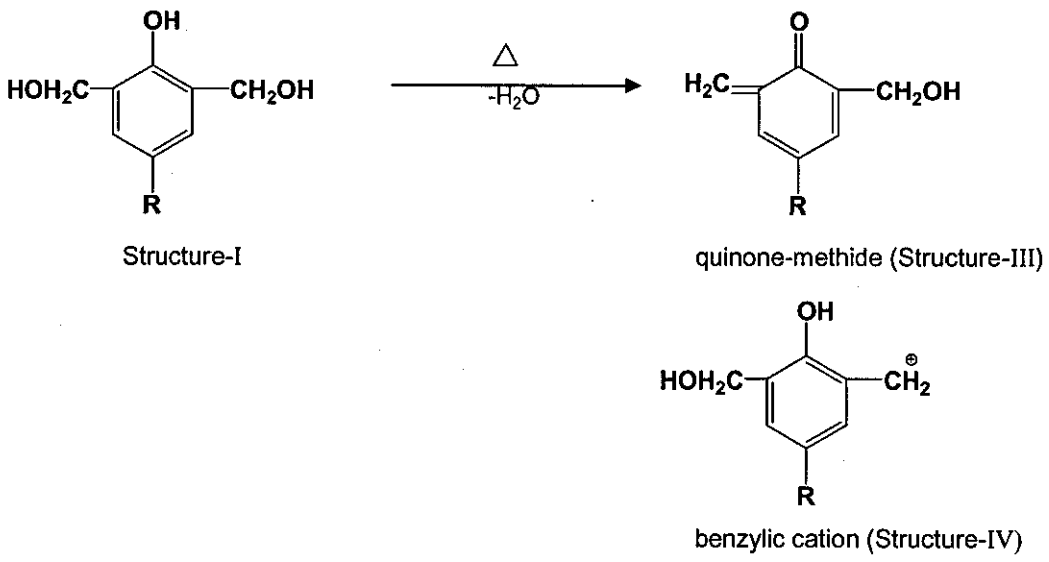

Structure-I quinone-methide (Structure-III)

benzylic cation (Structure-IV)

Scheme 6.11 Dehydration of SP resin to reactive species; quinone-methide and benzylic cation

The dehydration reaction is catalyzed in an acidic environment [212, 246]. The intermediates obtained in previous studies [245, 294] were identified as quinone-methide

(Structure-III or Structure-VI) and/or benzylic cations (Structure-IV). Of them, quinone-methide is commonly observable. The quinone-methide intermediate then combines with a double bond on a rubber molecule, by virtue of one of two mechanisms as proposed in previous studies; namely a chroman mechanism, and an allyl hydrogen mechanism [245, 293, 294]. Subsequent dehydration and the addition of a second rubber molecule produce crosslinks in the rubber phase. These two mechanisms are illustrated in Schemes 6.12 and 6.13, and 6.14 respectively.

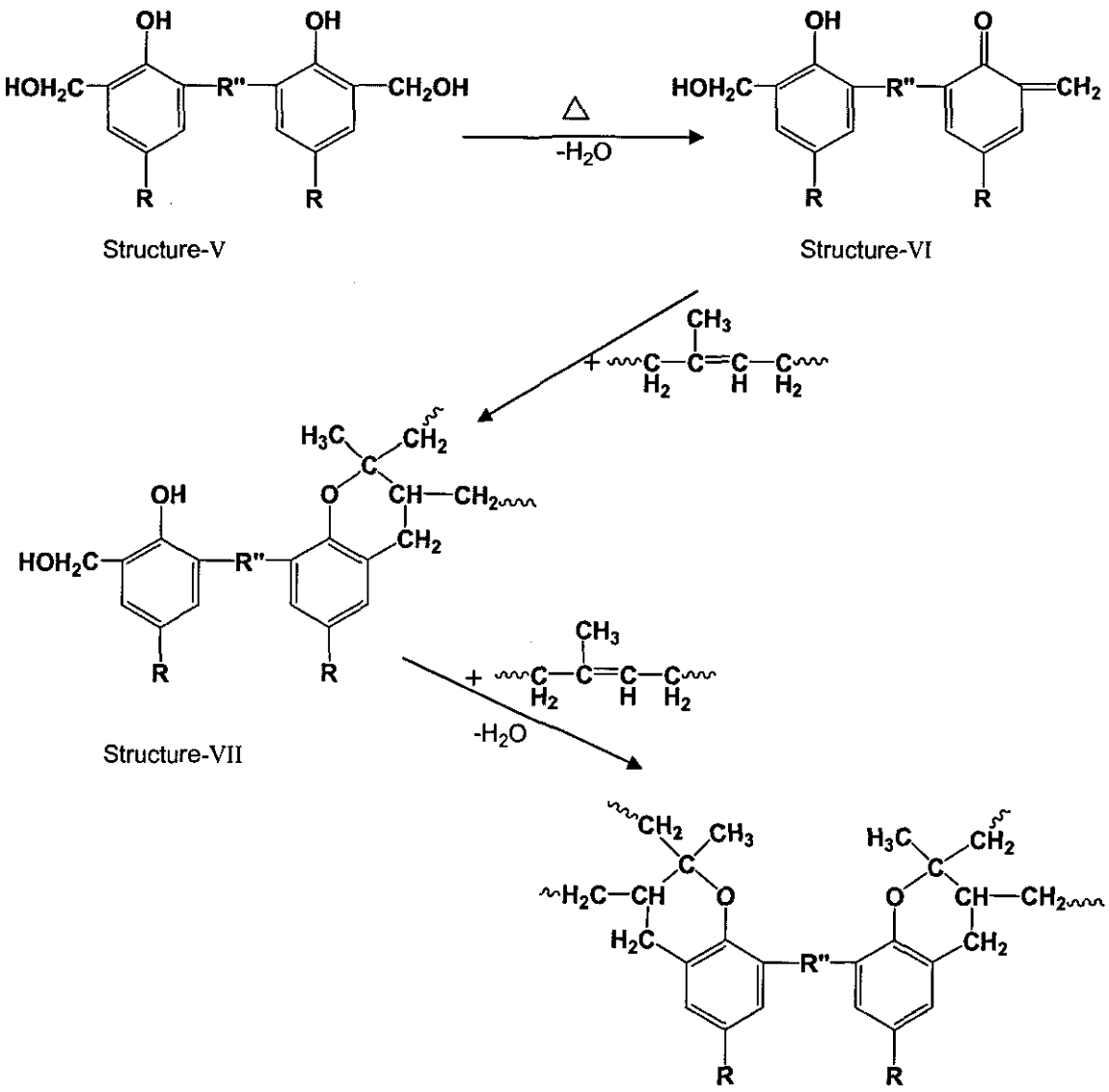

Scheme 6.12 Formation of crosslinks by the chroman mechanism (with bisphenol) [293]

In the chroman mechanism (Scheme 6.12), the intermediate combines with a rubber double bond in a cyclo-addition reaction to produce the chroman ring structure

(Structure-VII) [244, 293]. This mechanism requires at least a bisphenol (Structure-IV), and destroys the rubber unsaturation upon crosslink formation. However, the self-condensed product (Structure-II), formed by monophenol (Structure-I), will also combine with rubber double bonds to form a crosslink within the rubber phase (Scheme 6.13). This reaction could be expected to occur as the melt mixing temperature (180 ^{0}C) is well above the temperature necessary for self-condensation (80 ^{0}C) [293].

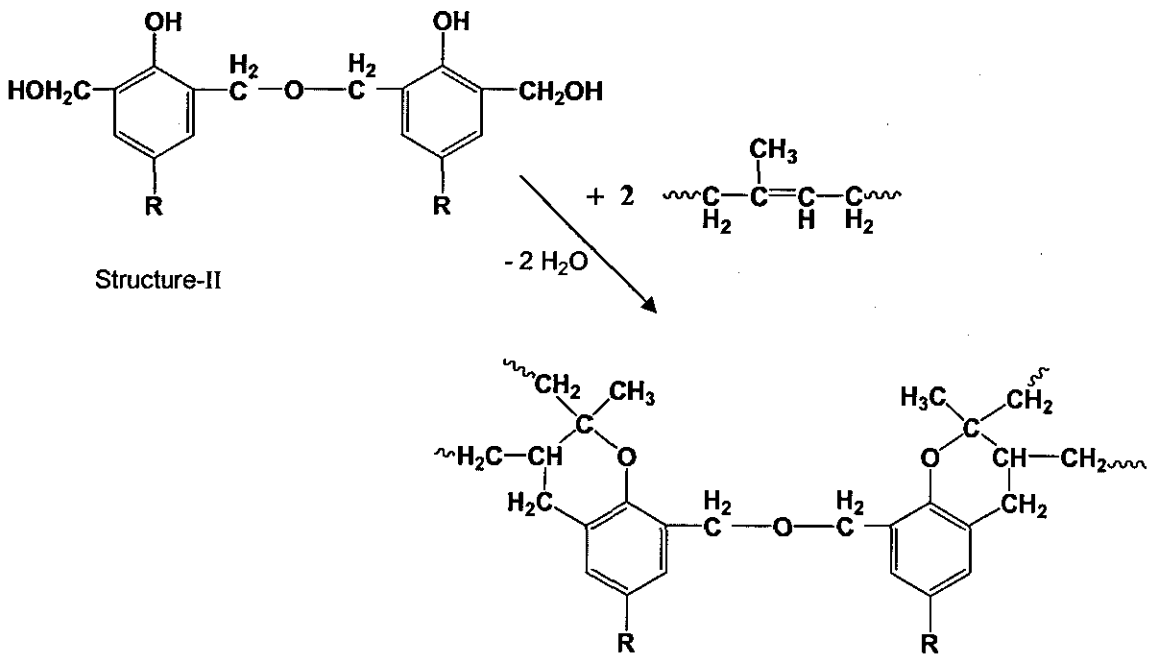

Scheme 6.13 Formation of crosslinks by the chroman mechanism (with self condensed SP resin) [293]

According to the allyl hydrogen mechanism (Scheme 6.14), the intermediate abstracts allyl hydrogen from the unsaturated rubber and forms a methylene bridge structure (Structure-VIII) [212, 293]. Under this mechanism a crosslink can be formed with a monophenol linkage. Rubber unsaturation is retained although the double bond is shifted. It remains unclear what parameters affect the selectivity of chroman versus methylene bridged structures (presence of activators, structure of olefin, etc.,). However, it was reported [199, 212, 244] that during melt mixing with SP resin, the methylol and hydroxyl groups were capable of reacting with the unsaturated sites in the NR molecules to produce chroman ring structures. Further, in the case of SP resin with $SnCl_2$, methylene bridged structures will be formed [167, 212]. In the case of $SnCl_2$ dihydrate, the reactions probably precede via a cationic mechanism with benzylic cations as reactive spices, adding to the least sterically hindered olefinic C-atom [294].

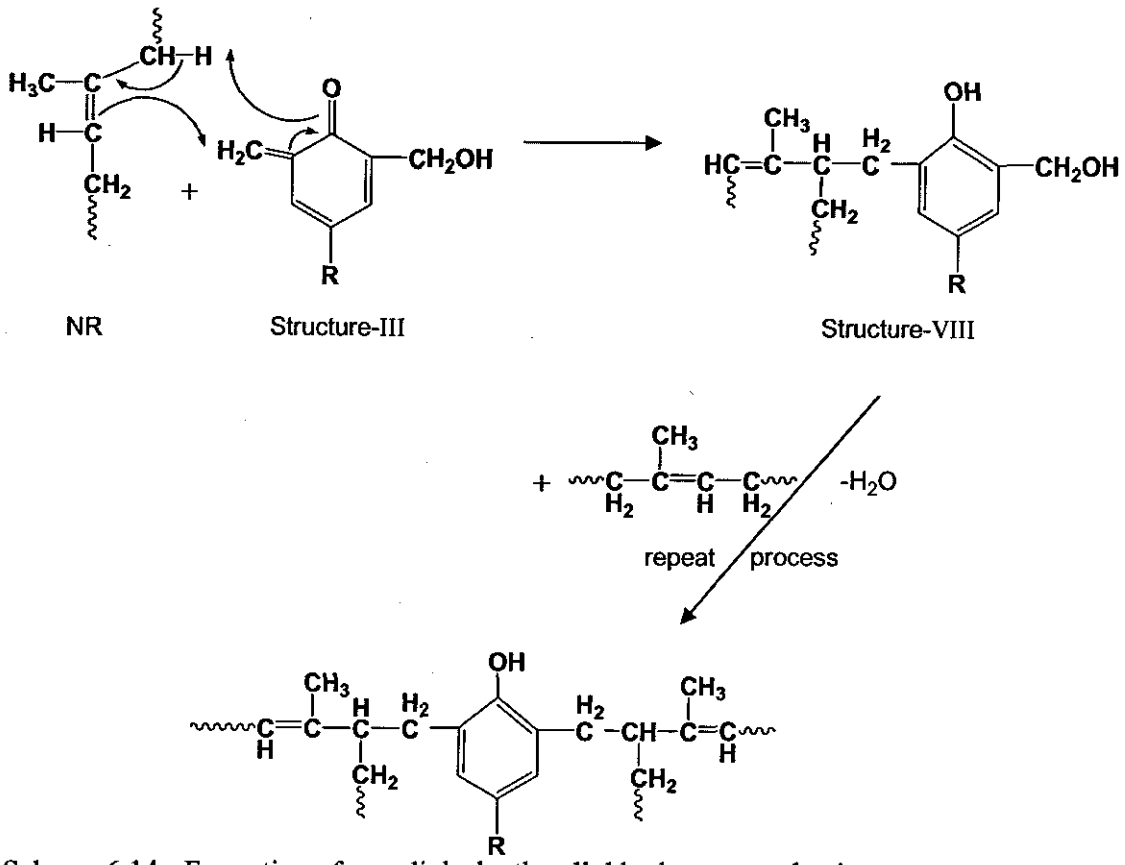

Scheme 6.14 Formation of crosslinks by the allyl hydrogen mechanism

Phenol resins could be used to crosslink essentially saturated olefin polymers like PP and EPR [165, 212]. As with the reaction of quinone-methide and diene rubber (Scheme 6.12), WPP will also react with SP resin to form methylolhydroxyphenyl-substituted WPP, also called resin modified WPP (Structure-IX). The WPP modification is given in Scheme 6.15.

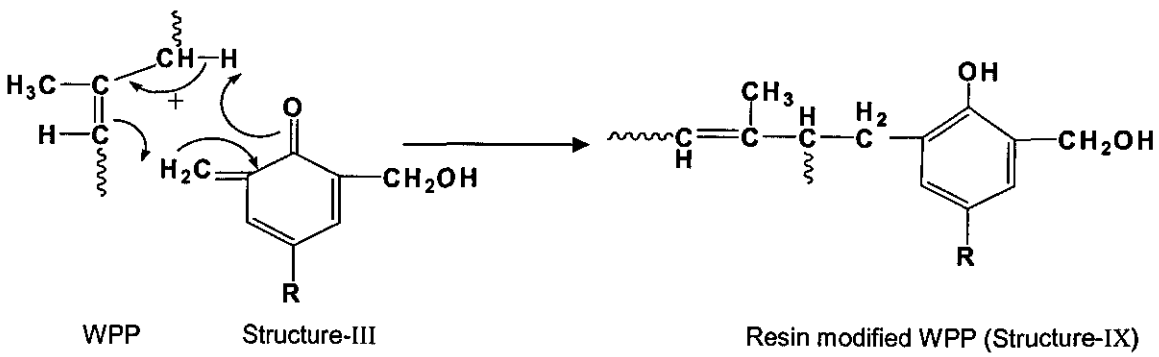

Scheme 6.15 Modification of WPP by SP resin [106, 165, 212]

The remaining methylol groups can then similarly react with unsaturated diene rubber molecule. The overall effect is the formation of interfacial crosslinks, as shown in Scheme 6.16. For this mechanism, it is essential to have at least a few double bonds in the WPP in order to react with methylol and the hydroxyl groups of the resin. Some unsaturation was noticed in the WPP (Section 4.1.3). It should be noted that stoichiometry demands, on average, one double bond per WPP molecule as seen in Scheme 6.15. A similar reaction scheme was proposed in several studies for PP/NBR blends [104, 106, 166, 167].

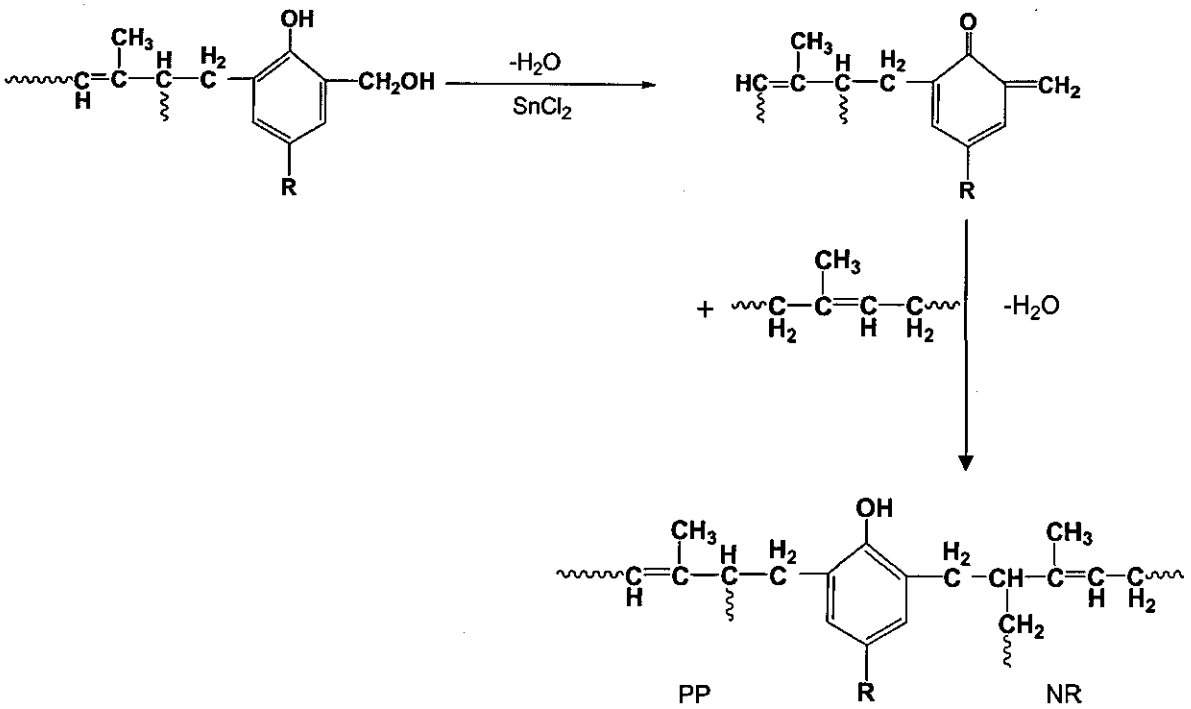

Scheme 6.16 Formation of interfacial crosslinks between WPP and NR [106]

6.2.2 Processing Characteristics

Typical torque-time curves for the blends prepared with the SP resin system, under the schedule–a, in which both the GTR and the WPP were added together before adding the compatibilizing system, showed the same trend in torque developments as with the control blend (Figure 6.31), and with the blends with HVA-2 alone (Figure 6.3). No increase in torque was observed after the addition of the compatibilizing system. This suggests that there was no involvement of the WPP phase in the crosslinking process after the addition of the SP resin system, although a suitable mechanism is proposed by

Scheme 6.16. This is in contrast to the torque development for the maleimide compatibilizing system (Figure 6.5). However, the torque at the completion of melt mixing (steady state torque), which is given in Table 6.16, increases with the SP resin level before finally levelling off. This increase is observed with blends containing SP resin both with and without a constant level (0.2 pphp) of $SnCl_2$. This torque increase is an indication of crosslink formation in the GTR phase as proposed by either the chroman mechanism (Scheme 6.12 or 6.13) or by the allyl hydrogen mechanism (Scheme 6.14). Alternatively, this torque increase could be due to modification of the WPP phase (Scheme 6.15), which increases the viscosity of the WPP (Section 6.2.12) and thereby the viscosity of the blend. Once the active sites available, i.e. unsaturation, both in the GTR phase and the WPP phase, were fully utilized, torque remains unchanged.

Table 6.16 Steady sate torques for blends containing SP resin with and without 0.2 pphp of activators

SP Resin, pphp	Steady State Torque, N/m	
	Without activator	With 0.2 pphp of $SnCl_2$
0	8.4(8.3)	-
1	8.8(8.7)	8.9(9.0)
2	9.1(9.1)	9.2(9.4)
3	9.3(9.3)	9.5(9.9)
4	9.8(9.6)	10.0(10.2)
5	10.2(10.2)	10.3(10.5)
6	10.5(10.5)	-
7	11.1(10.8)	-
8	10.9(10.9)	-

duplicate results are given in parenthesis

Table 6.17 shows the steady state torque at different levels of $SnCl_2$. This does not show a significant variation with increase in $SnCl_2$ level up to 1 pphp. This suggests that either there was no further formation of crosslinks in the GTR phase or no modification of the WPP phase with increase in $SnCl_2$ for the levels studied.

Table 6.17 Steady sate torques for blends containing 3 pphp of SP resin with different levels of activators

$SnCl_2$, pphp	Steady State Torque, N/m
0.2	9.5(9.9)
0.4	9.6(9.5)
0.6	9.6(9.8)
0.8	9.8(9.6)
1	9.5(9.6)

duplicate results are given in parenthesis

Typical torque-time curves for the blends prepared with the SP resin system according to schedule–b are shown in Figure 6.31. In this mixing schedule, the WPP was first added, then the compatibilizing system and finally the GTR. In these blends, the ratio by weight of SP resin to $SnCl_2$ was kept at 5:1. The steady state torque for all blends prepared under mixing schedule-b is given in Table 6.18. Figure 6.31 and Table 6.18 show that the steady state torque increases with increase in SP resin level with a further slight increase with the addition of $SnCl_2$. This may be again due to crosslinking in the GTR phase, or to modification of the WPP phase, or due to a combined effect.

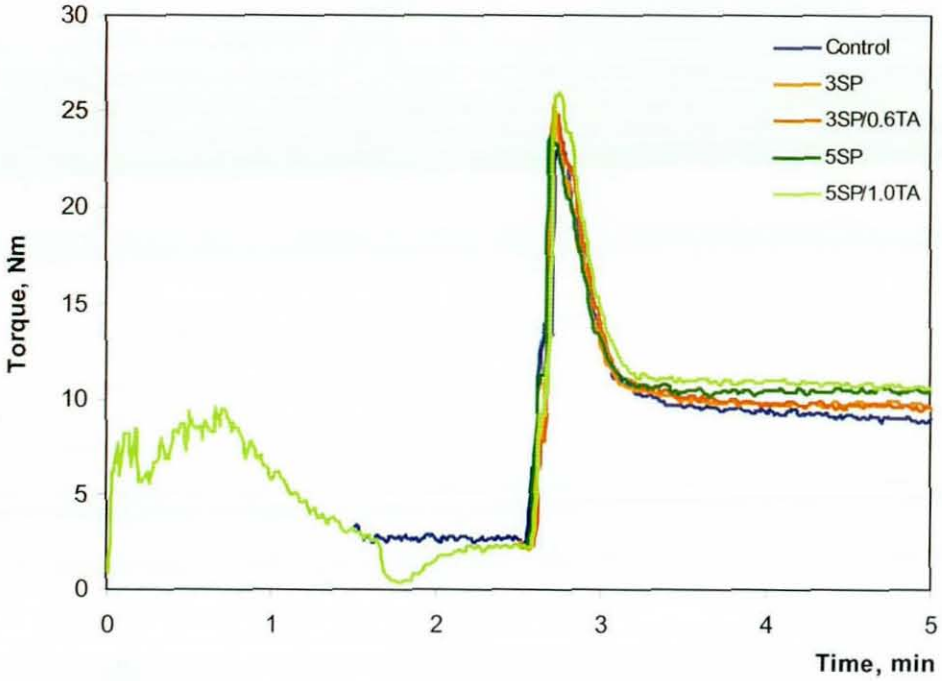

Figure 6.31 Torque vs. time curves for blends containing SP resin with and without activator, prepared under schedule-b

Table 6.18 Steady sate torques for blends containing SP resin with and without $SnCl_2$ prepared under schedule-b

Sample Code	Steady State Torque, N/m
Control-b	9.0(8.9)
2S-b	9.2(9.3)
3S-b	9.5(9.6)
4S-b	10.1(10.3)
5S-b	10.5(10.7)
2S/0.4TA-b	9.4(9.6)
3S/0.6TA-b	9.7(9.8)
4S/0.8TA-b	10.4(10.5)
5S/1.0TA-b	10.7(10.7)

duplicate results are given in parenthesis

6.2.3 Swelling Behaviour

SP resin will dissolve in toluene at room temperature, and hence any uncombined SP resin in the blends will migrate to the sol when swollen. In addition, the sol may contain soluble low-molecular weight materials from the WPP, soluble non-crosslinkable materials in the GTR, soluble by-products of the compatibilizing system, and non-crosslinked rubber in the GTR [153]. Table 6.19 shows the swelling indices and the %solvent extraction residues of the blends containing SP resin alone, for test in toluene at room temperature. The swelling index increases initially with the addition of the SP resin, and decreases with further addition. The formation of low levels of crosslinks allow the GTR phase to swell without dissolving in toluene, and hence increase both the swelling index. However, the formation of more crosslinks restricts the further swelling of the GTR phase and thereby swelling of the blend, and hence decreases the swelling index. The %solvent extraction residue remains unchanged. These results confirm the formation of crosslinks in the GTR phase. The involvement of the WPP phase in the crosslinking process, or the modification of the WPP phase, cannot be analyzed by these swelling characteristics as even the un-crosslinked WPP does not dissolve in toluene.

Table 6.19 Swelling characteristics of blends containing different levels of SP resin

SP Resin, pphp	Swelling Index	%Solvent Extraction Residue
0	0.50(0.01)	92 (0)
1	0.56(0.03)	93(0)
2	0.55(0.03)	93(0)
3	0.48(0.03)	93(1)
4	0.52(0.03)	92(1)
5	0.49(0.03)	93(1)
6	0.51(0.03)	93(1)
7	0.42(0)	94(0)
8	0.42(0)	94(0)

6.2.4 Tensile Properties

Tensile stress-strain curves for the blends containing SP resin with and without $SnCl_2$ were similar to each other. These curves were also similar to the curve for the control blend (Figure 6.6). The tensile properties obtained for the blends containing SP resin with and without 0.2 pphp of $SnCl_2$ are given in Table 6.20. For the blends with SP resin alone, the tensile strength initially increases with the SP resin level and then decreases passing through a maximum at 3 pphp. The elongation at break and the secant modulus at 2% strain show similar trends, but the variations with SP resin level are marginal. These variations are due to the formation of increased levels of crosslinks in the GTR phase with the SP resin level, or to modification of the WPP, or to a combined effect, as observed with the processing characteristics (Section 6.2.2). An increase in crosslinking in the GTR phase with SP resin level is proven by the swelling characteristics (Section 6.2.3). The shift in the T_g of the GTR phase to a higher temperature is also evidence for crosslinking in the GTR phase (Table 6.29).

Table 6.20 Tensile properties of blends containing SP resin with (0.2pphp) and without $SnCl_2$ prepared under schedule-a

SP Resin, pphp	Without activator			With 0.2 pphp of $SnCl_2$		
	T/S, MPa	%Eb	Modulus, MPa	T/S, MPa	%Eb	Modulus, MPa
0	8.0(0.3)	12.6(0.8)	184(8)	-	-	-
1	8.8(0.4)	13.3(1.5)	198(2)	9.2(0.3)	19.4(0.6)	194(5)
2	9.1(0.3)	13.7(0.9)	196(3)	9.8(0.2)	20.4(0.8)	196(6)
3	10.3(0.2)	14.8(0.6)	203(3)	9.9(0.1)	21.2(0.8)	197(3)
4	10.0(0.4)	15.5(1.3)	205(6)	9.7(0.2)	20.1(0.7)	198(2)
5	10.0(0.3)	15.1(1.3)	207(4)	9.7(0.2)	19.2(1.2)	201(4)
6	9.7(0.3)	15.6(1.0)	208(4)	-	-	-
7	9.1(0.3)	14.2(0.8)	210(9)	-	-	-
8	9.0(0.5)	12.6(1.2)	207(9)	-	-	-

With the addition of a constant level (0.2 pphp) of $SnCl_2$ into the SP resin, the elongation at break significantly improved for all SP resin levels studied. The tensile strength increased for low SP resin levels, but remained unchanged at high levels. The modulus did not change with the addition of $SnCl_2$. These property variations could be due to a combined effect of crosslinking in the GTR phase and modification of the WPP phase. Crosslinking in the GTR phase improves both tensile strength and elongation at break. Modification of the WPP phase would lower the tensile strength of the WPP (Section 6.2.12), and thereby lowers the tensile strength of the blend. The tensile property variation could also be due to the characteristics of the two types of crosslinks formed in the GTR phase. It has been reported that the SP resin alone would produce crosslinks in diene rubbers under the chroman mechanism (Schemes 6.12 and Section 6.13) [244]. The SP resin with $SnCl_2$ produces crosslinks by the chroman mechanism and/or by the allyl hydrogen mechanism (Scheme 6.14) [167, 212]. However, the type of crosslinks formed in the diene rubbers with the SP resin system is yet to be established.

The above results also suggest that the $SnCl_2$ level used (0.2 pphp) was not sufficient to activate the SP resin at higher levels. Both reactions were required for enhancement in tensile properties. Table 6.21 gives the variation of tensile properties with $SnCl_2$ level. It shows maximum tensile properties (but marginal) at 0.6 pphp level thus confirming that insufficient $SnCl_2$ was added to the SP resin. This optimum level is for the blend containing a constant level of 3 pphp of SP resin, which suggests an optimum blend composition of 5:1 by weight of SP resin:$SnCl_2$. With $SnCl_2$ levels greater than 0.6 pphp, relatively inferior tensile properties result. The excess $SnCl_2$ will remain un-reacted in the blend as a filler, or it could be utilized in modification of the WPP phase.

Tensile properties for the blends, prepared according to the schedule-b, are given in Table 6.22. All three properties slightly increase with the addition of SP resin and further increase with the SP resin level. The blends with SP resin alone prepared according to schedule-b exhibit greater elongations at break compared to those made according to schedule-a. This implies that blending GTR with modified WPP will provide better properties.

This tensile property improvement with the addition of the SP resin is again due to the combined effect of crosslinking in the GTR phase and modification of the WPP phase.

This improvement is also related to the improvement in compatibility between phases, which is revealed through an increase in viscosity of the WPP phase due to its modification (Table 6.32) and to the improved crystallinity of the WPP phase (Table 6.28). The closeness of the T_g of the two phases (Table 6.29) is evidence for the improvement in blend's compatibility. Further improvement in the properties with SP resin and $SnCl_2$ is a result of the more stable morphology noted in the tensile fractographs (Figure 6.32). This property improvement could also be due to the effect of the formation of smaller crystals in the WPP phase (Section 6.2.7), although the %crystallinity is similar.

Table 6.21 Tensile properties of blends containing (3 pphp) SP resin with different levels of $SnCl_2$

$SnCl_2$, pphp	T/S, MPa	%Eb	Secant Modulus, MPa
0.2	9.9(0.1)	21.4(0.9)	197(3)
0.4	10.0(0.2)	21.0(0.8)	205(4)
0.6	10.3(0.2)	21.6(0.8)	209(3)
0.8	10.2(0.2)	17.2(0.2)	201(3)
1	10.4(0.1)	12.8(0.2)	203(4)

Table 6.22 Tensile properties of blends containing SP resin with and without $SnCl_2$ prepared under schedule-b

Sample Code	T/S, MPa	%Eb	Secant Modulus, MPa
Control-b	8.0(0.1)	12.6(0.8)	184(8)
2S-b	8.2(0.1)	13.3(0.3)	195(4)
3S-b	10.1(0.1)	19.5(1.0)	197(3)
4S-b	9.8(0.3)	19.7(1.0)	206(5)
5S-b	9.7(0.2)	20.0(1.3)	209(5)
2S/0.4TA-b	9.6(0.2)	19.2(0.9)	193(4)
3S/0.6TA-b	10.6(0.1)	21.9(1.0)	210(7)
4S/0.8TA-b	10.6(0.2)	24.3(0.9)	211(8)
5S/1.0TA-b	10.1(0.2)	19.2(0.5)	208(4)

The maximum increase in tensile strength for the blends with the resin compatibilizing system (4 pphp of SP resin and 0.8 pphp of $SnCl_2$), when compared to the control blend, was 33%, while elongation at break was 93% and secant modulus was 15%. Maximum increases in tensile strength, and elongation at break, were reported [111] as 29% and 20% respectively for waste-SBR/PP (50/50) blends when compatibilized with SP resin (5 pphp) and $SnCl_2$ (0.5 pphp). However, no such increment was reported in the same study for recycled-NR/SBR mix/PP blends. The results of the study imply that the tensile property improvements obtained with the resin compatibilizing system for blends of WPP or PP with waste rubbers are small, and are in agreement with the results obtained in the present study. However, remarkable improvements in tensile properties, (tensile strength up to 400% and elongation at break up to 600%), were reported for EPDM/PP blends [164] and NBR/PP blends [106, 167] made with the resin compatibilizing system. These studies showed that the property enhancement was due to the formation of homogeneous blends with the formation of block/graft copolymers from the respective homopolymers. Tensile property enhancements were also reported for SBR/PP blends and NR/PP blends prepared with SP resin with and without activators [152, 153]. Greater improvements were also shown with a ZnO activator, compared with SP alone and also with $SnCl_2$ activator [152]. The inferior tensile properties for the blends prepared in the present study, compared to those reported for blends with virgin polymers, are mainly due to lack of interfacial adhesions between phases (Section 6.2.9) and hence due to non-homogeneous blend morphology (Figure 6.32). This could also be due to a lack of vinyl moieties, or unsaturation in the rubbers in the GTR and in the WPP, which is essential to produce crosslinks with SP resin.

6.2.5 Tensile Fracture

SEM images of the tensile fracture surfaces of the two selected blends compatibilized with the SP resin system are given in Figure 6.32. Both fractographs exhibit overall non-homogeneous surfaces with micro voids at interfaces, within the GTR phase, and with macro voids created due to the removal of GTR particles from the WPP phase due to poor interfacial and/or inter-particle adhesions during melt-mixing. In addition, some fibrillation is exhibited around the GTR particles, which represents shear yielding failure. Also regions of rough surfaces represent brittle failure of the WPP phase. When

comparing the two fractographs, a slightly stable surface is illustrated for the 4S/0.8TA-b blend. However, the SEM images show that interfacial debonding is the preferred failure mechanism for all these blends. Similar fracture surfaces were observed for the control blend and blends containing HVA-2 with and without MBTS (Figure 6.12). Further, the surfaces of the tensile fractured specimens of the blends with SP resin with and without $SnCl_2$ were similar to those for blends with HVA-2 with and without MBTS, which were also similar to simple blends (Figure 5.12).

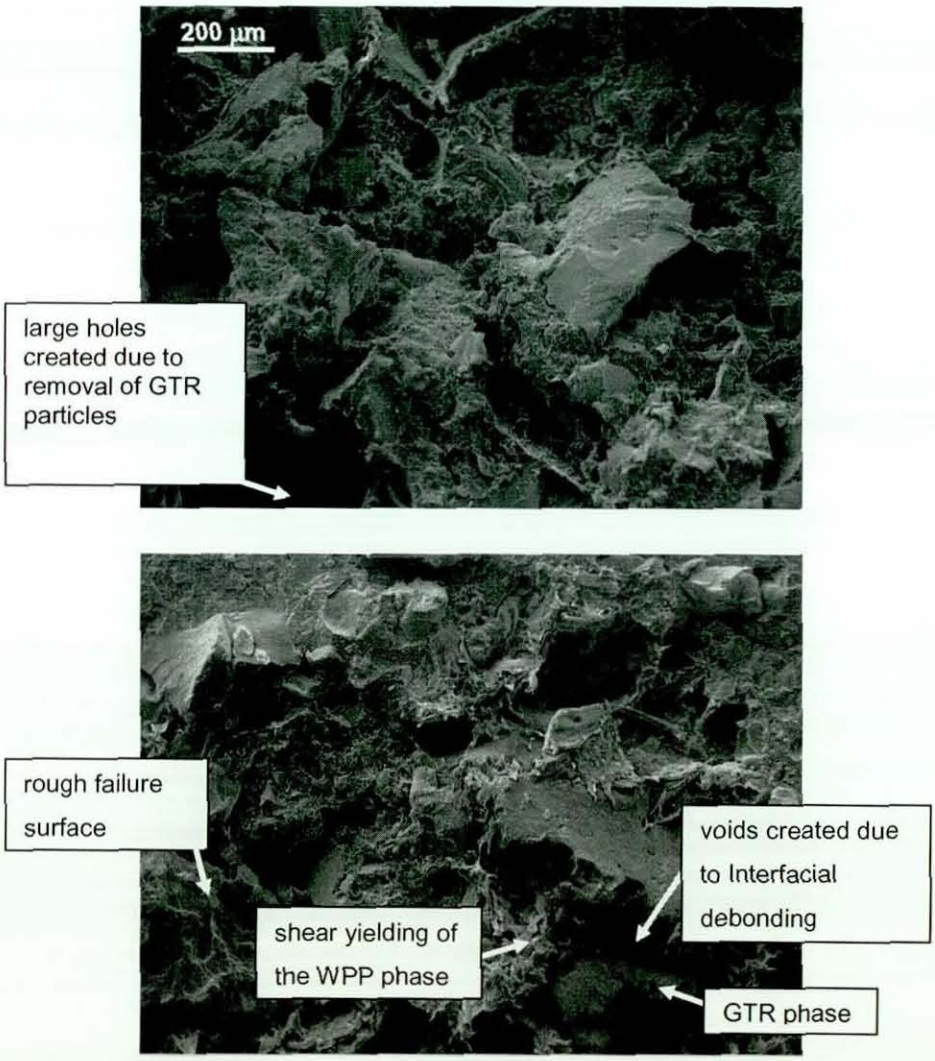

Figure 6.32 Tensile fractographs of 50:50 blends (a) 4S-a (b) 4S/0.8TA-b

6.2.6 Impact properties

Table 6.23 gives the impact properties for the blends containing SP resin at different levels obtained from the falling dart impact test performed at 20±1^{0}C. These properties include failure mode, peak force, and fracture initiation, propagation and failure energies. The peak force, and fracture imitation energy, increases with the addition of SP resin, while the propagation energy decreases, as the failure mode changes from ductile to semi brittle. The normalized stiffness of the blends at all SP resin levels were constant at 8±1 N/mm^2. An increase in peak force, with a constant stiffness, implies greater deformations at fracture initiation with the addition of SP resin. These results are again due to the formation of crosslinks in the GTR phase and to modifications in the WPP phase. The decrease in propagation energy is due to further phase separation which occurred with modifications in both phases without the formation of interfacial adhesions. However, the overall failure energy remains constant for all the SP resin levels studied. All these properties show lower values at high SP resin level (8 pphp), with brittle fracture due to enhanced modifications in both phases.

Table 6.23 Impact properties of blends containing different SP resin levels

SP Resin, pphp	Failure Mode	Peak Force*, N/mm	Initiation Energy*, J/m	Propagation Energy*, J/m	Failure Energy*, J/m
0	Ductile	67(2)	223(11)	500(40)	723(18)
1	Semi Brittle	72(4)	388(12)	386(23)	773(12)
2	Semi Brittle	71(4)	383(20)	377(25)	760(24)
3	Semi Brittle	74(2)	440(19)	361(30)	779(33)
4	Semi Brittle	70(3)	411(23)	387(25)	798(19)
5	Semi Brittle	75(3)	437(19)	392(20)	780(18)
6	Semi Brittle	67(4)	415(25)	384(19)	799(14)
7	Semi Brittle	62(3)	396(18)	377(16)	784(25)
8	Brittle	62(3)	388(24)	249(20)	636(23)

** normalized by dividing by the thickness of the specimen*

Impact properties for the blends containing SP resin with $SnCl_2$ are given in Table 6.24 Table 6.25 and Table 6.26. These blends exhibit a semi brittle mode of failure with no improvement in failure energy at any SP resin level. An increase in the $SnCl_2$ level slightly increases the failure energy. However, this increment is not so pronounced as with the tensile property improvements observed for the same blends (Table 6.21).

Table 6.24 Impact properties of blends containing different levels of SP resin with 0.2 pphp of $SnCl_2$

SP resin, pphp	Failure Mode	Peak Force*, N/mm	Failure Energy*, J/m
1	Semi Brittle	71(4)	761(24)
2	Semi Brittle	69(5)	756(16)
3	Semi Brittle	67(5)	773(27)
4	Semi Brittle	66(5)	782(24)
5	Semi Brittle	69(6)	815(24)

** normalized by dividing by the thickness of the specimen*

Table 6.25 Impact properties of blends containing 3 pphp of SP resin with different $SnCl_2$ levels

$SnCl_2$, pphp	Failure Mode	Peak Force*, N/mm	Failure Energy*, J/m
0.2	Semi Brittle	67(5)	773(27)
0.4	Semi Brittle	66(3)	808(34)
0.6	Semi Brittle	68(1)	815(24)
0.8	Semi Brittle	66(2)	810(33)
1.0	Semi Brittle	67(2)	811(24)

** normalized by dividing by the thickness of the specimen*

The blends processed according to schedule-b, compared to those prepared according to schedule-a, show relatively greater peak forces due to the combined effect of GTR crosslinking, WPP modification and thereby improved blend's compatibility. At optimum level, the 4S/0.8TA-b blend exhibits maximum failure energy, with ductile fracture. Most of the other blends show semi brittle fracture. However, the stiffness was same for all

blends with the resin compatibilizing system. Although an overall significant improvement in impact properties is noticed with the resin compatibilized blends, it is not remarkable. This inadequate property improvement is possibly due to the non-homogeneous blend morphology (Figure 6.32).

Table 6.26 Impact properties for the blends with the SP resin compatibilizing system prepared according to mixing schedule-b

Sample Code	Failure Mode	Peak Force*, N/mm	Failure Energy*, J/m
Control	Semi Brittle	66(3)	764(5)
2S-b	Semi Brittle	70(2)	772(14)
3S-b	Semi Brittle	73(2)	778(14)
4S-b	Semi Brittle	72(2)	775(8)
5S-b	Semi Brittle	65(2)	802(15)
2S/0.4TA-b	Ductile	71(1)	793(10)
3S/0.6TA-b	Ductile	72(2)	834(8)
4S/0.8TA-b	Ductile	73(2)	896(16)
5S/1.0TA-b	Semi Brittle	62(2)	790(5)

** normalized by dividing by the thickness of the specimen*

6.2.7 Melting and Crystallization Behaviour

Thermal properties obtained from the DSC thermograms of the blends containing SP resin with and without $SnCl_2$ are given in Table 6.27 and Table 6.28. With the addition of SP resin, both the onset and peak crystallization temperatures (T_{co} and T_p, respectively) drop by nearly 1 ^{0}C, while the melting temperature (T_m) remains constant at 163.5±0.5 ^{0}C (Table 6.27). As a result, the super cooling temperature (ΔT) increases, indicating an anti-nucleating effect for crystal formation, caused either by the resin modified WPP phase or by the crosslinked GTR phase. However, the addition of the SP resin results in a relatively rapid rate of crystallization indicated by a larger S_i, and a narrow crystal size distribution indicated by a smaller ΔW. As a combined effect, many smaller crystals are

formed in the blends with the SP resin. The heat of fusion and thereby the degree of crystallinity also increases with the addition of SP resin.

Table 6.27 Thermal properties determined from the DSC thermograms of blends containing SP resin with $SnCl_2$

Sample Code	T_{co}, ^0C	T_p, ^0C	T_m, ^0C	ΔT, ^0C	S_i, mW/g^0C	ΔW, ^0C
Control	128.8(0.6)	120.2(0.3)	163.5(0.5)	35	0.3(0.0)	5.2(0.1)
3S-b	127.5(0.5)	119.2(0.2)	163.3(0.4)	36	0.6(0.0)	4.5(0.2)
4S-b	127.8(0.4)	119.6(0.3)	163.4(0.4)	36	0.6(0.0)	4.4(0.2)
5S-b	127.8(0.5)	119.7(0.4)	163.3(0.3)	36	0.6(0.0)	4.2(0.3)
3S/0.6TA-b	126.5 (0.3)	119.4(0.2)	162.9(0.5)	36	0.7(0.0)	4.1(0.1)
4S/0.8TA-b	126.4(0.5)	119.4(0.4)	162.8(0.3)	36	0.7(0.0)	4.1(0.2)
5S/1.0TA-b	126.1(0.4)	119.3(0.3)	162.0(0.5)	36	0.7(0.0)	3.7(0.2)

The incorporation of $SnCl_2$ into the SP resin further reduces the T_{co} and crystal size distribution, while increasing the rate of crystallization. The delay in nucleation and the changes in crystal structure are associated with the enhancement of the WPP modification caused by the SP resin in the presence of $SnCl_2$. The incorporation of $SnCl_2$ also reduces T_m providing the same super cooling effect, similar to that for blends with SP resin alone. The resin modified WPP will introduce defects into the crystals thus reducing T_m. Therefore the slight drop in T_m confirms the modification of the WPP phase to a small extent. The degree of crystallinity remains increased as with the blends containing SP resin alone. This improved crystallinity and the changes in crystalline structure should improve blend properties extensively. However, due to the lack of interfacial adhesions (Figure 6.32) and thereby lack of effective load transfer between phases, the property improvement in the present study is not remarkable.

Table 6.28 Enthalpies and degrees of crystallinity from DSC thermograms of blends containing SP resin with $SnCl_2$

Sample Code	ΔH_f, J/g	$\%X_c$ (Blend)	$\%X_c$ (WPP)
Control	44(1)	21(1)	43(1)
3S-b	50(2)	24(1)	49(2)
4S-b	50(2)	24(1)	50(2)
5S-b	48(2)	23(1)	48(2)
3S/0.6TA-b	50(2)	24(1)	50(1)
4S/0.8TA-b	49(1)	23(1)	49(1)
5S/1.0TA-b	47(1)	23(1)	48(1)

6.2.8 Dynamic Mechanical Properties

Table 6.29 gives the glass transition temperatures (T_g) determined from tan δ curves for both phases, and storage modulus at 20 ^{0}C for selected blends containing SP resin with and without $SnCl_2$. The T_g of the GTR phase shifts to a higher temperature with the addition of SP resin due to the formation of additional crosslinks in the GTR phase. The T_g of the WPP phase shifts to a lower temperature, resulting a small difference in T_g between phases. This closeness of the T_g of the phases suggest an improved compatibility between phases. No further variation in T_g is noticed for the blends containing SP resin with $SnCl_2$. Similar variations in T_g were observed for the blends containing HVA-2 with and without MBTS (Table 6.13).

The addition of SP resin increases the storage modulus at 20 ^{0}C. The addition of $SnCl_2$ into the blends containing SP resin further increases the storage modulus. These results are in agreement with the secant modulus determined under tensile testing (Table 6.22).

Table 6.29 Dynamic mechanical properties of selected blends containing SP resin with and without $SnCl_2$

Sample Code	T_g of GTR, ^0C	T_g of WPP, ^0C	Temperature Difference, ^0C	Storage Modulus @ 20 ^0C, MPa
Control	-42	15	57	574
4S-b	-38	14	52	660
4S/0.8TA-b	-38	14	52	673

6.2.9 Boiled Xylene Extraction

The xylene insoluble fractions of the blends containing SP resin at different levels, prepared according to schedule-a, are given in Figure 6.33. This figure shows a drastic increase in the xylene insoluble fraction, and hence the degree of crosslinking, with the addition of SP resin to the control blend. However, no further increase in either xylene insoluble fraction or the degree of crosslinking was observed up to 3 pphp. A certain level of crosslinks needs to be formed to initiate a significant difference. At higher SP resin levels, both properties increase and hence confirm the formations of crosslinks at higher SP resin levels.

The addition of $SnCl_2$ activator to the SP resin did not produce any further increase in degree of crosslinking. This is in agreement with the swelling characteristics (Section 6.2.3), and with the mechanical properties obtained (Section 6.2.4 and Section 6.2.6). Further, the degrees of crosslinking obtained for these blends remain less than 100% indicating no involvement of the WPP in the crosslinking process and thereby no adhesion between phases during the melt-mixing process. The resin modified WPP will be dissolved in boiled xylene, and therefore WPP modification level cannot be measured by this technique.

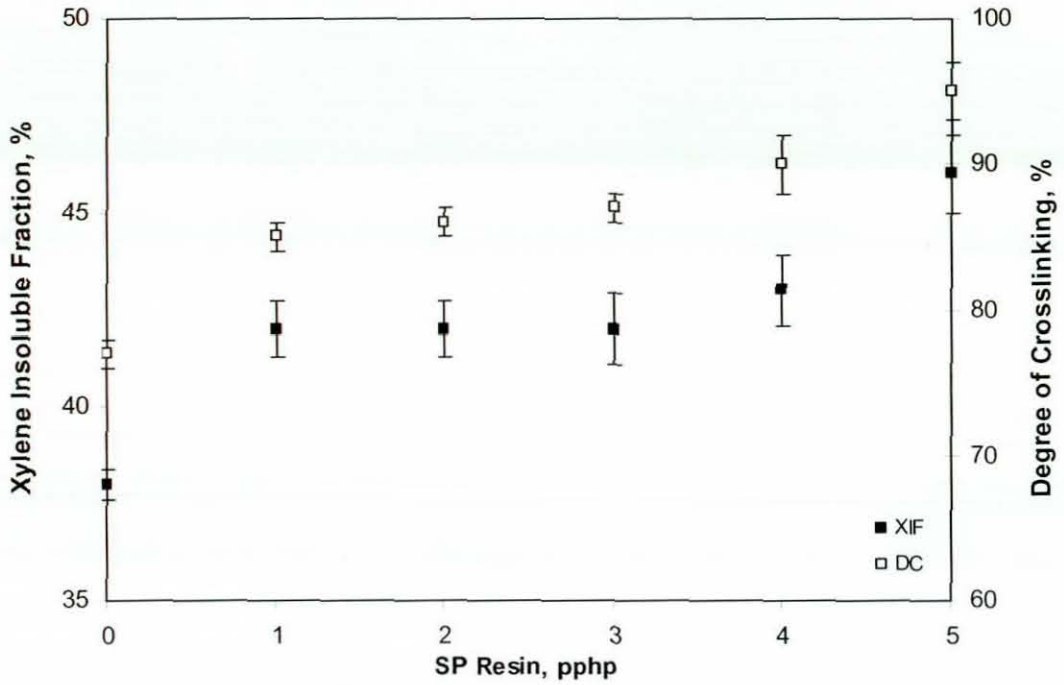

Figure 6.33 Xylene insoluble fraction and degree of crosslinking of blends containing SP resin

The appearances of gel fractions and sol fractions of the blends containing 3 pphp of SP resin with 0.6pphp of $SnCl_2$, and without $SnCl_2$, obtained during boiled xylene extraction are illustrated in Figure 6.34. The gels from the blends with and without $SnCl_2$ are very similar in appearance. They are of free flowing coarse particles, which could be crushed under finger pressure. But the appearances of the sols slightly differed from each other. The sol of the blend with SP resin alone has a black precipitate with fine black particles dispersed in the xylene, while that of the blend with SP resin and $SnCl_2$ does not show any dispersed particles. This occurs as those fine black particles are separated from the xylene based solvent and added to the precipitate, due to the relatively lower density of the solvent. This implies that the polymer content dissolved in the solvent is relatively low. In other words the gel content of this blend is relatively high.

The DSC thermograms of the gel fractions of the two blends are shown in Figure 6.35. The thermograms of both blends do not show any endothermic peak assigned to melting of the WPP around 166 ^{0}C. This observation confirms that f the WPP had no involvement

in the crosslinking process and hence there were no interfacial adhesions formed by the resin compatibilizing system.

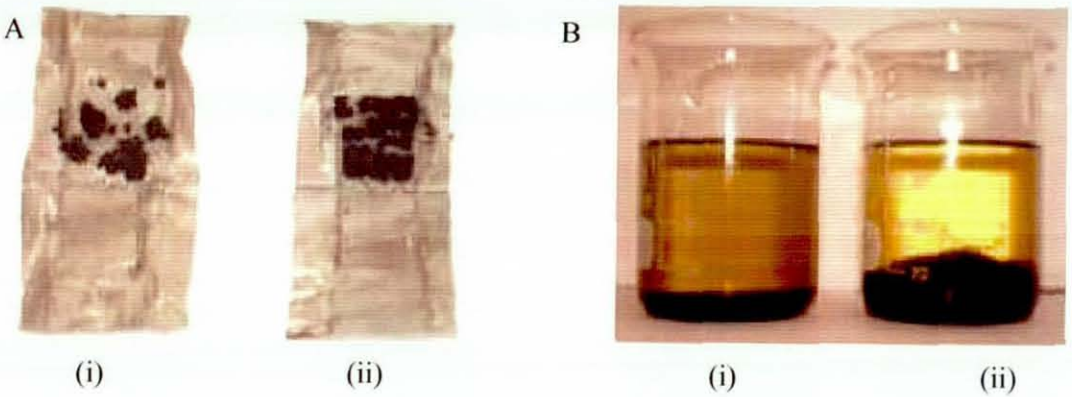

Figure 6.34 Gels and sols from the blends after boiled xylene extraction; A- gel, B-sol

(i) 3SP (ii) 3SP/0.6TA

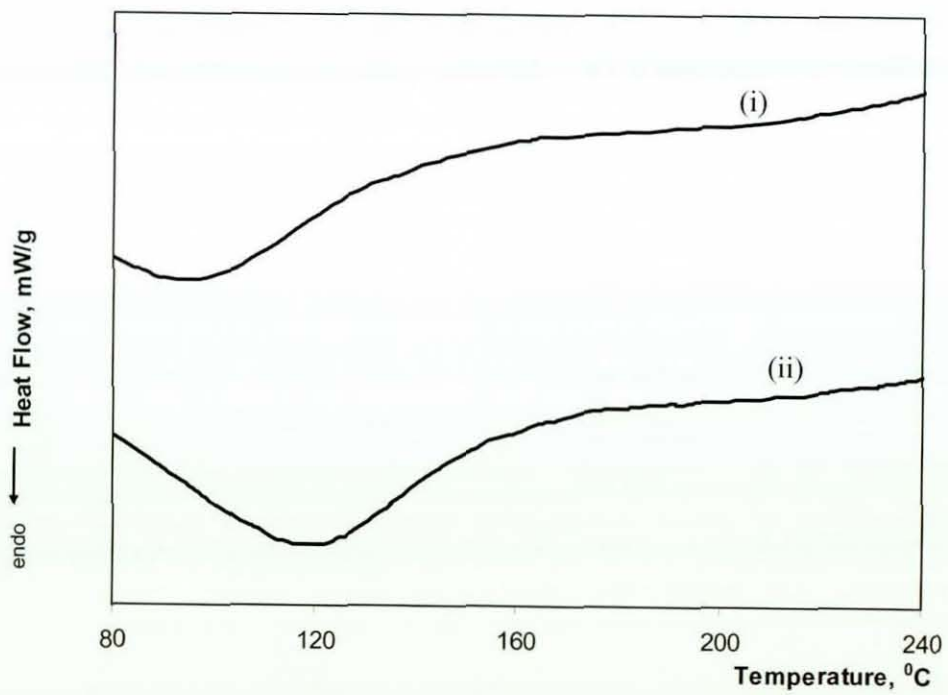

Figure 6.35 DSC thermograms of gels of blends after boiled xylene extraction

(i) 3SP (ii) 3SP/0.6TA

The FTIR spectra of the control blend, the blend containing 3 pphp pf SP resin and the spectrum of the SP resin are illustrated in Figure 6.36. These are similar to the spectra of gels from the blend containing HVA-2 alone (Figure 6.29b), The spectra for the blend containing SP alone (Figure 6.36b) shows increased intensity of specific peaks assigned to alkenes, indicating the presence of the GTR phase in the gels (Section 6.1.12). Most of the peaks can also be clearly seen in the spectrum for the SP resin (Figure 6.36c). These observations confirm the presence of SP resin combined in the GTR in such gels. However, no specific peak shown confirms the presence of the WPP in the gel.

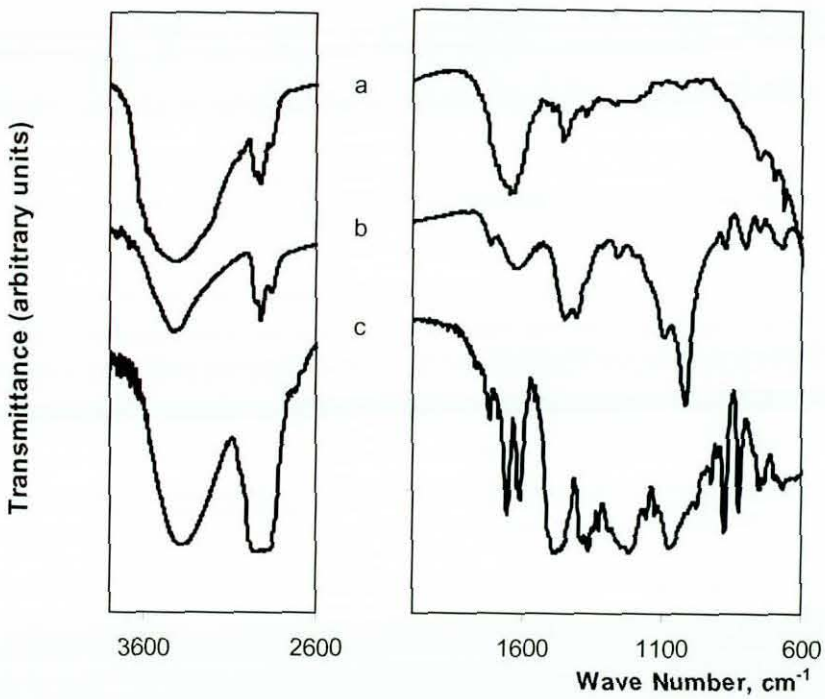

Figure 6.36 FITR spectra (pyrolytic) of gels from blends after boiled xylene extraction a. Control b. 3S-a and c. FTIR spectrum of SP resin (KBr pellet)

6.2.10 Activator Effect: Stannous Chloride Anhydrous vs. Dihydrate

The effect of the two forms of stannous chloride used, stannous chloride anhydrous ($SnCl_2$) and stannous chloride dihydrate ($SnCl_2.2H_2O$) were investigated based. These blends (Table 3.8) contain 4 pphp of SP resin and 0.8 pphp of activator, and were

prepared according to mixing schedule-b (Section 3.2.6). The above properties are tabulated in Table 6.30.

Table 6.30 Mechanical and thermal properties for blends containing SP resin with two forms of stannous chloride activators

Property	Sample Code	
	4S/0.8TA-b	4S/0.8TD-b
Steady state torque**, Nm	10.4(10.5)	10.3(10.4)
Tensile strength, MPa	10.6(0.1)	10.5(0.3)
%Elongation at break	24.3(0.9)	24.0(0.9)
Modulus @ 2% strain, MPa	211(8)	188(5)
Failure Mode	Ductile	Ductile
Peak force*, N/mm	73(2)	74(4)
Impact failure energy*, J/m	896(16)	940(30)
%Crystallinity of WPP	49(1)	50(1)
T_g of GTR, ^{0}C	-38	-38
T_g of WPP, ^{0}C	14	14
Storage modulus @ 20 ^{0}C, MPa	673	640

** normalized by dividing by the thickness of the specimen*

*** duplicate results are given in parenthesis*

The blend with $SnCl_2.2H_2O$ (4S/0.8TA-b), compared to the blend with $SnCl_2$ (4S/0.8TD-b), shows a lower modulus at 2% strain, a lower storage modulus at 20 ^{0}C, and a higher impact failure energy. All the other properties show no significant differences. The above property variations could be due to the differences in properties of the WPP phase when modified with SP resin with $SnCl_2.2H_2O$ or with $SnCl_2$ (Section 6.2.12). The GTR modified by SP resin with $SnCl_2.2H_2O$ or with $SnCl_2$ were almost similar (Section 6.2.11). The tensile fractures of both blends were also similar (Figure 6.32). Both fractographs did not exhibit improved interfacial adhesions to provide considerable improvement in properties. The overall results imply that the activity of $SnCl_2.2H_2O$ or $SnCl_2$ as an activator for the SP resin in the GTR/WPP blends is more or less similar. However, it has been reported [245] that $SnCl_2.2H_2O$, compared to $SnCl_2$, was more

effective in catalyzing quinone-methide formation (Scheme 6.11), and hence is effective in vulcanizing EPDM with the resin vulcanizing system. The reason given in that study was the more acidic properties of $SnCl_2.2H_2O$ due to the formation of $H^+[SnCl_2(OH).nH_2O]$ complexes. However, at the processing temperature used in the present study (180 ^{0}C), the catalyzing effect of $SnCl_2.2H_2O$ should be similar to that of $SnCl_2$. The water present in the dihydrate form will evaporate, and hence $SnCl_2.2H_2O$ will convert into the anhydrous form during melt mixing.

6.2.11 Crosslinking of GTR with the SP Resin System

The steady state torques and the appearances of the GTR after melt mixing with and without the resin compatibilizing system are given in Table 6.31. This table also details the appearance of the moulded sheets. The GTR after processing produced some GTR agglomerants, which were easily broken under slight finger pressure. It also consisted of some free flowing GTR particles. At high shear melt mixing, GTR alone produces free radicals due to main chain and/or crosslink scission and combines to form some agglomerants. These agglomerants were re-linked under compression moulding at high temperatures to form smooth sheets, which were suitable for making the test specimens.

Table 6.31 Appearances and some properties of GTR with and without resin compatibilizing system

Sample Code	GTR	8S/1.6TA/GTR	8S/1.6TA/GTR
T_{ss}, Nm	6.5(6.7)	10.3(10.2)	10.3(10.4)
Appearance after melt mixing	Some agglomerants with free flowing particles	free flowing particles only	
Appearance after compression moulding	Smooth sheet	Sheet, which is easily breakable	

The addition of the resin compatibilizing system into the GTR produced free flowing GTR particles due to crosslinking within each particle. Increase in steady state torque with the addition of resin compatibilizing system is evidence for crosslinking of the GTR particles. However, the gel content after acetone extraction (Section 3.9.2) for the GTR with and without the resin compatibilizing system was kept constant at 90±1%. The crosslinked GTR particles prevented agglomeration during blending or during moulding and produced moulded sheets with loosely bound particles. The crosslinking effect of $SnCl_2.2H_2O$ and $SnCl_2$ activators were difficult to compare using mechanical properties, as it was impossible to cut test specimens from those sheets.

6.2.12 WPP Modification by SP Resin

The steady state torques for the WPP, the PP and their resin modified polymers are given in Table 6.32. It is clearly shown that the steady state torque for the WPP is much lower than that for the PP. This may be due to the lower viscosity of the WPP, which is associated with its degradation during previous processes. With the addition of the resin compatibilizing system either to the WPP or to the PP, the steady state torque increases. The torque appears greater at higher levels of compatibilizing system. The torque increase is an indication of the degree of structural modification during processing. However, the steady state torque does not vary with the form of the stannous chloride used.

Table 6.32 Steady state torque for the resin modified WPP and PP

Sample Code	T_{ss}, Nm	Sample Code	T_{ss}, Nm
WPP	5.8(5.7)	PP	10.5(10.8)
4S/0.8TA/WPP	6.0(6.1)	4S/0.8TA/PP	14.6(14.4)
8S/1.6TA/WPP	6.3(6.4)	8S/1.6TA/PP	15.0(14.8)
8S/1.6TD/WPP	6.4(6.3)	8S/1.6TD/PP	14.7(14.8)

Tensile properties for the PP, the WPP and their resin modified polymers are given in Table 6.33. Young's modulus was calculated considering stresses at 0.05% and 0.25%

strains (Section 3.7.2). The PP, when compared to the WPP, show a higher tensile strength and a remarkably greater elongation at break associated with cold drawing during tensioning. The WPP fractured at yielding without drawing (Figure 5.7). The inferior properties of the WPP are due to the presence of additives and impurities and especially due to degradation during previous processes. With modification of the PP by the resin compatibilizing system, elongation at break drastically drops and a brittle fracture occurs. The tensile strength also drops, but slightly, providing a higher Young's modulus for the resin modified PP. The WPP also shows a slight drop in both tensile strength and elongation at break. These results are in agreement with the processing characteristics (Table 6.32).

Table 6.33 Tensile properties for the resin modified WPP/PP with SP resin system

Sample Code	T/S, MPa	% Eb	Young's Modulus, MPa
WPP	29.4(0.2)	20.8(1.5)	958(37)
4S/0.8TA/WPP	25.3(0.9)	13.2(0.8)	790(21)
8S/1.6TA/WPP	26.7(0.5)	14.0(1.4)	826(16)
8S/1.6TD/WPP	25.9(0.5)	16.2(1.0)	812(15)
PP	33.5(0.2)	844(5)	417(10)
4SP/0.8TA/PP	32.6(1.0)	20.2(0.6)	784(30)
8SP/1.6TA/PP	32.2(0.6)	20.0(1.2)	775(27)
8SP/1.6TD/PP	31.1(1.3)	27.2(2.4)	821(30)

Both tensile strength and the elongation at break for the resin modified polymers are independent of the level of the compatibilizing system. The tensile strength for these polymers is also independent of the form of stannous chloride, but the resin modified polymer containing $SnCl_2.2H_2O$, compared to that containing $SnCl_2$, showed a slightly higher elongation at break. This may be due to effective utilization of the SP resin for WPP/PP modification, in presence of $SnCl_2.2H_2O$. The non-utilized SP resin could be entrapped in the WPP/PP as a filler. All these results imply that the WPP can be modified by the resin compatibilizing system in a similar manner to PP modification. This is confirmed with the marginally different tensile properties obtained for the GTR/WPP

blend and GTR/PP blend containing 4 pphp of SP resin with 0.8 pphp of $SnCl_2.2H_2O$. The tensile strength and elongation at break for the GTR/WPP blend was 10.1±0.2 MPa and 21.3±1.0%, respectively, while those for the GTR/PP blend was 11.3±0.9 MPa and 21.2±0.9%, respectively.

Figure 6.37 illustrates typical FTIR spectra for the WPP and the resin modified WPP taken before and after acetone or xylene extraction. The spectra for the resin modified WPP (Figure 6.37c-e), compared to the spectra for the WPP (Figure 6.37a), show additional peaks at 3370, 1640 and 1220 cm^{-1} which corresponds to hydrogen bonding of phenol, -C=C- stretching vibration of aromatic rings, and –C-O- stretching vibration, respectively. The appearance of these peaks indicates the presence of SP resin in the WPP. As expected, the FTIR spectrum for the acetone extracted resin modified WPP ((Figure 6.37f), shows a similar spectrum to that for the resin modified WPP (Figure 6.37e). The uncombined/non-grafted SP resin in the resin modified WPP does not move to acetone, as there is no or low swelling of the specimen in acetone. In xylene, the specimen swells, the uncombined SP resin migrates to xylene and hence the FTIR spectrum for the xylene extracted resin modified WPP ((Figure 6.37g and h), shows lower peak heights at 3370 and at 1220 cm^{-1}. However, no significant variation of peaks or the peak heights in the FTIR spectra are noticed for the resin modified WPP with $SnCl_2.2H_2O$ or with $SnCl_2$, whether they are xylene extracted or not (Figure 6.37d and e, and Figure 6.37g and h). The FTIR spectra for both xylene extracted WPP and resin modified WPP exhibits an additional peak at 1610 cm^{-1}, which is a characteristic peak for xylene (Figure 6.30). These observations reveal that, the WPP can be modified with the resin compatibilizing system, even though some non-utilized SP resin is present in the resin modified WPP.

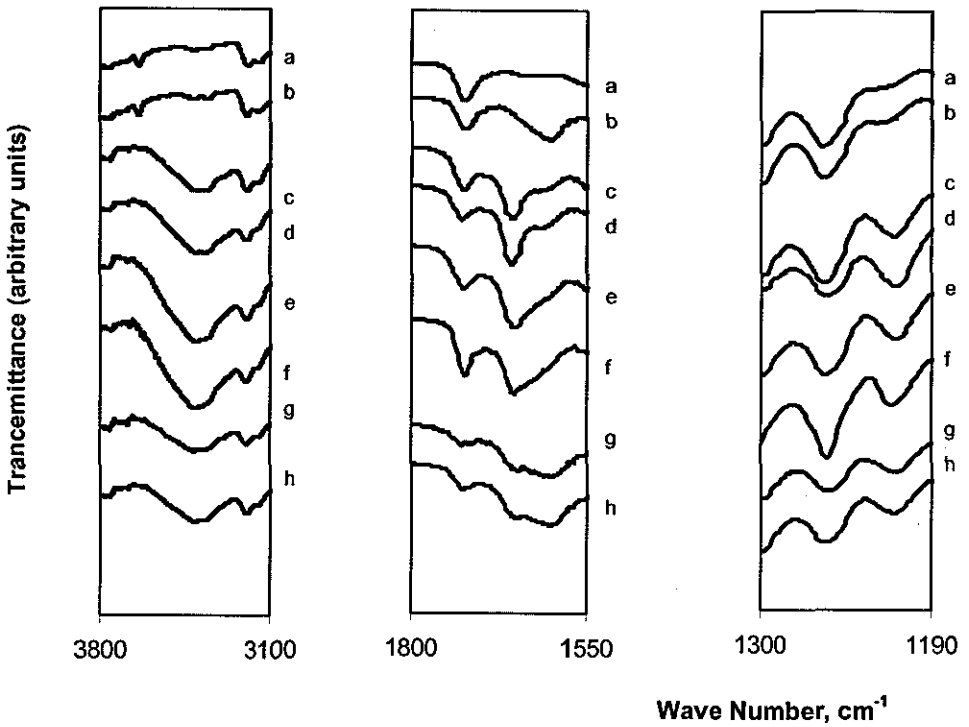

Figure 6.37 FTIR spectra for: (a) WPP (b) xylene extracted WPP (c) 4S/0.8TA/WPP (d)8S/1.6TD/WPP (e)8S/1.6TA/WPP (f) acetone extracted 8S/1.6TA/WPP (g) xylene extracted 8S/1.6TD/WPP (h) xylene extracted 8S/1.6TA/WPP

6.3 Comparison of Compatibilizing Systems

Dynamic vulcanization of the GTR/WPP by the dimaleimide compatibilizing system is based on the free radical mechanism, while that by the resin compatibilizing system is based on the ionic mechanism. Crosslinking by resin compatibilizing would occur if vinyl moieties, or unsaturation, present in the GTR were sufficient. However, both systems produce heat resistant C-C crosslinks in the GTR phase, which are stronger than the C-S and S-S crosslinks present in the GTR. Formation of additional crosslinks in the GTR phase with increasing levels of compatibilizing agent, with both HVA-2 and SP resin, were evident by the increase in steady state torque and the decrease in melt flow index. This was further confirmed by the increase in xylene insoluble fraction, crosslink density, % solvent extraction residue, shift in T_g of the GTR to a higher temperature, and also by the decrease in swelling index.

Due to the formation of additional crosslinks in the GTR phase by the HVA-2 (Scheme 6.3), hardness, tensile properties, impact failure energy and storage modulus initially increased with the HVA-2 level, before reaching a plateau or slightly decreasing. The optimum properties were obtained at 3 pphp level. Although crosslinking in the GTR phase increased its strength, the highly crosslinked GTR phase separated easily from the WPP phase. The variation in the tensile properties with resin level, for the blends containing SP resin, showed a similar trend. The tensile and impact properties of the two systems at a constant level of 3 pphp of compatibilizing agent and 0.6 pphp level of activator are given in Figure 6.38 and Figure 6.39, respectively. The increase in elongation at break for the blends with SP resin was marginal and was similar to those for the blends with HVA-2 at each level. However, the tensile strengths for those blends, compared to blends with HVA-2 at the same levels, were relatively lower. This variation is due to the formation of more crosslinks and/or shorter and hence stronger crosslinks with the HVA-2. It was noticed that high shear melt mixing generated free radicals (Scheme 6.1 and Scheme 6.2), which provided facilities for HVA-2 to produce more crosslinks with these active sites. The modification of the WPP phase by the SP resin (Scheme 6.15) decreased the strength of the WPP phase and hence strength of the blend. The modification also increased the brittleness of the WPP phase and hence the impact failure energy did not increase with the SP resin level. The enhancements in properties for the blends with HVA-2 and SP resin were not as high as expected. This was probably due to the lack of vinyl moieties in the GTR phase, which are required for effective crosslinking. This is also associated with the premature failure of the test specimens due to interfacial debonding. The tensile fracture surfaces were non-homogeneous and had large holes created due to removal of the GTR particles from the WPP matrix phase. The DSC thermograms, and the FTIR spectra of the gels obtained after boiled xylene extraction, reveal that the WPP phase was not involved in the crosslinking process.

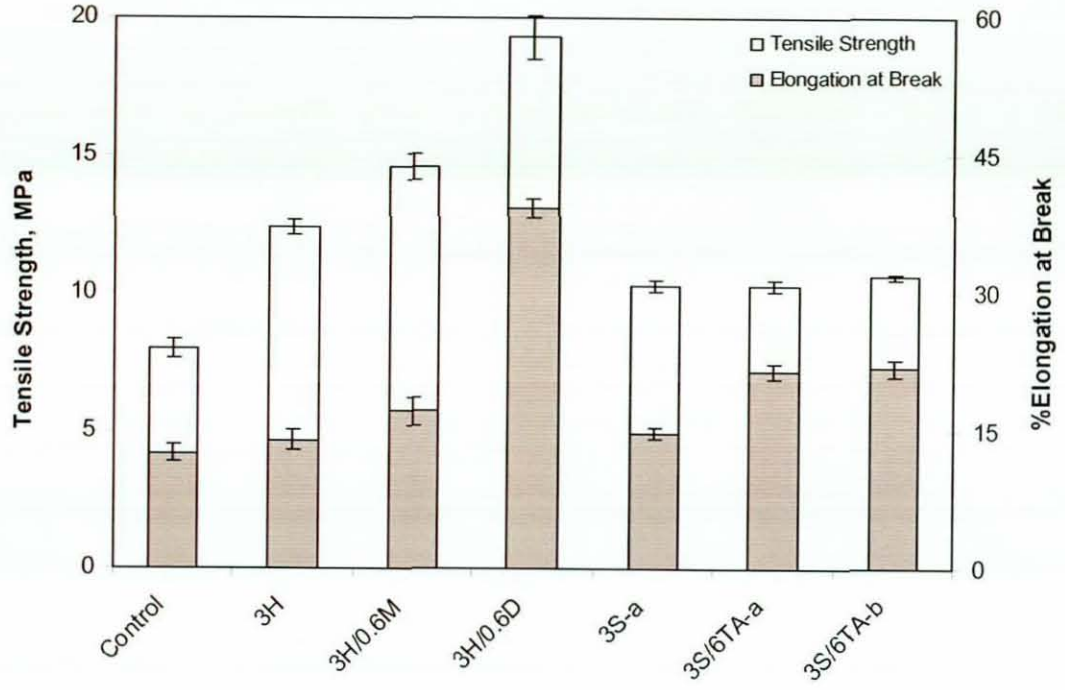

Figure 6.38 Tensile properties of the control blend, and blends with two compatibilizing systems

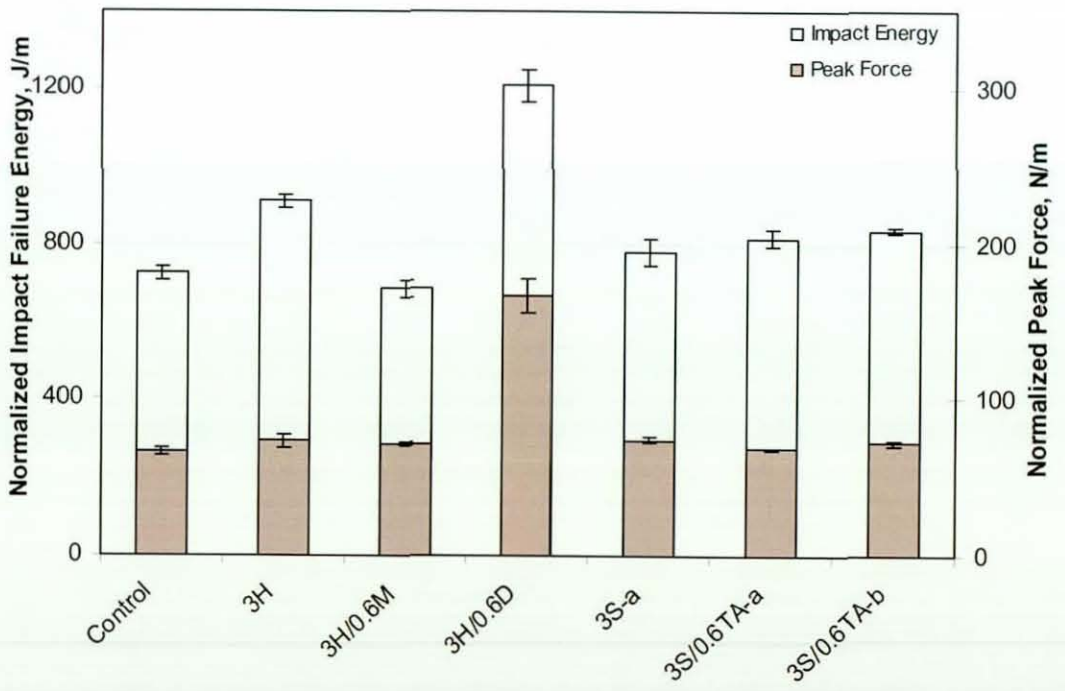

Figure 6.39 Impact properties of the control blend and blends with two compatibilizing systems

With the addition of MBTS into the blends containing HVA-2, the tensile properties further improved, but not greatly. The impact properties decreased with the MBTS level. The slight enhancement in tensile properties suggested the formation of some more crosslinks in the GTR phase and hence the behaviour of MBTS as a crosslinking promoter for HVA-2 in the GTR/WPP blends. That was further confirmed by the processing characteristics, the chemical characteristics and by the thermal properties investigated. However, the blend morphology was not changed, and did not show any improvement in its homogeneity. Failure occurred mainly due to interfacial debonding. The addition of DTBPIB into the blends containing HVA-2 improved the mechanical properties drastically. More stable blend morphology was exhibited with the formation of crosslinks at the interface (Scheme 6.9), which increased the adhesion between phases. The participation of the WPP phase in interfacial crosslinking was revealed by the FTIR spectra and DSC thermograms of the gels after the boiled xylene extractions. Further, this was confirmed by the closeness of the T_g of both phases observed in the tan δ curves. The increased interfacial adhesions permitted interaction of stress concentration zones, developed from the GTR particles under deformation, and promoted shear yielding in the WPP phase. These results suggested that the DTBPIB is better than MBTS as an activator for HVA-2. Further, optimum levels of HVA-2 and activators are required to achieve best balanced properties. In the case of the HVA-2 with MBTS system, better tensile properties were obtained at higher HVA-2 levels (5 pphp), and at lower MBTS levels (0.2 pphp). HVA-2 with DTBPIB blends also exhibited better properties at higher HVA-2 levels. However, similar properties were obtained at 3 pphp of HVA-2 with 0.6 pphp of DTBPIB. Further increases in either MBTS or DTBPIB did not produce significant property improvement.

With the addition of both $SnCl_2$ activator and the SP resin to the mix of GTR and WPP (schedule-a), elongation at break drastically increased and was greater than the maximum increase exhibited for the blends containing HVA-2 with MBTS. This greater elongation is attributed to the improved compatibility between phases which occurred through modification of the WPP phase. The tensile strength and the impact strength did not show further significant increase with the addition, and then with the increase, in the $SnCl_2$ level. The blends prepared by melt mixing of the GTR with the resin modified WPP (schedule-b) exhibited slightly improved tensile and impact properties associated with

improved compatibility. This was evident by the closeness of the glass transition temperatures of the two phases, and by the slightly improved blend homogeneity. The maximum properties were exhibited at 4 pphp of SP resin and at 0.8 pphp of $SnCl_2$. The blends prepared with $SnCl_2$ and with $SnCl_2.2H_2O$ exhibited similar characteristics, indicating that the activity of any form of stannous chloride as an activator for SP resin in the GTR/WPP blends is more or less similar. Even though an improvement in properties for the blends with resin compatibilizing system was obtained, it was considerably lower than that for the blends containing HVA-2 with DTBPIB. The results of the present study clearly showed that the WPP could be modified by the SP resin system in a similar manner to the virgin PP. The GTR phase could also be crosslinked with the SP resins system. Therefore, the main reason for the inferior properties of the blends with the resin compatibilizing system is lack of interfacial adhesions developed by the resin compatibilizing system (Scheme 6.16). This was evident by interfacial debonding on the tensile fractographs and no peak assignments given for the WPP on the DSC thermograms of the gels from boiled xylene extraction and on the FTIR spectra of the blends after xylene extraction.

Chapter 7 Results and Discussion - Part IV

Delink Treated Ground Tyre Rubber and Its Blends

The ground tyre rubber (GTR) was first treated with Delink, according to the mixing schedule-d, under the processing conditions given in Section 3.2.10.2. The Delink consisted of zinc dimethyldithiocarbomate (ZDMC), 2-mercaptobenzothiazole (MBT), zinc oxide, stearic acid, sulfur and diethylene glycol as given in the formulation in Section 3.1.2. The optimum Delink level and the treatment conditions were investigated using tensile properties. The Delink treated GTR at the optimum level of 3 phr (DGTR), was then mixed with the waste polypropylene (WPP) to prepare DGTR/WPP blends. The DGTR/WPP blends were also prepared with the selected compatibilizing systems used in previous studies (Chapter 6). The effect of Delink treatment on the GTR in the DGTR/WPP blends was investigated by comparing their tensile and impact properties with those for the processed-GTR/WPP blends. The processed-GTR (PGTR) was prepared according to the same mixing schedule-d, but without the Delink. This chapter considers the optimum Delink level and the treatment conditions, and discusses the properties of DGTR/WPP and PGTR/WPP blends.

7.1 Delink Treatment of GTR

The GTR was treated with Delink at three different levels, 3, 6 and 9 phr, in the Haake mixer (Figure 3.9) at a rotor speed of 90 rpm and at a selected temperature of 40 ^{0}C. Delink treatment was carried out first for 7 minutes and then for 10 minutes. The Delink treated GTR was vulcanized at two different temperatures, at 150 ^{0}C the normal rubber vulcanizing temperature and at 200 ^{0}C, the temperature at which the sheets from the blends were moulded. The optimum Delink level and the treatment conditions were investigated. The results obtained at different Delink levels and at different treatment conditions are discussed in this section. The possible chemical reactions that could occur during Delink treatment are also discussed.

7.1.1 Possible Chemical Reactions during Delink Treatment

The GTR will undergo bond scissions on the sulfur crosslinks and on the rubber chains, and form active free radicals due to the high mechanical shearing forces generated, especially at low temperatures, as given by Scheme 6.1.

MBT, the major component of the Delink, exists in two forms namely, thione and thiol (Scheme 7.1) [295]. The thione form has less energy and hence it is more stable than thiol form [195]. The highly active thiol form would also be expected to produce free radicals under high shearing forces by homolytic fission of the S-H bond in the thioketone group in the MBT (Scheme 7.2) Alternatively, MBT can be oxidized to the disulfide, 2,2-dithiobisbenzothiazole (MBTS) [252]. The central S-S bond of MBTS, which has the weakest bond energy, will undergo homolytic fission to produce free radicals (Scheme 7.2), which could then be notated as Ac-S radicals (Ac is the accelerator fragment, 2-benzothiazolyl group). Another reaction for the MBT with zinc oxide to form the zinc salt, zinc mecaptobenzothiazole (ZMBT) was suggested in the chemistry of unsaturated rubber vulcanization [251, 252], but it could not be expected to occur at the Delink treatment conditions, 40 ^{0}C. This is evident from the DSC thermograms of the Delink chemicals (see Figure 7.2). ZDMC may also undergo homolytic fission to form active radicals simultaneously, in lesser amounts (Scheme 7.3). The presence of ZDMC in the Delink is relatively low, in a molar ratio 15:2 for MBT:ZDMC.

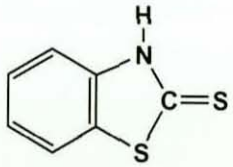

thione

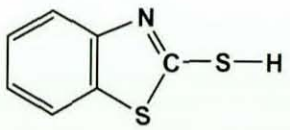

thiol

Scheme 7.1 Structural formulas of MBT

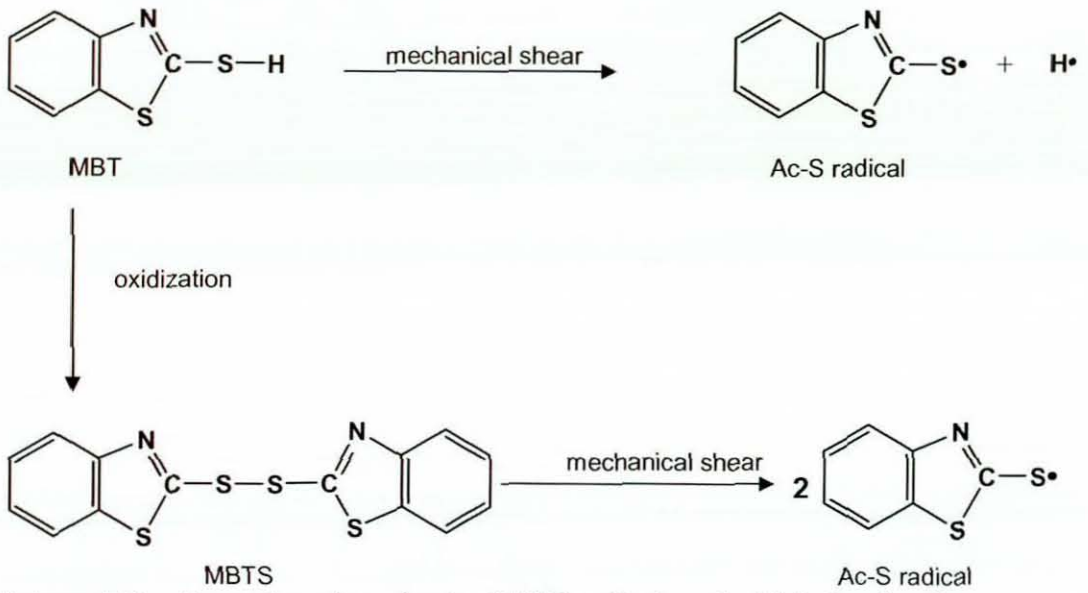

Scheme 7.2 Formation of accelerator (MBT) radicals under high shearing forces

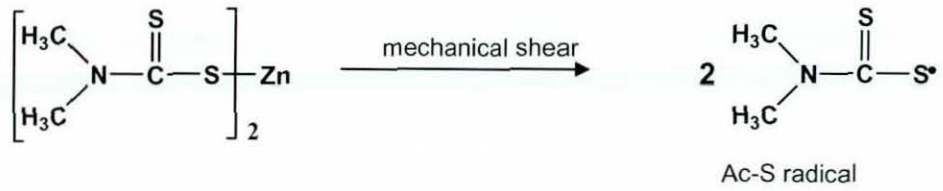

Scheme 7.3 Formation of accelerator (ZDMC) radicals under high shearing forces

The accelerator radicals will then combine with the radicals formed on the crosslinks and on the rubber chains (Scheme 6.1) in order to form rubber bound accelerator fragments (rubber-S_n-S-Ac), which are then available for a new vulcanization reaction. The proposed reaction is shown in Scheme 7.4. The rubber bound accelerator fragments are similar to the accelerator-derived polysulfides formed as crosslink precursors in the course of sulfur vulcanization of unsaturated rubbers [81, 251]. These highly active accelerator radicals may also attack the weaker S-S and S-C bonds in the crosslinks in the GTR and may generate more free radicals. As a result, the GTR undergoes devulcanization than depolymerization, in the presence of the Delink. However, it is known that the MBT has a slight depolymerizing activity on rubber [251]. The inventors of the Delink process [169, 247] also proposed a similar reaction scheme (Figure 2.18).

During mixing for longer periods, once the accelerator radicals are fully consumed in radical capping, the radicals formed in the GTR may couple themselves to chain extensions during the final part of the Delink treatment. However, no reactions between the Delink chemicals could occur at the treatment conditions used in the present study. Figure 7.1, the DSC thermograms for the PGTR with 3 phr of Delink performed at different isothermal temperatures, shows no reaction at 40 and 50 ^{0}C. A slight increase in the heat flow with time when processed at 60 ^{0}C suggests the commencement of a reaction however the reaction will not progress to a significant extent within 10 minutes. The thermograms at 70 ^{0}C and above indicate the completion of a chemical reaction to a considerable extent. These results are supported by the DSC thermograms obtained for individual Delink chemicals and their combinations (Figure 7.2).

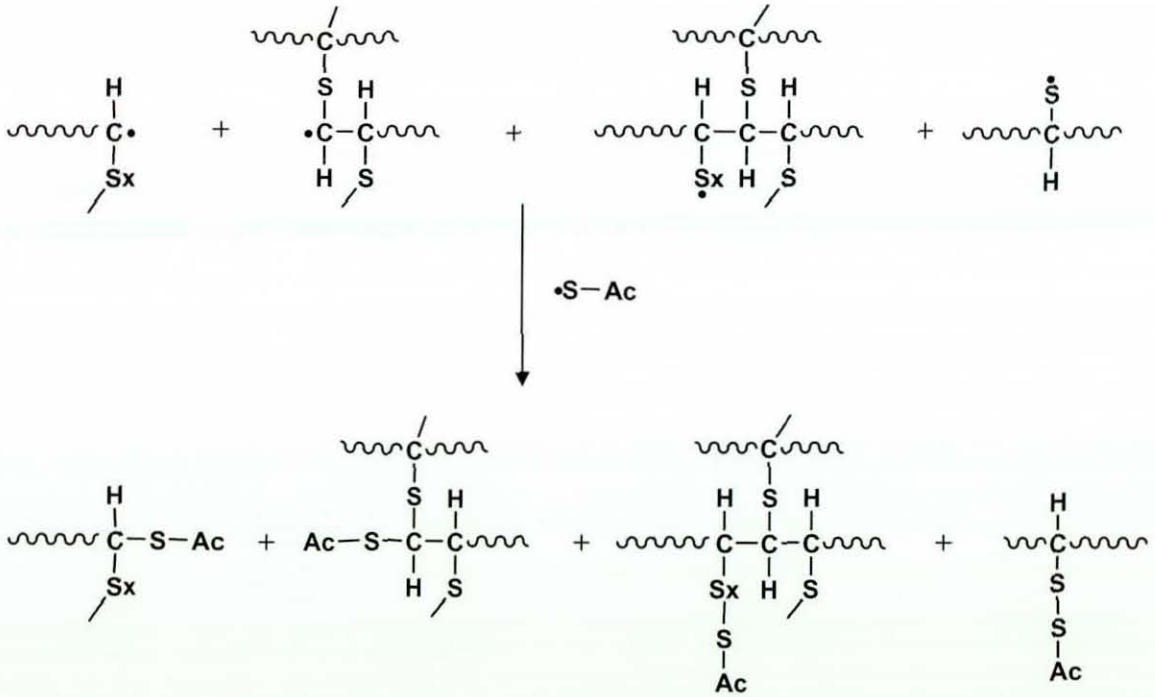

Scheme 7.4 Radical capping for Delink devulcanization

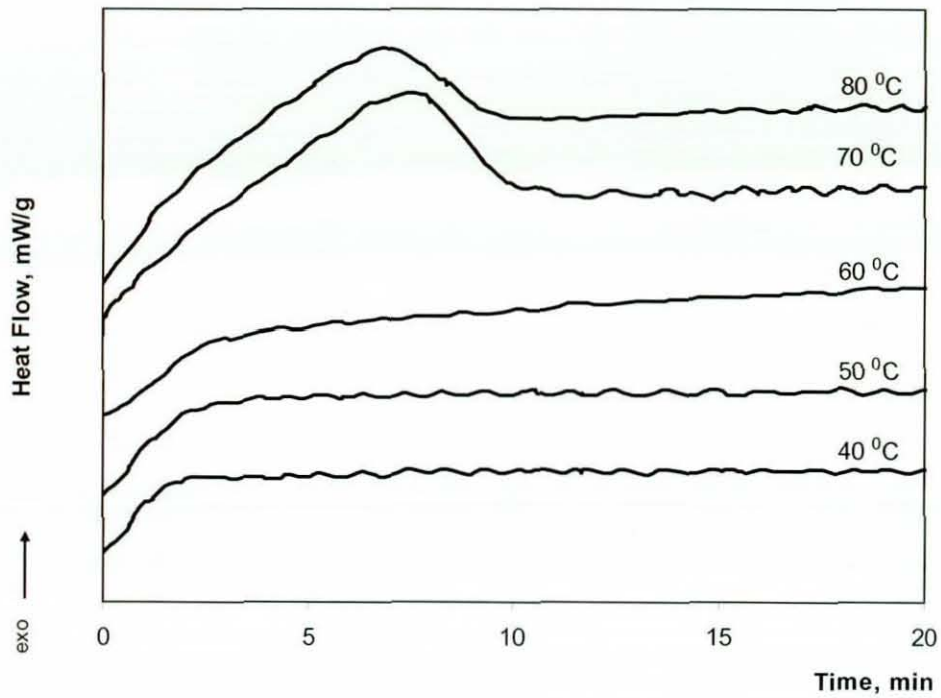

Figure 7.1 DSC thermograms for PGTR with 3 phr of Delink obtained at isothermal conditions

7.1.2 Re-vulcanization of Delink Treated GTR

The Delink treated rubber consists of rubber bound accelerator fragments, the non-utilized Delink chemicals, and the broken rubber radicals generated due to high shearing forces. During vulcanization, moulding at high temperature and pressure, the rubber bound accelerator fragments will break back and form accelerator radicals/fragments, and broken sulfur crosslink ends and rubber chains. Simultaneously, the Delink chemicals will react with each other to finally form a crosslinked rubber network. The reactivity of the Delink chemicals was studied by observing the DSC thermograms of the chemicals and their combinations performed at a heating rate of 10 ^{0}C/min, which are shown in Figure 7.2.

The MBT accelerator fragments will not react effectively with rubber if MBT is used alone below its melting temperature of 182 ^{0}C. However, in the presence of sulfur, the MBT accelerator will first react to produce accelerator derived polysulfides (Ac-S_x-Ac)

and then interact with rubber in the GTR to produce macromolecular polysulfidic intermediates (rubber- S_x-Ac), in a similar way to the initial step of the accelerated sulfur vulcanization of unsaturated rubbers [81, 251]. Finally, the rubber polysulfides react either directly or through an intermediate to give crosslinks (rubber-S_x-rubber).

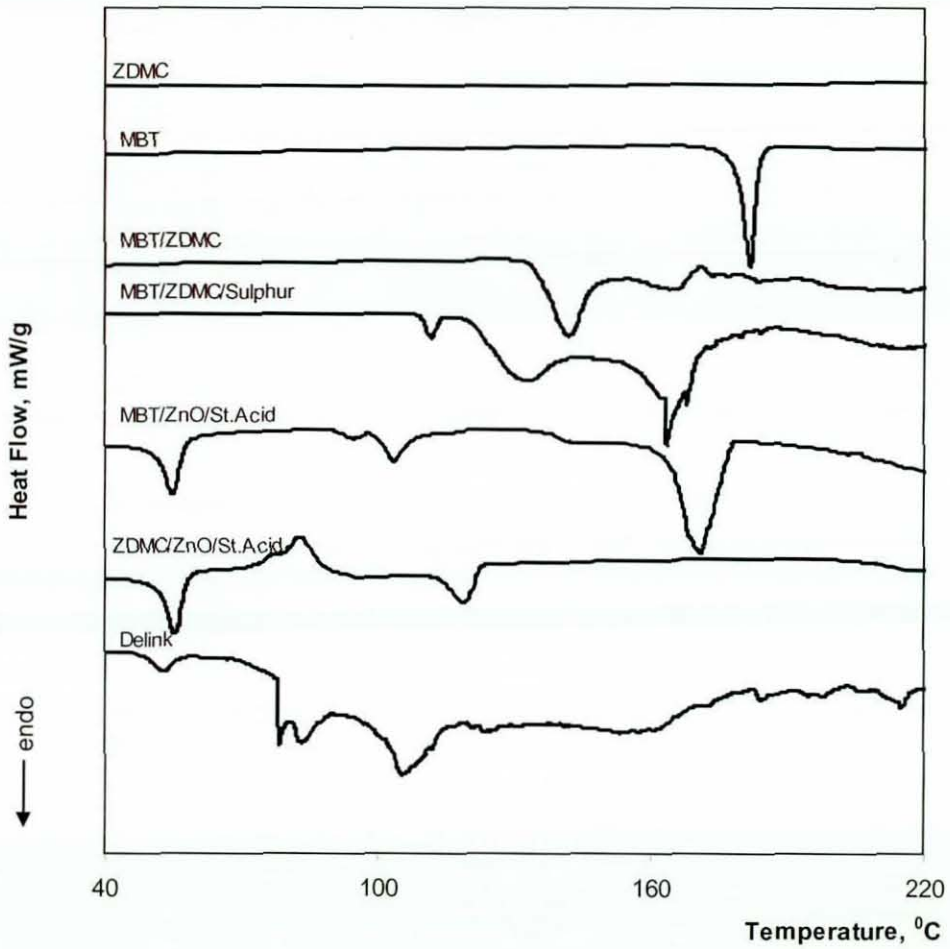

Figure 7.2 DSC thermograms of Delink chemicals and their combinations

The addition of Zn^{++} ions, by the addition of zinc salt and/or of ZnO, promotes the formation of more di- and mono-sulfidic crosslinks [81, 296]. This is attributed to the formation of zinc accelerator complexes, which catalyze crosslink formation. These complexes may act as sulfur-atom carrier, transporting them from sulfur-rich to sulfur-poor areas, in the Delink treated GTR [296]. In support of this theory it is clearly shown in Figure 7.2 that the addition of ZnO and stearic acid to MBT drops its melting point to 170 ^{0}C, and broadens the melting endotherm, which is evident for the formation of zinc

accelerator complexes at lower vulcanizing temperatures. The melting endotherm broadens due to change in MBT morphology. The formation of complex structures, in the MBT, in the presence of ZnO and further with stearic acid when heated to 130-150 ^{0}C has been reported previously [295, 297]. The two small endotherms in the DSC thermogram of MBT with ZnO and stearic acid, observed at 55 ^{0}C and 104 ^{0}C, are attributed to the melting of stearic acid and the formation of zinc stearate, respectively [298]. No indications were seen for the formation of zinc stearate immediately after melting of the stearic acid, in the absence of water, although it was reported in a previous study [298].

The addition of Zn^{++} to MBT by the addition of ZDMC in a molar ratio of 2 to 15 of MBT is also shown as effective in the formation of zinc accelerator complexes, which is indicated by a broader melting endotherm for the MBT at 142 ^{0}C. The melting point of ZDMC is 240 ^{0}C [298] and hence ZDMC alone did not show a melting endotherm within the temperature range studied. The formation of synergistic accelerator complexes from MBT and ZDMC was reported previously [252]. This accelerator complex is shown in Figure 3.7. It has been reported [251] that a small quantity of ZDMC is a good activator for MBT in sulfur vulcanization. The addition of larger quantities of ZDMC to the sulfur vulcanizing system reduces the processing safety of the rubber compound, and hence vulcanization would occur at a low temperature in the range110-120 ^{0}C [251]. Further, the addition of free ZnO to the sulfur vulcanizing system with ZDMC is essential, to react with the H_2S formed, and not to produce zinc complexes.

The addition of sulfur to the MBT/ZDMC mix, further broadens the melting endotherm of MBT and drops its melting point to 134 ^{0}C. This is associated with the dissolution of MBT in sulfur once it is melted at 112 ^{0}C. A melting endotherm at 133 ^{0}C was also obtained in a previous study [298] for a MBT/sulfur mix of 1:1 mole ratio. Therefore, an effective re-vulcanization through the formation of a higher concentration of di- and mono-sulfidic crosslinks could be expected with the Delink composition that was used in the present study. As the ratio of the concentration of accelerator to that of sulfur in the Delink treated GTR, compared to those in the PGTR, increases, the proportion of mono- and di-sulfidic crosslinks increases and hence results in stronger crosslinks in the GTR phase. It is well known that the ZDMC has a good crosslink shortening activity through desulfuration of the rubber polysulfides [251, 296, 299]. The crosslink shortening during

re-vulcanization of the Delink treated rubber was previously reported by the inventors of the Delink process [247].

7.1.3 Evaluation of Optimum Delink Level

The optimum Delink level was evaluated using the tensile properties of the vulcanizates of the Delink treated GTR. The processing characteristics, gel content, and macroscopic images of the moulded sheets were also used to evaluate the optimum Delink level. For this study, the GTR was treated with the Delink at 3, 6 and 9 phr levels at 40 ^{0}C for 7 min. Vulcanizates were prepared at 150 ^{0}C. The results obtained at the three different Delink levels are discussed in this section.

7.1.3.1 Processing Characteristics

Torque vs. time curves for the GTR and the GTR treated at different Delink levels are shown in Figure 7.3. The torque development curve for the GTR shows an initial torque increase with loading of the GTR and then a decrease towards stabilization. The resultant product (PGTR) was a free flowing powder.

With the addition of 3 phr of the Delink after 2 minutes, a sudden increase in torque was exhibited due to loading cold materials. Therefore the torque drops with the mixing of the chemicals and stabilized at the processing temperature. Due to the formation of free radicals on the crosslinks and on the rubber chains (Scheme 6.1), and to the radical capping reactions (Scheme 7.4), the torque again increases and stabilizes with time. This is also associated with the GTR particle agglomeration, which was observed after the completion of mixing. The Delink treated GTR at this 3 phr level was wet and sticky.

The GTR treated with 6 and 9 phr of the Delink shows a slight decrease in torque at the latter stage of mixing being greater with the 9 phr level. This torque decrease is associated with the reduced levels of particle agglomeration, which occurs in the presence of excess Delink chemicals. The resultant Delink treated GTR at the higher levels behaved as free flowing particles. This torque decrease may also be due to excessive dissociation of the

rubber chains without causing an effective dissociation of the crosslinks at higher Delink levels. The dissociation of rubber chains results in a reduction in the molecular weight of the treated GTR. The decrease in stabilization torque with the Delink level, when added to rubber powder waste was also reported in literature [38].

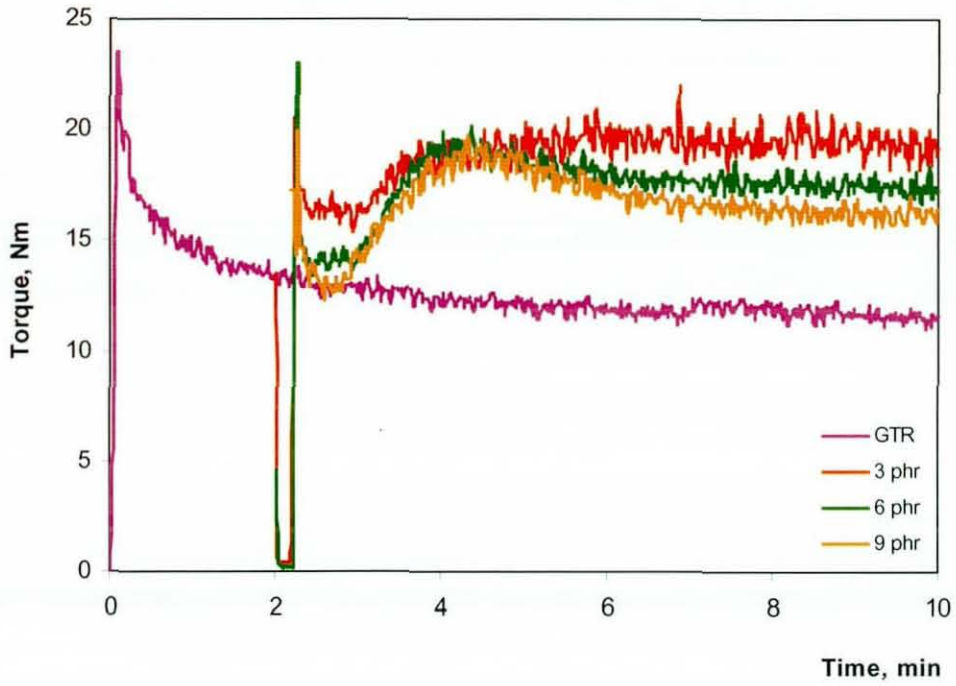

Figure 7.3 Torque-time curves (at 40 ^{0}C) for the GTR, and the GTR treated at different Delink levels

7.1.3.2 Surface Characteristics of Vulcanizates

The moulded sheets prepared at 150 ^{0}C from the PGTR, and the Delink treated GTR at all three levels, were smooth and did not show any imperfections on their surfaces. However, after six weeks, a certain level of blooming was noticed on the moulded sheets prepared from the Delink treated GTR with 9 phr of the Delink (Figure 7.4b). Surface blooming was due to the migration of one or more Delink chemical, which was not involved in the re-vulcanization process. No blooming was observed on the sheets with 3 and 6 phr Delink. An optical image of a non-bloomed surface is shown in Figure 7.4a. This implies that the added Delink, at 3 and 6 phr levels, was effectively utilized in the re-

vulcanization process, and less or no free Delink chemicals were present in those vulcanizates.

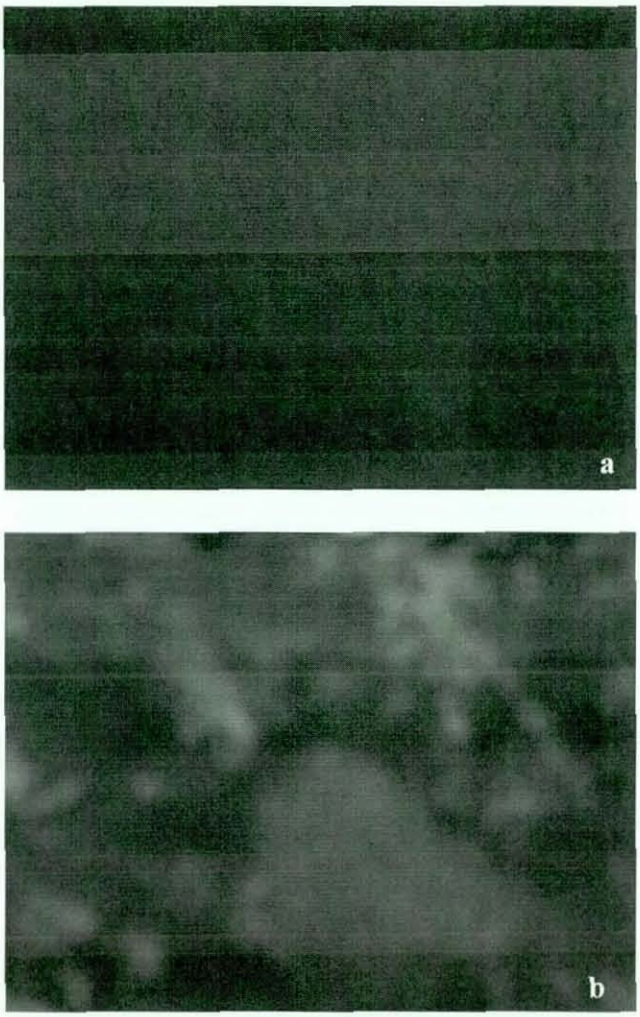

Figure 7.4 Optical images of vulcanizate surfaces of the Delink treated GTR

(a) non-bloomed (b) bloomed

FTIR spectra for the bloomed and the non-bloomed surfaces are given in Figure 7.5. This figure clearly shows some additional peak assignments in the spectra for the bloomed surface. The presence of stearic acid and/or the zinc stearate in the bloomed surface is revealed by the additional peak assignments observed at 3400, 1712, and 1260 cm^{-1} for O-H, C=O and C-O stretching vibrations, respectively. In addition, the appearance of peaks at 1506 and 1602 cm^{-1}, assigned to C=C in aromatic rings, at 1411 cm^{-1} assigned to C=S stretching vibrations, at 1340 and 1132 cm^{-1} assigned to C-N stretching vibrations, at

870 cm^{-1} assigned to C-S stretching vibrations and at 670 cm^{-1} assigned to N-H wagging vibrations suggests the presence of MBT and ZDMC in the bloomed surface [300]. These observations confirm the migration of excess Delink chemicals to the surface as bloom.

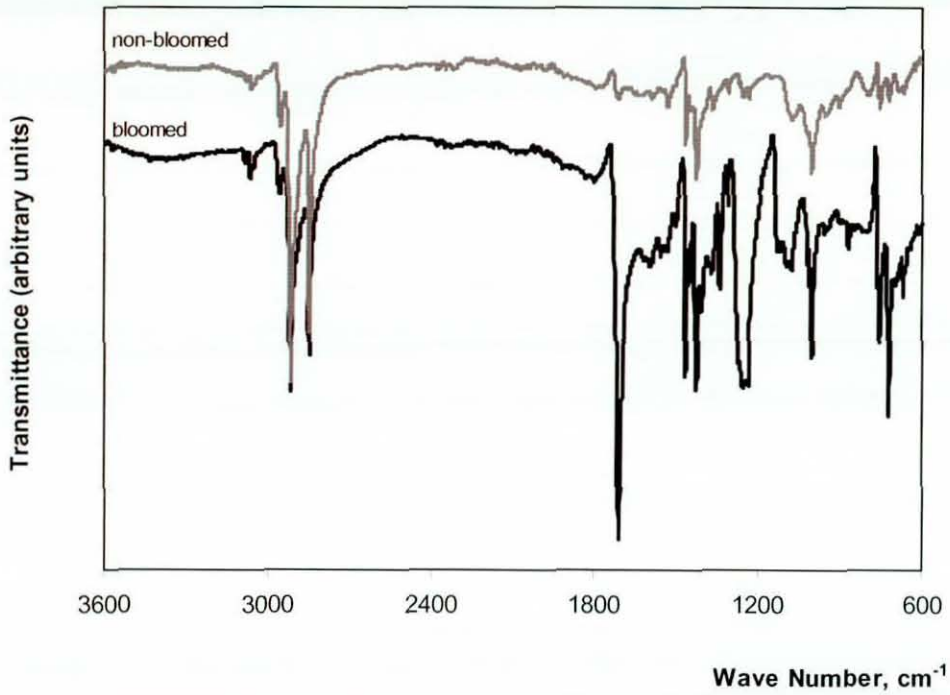

Figure 7.5 FTIR spectra for the surfaces of the moulded sheets

7.1.3.3 Gel Content and Swelling Index

The gel contents for the PGTR, the Delink treated GTR, and the vulcanizates of the Delink treated GTR determined by immersing in toluene at 40 ^{0}C for 7 days and then drying at 70 ^{0}C for 2 hours in a vacuum oven, are given in Figure 7.6. The %gel content was calculated per sample weight in psw according to Equation 3.17 and per GTR weight in prsw according to Equation 3.18. The gel content of the PGTR was 85.3±0.3% which is very high due to the crosslinked structures formed during the previous vulcanization processes, although some degradation occurred during processing under high shear forces. The Delink treated GTR, within the Delink levels studied, was also not fully dissolved in toluene, unlike un-vulcanized rubbers which are completely soluble in toluene. A considerable fraction remained as a swollen gel. This implies that no scission occurred in the rubber chains and hence no severe degradation occurred with the Delink

treatment of the GTR. The dissociated crosslinks remain entrapped in the gel, when the rubber chains are long, and hence no information can be obtained on the degree of crosslink dissociation from the gel content results.

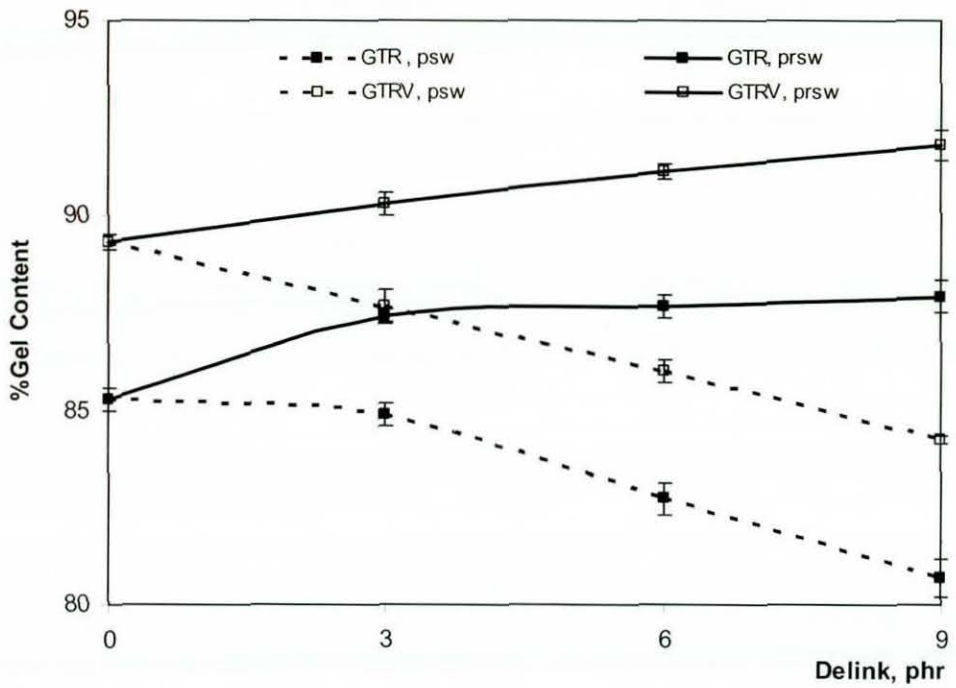

Figure 7.6 Gel content of the Delink treated GTR and their vulcanizates (GTRV)

The gel content of the sample for the Delink treated rubber at 3 phr was similar to that for the PGTR. However, the gel content of the samples decreased considerably when the Delink level was above 3 phr, indicating a certain level of dissociation of either crosslinks and/or rubber chains, or removal of the Delink chemicals, which were not utilized in the Delink process. This explanation is in agreement with the drop in torque noticed at the latter stage of mixing for GTR treated with 6 and 9 phr of the Delink (Figure 7.3). However, the gel content per GTR in the sample increases significantly at 3 phr of the Delink, and the increase is not gradual and not so great at 6 and 9 phr levels. This increase in gel content at 3 phr level explains that the dissolution of GTR and Delink chemicals in toluene, after the Delink process, is lower in quantity than the Delink added. If the scission of the rubber chains occurred during the Delink process, with the Delink level, the dissolution of the GTR in toluene is greater, and hence both the gel content per

sample and the gel content per GTR in the sample will decrease. These results confirm that the Delink utilization is optimum at 3 phr.

The gel content of the PGTR vulcanizate increased by 4% due to the formation of new crosslinks during re-vulcanization through a combination of radicals formed on crosslinks, and on rubber chains, during the high shear processing (Scheme 6.1) or with the radicals or active sites available with the GTR itself. The gel contents of the vulcanizates of the Delink treated GTR increased by approximately 3% at each Delink level, which is also due to the formation of new crosslinks (Figure 2.18). The crosslinks would be formed through rubber bound accelerators generated during Delink treatment (Scheme 7.4). Furthermore, due to side reactions, cyclic sulphides, mono-sulphidic pendent groups and other non active groups, which would account for the gel, could also be produced. However, the gel contents for the vulcanizates of the Delink treated GTR were lower than those for the PGTR vulcanizate, and also showed a linear decrease with the Delink level. These differences in gel contents are due to removal of non-utilized Delink chemicals. This may also be due to the relatively lower degree of crosslinks formed during re-vulcanization compared to those due to dissociation during Delink treatment. Further, a gradual increase in the gel content per GTR in the sample indicates lower levels of dissociation of rubber chains in the vulcanizates of the Delink treated GTR. All these results are evidence for the dissociation of crosslinks rather than those of rubber chains, during Delink treatment at lower temperatures, and the formation of new crosslinks during re-vulcanization at higher temperatures.

The swelling indices for the vulcanizates of the PGTR, and Delink treated GTR, were determined by immersion in toluene and calculated according to the Equation 3.16. These indices are given in Table 7.1. The swelling index decreases with the addition of the Delink and further decreases with the Delink content up to 6 phr. This also confirms the formation of new crosslinks during re-vulcanization. Although the formation of crosslinks in the vulcanizate with 9 phr of the Delink was expected to be greater, due to entrapment of more toluene in the specimen, in places where the specimen consisted of loosely bounded GTR particles and/or voids, this vulcanizate showed a greater swelling index, even greater than that of the vulcanizate of the PGTR.

Table 7.1 Swelling indices for the vulcanizates of the PGTR and Delink treated GTR

Delink, phr	% Swelling Index
0 (PGTR)	1.97
3	1.62
6	1.52
9	2.13

7.1.3.4 Tensile Properties

Tensile properties of the Delink treated GTR are given in Figure 7.7. With the addition of 3 phr of the Delink to the GTR, tensile strength, secant modulus at 2% strain and elongation at break increased significantly. This increase in tensile properties is probably a result of the formation of shorter and stronger crosslinks between GTR particles, as explained in Section 7.1.2. An increase in gel content per GTR in the sample, and decrease in swelling index for vulcanizates of the Delink treated GTR, also indicated the formation of new crosslinks during the re-vulcanization process (Section 7.1.3.3).

With further increases in the Delink level, more crosslinks are dissociated during Delink treatment, and more crosslinks and chain modifications are developed during re-vulcanization. Similarly, more non-utilized Delink chemicals are entrapped in the Delink treated GTR. These chemicals would liberate some gasses due to their decompositions at 150 ^{0}C (Section 7.1.2) and moulded sheets with loosely bounded GTR particles would result. The tensile test specimens cut from these sheets split upon straining during the tensile test, and also exhibited blooming due to the migration of these chemicals to the surface (Figure 7.8). As a result, the vulcanizates of the Delink treated GTR, at higher Delink levels produced inferior tensile strength and elongation at break. However, due to the increase in non-rubbery components such as fillers in the vulcanizates, secant modulus slightly increases with the Delink level

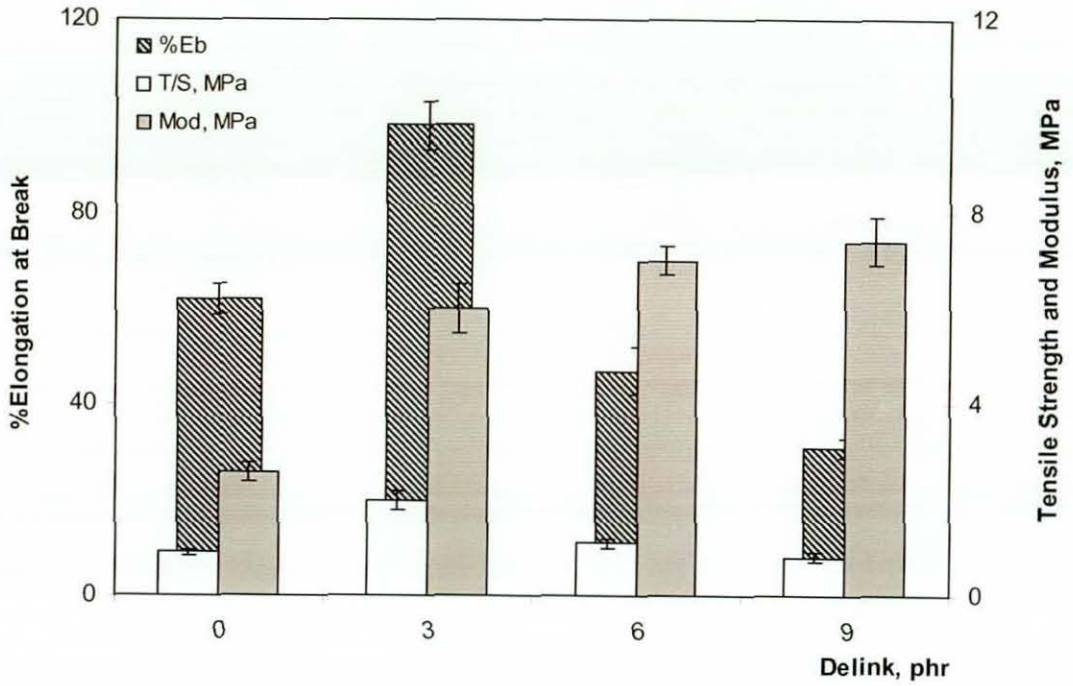

Figure 7.7 Tensile properties for the vulcanizates of the Delink treated GTR

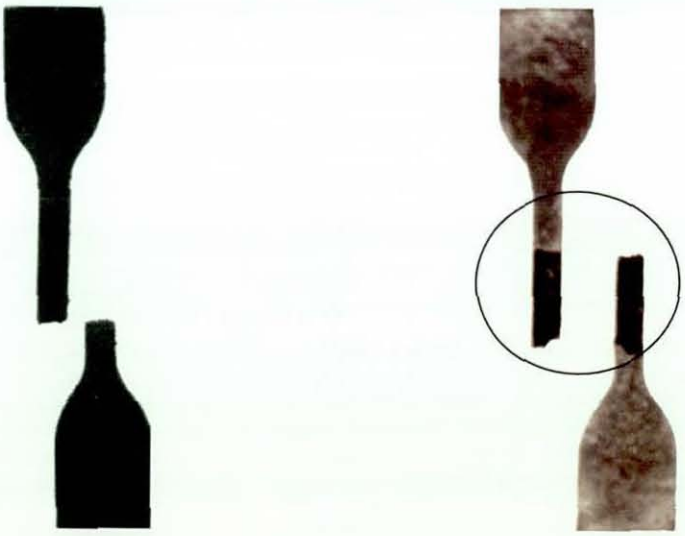

(a) (b)

Figure 7.8 Fractured tensile test specimens of Delink treated GTR with (a) 3 and (b) 9 phr, when re-vulcanized at 150 ^{0}C

A previous study [169] suggested the use of 2-6 pphp of Delink as the amount required depends on the type of rubber being devulcanized and the final form of the devulcanized

product desired. An optimum Delink level as 6 pphp was found when 30% treated rubber was blended with virgin natural rubber [38]. Further, 6 pphp of Delink was used in treating buffing dust in order to incorporate it in virgin natural rubber at 0-50 % levels [171]. Further, 6 pphp of Delink was used in treating tyre crumbs with 100% natural rubber resulting comparable properties to virgin rubbers [42]. However, with the selected Delink formulation, and under the process conditions used in mixing and moulding in the present study, the best tensile properties were obtained at 3 phr of the Delink.

7.1.4 Effect of Delink Treatment Conditions

The influence of the Delink treatment conditions, such as processing time and re-vulcanizing temperature, were investigated using tensile strength and elongation at break of the vulcanizates of the Delink treated GTR. The Delink treatment was carried out at 40 ^{0}C in order to prevent re-vulcanization during the treatment. The processing time was either 7 min. or 10 min., while the re-vulcanization temperature and time were kept constant at 150 ^{0}C and 8 min., respectively. The effect of re-vulcanizing temperature of 200 ^{0}C on the tensile properties of the Delink treated GTR was also investigated after treating with the Delink for 10 min.

7.1.4.1 Processing Time

The tensile strength and the elongation at break for the Delink treated GTR at 7 and 10 min. processing time are given in Table 7.2. The GTR treated with the Delink for 10 min, compared to 7 min, showed better properties, due to completion of the Delink treatment process. However, GTR with 9 phr of the Delink showed slightly lowered tensile properties when processed for 10 min. This is associated with the greater levels of gas liberation with increase in processing time, which create imperfections in the moulded sheets. The torque-time curves recorded for the GTR treated with the Delink at the selected levels were also an evidence for completion of the treatment process. These curves exhibited torque stabilization at 10 min (Figure 7.3). The inventors of the Delink process reported that the Delink treatment will complete within 8 min. in a two-roll mill and in 5 to 6 min. in an internal mixer [169]. Therefore, it was recommended that the

waste rubber be treated with the Delink for less than 10 min. at a temperature below 70 ^{0}C, to avoid premature vulcanization [42].

Table 7.2 Tensile properties of Delink treated GTR at different processing times

Delink, phr	Tensile Strength, MPa		%Elongation at Break	
	7 min.	10 min.	7 min.	10 min.
0 (PGTR)	0.9(0.1)	1.0(0.1)	62(2)	80(3)
3	2.0(0.2)	2.9(0.2)	98(2)	141(5)
6	1.1(0.1)	1.4(0.2)	47(3)	62(5)
9	0.8(0.1)	0.7(0.1)	31(1)	27(2)

7.1.4.2 Re-vulcanization Temperature

Sheet moulded at 200 ^{0}C from the PGTR was smooth but slightly sticky unlike the sheets prepared at 150 ^{0}C from the PGTR (Section 7.1.3.2). This stickiness was due to degradation of the GTR to a certain extent. Sheets moulded at 200 ^{0}C from the Delink treated GTR exhibited surface bulges, as shown in Figure 7.9. However, no surface imperfections appeared on the sheets prepared at 150 ^{0}C. The formation of bulges at 200 ^{0}C is associated with gas entrapment in the GTR which occurred due to severe decomposition of one or more of the Delink chemicals, and the properties of the Delink treated GTR such as early vulcanizing capability due to the presence of still active crosslinking sites. A burning smoke and odor observed during moulding at 200 ^{0}C confirmed the severe decomposition of Delink chemicals and/or the GTR. The decomposition of Delink chemicals at higher temperatures was also noticed on the DSC thermogram for the Delink (Figure 7.2). The decomposition of Delink chemicals were reconfirmed with the surface blooming observed on all sheets prepared from the Delink treated GTR at 200 ^{0}C. This is due to migration of low molecular weight species generated by the decompositions of non-utilized Delink chemicals. The bloom was great at high Delink levels and was observed on the sheets with 9, 6 and 3 phr of the Delink after 1, 3 and 6 weeks, respectively. The bloom yield, which is a measure of the thickness

of the layer and the colour [38], increased with the Delink level, due to the presence of more non-utilized Delink chemicals. This is supported by the lower gel contents obtained for higher Delink levels (Section 7.1.3.3). In addition to surface bulging and blooming, the sheets moulded from the Delink treated GTR at 6 and 9 phr levels exhibited splits throughout their thicknesses. Such imperfections will give a bad product appearance, disturbance during tensile tests, and will result in unreliable measurements [37].

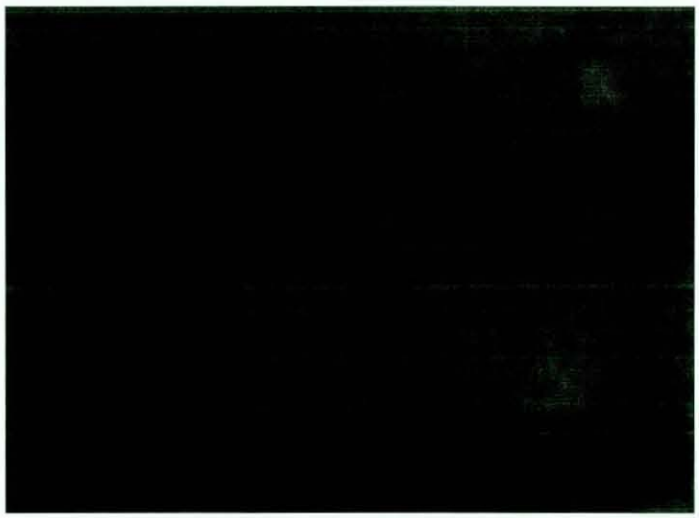

Figure 7.9 Surface bulges d on the moulded sheets prepared at 200 ^{0}C from the Delink treated GTR

Tensile strength and %elongation at break for the Delink treated GTR re-vulcanized at 150 ^{0}C and at 200 ^{0}C for 8 min. are given in Figure 7.10. The PGTR exhibited better tensile properties when re-vulcanized at 200 ^{0}C, compared to that at 150 ^{0}C. This may be due to improvement in cohesive strength of the GTR particles gained through better adhesion between GTR particles due to degradation of the GTR at 200 ^{0}C. Because of this degradation, the elongation at break of the Delink treated GTR at every Delink level slightly increased. However, the tensile strength of the Delink treated GTR decreased, when re-vulcanized at 200 ^{0}C. This is attributed to the decomposition of the Delink chemicals leading to poor adhesion between GTR particles, and also to chain modifications which occurred through side reactions without forming effective crosslinks during re-vulcanization. Of the Delink levels studied, the best tensile properties were obtained at 3 phr even when re-vulcanized at 200 ^{0}C, the temperature at which the sheets were moulded from the GTR/WPP blends.

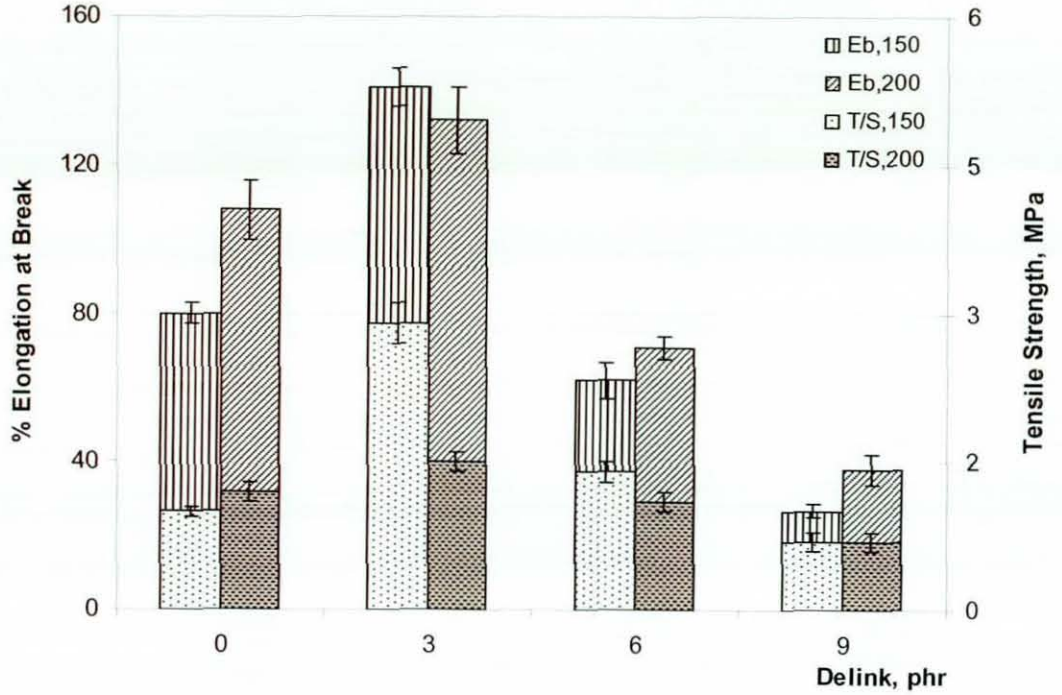

Figure 7.10 Tensile properties for the Delink treated GTR re-vulcanized at 150 ^{0}C and at 200 ^{0}C

These results revealed that processing for 10 min. at 40 ^{0}C produced the best tensile properties for the Delink treated GTR up to 6 phr. Further, 150 ^{0}C was the best re-vulcanization temperature for the Delink treated GTR, moulded alone (without the WPP) for 8 min. This is in agreement with the recommendations made by the inventors to re-vulcanize at 150 ^{0}C for 5-30 minutes with 6 phr of the Delink [42]. This is further supported by the DSC thermogram recorded at 150 ^{0}C under isothermal conditions, which is illustrated in Figure 7.11. The two thermograms at 150 ^{0}C and at 200 ^{0}C exhibited broad endotherms associated with crosslink formation. The crosslink formation processes were completed within 14 min., indicating that the completion of crosslink formation during moulding under high pressure occurs within a shorter time period.

7.1.5 WPP Blends with Delink Treated GTR at 3 and 6 phr Levels

The effect of Delink level on the tensile and the impact properties of the blends of Delink treated GTR and WPP was investigated using GTR treated with 3 and 6 phr of the Delink

at 40 ^{0}C and 90 rpm for 10 min. The blend composition of these blends was 50 wt% of each polymer. These blends were moulded at 200 ^{0}C, and according to the process conditions given in Section 3.6.

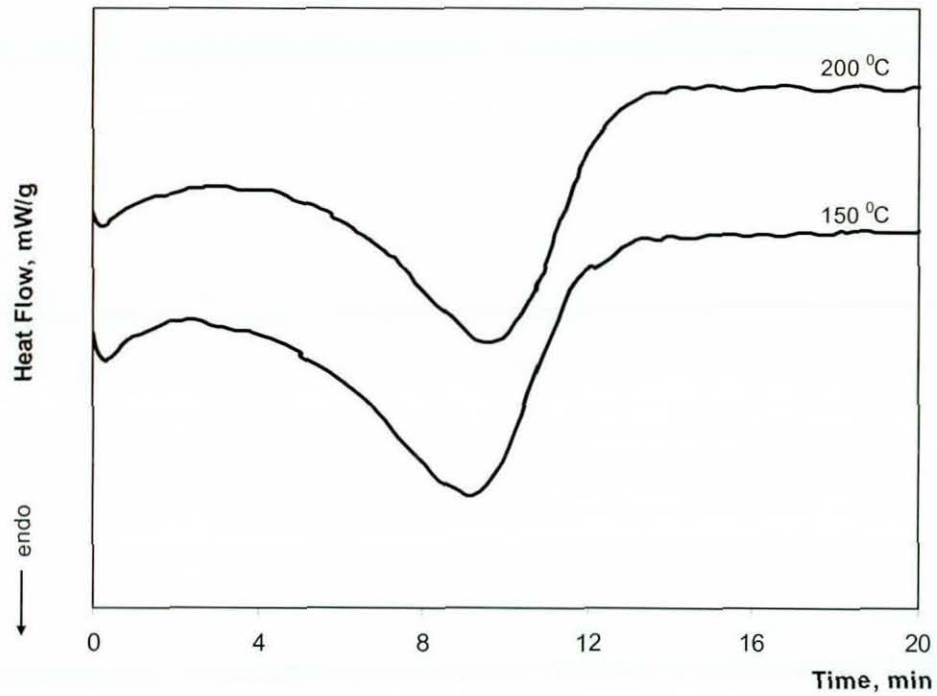

Figure 7.11 DSC thermograms for the Delink treated GTR (3 phr) recorded at 150 ^{0}C and 200 ^{0}C

The Torque vs. time curves developed during melt mixing were similar for both Delink treated GTR/WPP blends, and also similar to that of the PGTR/WPP blend, and the control GTR/WPP blend (Section 6.1.2).

The tensile and the impact properties for these blends are given in Table 7.3, while the thermal properties obtained from the DSC thermograms (Section 3.8.2.2) are given in Table 7.4. The tensile strength, elongation at break and secant modulus at 2% strain increase by approximately 15%, 18% and 12%, respectively, with the addition of 3 phr of the Delink. This slight property improvement is attributed to the improvement in cohesive strength within the GTR phase gained through crosslink formation due to the Delink treatment. This could also be associated with the slight increase in crystallinity in the WPP phase of the blend (%X_c-WPP). However, no significant variations were shown in

the melting temperature (T_m) and the peak crystallization temperature (T_p). The supper cooling temperature was obtained as 36 ^{0}C for all blends. These thermal properties indicate that there is no influence of the Delink treatment on the crystal nucleation and propagation process. The increase in Delink level to 6 phr did not produce any further improvement in the properties. The normalized impact peak force and the impact failure energy also had similar values for all blends. These results reveal that there was no significant effect of the Delink level on the blend properties, although a remarkable difference in properties has been shown for Delink treated GTR when vulcanized without the WPP (Sections 7.1.3 and 7.1.4). Therefore, the Delink level of 3 phr was selected for future studies discussed in detail in Sections 7.2 and 7.3.

Table 7.3 Tensile and impact properties for Delink treated GTR/WPP blends

Delink, phr	0 (PGTR)	3	6
Tensile Strength, MPa	8.8(0.3)	10.1(0.9)	10.1(0.3)
%Elongation at Break	15.9(1.2)	18.7(1.2)	19.9(1.4)
Secant Modulus@ 2% Strain, MPa	181(7)	202(1)	200(5)
Impact Peak Force, *N/mm	66(5)	71(1)	71(4)
Impact Failure Energy*, J/m	764(10)	763(23)	766(25)

** normalized by dividing by the thickness of the specimen*

Table 7.4 Thermal Properties for Delink treated GTR/WPP blends

Delink, phr	0 (PGTR)	3	6
Melting Temperature, ^{0}C	164.1(0.3)	164.8(0.1)	164.7(0.1)
Peak Crystallization Temperature, ^{0}C	119.1(0.2)	119.3(0.1)	118.9(0.3)
Onset Crystallization, Temperature ^{0}C	128.5(0.2)	128.8(0.3)	128.5(0.2)
% Crystallinity of WPP phase	37(1)	39(0)	39(0)

7.2 DGTR/WPP Simple Blends

The Delink treated GTR at the optimum Delink level of 3 phr (DGTR), was blended with the WPP to prepare DGTR/WPP blends, according to the mixing schedule-e (Section 3.2.11). In the mixing schedule-e, the WPP was added at the commencement of the mixing, and the DGTR was added to the molten WPP after 2 min. This mixing schedule differed to that practiced in preparing GTR/WPP blends (schedule-a), in which both polymers were added together to the internal mixer at the commencement of mixing. DGTR/WPP blends were moulded in a similar way to GTR/WPP blends and according to the moulding conditions given in Section 3.6. The effect of blend composition on tensile and impact properties was studied at different DGTR contents ranging from 10 to 100 wt%, at 10 wt% intervals. The processing characteristics and the mechanical properties of DGTR/WPP blends were compared with those of PGTR/WPP blends. PGTR/WPP blends were prepared according to the same mixing schedule-e, and moulded at the same conditions given above. The surfaces of the moulded sheets, tensile facture surfaces, and morphology of these blends, were studied by examining their microscopic images, in order to explain their mechanical properties. In addition, the pure DGTR and the pure PGTR were reprocessed at 180 ^{0}C in a similar way to the processing of the PGTR/WPP blends at different compositions and moulded under the same conditions given in Section 3.6. The tensile and impact properties of the two blends were compared with the DGTR and the PGTR, which were not reprocessed at 180 ^{0}C, but moulded as the same way. These two blends labelled reprocessed-DGTR (RDGTR) and reprocessed-PGTR (RPGTR). The notations used for all blends discussed in this section are given in Section 3.2.11.

7.2.1 Processing Characteristics

Torque-time curves recorded for DGTR/WPP blends were similar to those for PGTR/WPP, and also for GTR/WPP (simple) blends prepared at every GTR content (Section 5.1.1.1). The steady state torques, which were taken as the torques on completion of mixing at 7 min., for DGTR/WPP and PGTR/WPP blends are given in Table 7.5. This table shows increases in steady state torque with DGTR or PGTR content for both blends. This torque increase is associated with an increase in the highly viscous DGTR or PGTR

contents in the blends. However, pure DGTR or pure PGTR recorded lower steady torques due to their free flowing particulate nature. A similar variation of steady state torque versus GTR content was obtained for GTR/WPP blends (Section 5.1.1.2).

The steady state torques recorded for DGTR/WPP blends were similar to those recorded for PGTR/WPP blends up to 70 wt% DGTR or PGTR content. However, a relatively greater steady state toque was recorded for the DGTR/WPP blend at 90 wt% DGTR content. In this blend, the GTR phase was the continuous phase (Section 7.2.7), and hence the greater torque recorded was due to an increase in melt viscosity developed due to the formation of new crosslinks within the GTR phase when processed at 180 ^{0}C in the presence of Delink chemicals. In the blends at lower DGTR contents (up to 70 wt%), the GTR phase was the dispersed phase (Figure 7.24a and Figure 7.24c), and hence there was no impact, due to the formation of new crosslinks within the GTR phase, on the blend's melt viscosity. The new crosslink formation within the GTR phase in the DGTR/WPP blends was confirmed by the remarkably greater steady state torque recorded for the pure DGTR compared to the pure PGTR.

Table 7.5 Steady state torques for DGRT/WPP and PGTR/WPP blends

DGTR/PGTR	Steady State Torque, Nm	
level, wt%	DGTR/WPP Blend	PGTR/WPP Blend
10	6.5(6.4)	6.3 (6.4)
30	7.1(7.1)	7.1(7.0)
50	8.5(8.6)	8.3(8.4)
70	9.9(9.8)	9.8(9.7)
90	12.4(12.5)	11.9(12.0)
DGTR/PGTR	6.4(6.5)	5.4(5.3)

duplicate results are given in parenthesis

7.2.2 Surface Appearance of Moulded Sheets

The pure PGTR, when reprocessed at 180 ^{0}C had similar processing characteristics to the PGTR/WPP blends at different compositions, but became less sticky compared to the PGTR. This implies that the PGTR particles will undergo crosslinking within each particle during reprocessing, without forming crosslinks between particles. The free radicals formed both on the rubber chains and on crosslinks during processing at 40 ^{0}C under high shear forces will be involved in this re-vulcanization process. Due to the presence of these loosely bound crosslinked particles, the sheets moulded from the reprocessed-PGTR (RPGTR) showed surface imperfections including visible cracks (Figure 7.12). The sheets moulded from the reprocessed-DGTR (RDGTR) also exhibited surface imperfections. Therefore, properties of the 100 wt% PGTR/DGTR cannot be included in property variation comparison. Unlike the sheets moulded from the RPGTR and the RDGTR, the sheets moulded from the PGTR and the DGTR showed smooth and uniform surfaces. This uniformity of the sheets is due to particle agglomeration, and to the formation of new crosslinks between particles, when re-vulcanized under high pressure. The sheets moulded from DGTR/WPP blends and PGTR/WPP blends, at every composition, produced smooth surfaces without imperfections.

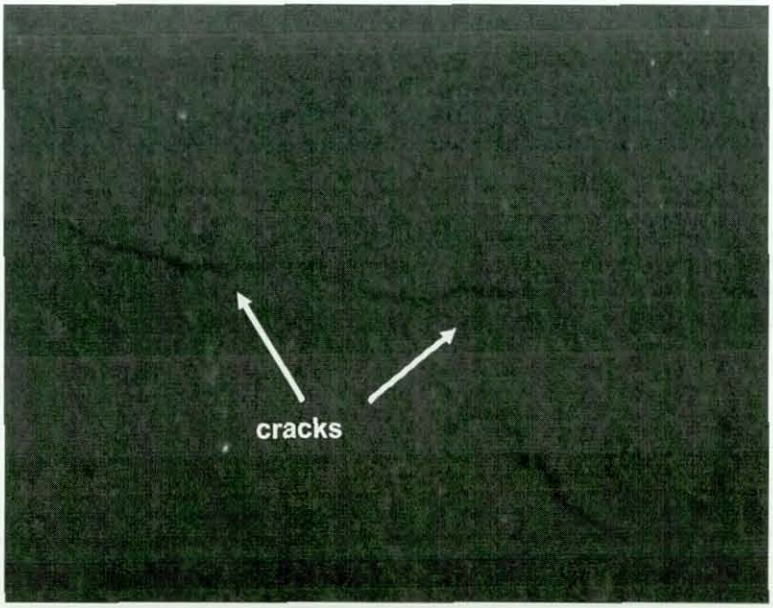

Figure 7.12 Surface appearances of RPGTR or RDGTR moulded sheets

7.2.3 Tensile Properties

Tensile properties, such as tensile strength, elongation at break and secant modulus at 2% strain, were studied firstly for the DGTR and the RDGTR, and were compared with those for the PGTR and the RPGTR. Secondly, these properties for DGTR/WPP blends at different compositions were studied and were compared with PGTR/WPP blends at all compositions.

7.2.3.1 Tensile Properties for PGTR and DGTR

Table 7.6 gives tensile properties for the PGTR, the DGTR, and their reprocessed polymers. The DGTR compared to the PGTR exhibited greater tensile strength and elongation at break. The secant modulus at 2% strain was the same. These increased properties are associated with the formation of shorter and stronger crosslinks between GTR particles through chemical reactions between rubber bound accelerator fragments (Section 7.1.2). In the PGTR, a lower level of crosslinks will be formed with limited free radicals generated during processing under high shearing forces (Scheme 6.1). Both RDGTR and RPGTR exhibited poor tensile properties, as expected. These inferior properties are a result of the weakly moulded sheets (Figure 7.12).

Table 7.6 Tensile properties of PGTR, DGTR and their reprocessed polymers

Sample	Tensile Strength, MPa	% Elongation at Break	Modulus@2% Strain, MPa
PGTR	0.98(0.05)	108(10)	5.6(0.5)
RPGTR	0.50(0.03)	47(2)	2.9(0.2)
DGTR	1.5(0.1)	132(9)	5.6(0.2)
RDGTR	0.45(0.04)	52(2)	2.6(0.3)

7.2.3.2 Tensile Properties of DGTR/WPP and PGTR/WPP Blends

Figure 7.13 shows the tensile strength for DGTR/WPP blends and for PGTR/WPP blends at different DGTR or PGTR contents, while Figure 7.14 and Figure 7.15 show elongation at break and secant modulus at 2% strain for those blends, respectively. These figures show that tensile strength and secant modulus decrease with the DGTR or PGTR content, while elongation at break increases. Similar trends in tensile property variations were obtained for GTR/WPP blends (Section 5.1.3.2). However, the DGTR/WPP blend and the PGTR/WPP blend at 10 wt% DGTR or PGTR content, compared to the GTR/WPP blend at respective composition, showed greater tensile strengths and elongations at break. These enhancements may be associated with the expected size reduction in the dispersed rubber phase when crosslinked. The free radicals formed during the additional processing step carried out at 40 ^{0}C for the GTR, with or without the Delink, would react with each other during blending with the WPP to form new crosslinks within the rubber phase, as discussed in Section 7.1.2. Although the degree of crosslinking increases with the DGTR or PGTR content, further particle reduction in the dispersed phase of the blends could not be expected. Like rubber particles in the blends will agglomerate to increase the size of the dispersed phase, and this effect is greater at higher DGTR or PGTR contents. An increase in particle agglomeration with GTR content was observed for DGTR/WPP blends (Figure 7.41) and for GTR/WPP blends (Figure 5.22).

The DGTR/WPP blends, compared to the PGTR/WPP blends, exhibited slightly increased tensile properties at every DGTR or PGTR content. Further, the increment is greater at higher DGTR or PGTR contents. The enhanced properties for the DGTR/WPP blends are due to the formation of new crosslinks within the DGTR phase due to the Delink treatment. This is supported by the smaller glass transition temperature difference observed for the two phases in the DGTR/WPP blends (Section 7.2.6). However, due to decomposition of Delink chemicals at higher temperatures (Section 7.1.4.2), no significant comparative increase is shown even at higher DGTR contents. The maximum increase observed at 90 wt% DGTR or PGTR content is only 30 to 40%. This poor tensile property improvement is due to poor interaction between the DGTR and WPP phases (Figure 7.16). These results indicate that the Delink treatment for the GTR alone is not

sufficient for property enhancement in the GTR/WPP blends, and further suggest a necessity for a compatibilizer to improve interfacial adhesions.

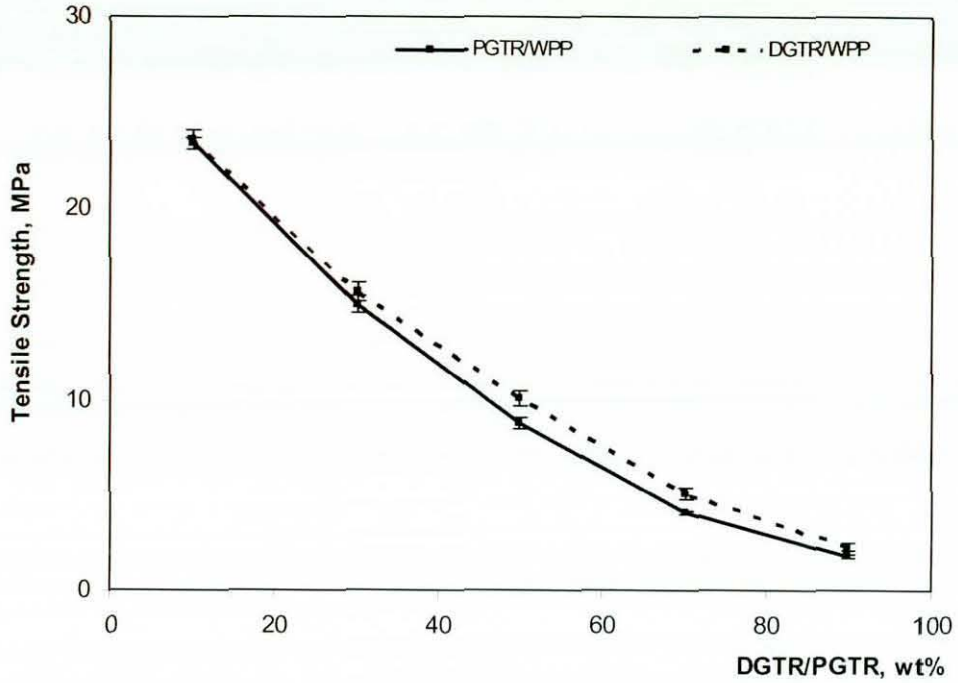

Figure 7.13 Tensile strength vs. DGTR/PGTR content

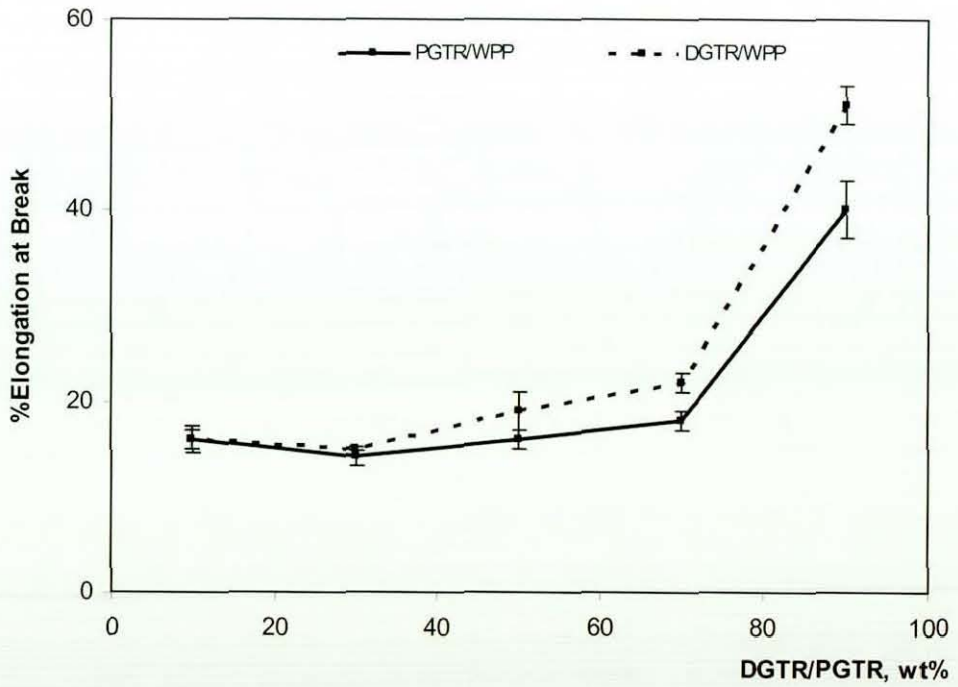

Figure 7.14 Elongation at break vs. DGTR/PGTR content

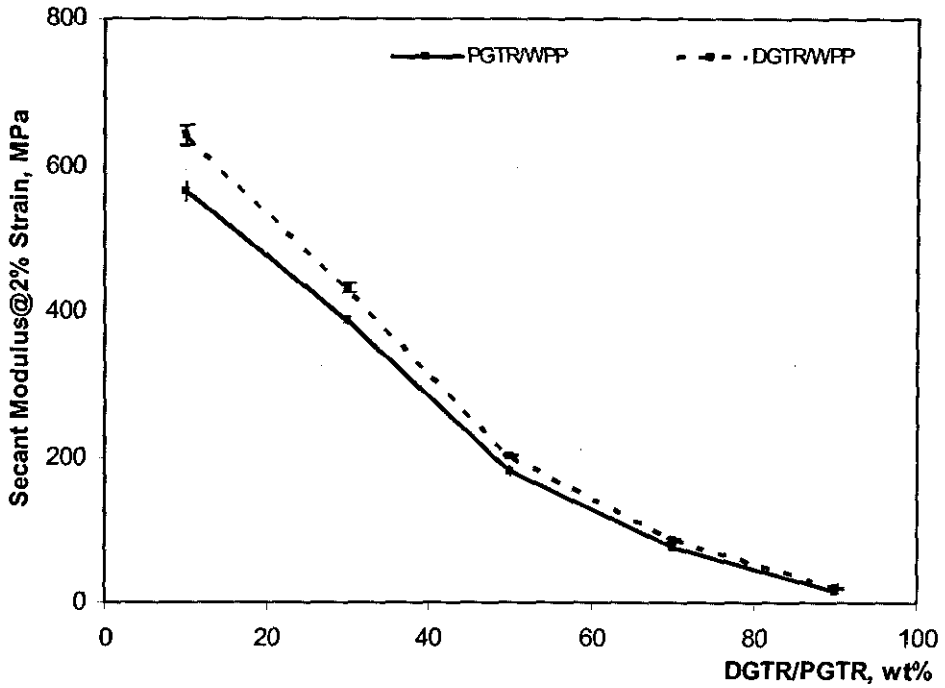

Figure 7.15 Secant modulus vs. DGTR/PGTR content

7.2.4 Tensile Fracture

Figure 7.16 and Figure 7.17 illustrate the tensile fracture surfaces of DGTR/WPP blends containing 30 wt% (30:70-DGTR-e) and 70 wt% DGTR content (70:30-DGTR-e), respectively obtained using a field emission gun scanning electron microscope (FEGSEM). The fracture surface of the 30:70-DGTR-e blend shows two distinct regions, with big holes created due to removal of DGTR particles from the WPP matrix at the fracture. One region shows interfacial debonding with some fibrillation in the WPP phase around the separated DGTR particles (Figure 7.16a). The other region shows a rough brittle fracture surface for the WPP phase. These observations suggest that the fracture mode for the 30:70-DGTR-e blend is a combination of interfacial debonding, shear yielding and crazing. However, the fracture surface of the 70:30-DGTR-e (Figure 7.17) did not show a brittle fracture in the WPP phase as appeared in Figure 7.16b. The fracture surface contained big holes, de-bonded DGTR particles, and a little fibrillation in the WPP phase. Therefore, the predominant fracture mode for the DGTR/WPP blends at any blend composition was identified as interfacial debonding. This implies that no interfacial crosslinks developed with the addition of the DGTR to the WPP.

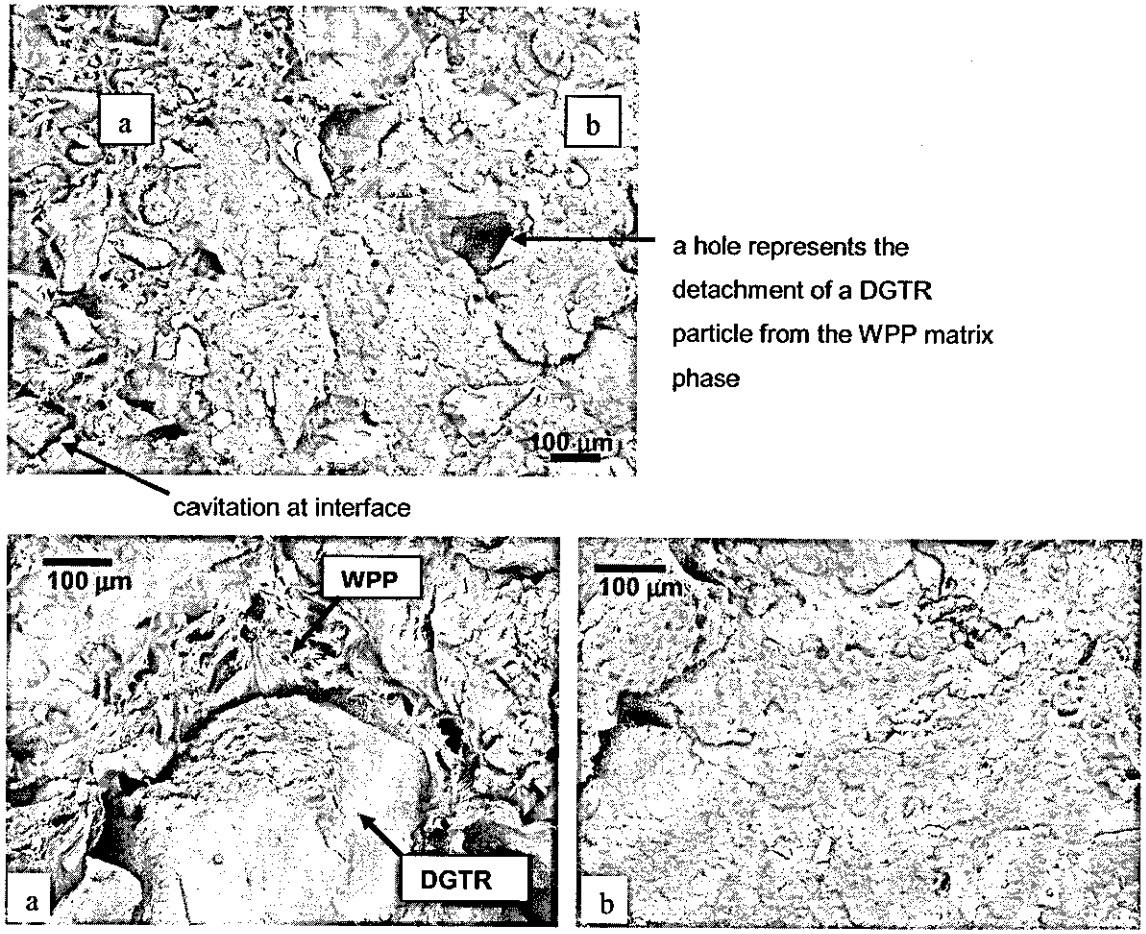

Figure 7.16 Tensile fractograph of 30:70-DGTR-e blend with two specific regions at higher magnification

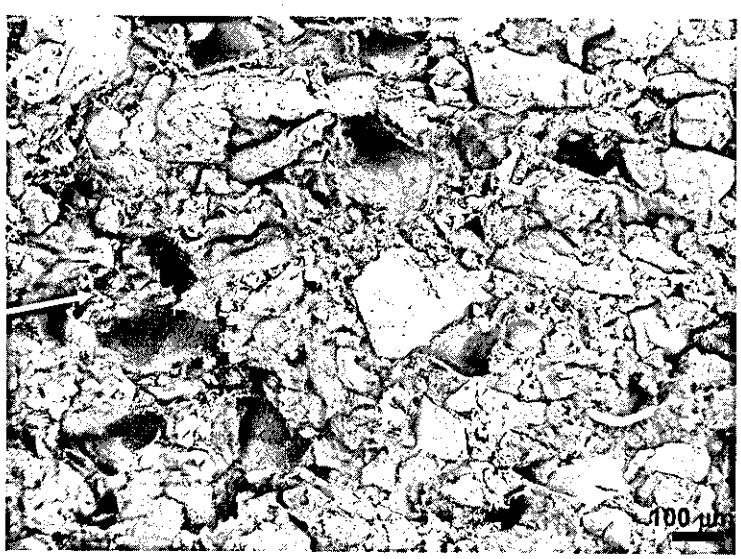

Figure 7.17 Tensile fractograph of 70:30-DGTR-e blend

7.2.5 Impact Properties

Normalized impact properties, such as peak force and fracture initiation, propagation, and failure energies, for the DGTR/WPP and PGTR/WPP blends prepared at different blend compositions are given in Figure 7.18 and Figure 7.19. The PGTR/WPP blends exhibit variations in the peak force, and the fracture energies, with PGTR content similar to the GTR/WPP (simple) blends (Section 5.1.3.5). The DGTR/WPP blends also show a similar trend, except at 10 wt% DGTR. At 10 wt%, the peak force, and hence the initiation energy for the DGTR/WPP blend are remarkably greater than for the PGTR/WPP blend. This greater improvement in impact properties, observed at 10 wt%, suggests that the crosslinking within the GTR phase through Delink treatment is effective when the DGTR content in the blend is low. The tiny crosslinked DGTR particles formed at lower DGTR contents, which are physically anchored to the WPP matrix phase, will act as stress concentrators and finally will increase the fracture initiation energy. Due to the increase in DGTR particle size with DGTR content (Figure 7.41), and due to interfacial debonding (Figure 7.16 and Figure 7.17), the DGTR/WPP blends at higher DGTR contents exhibited similar or only slightly different impact properties relative to the PGTR/WPP blends. However, the pure DGTR, compared to the pure PGTR, exhibited lower impact properties (Table 7.7). This is associated with the surface bulges, and DGTR particle separation (Section 7.1.4.2). The poor impact properties obtained for the DGTR/WPP blends confirm the necessity of a suitable compatibilizer to enhance the mechanical properties by improving the interfacial adhesions between the two phases.

Table 7.7 Impact properties for PGTR and DGTR

Sample	Peak Force*, N/mm	Initiation Energy*, J/m	Propagation Energy*, J/m	Failure Energy*, J/m
PGTR	82(4)	771(18)	275(13)	1046(32)
DGTR	76(4)	608(35)	172(14)	780(44)

**normalized by dividing by the thickness of the specimen*

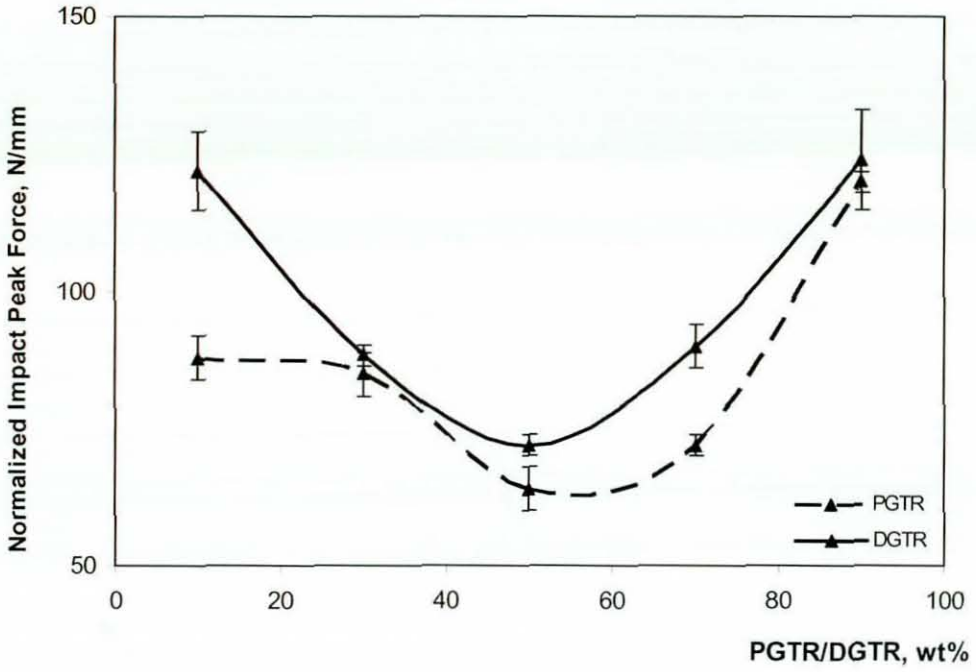

Figure 7.18 Impact peak force vs. DGTR/PGTR content

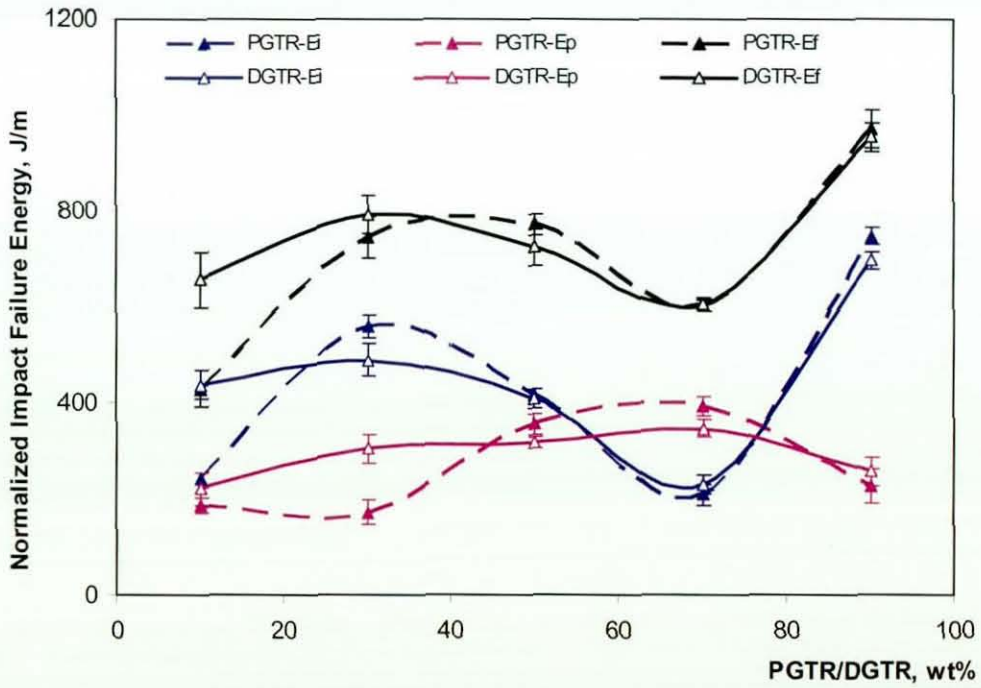

Figure 7.19 Impact (initiation, propagation and failure) energies vs. DGTR/PGTR content

7.2.6 Dynamic Mechanical Properties

Figure 7.20 shows the storage modulus variation with temperature for DGTR/WPP blends containing 30, 50 and 70 wt% of the DGTR. The storage modulus decreases with increase in temperature for all blends due to increase in polymer main chains mobility with temperature. Further, the decrease in modulus is greater with the DGTR content, due to an increase in soft regions in the blend. This result is supported by the secant modulus values obtained (Figure 7.15).

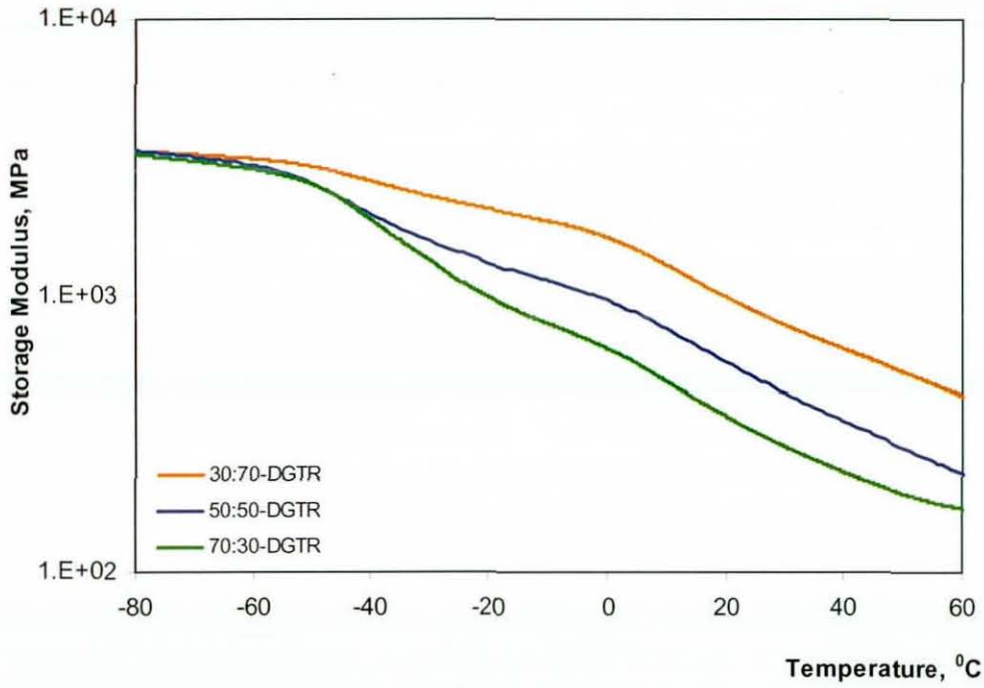

Figure 7.20 Storage modulus vs. temperature for DGTR/WPP blends

Figure 7.21 shows loss factor (tan δ) variation with temperature for the three blends. These curves show two distinct peaks corresponding to the glass transitions of the two phases, representing a two phase system. This is in agreement with the microscopic studies (Figure 7.24). As expected, the magnitude of the transition peak corresponding to the DGTR recorded at lower temperature increases with DGTR content, while that corresponding to the WPP decreases. The glass transition temperatures determined from the tan δ curves for each phase are given in Table 7.8. Figure 7.21 and Table 7.8 show an increase in the T_g of the GTR with an increase in DGTR or PGTR content, but no shift is

noticed for the T_g of the WPP. These T_g shifts were similar to those for the GTR/WPP blends (Section 5.1.4). A slightly greater shift in T_g of GTR observed for DGTR/WPP blends is attributed to the lowering of chain flexibility by the formation of additional crosslinks with Delink treatment. The shift in T_g of WPP for DGTR/WPP blends may be due to a plasticizing effect caused by the DGTR on the WPP phase. Hence, a relatively smaller difference in T_g for the two phases obtained in the DGTR/WPP blend suggests a slight improvement in compatibility between phases, which would result in an enhancement in tensile properties (Section 7.2.3.1).

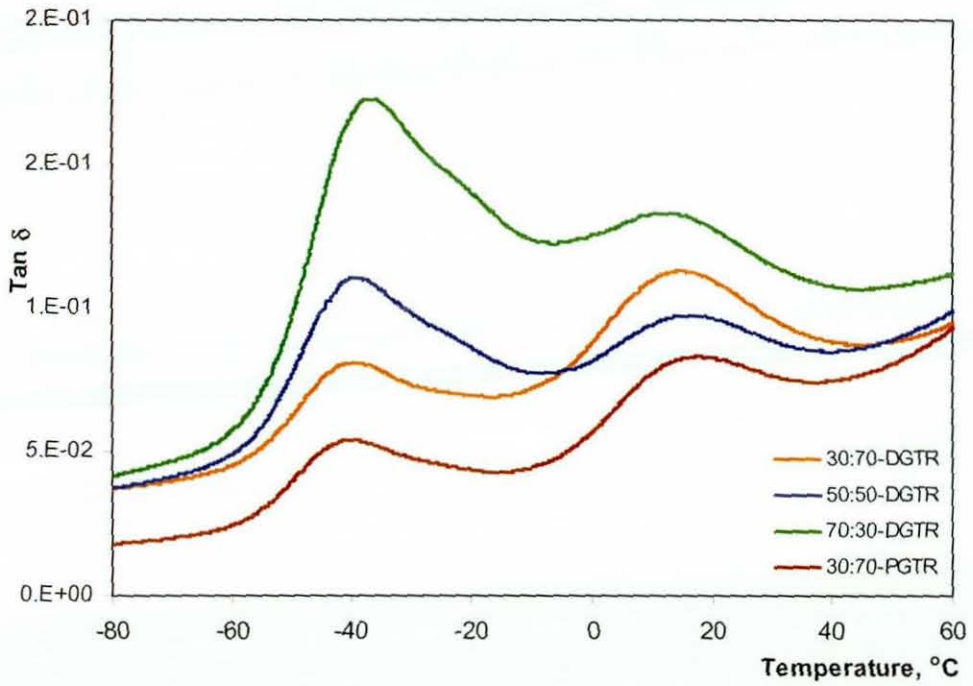

Figure 7.21 Tan δ vs. temperature for DGTR/WPP and PGTR/WPP blends

Table 7.8 Glass transition temperature of each phase in DGTR/WPP or PGTR/WPP blends

DGTR/PGTR,	DGTR/WPP Blends		PGTR/WPP Blends	
wt%	T_g of GTR, ^{0}C	T_g of WPP, ^{0}C	T_g of GTR, ^{0}C	T_g of WPP, ^{0}C
30	-40	14	-41	15
50	-39	14	-40	15
70	-37	13	-38	15

7.2.7 Morphology

Scanning electron micrographs of the fracture surfaces, for the DGTR/WPP blends at two different compositions are shown in Figure 7.22. These surfaces were fractured cryogenically using liquid nitrogen. The two phases, DGTR and WPP, were clearly visible on both micrographs. Both phases show rough fracture surfaces leading to a total brittle fracture. Further, no phase separation is shown on any micrograph, although considerable phase separations appeared on tensile fracture surfaces (Figure 7.16 and Figure 7.17). Figure 7.23, which was taken at a higher magnification, shows a clear interface with no phase separation. These results confirm that the two phases are not separated in the DGTR/WPP blends in the normal or unstrained conditions, but separate during tensile fracture on straining.

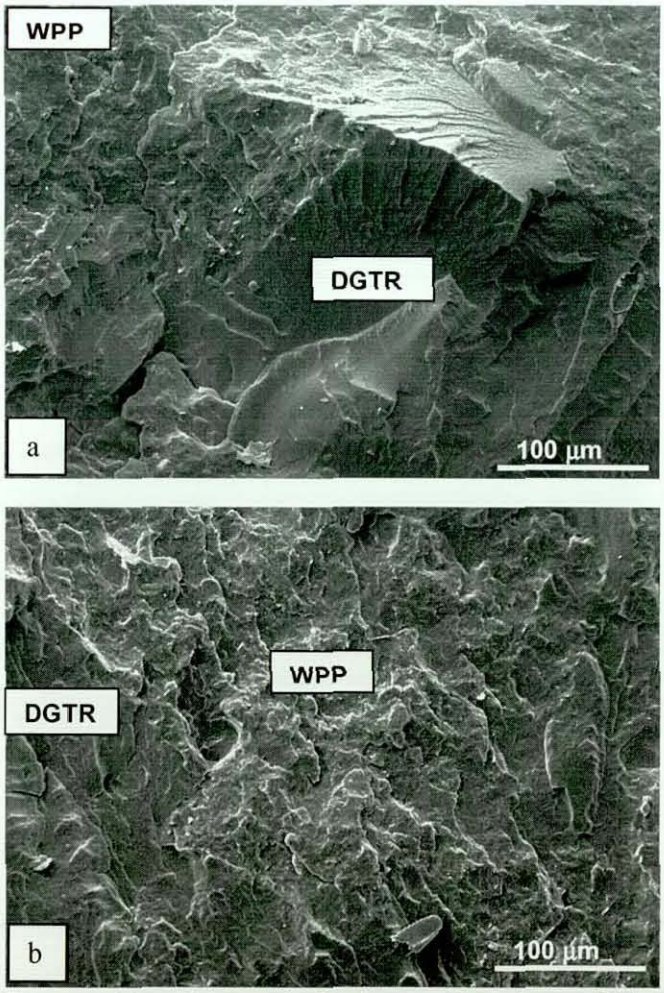

Figure 7.22 Cryogenically fractured surfaces of blends
(a) 30:70-DGTR-e (b) 70:30-DGTR-e

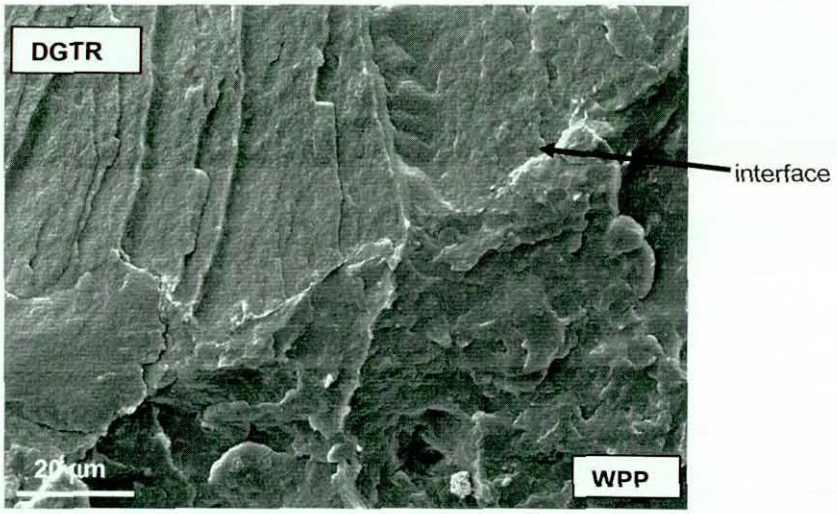

Figure 7.23 Interface on a cryogenically fractured surface of a DGTR/WPP blend

Optical micrographs of the microtome films of the DGTR/WPP blends at three different DGTR contents (30, 50 and 70 wt%) are given in Figure 7.24. The microtome films were cut in the same orientation, on each occasion corresponding to a cross-sectional area being across the middle of a tensile bar, or across the piece of material left after press-cutting two tensile bars. The micrographs show two different phases, as expected, due to incompatibility between the GTR and the WPP. Small voids are also seen around DGTR particles in every micrograph, and these are thought to arise due to the microtoming process. The micrographs for the blends containing 30 and 50 wt% of the DGTR show DGTR particles of different sizes in the dispersed phase (Figure 7.24a and Figure 7.24b). Confirmation of particle agglomeration is given with the appearance of larger DGTR particles as DGTR content increases. Further, the blend containing 70 wt% DGTR, exhibits DGTR in a continuous phase (Figure 7.24c). Similar micrographs were recorded for the GTR/WPP blends at respective blend compositions (Figure 5.23).

In order to study the effect of DGTR content on the WPP crystalline structure, the microtome films were viewed in polarised light. However, these images did not reveal any alterations in the WPP crystalline structure due to the DGTR phase. In the case of 70 wt% DGTR, too little WPP could be seen to make any valid comment on its structure.

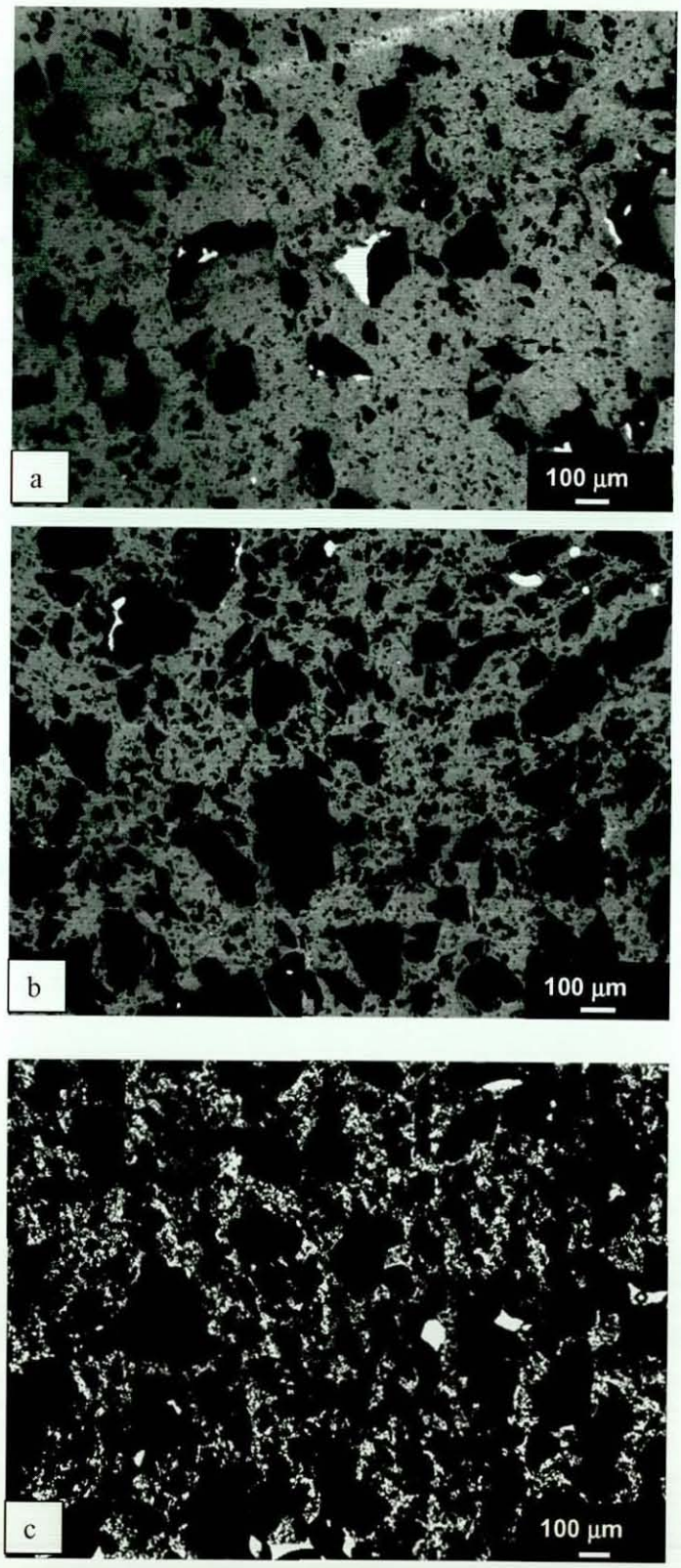

Figure 7.24 Optical micrographs of DGTR/WPP blends

(a) 30:70-DGTR-e (b) 50:50-DGTR-e (c) 70:30-DGTR-e

7.3 DGTR/WPP Reactive Blends

The tensile and impact properties of the DGTR/WPP simple blends did not show significant improvement with the addition of the DGTR, and revealed the necessity of a suitable compatibilizer to improve the interfacial adhesions. Therefore, the two compatibilizing systems used in a previous part of the study (Chapter 6), were incorporated into the DGTR/WPP blends. The selected dimaleimide compatibilizing system comprised of N-N'metaphenylene dimaliemide (HVA-2) and di(tert-butylperoxyisopropyl) benzene (DTBPIB) activator. The resin compatibilizing system comprised of SP resin (HVA-2) and stannous chloride ($SnCl_2$) activator. The compatibilizing systems at their optimum levels recorded for the GTR/WPP (50/50) blend (Section 6.3) were used in this section of the study. The blends with the dimaleimide compatibilizing system were prepared according to the mixing schedule-e (Section 3.2.11) and the schedule-f (Section 3.2.12.1). The blends with the resin compatibilizing system were prepared according to the mixing schedule-g (Section 3.2.12.2). The DGTR/WPP blends with compatibilizing systems were also moulded according to the conditions given in Section 3.6. The processing characteristics, the tensile and the impact properties, and the thermal properties, of the DGTR/WPP blends with the compatibilizing systems were measured and were compared with those of PGTR/WPP blends. The PGTR/WPP blends were prepared according to the respective mixing procedures, and moulded at the same conditions given above. Cryogenically fractured surfaces, tensile facture surfaces, and the microtome sections of these blends, were examined in order to explain their mechanical properties. The property variations with the incorporation of the two compatibilizing systems are discussed in this Section.

7.3.1 Dimaleimide Compatibilizing System

The dimaleimide compatibilizing system is a two component system, which consists of HVA-2 and DTBPIB at their optimum levels, 3 pphp and 0.6 pphp, respectively. HVA-2 is the compatibilizer and DTBPIB the activator. This system was added to the DGTR/WPP (50:50) blend under the two mixing schedules given above to find the effective mixing procedure. The effect of compatibilizer alone on the blend prepared according to the mixing schedule-e was also investigated.

7.3.1.1 Processing Characteristics

Figure 7.25 shows typical torque-time curves recorded for the DGTR/WPP (50/50) blends with and without the compatibilizing system. This figure, further, shows the curves for the blends with the compatibilizing system prepared under two mixing procedures and with the HVA-2 compatibilizer alone.

The torque-time curve for the blend with HVA-2 alone exhibit slightly higher toque, compared to the blend without a compatibilizing system, due to the formation of additional crosslinks within the DGTR phase. This observation is similar to that observed for the respective GTR/WPP blends (Section 6.1.2). As expected, the blends containing the compatibilizing system exhibited greater torques at their additions. This is due to the formation of interfacial crosslinks in addition to the formation of crosslinks within the DGTR phase (Section 6.1). The blends prepared according to the mixing schedule-e, in which DGTR was added with HVA-2 together after 2 minutes, produce greater torques compared to the blends prepared with the schedule-f. In the schedule-f the compatibilizing system was added to the DGTR/WPP melt mix at the 4^{th} minute. When the system is added together with the DGTR, the active free radicals formed on crosslinks and/or on rubber chains (Scheme 6.1), the accelerator radicals (Schemes 7.2 and 7.3), and/or rubber bound accelerator fragments (Scheme 7.4) present in the DGTR will react with the radicals formed on the WPP by the HVA-2 and DTBPIB to form interfacial crosslinks (Scheme 6.9) and additional crosslinks within the DGTR phase (Scheme 6.3). When the system is added to the DGTR/WPP melt mix, the DGTR added initially will form crosslinks within the DGTR phase (Scheme 6.3). The non-utilized radicals on crosslinks and/or on rubber chain, which were formed during Delink treatment, will participate in the formation of interfacial crosslinks with the addition of the compatibilizing system. This results in the development of lower torques towards completion of mixing, when processed according to the mixing schedule-f.

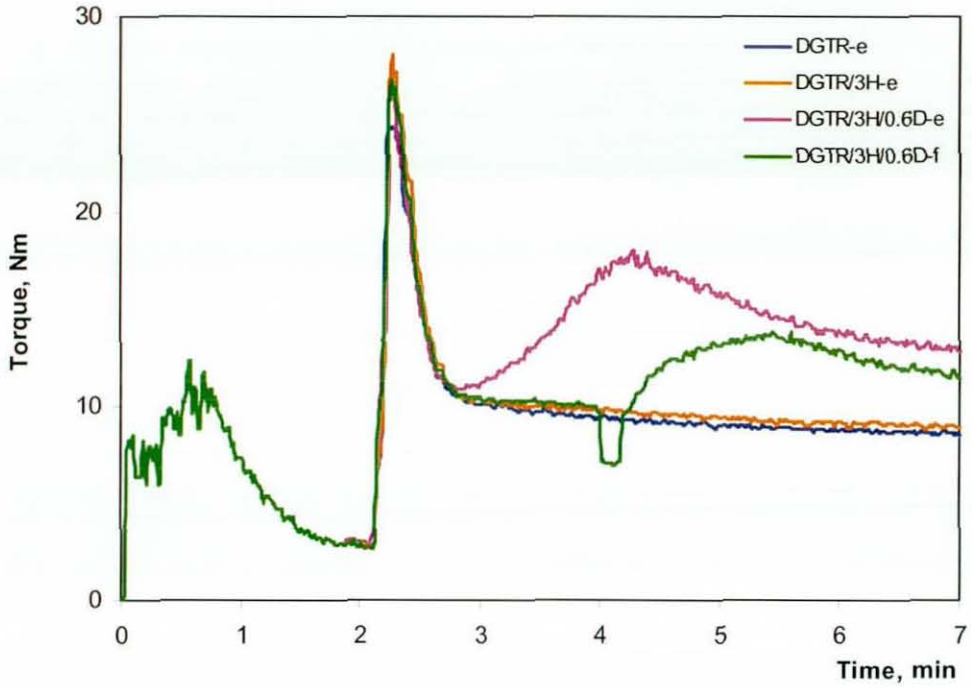

Figure 7.25 Torque vs. time for the DGTR/WPP (50/50) blends with the dimaleimide compatibilizing system

7.3.1.2 Tensile Properties

Tensile properties for the above blends, such as tensile strength, elongation at break and secant modulus at 2% strain, are given in, Figure 7.26 Figure 7.27 and, Figure 7.28 respectively. These figures show that tensile strength and secant modulus increase with addition of HVA-2 alone to the DGTR/WPP blend. However, elongation at break does not show a significant change. These property variations are due to the formation of crosslinks within the DGTR phase, as evidenced by the processing characteristics (Section 7.3.1.1). The tensile strength enhancement for the DGTR/WPP blend with HVA-2 alone is low. This would suggest the formation of flexible sulfidic crosslinks in the GTR phase by the HVA-2 in conjunction with rubber bound accelerator fragments, which were developed during Delink treatment. The HVA-2 alone will produce shorter C-C crosslinks within the GTR phase in PGTR/WPP blends (Scheme 6.3). However, a slight increase in mechanical properties through improvement in compatibility between

phases, due to Delink treatment was observed for DGTR/WPP blends, compared to the PGTR/WPP blends (Section 7.3.3.5).

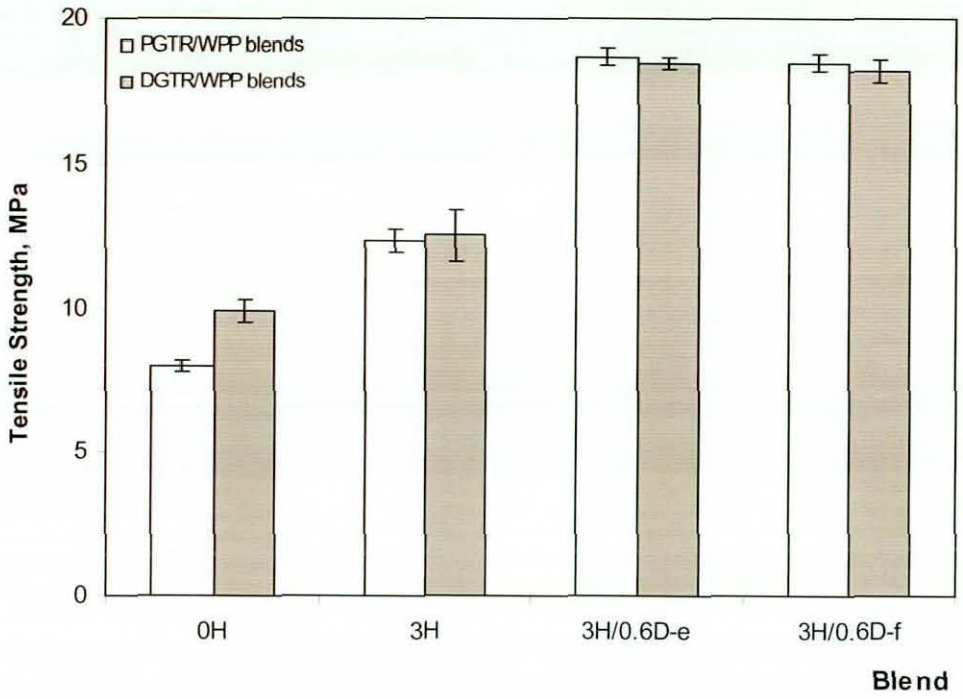

Figure 7.26 Tensile strength for DGTR/WPP and PGTR/WPP (50/50) blends with the dimaleimide compatibilizing system

With the addition of HVA-2 with DTBPIB to the DGTR/WPP blend, both tensile strength and elongation at break increase remarkably. Similarly, PGTR/WPP blends also exhibit drastic increases in tensile properties. This increase is associated with the formation of interfacial crosslinks, in addition to the formation of crosslinks within the GTR phase. Further, a prominent increase in elongation at break is noticed when the compatibilizing system was added to the DGTR, as it forms flexible sulfidic crosslinks between phases. In the PGTR/WPP blends, C-C crosslinks will mostly develop, which would result in a low elongation at break. The variations in secant modulus for both DGTR/WPP and PGTR/WPP blends are marginal, and the modulus does not depend on the mixing schedule. These results are supported by the variations in processing characteristics (Section 7.3.1.1). All these results reveal that the degree of crosslinking in the DGTR/WPP and PGTR/WPP blends is not significantly different, and further the type of crosslinks formed within the phases and between the phases is different.

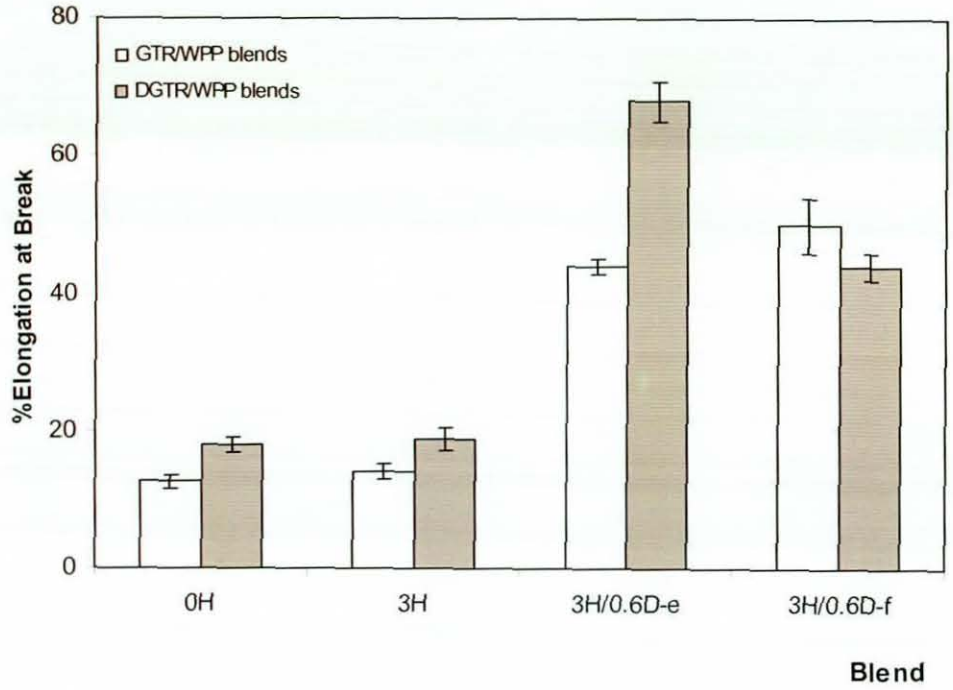

Figure 7.27 Elongation at break for DGR/WPP and PGTR/WPP (50/50) blends with dimaleimide compatibilizing system

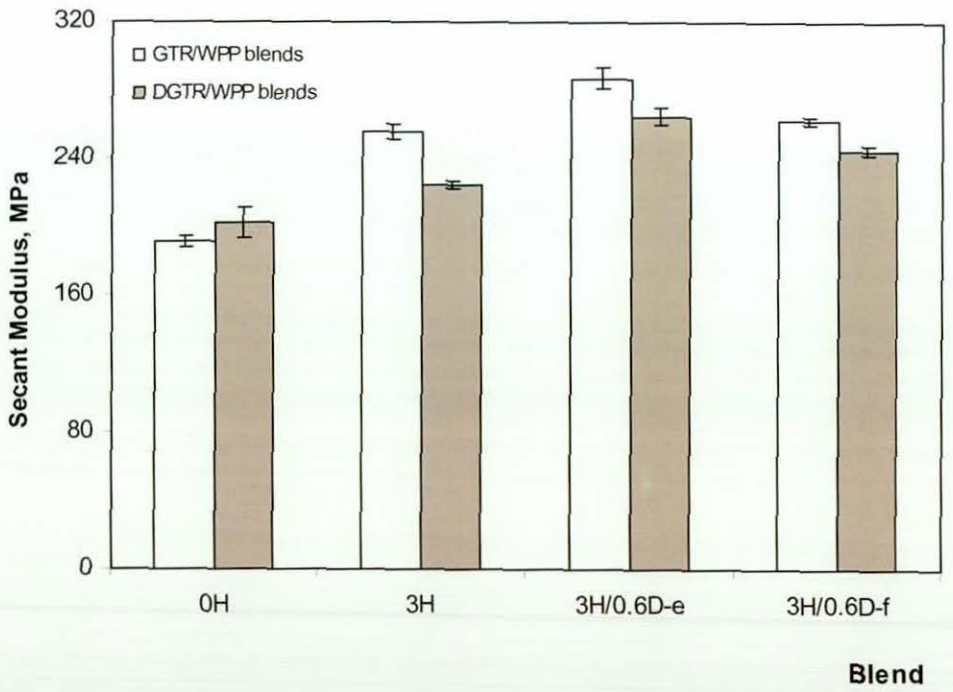

Figure 7.28 Secant modulus for DGTR/WPP and PGTR/WPP (50/50) blends with the dimaleimide compatibilizing system

Tensile fractographs recorded for the DGTR/WPP (50/50) blends with the dimaleimide compatibilizing system showed quite regular shapes and homogeneous blend, and a rough brittle fracture surface. In addition, low level of shear yielding in the WPP phase around loosely boned DGTR particles was observed. Similar fractographs were recorded for the respective GTR/WPP (50/50) blends (Section 6.1.7).

7.3.1.3 Impact Properties

Figure 7.29 shows force-deformation curves recorded under impact loading for DGTR/WPP blends with the dimaleimide compatibilizing system. All blends exhibited ductile fracture (Figure 6.19). The impact properties determined from the curves are given in Table 7.9. This table shows an increase in peak force with the addition of 3 pphp of the HVA-2, and further with the addition of 0.6 pphp of the DTBPIB. The increase is greater with the addition of DTBPIB to the HVA-2 due to the formation of interfacial crosslinks, which facilitate load transfer between phases effectively. The impact failure energy also increases accordingly. This trend is observed for both DGTR/WPP and PGTR/WPP blends.

The DGTR/WPP blend containing the dimaleimide system, compared to the respective PGTR/WPP blend, exhibit greater force and deformation before fracture was initiated, providing greater fracture initiation energy. However, due to lack of rubber bound accelerator fragments available to react with the dimaleimide system, the DGTR/WPP blends processed according to mixing schedule-f, exhibit relatively lower properties. This property variation is supported by the variation in elongation at break observed for the respective blends (Figure 7.35). Further, the variations are in agreement with the processing characteristics (Figure 7.25). These results confirm that the mechanical properties of a DGTR/WPP blend are depended on the type and extent of crosslinks formed in the blend. The property variation is also dependent on the blend morphology, which is a result of the nature of crosslinking within the blend.

Figure 7.33 shows optical micrographs recorded for the DGTR/WPP blend with and without the dimaleimide compatibilizing system. Different sizes of DGTR particles are apperant on both micrographs, however, the particle size distribution is small for the

DGTR/WPP blend containing the dimaleimide system. This is a result of the formation of strong crosslinks between DGTR particles and between two phases.

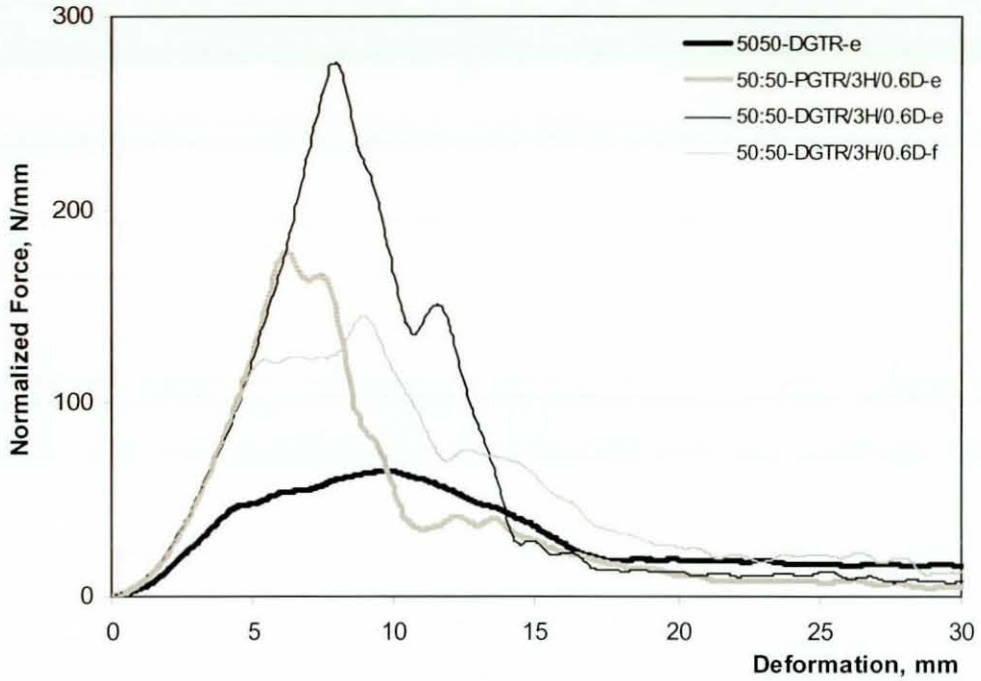

Figure 7.29 Force vs. deformation for the DGTR/WPP (50/50) blends with the dimaleimide compatibilizing system

Table 7.9 Impact properties for the DGTR/WPP (50/50) blends with the dimaleimide compatibilizing system

Sample Code	Peak Force*, N/mm	Initiation Energy*, J/m	Propagation Energy*, J/m	Failure Energy*, J/m
50:50-DGTR-e	66(4)	408(13)	316(20)	724(18)
50:50-DGTR/3H-e	78(3)	442(29)	450(28)	892(21)
50:50-DGTR/3H/0.6D-e	288(14)	838(33)	905(36)	1743(37)
50:50-DGTR/3H/0.6D-f	161(7)	799(15)	880(18)	1679(16)
50:50-PGTR-e	66(2)	223(10)	525(51)	737(31)
50:50-PGTR/3H-e	73(4)	448(45)	475(43)	910(17)
50:50-PGTR/3H/0.6D-e	160(11)	422(26)	785(30)	1207(42)

**normalized by dividing by the thickness of the specimen*

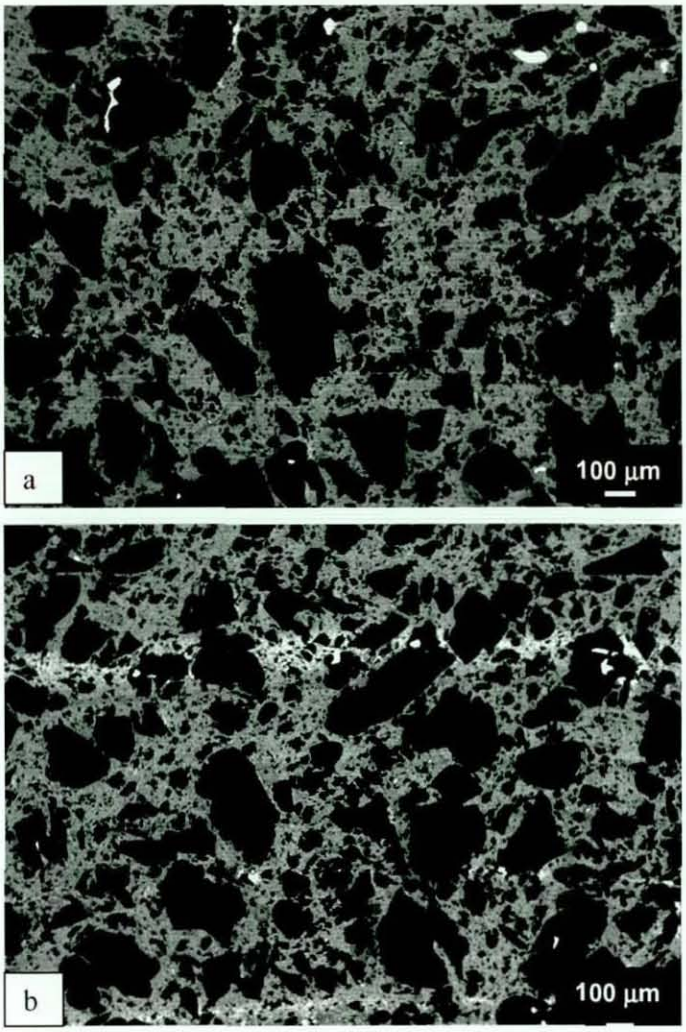

Figure 7.30 Optical micrographs of DGTR/WPP blends (a) 50:50-DGTR-e (b) 50:50-DGTR/3H/0.6D-e

7.3.2 Resin Compatibilizing System

The resin compatibilizing system used in this part of the study consists of SP resin compatibilizer and $SnCl_2$ activator at their optimum levels, 4 pphp and 0.8 pphp, respectively. This system was added to the DGTR/WPP (50:50) blend under mixing schedule-g. In this schedule, the WPP was first modified with the resin system and then the DGTR was added after 4 minutes from the commencement of mixing. This schedule was further compared with the mixing schedule-e, in which the DGTR and the resin system together were added to the molten WPP at the second minute.

7.3.2.1 Processing Characteristics

Torques-time curves for the DGTR/WPP blends containing the resin compatibilizing system produced similar curves to the GTR/WPP blends (Figure 6.32). No torque increase was shown with the addition of the DGTR to the modified WPP. Table 7.10 shows the steady state torque taken at the completion of melt mixing at the 7th minute. With the addition of SP resin alone, the steady state torque increases considerably due to the formation of crosslinks within the GTR phase (Schemes 6.12, 6.13 and 6.14). However, the increase in torque with the addition of $SnCl_2$ activator, either in anhydrous form or in dihydrate form, is not so significant. Alternatively, no change in torque is noticed with the mixing schedule. These lower steady state torques indicate that no interfacial crosslinks were generated during melt mixing with the resin system.

Table 7.10 Steady state torques for DGTR/WPP blends with the resin compatibilizing system

Sample Code	Steady State Torque, Nm
DGTR-e	8.5(8.1)
DGTR/4S-g	9.0(8.9)
DGTR/4S/0.8TA-g	9.2(9.1)
DGTR/4S/0.8TD-g	9.1(9.2)
DGTR/4S/0.8TA-e	9.1(9.2)
DGTR/4S/0.8TD-e	9.3(9.2)

duplicate results are given in parenthesis

7.3.2.2 Tensile Properties

Table 7.11 illustrates the tensile strength and the elongation at break for DGTR/WPP blends and PGTR/WPP blends. In agreement with the processing characteristics of the DGTR/WPP blends (Section 7.3.2.1), the tensile strength and the elongation at break do not show significant improvements with the addition of the resin system. However, considerable increases in tensile properties are observed for the PGTR/WPP blends, with

the addition of the resin system. This is due to a combined effect of crosslink formation within the GTR phase, and modification of the WPP phase (Section 6.2.4). In the DGTR/WPP blends, the Delink itself will form crosslinks within the GTR phase, without leaving active sites to react with the resin system to generate more crosslinks. Hence, the two systems, Delink and the resin system, did not give synergistic effects towards crosslink formation.

Table 7.11 Tensile properties for DGRT/WPP blends with the resin compatibilizing system

Sample Code	Tensile Strength, MPa	%Elongation at Break
50:50-DGTR-e	10.1(0.4)	19(2)
50:50-DGTR/4S-g	10.1(0.4)	18(1)
50:50-DGTR/4S/0.8TA-g	10.4(0.4)	20(2)
50:50-DGTR/4S/0.8TD-g	10.3(0.3)	20(2)
50:50-DGTR/4S/0.8TA-e	10.3(0.3)	21(2)
50:50-DGTR/4S/0.8TD-e	10.6(0.5)	20(1)
50:50-PGTR/4S-e	9.8(0.3)	18(1)
50:50-PGTR/4S/0.8TA-g	10.7(0.4)	22(1)
50:50-PGTR/4S/0.8TD-g	9.9(0.3)	21(2)

Figure 7.31, which is a representative of resin compatibilized blends, illustrates a typical tensile fractograph for the 50:50-DGTR/4S/0.8TA-e blend. Tensile fracture surfaces of the DGTR/WPP blends containing the resin system, exhibited interfacial debonding, with a little brittle fracture in certain areas. The DGTR particles could not be seen in the areas where the rough brittle fracture is shown (Figure 7.31a). In contrast, the DGTR particles are clearly visible in the other areas with shear yielding of the WPP phase around the loosely bound DGTR particles (Figure 7.31b). This fractograph clearly shows that the predominant tensile fracture mode for these blends is interfacial debonding, which is the cause of poor mechanical properties.

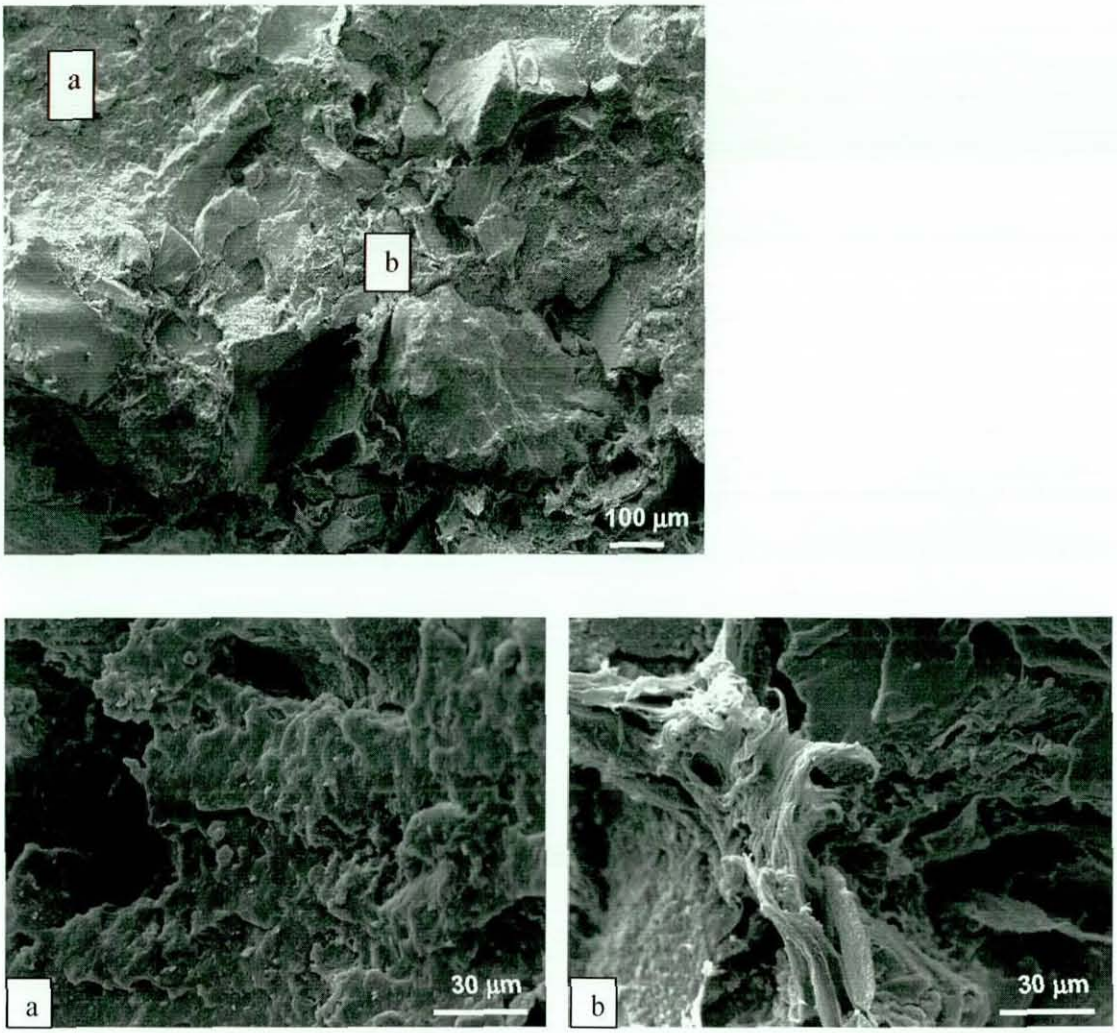

Figure 7.31 Tensile fractograph of 50:50-DGTR/4S/0.8TA-e blend showing different fracture modes, (a) brittle fracture (b) shear yielding

7.3.2.3 Impact Properties

Typical force-deformation curves recorded under impact loading for selected DGTR/WPP blends containing resin compatibilizing systems are given in Figure 7.32. These blends exhibited a ductile fracture. The impact properties determined from the curves for all DGTR/WPP blends, and PGTR/WPP blends containing resin compatibilizing system, are given in Table 7.12. The peak force and the impact failure energy increase slightly with the addition of SP resin and further with the resin system. A

greater increase in propagation energy compared to initiation energy is shown. This increase in propagation energy indicates a greater tendency for load transfer between phases in the DGTR/WPP blends containing resin system, which occurred through increase in compatibility between phases. This is supported by the closeness of the glass transition temperatures of the two phases observed in dynamic mechanical measurements (Table 7.13). However, this increase is small, hence confirming that no interfacial crosslinks formed in these blends. The tensile fractographs reveal an absence of interfacial crosslinks in these blends. These DGTR/WPP blends containing the resin system, compared to respective PGTR/WPP blends, exhibited slightly greater fracture initiation energies. This increase is associated with greater levels of crosslinks developed within the GTR phase due to the Delink treatment. All these results finally reveal that no actives double bonds were formed in diene rubbers in the GTR during Delink treatment, thus prohibiting the development of interfacial crosslinks in the resin modified WPP.

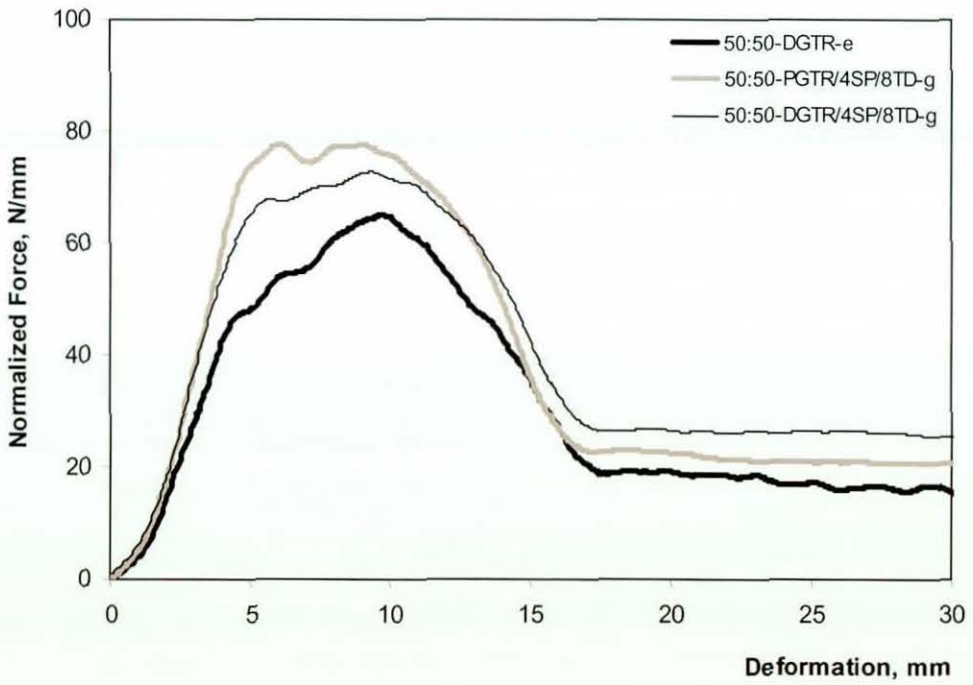

Figure 7.32 Force vs. deformation for DGTR/WPP (50/50) blends containing the resin compatibilizing system

Table 7.12 Impact properties for DGTR/WPP blends and PGTR/WPP blends containing the resin compatibilizing system

Sample Code	Peak Force*, N/mm	Initiation Energy*, J/m	Propagation Energy*, J/m	Failure Energy*, J/m
50:50-DGTR-e	66(4)	408(13)	316(20)	724(18)
50:50-DGTR /4S-g	62(3)	382(16)	385(23)	766(25)
50:50-DGTR/4S/0.8TA-g	69(2)	335(14)	496(9)	831(25)
50:50-DGTR/4S/0.8TD-g	74(2)	415(15)	461(17)	876(19)
50:50-DGTR/4S/0.8TA-e	68(3)	348(14)	415(35)	763(35)
50:50-DGTR/4S/0.8TD-e	67(4)	382(18)	408(17)	790(31)
50:50-PGTR-e	66(5)	353(17)	391(28)	744(10)
50:50-PGTR /4SP-g	71(3)	359(18)	419(20)	778(40)
50:50-PGTR/4S/0.8TA-g	71(1)	212(15)	585(13)	797(11)
50:50-PGTR/4S/0.8TD-g	76(4)	228(28)	614(30)	842(21)

**normalized by dividing by the thickness of the specimen*

7.3.2.4 Dynamic Mechanical Properties

The glass transition temperatures determined from the tan δ vs. temperature curves recorded in the dynamic mechanical tests are given in Table 7.13. The shift of the T_g of the GTR phase to high temperature side is an indication of the formation of crosslinks in the GTR phase due to the resin system. The closeness of the T_g values in the DGTR/WPP blends containing the resin system, compared to the respective PGTR/WPP blends proved that there was an improvement in compatibility between phases of the blend. This slight enhancement in compatibility between phases is responsible for the slight improvement in tensile and impact properties of the DGTR/WPP blends containing SP resin with $SnCl_2.2H_2O$. However, this property improvement obtained by replacing GTR with DGTR in GTR/WPP blends containing resin system is not remarkable. Hence, the addition of a pre-treatment process like Delink treatment is not economical when compatibilized with the resin system.

Table 7.13 Glass transition temperature of each phase in DGTR/WPP or PGTR/WPP blends containing the resin compatibilizing system

Sample Code	T_g of GTR, ^0C	T_g of WPP, ^0C
50:50-DGTR-e	-39	13
50:50-DGTR/4S/0.8TD-g	-36	14
50:50-PGTR/4S/0.8TD-g	-38	14

The DGTR/WPP (50/50) blends compatibilized with the dimaleimide system, however, exhibited remarkable improvements in mechanical properties with their stable morphology obtained through the formation of strong interfacial adhesions. Therefore, an investigation of the effect of the incorporation of the dimaleimide system to the DGTR/WPP blends, at different blend compositions, is valued.

7.3.3 Effect of the Dimaleimide Compatibilizing System on DGTR/WPP Blends at Different Compositions

The DGTR/WPP blends compatibilized with the dimaleimide system were prepared according to the mixing schedule-e, at three different DGTR contents, 30, 50 and 70 wt%. A constant amount of the dimaleimide system, which contained 3 pphp of the HVA-2 and 0.6 pphp of the DTBPIB, was used for this study. The processing characteristics, the tensile and the impact properties of these blends were measured, and were compared with the respective DGTR/WPP simple blends. The morphology of such blends and thermal properties of such blends were also studied, and were used to explain the mechanical property variations.

7.3.3.1 Processing Characteristics

Table 7.14 illustrates the steady state torques determined from the torque-time curves recorded for the DGRT/WPP blends containing the dimaleimide system at the three

different DGTR contents. The steady state torque increases with increase in DGTR content as observed for the DGTR/WPP simple blends (Table 7.5). Remarkable increases in steady state torques are recorded for the DGRT/WPP blends containing the dimaleimide system at every DGTR content (Table 7.5 and Table 7.14).

Table 7.14 Steady state torques for DGRT/WPP blends with the dimaleimide compatibilizing system at different blend compositions

Sample Code	Steady State Torque, Nm
30:70-DGTR/3H/0.6D-e	11.0(10.9)
50:50-DGTR/3H/0.6D-e	12.7(12.6)
70:30-DGTR/3H/0.6D-e	13.0(13.2)

duplicate results are given in parenthesis

7.3.3.2 Tensile Properties

The stress-strain curves for the DGTR/WPP blends with and without the dimaleimide system are given in Figure 7.33. The dimaleimide compatibilized blends exhibited much greater tensile strengths and deformations before fracture. The tensile properties such as tensile strength, elongation at break, and secant modulus at 2% strain, determined from these curves are given in Figure 7.34, Figure 7.35, and Figure 7.36, respectively. Tensile strength, and secant modulus, linearly decreases with the DGTR content, in a similar way to those for the DGTR/WPP simple blends. This is due to the replacement of the high strength WPP by the low strength GTR. The dimaleimide compatibilized DGTR/WPP blends and PGTR/WPP blends do not show any differences in the two properties, although significant differences are shown from their simple blends. However, the compatibilized DGTR/WPP blends compared to the corresponding PGTR/WPP bends exhibited significant increases in elongation at break. Hence believed no additional crosslinks will be developed in the dimaleimide compatibilized blends when the PGTR is replaced by the DGTR, and the significant difference in elongation at break is associated with the types of crosslinks formed.

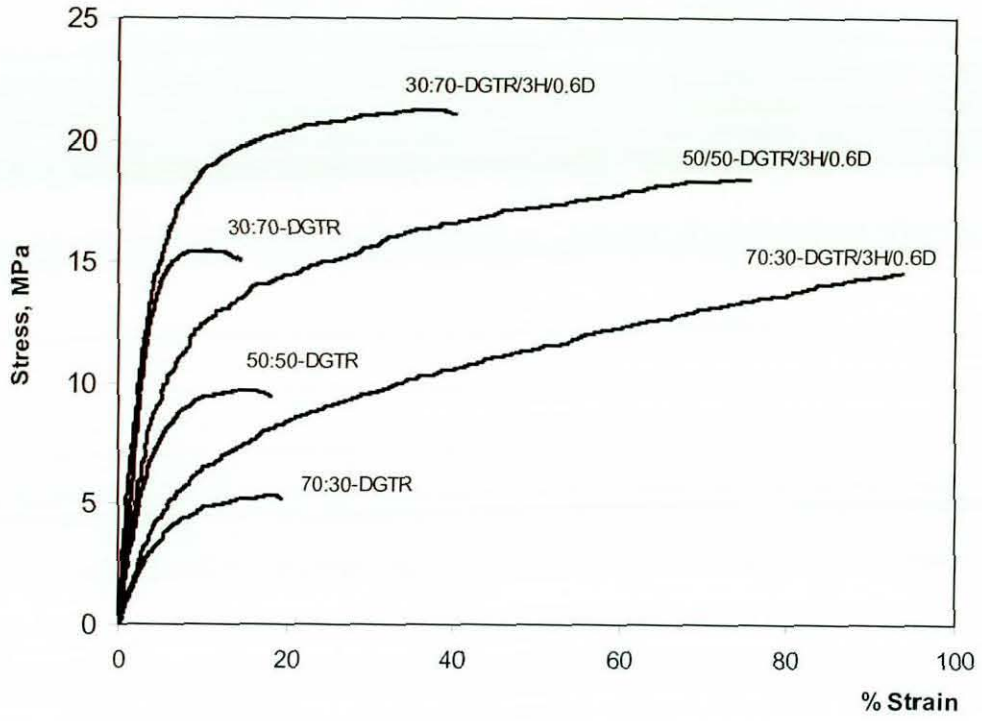

Figure 7.33 Stress vs. strain curves for DGTR/WPP blends at different DGTR contents

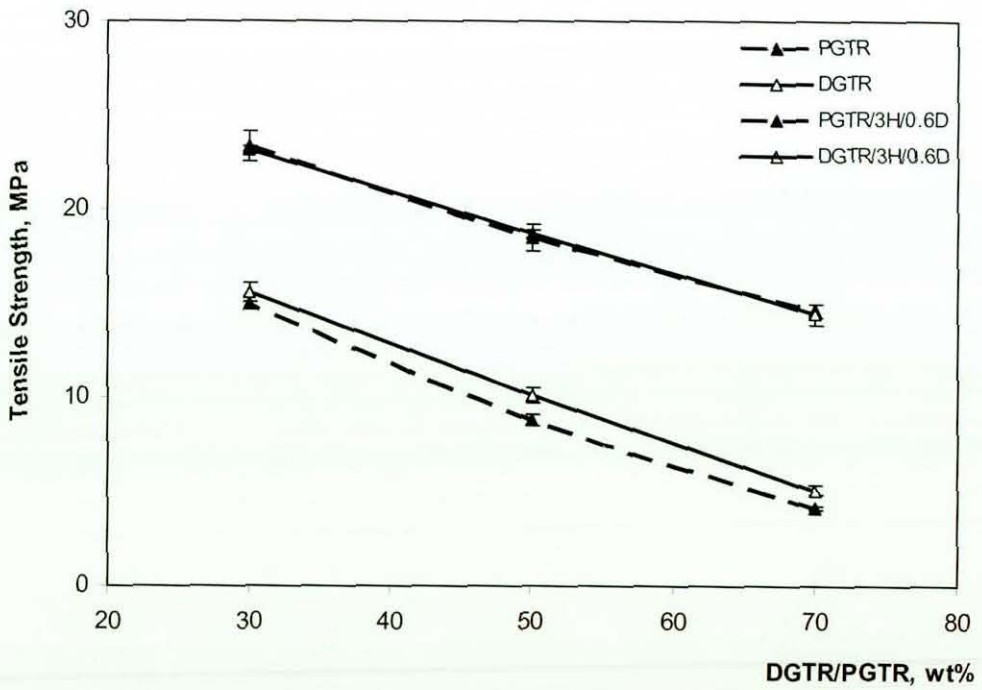

Figure 7.34 Tensile strength vs. DGTR or PGTR content

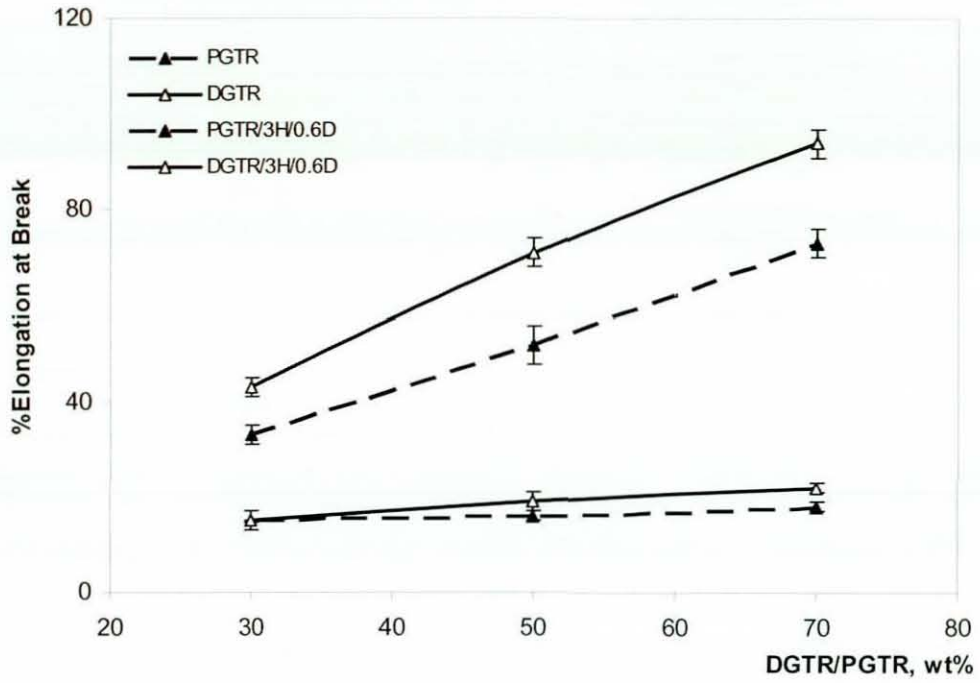

Figure 7.35 Elongation at break vs. DGTR or PGTR content

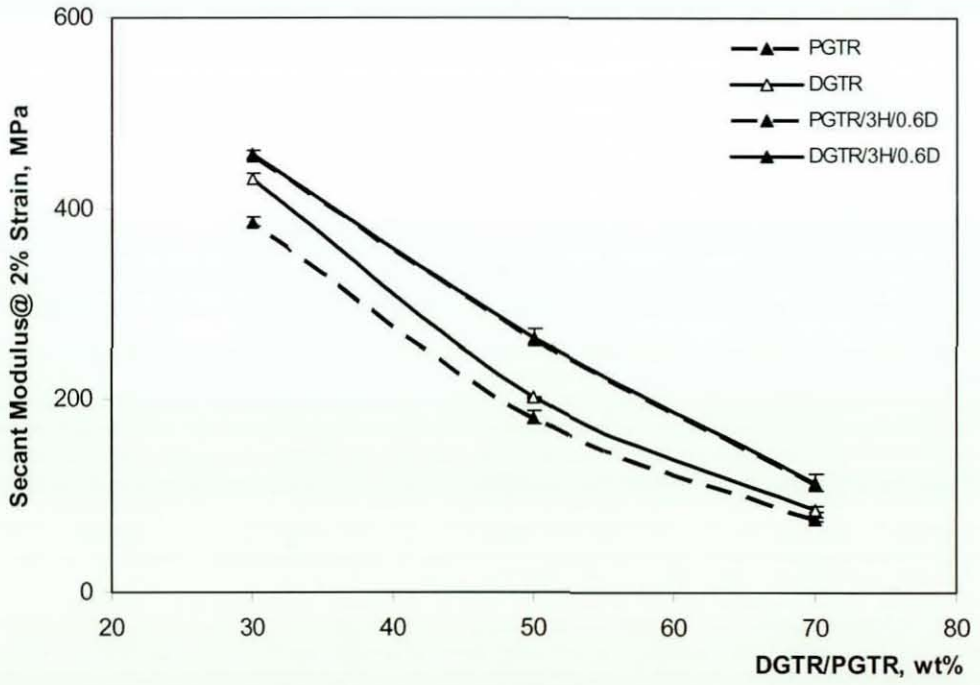

Figure 7.36 Secant modulus vs. DGTR or PGTR content

The compatibilized GTR/WPP blends prepared according to the mixing schedule-a produced lower tensile properties than those for the PGTR/WPP blends. Tensile strength, secant modulus and elongation at break recorded for the GTR/WPP blends at 70 wt% GTR were 12.9 MPa, 83 MPa and 60%, respectively. This difference may be a result of additional free radicals developed during processing of the PGTR.

7.3.3.3 Tensile Fracture

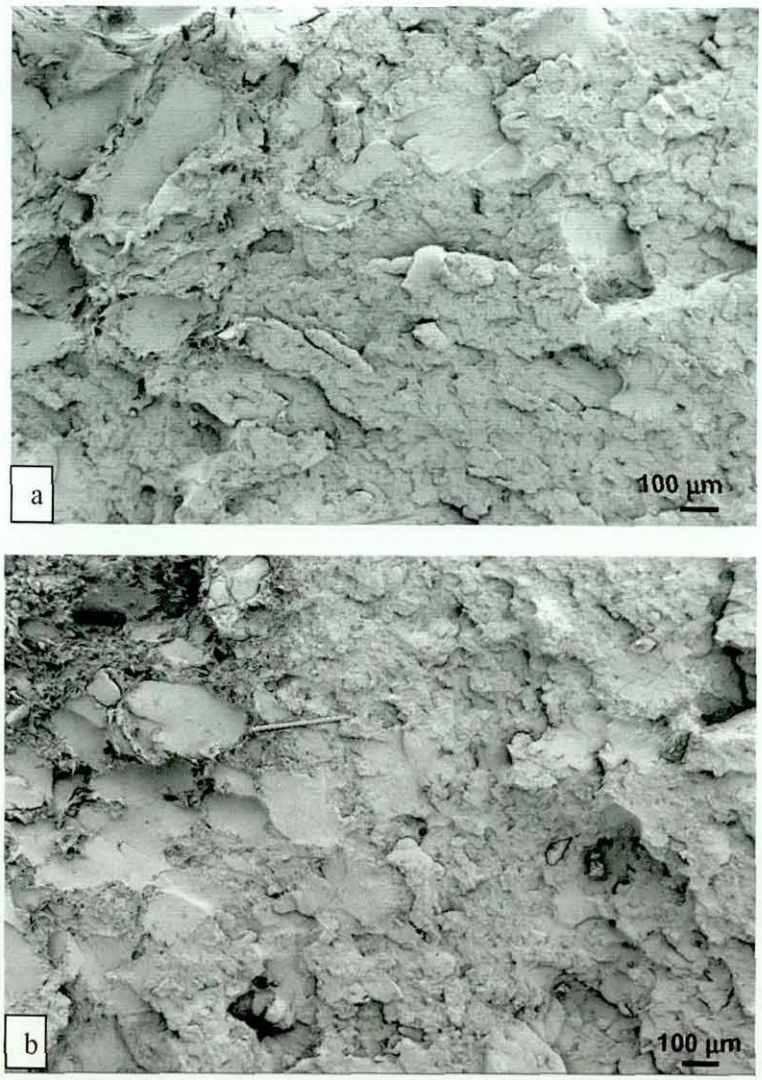

Figure 7.37 Tensile fractographs of dimaleimide compatibilized DGTR/WPP blends

a. 30:70-DGTR/3H/0.6D b.70:30-DGTR/3H/0.6D

Micrographs of the tensile fracture surfaces for the dimaleimide compatibilized DGTR/WPP blends at 30 and 70 wt% DGTR contents are given in Figure 7.37. Both micrographs exhibited quite regular shapes and a homogeneous blend, with a rough fracture surface. However, two different phases with a little interfacial debonding and yielding in the WPP phase around loosely bound GTR particles are apparent in certain areas. These are the places of imperfections, where the fracture was initiated. The strong interfacial adhesions formed in the blends containing the dimaleimide compatibilizing system will suppress the formation of voids at the interface. As a result of such adhesions large holes, created due to removal of the GTR particles could not be seen.

Figure 7.38 is a micrograph of a tensile fracture surface of a dimaleimide compatibilized blend recorded at a higher magnification. This micrograph clearly shows two distinct phases, the DGTR phase and WPP phase, and also a properly bound interface between them. The interface in this micrograph is similar to the interface on the cryogenically fractured surfaces taken under zero strain (Figure 7.43). The strong interfaces in the dimaleimide compatibilized blends raise the critical stress required for a permanent fracture, and provide larger deformations before failure.

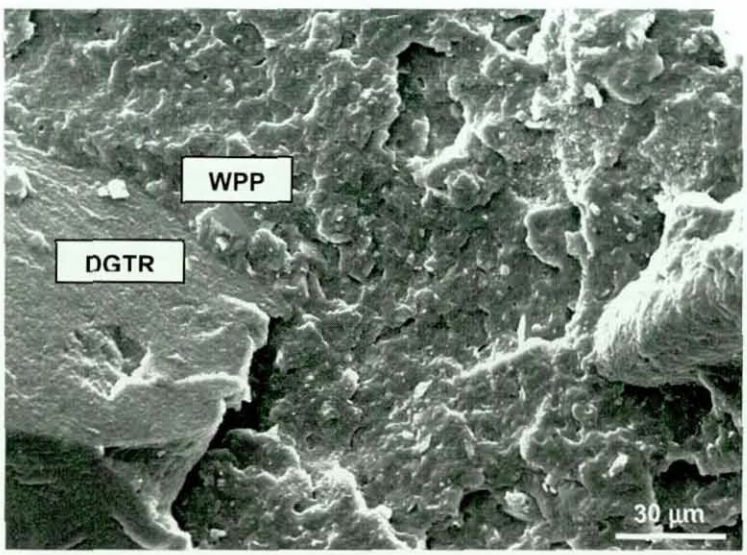

Figure 7.38 Tensile fractograph of a 70:30-DGTR/3H/0.6D blend showing a strong interface

7.3.3.4 Impact properties

The force-deformation curves recorded under impact loading for DGTR/WPP blends containing the dimaleimide system and for DGTR/WPP simple blends prepared at 30 and 70 wt% DGTR contents are given in Figure 7.39. The dimaleimide compatibilized DGTR/WPP blends exhibited greater peak forces and hence greater impact failure energies compared to those for the DGTR/WPP blends at every DGTR content. The peak force increases are the result of the formation of interfacial crosslinks, and crosslinks within the GTR phase, in the dimaleimide compatibilized DGTR/WPP blends. These observations are supported by the greater tensile properties obtained (Figure 7.34), and by the blends homogeneity observed in tensile fracture surfaces (Figure 7.37).

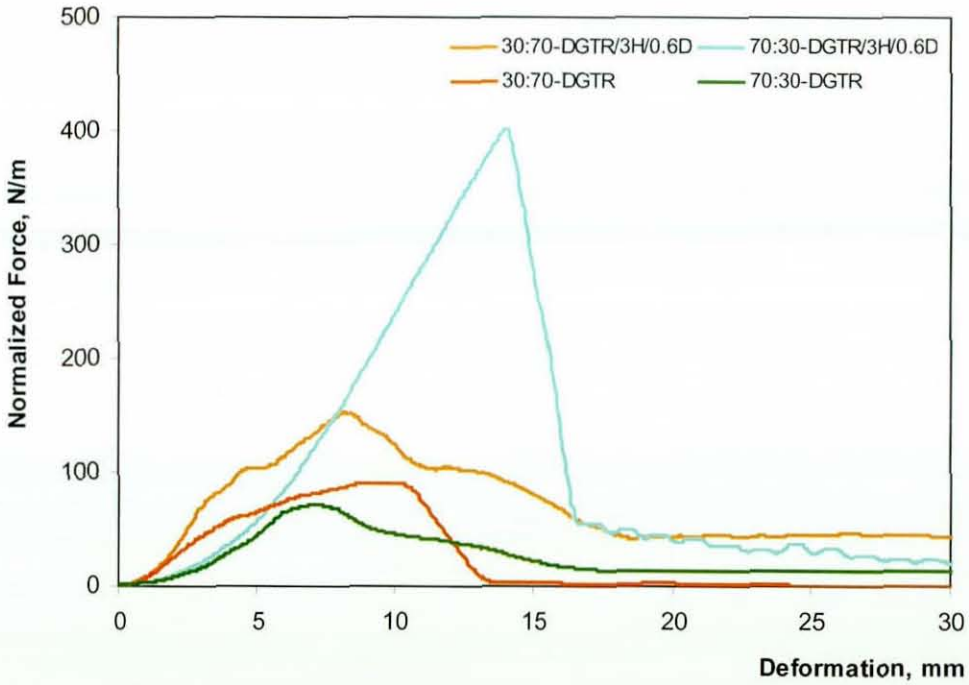

Figure 7.39 Force vs. displacement for DGTR/WPP blends with the dimaleimide compatibilizing system under impact loading

The dimaleimide compatibilized DGTR/WPP blend with 30 wt% DGTR, exhibited a smaller improvement (80%) in impact failure energy when compared with the respective DGTR/WPP simple blend. The corresponding blend at 70 wt% of the DGTR exhibited a greater increase (350%). At 70 wt% DGTR content, the DGTR/WPP simple blend had

inferior impact failure energy (Figure 7.19 and Table 7.7) associated with severe DGTR particle separation and interfacial debonding at failure (Figure 7.17). In contrast, the dimaleimide compatibilized DGTR/WPP blends at 70 wt% of the DGTR produced a stable blend with strong interactions between DGTR particles, and between phases (Figure 7.37). The optical micrographs for the compatibilized blend, which exhibited a lower size distribution for the DGTR agglomerants, are also evidence for this stable blend morphology (Section 7.3.3.6). These interactions enhance load transfer between phases and provide maximum toughness to the WPP phase. At 30 wt%, the toughening effect of the WPP caused by the DGTR is reduced due to lack of DGTR particles, which act as stress concentration zones in the dimaleimide compatibilized DGTR/WPP blends. Further, both blends exhibit similar blend morphology. These results reveal that the impact energy could be enhanced remarkably when the DGTR/WPP blends at higher DGTR contents are dynamically vulcanized with the dimaleimide system.

Table 7.15 gives the impact properties obtained for the DGTR/WPP and PGTR/WPP blends containing the dimaleimide compatibilizing system. Compared to the compatibilized PGTR/WPP blends, the corresponding DGTR/WPP simple blends showed slightly higher impact properties. It is found that the increase in failure energies for blends containing 30 wt% and 70 wt% GTR are 20% and 50%, respectively. This increase in failure energy for the DGTR/WPP blends containing the dimaleimide compatibilizing system is related to the relatively greater fracture initiation energy. This is correlated to the type of crosslinks present in the blend. Further, the difference in increment between 30 and 70 wt% of the DGTR is again due to the phase morphologyand also toquantitative difference in stress concentration zones in the dimaleimide compatibilized DGTR/WPP blends.

Table 7.15 Impact properties for DGTR/WPP and PGTR/WPP blends

Sample Code	Peak Force*, N/mm	Initiation Energy*, J/m	Propagation Energy*, J/m	Failure Energy*, J/m
30:70-DGTR/3H/0.6D	166(10)	509(40)	909(40)	1418(125)
50:50-DGTR/3H/0.6D	288(14)	838(40)	905(39)	1743(100)
70:30-DGTR/3H/0.6D	402(10)	2007(80)	731(38)	2737(120)
30:70-PGTR/3H/0.6D	133(11)	427(35)	743(18)	1170(80)
50:50-PGTR/3H/0.6D	210(14)	513(33)	640(46)	1153(87)
70:30-PGTR/3H/0.6D	327(18)	1288(84)	560(18)	1848(75)

**normalized by dividing by the thickness of the specimen*

7.3.3.5 Dynamic Mechanical Properties

Typical tan δ vs. temperature curves for the selected DGTR/WPP blends containing the dimaleimide compatibilizing system are shown in Figure 7.40. Similar to the curves for the DGTR/WPP simple blends (Figure 7.21), these curves also show two distinct peaks corresponding to the glass transitions of the two phases. The magnitude of the transition peak also varies according to the content of each phase. The glass transition temperatures determined from the tan δ curves for each phase are given in Table 7.16. As expected, the T_g of the GTR phase shifted to the high temperature side with an increase in DGTR content, while the T_g of the WPP phase shifted to the low temperature side. This shift in T_g of the GTR phase is much greater for the DGTR/WPP blends containing the dimaleimide system than that for the DGTR/WPP simple blends (Table 7.8). This greater shift makes the difference between the glass transitions of the phases smaller, and hence indicates enhanced compatibility between phases in such blends. This is also an indication of better mechanical properties from the DGTR/WPP blends containing dimaleimide compatibilizing system, especially at higher GTR/DGTR contents.

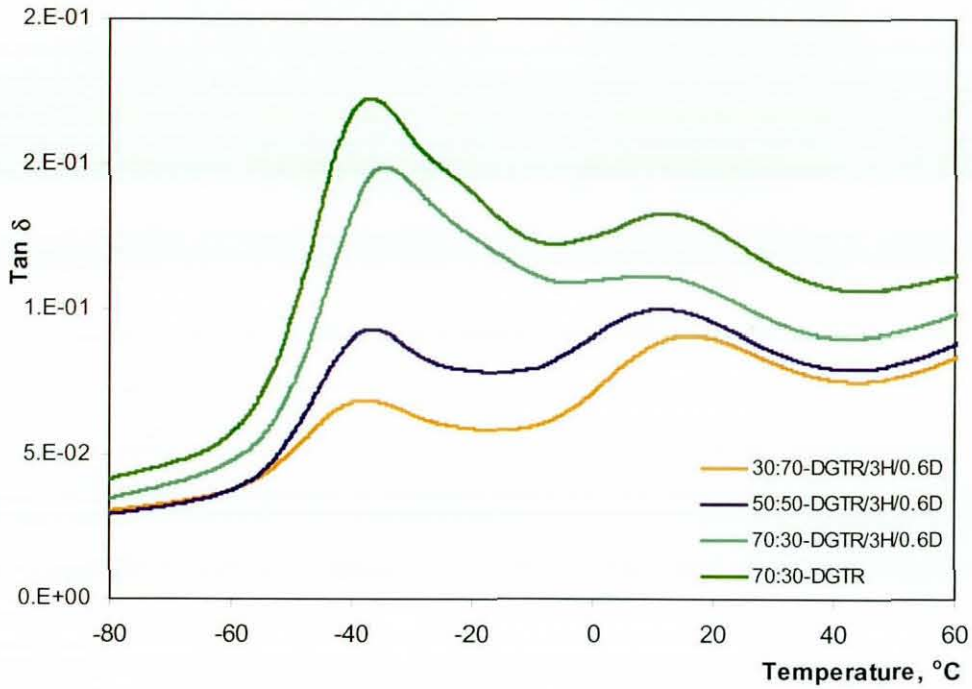

Figure 7.40 Tan δ vs. temperature for DGTR/WPP blends containing dimaleimide compatibilizing system at different DGTR contents

Table 7.16 Glass transition temperature of each phase in DGTR/WPP blends containing dimaleimide compatibilizing system

DGTR, wt%	T_g of GTR, ^0C	T_g of WPP, ^0C
30	-37	14
50	-36	13
70	-33	13

7.3.3.6 Morphology

Figure 7.41 shows typical optical micrographs recorded for the microtomed films of the DGTR/WPP blends containing the dimaleimide compatibilizing system, at 30 and 70 wt% DGTR. Both micrographs show two phases. The micrograph for the blend at 30 wt% of the DGTR exhibits many small DGTR agglomerants with less large DGTR agglomerants dispersed in the WPP matrix (Figure 7.41a). The micrograph for the blend

at 70 wt% of the DGTR exhibits many large DGTR agglomerants and less small DGTR agglomerants combined to form a continuous DGTR phase (Figure 7.41b). Further, the DGTR agglomerant size distribution in these micrographs, when compared to those in the micrographs for the respective DGTR/WPP simple blends (Figure 7.24), is narrow. The narrow agglomerant size distribution is associated with the strong interfacial adhesions present in the compatibilized blend. Further, it is an indication of enhanced blend compatibility (Section 7.3.3.5), and better mechanical properties (Section 7.3.3.2 and Section 7.3.3.4).

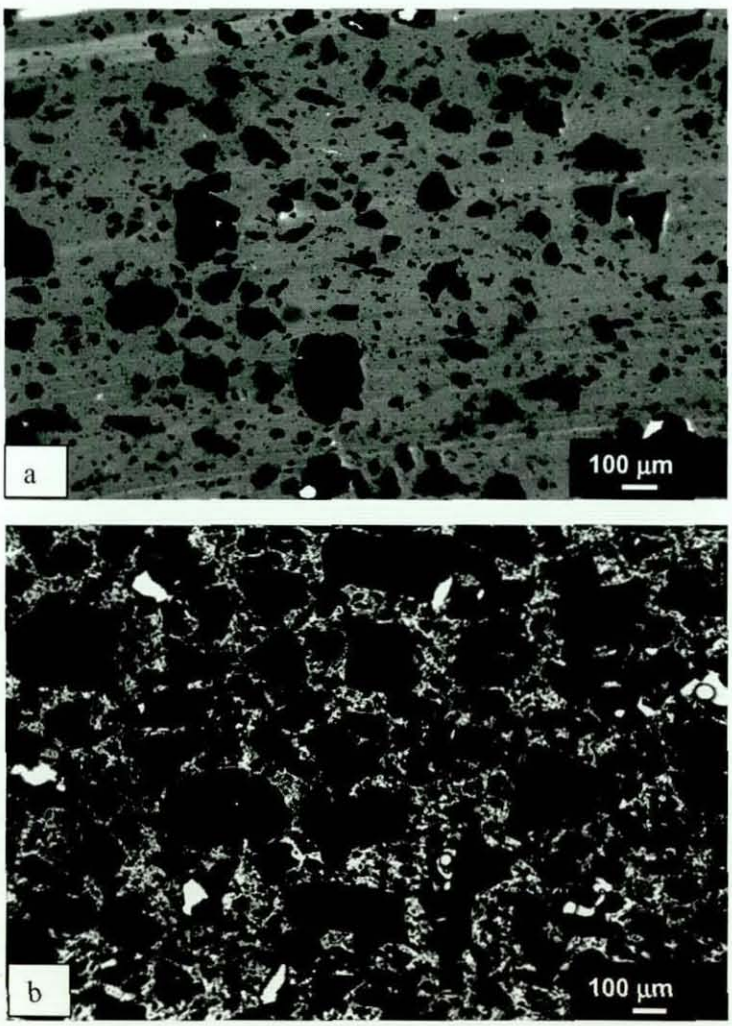

Figure 7.41 Optical micrographs of DGTR/WPP blends containing dimaleimide compatibilizing system

(a) 30:70-DGTR/3H/0.6D-e (b)70:30-DGTR/3H/0.6D-e

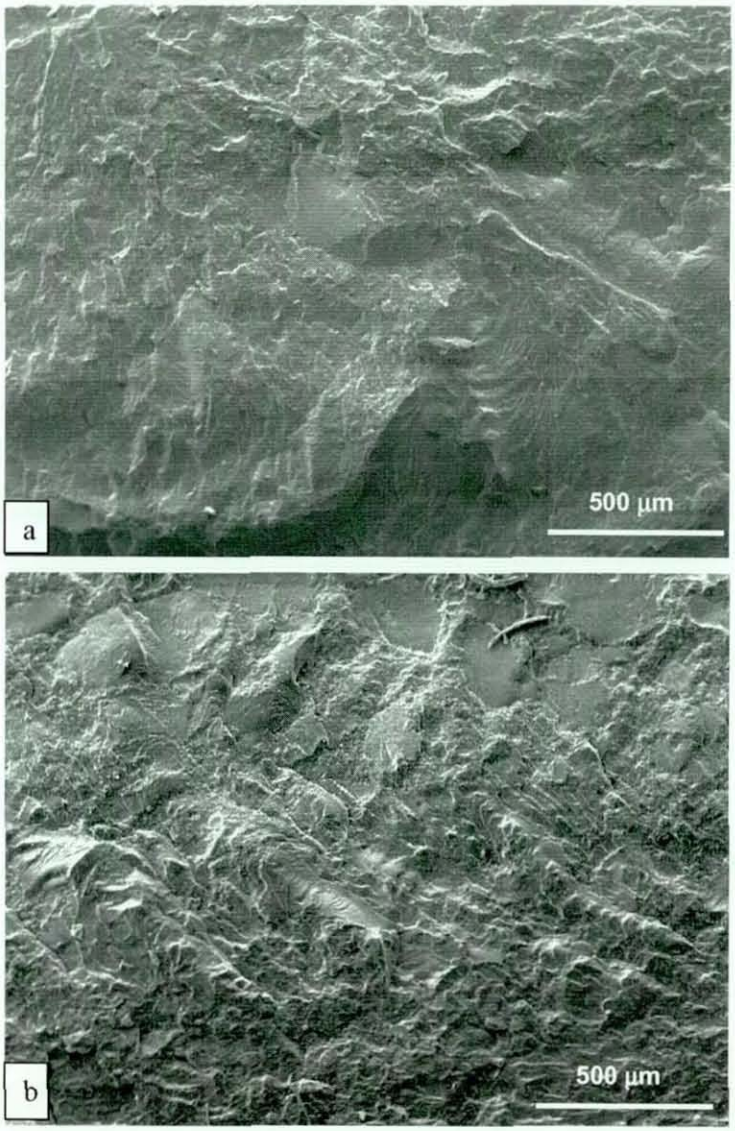

Figure 7.42 Cryogenically fractured surfaces of DGTR/WPP blends

a. 30:70-DGTR/3H/0.6D-e b. 70:30-DGTR/3H/0.6D-e

Typical SEM images of the cryogenically fractured surfaces of DGTR/WPP blends containing the dimaleimide compatibilizing system, prepared at 30 and 70 wt% of the DGTR content, are shown in Figure 7.42 and Figure 7.43. Both micrographs exhibited two phases, which underwent brittle fracture. However, the micrograph for the blend at 30 wt % of the DGTR (Figure 7.42a) shows more regular WPP phase shapes, with no clear interfaces, indicating stability of the blend. The micrograph for the blend at 70 wt % of the DGTR (Figure 7.42b) exhibits more DGTR phase, with no clear interfaces. However, clear interfaces could be seen around DGTR particles which were entrapped in

the WPP phase (Figure 7.43). These might be the places where the interfacial debonding occurred during straining. These differences are due to the presence of high DGTR contents in the blend.

The optical micrographs of the microtome films and the scanning electron micrographs of the cryogenically fractured surfaces for the DGTR blends containing the dimaleimide system represent stable blend morphology, which is caused by the strong interfacial adhesions formed during the melt mixing process. The blends with stable morphology will provide enhanced mechanical properties.

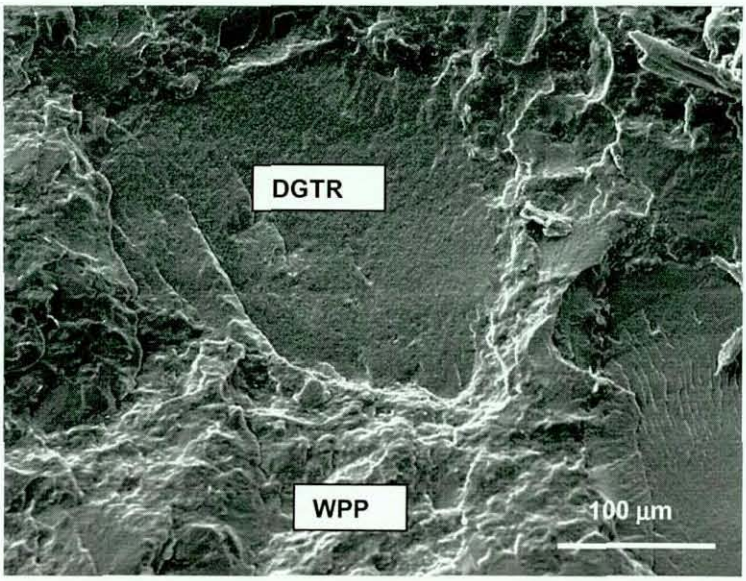

Figure 7.43 Entrapment of GTR particles in a cryogenically fractured surface of a 70:30-DGTR/3H/0.6D-e blend

7.4 Summary

The GTR was treated with the Delink at 3, 6 and 9 phr levels. The Delink treatment was carried out in the Haake mixer at 40 ^{0}C at 90 rpm, for 7 minutes, and the test specimens were moulded at 150 ^{0}C for 10 minutes. The processing characteristics, the gel content and the swelling index of the Delink treated GTR revealed that scission of crosslinks, rather than of rubber chains, is the predominant reaction, when treated with 3 phr of the

Delink. At higher Delink levels, these properties indicated rubber chain scission to some degree. In addition, at higher levels, surface blooming caused by decomposition of excess or unutilized Delink chemicals was noticed. Hence, the GTR treated with 3 phr of the Delink produced the optimum tensile properties. These properties were maximized when treated with Delink for 10 minutes. The Delink level of 3 phr produced maximum properties even when moulded at 200 ^{0}C, the temperature at which the blends were moulded. At higher Delink levels, pronounced odour and surface blooming was observed, when moulded at 200 ^{0}C. The odour and the bloom are associated with the decomposition of excessive Delink chemicals present in the blend.

The Delink treated GTR at the optimum level of 3 phr (DGTR), was melt mixed with the WPP to prepare DGTR/WPP simple blends at different compositions. The Delink level ranged from 10 to 90 wt% of the Delink at 20 wt% intervals. The steady state torque of the DGTR/WPP simple blends increased with the DGTR content due to an increase in the highly viscous GTR content of the blend. The tensile strength and secant modulus at 2% strain decreased with the DGTR content, while the elongation at break increased. Compared to the PGTR/WPP simple blends, the DGTR/WPP simple blends at every DGTR content exhibited slight improvements in tensile properties. The maximum improvement of 30% was obtained at 90 wt% DGTR content. These improvements are due to the increase in cohesive strength of the DGTR phase gained through the formation of additional crosslinks within the DGTR phase. The slightly stable blend morphology and the closeness of the glass transitions, of the phases of the DGTR/WPP blends, produced a slight improvement in compatibility between phases. However, the impact properties did not show any enhancement with the Delink treatment of the GTR, especially at higher GTR contents. The blend at 10 wt% DGTR exhibited a slight improvement in impact failure energy. At this DGTR content, small DGTR agglomerants, which were anchored to the WPP matrix phase, behave as effective stress concentration zones. Due to an increase in DGTR agglomerant size, with the increase in the DGTR content, and to lack of interfacial adhesions, the larger DGTR agglomerants detached from the WPP phase under impact loading. These poor tensile and impact properties recorded for the DGTR/WPP simple blends suggested the necessity of a suitable compatibilizer to improve the interfacial adhesions between the two phases and hence to produce better mechanical properties.

The two compatibilizing systems, dimaleimide system and resin system were used to prepare DGTR/WPP (50/50) reactive blends. The dimaleimide system consisted of 3 pphp of HVA-2 and 0.6 pphp of DTBPIB activator, while the resin system consisted of 4 pphp of SP resin and 0.8 pphp of $SnCl_2$ activator. The blends with the SP resin alone, and those with the resin compatibilizing system, exhibited slightly enhanced impact properties. However, the tensile properties did not show any significant improvement. This poor property enhancement is related to the severe interfacial debonding observed in the micrographs. In contrast, the DGTR/WPP blends containing HVA-2 alone exhibited significant improvement in tensile and impact properties. This was further enhanced with the incorporation of the DTBPIB activator to the HVA-2. These remarkable property enhancements are associated with the stabilized blend morphology. Further, the glass transitions of the phases shifted towards each other, indicating improved compatibility between phases. The improvement in tensile strength, elongation at break, secant modulus, and impact failure energy for the DGTR/WPP (50/50) blends containing the dimaleimide system, compared to the DGTR/WPP (50/50) simple blends were 85%, 275%, 30% and 140%, respectively. Further, improvements in elongation at break and impact failure energy for the DGTR/WPP blends containing the dimaleimide system compared to the respective PGTR/WPP blends was observed, and the maximum improvement was limited to 35%. This improvement may be related to the more flexible sulfidic crosslinks available.

The DGTR/WPP blends containing the dimaleimide system prepared at 30 wt% and 70 wt% of the DGTR content also exhibited remarkable improvements in tensile and impact properties compared to the corresponding DGTR/WPP simple blends. The tensile strength and the secant modulus decreased with the DGTR content, while the elongation at break and the impact failure energy increased. As expected, due to the effect of the Delink treatment of the GTR, the blends containing higher DGTR contents (70 wt% was the highest) exhibited maximum improvement in properties. The improvement in tensile strength, elongation at break, secant modulus and impact failure energy for the DGTR/WPP (70/30) blends containing the dimaleimide system, were 180%, 325%, 33% and 350%, respectively. Further, the improvements in elongation at break and impact failure energy for the blend containing DGTR/WPP (70/30) were recorded as 29% and 48%, respectively, over the PGTR/WPP (70/30) blend. The improvements in tensile strength, elongation at break and impact failure energy were recorded as 12% and 58%

and 52% over the GTR/WPP (70/30) blends. These property enhancements suggested to use DGTR in place of GTR in producing blends GTR/WPP blends. However, the use of DGTR in GTR/WPP blends is debatable and depends on the properties required for the specific application against its price (1000 kg of 40 mesh tyre rubber, and Delink treated tyre rubber, are GBP 12.80 and 35.50, respectively at DSI Industries PLC, Sri Lanka).

7.5 Property Comparison of Experimental Blends and Commercial Products

A wide range of properties obtained for the GTR/WPP and DGTR/WPP blends suggested their use in different commercial applications. Table 2.1Table 7.17 gives the property comparison of experimental blends and some commercial products. The experimental results suggested that the suitability of simple blends in low performance applications and reactive blends in high performance applications.

Table 7.17 Properties of experimental blends and commercial products

Blend/product	Hardness, IRHD	T/S, MPa	%Eb
Simple blends	56 -86	4.1- 18.7	15-28
Reactive blends	88-89	14.4-23.3	15-94
Carpet Underlay (Damtech™)	-	0.6	20
Commercial Flooring [102]	55	3.0±0.7	>60
Roof slate [130]	-	15	10

Chapter 8

Conclusions and Recommendations for Future Work

8.1 Conclusions

A wide spectrum of properties of the blends prepared from the ground tyre rubber (GTR) and waste polypropylene (WPP) revealed that the useful materials could be produced with the specified waste polymers, especially with the addition of a dimaleimide compatibilizing system. The main conclusions drawn from this present study are discussed under three sub sections namely GTR/WPP simple blends, compatibilization, and GTR pretreatment.

8.1.1 GTR/WPP Simple Blends

The melting temperature of the WPP at 166 ^{0}C, and the onset degradation temperatures of the GTR and the WPP at 200 ^{0}C and 230 ^{0}C, respectively, indicated that the two polymers can be processed at 180 ^{0}C under high shear forces in the presence of a suitable antioxidant.

The smooth compression moulded sheets made from small pieces of the melt-mixed materials at every composition showed that the GTR and the WPP, although contained considerable amounts of polymer chemicals and other contaminants, are suitable for the production of blends.

The morphology of the blends and the tan δ curves in the dynamic mechanical analysis showed a two-phase system, indicating immiscible behaviour of the blends, thus confirming the incompatibility between the GTR and the WPP.

The GTR was dispersed as domains in the continuous WPP matrix at low GTR contents up to 60 wt%. At 70 wt% GTR, the GTR dispersed phase changed to a continuous phase.

This morphology change confirmed the suitability of the GTR and the WPP for producing rubber-thermoplastic blends.

The processing and flow characteristics, and the mechanical properties, of the GTR/WPP simple blends were found to be strongly affected by the blend composition, which directly influenced the degree of crystallinity and the phase morphology. The melt flow index, hardness, tensile strength, secant modulus at 2% strain and tear resistance of the blends decreased with GTR content, whilst torque developed at the completion of the melt-mix process, elongation at break and impact failure energy increased. The best balance properties were obtained at 50 wt% of each polymer.

The change in properties is small at low GTR contents, but increases above 30 wt% GTR and shows significant change from 70 wt% GTR. The slow variations in properties at low GTR contents suggest that at least 30 wt% of GTR is required to give rubbery properties to a GTR/WPP simple blend.

The optimum processing parameters were identified; as a processing temperature of 180 ^{0}C, as a processing speed of 90 rpm, and as a processing time of 5 minutes, when processed under a single step adding procedure.

The small variation in tensile properties of the GTR/WPP (50/50) simple blend suggests that the shear induced phase adhesion cannot be sufficiently developed by varying the processing parameters. This led to a conclusion that the properties of the GTR/WPP blends cannot be remarkably enhanced by varying processing parameters.

8.1.2 Compatibilization

A significant mechanical property enhancement can be achieved by incorporating HVA-2 compatibilizer into the GTR/WPP (50/50) simple blend due to the formation of crosslinks at the GTR phase. The best balance of properties for these blends was obtained at 3 pphp of HVA-2. The increases in tensile strength, elongation at break and impact failure energy of this blend over the simple blend were obtained as 55%, 11% and 26%, respectively.

The tensile properties could be further enhanced (tensile strength by 14%) by the addition of the MBTS activator into the HVA-2 compatibilizer, but with a decrease in the impact properties. This property variation showed that the additional crosslinks were formed only at the GTR phase. The best balance of properties for these blends was obtained at 5 pphp of HVA-2 and 0.2 pphp of MBTS within the compatibilizer component levels studied.

A remarkable property enhancement (increase in tensile strength by 56%) could be achieved by the addition of the DTBPIB activator into the HVA-2 compatibilizer. This enhancement was associated with the stable blend morphology developed due to the formation of crosslinks at the GTR phase and the interface. The best balance of properties for these blends was obtained at 3 pphp of HVA-2 and at 0.6 pphp of DTBPIB. The properties of the GTR/WPP blends obtained were comparable with virgin NR/PP blends.

The differences in property enhancements between the DTBPIB and the MBTS indicate that DTBPIB is an effective activator for HVA-2 in compatibilizing the phases in the GTR/WPP blend.

A significant property enhancement (increase in tensile strength by 23%) could also be achieved by incorporating a SP resin compatibilizer to the GTR/WPP (50/50) simple blend. This property enhancement could be further improved (increase in tensile strength by 8%) by the addition of the $SnCl_2$ activator to the SP resin, due to improved compatibility between phases which occurred through modification of the WPP phase. The addition of GTR to the modified-WPP by the SP resin system produced optimum properties at 4 pphp of SP resin and at 0.8 pphp of $SnCl_2$.

The $SnCl_2$ activator, in both anhydrous and dihydrated forms, produced similar catalyzing effect at the 180 ^{0}C processing temperature used in the present study. This observation led to a conclusion that any form of $SnCl_2$ can be used as an activator for the resin compatibilizing system.

The maximum increases in the tensile strength, the elongation at break and the impact failure energy, for the blend containing the dimaleimide compatibilizing system (3 pphp of the HVA-2 and 0.6 pphp of the DTBPIB) over the simple (50/50) blend were 141%, 211% and 76%, respectively, while those for the blends containing the resin

compatibilizing system (4 pphp of the SP resin and 0.8 pphp of the $SnCl_2$) were 30%, 93% and 24%, respectively. These great differences in the mechanical properties clearly proved that the dimaleimide system was more effective than the resin system as a compatibilizer for GTR/WPP blends.

8.1.3 GTR Pre-treatment

Of the Delink levels investigated in the present study, 3 phr produced the best tensile properties. The tensile properties were maximized when the GTR was treated with Delink for 10 minutes.

A considerable improvement in the tensile properties, at every GTR content, could be obtained by the replacement of GTR with Delink treated GTR at the optimum level of 3 phr (DGTR) in the GTR/WPP blends. However, the impact properties remained unchanged. The maximum improvement of 28% obtained at 90 wt% DGTR revealed that the Delink treatment was limited to an increase in cohesive strength of the GTR phase.

A greater enhancement in the mechanical properties could be obtained with the addition of the dimaleimide system into the DGTR/WPP blends. Tensile strength, elongation at break and impact failure energy for the DGTR/WPP (70/30) blends containing dimaleimide system increased by 180%, 325% and 350%, respectively, over the DGTR/WPP (70/30) simple blend. However, considerable property improvements cannot be achieved by the addition of the resin system into the DGTR/WPP blends.

A significant property enhancement (increases in tensile strength and elongation at break by 12% and 58%, respectively) obtained for the DGTR/WPP (70/30) blend containing the dimaleimide system over the respective GTR/WPP (70/30) blend proved the DGTR is more suitable for the production of blends with the WPP. The effectiveness of using DGTR in GTR/WPP blends is debatable when the increased price of the Delink treated tyre rubber is considered.

The mechanical properties obtained for the GTR/WPP blends in the present study extended over a wide range, and varied according to the blend composition and the

compatibilizing system. Hence, a range of viable blends could be produced for different applications; low performance applications using simple blends and high performance applications from reactive blends.

8.2 Recommendation for Future Work

The dimaleimide compatibilizer used in the present study (HVA-2) generated the best mechanical properties for the GTR/WPP blends and DGTR/WPP blends. However, HVA-2 is more volatile and toxic than some bismaleimides commercially used in the polymer industry, eg. N-N'- (4, 4'-diphenylmethane) bismaliemide. Therefore, an investigation into the suitability of the bismaleimides use in the GTR/WPP blends is suggested for future work.

The results of the present study revealed that the mechanical properties could not be remarkably enhanced by the resin system, when the blends processed at 180 ^{0}C. However, it has been reported [294] that model crosslinks were formed in the low molecular weight EPDM by the SP resin and stannous chloride only at 225 ^{0}C. Temperatures below this, showed only model crosslink precursors, and not model crosslinks. These findings suggest further investigations on processing GTR/WPP blends with the resin system at temperatures higher than 180 ^{0}C. However, measures will have to be taken to prevent property deterioration of the principal polymers when exposed to elevated temperatures.

The replacement of the GTR by the DGTR in the GTR/WPP blends at 10 wt% of the DGTR produced a 50% increase in its impact strength, although other compositions did not produce such an increase. This improvement was obtained without incorporating any compatibilizing system. Therefore, future work can be focused on a detailed study of this blend composition.

The replacement of the GTR by the DGTR in the GTR/WPP blends at other DGTR contents did not produce remarkable improvements in mechanical properties. The main reason for this was the decomposition of unutilized Delink chemicals at 180 ^{0}C. Further, it was revealed that a severe decomposition of Delink chemicals would not occur at 150 ^{0}C, the temperature at which the polyethylene (PE) could be processed. Hence, it is

recommended that the effect of Delink treatment on the GTR in the GTR/waste PE (WPE) blends be evaluated in future work.

The properties of the GTR/WPP blends produced in the present study suggested that they could be used in a range of applications. These blends were produced without filler or other polymer additives. Therefore, further studies can be focused onto specific applications with the development of a suitable compound.

The scope of this project was to develop useful materials with polymer waste, and hence it could be recommended that future studies should concentrate on developing simple rubber-thermoplastic blends from waste rubber and mixed waste plastics containing PP. In addition, studies on the incorporation of a dimaleimide compatibilizing system into blends should be undertaken. As an overall solution for the waste disposal problem, certain natural waste materials like wood flour, coir dust, etc. could be investigated for incorporation in GTR/WPP blends in place of fillers and other polymer additives.

APPENDIX

A.1 Thermal Expansivity

Thermal Expansion coefficients of polymers used in the present study are given in Table A.1.

Table A.1 Thermal expansivities of polymers used in the present study

Polymer	Coefficient of Expansion, volume, K^{-1} [217]
NR	670×10^{-6}
SBR	660×10^{-6}
PP	6.8×10^{-5}

A.2 Solubility Parameter

Solubility parameters of NR and PP are 16.2 and 18.8 $(J/cm^3)^{1/2}$ respectively [217]. These values are for homopolymers of the repeating unit. SBR has a range of solubility parameters, 16.45-17.8 $(J/cm^3)^{1/2}$. The values vary with the composition of homopolymers present in the SBR copolymer. The solubility parameter of SBR containing 12.5% styrene of 17.6 $(J/cm^3)^{1/2}$ is taken for the calculation.

A.3 Flory Interaction Parameter

Flory interaction parameters for NR-PP and SBR-PP systems were calculated according to Equation 2.11. These parameters were calculated at 478 K (180 ^{0}C). The universal gas constant is taken as 8.314 J mol^{-1} K^{-1}. The arbitrary reference volumes,v ($=\sqrt{v_1 v_2}$), of the two systems were calculated using the molar volume of each polymer. These values are given in Table A.2. Molar volumes of polymers were taken as the ratio of the molecular

weight of the repeating unit of the polymer to the density of the polymer and are given in Table A.3. The density of SBR was also taken for SBR containing 12.5% styrene.

Table A.2 Flory Interaction Parameters

System	v, cm^3/mol	χ_{12}
NR-PP	57.8	0.09
SBR-PP	53.0	0.03

Table A.3 Molar Volume of Polymers

Polymer	Density, g/cm^3 [217]	Molecular weight of repeating unit, g/mol	Molecular weight of polymer*, g/mol	Molar volume, v_i, cm^3/mol
NR	0.913	68	1×10^6	74.5
SBR	0.933	58.5	1.76×10^5	62.7
PP (isotactic)	0.938 (av.)	42	5×10^5	44.8

**estimated values*

Critical values of the interaction parameter for the two systems can be calculated according to Equation 2.7 and also an approximated value containing equal amounts of segments of each polymer can be obtained using $(\chi_{12})_{crit} = 2/r$. The molecular weights for rubbers are in the range $1x10^4$ to $1x10^7$ and that for PP is in the range 2.0 - 7.7 $x10^5$ [217]. If the average molecular weight of the polymers is taken as 1.0 $x10^5$, then the degree of polymerization will be 2000. The average value of the molecular weight of repeating units was taken as 50. Finally, the critical value of the interaction parameter for GTR and WPP blends will be 0.001.

REFERENCES

1 Environmental Review in Germany, Available at http://www.conti.online/generator (1999).

2 De, S. K., Isayev, A. I. and Khait, K., *Rubber Recycling* (Taylor & Francis, USA, 2005).

3 Marcher, F., Waste Statistics 2004 Report No. 1 (Danish Environmental Protection Agency, Denmark, 2006).

4 Marcher, F., Waste Statistics 2005 Report No. 6 (Danish Environmental Protection Agency, Denmark, 2007).

5 Recycling and recovering plastics; West Europe, Available at http://www.isopa.org/htdocs/isopa_site/documents_ns/pu_perspec.pdf4. (2004).

6 Stribling, J. B., Solution to the scrap tyre problem. *Rubber Journal (Changed to European Rubber Journal),* **155**, 40-42 (1973).

7 Aisien, F. A., Hymore, F. K. and Ebewele, R. O., Potential application of recycled rubber in oil pollution control. *Environmental Pollution and Assessment,* **85**, 175-190 (2003).

8 Youwai, S. and Bergoda, D. T., Strength and deformation characteristics of shredded rubber tire - sand mixtures. *Canadian Geotechnical Journal,* **40**, 254-265 (2003).

9 Liu, H. S., Mead, J. L. and Stacer, R. G., Environmental effects of recycled rubber in light-fill applications. *Rubber Chemistry and Technology,* **73**, 551-564 (2000).

10 Mustafa, N., *Plastic Waste Management- Disposal, Recycling and Reuse*, 1st ed. (Marcel Dekker Inc., New York, 1993).

11 Iuga, A., Calina, L., Neamtua, V. M., Mihalcioiua, A. and Dascalescu, L., Tribocharging of plastics granulates in a fluidized bed device. *Journal of Electrostatics,* **63**, 937-942 (2005).

12 Ha, M. Y., Jeon, C. H., Choi, D. S. and Hae-Jin, C., A numerical study on the triboelectrostatic separation of PVC materials from mixed plastics for waste plastic recycling. *KSME International Journal,* **17**, 1485-1495 (2003).

13 Lee, J. K. and Shin, J. K., Triboelectrlostatic separation of PVC materials from mixed plastics for waste plastic recycling. *Korean Journal of Chemical Engineering,* **19**, 267-272 (2002).

14 Jonna, S. and Lyons, J., Processing and properties of cryogenically milled post-consumer mixed plastic waste. *Polymer Testing,* **24**, 428-434 (2005).

15 Freitag, H., Huth-Fehre, T. and Cammann, K., Rapid identification of plastics from electronic devices with NIR-spectroscopy. *Analytical Letters,* **33**, 1425-1431 (2000).

16 Gente, V., Marca, F. L., Lucci, F., Massacci, P. and Pani, E., Cryo-comminution of plastic waste. *Waste Management,* **24**, 663-672 (2004).

17 Reijnders, L., Recycling and reuse of materials, materials processing and manufacturing technologies, Available at http://www.greenplanet.eolss.net//Elosslogn/view.Chapter,aspx (2005).

18 Holst, O., Stenberg, B. and Christiansson, M., Biotechnological possibilities for waste tyre-rubber treatment. *Biodegradation,* **9**, 301-310 (1998).

19 Wagener, K., Nel, J., Duttweiler, R., Hillmyer, M., Boncella, J., Konzelman, J., Smith, J., D.W., Puts, R. and Willoughby, L., Metathesis polycondensation chemistry as a route to unsaturated elastomers. *Rubber Chemistry and Technology,* **64**, 83 (1991).

20 Adam, G., Sebenik, A., Osredkar, U., Veksli, Z. and Ranogaje, C., Grafting of waste rubber. *Rubber Chemistry and Technology,* **63**, 660-668 (1990).

21 Saville, B. and Watson, A. A., Structural characterization of sulfur-vulcanized rubber networks. *Rubber Chemistry and Technology,* **40**, 100-148 (1967).

22 Nicholas, P. P., The scission of polysulfide crosslinks in scrap rubber particles. *Rubber Chemistry and Technology,* **55**, 1499-1515 (1982).

23 Maduwage, S., Amarasinghe, A. D. U. S. and Munindradasa, A. D. I., Ultrasonic devulcanization of sulfur vulcanized natural rubber, presented at the Technical Sessions of the Institute of Engineers (Sri Lanka, 2004).

24 Kleps, T., Piaskiewicz, M. and Parasiewicz, W., The use of thermogravimetry in the study of rubber devulcanization. *Journal of Thermal Analysis and Calorimetry,* **60**, 271-277 (2000).

25 Dioa, B., Isayev, A. I. and Levin, V. Y., Basic study of continuous ultrasonic devulcanization of unfilled silicone. *Rubber Chemistry and Technology,* **72**, 152-164 (1999).

26 Levin, V. Y., Kim, S. H. and Isayev, A. I., Effect of crosslink type on the ultrasound devulcanization of SBR vulcanizates. *Rubber Chemistry and Technology,* **70**, 641-649 (1997).

27 Levin, V. Y., Kim, S. H., Isayev, A. I., Massey, J. and Meerawall, E. V., Ultrasound devulcanization of sulfur vulcanized SBR : Crosslink density and molecular mobility. *Rubber Chemistry and Technology,* **69**, 104-114 (1996).

28 Isayev, A. I., Chen, J. and Tukachinsky, A., Novel ultrasonic technology for devulcanization of waste rubbers. *Rubber Chemistry and Technology,* **68**, 267-280 (1995).

29 Warner, W., Methods of devulcanization. *Rubber Chemistry and Technology,* **67**, 559-566 (1994).

30 Wang, P. and Liu, S. Y., Recovery of waste rubber through pulverization at a low temperature of refrigeration by an air turbine. *Journal of Process Mechanical Engineering,* **213**, 135-138 (1999).

31 Burgoyne, M. D. and Evans, R. J. *Abstracts in Rubber Chemistry and Technology,* **51**, 385 (1978).

32 Beau, D. S. L., Science and technology of reclaimed rubber. *Rubber Chemistry and Technology,* **40**, 217-237 (1967).

33 Kawabata, N., Okuyama, B. and Yamashita, S., Reclamation of vulcanized rubber by chemical degradation. XV. Degradation of vulcanized synthetic isoprene by the phenylhydrazine-iron (II) chloride system. *Journal of Applied Polymer Science,* **26**, 1417-1419 (1981).

34 Klingensmith, B., Recycling, production and use of reprocessed rubbers. *Rubber World,* **203**, 16-21 (1991).

35 Yamashita, S., Kawabata, N., Sagan, S. and Hayashi, K., Reclamation of vulcanized rubbers by chemical degradation V. Degradation of vulcanized synthetic isoprene rubber by the phenylhydrazine-ferrous chloride system. *Journal of Applied Polymer Science,* **21**, 2201-2209 (1977).

36 SBP Board of Consultants and Engineers, *SBP Handbook of Rubber Projects, Technology and Product Formulary*, 3rd ed. (SBP Consultants and Engineers, Delhi, 1991).

37 Sutanto, P., Picchion, F., Janseen, L. P. B. M., Dijkhuis, K. A. J. and Dierkes, W. K., EPDM rubber reclaim from devulcanized EPDM. *Journal of Applied Polymer Science,* **102**, 5948-5957 (2006).

38 Ishiaku, U. S., Chong, C. S. and Ismail, H., Determination of optimum De-Link R concentration in a recycled rubber compound. *Polymer Testing,* **18**, 621-633 (1999).

39 De, D., Das, A., De , D., Dey, B., Debnath, S. C. and Roy, B. C., Reclaiming of ground rubber tire by a novel reclaiming agent. *European Polymer Journal,* **42,** 917-927 (2006).

40 Dodbiba, G., Haruki, N., Shibayama, A., Miyazaki, T. and Fujita, T., Combination of sink-float separation and flotation technique for purification of shredded PET-bottle from PE or PP flakes. *International Journal of Mineral Processing,* **65,** 11-29 (2002).

41 Ferrara, G., Bevilacqua, P., De Lorenzi, L. and Zanin, M., The influence of particle shape on the dynamic dense medium separation of plastics. *International Journal of Mineral Processing,* **59,** 225-235 (2000).

42 Sekhar, B. C., Kormer, V. A., Sotnikova, E. N., Mironyuk, V. P., Trunova, L. N. and Nikitina, N., Reclaiming of elastomeric materials Patent No. 5770632 (USA, 1998).

43 Department of Environment, F. a. R. A., Waste strategy 2000 for England and Wales Part 2, Available at www.defra.gov.uk/Environment/waste/strategy/cm4693/index.htm (2003).

44 Borgiannia, C., Filippisa, P. D., Pochetti, F. and Paolucci, M., Gasification process of wastes containing PVC. *Fuel,* **81,** 1827-1833 (2001).

45 Munoz, I., Rieradevall, J., Domenech, X. and Mila, L., LCA Application to integrated waste management planning in Gipuzkoa (Spain). *International Journal of Life Cycle Assessment,* **9,** 272-280 (2004).

46 Garforth, A. A., Ali, S., Martinez, J. H. and Akah, A., Feedstock recycling of polymer wastes. *Current Opinion in Solid State and Material Science,* **8,** 419-425 (2004).

47 Nomura, S. and Kato, K., Basic study on separate charge of coal and waste plastics in coke oven chamber. *Fuel,* **84,** 429-434 (2005).

48 Ali, S., Garforth, A. A., Harris, D. H., Rawlence, D. J. and Uemichi, Y., Polymer waste recycling over an used catalysts. *Catalysis Today,* **75,** 247-255 (2002).

49 Yoshioka, T., Kitagawa, E., Mizoguchi, T. and Okuwaki, A., High selective conversion of poly(ethylene terephthalate) into oil using Ca(OH)2. *Chemistry Letters,* **33,** 282-283 (2004).

50 Mastellone, M. L. and Arena, U., Bed defluidisation during the fluidised bed pyrolysis of plastic waste mixtures. *Polymer Degradation and Stability,* **85,** 1051-1058 (2004).

51 Uemura, Y., Azeura, M., Ohzuno, Y. and Hatate, Y., Flash-pyrolyzed product distribution of major plastics in a batch reactor. *Journal of Chemical Engineering of Japan,* **34**, 1293-1299 (2001).

52 Manos, G., Garforth, A. A. and Dwyer, J., Catalytic degradation of high-density polyethylene over different zeolitic structures. *Industrial and Engineering Chemistry Research,* **39**, 1198-1202 (2000).

53 Ding, W., Liang, J. and Anderson, L. L., Thermal and catalytic degradation of high density polyethylene and commingled post-consumer plastic waste. *Fuel Processing Technology,* **51**, 47-62 (1997).

54 Gobin, K. and Manos, G., Polymer degradation to fuels over microporous catalysts as a novel tertiary plastic recycling method. *Polymer Degradation and Stability,* **83**, 267-279 (2004).

55 Walendziewski, J. and Steininger, M., Thermal and catalytic conversion of waste polyolefines. *Catalysis Today,* **65**, 323-330 (2001).

56 Murthy, M. V. S., Rangarajan, P., Grulke, E. A. and Bhattacharyaa, D., Thermal degradation/hydrogenation of commodity plastics and characterization of their liquefaction products. *Fuel Processing and Technology,* **49**, 75-90 (1996).

57 Kaminsky, W., Predel, M. and Sadiki, A., Feedstock recycling of polymers by pyrolysis in a fluidised bed. *Polymer Degradation and Stability,* **85**, 1045-1050 (2004).

58 British Plastic Federation-Plastic Waste Management, Available at http://www.bpf.co.uk/bpfissues/waste/management.cfm (2003).

59 Kim, D., Shiu, F. J. Y. and Teh, F. Y., Devulcanization of scrap tire through matrix modification and ultrasonication. *Energy Sources,* **25**, 1099-1112 (2003).

60 San Miguel, G., Fowler, G. D., Dall'Orso, M. and Sollars, C. J., Porosity and surface characteristics of activated carbons produced from waste tyre rubber. *Journal of Chemical Technology and Biotechnology,* **77**, 1-8 (2002).

61 Uemura, Y., Ohe, H., Ohzuno, Y. and Hatate, Y., Formation of carbon and hydrogen from lower hydrocarbons in a packed bed of nickel-plated alumina balls. *Journal of Chemical Engineering of Japan,* **36**, 578-585 (2003).

62 Kawser, M. J. and Farid, N. A., Thermochemical processing of rubber waste to liquid fuel. *Plastics, Rubber and Composites,* **29**, 100-104 (2000).

63 Beckman, J. A., Crane, G., Kay, E. L. and Laman, J. R., Scrap tire disposal. *Rubber Chemistry and Technology,* **47**, 597-624 (1974).

64 Duraiappah, A. K., Xin, Z., Pieter, J. H. and Beukering, V., Issues in production, recycling and international trade: analyzing the Chinese plastic sector using an optimal life cycle (OLC) model. *Environment and Development Economics,* **7**, 47-74 (2002).

65 Constantine, H., The USA plastics recycling industry: a survey of manufacturers and vendors of recycled plastic products. *Environmental Conservation,* **26**, 125-135 (1999).

66 Perugini, F., Mastellone, M. L. and Arena, U., Life cycle assessment of mechanical and feedstock recycling options for management of plastic packaging wastes. *Environmental Progress,* **24**, 137-154 (2005).

67 Lebreton, B. and Tuma, A., A quantitative approach to assessing the profitability of car and truck tire remanufacturing. *International Journal of Production Economics,* **104**, 639-652 (2006).

68 Boughton, B. and Horvath, A., Environmental assessment of shredder residue management. *Resources, Conservation and Recycling,* **47**, 1-25 (2006).

69 Corti, A. and Lombardi, L., End life tyres: Alternative final disposal processes compared by LCA. *Energy,* **29**, 2089-2108 (2004).

70 Arena, U., Mastellone, M. L. and Perugini, F., Life cycle assessment of a plastic packaging recycling system. *International Journal of Life Cycle Assessment,* **8**, 92-98 (2003).

71 Tripathy, A. R., Morin, J. E., Williams, D. E., Eyles, S. J. and Farris, R. J., A novel approach to improving the mechanical properties in recycled vulcanized natural rubber and its mechanism. *Macromolecules,* **35**, 4616-4627 (2002).

72 Lapcik, L., Augustin, P., Pistek, A. and Bujnoch, L., Measurement of the dynamic stiffness of recycled rubber based railway track mats according to the DB-TL 918.071 standard. *Applied Acoustics,* **62**, 1123-1128 (2001).

73 Cruz, S. A. and Zanin, M., Evaluation and identification of degradative processes in post-consumer recycled high-density polyethylene. *Polymer Degradation and Stability,* **80**, 31-37 (2003).

74 Accetta, A. and Vergnaud, J. M., Rubber recycling- upgrading of scrap rubber powder by vulcanization. II. *Rubber Chemistry and Technology,* **55**, 961-966 (1982).

75 Accetta, A. and Vergnaud, J. M., Rubber Recycling-upgrading of scrap rubber powder by vulcanization without new rubber. *Rubber Chemistry and Technology,* **54**, 302-310 (1981).

76 Ambrose, C. A., Hooper, R., Potter, A. K. and Singh, M. M., Diversion from landfill: quality products from valuable plastics. *Resources, Conservation and Recycling,* **36**, 309-318 (2002).

77 Jacob, C., Bhowmick, A. K. and De, S. K., Studies on ground EPDM vulcanizate as filler in window seal formulation. *Plastics, Rubber and Composites,* **31**, 212-219 (2002).

78 Phadke, A., Bhattacharya, A., Chakraborty, S. and De, S. K., Studies of vulcanization of reclaimed rubber. *Rubber Chemistry and Technology,* **56**, 726-736 (1983).

79 Burgoyne, M. D., Leaker, G. and Krekic, Z., The effect of reusing ground flash and scrap rubber in parent compound. *Rubber Chemistry and Technology,* **49**, 375-378 (1976).

80 Peterson, L. B., Moriartyt, J. T. and Bryant, W. C., Use of cryogenically ground rubbers. *Abstracts in Rubber Chemistry and Technology,* **51**, 386 (1978).

81 Frantzis, P., Development of crumb rubber reinforced bituminous binder under laboratory conditions. *Journal of Materials Science,* **38**, 1397-1401 (2003).

82 Segre, N., Monteiro, P. J. M. and Sposito, G., Surface characterization of recycled tire rubber to be used in cement paste matrix. *Journal of Colloid and Interface Science,* **248**, 521-523 (2002).

83 Raghavan, D., Study of rubber-filled cementitious composites. *Journal of Applied Polymer Science,* **77**, 934-942 (2000).

84 Nehdi, M. and Khan, A., Cementitious composites containing recycled tire rubber: An overview of engineering properties and potential applications. *Cement, Concrete and Aggregates,* **23**, 3-10 (2001).

85 Kim, J. K., Experimental and theoretical studies on crumb rubber/polyurethane blend system. *Korea Polymer Journal,* **5**, 241-247 (1997).

86 Myhre, M. J. M., D. A., Rubber recycling. *Rubber Chemistry and Technology,* **75**, 429-474 (2002).

87 Ishiaku, U. S., Chong, C. S. and Ismail, H., Cure characteristics and vulcanizate properties of a natural rubber compound extended with convoluted rubber powder. *Polymer Testing,* **19**, 507-521 (2000).

88 Burford, R. P. and Pittolo, M., Fracture morphology of rubber compounds containing recycled rubber powder. *Journal of Materials Science Letters,* **2,** 422-424 (1983).

89 Ismail, H. and Suryadiansyah, H., Thermoplastic elastomers based on polypropylene/natural rubber and polypropylene/recycle rubber blends. *Polymer Testing,* **21,** 389-395 (2002).

90 Kumnuantip, C. and Sombatsompop, N., Dynamic mechanical properties and swelling behaviour of NR/reclaimed rubber blends. *Materials Letters,* **57,** 3167-3174 (2003).

91 Mathew, G., Singh, R. P., Nair, N. R. and Thomas, S., Development and characterization of novel EPDM/NR prophylactic waste composites. *Journal of Materials Science,* **38,** 2469-2481 (2003).

92 Fukumori, K., Matsushita, M., Okamoto, H., Sato, N., Suzuki, Y. and Takeuchi, K., Recycling technology of tire rubber. *JSAE Review,,* **23,** 259-264 (2002).

93 Cavalieri, F. and Padella, F., Development of composite materials by mechanochemical treatment of post-consumer plastic waste. *Waste Management,* **22,** 913-916 (2002).

94 Bertin, S. and Robin, J.-J., Study and characterization of virgin and recycled LDPE/PP blends. *European Polymer Journal,* **38,** 2255-2264 (2002).

95 Sonnier, R., Leroy, E., Clere, L., Bergeret, A. and Lopez-Cuesta, J. M., Polyethylene/ground tyre rubber blends: Influence of particle morphology and oxidation on mechanical properties. *Polymer Testing,* **26,** 274-281 (2007).

96 Jose, J., Satapathy, S., Nag, A. and Nando, B., Modification of waste polypropylene with waste rubber dust from textile industry and its characterization. *Process Safety and Environmental Protection,* **85,** 318-326 (2007).

97 Gabriele, M. C., Move over rubber- today's TPEs have more to give. *Plastics Technology,* **41,** 42-47 (1995).

98 Begin, S., Problem solver- Evans tackles recycling with rubber-plastic combo. *Rubber and Plastic News,* **September 20,** 70-73 (1999).

99 Statham, B., Introduction to TPE technology. *European Rubber Journal,* **186,** 28 (2004).

100 Ibrahim, A. and Dahlan, M., Thermoplastic-natural rubber blends. *Progress in Polymer Science,* **23,** 665-706 (1998).

101 Rajalekshmi, S. and Joseph, R., Studies on the blends of low density polyethylene and linear low density polyethylene with modified latex product waste. *Polymer Recycling,* **6**, 99-107 (2001).

102 Liu, H. S., Richard, C. P., Mead, J. L. and Stacer, R. G., Development of novel applications for using recycled rubber in thermoplastics Report No. 18 (Chelsea Center for Recycling and Economic Development, Massachusetts, 2000).

103 Van der Wal, A. M., J. J., Oderkerk, J. and Gaymans, R. J., Polypropylene-rubber blends- 1. The effect of the matrix properties on the impact behaviour. *Polymer,* **39**, 6781-6787 (1998).

104 George, S., Joseph, R., Thomas, S. and Varughese, K. T., Blends of isotactic polypropylene and nitrile rubber: morphology, mechanical properties and compatibilization. *Polymer,* **36**, 4405-4416 (1995).

105 Halimatuddahliana, Ismail, H. and Akil, H., The effect of HVA-2 addition on the properties of PP-EPDM-NR ternary blends. *Journal of Elastomers and Plastics,* **37**, 55-72 (2005).

106 George, S., Prasannakumari, L., Koshy, P., Varughese, K. T. and Thomas, S., Tearing behavior of blends of isotactic polypropylene and nitrile rubber: Influence of blend ratio, morphology and compatibilizer loading. *Materials Letters,* **26**, 51-58 (1996).

107 Kocsis, J. K., *Polypropylene- Structure, Blends and Composites -Volume II* (Chapman and Hall, UK, 1995).

108 Utracki, L. A., *Polymer Alloys and Blends* (Hanser, New York, 1989).

109 George, J., Varughese, K. T. and Thomas, S., Dynamically vulcanized thermoplastic elastomer blends of polyethylene and nitrile rubber. *Polymer,* **41**, 1507-1517 (2000).

110 Halimatuddahliana and Ismail, H., Thermoplastic elastomer based on PP/EPDM/ENR25 and PP/EPDM/NR blends. *Polymer - Plastics Technology and Engineering,* **43**, 357-368 (2004).

111 Liu, H. S., Mead, J. L. and Stacer, R. G., Process development of scrap rubber / thermoplastic blends Report No. 36 (Chelsea Center for Recycling and Economic Development, Massachusetts, 2001).

112 Liu, H. S., Mead, J. L. and Stacer, R. G., Thermoplastic elastomers and rubber-toughened plastics from recycled rubber and plastics. *Rubber Chemistry and Technology,* **75**, 49-64 (2002).

113 Pramanik, P. K. and Baker, W. E., Toughening of ground rubber tire filled thermoplastic compounds using different compatibilizer systems. *Plastics, Rubber and Composites Processing and Applications,* **24,** 229-237 (1995).

114 Goncharuk, G. P., Knunyants, M. I., Kryuchkav, A. N. and Obolonkova, E. S., Effect of the specific surface area and the shape of rubber crumb on the mechanical properties of rubber-filled plastics. *Polymer Science. Series B,* **40,** 166-169 (1998).

115 Sonnier, R., Leroy, E., Bergeret, J.-M., A.-S., L. C. and Bretella, P. L., Compatibilizing Thermoplastic/ground tyre rubber powder blends: Efficiency and Limits. *Polymer Testing,* **27,** 901-907 (2008).

116 Ismail, H., Awang, M. and Hazizan, M. A., Effect of waste tire dust size on the mechanical and morphological properties of polypropylene/waste tire dust blends. *Polymer Plastics Technology and Engineering,* **45,** 463-468 (2006).

117 Zhang, S. L., Xin, Z. X., Zhang, Z. X. and Kim, J. K., Characterizing of the properties of thermoplastic elastomers conatining waste rubber tyre powder. *Waste Management,* **29,** 1480-1485 (2009).

118 Rajalingam, P. and Baker, W. E., The role of functional polymers in ground rubber tire-polyethylene composite. *Rubber Chemistry and Technology,* **65,** 908-916 (1992).

119 Pramanik, P. K. and Baker, W. E., LLDPE composites filled with corona discharge treated ground rubber tire crumb. *Journal of Elastomers and Plastics,* **27,** 253 (1995).

120 Brydson, J. A., *Plastics Materials,* 7th ed. (Butterworth-Heinemann, Oxford, 1999).

121 Kumar, C. R., Fuhrmann, I. and Kocsis, J. K., LDPE-based thermoplastic elastomers containing ground tire rubber with and without dynamic curing. *Polymer Degradation and Stability,* **76,** 137-144 (2002).

122 Scaffaro, R., Dintcheva, T., La Mantia, F. P. and Nocilla, M. A., Formulation, characterization and optimization of the processing condition of blends of recycled polyethylene and ground tyre rubber: Mechanical and rheological analysis. *Polymer Degradation and Stability,* **90,** 281-287 (2005).

123 Ismail, H., Nordina, R. and Noorb, A. M., Cure characteristics, tensile properties and swelling behaviour of recycled rubber powder-filled natural rubber compounds. *Polymer Testing,* **21,** 565-569 (2002).

124 Malaika, S. A., *Reactive Modifiers for Polymers* (Blackie Academic and Professional, UK, 1997).

125 Mousa, A., Ishiaku, U. S. and Ishak, Z. A. M., Rheological properties of dynamically vulcanized poly(vinyl chloride)/epoxidized natural rubber thermoplastic elastomers: Effect of processing variables. *Polymer Testing,* **19,** 193-204 (2000).

126 Bhowmick, A. K. and White, J. R., Thermal, UV- and sunlight ageing of thermoplastic elastomeric natural rubber-polyethylene blends. *Journal of Materials Science,* **37,** (2002).

127 Asaletha, R., Kumarana, M. G. and Thomas, S., Thermoplastic elastomers from blends of polystyrene and natural rubber: morphology and mechanical properties. *European Polymer Journal,* **35,** 253-271 (1999).

128 Dao, K. C., Mechanical properties of polypropylene/crosslinked rubber blends. *Journal of Applied Polymer Science,* **27,** 4799-4806 (1982).

129 Burford, R. and Pittolo, M., Characterization and performance of powdered rubber. *Rubber Chemistry and Technology,* **55,** 1233-1249 (1982).

130 Pedersen, T., Reynolds, C. and Pool, M., Recycling ultra-fine car tyre rubber in synthetic roof slates (Airport Business Centre, Oxon, 2007).

131 Rajalingam, P., Sharpe, J. and Baker, W. E., Ground rubber tire / thermoplastic composites: effect of different ground rubber tires. *Rubber Chemistry and Technology,* **66,** 664-692 (1993).

132 Anandhan, S., De, P. P., De, S. K., Bhowmick, A. K. and Swayajith, S., Thermorheological properties of thermoplastic elastomeric blends of NBR/SAN containing waste nitrile rubber vulcanizate powder. *Polymer Library (formerly Rapra Abstracts),* **57,** 599-608 (2004).

133 Mangaraj, D., in *Rubber Recycling,* edited by De, S. K., Isayev, A. I., and Khait, K. (American Chemical Society, USA, 2004).

134 Shaltout, N. A., Zeid, A. M. M., Aziz, A. M. M. and Miligy, A. A., Yielding behaviour of thermoplastic/elastomer blends cured by gamma irradiation. *Polymer International,* **50,** 263-270 (2001).

135 Oh, J. S., Isayev, A. I. and Rogunova, M. A., Continuous ultrasonic process for in situ compatibilization of polypropylene/natural rubber blends. *Polymer,* **44,** 2337-2349 (2003).

136 Isayev, A. I. and Hong, C. K., Novel ultrasonic process for in-situ copolymer formation and compatibilization of immiscible polymers. *Polymer Engineering and Science,* **43**, 91-101 (2003).

137 Hong, C. K. and Isayev, A. I., Plastic/rubber blends of ultrasonically devulcanized GRT with HDPE. *Journal of Elastomers and Plastics,* **33**, 47-71 (2001).

138 Shanmugharaj, A. M., Kim, J. K. and Ryu, S. H., UV surface modification of waste tire powder: Characterization and its influence on the properties of polypropylene/waste powder composites. *Polymer Testing,* **24**, 739-745 (2005).

139 Hassani, A., Ganjidoust, H. and Maghanaki, A. A., Use of plastic waste (poly-ethylene terephthalate) in asphalt concrete mixture as aggregate replacement. *Waste Management and Research,* **23**, 322-327 (2005).

140 Phynyocheep, P., Axtell, F. H. and Laosee, T., Influence of compatibilizers on mechanical properties, crystallization, and morphology of polypropylene/scrap rubber dust blends. *Journal of Applied Polymer Science,* **86**, 148-159 (2002).

141 Choudhury, N. R. and Bhowmick, A. K. *Journal of Adhesion Science Technology,* **2**, 357-368 (1998).

142 Choudhury, N. R. and Bhowmick, A. K., Influence of interaction promoter on the properties of thermoplastic elastomeric blends of natural rubber and polyethylene. *Journal of Materials Science,* **23**, 2187-2194 (1988).

143 Qin, C., Yin, J. and Huang, B., Compatibilization of natural rubber/polyethylene blends by polyethylene-b-polyisoprene diblock copolymers. *Polymer,* **31**, 663-667 (1990).

144 Kuriakose, B., Chakraborthy, S. K. and De, S. K., Scanning electron microscopy studies on tensile failure of thermoplastic elastomers from polypropylene- natural rubber blends. *Materials Chemistry and Physics,* **12**, 157-170 (1985).

145 De, S. K. and Bhowmick, A. K., *Thermoplastic Elastomers from Rubber Thermoplastic Blends* (Ellis Harwood, England, 1990).

146 Thitithammawonga, A., Nakasona, C., Sahakaroa, K. and Noordermeerb, J., Effect of different types of peroxides on rheological, mechanical, and morphological properties of thermoplastic vulcanizates based on natural rubber/polypropylene blends. *Polymer Testing,* **26**, 537-546 (2007).

147 Varughese, S., Alex, R. and Kuriakose, B., Natural rubber-isotactic polypropylene thermoplastic blends. *Journal of Applied Polymer Science,* **92**, 2063-2068 (2004).

148 Elliott, D. J., in *Thermoplastic Elastomers from Rubber Thermoplastic Blends*, edited by De, S. K. and Bhowmick, A. K. (Ellis Horwood, England, 1990).

149 Norzalia, S., Hanim, H. and Faud, M. Y. A., The effect of addition of bismaleimide and maleated PP wax on the crystallization and mechanical properties of PP/NR blends. *Plastics, Rubber and Composites Processing and Applications,* **22**, 185-193 (1994).

150 Coran, A. Y. and Patel, R. P., Thermoplastic compositions of high unsaturation diene rubber and polyolefin resin Patent No. U. S. Patent 4,104,210 (USA, 1978).

151 Tinker, A. J., Preparation of polypropylene/natural rubber blends having high impact strength at low temperatures. *Polymer Communication,* **25**, 325-326 (1984).

152 Kuriakose, B., The effect of PF resin-zinc oxide system as curative for soft thermoplastic NR:PP blends. *Rubber World,* **August, 1**, (1990).

153 Coran, A. Y. and Patel, R. P., Elastoplastic compositions of cured diene rubber and polypropylene Patent No. 4271049 (United States, 1981).

154 Nakason, C., Wannavilai, P. and Kaesaman, A., Effect of vulcanization system on properties of thermoplastic vulcanizates based on epoxidized natural rubber/ polypropylene blends. *Polymer Testing,* **25**, 34-41 (2006).

155 Tantayanon, S. and Juikham, S., Enhanced toughening of polypropylene with reclaimed tire rubber. *Journal of Applied Polymer Science,* **91**, 510-515 (2004).

156 Shanmugharaj, A. M., Modification of rubber powder with peroxide and properties of polypropylene/rubber composites. *Journal of Applied Polymer Science,* **104**, 2237-2243 (2007).

157 Sain, M. M., Lacok, J., Beniska, J. and Bina, J., Estimation of cure charcateristics of natural rubber -polyethylene blends by use of a rheometer. *Acta Polymerica,* **2**, 136 (1989).

158 Naskar, A. K., Bhowmick, A. K. and De, S., Thermoplastic elastomeric composition based on ground rubber tire. *Polymer Engineering and Science,* **41**, 1087-1098 (2001).

159 Awang, M. and Ismail, H., Preparation and characterization of polypropylene/waste tyre dust blends with addition of DCP and HVA-2 ($PP/WTD_{P\text{-}HVA\text{-}2}$). *Polymer Testing,* **27**, 321-329 (2008).

160 Tawney, P. O., Wenisch, W. J., Van der Burg, S. and Relyea, D. I., Vulcanization with maleimides. *Journal of Applied Polymer Science,* **8**, 2281-2298 (1964).

161 Inoue, T., Selective crosslinking in polymer blends I Novel selective crosslink system for polypropylene/ unsaturated elastomer blends. *Journal of Applied Polymer Science,* **54**, 709-721 (1994).

162 Inoue, T., Selective crosslinking in polymer blends II Its effect on impact strength and other mechanical properties of polypropylene/ unsaturated elastomer blends. *Journal of Applied Polymer Science,* **54**, 723-733 (1994).

163 Medsker, R. E., Gilbertson, G. W. and Patel, R., Preferred structure of phenolic resin curative for thermoplastic vulcanizate Patent No. 5952425 (U S, 1999).

164 Abdous-Sabet, S., Puydak, R. C. and Rader, C. P., Dynamically vulcanized thermoplastic elastomers. *Rubber Chemistry and Technology,* **69**, 476 (1996).

165 Coran, A. Y., Patel, R. P. and D. Williams-Headd, D., Rubber-thermoplastic compositions. Part IX. Blends of dissimilar rubbers and plastics with technological compatibilization. *Rubber Chemistry and Technology,* **58**, 1014-1023 (1985).

166 Ghassem, N., Nouri, M. R., Mehrabzadeh, M. and Bakhshandeh, G. R., Studies on dynamic vulcanization of PP/NBR thermoplastic elastomer blends. *Indian Polymer Journal,* **8**, 37-42 (1999).

167 Coran, A. Y. and Patel, R. P., Rubber-thermoplastic compositions. Part VIII. Nitrile rubber polyolefin blends with technological compatibilization. *Rubber Chemistry and Technology,* **56**, 1045-1065 (1983).

168 Naskar, A. K., De, S. K. and Bhowmick, A. K., Thermoplastic elastomeric composition based on maleic anhydride -grafted ground rubber tire. *Journal of Applied Polymer Science,* **84**, 370-378 (2002).

169 Kohler, R., New technology for the devulcanization of sulfur-cured scrap elastomers. *Rubber World,* **216**, 32 (1997).

170 Sekhar, B. C., Kormer, V. A., Sotnikova, E. N., Mironyuk, V. P., Trunova, L. N. and Nikitina, N., Improvements in and relating to the reclaiming elastomeric materials Patent No. CA 2152641 (Canada, 1996).

171 Wellappilli, C. J., de Silva, K., Dharmatilake, M. and Denawaka, I., Effect of chemically treated buffing dust on technological properties of tyre tread compounds. *Progress in Rubber, Plastics and Recycling Technology,* **23**, 1-20 (2007).

172 Engineers, S. B. o. C., *SBP Handbook of Rubber Projects, Technology and Product Formulary*, 3d rev. ed. ed. (SBP Consultants & Engineers, Delhi, 1991).

173 Saeki, K., Funatsu, K. and Tanabe, K., Discrimination of poly(vinyl chloride) samples with different plasticizers and prediction of plasticizer contents in poly(vinyl chloride) using near-infrared spectroscopy and neural-network analysis. *Analytical Sciences,* **19**, 309-312 (2003).

174 Rouilly, A. and Rigal, L., Agro-materials: A bibliographic review. *Journal of Macromolecular Science - Polymer Reviews,* **42**, 441-479 (2002).

175 Kowalska, E., Wielgosz, Z. and Pelka, J., Use of post-life waste and production waste in thermoplastic polymer compositions. *Polymers and Polymer Composites,* **10**, 83-91 (2002).

176 Rodrigues, E. L., Effect of cryogenically ground rubber on some mechanical properties of an unsaturated polyester resin. *Polymer Engineering and Science,* **28**, 1455-1461 (1988).

177 Flory, P. J., *Principles of Polymer Chemistry* (Cornell University Press, New York, 1953).

178 Kumar, A. and Guptha, R. K., *Fundamentals for Polymer Engineering*, 2nd ed. (Marcel Dekker Inc., New York, 2003).

179 Lipatov, Y. S. and Nesterov, A. E., *Thermodynamics of Polymer Blends- Volume I* (Technomic Publishing Company, USA, 1997).

180 Datta, S. and Lahose, D. J., *Polymeric Compatibilizers* (Hanser Publications Inc., New York, 1996).

181 Feldman, D., Polyblend compatibilization. *Journal of Macromolecular Science - Pure and Applied Chemistry,* **42 A**, 587-605 (2005).

182 Solc, K., *Polymer Compatibility and Incompatibility- Principles and Practices* (Harwood Academic Publishers, New York, 1982).

183 Van Dijk, M. A. and Wakker, A., *Concepts of Polymer Thermodynamics* (Technomic Publishing Company Inc., USA, 1997).

184 Paul, R. D. and Newman, S., *Polymer Blends- Volume 1* (Academic Press, New York, 1981).

185 Utracki, L. A., *Commercial Polymer Blends* (Chapman and Hall, UK, 1998).

186 Rajeev, R. S. and De, S. K., Thermoplastic elastomers based on waste rubber and plastics. *Rubber Chemistry and Technology,* **77**, 569-577 (2004).

187 Danesi, S. and Porter, R. S., Blends of isotactic polypropylene and ethylene propylene rubbers: rheology, morphology and mechanics. *Polymer,* **19**, 448-457 (1978).

188 Volfson, S. A. and Nikolskii, V. G., Processing and re-use of scrap tyres and rubber products in the tyre and mechanical rubber goods. *International Polymer Science and Technology,* **25**, 93-99 (1998).

189 Koning, C., Van Duin, M., Pagnoulle, C. and Jerome, R., Strategies for compatibilization of polymer blends. *Progress in Polymer Science,* **23**, 707-757 (1998).

190 Yusof, A. M. M., PhD Thesis, Loughborough University, 1999.

191 White, J. L., Coran, A. Y. and Moet, A., *Polymer Mixing- Technology and Engineering* (Hanser Publishers, Munich, 1998).

192 Paul, D. C. and Bucknall, C. B., *Polymer Blends- Volume 2 : Performance* (John Willey and Sons, Canada, 2000).

193 Antony, P. and De, S. K., Ionic thermoplastic elastomers: A review. *Journal of Macromolecular Science - Polymer Reviews,* **41**, 41-77 (2001).

194 Mousa, A., The effect of dynamic vulcanization on the mechanical properties of EPDM/PP thermoplastic elastomers. *International Journal of Polymeric Materials,* **54**, 619-631 (2005).

195 Riahi, F., Benachour, D. and Douibi, A., Dynamically vulcanized thermoplastic elastomer blends of natural rubber and polypropylene. *International Journal of Polymeric Materials,* **53**, 143-156 (2004).

196 Jha, A. and Bhowmick, A. K., Mechanical and dynamic mechanical thermal properties of heat- and oil-resistant thermoplastic elastomeric blends of poly(butylene terephthalate) and acrylate rubber. *Journal of Applied Polymer Science,* **78**, 1001-1008 (2000).

197 Inoue, T. and Suzuki, T., Selective crosslinking reaction in polymer blends III The effect of the crosslinking of dispersed EPDM particles on the impact behaviour of PP/EPDM blends. *Journal of Applied Polymer Science,* **59**, 1113-1125 (1995).

198 Coran, A. Y. and Patel, R. P., Thermoplastic compositions of high unsaturation diene rubber and polyolefin resin Patent No. 4104210 (USA, 1975).

199 Nakason, C., Nuansomsri, K., Kaesaman, A. and Kiatkamjornwong, S., Dynamic vulcanization of natural rubber/high-density polyethylene blends:Effect of compatibilization, blend ratio and curing system. *Polymer Testing,* **25**, 782-796 (2006).

200 Awang, A., Ismail, H. and Hazizan, M. A., Processing and properties of polypropylene-latex modified waste tyre dust blends. *Polymer Testing,* **27**, 93-99 (2008).

201 Clark, D. E., Folz, D. C. and West, J. K., Processing materials with microwave energy. *Materials Science and Engineering A: Structural Materials: Properties, Microstructure and Processing,* **287**, 153-158 (2000).

202 Lai, C.-P., Tsai, M.-H., Chen, M., Chang, H.-S. and Tay, H.-H., Morphology and properties of denture acrylic resins cured by microwave energy and conventional water bath. *Dental Materials,* **20**, 133-141 (2004).

203 Zhou, J., Shi, C., Mei, B., Yuan, R. and Fu, Z., Research on the technology and the mechanical properties of the microwave processing of polymer. *Journal of Materials Processing Technology,* **137**, 156-158 (2003).

204 Boey, F. Y. C. and Lye, S. W., Void reduction in autoclave processing of thermoset composites. II: Void reduction in a microwave curing process. *Composites,* **23**, 266-270 (1992).

205 Antonio, C. and Deam, R. T., Comparison of linear and non-linear sweep rate regimes in variable frequency microwave technique for uniform heating in materials processing. *Journal of Materials Processing Technology,* **169**, 234-241 (2005).

206 Ku, H. S., Siu, F., Siores, E., Ball, J. A. R. and Blicblau, A. S., Applications of fixed and variable frequency microwave (VFM) facilities in polymeric materials processing and joining, presented at the 5th Asia Pacific Conference on Materials Processing (Seoul, 2001).

207 Dao, K. C., Toughness evaluation of blends of polypropylene/cross-linked rubber using the instrumented high-speed puncture test, presented at the ANTEC 83: Plastics -Engineering today for tomorrow's world (Chicago, 1983).

208 Anonymous, Mat Web Data Sheets, Available at www.matweb.com.

209 Muratoglu, O. K., Argon, A. S. and Cohen, R. E., Crystalline morphology of polyamide-6 near planar surfaces. *Polymer,* **36**, 2143-2152 (1995).

210 Nourry, A., *Reclaimed Rubber- It's Development, Applications and Future* (Mc. Learn & Sons Ltd., London, 1962).

211 Rodger, M. B., Rubber tires. *Encyclopedia of Materials: Science and Technology,* 8237-8242 (2007).

212 Mark, J. E., Erman, B. and Eirich, E. R., *Science and Technology of Rubbers*, 3rd ed. (Elseveir, USA, 2005).

213 Kocsis, J. K., *Polypropylene- Structure, Blends and Composites -Volume I* (Chapman and Hall, UK, 1995).

214 Jimenez, A., Torre, L. and Kenny, J. M., Processing and properties of recycled polypropylene modified with elastomers. *Plastics, Rubber and Composites,* **32**, 357-367 (2003).

215 Stromberg, E., Fransisco, V., Staffan, A. and Amparo, R. G. K., Quality assessment of recycled plastics, presented at the Identiplast 2005 - Identify the opportunities for plastics recovery (Brussels, 2005).

216 Morton, M., *Rubber Technology* (Van Nostrad Reinhold, New York, 1987).

217 Brandrup, J. and Immergut, E. H., *Polymer Handbook,* 2nd ed. (Willey Inter Science, 1975).

218 Ward, I. M., *An Introduction to Mechanical Properties of Solid Polymers* (John Wiley and Sons, New York, 1983).

219 Crazing, Available at http://www.specialchem4polymers.com/tc/MBS-Impact-Modifiers/index.aspx?id=crazing.

220 Kocsis, J. K., *Polypropylene- Structure, Blends and Composites- Volume III: Composites* (Chapman and Hall, UK, 1995).

221 Shear yielding Available at http://www.specialchem4polymers.com/tc/Acrylic-Impact-Modifiers/index.aspx?id=2908.

222 Bartczak, Z., Argon, A. S., Cohen, R. E. and Weinberg, M., Toughness mechanism in semi-crystalline polymer blends-I: High density polyethylene toughened with rubbers. *Polymer,* **40**, 2331-2346 (1999).

223 Zebarjad, S. M., Begheri, R., Lazzer, A., Reihani, S. M. S. S. and Frounchi, M., Fracture mechanism under dynamic loading of elastomer-modified polypropylene. *Materials Letters,* **57**, 2733-2741 (2003).

224 Zebarjad, S. M., Begheri, R., Lazzeri, A. and Serajzadeh, S., Fracture behaviour of isotactic propylene under static loading condition. *Materials and Design*, 105-109 (2003).

225 Van der Wal, A., Mulder, J. J., Thijs, H. A. and Gaymans, R. J., Fracture of polypropylene 1. The effect of molecular weight and temperature at low and high test speed. *Polymer,* **39**, 5467-5475 (1998).

226 Van der Wal, A., Mulder, J. J. and Gaymans, R. J., Fracture of polypropylene 2: The effect of crystallinity. *Polymer,* **39**, 5477-5481 (1998).

227 Wei, G. X., Fracture behaviour of styrene-ethylene-propylene rubber -toughened polypropylene. *Polymer Engineering and Science,* **40**, 1979-1988 (2000).

228 Wei, G. X., Sue, H. J., Chu, J., Haung, C. and Gong, K., Toughening and strengthening of polypropylene using the rigid-rigid polymer toughening concept. *Polymer,* **41**, 2947-2960 (2000).

229 Li, Y., Wei, G.-X. and Sue, H.-J., Morphology and toughening mechanisms in clay-modified styrene-butadiene-styrene rubber-toughened polypropylene. *Journal of Materials Science,* **37**, 2447-2459 (2002).

230 Dasari, A., Rohrmann, J. and Misra, R. D. K., Microstructural evolution during tensile deformation of polypropylenes. *Materials Science and Engineering,* **A351**, 200-213 (2003).

231 Liang, J. Z. and Li, R. K. Y., Rubber toughening in polypropylene. *Journal of Applied Polymer Science,* **77**, 409-417 (2000).

232 Argon, A. S. and Cohen, R. E., Toughenability of polymers. *Polymer,* **44**, 6013-6032 (2003).

233 Kolarik, J. and Jancar, J., Ternary composites of polypropylene/elastomer/calcium carbonate: Effect of functionalized components on phase structure and mechanical properties. *Polymer,* **33**, 4961-4967 (1992).

234 Chow, W. S., Bakar, A. A., Ishak, Z. A. M., Kocsis, J. K. and Ishiaku, U. S., Effect of maleic anhydride-grafted ethylene-propylene rubber on the mechanical properties of organoclay reinforced polyamide 6/ polypropylene nanocomposites. *European Polymer Journal,* **41**, 687-696 (2005).

235 Friedrich, K., Ruan, W. H. and Zhang, M. Q., Structure -property relationship if in-situ crosslinking modified nano-silica filled polypropylene composites, presented at the Polymers for Advanced Technologies International Symposium (Hungary, 2005).

236 Jang, B. Z., Uhlmann, D. R. and Sande, J. B. V., The rubber particle size dependence of crazing in polypropylene. *Polymer Engineering and Science,* **25**, 643-651 (1985).

237 Van der Wal, A., Nijhof, R. and Gaymans, R. J., Polypropylene-rubber blends 2: the effect pf the rubber content on the deformation and impact behaviour. *Polymer,* **40**, 6031-6044 (1999).

238 Van der Wal, A. and Gaymans, R. J., Polypropylene-rubber blends 3: The effect of the test speed on the fracture behaviour. *Polymer,* **40**, 6045-6055 (1999).

239 Hornsby, P. R. and Premphet, K., Fracture toughness of multiphase polypropylene composites containing rubbery and particulate inclusions. *Journal of Materials Science,* **32**, 4767-4775 (1997).

240 Van der Wal, A., Polypropylene-rubber blends 5: Deformation mechanism during fracture. *Polymer,* **40**, 6067-6075 (1999).

241 Kovacic, P. and Hein, R. W., Cross-linking of unsaturated polymers with dimaleimides. *Journal of the American Chemical Society,* **81**, 1190-1194 (1959).

242 Class, J. B., A review of fundamentals of crosslinking with peroxides. *Rubber World,* **220**, 35 (1999).

243 Naskar, K., PhD, University of Twente, 2004.

244 Lamb, J., Phenolic resins for curing elastomers, presented at the Xiamen pharmaceutical stopper seminar, 2003).

245 Van Duin, M. and Souphanthong, A., The chemistry of phenol-formaldehyde resin vulcanization of EPDM: Part I. Evidence for methylene crosslinks. *Rubber Chemistry and Technology,* **68**, 717 (1995).

246 Ignatz-Hoover, F., Review of vulcanization chemistry. *Rubber World,* **220**, 24 (1999).

247 Best practices in scrap tires and rubber recycling: Chemical devulcanization, Available at http://www.cwc.org/tire_bp/t_bp_pdf/T2-04-01.PDF (2007).

248 Rubber Recycling, Available at http://practicalaction.org/practicalanswers/product_infor.php?products_id=186{1}1.

249 Handbook of Fine Chemicals, in *Aldrich Catalogue* (2003), pp. T 848.

250 The Technical Adviser, *Product data sheet of SP 1045H* (SI Group Incorporation, USA).

251 Hofmann, W. ed., *Vulcanization and vulcanizing Agents.* (McLaren and Sons, London, 1967).

252 Ohm, R. F., Rubber chemicals, Available at http://mrw.interscience.willey.com/9780471238966/kirk/article/rubbohm.a01/current.pdf (1997).

253 Marques, M. F. V., Poloponsky, M. and Chaves, E. G., Influence of the elastomeric polypropylene addition on the properties of commercial metallocenic polypropylene. *Materials Research,* **4**, 251-254 (2001).

254 Plastics - Determination of the melt mass - flow rate and the melt volume - flow rate of thermoplastics Report No. BS EN ISO 1133: 2005 Procedure A (British Standards, 2005).

255 Brown, R., *Physical Testing of Rubbers*, 4th ed. (Springer Incorporation, USA, 2006).

256 Plastics - Determination of Tensile Properties Report No. BS EN ISO 527:1996 (British Standards, 1996).

257 Plastics- Films and Sheeting; Determination of Tear Resistance Report No. BS EN ISO 6383-1:2004 (British Standards, 2004).

258 Groenewood, W. M., *Characterisation of Polymers by Thermal Analysis* (Elsevier Science Netherlands, 2001).

259 Kong, X., Yang, X., Li, G., Zhao, X., Zhou, E. and Ma, D., Nonisothermal crystallization kinetics: Poly(ethylene terephthalate)-poly(ethylene oxide) segmented copolymer and poly(ethylene oxide) homopolymer. *European Polymer Journal,* **37**, 1855-1862 (2001).

260 Michico, S., *Comprehensive Handbook of Calorimetry and Thermal Analysis* (John Willey and Sons, England, 2004).

261 Mathot, V. B. F., *Calorimetry and Thermal Analysis of Polymers* (Hanser Publications, New York, 1994).

262 Available at http://en.wikipedia.org/wiki/Xylene (2007).

263 Polypropylene-European product range, Available at http://www.credum.cz/file.php?nid=1930&oid=472488.

264 Santos, A. S. F., Agnelli, J. A. M., Trevisan, D. W. and Manrich, S., Degradation and stabilization of polyolefins from municipal plastic waste during multiple extrusions under different reprocessing conditions. *Polymer Degradation and Stability,* **77**, 441-447 (2002).

265 *The Aldrich Library of FTIR Spectra*, 2nd ed. (Aldrich, USA, 1997).

266 Silverstein, R. M., Clayton, G. B. and Morril, C. R., *Spectroscopic Identification of Organic Compounds*, 5th ed. (Willey Inter Science, New York, 1991).

267 Perera, R., Albano, C., Gonzalez, J., Silva, P. and Ichazo, M., The effect of gamma radiation on the properties of polypropylene blends with styrene-

butadiene-styrene copolymers. *Polymer Degradation and Stability,* **85**, 741-750 (2004).

268 Mirabedini, M. S., Rahimia, H., Hamedifara, S. and Mohsenib, S. M., Microwave irradiation of polypropylene surface: a study on wettability and adhesion. *International Journal of Adhesion and Adhesives,* **24**, 163-170 (2004).

269 Chen, Y. and Li, H., Phase morphology evolution and compatibility improvement of PP/EPDM by ultrasound irradiation. *Polymer,* **46**, 7707-7714 (2005).

270 Brandolini, A. J. and Hills, D. D., *NMR Spectra of Polymers and Polymer Additives* (Marcel and Dekker Inc., New York, 2000).

271 Cambell, D. and White, J. R., *Polymer Characterization- Physical Techniques* (Chapman and Hall, London, 1989).

272 Jungang, G., Shurun, L. and Zhiting, L., Melting behavior and nonisothermal crystallization kinetics of metallocene polyethylene. *Chemistry Magazine,* **5**, 81 (2003).

273 Karian, H. G., *Handbook of Polypropylene and Polypropylene Composites* (Marcel Dekkar Inc., New York, 1999).

274 Rubber identification infrared spectroscopic method Report No. BS ISO 4650 2005).

275 Ferdinandez-Berridi, M. J., Gonzalez, N., Mugica, A. and Bernicot, C., Pyrolysis-FTIR and TGA techniques as tools in the characterization of blends of natural rubber and SBR. *Thermochemica Acta,* **444**, 65-70 (2006).

276 Williams, P. T. and Besler, S., Pyrolysis-thermogravimetric analysis of tyres and tyre components. *Fuel,* **74**, 1277-1283 (1995).

277 Bhowmick, A. K. R., S; Gallagher, K.; Seeger, R. Mclntyre, D., The degradation of guayule rubber and the effect of resin components on degradation at high temperature. *Journal of Applied Polymer Science,* **33**, 1125-1139 (1987).

278 David, T. B., *Plastics Compounding: Equipment and Processing* (Hanser Publications, Ohio, 1998).

279 Yokoyama, Y. and Ricco, T., Toughening of polypropylene by different elastomeric systems. *Polymer,* **39**, 3675-3681 (1998).

280 Samsuri, A. B., Thomas, A. G. and Gelling, I. R., Tearing characteristics of epoxidised natural rubber, presented at the International Rubber Conference (Kuala Lumpur, 1985).

281 Lotti, C., Correa, C. A. and Canevarolo, S. V., Mechanical and morphological characterization of polypropylene toughened with olefinic elastomer. *Materials Research,* **3**, 37-44 (2000).

282 Murayama, T., *Dynamic Mechanical Analysis and Polymeric Materials* (Elsevier Scientific, Netherlands, 1978).

283 Yu, J. and He, J., Crystallization kinetics of maleic anhydride grafted polypropylene ionomers. *Polymer,* **41**, 891-898 (2000).

284 Shonaike, G. O., Mechanical and thermal properties of copoly(styrene/acrylonitrile) compatibilized Nylon-thermoplastic elastomer blends. *Plastics, Rubber and Composites,* **20**, 494-499 (1999).

285 Assouline, E., Lustiger, A., Barber, A. H., Cooper, C. A., Klein , E., Wachtel, E. and Wagner, H. D., Nucleation ability of multiwall carbon nanotubes in polypropylene composites. *Journal of Polymer Science: Part B: Polymer Physics,* **41**, 520-527 (2003).

286 Sengupta, P. and Noordermeer, J. W. M., Effects of composition and processing conditions on morphology and properties of thermoplastic elastomer bends of SEBS-PP-oil and dynamically vulcanized EPDM-PP-oil. *Journal of Elastomers and Plastics,* **36**, 307-331 (2004).

287 Brydson, J. A., *Flow Properties of Polymer Melts*, 2nd ed. (Godwin in association with the Plastics and Rubber Institute, London, 1981).

288 Shenoy, A. V., *Rheology of Filled Polymer Systems* (Kluwer Academic Publishers, London, 1999).

289 da Silva, A. L. N., Rocha, M. C. G., Moraes, M. A. R., Valente, C. A. R. and Coutinho, F. M. B., Mechanical and rheological properties of composites based on polyolefin and mineral additives. *Polymer Testing,* **21**, 57-60 (2002).

290 Shih, C.-K., Tynan, D. G. and Denelsbeck, D. A., Rheological properties of multicomponent polymer systems undergoing melting or softening during compounding. *Polymer Engineering and Science,* **31**, 1670-1673 (1991).

291 Elliot, D., in *Polymer Blends Volume 2 - Performance*, edited by Paul, D. C. and Bucknall, C. B. (John Willey and Sons, Canada, 2000).

292 Ceresa, R. J., in *Reclaimed Rubber- It's Development, Applications and Future*, edited by Nourry, A. (Mc. Learn & Sons Ltd., London, 1962).

293 Lattimer, R. P., Kinsey, R. A. and Layer, R. W., The mechanism of phenolic resin vulcanization of unsaturated elastomers. *Rubber Chemistry and Technology,* **62,** 107 (1989).

294 Van Duin, M., The chemistry of phenol-formaldehyde resin crosslinking of EPDM as studied with low-molecular-weight models: Part II. Formation of inert species, crosslinking precursors and crosslinks. *Rubber Chemistry and Technology,* **73,** 706 (2000).

295 Shurkus, A. A., Pipiraite, P. P., Bolotin, A. B. and Simanenkova, L. B., Electronic structure and reactivity of 2-mercaptobenzothiazole derivatives in the vulcanization of rubbers. *Theoretical and Experimental Chemistry,* **20,** 590-594 (1985).

296 Nieuwenhuizen, P. J., Zinc accelerator complexes. versatile homogeneous catalysts in sulfur vulcanization. *Applied Catalysis A: General,* **207,** 55-68 (2000).

297 Morgan, B. and McGill, W. J., Benzothiazole-accelerated sulfur vulcanization IV -Effect of ZnO and Bis(2-mercaptobenzothiazole)Zinc(II) on 2-Bisbenzothiazole-2,2'-polysulfide formation in 2-bisbenzothiazole-2,2'-disulfide and 2-Bisbenzothiazole-2,2'-disulfide/sulfur. *Journal of Applied Polymer Science,* **76,** 1405-1412 (2000).

298 Luyt, A. S., William, J. M. and Shillington, D., DSC study of the interaction of 2-mercaptobenzothiazole, sulphur, Zno and stearic acid in the absence of rubber. *Polymer Journal,* **23,** 135-139 (1990).

299 Nieuwenhuizen, P. J., Ehlers, A. W., Hassnoot, J. G., Janse, S. R., Reedijk, J. and Baerends, E. J., The mechanism if zinc(II)-dicarbamate-accelerated vulcanization uncovered; Theoritical and experimental evidence. *Journal of American Chemical Society,* **121,** 163-168 (1999).

300 Rai, A. K., Singh, R. P., Singh, K. N. and SIngh, V. B., FTIR, Raman spectra and an initio calculations of 2-mercaptobenzothiazole. *Spectrochemica Acta Part A,* **63,** 483-490 (2006).